LINKING NEUROINFLAMMATION AND GLIAL PHENOTYPIC CHANGES IN NEUROLOGICAL DISEASES

EDITED BY: Yu Tang, Xuping Li and Xiaobo Mao
PUBLISHED IN: Frontiers in Cellular Neuroscience

frontiers Research Topics

frontiers

ISSN 1664-8714
ISBN 978-2-88963-410-1
DOI 10.3389/978-2-88963-410-1

About Frontiers

Frontiers is more than just an open-access publisher of scholarly articles: it is a pioneering approach to the world of academia, radically improving the way scholarly research is managed. The grand vision of Frontiers is a world where all people have an equal opportunity to seek, share and generate knowledge. Frontiers provides immediate and permanent online open access to all its publications, but this alone is not enough to realize our grand goals.

Frontiers Journal Series

The Frontiers Journal Series is a multi-tier and interdisciplinary set of open-access, online journals, promising a paradigm shift from the current review, selection and dissemination processes in academic publishing. All Frontiers journals are driven by researchers for researchers; therefore, they constitute a service to the scholarly community. At the same time, the Frontiers Journal Series operates on a revolutionary invention, the tiered publishing system, initially addressing specific communities of scholars, and gradually climbing up to broader public understanding, thus serving the interests of the lay society, too.

Dedication to Quality

Each Frontiers article is a landmark of the highest quality, thanks to genuinely collaborative interactions between authors and review editors, who include some of the world's best academicians. Research must be certified by peers before entering a stream of knowledge that may eventually reach the public - and shape society; therefore, Frontiers only applies the most rigorous and unbiased reviews.
Frontiers revolutionizes research publishing by freely delivering the most outstanding research, evaluated with no bias from both the academic and social point of view. By applying the most advanced information technologies, Frontiers is catapulting scholarly publishing into a new generation.

What are Frontiers Research Topics?

Frontiers Research Topics are very popular trademarks of the Frontiers Journals Series: they are collections of at least ten articles, all centered on a particular subject. With their unique mix of varied contributions from Original Research to Review Articles, Frontiers Research Topics unify the most influential researchers, the latest key findings and historical advances in a hot research area! Find out more on how to host your own Frontiers Research Topic or contribute to one as an author by contacting the Frontiers Editorial Office: researchtopics@frontiersin.org

LINKING NEUROINFLAMMATION AND GLIAL PHENOTYPIC CHANGES IN NEUROLOGICAL DISEASES

Topic Editors:
Yu Tang, National Clinical Research Center for Geriatric Disorders, Xiangya Hospital, Central South University, China
Xuping Li, Houston Methodist Research Institute, United States
Xiaobo Mao, School of Medicine, Johns Hopkins University, United States

Citation: Tang, Y., Li, X., Mao, X., eds. (2020). Linking Neuroinflammation and Glial Phenotypic Changes in Neurological Diseases. Lausanne: Frontiers Media SA. doi: 10.3389/978-2-88963-410-1

Table of Contents

frontiers in Cellular Neuroscience

EDITORIAL
published: 05 December 2019
doi: 10.3389/fncel.2019.00542

Editorial: Linking Neuroinflammation and Glial Phenotypic Changes in Neurological Diseases

Yu Tang[1]*, *Xuping Li*[2] and *Xiaobo Mao*[3]

[1] National Clinical Research Center for Geriatric Disorders, Department of Geriatrics, Xiangya Hospital, Central South University, Changsha, China, [2] Department of Systems Medicine and Bioengineering, Houston Methodist Research Institute, Houston, TX, United States, [3] Department of Neurology, Johns Hopkins University School of Medicine, Baltimore, MD, United States

Keywords: neurological diseases, neuroinflammation, glial phenotype, microglia, astrocyte, neuroprotection

Editorial on the Research Topic

Linking Neuroinflammation and Glial Phenotypic Changes in Neurological Diseases

Glial cells, a major population of cells in the human nervous system, play a critical role in mediating neuroinflammation and have been demonstrated to be tightly associated with neuronal alterations. They take the responsibility for maintaining homeostasis in the nervous system, by regulating neurogenesis and synaptogenesis, modulating neuronal excitability and shaping synaptic connectivity. However, dysfunctional glial cells contribute to the pathogenesis of a variety of neurological diseases such as Parkinson's disease (PD), Alzheimer's disease (AD), Amyotrophic lateral sclerosis (ALS), Multiple sclerosis (MS), Traumatic brain injury (TBI), Neuropathic pain, Autism spectrum disorder (ASD), and various psychiatric disorders, among others. Different types of glial cells including microglia, astrocytes, and oligodendrocytes possess different functions and basically crosstalk with each other to amplify their functions. An increasing number of studies have focused on the phenotypic variants of glial cells, such as M1/M2 microglia (Tang et al., 2014; Tang and Le, 2016) and A1/A2 astrocytes (Liddelow et al., 2017) to define their detrimental or neuroprotective effects. However, emerging studies have over time revealed different facets of glial phenotypic diversity, and the advent of single-cell RNA-Seq analysis has added new insights into glial heterogeneity (Ransohoff, 2016; Colonna and Butovsky, 2017). It is increasingly believed that the roles of glial cells are heterogeneous and context-dependent, echoing different disease conditions. With the help of newly developed techniques, their functions are underway to be fully revealed.

This Research Topic in *Frontier in Cellular Neuroscience*, therefore, has produced a highly informative collection of original research, reviews, and mini-reviews that covered multiple aspects in delving neuroinflammation and glial phenotypic changes in the pathogenesis of neurological diseases. Researchers have presented their work and views on the potential mechanisms of both microglia and astrocyte activation that are critically associated with a broad spectrum of neurological diseases.

This topic started by focusing on the pivotal role of glial activation in neurodegenerative diseases. First, Refolo and Stefanova provided a review of the current literature about glial phenotypic changes with respect to alpha-synucleinopathies, as well as their pathophysiological and therapeutic implications. The major diseases characterized by alpha-synucleinopathies are PD, multiple system atrophy (MSA) and dementia with Lewy bodies (DLB). The misfolding and accumulation of α-synuclein, a stretch of 140-amino-acid-protein encoded by the *SNCA* gene, associates with constant neuroinflammation and glial activation that are crucial factors during disease development. The authors thus comprehensively reviewed the emerging

OPEN ACCESS

Edited and reviewed by:
Arianna Maffei,
Stony Brook University, United States

***Correspondence:**
Yu Tang
tangyu-sky@163.com

Specialty section:
This article was submitted to Cellular Neurophysiology, a section of the journal Frontiers in Cellular Neuroscience

Received: *28 October 2019*
Accepted: *22 November 2019*
Published: *05 December 2019*

Citation:
Tang Y, Li X and Mao X (2019) Editorial: Linking Neuroinflammation and Glial Phenotypic Changes in Neurological Diseases. Front. Cell. Neurosci. 13:542. doi: 10.3389/fncel.2019.00542

notions of the glial phenotypic changes with alpha-synucleinopathies, both for microglia and astrocyte, and as well-pointed out the mysterious glial unknowns that await us to explore. Another study by Gao et al. did a nice work that linked the pro-inflammatory exosome release with the AD pathogenesis. Particularly, they observed the elevated level of glutaminase C (GAC) in early AD models that may shift the microglial phenotype toward pro-inflammatory states. Overexpression of GAC increased the release of exosomes, where classical pro-inflammatory miRNAs (such as miR-155, miR-130, miR-145a, miR-23b, and miR-146a, etc.) were enriched and specific anti-inflammatory miRNAs (such as miR-124 and let-7b) were downregulated. This study established a causal link of GAC elevation and microglial phenotypic changes, and thereby potentially introducing an important risk factor to the AD development.

Later on, Araujo et al. described the microglial dysfunctions in several other disorders including ASD, neuropathic pain, and drug addiction. They then paid great attention to the small, lipid-derived molecules known as endogenous cannabinoids, or endocannabinoids, which are one component of the endocannabinoid system (ECS). Notably, stimulation of cannabinoid receptor 2 (CB2) is associated with anti-inflammatory, neuroprotective glial phenotypes, suggesting that ECS signaling may be a novel entry for understanding microglial biology and its relationship to those disorders, particularly as it relates to the effects of chronic cannabis (marijuana) use. Bradford et al. studied prion infections, which cause extensive neuropathology, including abnormal accumulations of misfolded host prion protein, spongiform pathology, and neuronal loss as well as reactive glial responses, characterized by distinct morphological changes and upregulation of glial fibrillary acidic protein (GFAP). The authors figured out that the CD44 antigen, a transmembrane glycoprotein involved in cell-cell interactions, cell adhesion and migration, is highly expressed in a subset of reactive astrocytes in brain regions affected by prions. As the upregulation pattern of CD44 is unique to each prion agent strain, CD44 can thus be exploited as a novel marker to detect reactive astrocyte heterogeneity and for enhanced identification of distinct prion agent strains. Another original study by Smith et al. also focused on reactive astrocytes, but turned to the explanation of behavioral abnormality in a non-anaphylactic mouse model of cow's milk allergy (CMA). They investigated the neuroinflammatory changes in the CMA model sensitized by beta-lactoglobulin (BLG), and observed significantly increased anxiety- and depression-associated behaviors for male mice. Those GFAP-immunoreactive astrocytes were particularly evoked with hypertrophic morphologies and may account for those neuropsychiatric behaviors.

TBI is one of the leading causes of mortality, morbidity, and disability. The neuroinflammatory response is critical to both neurotoxicity and neuroprotection and has been proposed as a potentially modifiable driver of secondary injury in animal and human studies. The study by Izzy et al. thus documented the temporal course of changes in inflammatory factors of microglia isolated from injured mice brains at acute, subacute, and chronic time points after focal cerebral contusion. They identified a time-dependent, injury-associated change in the microglial gene expression profile, which gives us a more comprehensive picture of temporal microglial roles in TBI pathogenesis and probably hints an appropriate time window for therapeutic intervention. Similarly, glial activation is also a prominent feature of the demyelinating lesions and that progressive MS is basically associated with chronic glial activation in the central nervous system (CNS). The study by Roboon et al. investigated the role of CD38 in mediating neuroinflammation during the demyelination process. CD38 was found to be upregulated in both microglia and astrocytes in the demyelinating area after cuprizone (CPZ)-induced demyelination. It is then revealed that CD38 deficiency attenuated CPZ-induced glial activation and inflammatory responses, demyelination, and neurodegeneration. This renders CD38 as a potential target for the therapy of MS and other demyelinating diseases.

As an extension of the CNS, spinal cord is also affected in several neurological diseases. However, accumulative evidences show that microglia in the brain and spinal cord are quite different in development, cellular phenotypes, and biological functions. This notion is underpinned by studies on TBI and spinal cord injury (SCI) that acute inflammatory responses to traumatic injury are significantly greater in the spinal cord than in the cerebral cortex. Xuan et al. therefore pointed out the differences in development and phenotypes of microglia between those two regions and discussed whether such diversity may contribute to CNS development and functions as well as neurological diseases. By knowing that, it may be more valuable to locally rather than globally target microglia activation to reduce damages in treating spinal cord-related neurological diseases.

In the next section, we gathered several studies focusing on exploring the potential molecular mechanisms of glial activation. First, as earlier mentioned, miR-155 is one of the upregulated miRNAs that exerts pro-inflammatory effects by targeting different mediators of inflammatory signaling. Li et al. investigated the role of miR-155 in the inflammatory responses particularly in heat-stressed microglia and probed the underlying mechanisms. Specifically, miR-155 enhanced the NF-κB signaling activation and induced several pro-inflammatory factors including interleukin-1β (IL-1β), interleukin-6 (IL-6) and tumor necrosis factor-α (TNF-α), through targeting liver X receptor α (LXRα). This study thus described the cellular mechanisms underlying the neuroinflammation that may provide guidelines for heat stroke prevention and therapy. Next, Wu et al. documented a microglial phenotypic change by lipoxin A4 (LXA4). LXA4 is one of the synthetic lipoxins that possess desirable anti-inflammatory properties in respiratory inflammation, intestinal inflammation, nephritis, and cerebral infarction. The authors focused on the regulatory role of LXA4 on the Notch signaling pathway. They proved that LXA4 could inhibit the expression of Notch1 and Hes1 associated with the M1 microglial phenotype, along with the decreased M1 markers such as inducible nitric oxide synthase (iNOS), IL-1β, and TNF-α. In

parallel, LXA4 could upregulate the expression of the M2-associated Hes5, as well as M2 markers such as arginase 1 (Arg1) and IL-10. Therefore, LXA4 could mediate the microglial phenotypic switch, from the pro-inflammatory M1 toward anti-inflammatory M2.

Next, studies focused on the specific inflammatory roles of hemichannels and pannexons located on glial cells. The study by Gómez et al. demonstrated that adolescent alcohol consumption could activate the opening of hemichannels and pannexons in hippocampal astrocytes, thereby inducing the astrogliosis and altering neuroinflammatory profiles. Particularly, intermittent ethanol exposure enhanced the opening of connexin-43 (Cx43) hemichannels and pannexin-1 (Panx1) channels in hippocampal astrocytes from adolescent rats, and activated several pro-inflammatory mediators including p38 mitogen-activated protein kinase (MAPK), iNOS, cyclooxygenases (COXs), as well as pro-inflammatory cytokines such as IL-1β, TNF-α, and IL-6. This would be also of use to decipher the pathogenesis of alcohol use disorders in adulthood. And another original study by Chávez et al., in the same research group, further went to the mechanistic research of the opening of Cx43 hemichannels that alters hippocampal astrocyte functions. As the release of glutamate triggered by Cx43 activation approaches the excitotoxic levels, the functions of hippocampal neurons would be disturbed, including the dendritic arbor and spine density, as well as survival. This brings us the notion that astrocyte-neuron crosstalk is an important aspect when investigating related neurological disorders. The understanding of how glia-neuron crosstalk might be a promising avenue toward the development of common therapies. Thus, in the following review paper by Veremeyko et al., the authors stressed the microglia-neuron crosstalk and particularly summarized the role of neuronal soluble factors that may affect microglial phenotypes and functions, as well as its possible involvement in the pathology of neurodegenerative diseases.

Aging is one of the most important risk factors for the onset and progression of neurodegenerative diseases, however, almost all experimental studies were selectively carried out in young animals. In the study by Gil-Martínez et al., they evaluated the possible protective effects of an antioxidant (N-acetylcysteine, NAC) and anti-inflammatory agent (fasudil), respectively in aged PD mice. Although they produced beneficial effects individually, the combination usage gave rise to exacerbated dopaminergic neuron death accompanied by increased gliosis. This result raised the caveat that in elderly patients the combination of some drugs may unexpectedly have side effects, leading to the exacerbation of the neurodegenerative process.

Overall, this series of articles within the Research Topic have brought several interesting understandings of neuroinflammation in a range of neurological diseases, linking with glial phenotypic changes and novel neuroinflammation mechanisms. We expect that this topic would expand our knowledge on the biological basis of glia-mediated neuroinflammation, and also give exciting insights into new therapeutic approaches to efficiently treat neurological diseases, through targeting glial cells.

AUTHOR CONTRIBUTIONS

YT proposed and edited this Research Topic. XL and XM co-edited this Research Topic.

FUNDING

This study was supported by grants from the National Natural Sciences Foundation of China (No. 81801200) and Hunan Provincial Natural Science Foundation of China (No. 2019JJ40476).

ACKNOWLEDGMENTS

I would like to greatly thank XL and XM who acted as co-editors on this topic.

REFERENCES

Colonna, M., and Butovsky, O. (2017). Microglia function in the central nervous system during health and neurodegeneration. *Annu. Rev. Immunol.* 35, 441–468. doi: 10.1146/annurev-immunol-051116-052358

Liddelow, S. A., Guttenplan, K. A., Clarke, L. E., Bennett, F. C., Bohlen, C. J., Schirmer, L., et al. (2017). Neurotoxic reactive astrocytes are induced by activated microglia. *Nature* 541, 481–487. doi: 10.1038/nature21029

Ransohoff, R. M. (2016). A polarizing question: do M1 and M2 microglia exist? *Nat. Neurosci.* 19, 987–991. doi: 10.1038/nn.4338

Tang, Y., and Le, W. (2016). Differential roles of M1 and M2 microglia in neurodegenerative diseases. *Mol. Neurobiol.* 53, 1181–1194. doi: 10.1007/s12035-014-9070-5

Tang, Y., Li, T., Li, J., Yang, J., Liu, H., Zhang, X. J., et al. (2014). Jmjd3 is essential for the epigenetic modulation of microglia phenotypes in the immune pathogenesis of Parkinson's disease. *Cell Death Differ.* 21, 369–380. doi: 10.1038/cdd.2013.159

Conflict of Interest: The authors declare that the research was conducted in the absence of any commercial or financial relationships that could be construed as a potential conflict of interest.

frontiers in Cellular Neuroscience

ORIGINAL RESEARCH
published: 30 November 2018
doi: 10.3389/fncel.2018.00451

Unexpected Exacerbation of Neuroinflammatory Response After a Combined Therapy in Old Parkinsonian Mice

*Ana Luisa Gil-Martínez[1,2], Lorena Cuenca[1,2], Cristina Estrada[1,2], Consuelo Sánchez-Rodrigo[1,2], Emiliano Fernández-Villalba[1,2] and María Trinidad Herrero[1,2]**

[1] Clinical and Experimental Neuroscience Group (NiCE-IMIB), Department of Human Anatomy and Psychobiology, Institute for Aging Research, School of Medicine, University of Murcia, Murcia, Spain, [2] Biomedical Research Institute of Murcia (IMIB-Arrixaca), Campus of Health Sciences, University of Murcia, Murcia, Spain

The design of therapeutic strategies that focus on the repositioning of anti-inflammatory and antioxidant drugs are a great bet to slow down the progression of neurodegenerative disorders. Despite the fact that Parkinson's disease (PD) is an age-related pathology, almost all experimental studies are carried out in young animals. Here, we evaluated the possible neuroprotective effect of the combination of the antioxidant N-acetylcysteine (NAC) and the anti-inflammatory HA-1077 in aged 1-methyl-4-phenyl-1,2,3,6-tetrahydropyridine (MPTP)-treated mice (C57BL/6 mice, 20 months old), whose individual treatment has been shown to have neuroprotective effects in this Parkinsonism model. Interestingly, NAC+HA-1077-based treatment produced a significant increase in dopaminergic neuronal death accompanied by an increase in microglial and astroglial activation in the Substantia Nigra *pars compacta* (SNpc) and striatum of old-Parkinsonian mice compared to their control group. The astroglial response was also explored by co-immunostaining for GFAP and S100b together with p-JNK and it was found to be particularly exacerbated in the MPTP+NAC+HA-1077 group. The unexpected toxic effects found in the combined use of NAC and HA-1077 in old-Parkinsonian mice highlight the importance of taking into account that in elderly Parkinsonian patients the combination of some drugs (most of them used for other different age-related alterations) can have side effects that may result in the exacerbation of the neurodegenerative process.

Keywords: aging, drug-repositioning, glia, neuroinflammation, oxidative stress, Parkinsonism

OPEN ACCESS

Edited by:
Xiaobo Mao,
School of Medicine, Johns Hopkins University, United States

Reviewed by:
Jooho Shin,
School of Medicine, Sungkyunkwan University, South Korea
Jianmin Zhang,
Chinese Academy of Medical Sciences, China

****Correspondence:***
María Trinidad Herrero
mtherrer@um.es;
herreromt@gmail.com

Received: *25 September 2018*
Accepted: *08 November 2018*
Published: *30 November 2018*

Citation:
Gil-Martínez AL, Cuenca L, Estrada C, Sánchez-Rodrigo C, Fernández-Villalba E and Herrero MT (2018) Unexpected Exacerbation of Neuroinflammatory Response After a Combined Therapy in Old Parkinsonian Mice. Front. Cell. Neurosci. 12:451. doi: 10.3389/fncel.2018.00451

INTRODUCTION

Parkinson's disease (PD) is a pathology based on the chronic and the progressive loss of dopaminergic neurons in the Substantia Nigra *pars compacta* (SNpc) that results in a decrease of dopamine levels in the nigrostriatal pathway. This fact implies the development of motor alterations as stiffness, bradykinesia, resting tremor and postural instability. PD is the second most prevalent

Abbreviations: CNS, Central Nervous System; DA, dopaminergic; ERK, Extracellular signal-regulated kinase; GFAP, glial fibrillary acidic protein; Iba-1, ionized calcium-binding adapter molecule 1; JNK, c-Jun NH2-terminal kinase; MAPKs, Mitogen-activated protein kinases; MPTP, 1-methyl-4-phenyl-1,2,3,6-tetrahydropyridine; NAC, N-acetylcysteine; PD, Parkinson's Disease; ROS, Reactive Oxygen Species; SNpc, Substantia Nigra *pars compacta;* TH, Tyrosine hydroxylase; VTA, Ventral Tegmental Area.

neurodegenerative disorder that affects 100–200 per 100,000 people at the age of 65–70 years (Tysnes and Storstein, 2017). Although the cause of the disease is not clear yet, many studies emphasize aging as the main risk factor that contributes to the development of the disease (Collier et al., 2017) over other described risk factors, as genetic causes (Kalia and Lang, 2015) or exposure to environmental neurotoxins such as 1-methyl-4-phenyl-1,2,3,6-tetrahydropyridine (MPTP) (Kopin and Markey, 1988).

In this line, it is crucial to take into account the close relationship between aging and PD to understand the progression of the disease. An elderly condition exacerbates the main pathogenic pathways described as etiological bases of PD such as mitochondrial dysfunction (Bose and Beal, 2016), dysregulation of protein homeostasis (Sin and Nollen, 2015) and oxidative stress (Gaki and Papavassiliou, 2014). However, aging is a variable hardly ever incorporated in the studies with experimental animals as it entails a risk in the subjects' mortality and an increase in the associated costs. Only a few *post-mortem* analysis have been carried out in PD patients with genetic predisposition along with age-associated immunological alterations that have demonstrated an association between slight inflammation in the CNS and vulnerability to the degeneration of dopaminergic neurons (Tiwari and Pal, 2017). In the CNS, glial cells are the main responsible in the immune response. Firstly, after an injury microglial cells are activated and they migrate to the damaged area to phagocytize the apoptotic cells. If the pathological condition progresses, there is an imbalance of the pro-inflammatory over the anti-inflammatory processes that triggers the exacerbation of the response, probably activating astrocytes (Halliday and Stevens, 2011). Both PD and aged brains seem to share a similar inflammatory condition entitled "neuro-inflammaging," characterized by complex processes where astrocytes and microglial cells chronically produce several toxic agents (i.e., pro-inflammatory cytokines) which damage neighboring neurons (Rodriguez et al., 2015).

Different protein families mediate the activation and maintenance of glial-related processes (Dagda et al., 2009). Among them, we highlight the signaling pathway of the mitogen-activated protein kinases (MAPKs). This family is composed of an extracellular signal-regulated kinase (ERK), c-Jun NH2-terminal kinase (JNK), and p38 MAPK. In the last years, MAPKs have been shown to be involved in the development of some neurodegenerative diseases such as Alzheimer's or Parkinson's disease. The role of JNK is interesting as it has been demonstrated to be involved in the activation of cellular processes such as the release of pro-inflammatory cytokines and the oxidative stress response mediated by microglia and astroglia, thus contributing to the progression of neuroinflammation (Kim and Choi, 2015).

Considering the important role of inflammatory processes and oxidative stress, different research groups around the world focus their efforts on the study of the effect of anti-inflammatory drugs on dopaminergic neuronal death. In recent years, a new therapeutic strategy called "drug repositioning" has been introduced for the design and development of new treatments for PD patients. Drug repositioning consists of refocusing medicines indicated for other pathologies that have been demonstrated to have a positive effect in PD development (Brundin et al., 2015). The main advantage of this strategy is the availability of human clinical studies about the reliability and safety of these drugs (Maiti et al., 2017). This issue becomes especially controversial in PD and other age-related disorders whose patients are poly-medicated, both for the treatment of the disease and for the age-associated problems. The elderly patients have a less plastic brain and therefore, are more vulnerable to the severe toxicity produced by drug interaction (Savva et al., 2009).

Based on the previously described data, in the present study, we wanted to analyze the effect of an anti-inflammatory (fasudil, HA-1077) and antioxidant (N-acetylcysteine, NAC) in old-Parkinsonian mice. Both drugs have been shown to have an individual beneficial effect on both dopaminergic neuronal death and glial response. HA-1077 is a ROC-kinase inhibitor, a protein that is essential for the motility and phagocytic capacity of microglia. Previous studies from our research group showed that the use of HA-1077 decreases the activation of microglia in MPTP-intoxicated mice (Barcia et al., 2012). Additionally, Pan and co-workers demonstrated that treatment with the clinical commonly used antioxidant N-acetylcysteine (NAC), an inhibitor of the activation of JNK signaling pathway, has a protective effect on dopaminergic neuronal death in the young MPTP mouse model (Pan et al., 2009). Thus, our aim was to study the synergistic effect of a combined treatment of NAC and HA-1077 on dopaminergic neuronal death and inflammatory processes in old mice intoxicated with MPTP.

MATERIALS AND METHODS

Animals

The studies were performed on 64 male elderly C57BL/6J mice (20 months of age, weight 27–29 g) provided by Eleverge Janvier (Le Genest St Isle, France) and maintained in an isolated room with access to water and food *ad libitum*, under ambient conditions (20 ± 2°C) and light cycles: darkness of 12:12 h. All animal testing methods and procedures were approved by the Council of the European Community Committee (2010/63/EU) and by the Institutional Committee on Animal Ethics of the University of Murcia (REGA ES300305440012).

Experimental Design and Animal Model of Parkinsonism

Animals were divided into two main groups: non-MPTP group (n = 24) and MPTP group (n = 40). Parkinsonism was induced via intraperitoneal (i.p.) injection of the neurotoxin 1-methyl-4-phenyl-1,2,3,6-tetrahydropyridine (MPTP, Sigma-Aldrich), which specifically causes dopaminergic neuronal death. The dose administered per animal was 30 mg/kg, divided into two injections of 15 mg/kg each and spaced 5 h over a day (**Figure 1**; Jackson-Lewis and Przedborski, 2007; Annese et al., 2015).

Drug Administration

The animals belonging to the two main groups (both non-MPTP and MPTP) were divided into four subgroups according

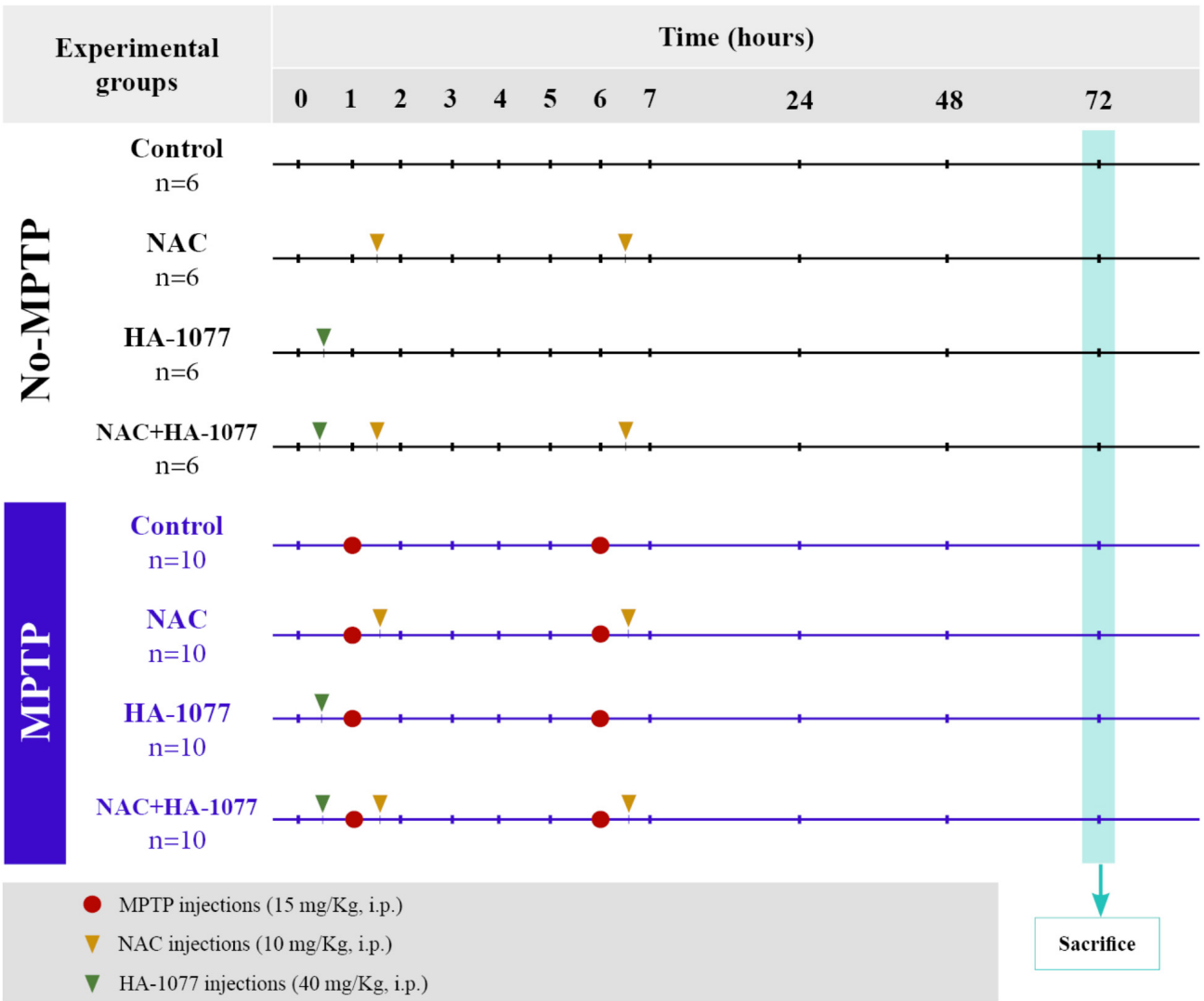

FIGURE 1 | Scheme of the experimental design and distribution of the groups and animals with their respective treatments.

to the treatment: (i) control (untreated); (ii) NAC; (iii) HA-1077; (iv) NAC+HA-1077. NAC treated groups received a dose of 100 mg/Kg (i.p.) of NAC (Sigma Aldrich) half an hour after each injection of MPTP (NAC and MPTP+NAC and MPTP+NAC+HA-1077), following the protocol described by Pan et al. (2009). A dose of 40 mg/Kg (i.p.) of HA-1077 (Sigma-Aldrich) half an hour before the first MPTP injection were administrated to HA-1077, MPTP+HA-1077, and MPTP+NAC+HA-1077 groups (**Figure 1**), following the protocol described by Barcia et al. (2012).

Sample Preparation

Seventy two hours after the drug treatment, the animals were sacrificed by cervical dislocation under an overdose of ketamine (50 mg/Kg, Imagene, Merial) and Xylazine (50 mg/Kg, Xilagesic, Calier Laboratories). For immunohistochemistry and immunofluorescence, brains were extracted, fixed overnight at 4°C in 4% paraformaldehyde in phosphate buffered saline or PBS (0.1 M, pH 7.4), washed with ethanol and embedded in paraffin. For Western Blot and ELISA, brains were extracted and immediately frozen. The cerebellum, midbrain and striatum were dissected according to the coordinates of the mouse brain atlas (Franklin and Paxinos, 2008). The tissue was homogenized with RIPA lysis buffer: 50 mM Tris-HCl pH 7.6, 150 mM NaCl, 5 mM EDTA, 1% Triton X-100, 1% SDS, 50 mM NaF, protease and phosphatases inhibitors (Abcam). Tissue extracts were incubated 2 h at 4°C under constant stirring. Samples were centrifuged (13,000 rpm, 20 min at 4°C) and the supernatant was collected. Total protein concentration was determined (Pierce BCA Protein Assay Kit, Thermo Scientific) and Western Blot and ELISA were performed according to the protocol detailed above.

The number of animals used for immunohistochemical (IHQ)/immunofluorescence (IF) analysis was $n = 3$ in the No-MPTP groups (control, NAC, HA-1077, NAC+HA-1077) and

TABLE 1 | Antibodies and protocols for the different techniques.

Primary antibodies	Host, code	Application	Antibody supplier, dilution, incubation period	Secondary antibodies, code	Antibody supplier, dilution, incubation period
Anti-TH	Mouse MAB318	IHQ[a]	Millipore, 1:500, ov	Anti-IgG mouse (Biotynilated) BA-9200	Vector Laboratories, 1:250, 1 h
		WB[c]	Millipore, 1:5000, ov	Anti-IgG mouse (HRP) 115-035-003	Jackson Immunoresearch, 1:5000, 2 h
		IF[b]	Millipore, 1:500, ov	Double Labeling Kit[d] DK-8818	Vector Laboratories, 30 min
Anti-Iba1	Rabbit B178846	IHQ[a]	Abcam, 1:1000, ov	Anti-IgG rabbit (Biotynilated) BA-1000	Vector Laboratories, 1:250, 1 h
		IF[b]	Abcam, 1:1000, ov	Double Labeling Kit[d] DK-8818	Vector Laboratories, 30 min
Anti-GFAP	Mouse MAB360	IHQ[a]	Millipore, 1:500, ov	Anti-IgG mouse (Biotynilated) BA-9200	Vector Laboratories, 1:250, 1 h
		IF[b]	Millipore, 1:500, ov	Double Labeling Kit[d] DK-8818	Vector Laboratories, 30 min
	Rabbit AB7260	IF[b]	Millipore, 1:500, ov	Double Labeling Kit[d] DK-8818	Vector Laboratories, 30 min
Anti-S100b	Rabbit AB52642	IF[b]	Abcam, 1:500, ov	Double Labeling Kit[d] DK-8818	Vector Laboratories, 30 min
Anti-JNK3	Rabbit AB87404	WB[c]	Abcam, 1:5000, ov	Peroxidase anti-rabbit IgG 111-035-144	Jackson Immunorearch, 1:5000, 2 h
Anti-GADPH	Mouse AB9684	WB[c]	Abcam, 1:5000, ov	Anti-IgG mouse (HRP) 115-035-003	Jackson Immunorearch, 1:5000, 2 h
Anti-Phopho-SAPK/JNK	Mouse #9255	IF[b]	Cell signaling, 1:200, ov	Double Labeling Kit[d] DK-8818	Vector Laboratories, 30 min

[a]*Immunohistochemistry.* [b]*Immunofluorescence.* [c]*Western Blot.* [d]*VectaFluor Duet Immunofluorescence Double Labeling Kit, DyLight 488 Anti-Rabbit (green)/DyLight 594 Anti-Mouse (red).*

$n = 5$ in the MPTP groups (control, NAC, HA-1077, NAC+HA-1077). For Western Blot and ELISA experiment, the number of animals used was $n = 3$ in the No-MPTP groups (control, NAC, HA-1077, NAC+HA-1077) and $n = 5$ in the MPTP groups (control, NAC, HA-1077, NAC+HA-1077).

Immunohistochemistry and Immunofluorescence

Coronal sections (7 μm) of SNpc and striatum were cut on microtome (Thermo Scientific HM 325 Rotary Microtome, Thermo Fisher Scientific). The sections were deparaffinized in xylene, rehydrated in a gradient of ethanol (100, 95, and 80%) and distilled water. Antigenic retrieval was performed in citrate buffer 30 min at 95°C (10 mM citric acid, pH 6.0). In immunohistochemistry, endogenous peroxidase was inhibited with a solution of 0.3% H_2O_2 for 20 min and non-specific binding of the antibodies was blocked (both in immunohistochemistry and immunofluorescence) in a blocking solution for 30 min: tris-buffered saline 0.1 M pH 8.4 (TBS_{IHQ}), 10% goat serum and 0.5% Triton X-100. After two washes with TBS_{IHQ} the samples were incubated with the corresponding primary antibody overnight at 4°C (**Table 1**). Primary antibodies used in immunohistochemistry and immunofluorescence were diluted in TBS_{IHQ}+Tween 0.5%+1% goat serum at the dilution indicated in **Table 1**. Following the primary antibody, two washes were performed with TBS_{IHQ} and sections were incubated with the secondary antibody diluted in TBS_{IHQ} at the concentrations indicated in **Table 1** for 30 min in immunohistochemistry (4 h in immunofluorescence). Sections were washed with TBS_{IHQ} and incubated at room temperature (RT) with avidin/biotin conjugated to peroxidase (ABC Elite Kit, Vector Laboratories), staining using the kit 3,3′-diaminobenzidine (DAB Peroxidase HRP Substrate Kit, Vector Laboratories) and, finally, assembly was performed for observation under the optical microscope. In the case of immunofluorescence, after washing with TBS_{IHQ} after incubation with the secondary antibody, the samples were assayed (VECTASHIELD Antifade Mounting Medium, Vector Laboratories).

Quantification of DAB and Immunofluorescence Labeling

For DAB labeling quantification, images were obtained by Hall 100 ZEISS optical microscope with an Axiocam ZEISS digital camera and were analyzed using the NIH ImageJ software (ImageJ; NIH, Bethesda, MD, United States). Field size was set at 1088 × 1040 pixels. All the analysis were performed without post-processing the images.

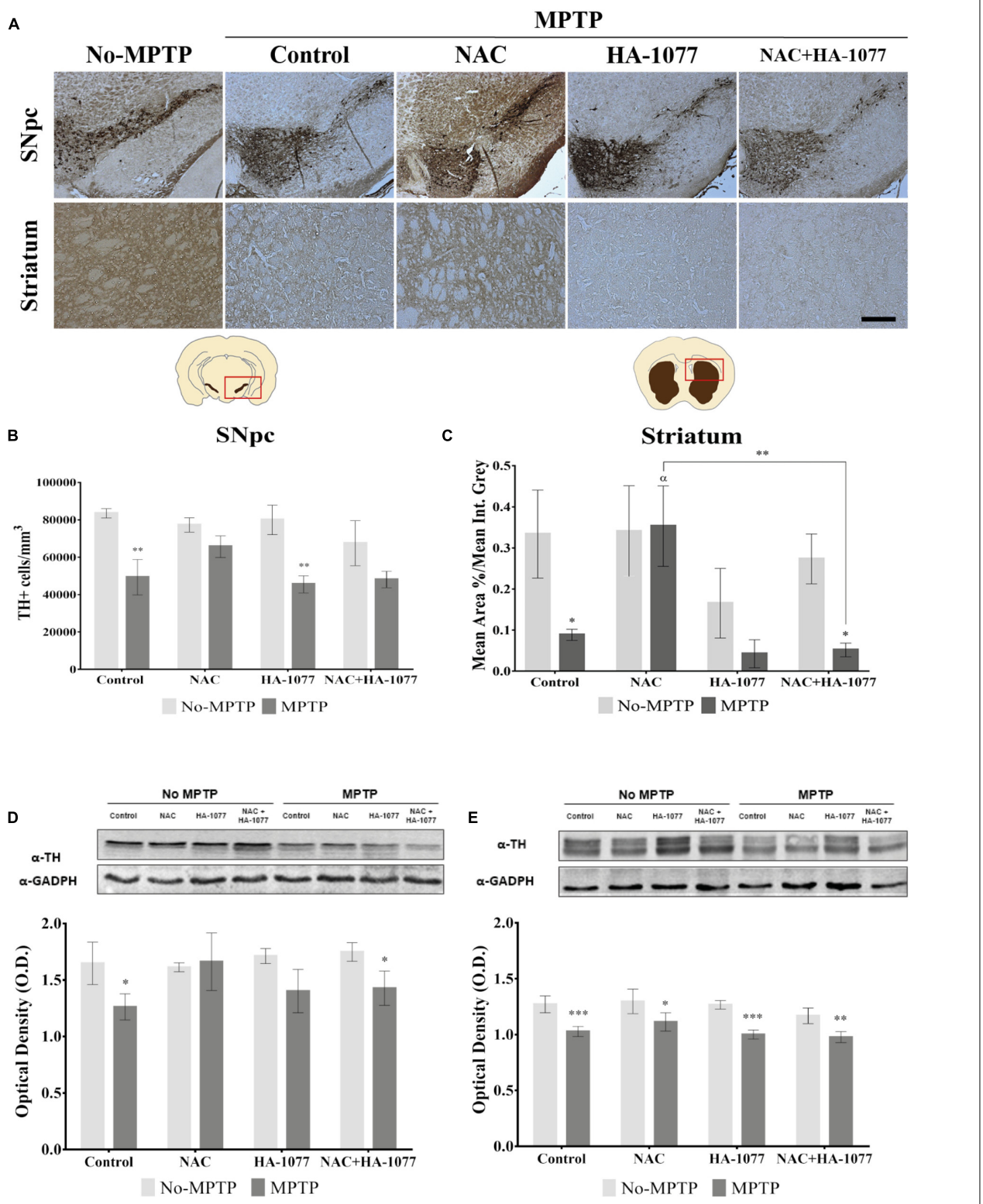

FIGURE 2 | Effect of the different treatments (NAC, HA-1077 and NAC+HA-1077) on dopaminergic neuronal death. **(A)** Representative micrographs of TH immunostaining in coronal sections at the SNpc and striatum levels: No-MPTP, MPTP, MPTP+NAC, MPTP+HA-1077, MPTP+NAC+HA-1077 (Magnification 10×, Scale bar = 100 μm). **(B,D)** Quantification of TH expression in SNpc by immunohistochemical analysis. **(B)** Very significant increase in dopaminergic neuronal death

(Continued)

FIGURE 2 | Continued
was in MPTP (**p = 0.0026) and MPTP+HA-1077 (**p = 0.0025) compared with their No-MPTP groups. **(D)** Western Blot results showed a significant decrease in TH expression in MPTP (*p = 0.0101) and MPTP+NAC+HA-1077 (*p = 0.0221). **(C,E)** Quantification of TH expression in the striatum. **(C)** Immunohistochemical analysis showed a significant decrease of TH expression in the innervations of the dopaminergic neurons in MPTP (*p = 0.0126) and MPTP+NAC+HA-1077 groups (*p = 0.0117) compared with their control groups. MPTP+NAC vs. MPTP (α = 0.0286) and MPTP+NAC vs. MPTP+NAC+HA-1077 (**p = 0.0046). **(E)** Quantification by Western Blot of TH protein expression showed significant differences in MPTP+NAC (*p = 0.0103) and a very significant in MPTP (***p = 0.0003), MPTP+HA-1077 (***p = 0.0006) and MPTP+NAC+HA-1077 (**p = 0.0076) compared with their No-MPTP groups.

SNpc and striatum areas were delimitated according to anatomical coordinates (Franklin and Paxinos, 2008). For each immunolabeling, eight serial sections of the SNpc and striatum of each animal were used at different rostrocaudal levels (1 section in every 10) and quantified following the conditions reported by Blesa et al. (2012). The serial sections used for the SNpc analysis were located in the anatomical coordinates between bregma -2.06 and -3.80 mm and for the striatum from bregma 0.02–0.26 mm (for more details see **Supplementary Figures S1, S2**). The quantification of all immunohistochemical analysis were performed in the striatum (both hemispheres in each slice) in micrographs covering the whole surface area of the dorsolateral region taken with the 20× magnification and using the principle of the optical dissector (Sterio, 1984). Positive cells were counted only when they touched the superior and left limit of the square. A representative image of the No-MPTP groups has been shown for each marker in the **Supplementary Figure S3**.

Quantification of TH-Positive (TH+) Cells

In SNpc, the total number of TH+ cells was determined using the 20× objective and results are expressed as the number of TH+ cells/mm^3. Counting unit was the nucleus surrounded by immunoreactive cytoplasm. The area of the SNpc was calculated by a systematic non-biased method. In the striatum, the dopaminergic innervations were quantified by measuring the optical density (O.D.) of DAB signal, expressed as Area (%)/mean gray value (Barcia et al., 2005).

Quantification and Stereological Analysis of Microglia

The study of microglia cells was performed using the marker Iba-1. Iba-1+ cells were counted in the SNpc and in the striatum and were expressed as Iba-1+ cells/mm^3. Counting unit was the nucleus surrounded by immunoreactive cytoplasm.

Quantification of GFAP+ Cells (Astrocytes) and Stereological Analysis of GFAP+ Astroglia

The number of GFAP+ cells in SNpc and striatum was determined following the same procedure as the one described for microglia analysis but using as counting unit the nucleus surrounded by GFAP-immunoreactive cytoplasm, and expressed as GFAP+ cells/mm^3.

Iba-1+ and GFAP+ Cells Morphological Analysis

For microglia and astroglia morphological analysis at SNpc and striatum level, immunolabeling of Iba-1 and GFAP was performed. For each label, we acquired z-stack images at 0.5 μm intervals using a confocal microscope Leica TCS-SP8 (SACE, University of Murcia) with the 63× glycol-immersion objective lens at optical zoom of 0.75 (x-axis x y-axis, 1024 × 1024 pixels). In order to avoid quantification and measurement bias, all the images were obtained under the same setting conditions. Morphological analysis was performed by O.D. measure following the protocol described by Otsu (1979) and, subsequently, developed by Tatsumi et al. (2016). We used ImageJ software (NIH, Bethesda, MD, United States) to convert the images to 8 bit grayscale images and to determine mean O.D. values. For each immunolabeling and area (GFAP or Iba-1, SNpc or striatum), 1/4 images out of a total 24 images in three different regions of each animal were measured to obtain the average O.D. value of the z-stack images.

Western Blot

Equal amounts of protein (30 μg) from each tissue extract were resolved in 12% polyacrylamide gels under denaturing conditions at constant voltage (110 V) at RT. After electrophoresis, proteins were transferred to PVDF membranes (Immobilon, Millipore) at constant voltage (20 V, 50 min, Trans-Blot SD Semi-Dry Transfer Cell, Bio-Rad) using the transfer buffer: 25 mM Tris-HCl, 192 mM glycine, 0.1% SDS, 20% methanol. Membranes were incubated for 1 h and constant stirring in blocking solution: 0.1 M TBS pH 7.5 (TBS_{WB}) + 0.05% Tween-20 (TBST) + 5% BSA. Membranes were then incubated with the specific primary antibody at 4°C overnight and constant stirring (**Table 1**). Primary antibodies used in Western Blot were diluted in TBST + 3% BSA at the dilution as referred in **Table 1**. Primary anti-glyceraldehyde-3-phosphate dehydrogenase (GADPH) antibody was added as the internal loading control of protein. After incubation with the primary antibody and 3 washes with TBST, the membranes were incubated with the corresponding peroxidase-conjugated secondary antibody (**Table 1**) diluted in TBST, at RT and constant agitation for 2 h. Protein detection was performed using the 3,3′-diaminobenzidine kit (DAB Peroxidase HRP Substrate Kit, Vector Laboratories). For TH, a specific band of approximately 60 kDa was detected in the SNpc and three specific bands of 55–60 kDa were detected at striatum level. The signal quantification was performed in the 60 kDa band as it has been described to be the functional isoform of the protein (Tabrez et al., 2012).

To calculate the intensity of the bands the membranes were scanned and analyzed by densitometry analysis using the ImageJ software. The optical density of each band corresponding to the protein of interest was normalized individually with the optical density of the GADPH band obtained for the sample from the same well. Densitometric analysis and quantification of the protein bands was performed using the ImageJ software.

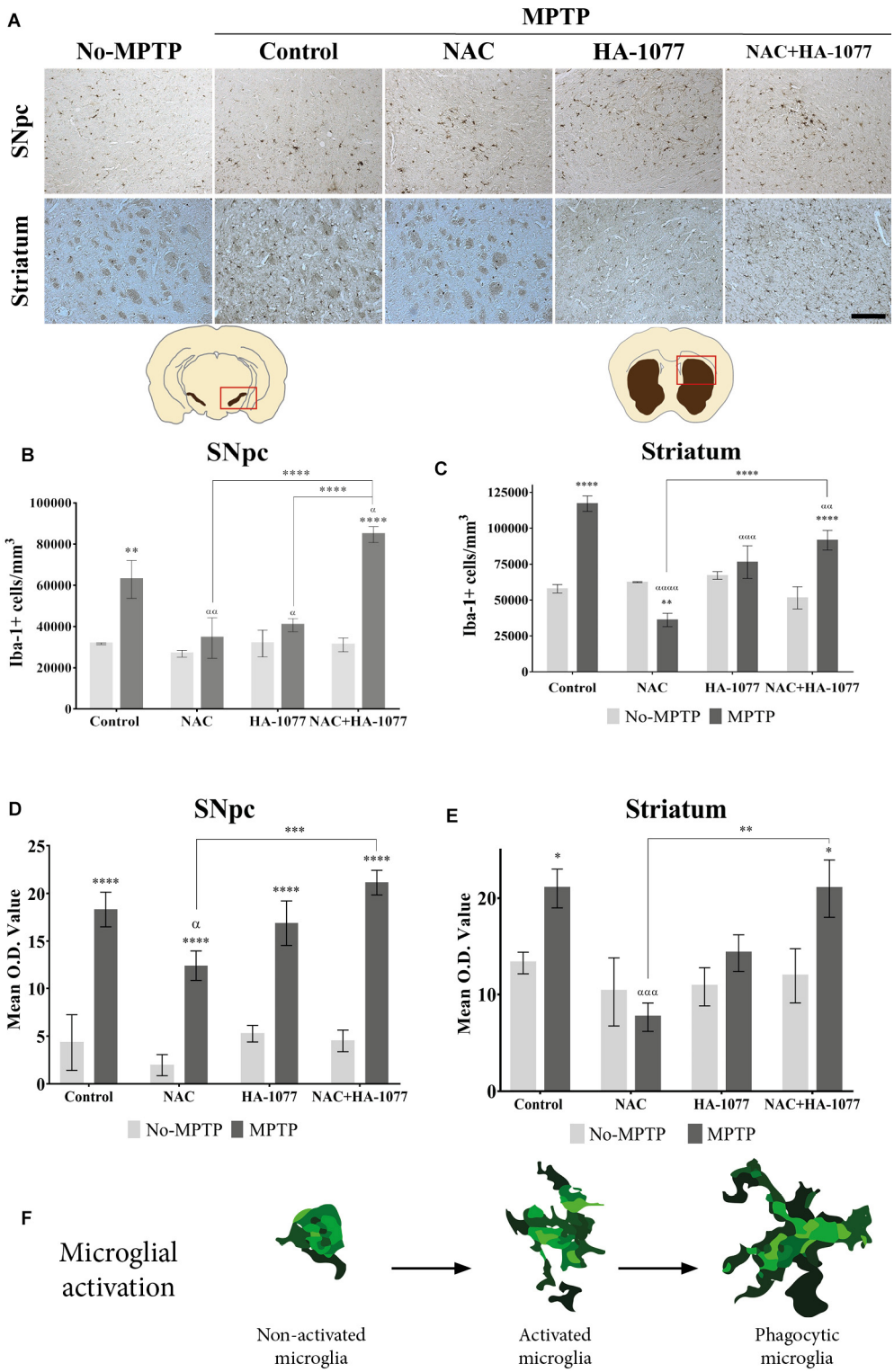

FIGURE 3 | Iba-1+ cell count depends on different treatments in old-Parkinsonian mice. **(A)** Immunohistochemical staining with Iba-1 of coronal sections of SNpc and striatum (Magnification 20×, Scale bar = 100 μm). **(B)** Quantification of Iba-1+ cells in the SNpc by immunostaining analysis. The results showed a significant increase of Iba-1+ cells in MPTP treated mice (**$p = 0.002$) and very significant in MPTP+NAC+HA-1077 (****$p < 0.0001$) compared with their control groups. MPTP vs. MPTP+NAC (αα = 0.0020); vs. MPTP+HA-1077 (α = 0.0196); and, vs. MPTP+NAC+HA-1077 (α = 0.0222). MPTP+NAC+HA-1077 vs. MPTP+NAC (****$p < 0.0001$) and vs. MPTP+HA-1077 (****$p < 0.0001$). **(C)** Mean O.D. value measurement for Iba-1+ cells in the SNpc for the morphological

(Continued)

FIGURE 3 | Continued
changes analysis. A very significant increase was found in MPTP, MPTP+NAC, MPTP+HA-1077 and MPTP+NAC+HA-1077 (****$p < 0.0001$) compared to their respective No-MPTP groups. MPTP vs. MPTP+NAC ($\alpha = 0.0344$) and MPTP+NAC vs. MPTP+NAC+HA-1077 (***$p = 0.0004$). **(D)** Iba-1+ cells quantification in the striatum. It was observed a significant increase of Iba-1+ cells in MPTP (**** $p < 0.0001$) and MPTP+NAC+HA-1077 (****$p < 0.0001$). In contrast, a significant decrease in the number of Iba-1+ cells was observed in the MPTP+NAC group compared to its control group (**$p = 0.0011$). MPTP vs. MPTP+NAC ($\alpha < 0.001$); vs. MPTP+HA-1077 ($\alpha = 0.0001$); vs. MPTP+NAC+HA-1077 ($\alpha < 0.0001$). **(E)** Mean O.D. value measurement for Iba-1+ cells in the striatum. MPTP (*$p = 0.0215$) and MPTP+NAC+HA-1077 (*$p = 0.0150$) showed a significant increase in the Mean O.D. value compared to No-MPTP groups (Control and HA-1077, respectively). MPTP vs. MPTP+NAC ($\alpha\alpha\alpha = 0.0005$) and MPTP+NAC vs. MPTP+NAC+HA-1077 (**$p = 0.0011$). **(F)** Illustration of microglial activation profiles found in the different experimental groups: non-activated microglia, activated microglia and phagocytic microglia.

ELISA

Total JNK1/2 levels and phosphorylated-JNK1/2 levels were measured using Enzyme-Linked Immunoabsorbent Assay (ELISA). The assay was conducted using JNK1/2 (pT183/Y185) + Total JNK1/2 SimpleStep ELISA^{TM} Kit (Abcam) according to the manufacturer's protocols. Signal generated was read as absorbance at 450 nm using CLARIOstar reader (BMG LABTECH).

Data and Statistical Analysis

Data are shown as mean ± SD. The statistical analysis were performed with GraphPrism 7.0 software using a two-way ANOVA test followed by *post hoc* analysis Sidak. The null hypothesis was rejected considering values of $p < 0.05$ in all cases.

RESULTS

The Combined Treatment NAC+HA-1077 Does Not Prevent Dopaminergic Neuronal Death in Parkinsonian Mice

To verify the possible neuroprotective effect of the combined treatment NAC+HA-1077 on the loss of dopaminergic neurons, immunohistochemical staining of TH in SNpc and in the striatum was performed (**Figure 2A**). As shown in **Figure 2**, dopaminergic neuronal death at the SNpc level was statistically very significant in the MPTP group ($p = 0.0026$) compared to the control group. These results validated our model for Parkinsonism. Similar results were obtained for the dopaminergic cell loss of the MPTP+HA-1077 group compared to its control ($p = 0.0025$). Surprisingly, no significant differences were observed in the TH+cells/mm^3 in the MPTP+NAC+HA-1077 group compared to the control group (**Figure 2B**). The levels of TH expression in the striatum were significantly decreased in the MPTP ($p = 0.0126$) and MPTP+NAC+HA-1077 ($p = 0.0117$) groups compared to their respective No-MPTP groups (**Figure 2C**). In contrast, TH levels in the striatum of the MPTP+NAC group were similar to those in the control group and significantly higher than in the MPTP group ($p = 0.0286$). These results demonstrate for the first time that NAC has a neuroprotective effect on dopaminergic neuronal death in old mice after MPTP insult, opening the action spectrum described by Pan et al. (2009). Western Blot analysis for TH expression (**Figures 2D,E**) reinforced the results obtained by immunohistochemical assay in which MPTP and MPTP+NAC+HA-1077 groups showed significantly decreased levels compared to their controls.

Treatment With NAC+HA-1077 Exacerbates Microglial Response in the MPTP Parkinsonism Model

In order to evaluate the anti-inflammatory properties of the combined and individual treatments in microglial activation, an immunohistochemical staining was performed in the ventral midbrain and in the striatum for Iba-1 (**Figure 3A**). Microglial activation was statistically very significant in the SNpc of MPTP ($p = 0.002$) and MPTP+NAC+HA-1077 ($p < 0.0001$), compared to their respective No-MPTP groups (**Figure 3B**). The morphological analysis by measuring the Mean O.D. value of Iba-1+ cells in the SNpc revealed that all Parkinsonian treated mice showed a very significant increase compared to their respective No-MPTP groups ($p < 0.0001$, **Figure 3C** and **Supplementary Figures S4i–viii**).

In the striatum (**Figure 3D**), there was also a statistically significant increase in Iba-1+ cells in the MPTP ($p < 0.0001$) and MPTP+NAC+HA-1077 ($p < 0.0001$) groups compared to their respective control groups. The number of Iba-1+ cells of MPTP+NAC and MPTP+HA-1077 groups in the striatum was not significantly increased compared to their control groups. These results support those obtained in relation to dopaminergic neuronal death and highlight the anti-inflammatory effect of individual treatment with NAC or with HA-1077. In contrast, Iba-1+ cells in the MPTP+NAC group was significantly lower compared to the NAC No-MPTP group ($p = 0.0011$).

Morphological analysis in the striatum, showed an significant increase in O.D. value in MPTP ($p = 0.0215$) and MPTP+NAC+HA-1077 ($p = 0.0150$) groups compared to their control animals (**Figure 3E** and **Supplementary Figures S4ix–xvi**). Interestingly, common morphological patterns were observed in the different stages of microglial activation after the MPTP insult: (i) non-active microglia; (ii) active microglia, and (iii) phagocytic microglia depending on the treatment (**Figure 3F**).

The Combined Treatment With NAC+HA-1077 Increases Reactive Astrogliosis in the Striatum

In order to analyze the effect of the different treatment on astrocytes' activation, immunohistochemical staining for GFAP was performed (**Figure 4A**). At the SNpc level

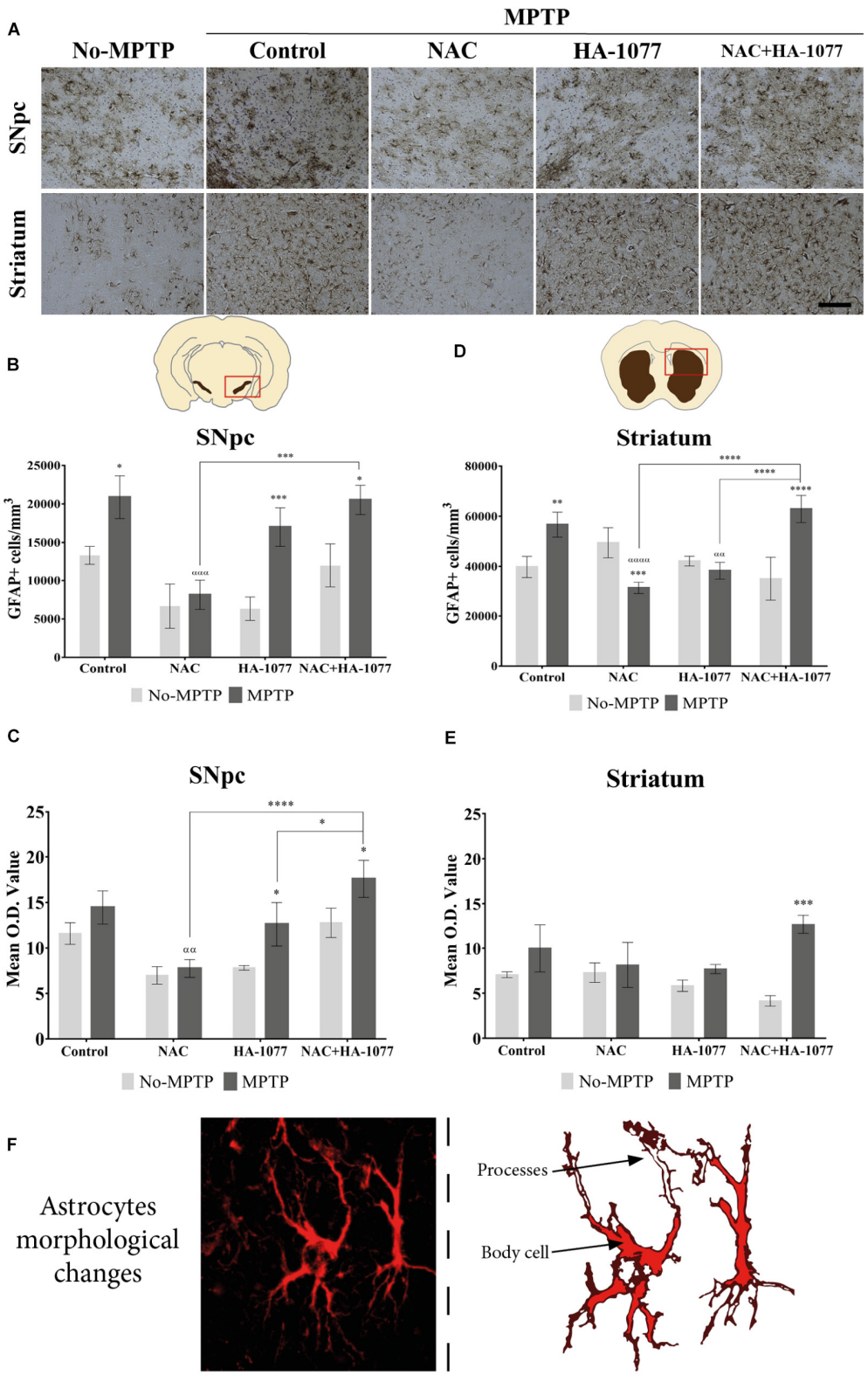

FIGURE 4 | GFAP expression in the SNpc and striatum in brains of old MPTP-intoxicated mice under different treatments. **(A)** Representative photomicrographs of GFAP immunostaining in the SNpc and striatum (Magnification 20×, Scale bar = 100 μm). **(B)** Quantification of GFAP+ cells/mm^3 in the SNpc. Significant differences were observed in MPTP (*P = 0.0235), MPTP+HA-1077 (***p = 0.0009) and MPTP+NAC+HA-1077 (*p = 0.0217). MPTP vs. MPTP+NAC (α = 0.0001)

(Continued)

FIGURE 4 | Continued
and MPTP+NAC vs. MPTP+NAC+HA-1077 (αααα = 0.0002). **(C)** Mean O.D. value measurement for GFAP+ cells in the SNpc for astrocytes' morphological changes analysis. Significant differences were found in MPTP+HA-1077 (p = 0.0208) and MPTP+NAC+HA-1077 (p = 0.0249) compared with their No-MPTP groups. MPTP vs. MPTP+NAC (αα = 0.0043). MPTP+NAC+HA-1077 vs. MPTP+NAC (****$p < 0.0001$); and, vs. MPTP+HA-1077 (*p = 0.0196). **(D)** Analysis of GFAP positive cells number/mm^3 in the striatum. GFAP+ cells density was significantly increased in MPTP (**p = 0.0023) and MPTP+NAC+HA-1077 (****$p < 0.0001$) groups compared with their controls, while a significant decrease was observed in MPTP+NAC group (***p = 0.0005) compared with its control group. MPTP vs. MPTP+NAC (αααα < 0.0001) and, vs. MPTP+HA-1077 (αα = 0.0035). MPTP+NAC+HA-1077 vs. MPTP+NAC (****$p < 0.0001$) and, vs. MPTP+HA-1077 (****$p < 0.0001$). **(E)** Mean O.D. value measurement for GFAP+ cells in the striatum for astrocytes' morphological changes analysis. MPTP+NAC+HA-1077 (*p = 0.0150) showed a significant increase in the Mean O.D. value compared to No-MPTP groups (Control and HA-1077, respectively). **(F)** Illustration of active astrocyte found in the different experimental groups characterized by ramified processes and body cell hypertrophy.

(**Figure 4B**), significant differences were found in GFAP expression in the MPTP (p = 0.0235), MPTP+HA-1077 (p = 0.0009), and MPTP+NAC+HA-1077 (p = 0.0217) groups compared with their No-MPTP groups. The astrocytes' morphological analysis in the SNpc showed a slight increase of Mean O.D. value of the GFAP immunostaining in the MPTP, MPTP+HA-1077 and MPTP+NAC+HA-1077 groups compared to their respective No-MPTP groups in the SNpc (**Figure 4C** and **Supplementary Figures S5i–viii**).

In addition, striatal GFAP expression was significantly increased in MPTP (p = 0.0023) and very significantly increased in MPTP+NAC+HA-1077 ($p < 0.0001$) compared with their respective control groups (**Figure 4D**). Importantly, NAC treatment in old-Parkinsonian mice produced a very significant decrease in the number of GFAP+ cells/mm^3 in the striatum (p = 0.0005). The study of morphological changes of astrocytes in the SNpc showed significant changes in MPTP+HA-1077 (p = 0.0208) and MPTP+NAC+HA-1077 (p = 0.0249) compared with their No-MPTP groups. Moreover, in the striatum showed that mean O.D. value was significantly increased in MPTP+NAC+HA-1077 (p = 0.0002) group compared to its No-MPTP group (**Figure 4E** and **Supplementary Figures S5ix–vi**). Activated astrocytes presented numerous and ramified processes as well as cell body hypertrophied depending on the treatment group (**Figure 4F**).

Astroglial Activation Processes Involved in the Dopaminergic Neuronal Death

To get deeper into the analysis of astroglial response among treatments, a double immunofluorescence was performed for TH and GFAP markers at the SNpc level. In **Figure 5Ai–viii**, it can be observed an indirect relationship in the expression of these markers in MPTP, MPTP+HA-1077, and MPTP+NAC+HA-1077 groups. Thus, a decrease in the expression of TH + cells is accompanied by an increase in the expression of GFAP+ cells. On the other hand, in the MPTP+NAC group, this relationship was not as pronounced.

In addition to the increase in GFAP expression, it has been shown that S100b levels increase during reactive astrogliosis in SNpc and striatum of PD patients, suggesting that this protein could play an important role in disease progression (Jackson-Lewis and Przedborski, 2007). Thus, immunofluorescence labeling for astrocyte markers GFAP and S100b was performed in the striatum. The double immunolabeling of these two markers revealed the existence of different profiles of astrocytes depending on the protein subcellular localization (**Figure 5Aix–xvi**). One astrocyte's profile is characterized by the presence of S100b only in the nucleus which is predominantly found in No-MPTP, MPTP+NAC, and MPTP+HA-1077. In MPTP and MPTP+NAC+HA-1077, the expression of S100b was found in the nucleus and in the perinuclear cytoplasm co-localizing with GFAP (**Figure 5B**). Taking all this data together, GFAP+S100b co-localization could have an important role in the dopaminergic neuronal death after MPTP intoxication in old mice.

Indirect Mediation of the JNK Pathway in Astroglial Response

Previous studies have demonstrated that dopaminergic neuronal death in the MPTP model is principally regulated by the JNK signaling pathway activation. It has been reported an increase in the p-JNK levels after MPTP intoxication mainly in response to the associated oxidative stress processes (Saporito et al., 1999; Lotharius et al., 2005; Pan et al., 2009). We have demonstrated that NAC treatment, an inhibitor of JNK, has a neuroprotective effect in old-Parkinsonian mice. Thus, we wanted to investigate whether the neuronal cell death was promoted by JNK signaling pathway activation in the SNpc.

Then, quantification of total JNK and p-JNK levels was performed by ELISA assay in the midbrain extracts (**Figures 6A,B**). The results showed a significant increase in total JNK levels in the MPTP group (p = 0.0321) and MPTP group treated with HA-1077 (p = 0.0129) compared to their respective controls. Furthermore, a significant increase in p-JNK levels was observed in the MPTP+HA-1077 group (p = 0.0007) and, reinforcing previous results, in the MPTP+NAC+HA-1077 group (p = 0.0219).

In addition, immunofluorescence staining for GFAP and S100b with p-JNK was performed at the SNpc level (**Figure 6C**) in order to examine possible changes in MAPK signaling pathway in astrocytes. In **Figures 6i–viii**, all MPTP treated groups, except those treated with NAC, showed hypertrophic astrocytes with an increase of GFAP, which does not co-localize with p-JNK. In **Figures 6Cix–xvi**, S100b expression was increased in the SNpc of MPTP, MPTP+HA-1077 and MPTP+NAC+HA-1077 groups, which co-localized with p-JNK (for more details see **Supplementary Figure S6**) (**Figure 6D**). These results suggest

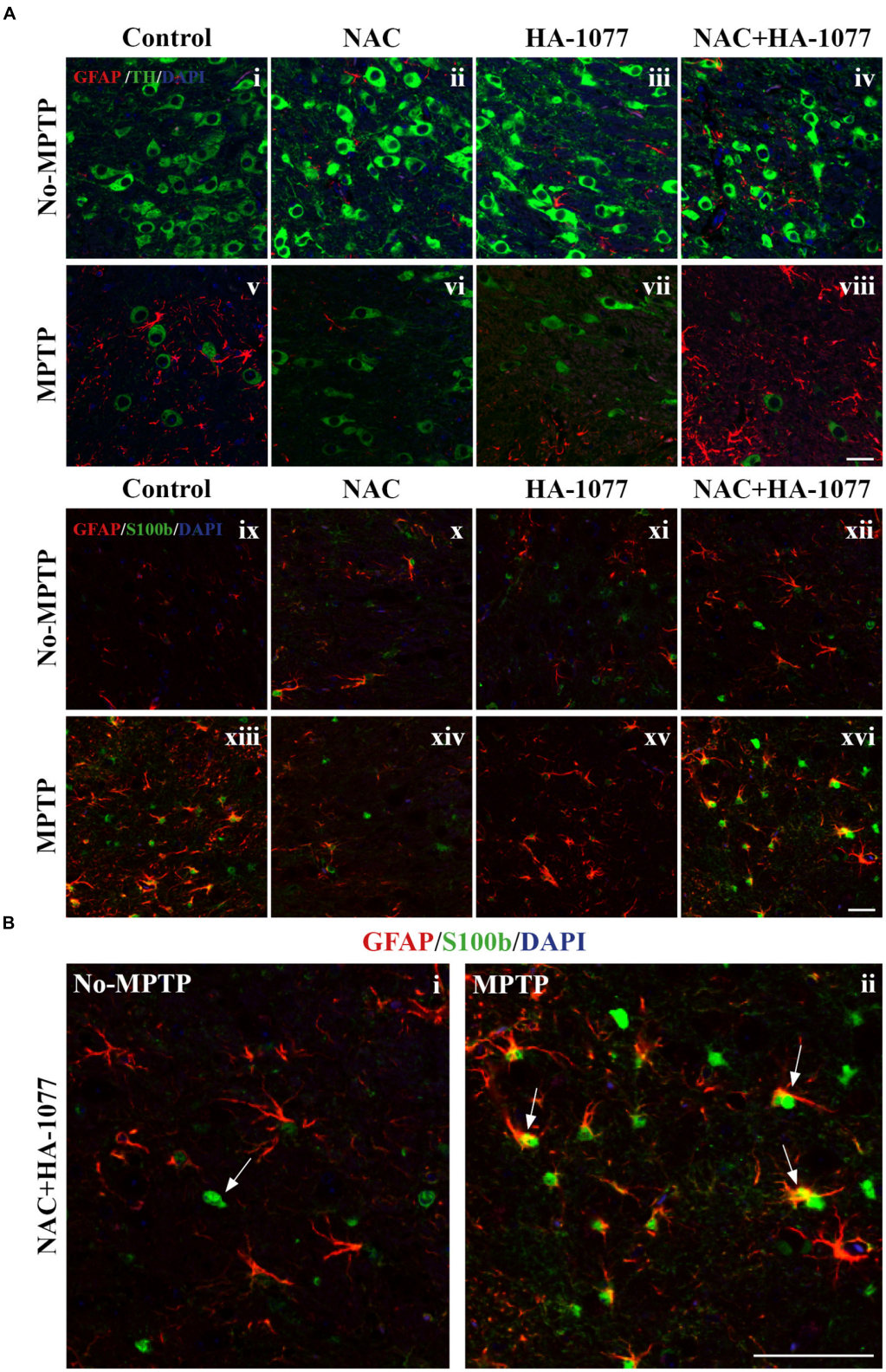

FIGURE 5 | Study of GFAP and S100b with TH in SNpc. **(A)** Representative micrographs of the double immunofluorescence assay for GFAP+TH **(i–viii)** and GFAP+S100b **(ix–xvi)** in the SNpc of the different experimental groups. **(B)** Representative figures for GFAP and S100b in the MPTP+NAC+HA-1077 group in which different astrocyte profiles were observed: S100b expressed in the nucleus and S100b co-located with GFAP in perinuclear cytoplasm. (Magnification 63×, Scale bar = 50 μm).

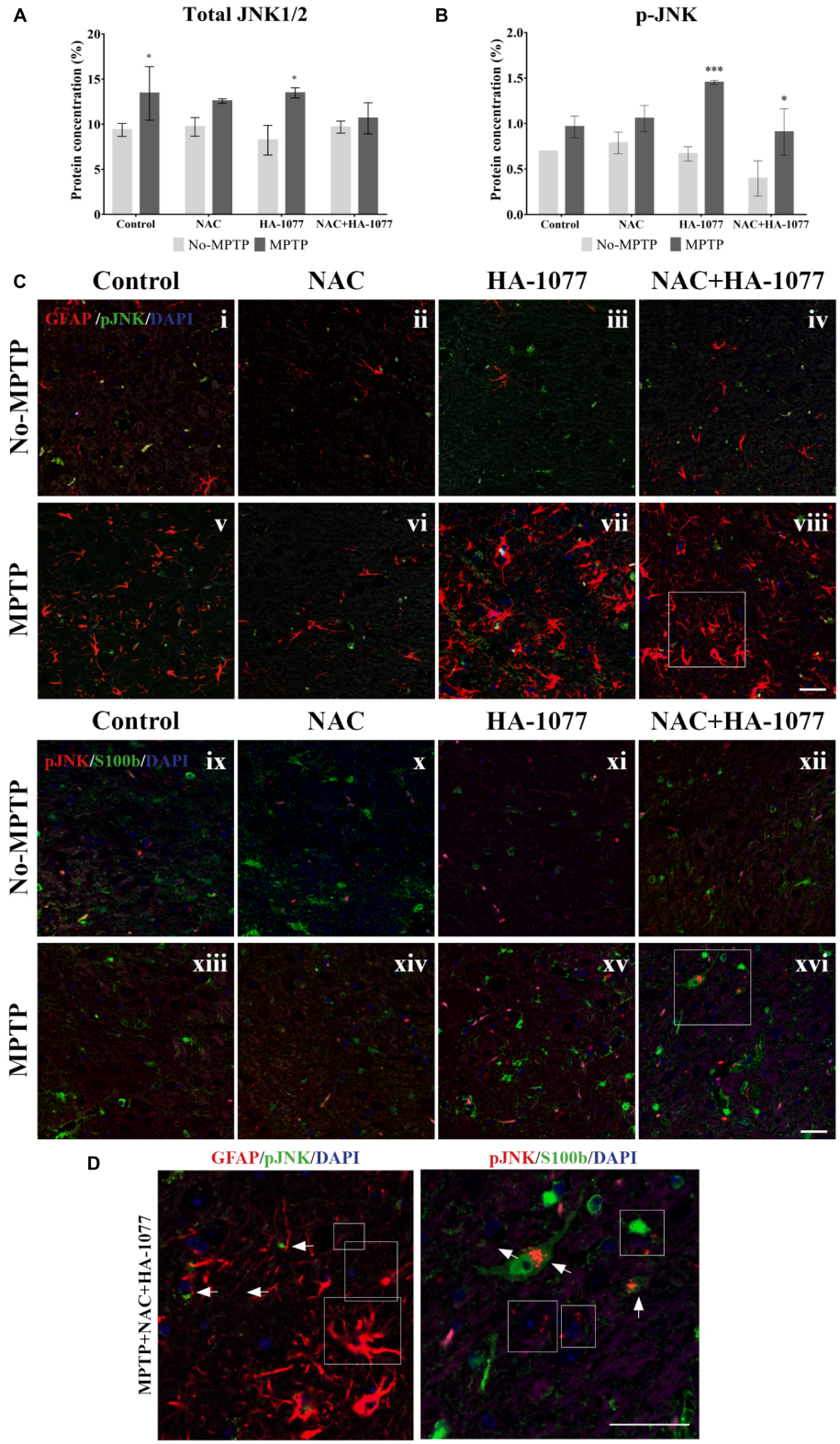

FIGURE 6 | Quantification of total and phospho-JNK1/2 expression by ELISA in midbrains of old-Parkinsonian mice. **(A)** There was a significant increase in protein concentration (%) of total JNK1/2 in MPTP (*p = 0.0321) and MPTP+HA-1077 (*p = 0.0129) groups compare with their controls. **(B)** Quantification of p-JNK concentration (%) by ELISA in midbrains of old-Parkinsonian mice. p-JNK expression was significantly increase in MPTP+HA-1077 (***p = 0.0007) and

(Continued)

FIGURE 6 | Continued
MPTP+NAC+HA-1077 (*p = 0.0219). **(C)** Confocal images for GFAP and p-JNK in SNpc **(i–viii)**. GFAP immune-reactive cells (red) were significantly increased in the MPTP **(v)**, MPTP+HA-1077 **(vii)** and MPTP+NAC+HA-1077 **(viii)** treated mice compared to their control groups (**i,iii,iv**, respectively). Phosphorilated JNK (pJNK, red) was not found in the GFAP+ cells' nucleus. Instead, this apoptotic protein appeared in the perinuclear region of the SNpc neurons. **(D)** Representative confocal images for S100b and p-JNK in SNpc **(ix–xvi)**. (Magnification 63×, Scale bar = 50 μm).

that the JNK pathway does not directly mediate astroglial activation. A deeper analysis of p-JNK expression in neurons may help in understanding its potential role in astroglial activation.

DISCUSSION

Recent studies in the literature have reported that inflammatory processes mediated by microglia and astrocytes might be an important key in the development and progression of PD (Wang et al., 2015; Tiwari and Pal, 2017). These mechanisms are exacerbated during aging, where there are a cell degeneration and glial dysfunction (Collier et al., 2017). Taking this background as a starting point, in the present study we decided to examine the possible synergistic effect of the combined treatment composed by an anti-inflammatory (HA-1077) and an antioxidant (NAC). Both HA-1077 and NAC, have been individually described to have beneficial effects on dopaminergic neuronal death in young MPTP intoxicated mice (Pan et al., 2009; Barcia et al., 2012). In *post-mortem* studies, we first analyzed dopaminergic neuronal death by TH immunostaining in the SNpc and the striatum (**Figure 2**). At the SNpc level, a significant decrease in the number of dopaminergic neurons in old MPTP treated mice was found (**Figures 2B,D**). On the other hand, in the striatum, a very significant decrease was observed in TH expression in DA fibers in MPTP, MPTP+HA-1077, and MPTP+HA-1077+NAC groups, but not in MPTP+NAC group (**Figures 2C,E**). These data may be explained by the fact that neurodegeneration, induced by MPTP injections, first affects the dopaminergic terminals in the striatum which project from the neuronal body at SNpc level (Morales et al., 2016).

These results are impressive because it was not expected to have a significant neuronal death within the combined treatment. These unexpected results were supported by the study of microglial activation. In the SNpc and in the striatum, an increase in the number of Iba-1+ cells was shown in all MPTP groups, with the exception of MPTP+NAC group (**Figures 3B,D**). In addition, morphological changes related with the different states of microglia cells under different pathological conditions were identified by measurement of Mean O.D value (**Figures 3C,E**). In No-MPTP groups, microglia was mainly not activated; in MPTP and MPTP+HA-1077 groups activated microglia was observed whereas phagocytic microglia was only identified in MPTP+NAC+HA-1077 group (**Figure 3** and **Supplementary Figure S4**). Barcia and co-workers also described this relationship between the exacerbation of neuronal death and microglial activation (Barcia et al., 2012).

On the other hand, the quantification of GFAP+ cells resulted significantly increased in MPTP+HA-1077 and MPTP+NAC+HA-1077 in the SNpc (**Figure 4B**). In the striatum, significant differences were observed in the groups treated with MPTP and MPTP+NAC+HA-1077 (**Figure 4D**). These data are consistent with the description of inflammatory events following damage in the CNS. The vicious cycle begins with the release of pro-inflammatory cytokines by dopaminergic neurons that stimulate microglia from an anti-inflammatory state to a pro-inflammatory state. If the damage persists, an uncontrolled release of pro-inflammatory cytokines is produced which stimulates astrocytes to a state of reactive astrogliosis and, consequently, exacerbating neuronal death.

The pro-neurotoxin MPTP is converted to the neurotoxin MPP+ by astrocytes and then released to dopaminergic neurons (Huang et al., 2017). In order to evaluate if the combined treatment was exacerbating reactive astrogliosis (and, in consequence, dopaminergic neuronal death) immunofluorescence staining for GFAP with TH and S100b in the SNpc was performed. In concordance with other studies, we found an increase of GFAP expression whereas there was a decrease in the number of TH+ neurons in MPTP, MPTP+HA-1077, and MPTP+NAC+HA-1077 groups (Huang et al., 2017).

Moreover, results showed astrocytes with different expression profiles depending on treatment: both the MPTP and the MPTP+NAC+HA-1077 had an increase in cytoplasmic S100b expression, whereas, in No-MPTP and MPTP+NAC groups, S100b was found only in the nucleus (**Figure 5**).

The following steps in our study were focused on answering why does a combination of drugs, which individually have neuroprotective effects, produce a toxic effect in old-Parkinsonian mice. One of the main basis of our hypothesis is supported by the fact that the elderly brains are more vulnerable to intoxication because, among other factors, they have a basal inflammatory condition that makes them more susceptible to cell degeneration (Savva et al., 2009). All our data discussed pointed out that NAC had a beneficial effect; HA-1077 had a toxic one and the combination of both showed a very toxic effect on neuronal death and glial associated response. Based on these results, we further study the possible metabolic pathway that could be affected by the combined treatment.

Many studies suggest that one of the possible metabolic pathways involved during a cellular stress condition (in this case by the administration of a neurotoxin) may be MAPKinases pathway (Kim and Choi, 2015). MAPKinases are a protein family composed by ERK, p38, and JNK. This last protein caught our

attention for being the target of one of our drugs, NAC (Pan et al., 2009). Then, we decided to analyze JNK expression in the different experimental groups and, surprisingly, an increase of its phosphorylated state was observed in thegroup MPTP+HA-077 and MPTP+HA-1077+NAC, but not in the group treated with MPTP+NAC (**Figures 6A,B**).Double immunofluorescence staining in the SNpc level for p-JNK together with GFAP and S100b was performed (**Figure 6C**). It was observed that p-JNK not co-localized neither with GFAP nor with S100b. These findings suggest that astroglial response could be indirectly mediated by the phosphorylation of JNK in damaged neurons. New research lines could further study the relationship between JNK pathway and neuroinflammation processes after an MPTP injection and, in this way, identified its crucial role in the degeneration of the nigrostriatal dopamine system.

According to the results obtained in the present study, we postulate that the combination of HA-1077 and NAC administrated in the most vulnerable brains, because of aging, has turned out to increase neuroinflammatory processes. With this, we conclude that personalized therapy should be supported in patients with different treatments based on the described data. Therefore, this work opens the door to consider the study of the effects of the combination of common drugs on neuronal death and inflammation, in order to design therapeutic strategies more adapted to PD patients (mainly in elderly people).

AUTHOR CONTRIBUTIONS

ALG-M and LC carried out all the experiments and wrote the manuscript. CS-R, CE, and EF-V participated in the experiments. MTH conceived the idea and design of the study, discussed the results, and worked in the manuscript preparation. All authors read and approved the final manuscript.

FUNDING

Research work of the authors was supported by the Spanish Ministry of Science and Innovation (FIS PI13 01293), Fundación Séneca (19540/PI/14) and "Prediction of cognitive properties of new drug candidates for neurodegenerative diseases in early clinical development" [European Community's Seventh Framework Programme (FP7/2007–2013) for the Innovative Medicine Initiative under Grant Agreement No. 115009] to MTH.

SUPPLEMENTARY MATERIAL

The Supplementary Material for this article can be found online at: https://www.frontiersin.org/articles/10.3389/fncel.2018.00451/full#supplementary-material

REFERENCES

Annese, V., Herrero, M. T., Di Pentima, M., Gomez, A., Lombardi, L., Ros, C. M., et al. (2015). Metalloproteinase-9 contributes to inflammatory glia activation and nigro-striatal pathway degeneration in both mouse and monkey models of 1-methyl-4-phenyl-1,2,3,6-tetrahydropyridine (MPTP)-induced Parkinsonism. *Brain Struct. Funct.* 220, 703–727. doi: 10.1007/s00429-014-0718-8

Barcia, C., De Pablos, V., Bautista-Hernández, V., Sánchez-Bahillo, Á., Bernal, I., Fernández-Villalba, E., et al. (2005). Increased plasma levels of TNF-α but not of IL1-β in MPTP-treated monkeys one year after the MPTP administration. *Parkinsonism. Relat. Disord.* 11, 435–439. doi: 10.1016/j.parkreldis.2005.05.006

Barcia, C., Ros, C. M., Annese, V., Carrillo-de Sauvage, M. A., Ros-Bernal, F., Gómez, A., et al. (2012). ROCK/Cdc42-mediated microglial motility and gliapse formation lead to phagocytosis of degenerating dopaminergic neurons in vivo. *Sci. Rep.* 2:809. doi: 10.1038/srep00809

Blesa, J., Pifl, C., Sánchez-González, M. A., Juri, C., García-Cabezas, M. A., Adánez, R., et al. (2012). The nigrostriatal system in the presymptomatic and symptomatic stages in the MPTP monkey model: a pet, histological and biochemical study. *Neurobiol. Dis.* 48, 79–91. doi: 10.1016/j.nbd.2012.05.018

Bose, A., and Beal, M. F. (2016). Mitochondrial dysfunction in Parkinson's disease. *J. Neurochem.* 139, 216–231. doi: 10.1111/jnc.13731

Brundin, P., Barker, R. A., Conn, P. J., Dawson, T. M., and Kieburtz, K. (2015). Linked clinical trials – the development of new clinical learning studies in Parkinson's disease using screening of multiple prospective new treatments. *J. Parkinsons Dis.* 3, 231–239. doi: 10.3233/JPD-139000

Collier, T. J., Kanaan, N. M., and Kordower, J. H. (2017). Aging and Parkinson's disease: different sides of the same coin? *Mov. Disord.* 32, 983–990. doi: 10.1002/mds.27037

Dagda, R. K., Zhu, J., and Chu, C. T. (2009). Mitochondrial kinases in Parkinson's disease: converging insights from neurotoxin and genetic models. *Mitochondrion* 9, 289–298. doi: 10.1016/j.mito.2009.06.001

Franklin, K., and Paxinos, G. (2008). *The Mouse Brain in Stereotaxic Coordinates*, 3rd Edn. Cambridge, MA: Academic Press.

Gaki, G. S., and Papavassiliou, A. G. (2014). Oxidative stress-induced signaling pathways implicated in the pathogenesis of Parkinson's disease. *Neuromolecular Med.* 16, 217–230. doi: 10.1007/s12017-014-8294-x

Halliday, G. M., and Stevens, C. H. (2011). Glia: initiators and progressors of pathology in Parkinson's disease. *Mov. Disord.* 26, 6–17. doi: 10.1002/mds.23455

Huang, D., Xu, J., Wang, J., Tong, J., Bai, X., Li, H., et al. (2017). Dynamic changes in the nigrostriatal pathway in the mptp mouse model of Parkinson's disease. *Parkinsons Dis.* 2017:9349487. doi: 10.1155/2017/9349487

Jackson-Lewis, V., and Przedborski, S. (2007). Protocol for the MPTP mouse model of Parkinson's disease. *Nat. Protoc.* 2, 141–151. doi: 10.1038/nprot.2006.342

Kalia, L. V., and Lang, A. E. (2015). Parkinson's disease. *Lancet* 386, 896–912. doi: 10.1016/S0140-6736(14)61393-3

Kim, E. K., and Choi, E. J. (2015). Compromised MAPK signaling in human diseases: an update. *Arch. Toxicol.* 89, 867–882. doi: 10.1007/s00204-015-1472-2

Kopin, I. J., and Markey, S. P. (1988). MPTP toxicity: implications for research in Parkinson's disease. *Annu. Rev. Neurosci.* 11, 81–96. doi: 10.1146/annurev.neuro.11.1.81

Lotharius, J., Falsig, J., Van Beek, J., Payne, S., Dringen, R., Brundin, P., and Leist, M. (2005). Progressive degeneration of human mesencephalic neuron-derived cells triggered by dopamine-dependent oxidative stress is dependent on the mixed-lineage kinase pathway. *J. Neurosci.* 25, 6329–6342. doi: 10.1523/JNEUROSCI.1746-05.2005

Maiti, P., Manna, J., and Dunbar, G. L. (2017). Current understanding of the molecular mechanisms in Parkinson's disease: targets for potential treatments. *Transl. Neurodegener.* 6:28. doi: 10.1186/s40035-017-0099-z

Morales, I., Sanchez, A., Rodriguez-Sabate, C., and Rodriguez, M. (2016). The astrocytic response to the dopaminergic denervation of the striatum. *J. Neurochem.* 139, 81–95. doi: 10.1111/jnc.13684

Otsu, N. (1979). A threshold selection method from gray-level histograms. *IEEE Trans. Syst. Man Cybern.* 9, 62–66. doi: 10.1109/TSMC.1979.4310076

Pan, J., Xiao, Q., Sheng, C. Y., Hong, Z., Yang, H. Q., Wang, G., et al. (2009). Blockade of the translocation and activation of c-Jun N-terminal kinase 3 (JNK3) attenuates dopaminergic neuronal damage in mouse model of Parkinson's disease. *Neurochem. Int.* 54, 418–425. doi: 10.1016/j.neuint.2009.01.013

Rodriguez, M., Rodriguez-Sabate, C., Morales, I., Sanchez, A., and Sabate, M. (2015). Parkinson's disease as a result of aging. *Aging Cell* 14, 293–308. doi: 10.1111/acel.12312

Saporito, M. S., Brown, E. M., Miller, M. S., & Carswell, S. (1999). CEP-1347/KT-7515, an inhibitor of c-jun N-terminal kinase activation, attenuates the 1-methyl-4-phenyl tetrahydropyridine-mediated loss of nigrostriatal dopaminergic neurons in vivo. *J. Pharmacol. Exp. Ther.* 288, 421–427.

Savva, G. M., Wharton, S. B., Ince, P. G., Forster, G., Matthews, F. E., Brayne, C., et al. (2009). Age, neuropathology, and dementia. *N. Engl. J. Med.* 360, 2302–2309. doi: 10.1056/NEJMoa0806142

Sin, O., and Nollen, E. A. A. (2015). Regulation of protein homeostasis in neurodegenerative diseases: the role of coding and non-coding genes. *Cell. Mol. Life Sci.* 72, 4027–4047. doi: 10.1007/s00018-015-1985-0

Sterio, D. C. (1984). The unbiased estimation of number and sizes of arbitrary particles using the disector. *J. Microsci.* 134, 127–136. doi: 10.1111/j.1365-2818.1984.tb02501.x

Tabrez, S., Jabir, N. R., Shakil, S., Greig, N. H., Alam, Q., Abuzenadah, A. M., et al. (2012). A synopsis on the role of tyrosine hydroxylase in Parkinson's Disease HHS public access. *CNS Neurol. Disord. Drug Targets* 1, 395–409. doi: 10.1007/978-1-4614-5915-6

Tatsumi, K., Okuda, H., Morita-Takemura, S., Tanaka, T., Isonishi, A., Shinjo, T., et al. (2016). Voluntary exercise induces astrocytic structural plasticity in the globus pallidus. *Front. Cell. Neurosci.* 10, 1–12. doi: 10.3389/fncel.2016.00165

Tiwari, P. C., and Pal, R. (2017). The potential role of neuroinflammation and transcription factors in Parkinson disease. *Dialog. Clin. Neurosci.* 19, 71–80.

Tysnes, O. B., and Storstein, A. (2017). Epidemiology of Parkinson's disease. *J. Neural. Transm.* 124, 901–905. doi: 10.1007/s00702-017-1686-y

Wang, Q., Liu, Y., and Zhou, J. (2015). Neuroinflammation in Parkinson's disease and its potential as therapeutic target. *Transl. Neurodegener.* 4:19. doi: 10.1186/s40035-015-0042-0

Conflict of Interest Statement: The authors declare that the research was conducted in the absence of any commercial or financial relationships that could be construed as a potential conflict of interest.

frontiers in Cellular Neuroscience

ORIGINAL RESEARCH
published: 04 December 2018
doi: 10.3389/fncel.2018.00472

Heavy Alcohol Exposure Activates Astroglial Hemichannels and Pannexons in the Hippocampus of Adolescent Rats: Effects on Neuroinflammation and Astrocyte Arborization

*Gonzalo I. Gómez[1,2], Romina V. Falcon[1], Carola J. Maturana[1], Valeria C. Labra[1], Nicole Salgado[3], Consuelo A. Rojas[1], Juan E. Oyarzun[1], Waldo Cerpa[4,5], Rodrigo A. Quintanilla[5,6] and Juan A. Orellana[1,5]**

[1]Departamento de Neurología, Escuela de Medicina and Centro Interdisciplinario de Neurociencias, Facultad de Medicina, Pontificia Universidad Católica de Chile, Santiago, Chile, [2]Instituto de Ciencias Biomédicas, Facultad de Ciencias de la Salud, Universidad Autónoma de Chile, Santiago, Chile, [3]Unidad de Microscopía Avanzada Medicina, Facultad de Medicina, Pontificia Universidad Católica de Chile, Santiago, Chile, [4]Laboratorio de Función y Patología Neuronal, Departamento de Biología Celular y Molecular, Facultad de Ciencias Biológicas, Pontificia Universidad Católica de Chile, Santiago, Chile, [5]Centro de Investigación y Estudio del Consumo de Alcohol en Adolescentes (CIAA), Santiago, Chile, [6]Laboratory of Neurodegenerative Diseases, Universidad Autónoma de Chile, Santiago, Chile*

OPEN ACCESS

Edited by:
Xuping Li,
Houston Methodist Research Institute, United States

Reviewed by:
Yedy Israel,
Universidad de Chile, Chile
Eliseo A. Eugenin,
The University of Texas Medical Branch at Galveston, United States

***Correspondence:**
Juan A. Orellana
jaorella@uc.cl

Received: *21 September 2018*
Accepted: *19 November 2018*
Published: *04 December 2018*

Citation:
Gómez GI, Falcon RV, Maturana CJ, Labra VC, Salgado N, Rojas CA, Oyarzun JE, Cerpa W, Quintanilla RA and Orellana JA (2018) Heavy Alcohol Exposure Activates Astroglial Hemichannels and Pannexons in the Hippocampus of Adolescent Rats: Effects on Neuroinflammation and Astrocyte Arborization. Front. Cell. Neurosci. 12:472. doi: 10.3389/fncel.2018.00472

A mounting body of evidence indicates that adolescents are specially more susceptible to alcohol influence than adults. However, the mechanisms underlying this phenomenon remain poorly understood. Astrocyte-mediated gliotransmission is crucial for hippocampal plasticity and recently, the opening of hemichannels and pannexons has been found to participate in both processes. Here, we evaluated whether adolescent rats exposed to ethanol exhibit changes in the activity of astrocyte hemichannels and pannexons in the hippocampus, as well as alterations in astrocyte arborization and cytokine levels. Adolescent rats were subjected to ethanol (3.0 g/kg) for two successive days at 48-h periods over 14 days. The opening of hemichannels and pannexons was examined in hippocampal slices by dye uptake, whereas hippocampal cytokine levels and astroglial arborization were determined by ELISA and Sholl analysis, respectively. We found that adolescent ethanol exposure increased the opening of connexin 43 (Cx43) hemichannels and pannexin-1 (Panx1) channels in astrocytes. Blockade of p38 mitogen-activated protein kinase (MAPK), inducible nitric oxide synthase (iNOS) and cyclooxygenases (COXs), as well as chelation of intracellular Ca^{2+}, drastically reduced the ethanol-induced channel opening in astrocytes. Importantly, ethanol-induced Cx43 hemichannel and Panx1 channel activity was correlated with increased levels of interleukin-1β (IL-1β), tumor necrosis factor-α (TNF-α), IL-6 in the hippocampus, as well as with profound alterations in astrocyte arbor complexity. Thus, we propose that uncontrolled opening of astrocyte hemichannels and pannexons may contribute not only to the glial dysfunction and neurotoxicity caused by adolescent alcohol consumption, but also to the pathogenesis of alcohol use disorders in the adulthood.

Keywords: alcoholism, glia, connexins, pannexins, astrocyte, cytokines, hippocampus

INTRODUCTION

Alcoholics exhibit a complex and multifactorial disorder featured as the repeated excessive use of alcoholic beverages, regardless of their prominent detrimental effects (Edenberg and Foroud, 2013). One pattern of alcohol misuse that has become popular among adolescents consist in consuming large amounts of alcohol in a single drinking session (∼2 h), the latter with the intention of get intoxicated (Cservenka and Brumback, 2017). Heavy alcohol intake by young people often causes serious impairments in executive functions and memory, which correspond with structural changes in prefrontal and hippocampal brain regions (Brown et al., 2000; De Bellis et al., 2000; Bava and Tapert, 2010; Cohen-Gilbert et al., 2017). Because its gradual development during adolescence, the hippocampus seems to be especially vulnerable to immediate consequences of alcohol misuse, including blackouts, hangovers and alcohol poisoning (Zeigler et al., 2005). Heavy ethanol exposure impairs both spatial hippocampal-dependent memory and hippocampal long-term potentiation (LTP) in adolescent rats (Fernandes et al., 2018; Tapia-Rojas et al., 2018). Multiple hypotheses have been proposed to explain the ethanol-induced impairment in hippocampal synaptic plasticity, including glutamate and N-methyl-D-aspartate (NMDA) receptor dysfunction (Sabeti and Gruol, 2008), lower BDNF levels (Fernandes et al., 2018), decreased neurogenesis (Liu and Crews, 2017), increased cytokine levels (Cippitelli et al., 2017), DNA double-strand break (Suman et al., 2016) and mGlu1 receptor alterations (Reynolds et al., 2015), among others. Nevertheless, the effect of ethanol treatment in the interaction between astrocytes and neurons has not been studied in detail.

Astrocytes embody a wide-ranging syncytial network that anatomically and functionally establish dynamic and often bidirectional interactions with neuronal synapses (Gundersen et al., 2015). In companion with pre- and postsynaptic neuronal elements, astrocytes establish the "tripartite synapse," a specialized functional platform in where they sense neurotransmission and respond to it by locally releasing paracrine substances called "gliotransmitters" (e.g., adenosine triphosphate (ATP), glutamate and D-serine; Araque et al., 1999; Perea et al., 2009). Astrocyte-mediated gliotransmission is crucial for hippocampal synaptic transmission and recently the opening of hemichannels and pannexons has been found to participate in this process (Ardiles et al., 2014; Chever et al., 2014; Meunier et al., 2017; Gajardo et al., 2018). Hemichannels are plasma membrane channels composed of six connexin subunits that oligomerize around a central pore that allow the passage of ions and small molecules, serving as a diffusional route of communication between the cytosol and the extracellular space (Montero and Orellana, 2015). In mammals, connexins exhibit an ubiquitous expression with 21 genes in humans and 20 in mice (Abascal and Zardoya, 2013). At the other end, pannexin channels or pannexons result from the oligomerization of six pannexins, a three-member family of proteins that have similar secondary and tertiary structures than connexins (Sosinsky et al., 2011). In astrocytes, hemichannels and pannexons allow the release of gliotransmitters that are necessary for different brain functions such as synaptic transmission and plasticity (Chever et al., 2014; Meunier et al., 2017), memory consolidation (Stehberg et al., 2012; Walrave et al., 2016), neuronal oscillations (Roux et al., 2015) and neuron-glia crosstalk (Torres et al., 2012). Despite the above, a mounting body of evidence have pointed out that homeostatic disturbances detected during brain diseases could be linked to enhanced and permanent opening of hemichannels and pannexons (Salameh et al., 2013; Orellana et al., 2014a, 2016).

Although several studies have demonstrated that alcohol exposure causes astrogliosis and alters the inflammatory profile of astrocytes (Blanco and Guerri, 2007; Adermark and Bowers, 2016), the molecular mechanisms and consequences of these phenomena are still poorly elucidated. Here, we show that intermittent ethanol exposure enhances the opening of connexin-43 (Cx43) hemichannels and pannexin-1 (Panx1) channels in hippocampal astrocytes from adolescent rats. In addition, we found that activation of (i) p38 mitogen-activated protein kinase (MAPK); (ii) inducible nitric oxide synthase (iNOS); (iii) cyclooxygenases (COXs); and (iv) cytoplasmic Ca^{2+}; appear to be critical for the latter response. In agreement with the idea of inflammation as major cause of the ethanol-evoked hemichannel/pannexon activity, we also observed elevated levels of cytokines (interleukin-1β (IL-1β), tumor necrosis factor-α (TNF-α), IL-6) and altered arborization of astrocytes in the hippocampus of adolescent rat exposed to ethanol.

MATERIALS AND METHODS

Reagents and Antibodies

The mimetic peptides gap19 (KQIEIKKFK, intracellular loop domain of Cx43), TAT-L2 (YGRKKRRQRRRDGANV DMHLKQIEIKKFKYGIEEHGK, second intracellular loop domain of Cx43) and ^{10}panx1 (WRQAAFVDSY, first extracellular loop domain of Panx1) were obtained from GenScript (Piscataway Township, NJ, USA). Ethanol was obtained from Merck Millipore (Darmstadt, Germany). HEPES, ns-398, sc-560, L-N6, SB203580, lanthanum (La^{3+}), anti-glial fibrillary acidic protein (GFAP) monoclonal antibody, BAPTA-AM, carbenoxolone (CBX), ethidium (Etd) bromide and probenecid were purchased from Sigma-Aldrich (St. Louis, MO, USA). Goat anti-mouse Alexa Fluor 488/555 and Hoechst 33342 were obtained from Thermo Fisher (Waltham, MA, USA). Normal goat serum (NGS) was purchased from Zymed (San Francisco, CA, USA).

Animals

Male Sprague-Dawley rat pups, postnatal day 25 (PDN25), were housed in groups of three rats per cage and maintained to 22°C on 12:12 h light-dark cycle, with food and water *ad libitum* previous to heavy ethanol administration. The animals were treated and handled according to the National Institutes of Health guidelines (NIH, Baltimore, MD, USA). This study was carried out in accordance with the recommendations of the Animal Care Guidelines of the Research Ethic Committee from the Pontificia Universidad Católica de Chile. The protocol was

approved by Research Ethic Committee from the Pontificia Universidad Católica de Chile.

Protocol of Intermittent Ethanol Exposure

Doses of ethanol (3.0 g/kg, 25% w/v mixed in isotonic saline) or saline solution were administrated via intraperitoneal (i.p.) injections beginning on PND25 as previously described (Pascual et al., 2007). A second dose was given on PND26 followed by alternating injections in PND 29, 30, 33, 34, 37 and 38. The injected i.p. volumes were dependent on the weight of each animal. According to these variations in the time, amounts administered were 1–3 ml. As previously reported (Pascual et al., 2007), a single dose of ethanol using this protocol result in a maximum blood ethanol concentration (BEC) of 210 ± 11 mg/dL at 30 min post-injection, followed by a gradual decline at 540 min later.

Enzyme-Linked Immunosorbent Assay (ELISA)

Enzyme-linked immunosorbent assay (ELISA) assays were performed to determine the amount of TNF-α, IL-1β and IL-6 in the hippocampus. Rats were anesthetized with ketamine/xylazine (10:1 mg/kg of body weight, i.p.) and then perfused and decapitated. Afterwards the hippocampus was removed and homogenized with an Ultra-Turrax homogenizer in buffer containing Tris-HCl 100 mM pH 7.4, EDTA 5 mM, SDS 1%, PMSF 1 μM and the protease inhibitor cocktail (ratio: 0.1 g hippocampus tissue: 1 ml lysis buffer; Pierce, Rockford, IL, USA). Protein concentrations were determined by using a detergent-compatible Bio-Rad protein assay kit (Bio-Rad, Richmond, CA, USA). Then, the samples were centrifuged at 14,000 *g* for 10 min. Supernatants were collected and protein content assayed by BCA method. Cytokines levels were determined by sandwich ELISA, according to the manufacturer's protocol (IL-6, IL-1β and TNF-α EIA kit, Enzo Life Science, Farmingdale, NY, USA). For the assay, 100 μL of samples were added per ELISA plate well and incubated at 4°C overnight. A calibration curve with recombinant cytokine was included. Detection antibody was incubated at room temperature for 2 h and the reaction developed with avidin–HRP and substrate solution. Absorbance was measured at 450 nm with reference to 570 nm with the microplate reader Synergy HT (Biotek Instruments). The results were normalized by protein amount in ng/ml.

Acute Brain Slices

Rats were anesthetized under isoflurane, decapitated and brains were extracted and cut into coronal slices (300 μm) using a vibratome (Leica, VT1000GS; Leica, Wetzlar, Germany) filled with ice-cold slicing solution containing (in mM): sucrose (222); KCl (2.6); $NaHCO_3$ (27); $NaHPO_4$ (1.5); glucose (10); $MgSO_4$ (7); $CaCl_2$ (0.5) and ascorbate (0.1), bubbled with 95% O_2/5% CO_2. Then, the slices were transferred at room temperature (20–22°C) to a holding chamber in ice-cold artificial cerebral spinal fluid (ACSF) containing (in mM): 125 NaCl, 2.5 KCl, 25 glucose, 25 $NaHCO_3$, 1.25 NaH_2PO_4, 2 $CaCl_2$ and 1 $MgCl_2$, bubbled with 95% O_2/5% CO_2, pH 7.4, for a stabilization period of 60 min before dye uptake experiments (see below).

TABLE 1 | Principal pharmacological agents used in this study.

Agent	Action
^{10}panx1	Mimetic peptide against Panx1 channels
BAPTA-AM	Intracellular calcium chelator
CBX	General hemichannel and pannexon blocker
Gap19	Mimetic peptide against Cx43 hemichannels
La^{3+}	General hemichannel blocker
L-N6	Selective inhibitor of iNOS
NS-398	Selective COX_2 inhibitor
Probenecid	Panx1 hemichannel blocker
SB203580	p38 MAP Kinase Inhibitor
SC-560	Selective COX_1 inhibitor
TAT-L2	Mimetic peptide against Cx43 hemichannels

Dye Uptake in Acute Brain Slices and Confocal Microscopy

For dye uptake and *ex vivo* "snapshot" experiments, acute brain slices were incubated with 5 μM Etd for 10 min in a chamber filled with ACSF and bubbled with 95% O_2/5% CO_2, pH 7.4. Some acute brain slices were pre-incubated for 15 min before and during Etd uptake experiments with the following agents: La^{3+} (200 μM), probenecid (500 μM), CBX (10 μM), gap19 (100 μM), TAT-L2 (100 μM), ^{10}panx1 (100 μM); and ns-398 (10 μM), sc-560 (40 μM), SB203580 (10 μM); L-N6 (1 μM) and BAPTA (10 μM; **Table 1**). Afterwards, the slices were washed three times (5 min each) with ACSF, and fixed at room temperature with 4% paraformaldehyde for 60 min, rinsed once with 0.1 mM glycine in phosphate buffered saline (PBS) for 5 min and then twice with PBS for 10 min with gentle agitation. Then, the slices were incubated two times for 30 min each with a blocking solution (PBS, gelatin 0.2%, Triton-X 100 1%) at room temperature. Afterwards, the slices were incubated overnight at 4°C with anti-GFAP monoclonal antibody (1:500, Sigma) to detect astrocytes. Later, the slices were washed three times (10 min each) with blocking solution and then incubated for 2 h at room temperature with goat anti-mouse Alexa Fluor 488 (1:1,000) antibody and Hoechst 33342. Further, the slices were washed three times (10 min each) in PBS and then mounted in Fluoromount, cover-slipped and examined in a confocal laser-scanning microscope (TBCS SP2, Nikon, Japan). Stacks of consecutive confocal images were taken with 40× objective at 100 nm intervals were acquired sequentially with three lasers (in nm: 408, 488 and 543), and Z projections were reconstructed using Nikon confocal software (NIS-elements) and ImageJ software. Dye uptake was calculated with the following formula: Corrected total cell Etd fluorescence = Integrated Density − ([Area of selected cell] × [Mean fluorescence of background readings]). At least six cells per field were selected from at least three fields in each brain slice.

Quantification of Astrocyte Morphology and Sholl Analysis

Image processing was performed using the Fiji-ImageJ software (Schindelin et al., 2012). All samples were coded and analyzed randomly by a researcher blinded to animal number and condition. A minimum of 10 astrocytes from each animal

where chosen for analysis and their image data were imported using the BioFormats plugin and then channels separated with the Split channels tool. Later, the GFAP channel was selected and Z-axis projection of the sum of planes was performed using the Z projection tool. Afterwards, astrocytes were selected and cut with the crop tool to facilitate their analysis when they fulfilled the following criteria: (i) presence of untruncated processes; (ii) consistent and strong GFAP staining along the entire arborization field; and (iii) relative isolation from neighboring astrocytes to avoid overlap. Afterwards, GFAP signal was segmented with the threshold tool and converted to binary mask before its skeletonization with the skeletonize tool. The latter tool allowed to obtain segment length and any possible bifurcation of the skeletonized image analyzed with the Fiji-ImageJ software. Then, maximum and total branch length of astroglial processes, as well as the number of branches were measured with the AnalizeSkeleton plugin of Fiji-ImageJ. Further, the plugin Sholl analysis of Fiji-ImageJ was used to place concentric circles around the cell starting from the soma and radiating outward at increasing radial increments of 5 μm (Sholl, 1953). Different parameters were measured including the number of intersections (points where the astrocytic processes cross concentric rings), area under the Sholl curve, the maximum number of intersections, the radius of highest count of intersections (maximum intersect. radius) and the sum of intersections divided by intersecting radii (mean of intersections).

Statistical Analysis

For each data group, results were expressed as mean ± standard error (SEM); n refers to the number of independent experiments. Detailed statistical results were included in the figure legends. Statistical analyses were performed using GraphPad Prism (version 7, GraphPad Software, La Jolla, CA, USA). Normality and equal variances were assessed by the Shapiro-Wilk normality test and Brown-Forsythe test, respectively. Unless otherwise stated, data that passed these tests were analyzed by unpaired *t*-test in case of comparing two groups, whereas in case of multiple comparisons, data were analyzed by one or two-way analysis of variance (ANOVA) followed, in case of significance, by a Tukey's *post hoc* test. When data were heteroscedastic as well as not normal and with unequal variances, we used Mann-Whitney test in case of comparing two groups, whereas in case of multiple comparisons data are analyzed by Kruskal-Wallis test followed, in case of significance, by Dunn's *post hoc* test. A probability of $P < 0.05$ was considered statistically significant.

RESULTS

Intermittent Heavy Ethanol Exposure Enhances Cx43 Hemichannel and Panx1 Channel Activity in Hippocampal Astrocytes From Acute Brain Slices of Adolescent Rats

In adolescent rodents, heavy ethanol exposure disrupts hippocampal-dependent synaptic plasticity and memory (Fernandes et al., 2018; Tapia-Rojas et al., 2018), as well as neuronal survival (Broadwater et al., 2014). Given that uncontrolled opening of astrocyte hemichannels and pannexons has been linked to synaptic impairment and neuronal loss (Orellana et al., 2011a,b; Abudara et al., 2015; Yi et al., 2016), we investigated whether intermittent heavy ethanol exposure affects the functional activity of these channels in the hippocampal CA1 region. To address this, we examined hemichannel and pannexon activity by measuring Etd uptake in acute brain slices from adolescent rats after different weeks following the last saline or ethanol injection. Etd enters to the cytoplasm of normal cells through plasma membrane channels with large pores, including hemichannels and pannexons. After its intercalation with base pairs of DNA and RNA, Etd becomes fluorescent, reflecting the activity of channels (Schalper et al., 2008; Sáez and Leybaert, 2014). Etd uptake by GFAP-positive astrocytes on acute brain slices was evaluated in "snapshot" experiments in the stratum oriens, stratum pyramidale and stratum radiatum of the hippocampal CA1 region.

Astrocytes observed in acute brain slices from control adolescent rats exhibited a low Etd uptake ratio in all CA1 regions analyzed (**Figures 1A**, **2A**, **3A**). However, during the 1-week period after the last ethanol injection, adolescent rats showed astrocytes with increased Etd uptake at the stratum oriens (∼560%, **Figures 1A–C**), stratum pyramidale (∼430%, **Figures 2A–C**) and stratum radiatum (∼325%, **Figures 3A–C**). Temporal analysis of these responses in acute brain slices revealed that astroglial Etd uptake rapidly augmented 1-week post ethanol exposure but progressively decreased as the weeks following ethanol injections increased (**Figures 1C**, **2C**, **3C**). Given that Cx43 hemichannels and Panx1 channels are major routes for dye influx in astrocytes (Contreras et al., 2002; Iglesias et al., 2009), the possible role of these channels in the ethanol-induced astroglial Etd uptake was examined. To do that, some acute brain slices were pre-incubated for 15 min before and during Etd uptake experiments with different pharmacological agents (**Table 1**). La^{3+} (200 μM), a general hemichannel blocker (Schalper et al., 2008), or the two Cx43 hemichannel mimetic peptides gap19 (100 μM) and TAT-L2 (100 μM; Wang et al., 2013), strongly reduced the astroglial Etd uptake observed in the stratum oriens after 1 week following ethanol exposure (from ∼560% to ∼52%, ∼33% and ∼100%, respectively; **Figure 1D**). These inhibitors caused similar counteracting actions in the ethanol-mediated Etd uptake detected in astrocytes from the stratum pyramidale (**Figure 2D**) and stratum radiatum (**Figure 3D**). To figure out the implication of Panx1 channels in the astroglial Etd uptake observed in acute brain slices of ethanol-exposed rats, we employed CBX and probenecid, two well-known blockers of these channels (Silverman et al., 2008; D'Hondt et al., 2009); as well as the Panx1 mimetic peptide: ^{10}panx1 (Pelegrin and Surprenant, 2006). CBX (5 μM), probenecid (500 μM) and ^{10}panx1 (100 μM) strongly blunted the astroglial Etd uptake induced by 1-week post-ethanol exposure in the stratus oriens (**Figure 1D**), stratum pyramidale (**Figure 2D**) and stratum radiatum (**Figure 3D**). Altogether, these data robustly denote that intermittent ethanol exposure increases the activity

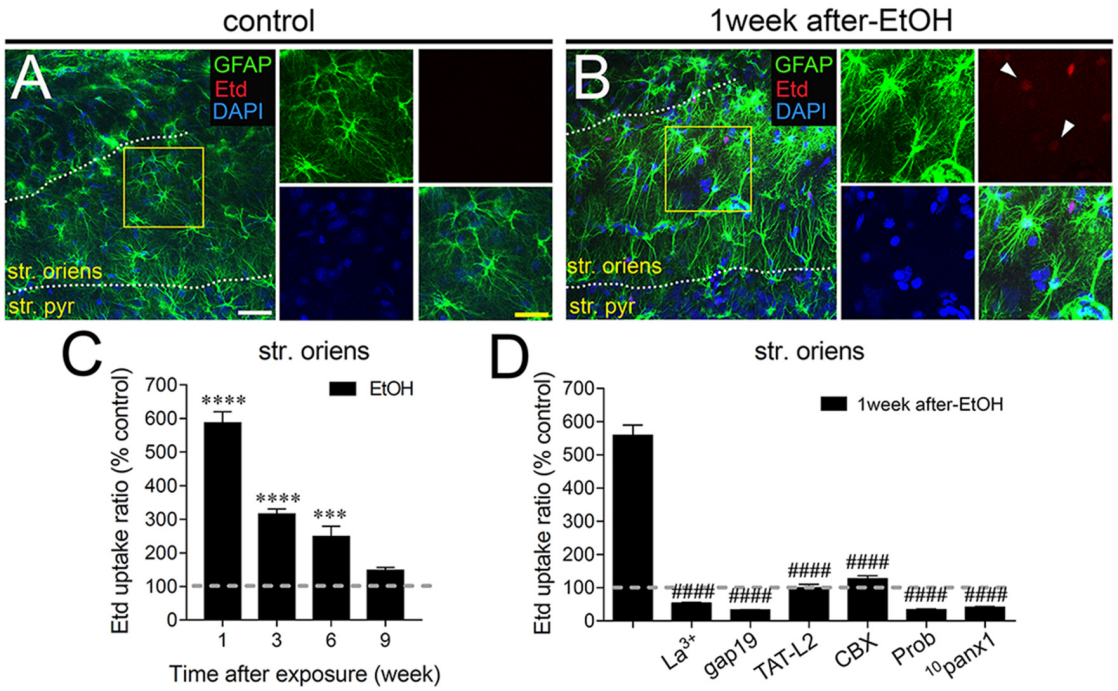

FIGURE 1 | Intermittent heavy ethanol exposure enhances astroglial connexin 43 (Cx43) hemichannel and pannexin-1 (Panx1) channel activity in the stratum oriens of adolescent rats. Representative images showing glial fibrillary acidic protein (GFAP; green), ethidium (Etd; red) and DAPI (blue) staining in the stratum oriens of control rats **(A)** and rats after 1-week following ethanol exposure **(B)**. Insets of astrocytes were taken from the area depicted within the yellow squares in **(A,B)**. **(C)** Averaged data of Etd uptake normalized to control conditions (dashed line) by astrocytes in the stratum oriens from rats after different weeks following ethanol exposure. $^{****}p < 0.0001$, $^{***}p = 0.0005$, for the effect of post-ethanol exposure compared to the respective control condition (two-way analysis of variance (ANOVA) followed by Tukey's *post hoc* test). Data were obtained from at least three independent experiments (≥59 cells analyzed for each independent experiment). **(D)** Averaged data of Etd uptake normalized to control conditions (dashed line) by astrocytes in the stratum oriens from rats after 1-week following ethanol exposure. Also shown are the effects of the following blockers applied during the Etd uptake assay: La^{3+} (200 μM), gap19 (100 μM), TAT-L2 (100 μM), CBX (5 μM), probenecid (Prob, 500 μM) and ^{10}panx1 (100 μM). $^{####}p < 0.0001$, for the effect of 1-week post-ethanol exposure compared to the respective blocker (one-way ANOVA followed by Dunnett's *post hoc* test). Data were obtained from at least three independent experiments (≥63 cells analyzed for each independent experiment). Calibration bars: white bar = 180 μm; yellow bar: 100 μm.

of Cx43 hemichannels and Panx1 channels in astrocytes from different hippocampal CA1 regions of adolescent rats.

Astrocyte Cx43 Hemichannel and Panx1 Channel Activity Mediated by Intermittent Heavy Ethanol Exposure Depends on p38 MAP Kinase/iNOS/COXs Pathways

In astrocytes, *in vivo* or *in vitro* ethanol exposure causes activation of iNOS and COX_2; (Blanco et al., 2004; Davis and Syapin, 2004; Vallés et al., 2004). Both enzymes generate NO and prostaglandins (PGs), respectively, two byproducts linked to the opening of astroglial Cx43 hemichannels (Retamal et al., 2006; Orellana et al., 2014b; Avendaño et al., 2015). Previous studies have revealed the involvement of p38 MAPK in the activity of Cx43 hemichannels (Retamal et al., 2006) and inflammatory activation of astrocytes (Pascual et al., 2003; Vallés et al., 2004; Blanco et al., 2005). Accordingly, we examined the influence of p38 MAPK, iNOS, COX_1 and COX_2 activation in the astrocyte Etd uptake observed in acute brain slices of ethanol-exposed adolescent rats. The Etd uptake triggered during the 1-week period following the last ethanol injection was strongly reduced by inhibition of p38 MAPK with 10 μM SB202190 or blockade of iNOS with 1 μM L-N6 in the three CA1 regions analyzed: stratus oriens (to ∼140% and ∼82%, respectively; **Figure 4A**), stratum pyramidale (to ∼150% and ∼60%, respectively; **Figure 4B**) and stratum radiatum (to ∼134% and ∼47%, respectively; **Figure 4C**). Likewise, sc-560 (40 μM) and ns-398 (10 μM), specific inhibitors for COX_1 and COX_2, respectively, prominently neutralized the Etd uptake caused by 1-week post-ethanol exposure in astrocytes from stratum oriens, stratum pyramidale and stratum radiatum (**Figures 4A–C**).

Prior evidence indicates that NO enhances COX_2 function and PG E_2 (PGE_2) production in macrophages (Swierkosz et al., 1995) and a similar phenomenon seems to occur in astrocytes treated with ethanol (Pascual et al., 2003; Blanco et al., 2005). Because activation of PGE_2 receptor 1 (EP_1) raises $[Ca^{2+}]_i$ levels (Woodward et al., 2011) and the latter is a broad-recognized cascade that elevates the opening of Cx43 hemichannels (De Bock et al., 2012) and Panx1 channels

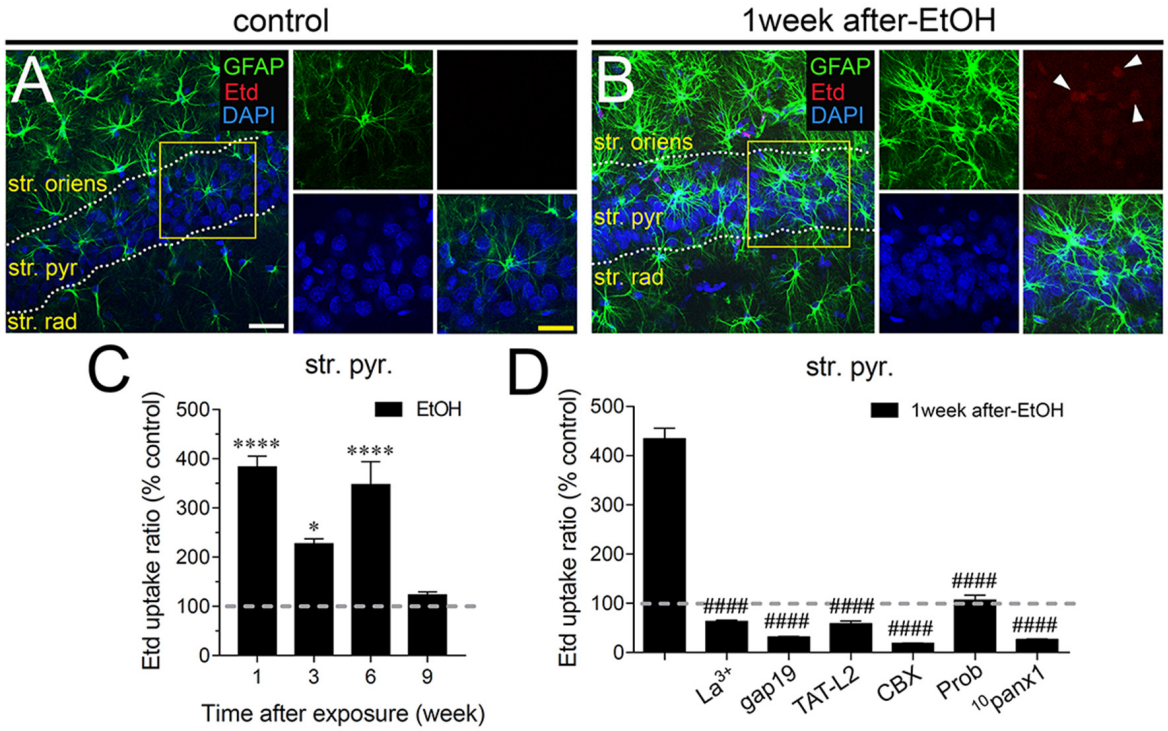

FIGURE 2 | Intermittent heavy ethanol exposure enhances astroglial Cx43 hemichannel and Panx1 channel activity in the stratum pyramidale of adolescent rats. Representative images showing GFAP (green), Etd (red) and DAPI (blue) staining in the stratum oriens of control rats **(A)** and rats after 1-week following ethanol exposure **(B)**. Insets of astrocytes were taken from the area depicted within the yellow squares in **(A,B)**. **(C)** Averaged data of Etd uptake normalized to control conditions (dashed line) by astrocytes in the stratum oriens from rats after different weeks following ethanol exposure. $^{****}p < 0.0001$, $^{*}p = 0.0126$ for the effect of post-ethanol exposure compared to the respective control condition (two-way ANOVA followed by Tukey's *post hoc* test). Data were obtained from at least three independent experiments (≥58 cells analyzed for each independent experiment). **(D)** Averaged data of Etd uptake normalized to control conditions (dashed line) by astrocytes in the stratum oriens from rats after 1-week following ethanol exposure. Also shown are the effects of the following blockers applied during the Etd uptake assay: La^{3+} (200 μM), gap19 (100 μM), TAT-L2 (100 μM), carbenoxolone (CBX, 5 μM), probenecid (Prob, 500 μM) and ^{10}panx1 (100 μM). $^{####}p < 0.0001$, for the effect of 1-week post-ethanol exposure compared to the respective blocker (one-way ANOVA followed by Dunnett's *post hoc* test). Data were obtained from at least three independent experiments (≥55 cells analyzed for each independent experiment). Calibration bars: white bar = 180 μm; yellow bar: 100 μm.

(Locovei et al., 2006), we examined whether $[Ca^{2+}]_i$ is involved in astrocyte Etd uptake observed in the hippocampus of ethanol-exposed rats. Treatment with 5 μM BAPTA, a Ca^{2+} chelator, was found to reduce the Etd uptake caused by 1-week post-ethanol exposure in stratus oriens (to ∼26%, **Figure 4A**), stratum pyramidale (to ∼28%, **Figure 4B**) and stratum radiatum (to ∼35%, **Figure 4C**). All these data suggest that Cx43 hemichannel and Panx1 channel opening in our system depends on the activation of p38 MAPK/iNOS/COXs–mediated pathway(s) and changes in cytoplasmic Ca^{2+} signaling.

Intermittent Heavy Ethanol Exposure Increases Hippocampal Cytokine Levels and Alters Astrocyte Arborization in Adolescent Rats

Once activated, astrocytes release relevant autocrine/paracrine amounts of inflammatory cytokines, which are capable of modify astrocyte properties at the molecular, morphological and functional level (Rossi and Volterra, 2009; Agulhon et al., 2012). Previous studies have shown that different cytokines such as IL-1β, IFN-γ, IL-6 and TNF-α elevate the opening of hemichannels and pannexons in different cell types (Takeuchi et al., 2006; Sáez et al., 2013; Mugisho et al., 2018), including astrocytes (Retamal et al., 2007; Froger et al., 2010). More relevantly, both hemichannels and pannexons have been proposed to contribute to the stimulation of the inflammasome route and its propagation through the release of cytokines to neighboring cells (Makarenkova and Shestopalov, 2014; Kim et al., 2016). Multiple lines of evidence have demonstrated that ethanol may increase the release of IL-1β, TNF-α and IL-6 from astrocytes through the activation of p38 MAPK/iNOS/COXs pathway(s). Given that inhibition of the latter pathways significantly reduced the astrocyte hemichannel/pannexon activity in ethanol-exposed rats, we evaluated whether ethanol could affect the levels of IL-1β, IFN-γ and IL-6 in the hippocampus. During the 1-week period after the last ethanol injection, the hippocampus of ethanol-exposed rats exhibited a prominent ∼5-fold increase in IL-1β levels that then dropped drastically during the following weeks (**Figure 5A**). Similarly, following 3-week of the last injection, ethanol caused a significant 2-fold steady-state increase in

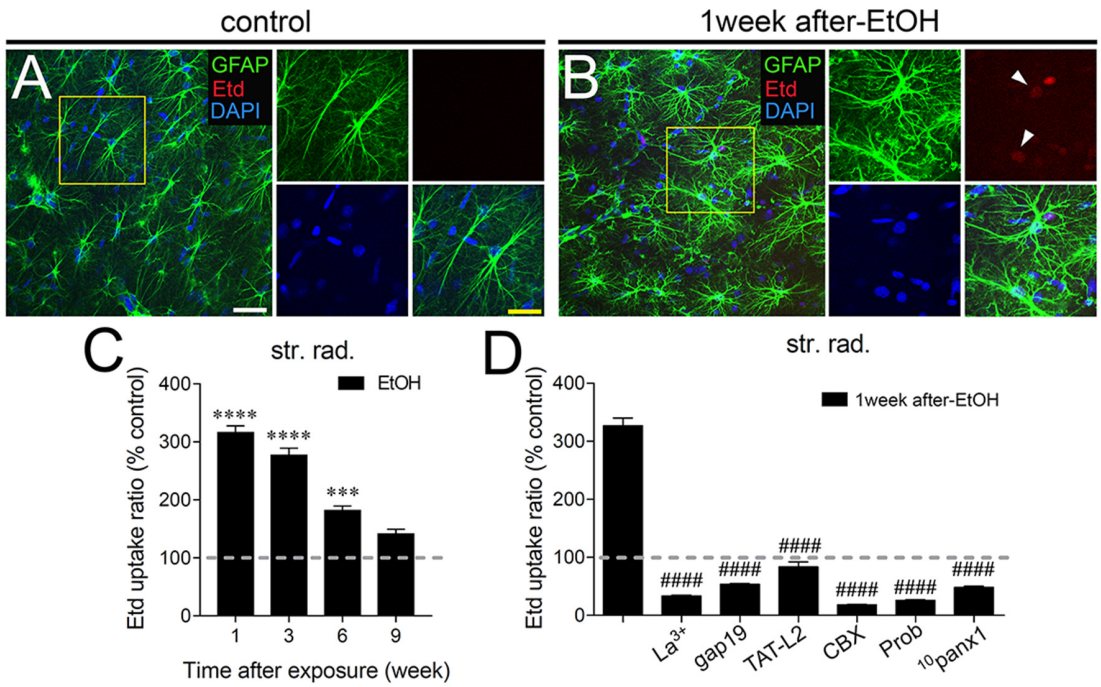

FIGURE 3 | Intermittent heavy ethanol exposure enhances astroglial Cx43 hemichannel and Panx1 channel activity in the stratum radiatum of adolescent rats. Representative images showing GFAP (green), Etd (red) and DAPI (blue) staining in the stratum oriens of control rats **(A)** and rats after 1-week following ethanol exposure **(B)**. Insets of astrocytes were taken from the area depicted within the yellow squares in **(A,B)**. **(C)** Averaged data of Etd uptake normalized to control conditions (dashed line) by astrocytes in the stratum oriens from rats after different weeks following ethanol exposure. $^{****}p < 0.0001$, $^{***}p = 0.0002$ for the effect of post-ethanol exposure compared to the respective control condition (two-way ANOVA followed by Tukey's *post hoc* test). Data were obtained from at least three independent experiments (≥59 cells analyzed for each independent experiment). **(D)** Averaged data of Etd uptake normalized to control conditions (dashed line) by astrocytes in the stratum oriens from rats after 1-week following ethanol exposure. Also shown are the effects of the following blockers applied during the Etd uptake assay: La^{3+} (200 μM), gap19 (100 μM), TAT-L2 (100 μM), CBX (5 μM), probenecid (Prob, 500 μM) and ^{10}panx1 (100 μM). $^{\#\#\#\#}p < 0.0001$, for the effect of 1-week post-ethanol exposure compared to the respective blocker (one-way ANOVA followed by Dunnett's *post hoc* test). Data were obtained from at least three independent experiments (≥52 cells analyzed for each independent experiment). Calibration bars: white bar = 180 μm; yellow bar: 100 μm.

hippocampal TNF-α levels that was maintained for 2 weeks after returning to control levels (**Figure 5B**). The hippocampus of rats injected with ethanol also exhibited a 2.5-fold increase in IL-6 levels during 3-weeks following ethanol exposure, which did not persist further (**Figure 5C**). Collectively, these results indicate that intermittent ethanol injections cause a rapid and transient inflammation in the hippocampus of adolescent rats.

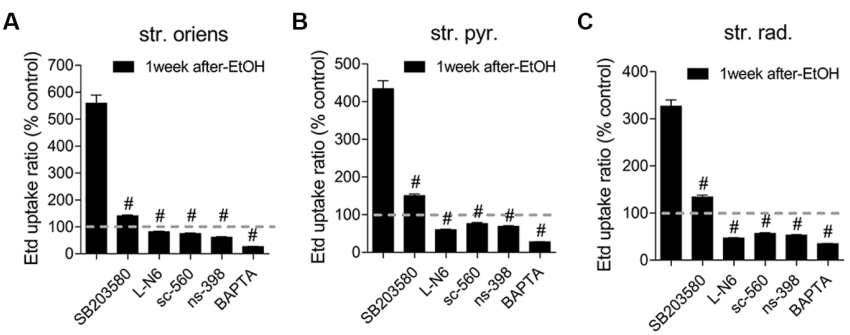

FIGURE 4 | Hemichannel and pannexon activity induced by intermittent heavy ethanol exposure depends on p38 mitogen-activated protein kinase (MAPK)/inducible nitric oxide synthase (iNOS)/cyclooxygenases (COXs) pathways. **(A–C)** Averaged data of Etd uptake normalized to control conditions (dashed line) by astrocytes in the stratum oriens **(A)**, stratum pyramidale **(B)** and stratum radiatum **(C)** from rats after 1-week following ethanol exposure. Also shown are the effects of the following blockers applied during the Etd uptake assay: SB203580 (10 μM, p38 MAPK inhibitor), LN-6 (1 μM, iNOS inhibitor), sc-560 (40 μM, COX_1 inhibitor), ns-398 (10 μM, COX2 inhibitor) and BAPTA (10 μM, Ca^{2+} chelator). $^{\#}p < 0.0001$, for the effect of 1-week post-ethanol exposure compared to the respective blocker (one-way ANOVA followed by Dunnett's *post hoc* test). Data were obtained from at least three independent experiments (≥90 cells analyzed for each independent experiment).

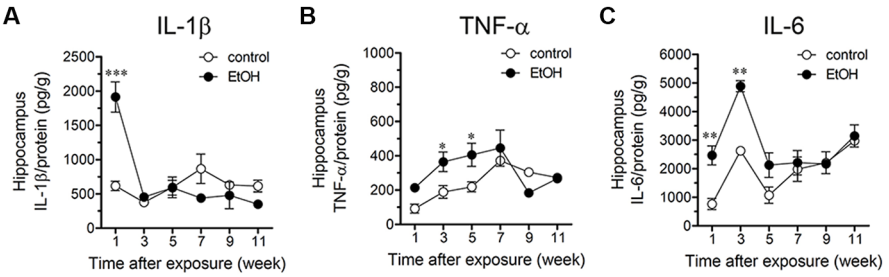

FIGURE 5 | Intermittent heavy ethanol exposure increases hippocampal levels of interleukin-1β (IL-1β), tumor necrosis factor-α (TNF-α) and IL-6. Averaged data of hippocampal levels of IL-1β **(A)**, TNF-α **(B)** and IL-6 **(C)** from control rats (white circles) or rats after different weeks following ethanol exposure (black circles). $^{*}p < 0.05$; $^{**}p < 0.0005$, $^{***}p < 0.0001$; effect of ethanol exposure compared with control conditions (two-way ANOVA followed by Bonferroni's *post hoc* test). Averaged data were obtained from at least three animals.

A large number of studies have shown that inflammation evoked by ethanol exposure is accompanied of reactive astrogliosis (Blanco and Guerri, 2007; Adermark and Bowers, 2016). The latter is a multiple stage and preserved process by which astrocytes undergo molecular, morphological and functional changes to counteract and limit brain damage (Pekny and Pekna, 2014). Hallmark features of reactive astrogliosis are the hypertrophy of cellular processes and profound alterations in the arborization and morphology of astrocytes (Pekny and Pekna, 2014). To examine whether ethanol exposure could affect the extent of astroglial arbor in the hippocampus, we measured the maximum and total branch length of astrocytes at the stratum oriens (**Figures 6A–D**), stratum pyramidale (**Figures 7A–D**) and stratum radiatum (**Figures 8A–D**). Measures beginning in the cell body throughout the end of each process, allowed us to calculate the length of the longest branch and the sum of all branch lengths of each astrocyte arbor, which were represented as maximum and total branch length, respectively. Temporal analysis of astrocyte arbor at the hippocampal CA1 area showed that maximum branch length remained unchanged between control rats and rats following different periods after ethanol exposure (**Figures 6C**, **7C**, **8C**). However, 1-week post-ethanol exposure strongly increased the total branch length of astrocytes in the stratum oriens (∼2-fold, **Figure 6D**) and stratum pyramidale (∼1.5-fold, **Figure 7D**) of adolescent rats. In an intriguing contrast, during the 3-week period after the last ethanol injection, adolescent rats exhibited astrocytes with a 2-fold reduction in total branch length in the stratum radiatum as compared to the control ones (**Figure 8D**). Similarly, 1-week post-ethanol exposure greatly elevated the number of astrocyte branches in the stratum oriens (∼2-fold, **Figure 6E**) and stratum pyramidale (∼2-fold, **Figure 7E**), nevertheless, an opposite response was observed in the stratum radiatum during the 3-week period after the last ethanol injection (**Figure 8E**).

To further scrutinize with major detail the arbor complexity of astrocytes in brain sections from control and ethanol-exposed rats, we used a Sholl analysis, which consist in place concentric rings at fixed intervals from the soma to further count branch intersections at each ring. Based on Sholl analysis, hippocampal astrocytes of ethanol-exposed rats are significantly different from hippocampal astrocytes of their saline-injected counterparts (**Figures 6F–M**, **7F–M**, **8F–M**). We found an increased number of intersections between branches and Sholl rings in ethanol-exposed rats, particularly in the stratum oriens and stratum pyramidale after 1-week but not in further periods following ethanol injections (**Figures 6F–I**, **7F–I**). In these hippocampal areas, 1-week post-ethanol exposure also augmented astrocyte branch complexity as assessed by the area under the Sholl curve for the total number of branch intersections at 5–60 μm from the soma (**Figures 6J**, **7J**). Ethanol exposure evoked similar increased values in the maximum number of intersections, the radius of highest count of intersections (maximum intersect. radius) and the sum of intersections divided by intersecting radii (mean of intersections; **Figures 6K–M**, **7K–M**). Although 1-week post-ethanol exposure significantly elevated the area under the Sholl curve and mean intersections in the stratum radiatum, a 2-fold decrease in all Sholl parameters was observed after 3-week following ethanol injections in this region (**Figures 8D–M**). These data indicate that ethanol modulates the complexity of astrocyte branch arbors in the hippocampus of adolescent rats in a time and spatial-depend manner.

DISCUSSION

In the present study, we showed that intermittent heavy ethanol exposure enhances the opening of Cx43 hemichannels and Panx1 channels in hippocampal astrocytes from acute brain slices of adolescent rats. This enhanced channel activity took place by a mechanism involving the stimulation of p38 MAP k/iNOS/COX-dependent pathways and intracellular Ca^{2+} signaling. The above responses were accompanied of elevated levels of IL-1β, TNF-α, IL-6 and altered arborization of astrocytes in the hippocampus. All these effects persisted during early adulthood but then were progressively compensated overtime.

Prior evidence indicates that heavy ethanol exposure during adolescence disturbs spatial hippocampus-mediated cognitive ability and LTP (Fernandes et al., 2018; Tapia-Rojas et al., 2018), as well as neuronal survival (Broadwater et al., 2014). Our study suggests that a portion of the above-mentioned alterations caused by ethanol exposure could base in the persistent opening of Cx43 hemichannels and Panx1 channels within the hippocampus. During the past decade, different lines of research

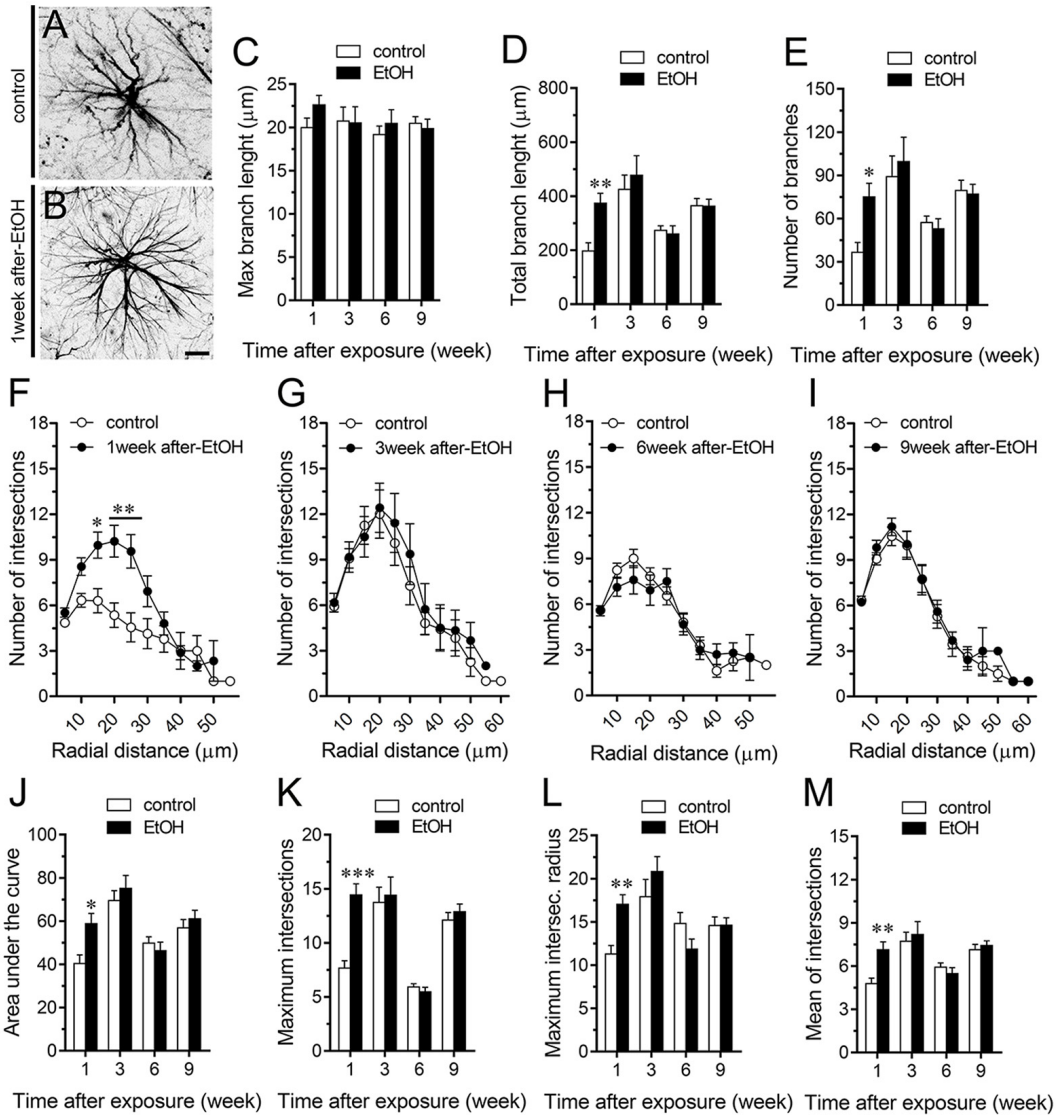

FIGURE 6 | Intermittent heavy ethanol exposure increases astrocyte arborization in the stratum oriens of adolescent rats. **(A,B)** Representative GFAP (black) positive astrocytes from the stratum oriens of control rats **(A)** and rats after 1-week following ethanol exposure **(B)**. **(C–E)** Averaged data of maximum branch length **(C)**, total branch length **(D)** and number of branches **(E)** by astrocytes in the stratum oriens from control rats (white bars) or rats after different weeks following ethanol exposure (black bars). $^{**}p < 0.0005$, $^{*}p < 0.002$, for the effect of post-ethanol exposure compared to the respective control condition (two-way ANOVA followed by Bonferroni's *post hoc* test). **(F–I)** Averaged data of Sholl analysis astrocytes from the stratum oriens of control rats (white circles) and rats after 1 **(F)**, 3 **(G)**, 6 **(H)** and 9 **(I)** weeks following ethanol exposure (black circles). $^{*}p < 0.005$, $^{**}p < 0.0001$ for the effect of post-ethanol exposure compared to the respective control condition (two-way ANOVA followed by Bonferroni's *post hoc* test). **(J–M)** Averaged data of area under the curve of Sholl analysis **(J)**, maximum intersection **(K)**, maximum intersection radius **(L)** and mean of intersections **(M)** by astrocytes in the stratum oriens from control rats (white bars) or rats after different weeks following ethanol exposure (black bars). $^{***}p < 0.0001$, $^{**}p < 0.005$, $^{*}p < 0.05$, for the effect of post-ethanol exposure compared to the respective control condition (two-way ANOVA followed by Bonferroni's *post hoc* test). Data were obtained from at least three independent experiments. Calibration bar = 25 μm.

have established that hemichannels and pannexons underpin multiple brain processes such as synaptic efficacy, neural activity, signal processing, cognition and behavior (Stehberg et al., 2012; Ardiles et al., 2014; Chever et al., 2014; Roux et al., 2015; Walrave et al., 2016; Meunier et al., 2017; Gajardo et al., 2018). However, during certain pathophysiological conditions, hemichannels and pannexons may favor brain disease progression by: (i) releasing excitotoxic levels of transmitters (e.g., ATP and glutamate); (ii) disturbing $[Ca^{2+}]_i$ handling; or (iii) altering cytoplasmic ionic and osmotic balance (Vicario et al., 2017). Here, we found that intermittent ethanol injections during adolescence increase the opening of Cx43 hemichannels and Panx1 channels in hippocampal astrocytes from the stratum oriens, stratum pyramidale and stratum radiatum. These responses were drastically blocked by La^{3+}, gap19, TAT-L2, CBX, probenecid and ^{10}panx1, indicating that both Cx43 hemichannels and

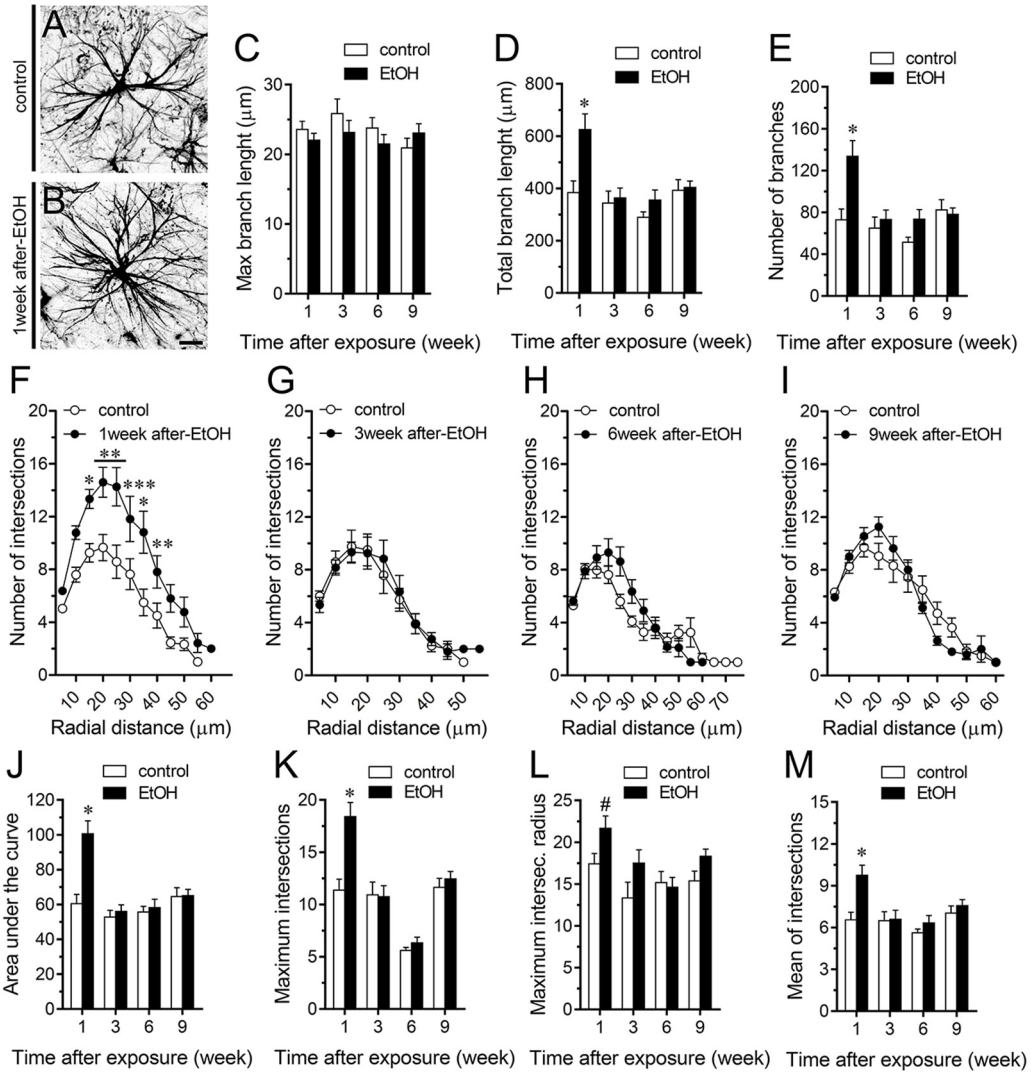

FIGURE 7 | Intermittent heavy ethanol exposure increases astrocyte arborization in the stratum pyramidale of adolescent rats. **(A,B)** Representative GFAP (black) positive astrocytes from the stratum pyramidale of control rats **(A)** and rats after 1-week following ethanol exposure **(B)**. **(C–E)** Averaged data of maximum branch length **(C)**, total branch length **(D)** and number of branches **(E)** by astrocytes in the stratum pyramidale from control rats (white bars) or rats after different weeks following ethanol exposure (black bars). $^{*}p < 0.0001$, for the effect of post-ethanol exposure compared to the respective control condition (two-way ANOVA followed by Bonferroni's *post hoc* test). **(F–I)** Averaged data of Sholl analysis astrocytes from the stratum pyramidale of control rats (white circles) and rats after 1 **(F)**, 3 **(G)**, 6 **(H)** and 9 **(I)** weeks following ethanol exposure (black circles). $^{***}p < 0.0006$, $^{**}p < 0.005$, $^{*}p < 0.05$, for the effect of post-ethanol exposure compared to the respective control condition (two-way ANOVA followed by Bonferroni's *post hoc* test). **(J–M)** Averaged data of area under the curve of Sholl analysis **(J)**, maximum intersection **(K)**, maximum intersection radius **(L)** and mean of intersections **(M)** by astrocytes in the stratum pyramidale from control rats (white bars) or rats after different weeks following ethanol exposure (black bars). $^{*}p < 0.0001$, for the effect of post-ethanol exposure compared to the respective control condition (two-way ANOVA followed by Bonferroni's *post hoc* test). $^{\#}p < 0.05$, for the effect of post-ethanol exposure compared to the respective control condition (Mann Whitney test). Data were obtained from at least three independent experiments. Calibration bar = 25 μm.

Panx1 channels were the principal responsible for the ethanol-mediated Etd uptake in astrocytes. The latter coincides with the increased activity described for both channels in astrocytes during several brain pathological scenarios including prenatal nicotine and postnatal high-fat diet (Orellana et al., 2014b), restraint stress (Orellana et al., 2015), epileptic seizures (Santiago et al., 2011), amyloid-β peptide treatment (Orellana et al., 2011b), spinal cord injury (Garré et al., 2016) and acute infection (Karpuk et al., 2011).

How does ethanol exposure during adolescence causes the opening of Cx43 hemichannels and Panx1 channels? Recent evidence indicates that hemichannel and pannexon activity in astrocytes result from the activation of a p38MAPK/iNOS/COX-dependent pathway (Retamal et al., 2006; Orellana et al., 2014b; Avendaño et al., 2015). Specifically, pro-inflammatory conditions (e.g., IL-1β and TNF-α) enhance the opening of Cx43 hemichannels via the stimulation of p38 MAPK and further NO-dependent S-nitrosylation of Cx43

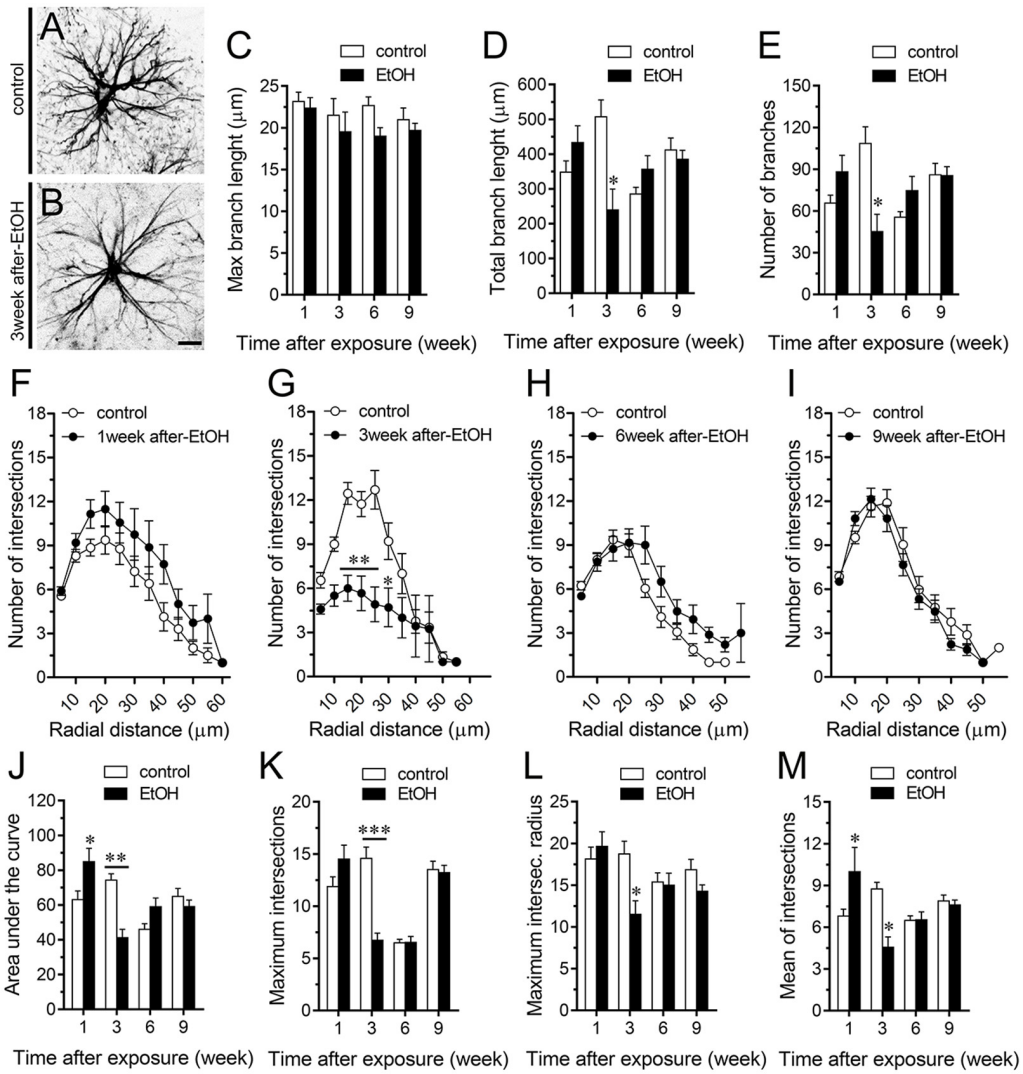

FIGURE 8 | Intermittent heavy ethanol exposure modulates astrocyte arborization in the stratum radiatum of adolescent rats. **(A,B)** Representative GFAP (black) positive astrocytes from the stratum radiatum of control rats **(A)** and rats after 3-week following ethanol exposure **(B)**. **(C–E)** Averaged data of maximum branch length **(C)**, total branch length **(D)** and number of branches **(E)** by astrocytes in the stratum radiatum from control rats (white bars) or rats after different weeks following ethanol exposure (black bars). $^{*}p < 0.002$, for the effect of post-ethanol exposure compared to the respective control condition (two-way ANOVA followed by Bonferroni's *post hoc* test). **(F–I)** Averaged data of Sholl analysis astrocytes from the stratum radiatum of control rats (white circles) and rats after 1 **(F)**, 3 **(G)**, 6 **(H)** and 9 **(I)** weeks following ethanol exposure (black circles). $^{**}p < 0.0002$, $^{*}p < 0.05$, for the effect of post-ethanol exposure compared to the respective control condition (two-way ANOVA followed by Bonferroni's *post hoc* test). **(J–M)** Averaged data of area under the curve of Sholl analysis **(J)**, maximum intersection **(K)**, maximum intersection radius **(L)** and mean of intersections **(M)** by astrocytes in the stratum radiatum from control rats (white bars) or rats after different weeks following ethanol exposure (black bars). $^{***}p < 0.0001$, $^{**}p < 0.001$, $^{*}p < 0.05$, for the effect of post-ethanol exposure compared to the respective control condition (two-way ANOVA followed by Bonferroni's *post hoc* test). Data were obtained from at least three independent experiments. Calibration bar = 25 μm.

(Retamal et al., 2006, 2007; Avendaño et al., 2015). Furthermore, COX_1/COX_2 stimulation is necessary for the persistent opening of Cx43 hemichannels and Panx1 channels elicited by prenatal nicotine and high-fat diet in the hippocampus (Orellana et al., 2014b). Similarly, iNOS and COX_2 activity, as well as $[Ca^{2+}]_i$ and NO, base the Panx1 channel-mediated release of ATP in LPS-treated microglia (Orellana et al., 2013). Here, we demonstrated that ethanol-mediated Etd uptake in hippocampal astrocytes is totally suppressed by blockers of p38MAPK, iNOS, COX_1 and COX_2, implicating that activation of Cx43 and Panx1 unopposed channels possibly took place downstream of these pathways (**Figure 9**). Importantly, the activity of these channels also depended on $[Ca^{2+}]_i$ signaling as BAPTA completely abolished the Etd uptake evoked by ethanol. The above findings are consistent with three facts observed in previous studies: (i) ethanol induces the activation of iNOS and COXs in astrocytes (Pascual et al., 2003; Blanco et al., 2005); (ii) iNOS and COX activity raises $[Ca^{2+}]_i$ due the release of PGE_2 and the subsequent stimulation of EP_1 receptors (Swierkosz et al., 1995; Woodward et al., 2011), which are expressed in astrocytes

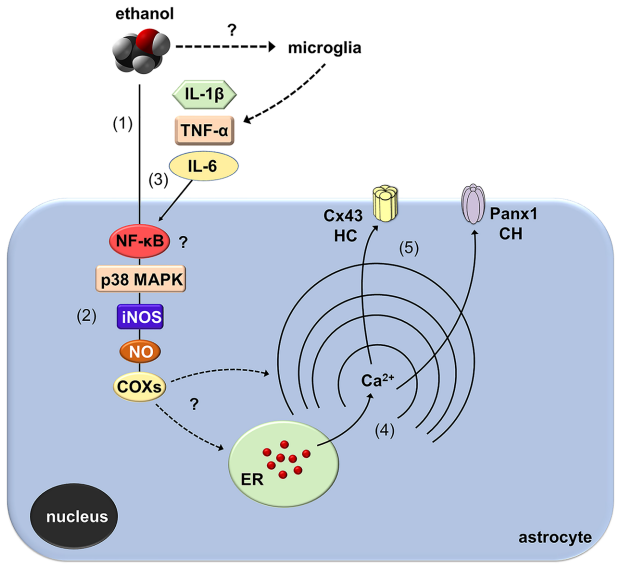

FIGURE 9 | Schematic diagram showing the possible pathways involved in the activation of astroglial Cx43 hemichannels and Panx1 channels evoked by *in vivo* ethanol exposure during adolescence. Ethanol could stimulate directly astrocytes (1) with a signal transduction that possibly involves NF-κβ signaling associated to p38 MAPK and iNOS activation, NO production and further stimulation of COXs (2). Alternatively, activation of NF-κβ signaling in astrocytes and/or microglia could evoke the autocrine/paracrine release of IL-1β, TNF-α, and IL-6, which are well-known inducers of the opening of hemichannel (HC) and pannexons via the stimulation of p38 MAPK/iNOS/COX pathway (3). The latter cascade through an unknown mechanism likely increase cytoplasmic levels of Ca^{2+} (4), which is known to open Cx43 HCs and Panx1 channels (CHs) (5).

(Fiebich et al., 2001); and (iii) the opening of hemichannels and pannexons rely on $[Ca^{2+}]_i$ increments (Locovei et al., 2006; De Bock et al., 2012; Meunier et al., 2017). Whether ethanol-induced hemichannel/pannexon activity occurs by parallel mechanisms affecting astrocytes, including post-translational modifications (e.g., S-nitrosylation) and $[Ca^{2+}]_i$ signaling, will be matter of future investigations. In addition, we cannot rule out the influence of microglia in the activity of Cx43 hemichannels and Panx1 channels observed in astrocytes from ethanol-exposed rats. Indeed, microglia are particularly sensitive to ethanol (Fernandez-Lizarbe et al., 2009) and also express functional Cx43 hemichannels and Panx1 channels (Gajardo-Gómez et al., 2016).

A keystone underlying the opening of hemichannels and pannexons in the nervous system came from the long-lasting production of pro-inflammatory cytokines due to the disrupted function of the brain innate and adaptive immune system (Sarrouilhe et al., 2017). Previous studies have demonstrated that several models of adolescent alcohol exposure raise cytokine levels in different brain areas (Pascual et al., 2018), including the hippocampus (Kane et al., 2014; Doremus-Fitzwater et al., 2015). Here, we observed that intermittent ethanol injections during adolescence cause rapid and transient augments in hippocampal levels of IL-1β, TNF-α and IL-6. Consequently, it is plausible to hypothesize that by activating the above signaling, IL-1β, TNF-α and IL-6 may be in part responsible of the opening of astroglial hemichannels and pannexons observed in our model of adolescent ethanol exposure (**Figure 9**). Supporting this idea, in astrocytes, the opening of Cx43 hemichannels and Panx1 channels is stimulated by IL-1β and TNF-α (Retamal et al., 2007; Avendaño et al., 2015), the latter cytokines being closely linked to the activation of p38 MAPK, iNOS and COXs (Clerk et al., 1999; Vinukonda et al., 2010; Sheng et al., 2011; Samy and Igwe, 2012). Alternatively, hemichannel and pannexon activity may result from alterations in redox status. During pathological scenarios, oxidant molecules increase the activity of Cx43 hemichannels and Panx1 channels (Retamal, 2014). In a recent work, we showed that the model of heavy ethanol exposure used in this study increases rapidly oxidative stress and mitochondrial dysfunction in the hippocampus (Tapia-Rojas et al., 2018). Whether astroglial hemichannel and pannexon opening evoked by ethanol exposure take places by an impairment in redox status and production of free radicals remains to be elucidated.

During neuroinflammation, among other changes, astrocytes undergo the remodeling of their dendritic arbor as well as multiple morphological alterations (Pekny and Nilsson, 2005). There is plenty of data demonstrating the detrimental effects of ethanol on astrocyte functions (Adermark and Bowers, 2016), but whether this occur in the adolescent brain is just beginning to be understood (Pascual et al., 2018). In the present study, we found that intermittent ethanol exposure modulates the complexity of astrocyte branch arbors in the hippocampus of adolescent rats in a time and spatial-depend manner. Particularly, ethanol exposure increased in a rapid and transient manner the arbor complexity of astrocytes in the stratum oriens and stratum pyramidale, but decreased branch arborization in the stratum radiatum after 3 weeks following ethanol exposure. These findings harmonize with previous studies showing the layer-specific arborization of astrocytes (Lanjakornsiripan et al., 2018) and the opposite regulation of this astroglial feature during different pathological conditions (Lechuga-Sancho et al., 2006; Torres-Platas et al., 2011; Tsai et al., 2018). Furthermore, in the hippocampus, astrocytes show a wide diversity and heterogeneity, particularly, astrocytes close to the stratum pyramidale are organized in networks that remain parallel to this layer, whereas astrocytes in the stratum radiatum have circular networks (Houades et al., 2006). Likewise, the electrophysiological features of hippocampal astrocytes also vary according to their location in different subregions of the hippocampus (Ben Haim and Rowitch, 2017). For example, astrocytes from the CA1 and CA3 areas of the hippocampus show different levels of cell-cell coupling (D'Ambrosio et al., 1998). This analysis becomes even more complex when the diversity of neuronal populations (e.g., pyramidal, baskets, etc.) and their projections (e.g., inhibitory, excitatory) are considered. These differences may explain not just the basal and ethanol-mediated heterogeneity in hippocampal astrocyte arborization, but also the diversity in ethanol-induced channel responses in the regions analyzed: stratum oriens > stratum pyramidale > stratum radiatum. Future studies are necessary to uncover the molecular and cellular mechanisms of these differential responses.

The fact that channel activity, cytokine production and astrocyte arborization were recovered to control levels during 3–7 weeks post-ethanol exposure is relevant and reveal the plasticity of astrocyte function and neural circuits. Our findings indicate that opening of hemichannels and pannexons occurs at early phases post alcohol exposure and is accompanied of neuroinflammation and astrocyte activation. We speculate that uncontrolled opening of astrocyte hemichannels and pannexons may contributes to the neurotoxicity caused by adolescent alcohol consumption. Future studies will elucidate whether these channels may participate in the pathogenesis of alcohol use disorders in the adulthood.

AUTHOR CONTRIBUTIONS

GG, RF, CM, VL, NS, CR, JEO, WC, RQ and JAO: conceived, performed and analyzed the experiments. JAO: wrote and edited the manuscript. All authors read and approved the final manuscript.

FUNDING

This work was supported by the Fondo Nacional de Desarrollo Científico y Tecnológico (FONDECYT) Grant 1160710 (to JAO), 1170441 (to RQ), the Comisión Nacional de Investigación Científica y Tecnológica (CONICYT), Proyecto de Cooperación Internacional (PCI)-BMBF 20150065 (to WC) and Programa de Investigación Asociativa (PIA) Grant Anillo de Ciencia y Tecnología ACT1411 (to WC, RQ and JAO).

ACKNOWLEDGMENTS

CONICYT, PIA, FONDECYT, Universidad Autónoma de Chile and Pontificia Universidad Católica de Chile.

REFERENCES

Abascal, F., and Zardoya, R. (2013). Evolutionary analyses of gap junction protein families. *Biochim. Biophys. Acta* 1828, 4–14. doi: 10.1016/j.bbamem.2012.02.007

Abudara, V., Roux, L., Dallerac, G., Matias, I., Dulong, J., Mothet, J. P., et al. (2015). Activated microglia impairs neuroglial interaction by opening Cx43 hemichannels in hippocampal astrocytes. *Glia* 63, 795–811. doi: 10.1002/glia.22785

Adermark, L., and Bowers, M. S. (2016). Disentangling the role of astrocytes in alcohol use disorder. *Alcohol. Clin. Exp. Res.* 40, 1802–1816. doi: 10.1111/acer.13168

Agulhon, C., Sun, M. Y., Murphy, T., Myers, T., Lauderdale, K., and Fiacco, T. A. (2012). Calcium signaling and gliotransmission in normal vs. reactive astrocytes. *Front. Pharmacol.* 3:139. doi: 10.3389/fphar.2012.00139

Araque, A., Parpura, V., Sanzgiri, R. P., and Haydon, P. G. (1999). Tripartite synapses: glia, the unacknowledged partner. *Trends Neurosci.* 22, 208–215. doi: 10.1016/S0166-2236(98)01349-6

Ardiles, A. O., Flores-Muñoz, C., Toro-Ayala, G., Cárdenas, A. M., Palacios, A. G., Muñoz, P., et al. (2014). Pannexin 1 regulates bidirectional hippocampal synaptic plasticity in adult mice. *Front. Cell. Neurosci.* 8:326. doi: 10.3389/fncel.2014.00326

Avendaño, B. C., Montero, T. D., Chávez, C. E., von Bernhardi, R., and Orellana, J. A. (2015). Prenatal exposure to inflammatory conditions increases Cx43 and Panx1 unopposed channel opening and activation of astrocytes in the offspring effect on neuronal survival. *Glia* 63, 2058–2072. doi: 10.1002/glia.22877

Bava, S., and Tapert, S. F. (2010). Adolescent brain development and the risk for alcohol and other drug problems. *Neuropsychol. Rev.* 20, 398–413. doi: 10.1007/s11065-010-9146-6

Ben Haim, L., and Rowitch, D. H. (2017). Functional diversity of astrocytes in neural circuit regulation. *Nat. Rev. Neurosci.* 18, 31–41. doi: 10.1038/nrn.2016.159

Blanco, A. M., and Guerri, C. (2007). Ethanol intake enhances inflammatory mediators in brain: role of glial cells and TLR4/IL-1RI receptors. *Front. Biosci.* 12, 2616–2630. doi: 10.2741/2259

Blanco, A. M., Pascual, M., Valles, S. L., and Guerri, C. (2004). Ethanol-induced iNOS and COX-2 expression in cultured astrocytes via NF-κB. *Neuroreport* 15, 681–685. doi: 10.1097/00001756-200403220-00021

Blanco, A. M., Vallés, S. L., Pascual, M., and Guerri, C. (2005). Involvement of TLR4/type I IL-1 receptor signaling in the induction of inflammatory mediators and cell death induced by ethanol in cultured astrocytes. *J. Immunol.* 175, 6893–6899. doi: 10.4049/jimmunol.175.10.6893

Broadwater, M. A., Liu, W., Crews, F. T., and Spear, L. P. (2014). Persistent loss of hippocampal neurogenesis and increased cell death following adolescent, but not adult, chronic ethanol exposure. *Dev. Neurosci.* 36, 297–305. doi: 10.1159/000362874

Brown, S. A., Tapert, S. F., Granholm, E., and Delis, D. C. (2000). Neurocognitive functioning of adolescents: effects of protracted alcohol use. *Alcohol. Clin. Exp. Res.* 24, 164–171. doi: 10.1097/00000374-200002000-00005

Chever, O., Lee, C. Y., and Rouach, N. (2014). Astroglial connexin43 hemichannels tune basal excitatory synaptic transmission. *J. Neurosci.* 34, 11228–11232. doi: 10.1523/JNEUROSCI.0015-14.2014

Cippitelli, A., Domi, E., Ubaldi, M., Douglas, J. C., Li, H. W., Demopulos, G., et al. (2017). Protection against alcohol-induced neuronal and cognitive damage by the PPARγ receptor agonist pioglitazone. *Brain Behav. Immun.* 64, 320–329. doi: 10.1016/j.bbi.2017.02.001

Clerk, A., Harrison, J. G., Long, C. S., and Sugden, P. H. (1999). Pro-inflammatory cytokines stimulate mitogen-activated protein kinase subfamilies, increase phosphorylation of c-Jun and ATF2 and upregulate c-Jun protein in neonatal rat ventricular myocytes. *J. Mol. Cell. Cardiol.* 31, 2087–2099. doi: 10.1006/jmcc.1999.1040

Cohen-Gilbert, J. E., Nickerson, L. D., Sneider, J. T., Oot, E. N., Seraikas, A. M., Rohan, M. L., et al. (2017). College binge drinking associated with decreased frontal activation to negative emotional distractors during inhibitory control. *Front. Psychol.* 8:1650. doi: 10.3389/fpsyg.2017.01650

Contreras, J. E., Sánchez, H. A., Eugenin, E. A., Speidel, D., Theis, M., Willecke, K., et al. (2002). Metabolic inhibition induces opening of unapposed connexin 43 gap junction hemichannels and reduces gap junctional communication in cortical astrocytes in culture. *Proc. Natl. Acad. Sci. U S A* 99, 495–500. doi: 10.1073/pnas.012589799

Cservenka, A., and Brumback, T. (2017). The burden of binge and heavy drinking on the brain: effects on adolescent and young adult neural structure and function. *Front. Psychol.* 8:1111. doi: 10.3389/fpsyg.2017.01111

D'Ambrosio, R., Wenzel, J., Schwartzkroin, P. A., McKhann, G. M. II., and Janigro, D. (1998). Functional specialization and topographic segregation of hippocampal astrocytes. *J. Neurosci.* 18, 4425–4438. doi: 10.1523/JNEUROSCI.18-12-04425.1998

Davis, R. L., and Syapin, P. J. (2004). Acute ethanol exposure modulates expression of inducible nitric-oxide synthase in human astroglia: evidence for a transcriptional mechanism. *Alcohol* 32, 195–202. doi: 10.1016/j.alcohol.2004.01.006

De Bellis, M. D., Clark, D. B., Beers, S. R., Soloff, P. H., Boring, A. M., Hall, J., et al. (2000). Hippocampal volume in adolescent-onset alcohol use disorders. *Am. J. Psychiatry* 157, 737–744. doi: 10.1176/appi.ajp.157.5.737

De Bock, M., Wang, N., Bol, M., Decrock, E., Ponsaerts, R., Bultynck, G., et al. (2012). Connexin 43 hemichannels contribute to cytoplasmic Ca^{2+} oscillations by providing a bimodal Ca^{2+}-dependent Ca^{2+} entry pathway. *J. Biol. Chem.* 287, 12250–12266. doi: 10.1074/jbc.M111.299610

D'Hondt, C., Ponsaerts, R., De Smedt, H., Bultynck, G., and Himpens, B. (2009). Pannexins, distant relatives of the connexin family with specific cellular functions? *Bioessays* 31, 953–974. doi: 10.1002/bies.200800236

Doremus-Fitzwater, T. L., Gano, A., Paniccia, J. E., and Deak, T. (2015). Male adolescent rats display blunted cytokine responses in the CNS after acute ethanol or lipopolysaccharide exposure. *Physiol. Behav.* 148, 131–144. doi: 10.1016/j.physbeh.2015.02.032

Edenberg, H. J., and Foroud, T. (2013). Genetics and alcoholism. *Nat. Rev. Gastroenterol. Hepatol.* 10, 487–494. doi: 10.1038/nrgastro.2013.86

Fernandes, L. M. P., Cartágenes, S. C., Barros, M. A., Carvalheiro, T., Castro, N. C. F., Schamne, M. G., et al. (2018). Repeated cycles of binge-like ethanol exposure induce immediate and delayed neurobehavioral changes and hippocampal dysfunction in adolescent female rats. *Behav. Brain Res.* 350, 99–108. doi: 10.1016/j.bbr.2018.05.007

Fernandez-Lizarbe, S., Pascual, M., and Guerri, C. (2009). Critical role of TLR4 response in the activation of microglia induced by ethanol. *J. Immunol.* 183, 4733–4744. doi: 10.4049/jimmunol.0803590

Fiebich, B. L., Schleicher, S., Spleiss, O., Czygan, M., and Hüll, M. (2001). Mechanisms of prostaglandin E2-induced interleukin-6 release in astrocytes: possible involvement of EP4-like receptors, p38 mitogen-activated protein kinase and protein kinase C. *J. Neurochem.* 79, 950–958. doi: 10.1046/j.1471-4159.2001.00652.x

Froger, N., Orellana, J. A., Calvo, C. F., Amigou, E., Kozoriz, M. G., Naus, C. C., et al. (2010). Inhibition of cytokine-induced connexin43 hemichannel activity in astrocytes is neuroprotective. *Mol. Cell. Neurosci.* 45, 37–46. doi: 10.1016/j.mcn.2010.05.007

Gajardo, I., Salazar, C. S., Lopez-Espíndola, D., Estay, C., Flores-Muñoz, C., Elgueta, C., et al. (2018). Lack of pannexin 1 alters synaptic GluN2 subunit composition and spatial reversal learning in mice. *Front. Mol. Neurosci.* 11:114. doi: 10.3389/fnmol.2018.00114

Gajardo-Gómez, R., Labra, V. C., and Orellana, J. A. (2016). Connexins and pannexins: new insights into microglial functions and dysfunctions. *Front. Mol. Neurosci.* 9:86. doi: 10.3389/fnmol.2016.00086

Garré, J. M., Yang, G., Bukauskas, F. F., and Bennett, M. V. (2016). FGF-1 triggers pannexin-1 hemichannel opening in spinal astrocytes of rodents and promotes inflammatory responses in acute spinal cord slices. *J. Neurosci.* 36, 4785–4801. doi: 10.1523/JNEUROSCI.4195-15.2016

Gundersen, V., Storm-Mathisen, J., and Bergersen, L. H. (2015). Neuroglial transmission. *Physiol. Rev.* 95, 695–726. doi: 10.1152/physrev.00024.2014

Houades, V., Rouach, N., Ezan, P., Kirchhoff, F., Koulakoff, A., and Giaume, C. (2006). Shapes of astrocyte networks in the juvenile brain. *Neuron Glia Biol.* 2, 3–14. doi: 10.1017/s1740925x06000081

Iglesias, R., Dahl, G., Qiu, F., Spray, D. C., and Scemes, E. (2009). Pannexin 1: the molecular substrate of astrocyte "hemichannels". *J. Neurosci.* 29, 7092–7097. doi: 10.1523/JNEUROSCI.6062-08.2009

Kane, C. J., Phelan, K. D., Douglas, J. C., Wagoner, G., Johnson, J. W., Xu, J., et al. (2014). Effects of ethanol on immune response in the brain: region-specific changes in adolescent versus adult mice. *Alcohol. Clin. Exp. Res.* 38, 384–391. doi: 10.1111/acer.12244

Karpuk, N., Burkovetskaya, M., Fritz, T., Angle, A., and Kielian, T. (2011). Neuroinflammation leads to region-dependent alterations in astrocyte gap junction communication and hemichannel activity. *J. Neurosci.* 31, 414–425. doi: 10.1523/JNEUROSCI.5247-10.2011

Kim, Y., Davidson, J. O., Gunn, K. C., Phillips, A. R., Green, C. R., and Gunn, A. J. (2016). Role of hemichannels in CNS inflammation and the inflammasome pathway. *Adv. Protein Chem. Struct. Biol.* 104, 1–37. doi: 10.1016/bs.apcsb.2015.12.001

Lanjakornsiripan, D., Pior, B. J., Kawaguchi, D., Furutachi, S., Tahara, T., Katsuyama, Y., et al. (2018). Layer-specific morphological and molecular differences in neocortical astrocytes and their dependence on neuronal layers. *Nat. Commun.* 9:1623. doi: 10.1038/s41467-018-03940-3

Lechuga-Sancho, A. M., Arroba, A. I., Frago, L. M., García-Cáceres, C., De Célix, A. D., Argente, J., et al. (2006). Reduction in the number of astrocytes and their projections is associated with increased synaptic protein density in the hypothalamus of poorly controlled diabetic rats. *Endocrinology* 147, 5314–5324. doi: 10.1210/en.2006-0766

Liu, W., and Crews, F. T. (2017). Persistent decreases in adult subventricular and hippocampal neurogenesis following adolescent intermittent ethanol exposure. *Front. Behav. Neurosci.* 11:151. doi: 10.3389/fnbeh.2017.00151

Locovei, S., Wang, J., and Dahl, G. (2006). Activation of pannexin 1 channels by ATP through P2Y receptors and by cytoplasmic calcium. *FEBS Lett.* 580, 239–244. doi: 10.1016/j.febslet.2005.12.004

Makarenkova, H. P., and Shestopalov, V. I. (2014). The role of pannexin hemichannels in inflammation and regeneration. *Front. Physiol.* 5:63. doi: 10.3389/fphys.2014.00063

Meunier, C., Wang, N., Yi, C., Dallerac, G., Ezan, P., Koulakoff, A., et al. (2017). Contribution of astroglial Cx43 hemichannels to the modulation of glutamatergic currents by D-serine in the mouse prefrontal cortex. *J. Neurosci.* 37, 9064–9075. doi: 10.1523/JNEUROSCI.2204-16.2017

Montero, T. D., and Orellana, J. A. (2015). Hemichannels: new pathways for gliotransmitter release. *Neuroscience* 286, 45–59. doi: 10.1016/j.neuroscience.2014.11.048

Mugisho, O. O., Green, C. R., Kho, D. T., Zhang, J., Graham, E. S., Acosta, M. L., et al. (2018). The inflammasome pathway is amplified and perpetuated in an autocrine manner through connexin43 hemichannel mediated ATP release. *Biochim. Biophys. Acta* 1862, 385–393. doi: 10.1016/j.bbagen.2017.11.015

Orellana, J. A., Avendaño, B. C., and Montero, T. D. (2014a). Role of connexins and pannexins in ischemic stroke. *Curr. Med. Chem.* 21, 2165–2182. doi: 10.2174/0929867321666131228191714

Orellana, J. A., Busso, D., Ramírez, G., Campos, M., Rigotti, A., Eugenín, J., et al. (2014b). Prenatal nicotine exposure enhances Cx43 and Panx1 unopposed channel activity in brain cells of adult offspring mice fed a high-fat/cholesterol diet. *Front. Cell. Neurosci.* 8:403. doi: 10.3389/fncel.2014.00403

Orellana, J. A., Froger, N., Ezan, P., Jiang, J. X., Bennett, M. V., Naus, C. C., et al. (2011a). ATP and glutamate released via astroglial connexin 43 hemichannels mediate neuronal death through activation of pannexin 1 hemichannels. *J. Neurochem.* 118, 826–840. doi: 10.1111/j.1471-4159.2011.07210.x

Orellana, J. A., Shoji, K. F., Abudara, V., Ezan, P., Amigou, E., Sáez, P. J., et al. (2011b). Amyloid β-induced death in neurons involves glial and neuronal hemichannels. *J. Neurosci.* 31, 4962–4977. doi: 10.1523/jneurosci.6417-10.2011

Orellana, J. A., Montero, T. D., and von Bernhardi, R. (2013). Astrocytes inhibit nitric oxide-dependent Ca^{2+} dynamics in activated microglia: involvement of ATP released via pannexin 1 channels. *Glia* 61, 2023–2037. doi: 10.1002/glia.22573

Orellana, J. A., Moraga-Amaro, R., Diaz-Galarce, R., Rojas, S., Maturana, C. J., Stehberg, J., et al. (2015). Restraint stress increases hemichannel activity in hippocampal glial cells and neurons. *Front. Cell. Neurosci.* 9:102. doi: 10.3389/fncel.2015.00102

Orellana, J. A., Retamal, M. A., Moraga-Amaro, R., and Stehberg, J. (2016). Role of astroglial hemichannels and pannexons in memory and neurodegenerative diseases. *Front. Integr. Neurosci.* 10:26. doi: 10.3389/fnint.2016.00026

Pascual, M., Blanco, A. M., Cauli, O., Miñarro, J., and Guerri, C. (2007). Intermittent ethanol exposure induces inflammatory brain damage and causes long-term behavioural alterations in adolescent rats. *Eur. J. Neurosci.* 25, 541–550. doi: 10.1111/j.1460-9568.2006.05298.x

Pascual, M., Montesinos, J., and Guerri, C. (2018). Role of the innate immune system in the neuropathological consequences induced by adolescent binge drinking. *J. Neurosci. Res.* 96, 765–780. doi: 10.1002/jnr.24203

Pascual, M., Valles, S. L., Renau-Piqueras, J., and Guerri, C. (2003). Ceramide pathways modulate ethanol-induced cell death in astrocytes. *J. Neurochem.* 87, 1535–1545. doi: 10.1046/j.1471-4159.2003.02130.x

Pekny, M., and Nilsson, M. (2005). Astrocyte activation and reactive gliosis. *Glia* 50, 427–434. doi: 10.1002/glia.20207

Pekny, M., and Pekna, M. (2014). Astrocyte reactivity and reactive astrogliosis: costs and benefits. *Physiol. Rev.* 94, 1077–1098. doi: 10.1152/physrev.00041.2013

Pelegrin, P., and Surprenant, A. (2006). Pannexin-1 mediates large pore formation and interleukin-1β release by the ATP-gated P2X7 receptor. *EMBO J.* 25, 5071–5082. doi: 10.1038/sj.emboj.7601378

Perea, G., Navarrete, M., and Araque, A. (2009). Tripartite synapses: astrocytes process and control synaptic information. *Trends Neurosci.* 32, 421–431. doi: 10.1016/j.tins.2009.05.001

Retamal, M. A. (2014). Connexin and Pannexin hemichannels are regulated by redox potential. *Front. Physiol.* 5:80. doi: 10.3389/fphys.2014.00080

Retamal, M. A., Cortés, C. J., Reuss, L., Bennett, M. V., and Sáez, J. C. (2006). S-nitrosylation and permeation through connexin 43 hemichannels in astrocytes: induction by oxidant stress and reversal by reducing agents. *Proc. Natl. Acad. Sci. U S A* 103, 4475–4480. doi: 10.1073/pnas.0511118103

Retamal, M. A., Froger, N., Palacios-Prado, N., Ezan, P., Sáez, P. J., Sáez, J. C., et al. (2007). Cx43 hemichannels and gap junction channels in astrocytes are regulated oppositely by proinflammatory cytokines released from activated microglia. *J. Neurosci.* 27, 13781–13792. doi: 10.1523/jneurosci.2042-07.2007

Reynolds, A. R., Williams, L. A., Saunders, M. A., and Prendergast, M. A. (2015). Group 1 mGlu-family proteins promote neuroadaptation to ethanol and withdrawal-associated hippocampal damage. *Drug Alcohol Depend.* 156, 213–220. doi: 10.1016/j.drugalcdep.2015.09.013

Rossi, D., and Volterra, A. (2009). Astrocytic dysfunction: insights on the role in neurodegeneration. *Brain Res. Bull.* 80, 224–232. doi: 10.1016/j.brainresbull.2009.07.012

Roux, L., Madar, A., Lacroix, M. M., Yi, C., Benchenane, K., and Giaume, C. (2015). Astroglial connexin 43 hemichannels modulate olfactory bulb slow oscillations. *J. Neurosci.* 35, 15339–15352. doi: 10.1523/jneurosci.0861-15.2015

Sabeti, J., and Gruol, D. L. (2008). Emergence of NMDAR-independent long-term potentiation at hippocampal CA1 synapses following early adolescent exposure to chronic intermittent ethanol: role for sigma-receptors. *Hippocampus* 18, 148–168. doi: 10.1002/hipo.20379

Sáez, J. C., and Leybaert, L. (2014). Hunting for connexin hemichannels. *FEBS Lett.* 588, 1205–1211. doi: 10.1016/j.febslet.2014.03.004

Sáez, P. J., Shoji, K. F., Retamal, M. A., Harcha, P. A., Ramirez, G., Jiang, J. X., et al. (2013). ATP is required and advances cytokine-induced gap junction formation in microglia *in vitro*. *Mediators Inflamm.* 2013:216402. doi: 10.1155/2013/216402

Salameh, A., Blanke, K., and Dhein, S. (2013). Mind the gap! Connexins and pannexins in physiology, pharmacology and disease. *Front. Pharmacol.* 4:144. doi: 10.3389/fphar.2013.00144

Samy, A. S., and Igwe, O. J. (2012). Regulation of IL-1β-induced cyclooxygenase-2 expression by interactions of Aβ peptide, apolipoprotein E and nitric oxide in human neuroglioma. *J. Mol. Neurosci.* 47, 533–545. doi: 10.1007/s12031-011-9670-8

Santiago, M. F., Veliskova, J., Patel, N. K., Lutz, S. E., Caille, D., Charollais, A., et al. (2011). Targeting pannexin1 improves seizure outcome. *PLoS One* 6:e25178. doi: 10.1371/journal.pone.0025178

Sarrouilhe, D., Dejean, C., and Mesnil, M. (2017). Connexin43- and pannexin-based channels in neuroinflammation and cerebral neuropathies. *Front. Mol. Neurosci.* 10:320. doi: 10.3389/fnmol.2017.00320

Schalper, K. A., Palacios-Prado, N., Orellana, J. A., and Sáez, J. C. (2008). Currently used methods for identification and characterization of hemichannels. *Cell Commun. Adhes.* 15, 207–218. doi: 10.1080/15419060802014198

Schindelin, J., Arganda-Carreras, I., Frise, E., Kaynig, V., Longair, M., Pietzsch, T., et al. (2012). Fiji: an open-source platform for biological-image analysis. *Nat. Methods* 9, 676–682. doi: 10.1038/nmeth.2019

Sheng, W., Zong, Y., Mohammad, A., Ajit, D., Cui, J., Han, D., et al. (2011). Pro-inflammatory cytokines and lipopolysaccharide induce changes in cell morphology and upregulation of ERK1/2, iNOS and sPLA(2)-IIA expression in astrocytes and microglia. *J. Neuroinflammation* 8:121. doi: 10.1186/1742-2094-8-121

Sholl, D. A. (1953). Dendritic organization in the neurons of the visual and motor cortices of the cat. *J. Anat.* 87, 387–406.

Silverman, W., Locovei, S., and Dahl, G. (2008). Probenecid, a gout remedy, inhibits pannexin 1 channels. *Am. J. Physiol. Cell Physiol.* 295, C761–C767. doi: 10.1152/ajpcell.00227.2008

Sosinsky, G. E., Boassa, D., Dermietzel, R., Duffy, H. S., Laird, D. W., Macvicar, B., et al. (2011). Pannexin channels are not gap junction hemichannels. *Channels* 5, 193–197. doi: 10.4161/chan.5.3.15765

Stehberg, J., Moraga-Amaro, R., Salazar, C., Becerra, A., Echeverria, C., Orellana, J. A., et al. (2012). Release of gliotransmitters through astroglial connexin 43 hemichannels is necessary for fear memory consolidation in the basolateral amygdala. *FASEB J.* 26, 3649–3657. doi: 10.1096/fj.11-198416

Suman, S., Kumar, S., N'Gouemo, P., and Datta, K. (2016). Increased DNA double-strand break was associated with downregulation of repair and upregulation of apoptotic factors in rat hippocampus after alcohol exposure. *Alcohol* 54, 45–50. doi: 10.1016/j.alcohol.2016.06.003

Swierkosz, T. A., Mitchell, J. A., Warner, T. D., Botting, R. M., and Vane, J. R. (1995). Co-induction of nitric oxide synthase and cyclo-oxygenase: interactions between nitric oxide and prostanoids. *Br. J. Pharmacol.* 114, 1335–1342. doi: 10.1111/j.1476-5381.1995.tb13353.x

Takeuchi, H., Jin, S., Wang, J., Zhang, G., Kawanokuchi, J., Kuno, R., et al. (2006). Tumor necrosis factor-α induces neurotoxicity via glutamate release from hemichannels of activated microglia in an autocrine manner. *J. Biol. Chem.* 281, 21362–21368. doi: 10.1074/jbc.m600504200

Tapia-Rojas, C., Carvajal, F. J., Mira, R. G., Arce, C., Lerma-Cabrera, J. M., Orellana, J. A., et al. (2018). Adolescent binge alcohol exposure affects the brain function through mitochondrial impairment. *Mol. Neurobiol.* 55, 4473–4491. doi: 10.1007/s12035-017-0613-4

Torres, A., Wang, F., Xu, Q., Fujita, T., Dobrowolski, R., Willecke, K., et al. (2012). Extracellular Ca^{2+} acts as a mediator of communication from neurons to glia. *Sci. Signal* 5:ra8. doi: 10.1126/scisignal.2002160

Torres-Platas, S. G., Hercher, C., Davoli, M. A., Maussion, G., Labonte, B., Turecki, G., et al. (2011). Astrocytic hypertrophy in anterior cingulate white matter of depressed suicides. *Neuropsychopharmacology* 36, 2650–2658. doi: 10.1038/npp.2011.154

Tsai, S. F., Wu, H. T., Chen, P. C., Chen, Y. W., Yu, M., Wang, T. F., et al. (2018). High-fat diet suppresses the astrocytic process arborization and downregulates the glial glutamate transporters in the hippocampus of mice. *Brain Res.* 1700, 66–77. doi: 10.1016/j.brainres.2018.07.017

Vallés, S. L., Blanco, A. M., Pascual, M., and Guerri, C. (2004). Chronic ethanol treatment enhances inflammatory mediators and cell death in the brain and in astrocytes. *Brain Pathol.* 14, 365–371. doi: 10.1111/j.1750-3639.2004.tb00079.x

Vicario, N., Zappala, A., Calabrese, G., Gulino, R., Parenti, C., Gulisano, M., et al. (2017). Connexins in the central nervous system: physiological traits and neuroprotective targets. *Front. Physiol.* 8:1060. doi: 10.3389/fphys.2017.01060

Vinukonda, G., Csiszar, A., Hu, F., Dummula, K., Pandey, N. K., Zia, M. T., et al. (2010). Neuroprotection in a rabbit model of intraventricular haemorrhage by cyclooxygenase-2, prostanoid receptor-1 or tumour necrosis factor-alpha inhibition. *Brain* 133, 2264–2280. doi: 10.1093/brain/awq107

Walrave, L., Vinken, M., Albertini, G., De Bundel, D., Leybaert, L., and Smolders, I. J. (2016). Inhibition of connexin43 hemichannels impairs spatial short-term memory without affecting spatial working memory. *Front. Cell. Neurosci.* 10:288. doi: 10.3389/fncel.2016.00288

Wang, N., De Bock, M., Decrock, E., Bol, M., Gadicherla, A., Bultynck, G., et al. (2013). Connexin targeting peptides as inhibitors of voltage- and intracellular Ca^{2+}-triggered Cx43 hemichannel opening. *Neuropharmacology* 75, 506–516. doi: 10.1016/j.neuropharm.2013.08.021

Woodward, D. F., Jones, R. L., and Narumiya, S. (2011). International union of basic and clinical pharmacology. LXXXIII: classification of prostanoid receptors, updating 15 years of progress. *Pharmacol. Rev.* 63, 471–538. doi: 10.1124/pr.110.003517

Yi, C., Mei, X., Ezan, P., Mato, S., Matias, I., Giaume, C., et al. (2016). Astroglial connexin43 contributes to neuronal suffering in a mouse model of Alzheimer's disease. *Cell Death Differ.* 23, 1691–1701. doi: 10.1038/cdd.2016.63

Zeigler, D. W., Wang, C. C., Yoast, R. A., Dickinson, B. D., Mccaffree, M. A., Robinowitz, C. B., et al. (2005). The neurocognitive effects of alcohol on adolescents and college students. *Prev. Med.* 40, 23–32. doi: 10.1016/j.ypmed.2004.04.044

Conflict of Interest Statement: The authors declare that the research was conducted in the absence of any commercial or financial relationships that could be construed as a potential conflict of interest.

frontiers in Cellular Neuroscience

ORIGINAL RESEARCH
published: 04 February 2019
doi: 10.3389/fncel.2019.00019

Lipoxin A4 Regulates Lipopolysaccharide-Induced BV2 Microglial Activation and Differentiation via the Notch Signaling Pathway

Jun Wu†, Dan-hua Ding†, Qian-qian Li, Xin-yu Wang, Yu-ying Sun and Lan-Jun Li*

Department of Neurology, The First Affiliated Hospital of Zhengzhou University, Zhengzhou, China

Inflammatory responses contribute to the pathogenesis of various neurological diseases, and microglia plays an important role in the process. Activated microglia can differentiate into the pro-inflammatory, tissue-damaging M1 phenotype or the anti-inflammatory, tissue-repairing M2 phenotype. Regulating microglia differentiation, hence limiting a harmful response, might help improve the prognosis of inflammation-related nervous system diseases. The present study aimed 1. to observe the anti-inflammatory effect of lipoxin A4 (LXA4) on the inflammatory response associated to lipopolysaccharide (LPS)-induced microglia activation, 2. to clarify that LXA4 modulates the activation and differentiation of microglia induced by LPS stimulation, 3. to determine whether LXA4 regulates the activation and differentiation of microglia through the Notch signaling pathway, 4. to provide a foundation for the use of LXA4 for the treatment of inflammatory related neurological diseases. To construct a model of cellular inflammation, immortalized murine BV2 microglia cells were provided 200 ng/ml LPS. To measure the mRNA and protein levels of inflammatory factors (interleukin [IL]-1β, IL-10, and tumor necrosis factor [TNF]-α) and M1 and M2 microglia markers (inducible nitric oxide synthase [iNOS], cluster of differentiation [CD]32, arginase [Arg]1, and CD206), we performed quantitative reverse transcription polymerase chain reaction (qRT-PCR) and enzyme-linked immunosorbent assay (ELISA), immunofluorescence, or flow cytometry. To determine the mRNA and protein levels of Notch signaling components (Notch1, Hes1, and Hes5), we performed qRT-PCR and western blot. LXA4 inhibits the expression of Notch1 and Hes1 associated with M1 type microglial differentiation and decreases the M1 type microglia marker iNOS and related inflammatory factors IL-1β and TNF-α. Moreover, LXA4 upregulates the expression of the M2-associated Hes5, as well as the expression of the M2 microglia marker Arg1 and the associated inflammatory factor IL-10. These effects are blocked by the administration of the γ-secretase inhibitor DAPT, a specific blocker of the Notch signaling pathway. LXA4 inhibits the microglia activation induced by LPS and the differentiation into M1 type with pro-inflammatory effect, while promoting the differentiation to M2 type with anti-inflammatory effect. LXA4 downregulates the inflammatory mediators IL-1β, TNF-α, and iNOS, while upregulating the anti-inflammatory mediator IL-10, which acts through the Notch signaling pathway.

Keywords: inflammatory response, microglia, lipopolysaccharide, LXA4, Notch signaling pathway

OPEN ACCESS

Edited by:
Xuping Li,
Houston Methodist Research Institute, United States

Reviewed by:
Hermona Soreq,
Hebrew University of Jerusalem, Israel
Tommaso Angelone,
Università della Calabria, Italy

****Correspondence:***
Jun Wu
wjun365@163.com

† These authors have contributed equally to this work as co-first authors

Received: *06 October 2018*
Accepted: *16 January 2019*
Published: *04 February 2019*

Citation:
Wu J, Ding D-h, Li Q-q, Wang X-y, Sun Y-y and Li L-J (2019) Lipoxin A4 Regulates Lipopolysaccharide-Induced BV2 Microglial Activation and Differentiation via the Notch Signaling Pathway. Front. Cell. Neurosci. 13:19. doi: 10.3389/fncel.2019.00019

INTRODUCTION

Numerous studies have shown that neuroinflammation plays an important role in the occurrence and development of central nervous system disorders such as ischemic stroke, Alzheimer's disease, and Parkinson's disease, and is associated to every stage of the disease process(Griffin, 2006; McColl et al., 2009; Naegele and Martin, 2014; Wang Q. et al., 2015; Cuello, 2017). The inflammatory response is an automatic defense response of the body to stimuli, which can promote the clearance of pathogenic factors and the healing of damaged tissue. It is usually beneficial, but it is a double-edged sword and is harmful in some cases. For example, the inflammatory response of the central nervous system sometimes aggravates the damage of nerve cells and tissues, and worsens the condition (Gordon, 2003; Mantovani et al., 2013). Simply inhibiting the inflammatory response will inevitably weaken its protective effect. A more principled approach is to take advantage of the benefits of the inflammatory mediator itself, while preventing the potential toxicity due to high concentrations of the mediator, and maintaining a good balance between its protective and detrimental effects.

Microglia plays an essential role in innate immunity, homeostasis, and neurotropic support in the central nervous system (Streit, 2002). Microglia is considered to be a resident macrophage in the brain and has important physiological functions. However, it is rapidly activated as a consequence of brain microenvironment changes, which induce microglia differentiation into M1 and M2 cell types (Nimmerjahn et al., 2005; Colton, 2009; Hu et al., 2015). M1 microglia is an activated form responsible of releasing large amounts of inflammatory and toxic factors with potential detrimental effects to central nervous system cells and tissues (Tang and Le, 2016; Xiong et al., 2016). M2 microglia is an alternative activation type, releasing a pool of modulatory factors including brain-derived neurotrophic factor, vascular endothelial growth factor and anti-inflammatory mediators, and promoting nerve tissue repair and nerve regeneration (Beyer et al., 2000; Jin et al., 2014; Tang and Le, 2016; Kanazawa et al., 2017; Ramirez et al., 2017). Therefore, it is of great significance to regulate the differentiation of microglia and counteract inflammatory damage.

In the central nervous system, the Notch signaling pathway is involved in dynamic changes at the cellular level which reflect into the regulation of the nervous system, which in turn plays an important role in the activation and differentiation of microglia (Grandbarbe et al., 2007). The Notch signaling pathway is mainly composed of receptors, ligand expressed on adjacent cell membranes, intracellular transcription factors, regulatory molecules and downstream effector molecules (Foldi et al., 2010). And γ-secretase catalysis is the key enzyme in the activation of Notch pathway. After the interaction between Notch receptor and ligand, the intracellular domain (notch intracellular domain) NICD was released into the cytoplasm and transferred into the nucleus under the catalysis of γ-secretase, which promoted the production of transcriptional activator and induced the expression downstream target genes in the Notch pathway, including hairy enhancer of split (Hes)1, Hes5, nuclear factor kappa-light-chain-enhancer of activated B cells (NF-κB), etc. (Oswald et al., 1998; Iso et al., 2003; Zhang et al., 2018). A growing number of studies have shown that the Notch signaling pathway is closely related to microglial activation and differentiation and might play a role in central nervous system diseases (Wei et al., 2011). The Notch pathway may represent a critical therapeutic target for regulating the activation and differentiation of microglia and inflammatory response. It is vital to identify drugs that regulate the activation of differentiation of Notch pathway and microglia.

Lipoxin is an endogenous anti-inflammatory lipid medium. It is released only in small amount under physiological conditions, but its synthesis is significantly increased under pathological conditions in response to inflammatory stimuli. It acts as a modulator of the inflammatory process, exerting anti-inflammatory and pro-inflammatory effects (Lee, 1995; Takano et al., 1997; Guo et al., 2016). Synthetic lipoxins such as lipoxin A4 (LXA4) possess desirable anti-inflammatory properties as shown in experimental studies of respiratory inflammation, intestinal inflammation and nephritis (Jin et al., 2007; Levy et al., 2007; Wu et al., 2007, 2009; Kure et al., 2010). Recent studies revealed that lipoxin has a protective role in central nervous system diseases such as cerebral infarction (Ye et al., 2010; Martin et al., 2014; Guo et al., 2016; Vital et al., 2016). There are very few studies investigating the interaction between LXA4 and Notch signaling pathways. Currently, only one study on transforming growth factor beta-1 (TGF-β1)-induced renal fibrosis found that LXA4 attenuated the expression of the Notch ligand Jagged1 (JAG1) and downstream molecule Hes1. Unfortunately, no further research has been carried on this important topic (Brennan et al., 2013). To date, there is no study exploring the regulatory role of LXA4 on the activation and differentiation of microglia induced by lipopolysaccharide (LPS) stimulation, nor the LXA4-mediated activation and differentiation of microglia through the Notch signaling pathway.

The purpose of this study is to clarify the modulatory effect of LXA4 on the inflammatory response associated to LPS-induced microglia activation, with a focus on the regulatory role of LXA4 on the Notch signaling pathway.

MATERIALS AND METHODS

Cell Culture and Passage

The BV2 murine microglia cell line was purchased from the Wuhan University China Culture Collection. BV2 microglia were placed in MEM/EBSS medium containing 10% fetal bovine serum (FBS) and 100 U/ml penicillin and streptomycin, and cultured at 37°C in an incubator with a 95% O_2/5% CO_2 atmosphere. Every 2–3 days, the cells were washed twice with phosphate-buffered solution (PBS). After adding 1–1.5 ml of 0.125% trypsin, the attached cells were allowed to detach from the surface of the cell cultures at 37°C; the trypsin was neutralized with culture medium, and the cells were transferred into a new flask containing MEM/EBSS medium (supplemented with 10% FBS and 100 U/ml penicillin and streptomycin) and placed in the incubator. When cells grew adherent and the cell body is branched, they were transferred into 24-well plates (10^5 cells/well

for enzyme-linked immunosorbent assay [ELISA], 10^4 cells/well for immunofluorescence), 6-well plates (2.5×10^5 cells/well for quantitative reverse transcription polymerase chain reaction [qRT-PCR], 5×10^5 cells/well for flow cytometry), or 100-mm culture dishes (1.2×10^6 cells/dish for western blotting).

Materials

In this study, we used the following materials: LXA4 (5S,6R,15R-trihydroxy-7,9,13-trans-11-cis-eicosatetraenoic acid; Cayman); Minimum essential medium (Eagle) with 2 mM L-glutamine and Earle's BSS (MEM-EBSS)medium (Hyclone); FBS (Biological Industries); interleukin (IL)-1β, IL-10, and TNF-α ELISA kits (Shanghai ExCell Biotechnology); mouse anti-β-tubulin monoclonal antibody, rabbit anti-mouse inducible nitric oxide synthase (iNOS) monoclonal antibody, rabbit anti-mouse arginase (Arg)1 monoclonal antibody, and rabbit anti-mouse Notch1 monoclonal antibody (Proteintech Group); rabbit anti-mouse CD32 monoclonal antibody and rabbit anti-mouse CD206 monoclonal antibody (Abcam); mouse anti-mouse Hes1 single-clone antibody (Tianjin Sungene Biotechnology); murine anti-mouse Hes5 monoclonal antibody (Zen BioScience Co); horseradish peroxidase (HRP)-labeled goat anti-mouse secondary antibody and fluorescently labeled goat anti-rabbit secondary antibody (Tianjin Sungene Biotechnology Co); HRP-labeled goat anti-rabbit secondary antibody and anti-β-tubulin (Proteintech Group); HiScript II Q RT SuperMix for qPCR (+gDNA wiper) reagent and AceQ® qPCR SYBR® Green Master Mix (Low ROX Premixed) kit (Vazyme Biotechnology Co); and 2-(4-Amidinophenyl)-6-indolecarbamidine dihydrochloride, DAPI dihydrochloride sealer and LPS (Sigma), DAPT (N-[N-(3,5-difluorophenacetyl)-l-alanyl]-S-phenylglycine t-butylester) (Sigma-Aldrich, München, Germany).

Cell Processing and Experimental Grouping

Cell treatment: BV2 microglia cultured *in vitro* stimulated by LPS as an inflammation model. Before each experiment, the cells were cultured in serum-free culture for 12 h, and LXA4 and Notch signaling pathway-specific blocker γ were administered to different groups. Pretreatment with the γ-secretase inhibitor DAPT. The concentration chosen for LPS is 200 ng/ml (Pan et al., 2016). The concentration selected for LXA4: our previous study compared the anti-inflammatory effects of 1, 10 and 100 nmol/l. It was found that the anti-inflammatory effect of 100 nmol/l was the best (Wu et al., 2011). Therefore, the study used LXA4. The concentration is 100 nmol/l. The concentration selected for DAPT is 10 μM (Wu et al., 2018).

Experimental grouping:

Part I LXA4 regulates the activation and differentiation of microglia (Results 3.1–3.2).

Control group: cells cultured in serum-free medium containing 0.035% ethanol.
LXA4 group: cells cultured in serum-free medium containing 100 nmol/l LXA4.
Lipopolysaccharide group: cells pretreated with serum-free medium containing 0.035% ethanol for 30 min, after which LPS was added to a final concentration of 200 ng/ml.
LXA4 group + LPS group: cells pretreated with serum-free medium containing 100 nmol/l LXA4 for 30 min, after which LPS was added to a final concentration of 200 ng/ml.

Part II Study on the regulation of Notch signaling pathway by LXA4 (Results 3.3).

1. LXA4 inhibits the expression of molecules downstream of the Notch signaling pathway.
   Grouped with the first part
2. LXA4 regulates Notch signaling pathway.

Control group: cells cultured in serum-free medium containing 0.035% ethanol.
LPS group: cells pretreated with serum-free medium containing 0.035% ethanol for 30 min, after which LPS was added to a final concentration of 200 ng/ml.
DAPT+LPS group: cells were pretreated with serum-free medium containing 10 μmol/l DAPT for 1 h, after which LPS was added to a final concentration of 200 ng/ml.
LXA4+LPS group: cells pretreated with serum-free medium containing 100 nmol/l LXA4 for 30 min, after which LPS was added to a final concentration of 200 ng/ml.
DAPT+LXA4+LPS group: after pretreatment with DAPT with a final concentration of 10 μM for 1 h, 100 nmol/l LXA4 was added for 30 min, and then added to a final concentration of 200 ng/ml LPS.

ELISA for IL-1β, IL-10, and TNF-α

The concentrations of IL-1β, IL-10, and TNF-α in cell supernatants were determined by ELISA, according to the ELISA kit manufacturer's protocol (Shanghai ExCell Biotechnology). BV2 microglia cultured on 24-well plates were treated with LPS for 6 h. Next, the cell supernatants were collected, and the total protein level therein contained was normalized for each sample prior to performing the ELISA measurements for IL-1β, IL-10, and TNF-α.

Quantitative Reverse Transcription Polymerase Chain Reaction

Total RNA was extracted from BV2 microglia using TRIzol reagent (Invitrogen, Carlsbad, CA, United States) according to the reagent instructions. The concentration of RNA was measured using Nanodrop-1000 (Nanodrop Technologies, United States) and the purity was evaluated by the absorbance ratio at 260 and 280 nm, and the RNA purity was between 1.9 and 2.1. The cDNA was synthesized according to HiScript II Q RT SuperMix for qPCR (+gDNA wiper) (Nanjing Vazyme Biotech Biotechnology) reagent and stored at −20°C. The mRNA expression level was detected by real-time fluorescent quantitative PCR using the AceQ® qPCR SYBR® Green Master Mix (Low ROX Premixed) kit. The expression level of the gene of interest was normalized using GAPDH (glyceraldehyde triphosphate dehydrogenase), the CT value represents a real-time fluorescent quantitative PCR value, and the $2^{-\Delta\Delta CT}$ method

was used to calculate relative change analysis data of gene expression. No treatment affected the expression of GAPDH mRNA. The primer sequences used are given in the **Table 1** below.

Western Blot Analysis

BV2 microglia cells were treated with LPS for 4 and 8 h, and the cell culture medium was discarded and washed three times with sterile phosphate buffered saline. A 100:1 mixture of 100 μl of ice-cold cell lysis buffer and protease inhibitor (PMSF) was added to the cell culture, then cells were incubated on ice for 30 min, and the lysate was clarified by spinning for 10 min at 4°C (12,000 rpm), leaving the supernatant for later use. Protein quantification was performed using the micro bicinchoninic acid method. A 5× sodium dodecyl sulfate loading buffer was added, before incubating at 99°C for 5 min. Then the samples were loaded at 15 μg protein/lane on 6 or 12% acrylamide gels and subjected to sodium dodecyl sulphate polyacrylamide gel electrophoresis for about 1.5 h at 80 mV (stacking gel) and 120 mV (resolving gel). Proteins were then transferred to a polyvinylidene fluoride membrane and blocking was made for 2 h in a 5% non-fat dry milk in Tris base/Tween-buffered saline (TBST). The molecular weights of the iNOS, Notch1, arginase (Arg)1, Hes1, Hes5, and β-tubulin proteins are 131, 120, 35/38, 35, 18, and 55 kDa, respectively. Samples were incubated at 4°C overnight with Rabbit anti-iNOS (1:500), Notch1 (1:500) and mouse anti-Arg1 (1:300), Hes1 (1:500), Hes5 (1:300), β-tubulin (1:1,000) primary antibodies. After washing three times with TBST, the samples were incubated for 1 h at room temperature with a secondary antibody of the IgG family, conjugated with HRP. Enhancement of the antibody reaction using an hypersensitive chemiluminescent (ECL) reagent (Beyotime Biotechnology) allowed for visualizing the protein. Protein bands were quantified using the ImageJ software and the band intensity was normalized to the band intensity of β-tubulin.

TABLE 1 | Primers used for qRT-PCR.

Primer name	Sequence (5′–3′)
GAPDH	F-GGGTGTGAACCACGAGAAAT
	R-CCTTCCACAATGCCAAAGTT
Arg1	F-GACCTGGCCTTTGTTGATGT
	R-CCATTCTTCTGGACCTCTGC
iNOS	F-ACGAGACGGATAGGCAGAGA
	R-CACATGCAAGGAAGGGAACT
CD206	F-GGGACTCTGGATTGGACTCA
	R-GCTCTTTCCAGGCTCTGATG
CD32	F-GCTCAAGGAAGACACGGTGA
	R-GTGTAGCTGGCTTGGACCTG
TNF-α	F-CCGATGGGTTGTACCTTGTC
	R-AGATAGCAAATCGGCTGACG
IL-1β	F-GCTGCTTCCAAACCTTTGAC
	R-AGCTTCTCCACAGCCACAAT
IL-10	F-CCAGTTTTACCTGGTAGAAGTGATG
	R-TGTCTAGGTCCTGGAGTCCAGCAGACTCAA
Notch1	F-GCCTTCGTGCTCCTGTTCTT
	R-CTTCTTGCTGGCCTCTGACA
Hes1	F-TCATGGAGAAGAGGCGAAGG
	R-CGGAGGTGCTTCACAGTCATT
Hes5	F-AGGCCGACATCCTGGAGAT
	R-TCGCTGTAGTCCTGGTGCAG

Immunofluorescence

To detect the expression of BV2 M1 and M2 microglia biomarkers, we first treated the cells with LPS. After treatment, the cells were washed 3 × 5 min with PBS (pH 7.4), and 4% paraformaldehyde was added for 30 min at room temperature, after which the cells were again washed 3 × 5 min with PBS. The membranes were disrupted with 0.5% Triton X-100 (PBS configuration) for 5 min. After washing three times with PBS for 5 min each, we added PBS containing 2% bovine serum albumin and 10% goat serum, and the plates were sealed at 37°C for 45 min. The following antibodies were added overnight at 4°C: rabbit anti-iNOS (1:200), rabbit anti-CD32 (1:200), rabbit anti-Arg1 (1:100), and rabbit anti-CD206 (1:100). After washing 3 × 5 min with PBS, we added a fluorescently labeled goat anti-rabbit IgG secondary antibody (1:500) for 1 h at room temperature. The cells were again washed 3 × 5 min with PBS, and counterstained in the dark with a mixture of 1 ml DAPI (1 mg/ml) + 1 ml H_2O. The cells were incubated at 37°C for 10 min, washed 3 × 5 min with PBS, observed under an Inverted fluorescence microscope (IX71 Japan OLYMPUS Corp.), and photographed.

Flow Cytometry

BV2 microglia were seeded at 5 × 10^5/well and treated according to their experimental group. After treatment, the culture supernatant was discarded, and cells were washed gently with 2 ml of PBS. Then, the PBS was aspirated and the adherent cells were digested with 1 ml of trypsin; 1 ml of MEM/EBSS medium was used to stop the digestion. The cells were centrifuged (1,000 rpm, 5 min, 4°C), washed twice with PBS, and resuspended at 1 × 10^5 cells/ml. To label the cells, we added PE/Cy5 anti-mouse CD16/CD32 monoclonal antibody (≤0.25 μg/10^6 cells, 100 μl) and Alexa Fluor® 488-labeled anti-mannose receptor antibody (1:500) for 20 min at room temperature in the dark, washed the cells twice with PBS, and resuspended them in 300 μl PBS. The cell surface expression of CD16/CD32 and CD206 was detected using a FACS Calibur flow cytometer (BD Company), and the data were analyzed using FlowJo software.

Statistical Analysis

All data are expressed as mean ± SD. Statistical analysis was performed using SPSS 21.0 statistical software. One-way analysis of variance (ANOVA) was used for comparison between groups, and pairwise comparison between sample means was performed using the Bonferroni method. Statistical significance was set at $p < 0.05$.

RESULTS

LXA4 Affects the Expression of Interleukin (IL)-1β, IL-10, and TNF-α in LPS-Treated BV2 Microglia

The expression of IL-1β, TNF-α and IL-10 mRNA was determined by qRT-PCR 6 h after the corresponding treatment. LPS induced a significant increase in IL-1β and TNF-α mRNA in BV2 microglia as compared to the control group ($p < 0.05$) (**Figures 1A,C**). LXA4 pretreatment reduced LPS-induced IL-1β and TNF-α mRNA levels (**Figures 1A,C**), while IL-10 mRNA expression increased significantly ($p < 0.05$) (**Figure 1E**). That is, LXA4 inhibited the expression of IL-1β and TNF-α mRNA in BV2 microglia induced by LPS, and upregulated the mRNA expression of IL-10.

Eight hours after the corresponding treatment, the ELISA method was used to detect the protein expression levels of IL-1β, TNF-α and IL-10. As compared to the control group, LPS induced a significant increase in IL-1β and TNF-α protein levels in BV2 microglial culture supernatants, and the difference was statistically significant ($p < 0.05$) (**Figures 1B,D**). LXA4 pretreatment inhibited the production of IL-1β and TNF-α induced by LPS ($p < 0.05$) (**Figures 1B,D**), while the protein level of IL-10 was significantly higher than that of the LPS group ($p < 0.05$) (**Figure 1F**). That is, LXA4 inhibited the expression of IL-1β and TNF-α mRNA induced by LPS in BV2 microglia, and upregulated the protein expression of IL-10.

Therefore, LXA4 inhibited the genes and protein expression of M-1 microglia-associated inflammatory factors IL-1β and TNF-α, and upregulated the expression of IL-10, an inflammatory factor associated with M2 microglia.

LXA4 Affects LPS-Induced BV2 Microglial Morphological Changes and Induces the Conversion of (M1) Microglia to (M2) Microglia

The expression of iNOS, cluster of differentiation (CD)32, Arg1 and CD206 mRNA was detected via qRT-PCR 6 h after the corresponding treatment. As compared to the control group, the relative expression of iNOS and CD32 mRNA in the LPS group was significantly increased ($p < 0.05$) (**Figures 2A,B**). However, the relative expression of mRNA of the M2 markers Arg1 and CD206 did not change significantly ($p > 0.05$). After LXA4 pretreatment, the expression of iNOS and CD32 was both significantly decreased ($p < 0.05$) (**Figures 2A,B**), and the expression of Arg1 and CD206 was both significantly increased ($p < 0.05$) (**Figures 2C,D**). Therefore, LXA4 inhibited the expression of the M1 markers iNOS and CD32 at the transcriptional level and upregulated the expression of the M2 markers Arg1 and CD206.

Each group was tested 8 h after the corresponding treatment. The levels of iNOS, Arg1, CD32 and CD206 proteins were determined by Western blot, cellular immunofluorescence and flow cytometry.

Western blot analysis showed that the expression of iNOS protein in LPS group was significantly increased as compared to the control group ($p < 0.05$) (**Figures 3A–C**), while the expression of Arg1 protein did not significantly increase ($p > 0.05$). As compared to the LPS group, the expression of iNOS protein was inhibited and the expression of Arg1 protein was increased in the LXA4 pretreatment group ($p < 0.05$) (**Figures 3A–D**).

Cellular immunofluorescence showed that BV2 microglia cells were activated in response to LPS treatment, the cell body became larger and rounder, the protrusion decreased and became thicker, and the morphology appeared as amoeba-like. LXA4 pretreatment weakened the response to LPS in terms of morphological changes (**Figures 4**–**7**). As compared to the control group, the expression of iNOS and CD32 after LPS treatment increased ($p < 0.05$) (**Figures 4**, **5**). As compared to the LPS group, the expression of iNOS and CD32 in the LXA4 pretreatment group was higher than that in the LPS group. The expression of Arg1 and CD206 significantly decreased in the LPS group ($p < 0.05$) (**Figures 6**, **7**).

CD32 is a M1 microglia surface marker molecule and can be detected by flow cytometry. As shown in **Figure 8**, we observed positive expression of CD32. The mean fluorescence intensity was only 17.6, indicating a low expression level. Treatment with LXA4 alone induced positive expression of CD32 and the mean fluorescence intensity was 11.6 (**Figure 8B**). In the LPS group, the average fluorescence intensity increased to 41.3, indicating that CD32 positive expression was significantly enhanced. In the LPS group pretreated with LXA4, positive expression was observed, but the mean fluorescence intensity was only 25.7. On the other side, CD206 is a M2 type microglia surface marker molecule. As shown in **Figure 8E**, the control group showed positive expression of CD206. However, the mean fluorescence intensity was only 30.2, indicating a low expression level. In the group treated with LXA4 alone, a positive expression was observed, with a mean fluorescence intensity value of 28.7, indicating a low expression level. In the LPS group, the mean fluorescence intensity increased to 27.2, showing low expression level. In the LPS group pretreated with LXA4, the average fluorescence intensity significantly increased to 51.2 ($p < 0.05$). That is, LXA4 inhibits the expression of CD32 and upregulates the expression of CD206.

Western blot, cellular immunofluorescence and flow cytometry were concordant in indicating that LXA4 inhibited the expression of M1 type biomarkers iNOS and CD32 at the protein expression and transcription levels, and upregulated the M2 type biomarkers Arg1 and CD206. In other words, LXA4 promoted the shift of M1 to M2 microglia.

Mechanism of LXA4 Regulation of Notch Signaling Pathway

Preliminary Observations of the Effect of LXA4 on the Expression of Downstream Effector Molecules in the Notch Signaling Pathway

The relative expression levels of Notch1, Hes1 and Hes5 mRNA were determined by qRT-PCR 3 h after the corresponding

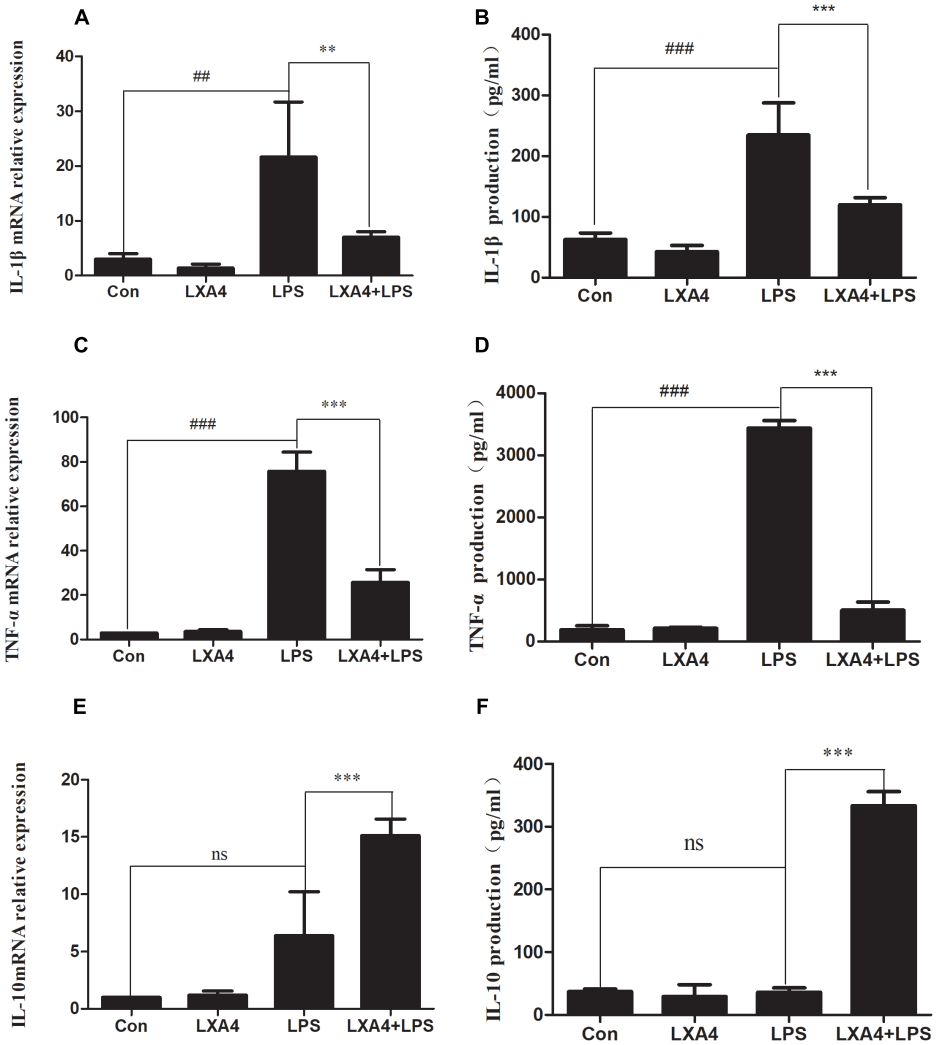

FIGURE 1 | LPS-induced microglia activation and release of inflammatory factors; After 6 h of LPS stimulating **(A,C,E)**: the mRNA expression levels of IL-1β, TNF-α were measured by real-time fluorescent quantitative PCR; 8 h after LPS treatment, **(B,D,F)** The concentration of IL-1β, TNF-α and IL-10 in the supernatant of the cells was detected by enzyme-linked immunosorbent assay (ELISA). LPS induces microglia activation, proinflammatory cytokines IL-1β, TNF-α and anti-inflammatory factor IL-10 release. With LXA4 intervention, IL-1β, TNF-α expression decreased, IL-10 expression increased significantly, $^{\#\#,**}p < 0.01$; $^{\#\#\#,***}p < 0.001$; n.s., no significance.

treatments were administered. As compared to the control group, the expression of Notch1 and Hes1 mRNA in the LPS group was significantly different ($p < 0.05$) (**Figures 9A,B**), while the relative expression of Hes5 mRNA was not significantly increased ($p > 0.05$) (**Figure 9C**). As compared to the LPS group, the expression of Notch1 and Hes1 mRNA in the LXA4 pretreatment group was decreased, and the expression of Hes5 mRNA was significantly increased ($p < 0.05$) (**Figures 9A–C**).

Each group was performed for 4 h with corresponding treatments and the expression levels of Notch1, Hes1, and Hes5 proteins were determined through Western blot. The expression of Notch1 and Hes1 protein in the LPS group was significantly higher than in the control group ($p < 0.05$), but the expression of Hes5 was not significantly increased. The difference was not statistically significant ($p < 0.05$). As compared to the LPS group, the expression of Notch1 and Hes1 protein in the LXA4 pretreatment group was decreased, and the protein expression of Hes5 was significantly increased ($p < 0.05$) (**Figure 10**).

Therefore, LXA4 affected the expression of downstream effector molecules within the Notch signaling pathway at the level of genes and protein; inhibited the expression of Notch1 and Hes1, and upregulated the expression of Hes5.

LXA4 Regulation of the Notch Signaling Pathway

LXA4 regulation on downstream effector molecules of the Notch signaling pathway

Each group was performed for 6 h with corresponding treatments and the expression levels of Notch1, Hes1, and Hes5 proteins were determined through Western blot. The levels of Notch1 and Hes1 protein in the LPS group were significantly higher

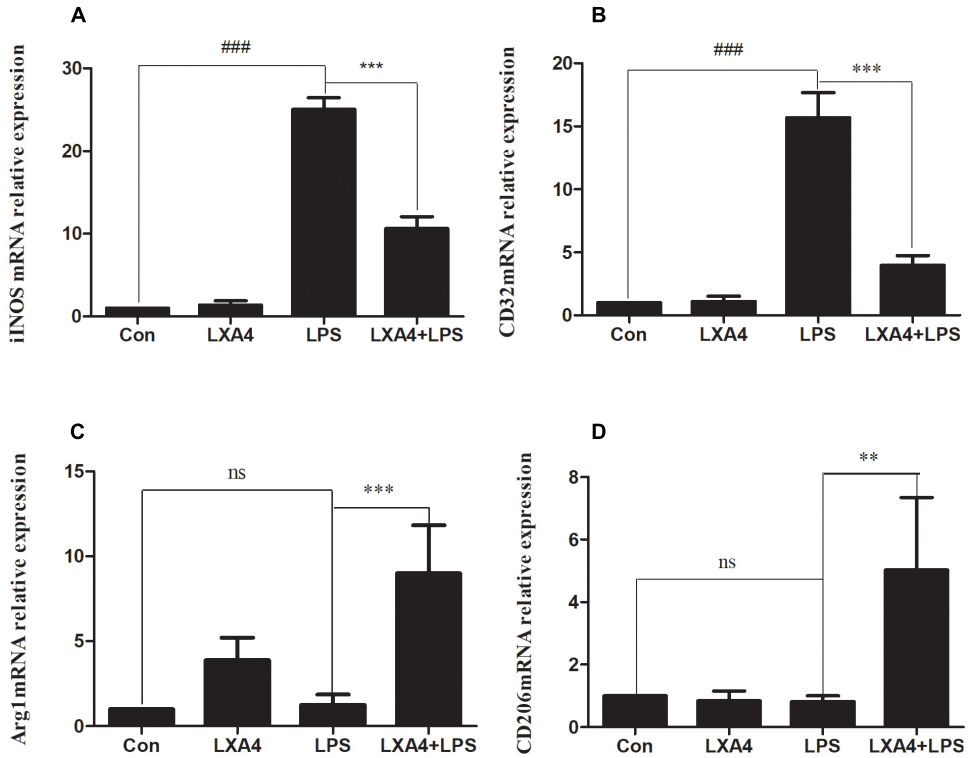

FIGURE 2 | Quantitative RT-PCR analysis of iNOS, CD32, Arg1, CD206 mRNA levels in the BV2microglia 6 h after LPS treatment. **(A,B)** Quantitative RT-PCR analysis of iNOS, CD32 mRNA levels. **(C,D)** Quantitative RT-PCR analysis of Arg1, CD206 mRNA levels. LPS upregluated M1 microglia biomarkers iNOS, CD32. With LXA4 intervention, iNOS, CD32 expression decreased, M2 microglia biomarkers Arg1, CD206 expression increased significantly. $^{\#\#,**}p < 0.01$; $^{\#\#\#,***}p < 0.001$; n.s., no significance.

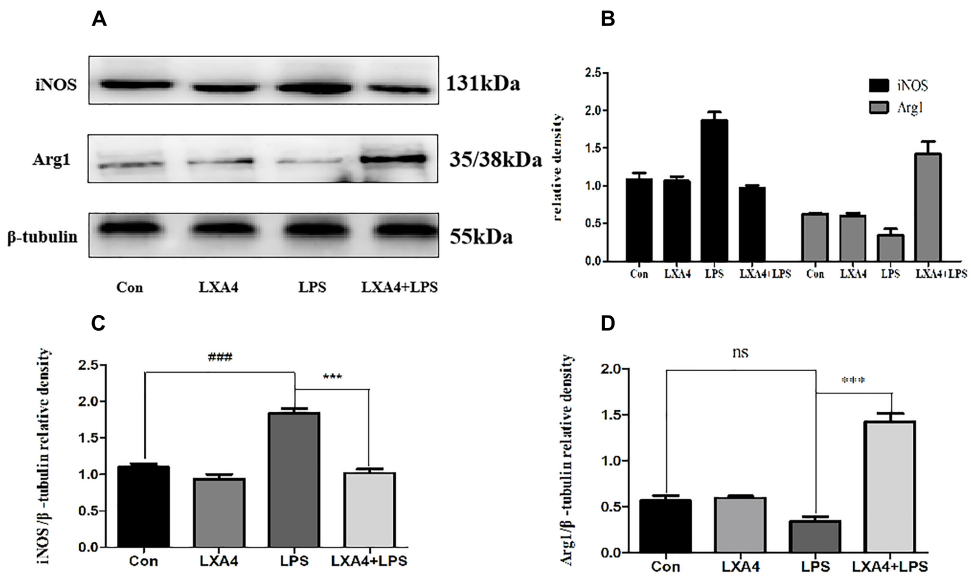

FIGURE 3 | Western blot analysis of the effect of LXA4 on iNOS and Arg1. **(A–C)** Western blot analysis of the protein level of iNOS in microglia. **(A,B,D)** Western blot analysis of the protein level of Arg1 in microglia, LPS upregluated M1 microglia biomarkers iNOS. With LXA4 intervention, iNOS expression decreased, M2 microglia biomarkers Arg1 expression increased significantly. $^{\#\#\#,***}p < 0.001$; n.s., no significance.

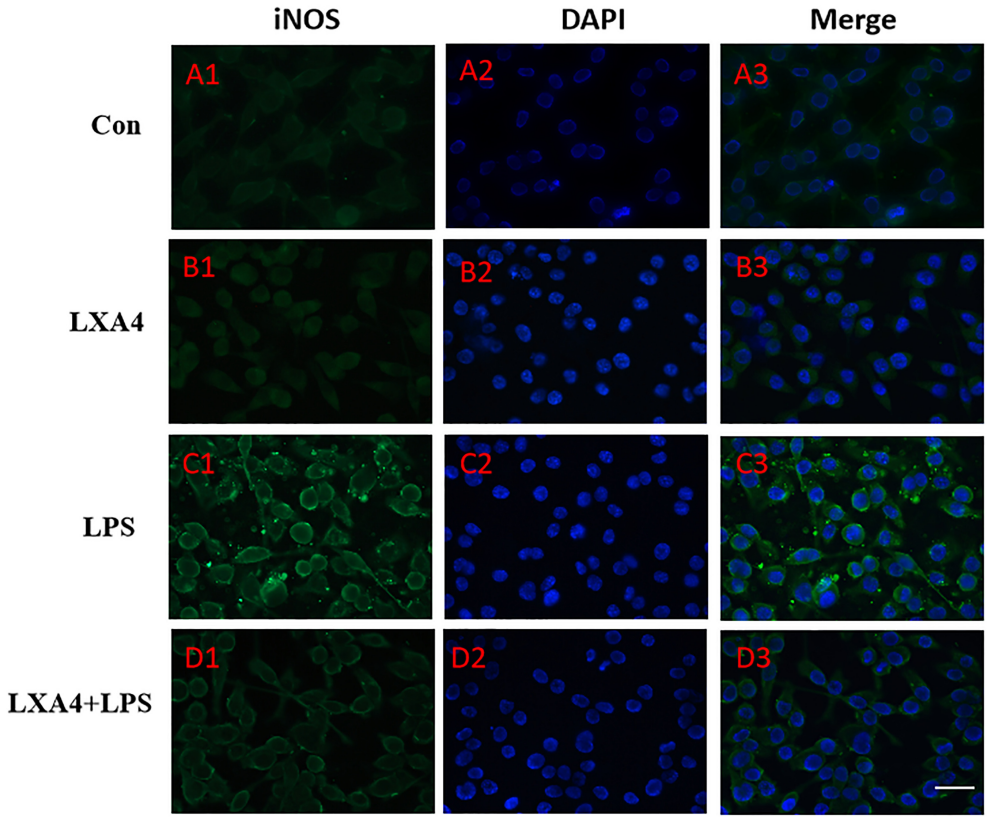

FIGURE 4 | Immunofluorescence images showing the BV2 microglia after LPS stimulates which were labeled with iNOS antibody, with LXA4, the expression of iNOS is decreased. Green fluorescence indicated iNOS positive cells, while blue fluorescence indicated DAPI-labeled nuclei. Scale bar: 20 μm.

than in the control group ($p < 0.05$), and there was no significant Hes5 upregulation ($p > 0.05$) (**Figures 11A,D–F**). In the DAPT-pretreatment group as compared to the LPS group, the Hes1 protein level was significantly decreased ($p < 0.05$) (**Figures 11A,E**), the Notch1 protein decreased slightly, and the Hes5 protein increased, but the change was not statistically significant ($p > 0.05$). In the LXA4 pretreatment group, the levels of Notch1 and Hes1 protein significantly decreased ($p < 0.05$) and the Hes5 protein was significantly upregulated ($p < 0.05$) (**Figures 11A,D–F**). After combined DAPT/LXA4 pretreatment, Notch1, Hes1 and Hes5 group were significantly decreased ($p < 0.05$). There was no change between Hes1 and Hes5 as compared to the control group.

Therefore, LXA4 downregulated the expression of Notch1 and the downstream effector Hes1 in M1 microglia differentiation (Wang et al., 2010; Liu et al., 2012; Wu et al., 2018), and upregulated the downstream effector Hes5 associated with the M2 differentiation (Liu et al., 2012), promoting the transformation of M1 to M2 microglia. However, after blocking the Notch signaling pathway with the γ-secretase inhibitor DAPT, the LXA4 regulation on the downstream effector molecules Hes1 and Hes5 of the Notch signaling pathway was abolished, indicating that LXA4 regulates the differentiation of microglia through the Notch signaling pathway.

Effect of LXA4 on microglia differentiation

Each group was performed for 6 h with corresponding treatments and the expression levels of microglia M1 biomarker iNOS and M2 biomarker Arg1 proteins were determined through Western blot. The expression of the iNOS protein increased in the LPS group as compared to the control group (**Figures 11A–C**). After treatment with DAPT and LXA4, the level of the iNOS protein was decreased, while after LXA4 pretreatment, the level of Arg1 protein was upregulated (**Figures 11A–C**). That is, LXA4 promotes the conversion of M1–M2 phenotype; the action of LXA4 can be abolished by the Notch signaling pathway blocker DAPT. The figure shows that the expression of the iNOS protein in the DAPT+LXA4+LPS group was increased, and the expression of Arg-1 was not, confirming that LXA4 regulates the differentiation of microglia through the Notch signaling pathway.

Effect of LXA4 on Notch signaling pathway and microglial differentiation on expression of inflammatory mediators

Each group was performed for 6 h with corresponding treatments and the ELISA method was used to detect the expression levels of M1 microglia-associated inflammatory cytokines IL-1β and TNF-α and M2 microglia-associated inflammatory factor IL-10. As compared to the control group, the expression of IL-1β and TNF-α protein in the LPS group increased (**Figures 12A,B**); as compared to the LPS group, the expression of IL-1β and TNF-α

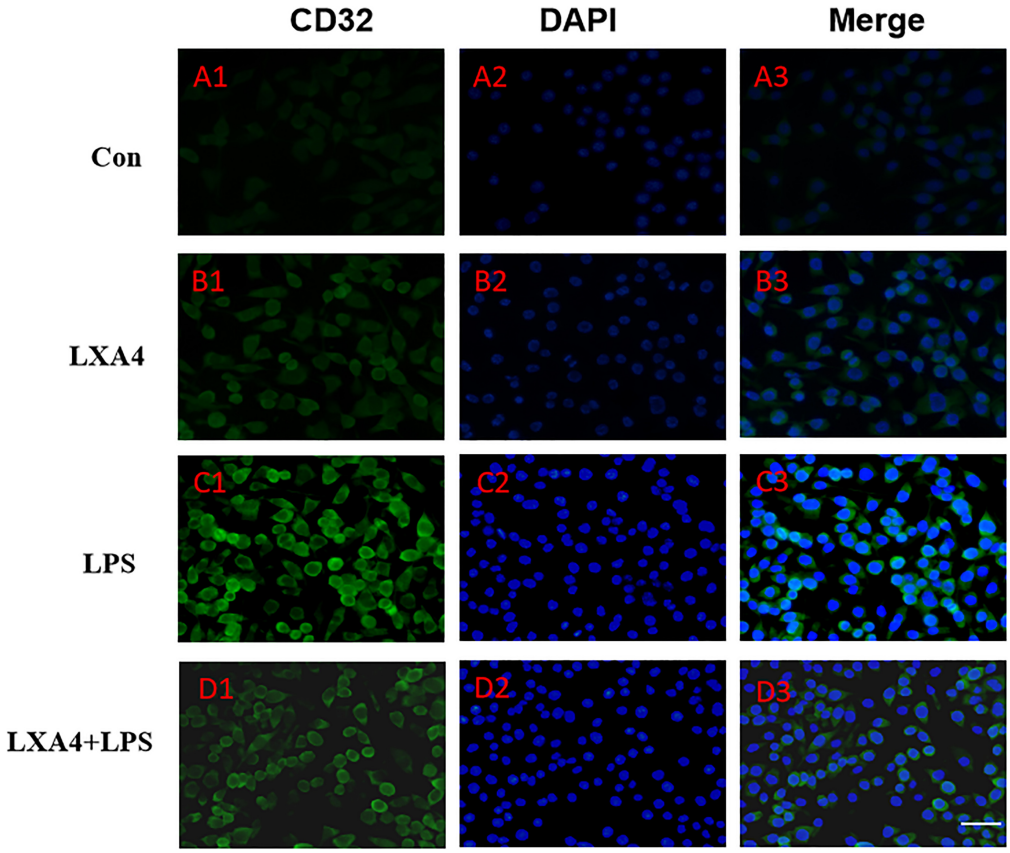

FIGURE 5 | Immunofluorescence images showing the BV2 microglia after LPS stimulates which were labeled with CD32 antibody, with LXA4, the expression of iNOS is decreased. Green fluorescence indicated CD32 positive cells, while blue fluorescence indicated DAPI-labeled nuclei. Scale bar: 20 μm.

in the DAPT+LPS group was significantly decreased ($p < 0.05$) (**Figures 12A,B**). The expression of IL-10 was upregulated in the LXA4+LPS group (**Figures 12A,B**), while IL-1β and TNF-α significant decreased (**Figure 12C**), suggesting that LXA4 promoted the conversion of M1 to the M2 phenotype, and this effect was abolished by the Notch signaling pathway blocker DAPT. As shown in **Figure 12C**, the inflammatory factors IL-1β and TNF-α are upregulated in the DAPT+LXA4+LPS group, while IL-10 showed no significant upregulation, confirming that the LXA4 modulates the expression of inflammatory cytokines by regulating the differentiation of microglia through the Notch signaling pathway.

DISCUSSION

An increasing number of studies reveal that inflammatory reactions exert a significant influence on the occurrence and development of central nervous system conditions such as ischemic stroke, Alzheimer's disease, Parkinson's disease, and multiple sclerosis, at multiple stages of the disease process. Inflammation aggravates the damage to nerve cells and tissues, worsening the pathological condition (Lucas et al., 2006; Xanthos and Sandkuhler, 2014; Meng et al., 2016).

The role of microglia in the neuroinflammatory response is important (Streit, 2002; Ramirez et al., 2017). Microglia cells are related to mononuclear/macrophage cell lines as for morphology, immunophenotype, and biological function, and are considered to be resident macrophages in the brain (Streit, 2000). Under physiological conditions, microglia plays an important role in the development, structural formation and functional regulation of the nervous system (Kim and de Vellis, 2005; Gomez-Nicola and Perry, 2015; Wolf et al., 2017). After exogenous stimulation or microenvironment changes in the brain, microglia is rapidly activated, and a series of changes occur in cell morphology, immunophenotype and function. Activated microglia mainly differentiate into M1 and M2 types (Kloss et al., 2001; Hu et al., 2014). M1 type is a classical activated microglia, and the corresponding biological molecular markers include iNOS and CD32. M1 microglia releases a large number of inflammatory factors such as TNF-α and IL-1β, causing damage to central nervous system cells and tissues. Increased expression of iNOS produces a large amount of NO in the brain, and high-load NO can exert toxic effects through various mechanisms such as mitochondrial damage, peroxidation, activation and inhibition of various signaling pathways, and DNA damage (Pacher et al., 2007; Martinez et al., 2009). The M2 type is an alternative activation type, and the corresponding biological

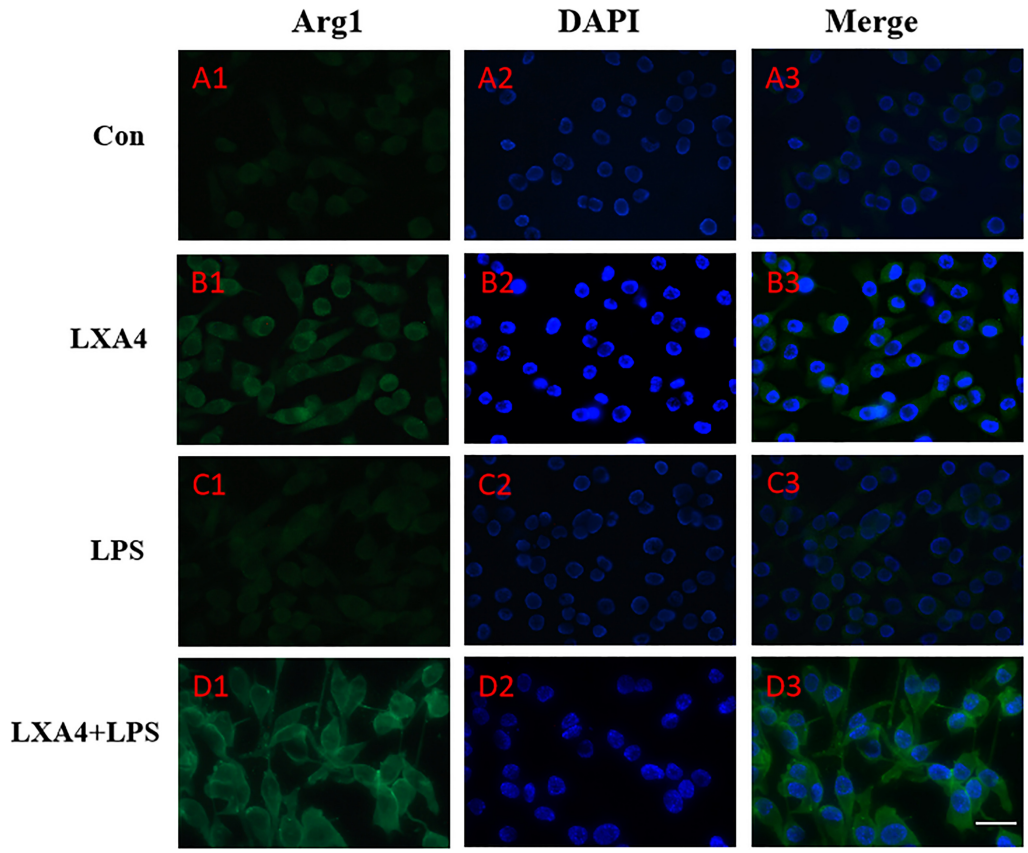

FIGURE 6 | Immunofluorescence images showing the BV2 microglia after LPS stimulates which were not labeled with Arg1 antibody, with LXA4, the expression of Arg1 is expressed at high levels. Green fluorescence indicated Arg1 positive cells, while blue fluorescence indicated DAPI-labeled nuclei. Scale bar: 20 μm.

molecular markers include Arg1 and CD206. M2 microglia can release chemokines, induce resting microglia to focus on the lesion, phagocytose toxic molecules and cell debris, and release brain-derived neurotrophic factor, vascular endothelial growth factor and the anti-inflammatory mediator IL-10 which inhibits immune inflammation, promotes inflammation regression, as well as nerve tissue repair and nerve regeneration (Jin et al., 2014; Beyer et al., 2015; Tang and Le, 2016; Kanazawa et al., 2017; Ramirez et al., 2017). M2 microglia releases Arg1, which competes with iNOS for arginine substrate, downregulates NO production, reduces tissue damage, and participates in tissue damage repair (Yang et al., 2016). Regulating the differentiation of microglia, and avoiding harm, is of great significance for the improvement of the prognosis of various inflammatory related nervous system diseases.

Activation and differentiation of microglia involves multiple signaling pathways, such as the Notch signaling pathway, NF-κB, tyrosine protein kinase (JAK) signal transduction/transcriptional activator (STAT), peroxisome proliferator-activator receptor-γ (PPAR-γ) and cAMP response element binding protein (CREB) (Grandbarbe et al., 2007; Xu et al., 2015; Ghosh et al., 2016; Chen J. et al., 2017; Qin et al., 2017; Wei et al., 2017; Liu et al., 2018). The Notch signaling pathway is highly conserved and participates in almost all physiological and pathological processes such as differentiation, proliferation and apoptosis of all cellular types. It can precisely regulate cell differentiation by translocating signals directly from adjacent cells to the cell nucleus to activate transcription factors, affecting embryonic development and the homeostasis of adult tissues and organs (Gazave et al., 2009; Oya et al., 2009; Ables et al., 2011; Andersson et al., 2011). In the central nervous system, the Notch signaling pathway is actively involved in dynamic changes at all scales, from cellular structure to nervous system function, inhibiting neuronal differentiation and promoting differentiation of glial subtypes (Tanigaki et al., 2001), especially during microglia activation. Moreover, it plays a very important role in differentiation (Grandbarbe et al., 2007; Yuan et al., 2015). The Notch signaling pathway is mainly composed of receptors, ligands expressed on adjacent cell membranes, intracellular transcription factors, regulatory molecules, and downstream effector molecules (Shang et al., 2016). After the interaction between the Notch receptor and the ligand, the NICD is released into the cytosol, thanks to the cleavage operated by the key enzyme γ-secretase which directly affected the activation of Notch pathway, and transferred to the nucleus. The activated NICD promotes the production of transcriptional activators, thereby inducing the expression of downstream migratory molecules including Hes1, Hes5 and NF-κB. Some studies have shown that elevated levels of

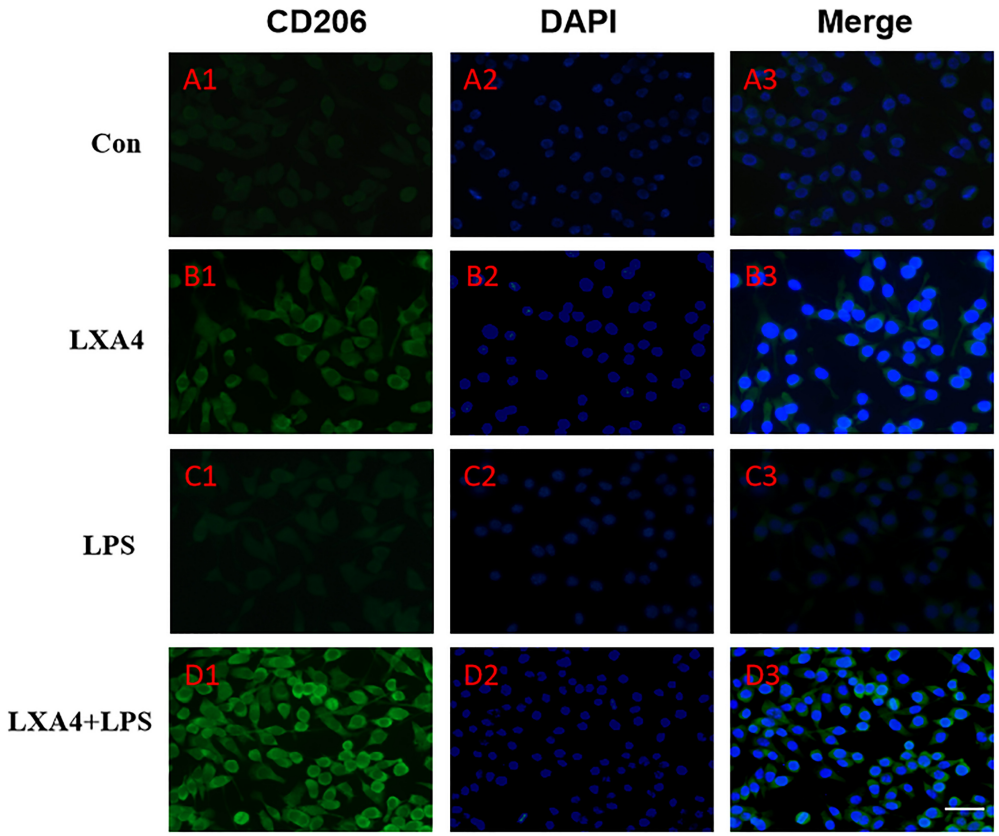

FIGURE 7 | Immunofluorescence images showing the BV2 microglia after LPS stimulates which were not labeled with CD206 antibody, with LXA4, the expression of Arg1 is expressed at high level. Green fluorescence indicated CD206 positive cells, while blue fluorescence indicated DAPI-labeled nuclei. Scale bar: 20 μm.

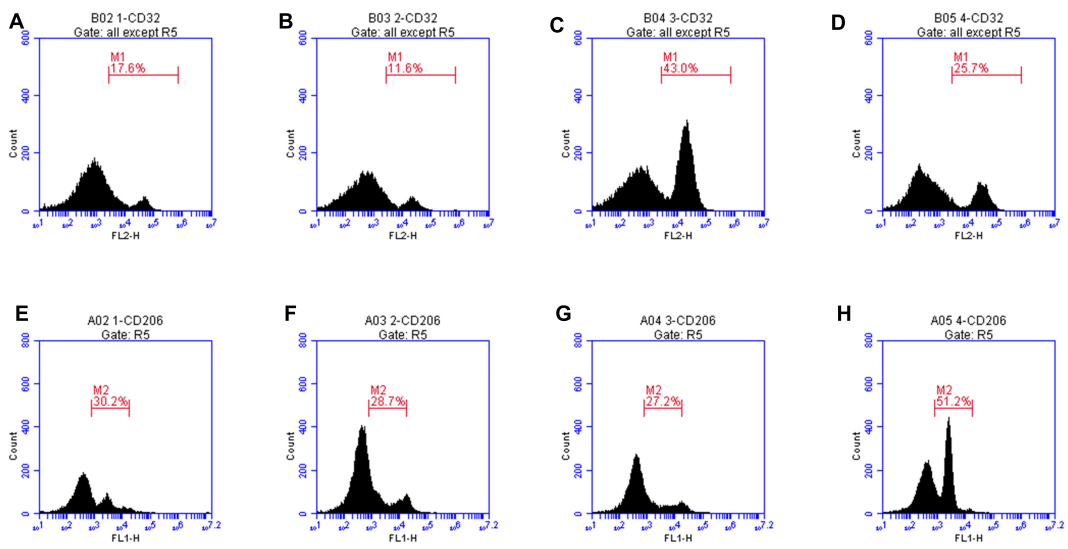

FIGURE 8 | Protein expression levels of CD32 and CD206 were measured by flow cytometry. **(A)** The mean fluorescence intensity of CD32 was only 17.6. **(B)** Treatment with LXA4 alone, the mean fluorescence intensity was 11.6. **(C)** In the LPS group, the average fluorescence intensity increased to 41.3. **(D)** In the LPS group pretreated with LXA4, the mean fluorescence intensity was only 25.7. **(E)** In the control group, the mean fluorescence intensity of CD206 was only 30.2, **(F)** In the group treated with LXA4 alone, the mean fluorescence intensity of CD206 was 28.7. **(G)** In the LPS group, the mean fluorescence intensity of CD206 was 27.2. **(H)** In the LPS group pretreated with LXA4, the average fluorescence intensity significantly increased to 51.2.

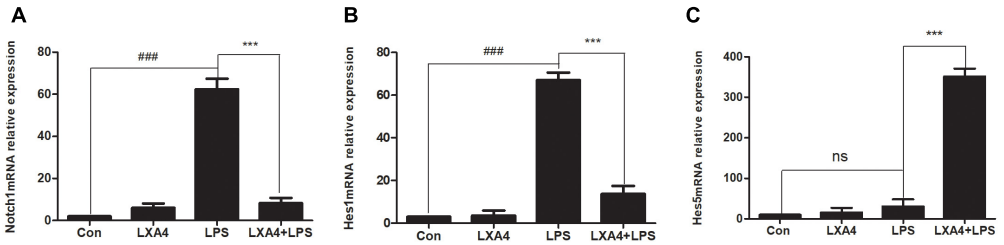

FIGURE 9 | Quantitative RT-PCR analysis of Notch1, Hes1 and Hes5 mRNA levels in the BV2 microglia. **(A)** Quantitative RT-PCR analysis of Notch1 mRNA levels. **(B)** Quantitative RT-PCR analysis of Hes1 mRNA levels. **(C)** Quantitative RT-PCR analysis of Hes5 mRNA levels.LPS upregluated M1 microglia related signal molecule Notch1, Hes1. With LXA4 intervention, Notch1, Hes1 expression decreased, M2 microglia related signal molecule Hes5 expression increased significantly. $^{###,***}p < 0.001$; n.s., no significance.

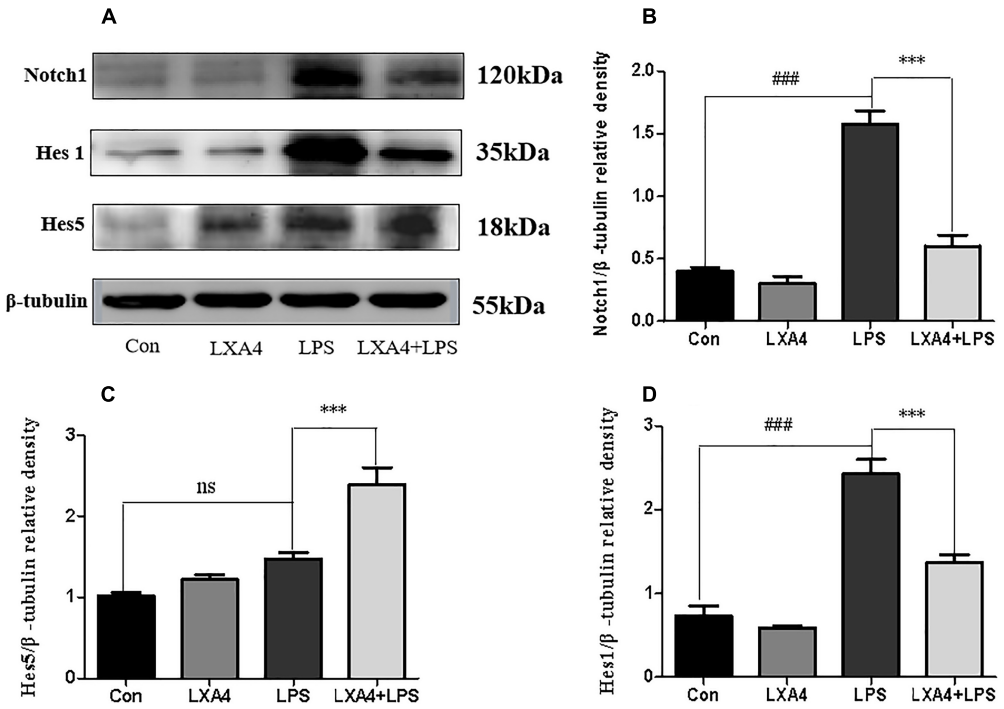

FIGURE 10 | Western blot analysis of the effect of LXA4 on Notch1, Hes1 and Hes5. **(A,B,D)** Western blot analysis of the protein level of Notch1, Hes1 in microglia. **(A,C)** Western blot analysis of the protein level of Hes5 in microglia, LPS upregluated M1 microglia related signal molecule Notch1, Hes1. With LXA4 intervention, Notch1, Hes1 expression decreased, M2 microglia related signal molecule Hes5 expression increased significantly. $^{###,***}p < 0.001$; n.s., no significance.

Notch1 receptor and downstream effector Hes1 are associated to microglia differentiation into the M1 type (Wang et al., 2010; Liu et al., 2012; Wu et al., 2018), while Hes5 is involved in M2 differentiation (Liu et al., 2012). Downstream target genes of the Notch pathway include Hes1, Hes5, NF-κB, Cyclin D1, and C-myc. The Notch pathway may act as a cascade with complex interactions with the NF-κB, Wnt, TGF/BMP, TLR and other pathways (Wei et al., 2011). The Notch pathway may be important for regulating the activation and differentiation of microglia and the inflammatory response. More and more studies show that the Notch signaling pathway and microglia activation and differentiation are involved in central nervous system diseases. The modulation of these processes is expected to be a key to the treatment of several central nervous system conditions. It is therefore imperative to identify drugs that regulate the Notch pathway and microglia activation and differentiation.

Lipoxins (LXs) are a class of arachidonic acid-derived mediators formed via lipoxygenase-catalyzed reactions, which carry anti-inflammatory and pro-inflammatory properties, and are classified according to the position and conformation of the hydroxyl groups in the molecule. LXA4 and LXB4, and their epimers 15-epi-LXA4 and 15-epi-LXB4, are synthesized only in small amount under physiological conditions. However, their levels significantly rise under various pathological conditions involving inflammatory stimuli, to act as downregulators of the inflammatory process. LXs play a role in anti-inflammatory and

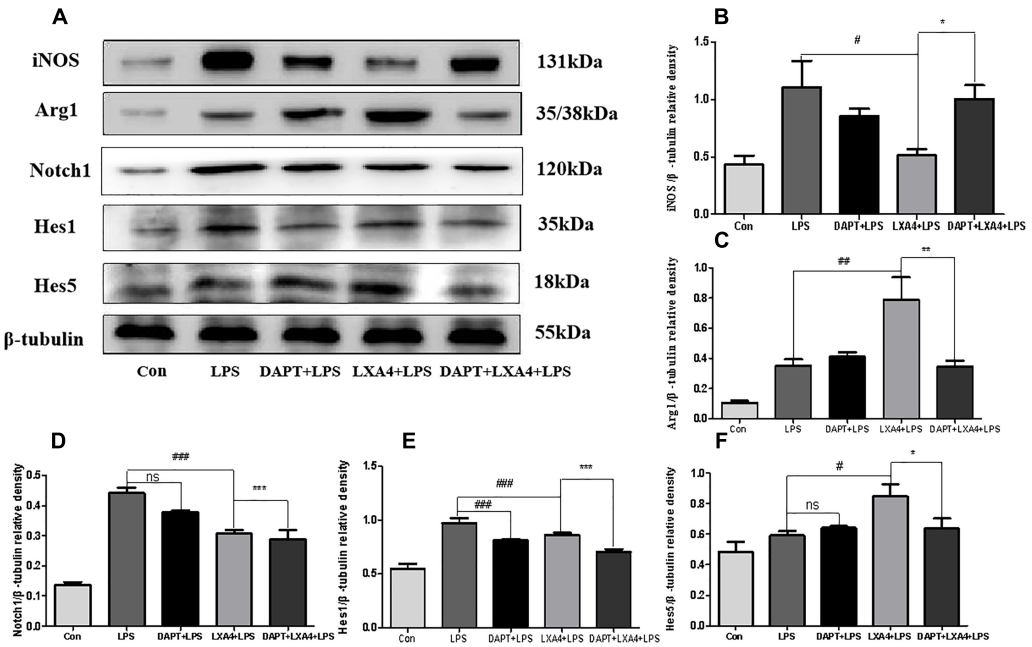

FIGURE 11 | Western blot analysis of the Notch1, Hes1, Hes5, iNOS and Arg1 effect after DAPT pretreatment. **(A–C)** Western blot analysis of the protein level of iNOS, Arg1 in microglia. **(A,D–F)** Western blot analysis of the protein level of Notch1, Hes1, Hes5 in microglia. $^{\#,*}p < 0.05$; $^{\#\#,**}p < 0.01$; $^{\#\#\#,***}p < 0.001$; n.s., no significance.

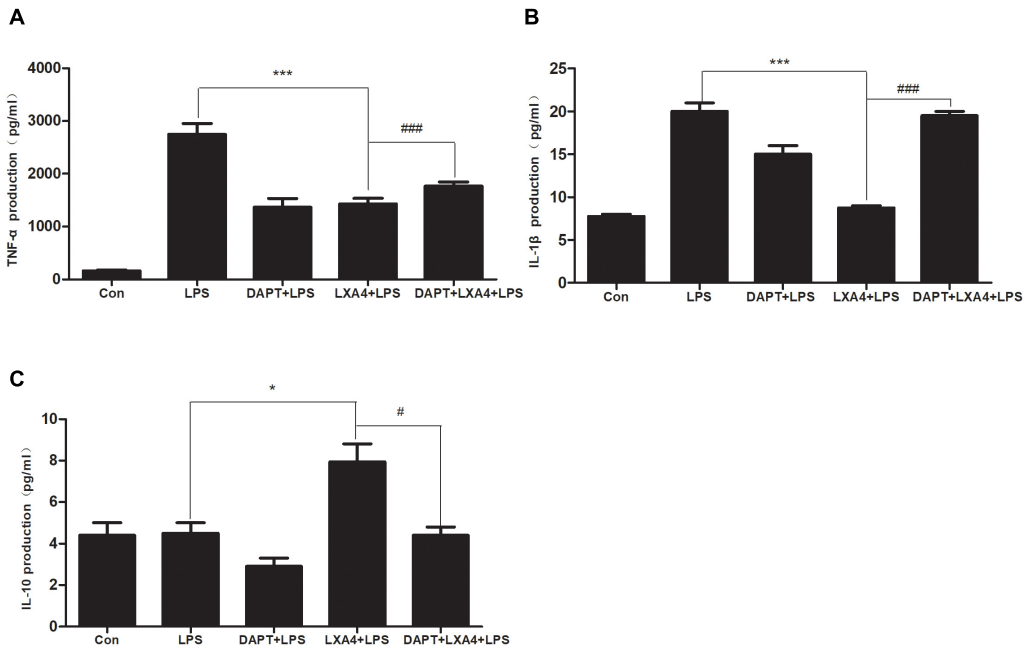

FIGURE 12 | LPS-induced microglia activation and release of inflammatory factors; After 6 h of LPS stimulating **(A–C)**: the protein expression levels of IL-1β, TNF-α, IL-10 were measured by enzyme-linked immunosorbent assay (ELISA). $^{\#,*}p < 0.05$; $^{\#\#,**}p < 0.01$; $^{\#\#\#,***}p < 0.001$; n.s., no significance.

pro-inflammatory decline. Some synthetic lipoxins such as LXA4 have exhibited anti-inflammatory effects in experimental studies on respiratory tract infections, lung injury, peritonitis, enteritis, nephritis, gynecological inflammation, and various tumor-related inflammations (Gewirtz et al., 2002; Chen et al., 2010; Xu et al., 2012, 2014; Okano Kwangbo Department of Medical Science and Research of Okayama University Department of Otolaryngology, 2015; Borgeson et al., 2015; Qi et al., 2015;

Wang Z. et al., 2015; Chen X.Q. et al., 2017; Xu et al., 2018). Experimental studies conducted in recent years have also found that lipoxin has a regulatory effect on central nervous system diseases such as cerebrovascular diseases and Alzheimer's disease (Wu et al., 2013; Guo et al., 2016; Han et al., 2016; Kantarci et al., 2018). The LXA4 receptor is represented on the microglia surface (Cui et al., 2002; Chen et al., 2006), which means that microglia may also be a target for the LXA4 in the central nervous system. There is very little research on whether LXA4 can act on the Notch signaling pathway. Only one study found that the LXA4 attenuates TGF-β1-induced renal fibrosis by suppressing the Notch signaling pathway (Brennan et al., 2013). However, whether the LXA4 can function through the Notch signaling pathway in the central nervous system diseases has not been reported before, especially in reference to the regulation of microglia activation and differentiation. Our study clarified that the LXA4 regulates microglia activation and differentiation through the Notch signaling pathway and plays an anti-inflammatory role, providing a new therapeutic target for the treatment of inflammatory-related nervous system diseases.

In this study, the immortalized murine microglial cell line BV-2 was used to construct an inflammatory model. BV2 microglia retains many morphological features, phenotypical characterization, and functional characteristics of the microglia, and is consequently an ideal model for studying microglia. We found that after LPS stimulation of BV2 microglia, the microglia cells were activated, and the round, swelling, and thin processes of the cell body retracted from branching to an amoeba-like asset. After pretreatment with LXA4, microglia cells showed small bodies and many branches.

This investigation capitalized on a complete set of analyses, including qRT-PCR, ELISA, western blot, cell immunofluorescence, and flow cytometry. A first part of the study explored the regulatory role of the LXA4 on the activation and differentiation of the microglia. We found that LXA4 could inhibit gene and protein expression of M1 biomarkers iNOS, CD32 and M1 related inflammatory cytokines IL-1β and TNF-α. Conversely, LXA4 caused upregulation of the expression of M2 biomarkers Arg1 and CD206 and M2 microglia-associated inflammatory factor IL-10. LXA4 can regulate the switch from M1 to M2 microglia and alleviate inflammation. A second part of this study focused on the LXA4 regulation of the Notch signaling pathway. LXA4 could affect the expression of downstream effector molecules of the Notch signaling pathway at both the gene and protein levels: it inhibited the expression of Notch1 and Hes1 related to the differentiation of M1 microglia. Upregulating the expression of Hes5 in association with M2 differentiation suggests that LXA4 promotes the transformation of M1 type to M2 microglia through the Notch signaling pathway.

It was subsequently found that the specific blocker Notch signaling pathway and the regulation of Notch downstream effector molecules Hes1 and Hes5 by LXA4 were blocked after the treatment of γ-secretase inhibitor DAPT. The results suggest that LXA4 regulates the differentiation of microglia through Notch signaling pathway.

Further studies showed that LXA4 decreased the expression of M1 related biomarkers iNOS and the related inflammatory cytokines IL-1β and TNF-α. The upregulation of the expression of Arg1 and the related inflammatory factor IL-10 can also be blocked by the DAPT. Therefore, we finally confirmed that LXA4 can exert its anti-inflammatory effects by regulating the differentiation of microglia through the Notch signaling pathway.

In conclusion, LXA4 inhibited the activation of microglia induced by LPS, promoted the transformation of M1–M2, and reduced the expression of IL-1β, TNF-α, and iNOS, while enhancing the expression of the anti-inflammatory mediator IL-10 through the Notch signaling pathway. This study shows: 1. LPS stimulation induced M1 microglia activation and increased the secretion of pro-inflammatory factors; 2. The Notch1 receptor and downstream effector Hes1 increased, suggesting that microglia differentiated into M1 type; 3. We revealed that LXA4 has desirable anti-inflammatory properties, which is consistent with previous studies (Wang et al., 2011; Zhou et al., 2011). But most importantly, we proved for the first time that LXA4 can regulate the differentiation of microglia and inhibit the inflammatory response induced by LPS, especially through the Notch signaling pathway, which is the focus and bright spot of this study.

It should be highlighted that γ-secretase is a key enzyme in the activation of the Notch pathway. DAPT can inhibit the activation of the Notch pathway by inhibiting the γ-secretase. However, the expression of the Notch1 protein was not affected in theory. Therefore, the expression of Hes1 and Hes5 was mainly inhibited after DAPT administration, and the change of Notch1 was not significant. Previous studies have shown that the γ-secretase enzyme blockers affect the Notch signaling pathway and produce a series of side effects at the level of the gastrointestinal tract and hematopoietic system, as well as induce thymocyte damage (Mumm et al., 2000; Real and Ferrando, 2009; Coric et al., 2012). Therefore, γ-secretase blockers are relatively far away from clinical use. A large number of studies have confirmed that lipoxin has the ability of inhibiting the further deterioration of inflammation *in vivo* and *in vitro*, promoting the timely regression of inflammation (Wang et al., 2014; Yao et al., 2014). Lipoxin acts in local tissues after its production, and then rapidly deactivates, it does not interfere with normal physiological function, is safe, has no toxic side effects, and can be used as an anti-inflammatory and modulating substance. Based on these advantages, and on its ability to maintain a balance between the benefits of the inflammatory mediators themselves and their potential toxicity at high concentrations (Zhou et al., 2011; Zhao et al., 2013), Lipoxin is expected to be a new anti-inflammatory drug, especially in the treatment of inflammatory nervous system diseases. Previous studies have also emphasized the expression of LXA4 receptors in neurons, microglia, astrocytes, and neural stem cells in the central nervous system (Wada et al., 2006; Decker et al., 2009; Wang et al., 2011). This suggests that they may be the target of lipoxin action in the central nervous system. Future studies will focus on ascertain the interplay between lipoxin-mediated pathways and other cells, notably neurons, astrocytes, and neural stem cells, to

further confirm the anti-inflammatory effect of lipoxin, reveal its anti-inflammatory mechanisms, and provide more evidence for clinical applications.

AUTHOR CONTRIBUTIONS

JW and D-hD participated in the design of this study and they both carried out the study and performed the statistical analysis. JW collected important background information and D-hD drafted the manuscript, and JW repeatedly modified the text structure and Details. Q-qL, X-yW, Y-yS, and L-JL participate in the original article and discussion about article writing and revision. All the authors revised and approved final version of the manuscript.

FUNDING

This work was supported by the National Natural Science Foundation of China to JW (Grant Number U1604181) and the Department of Science and Technology of Henan Province to JW (Grant Number 142300410390).

REFERENCES

Ables, J. L., Breunig, J. J., Eisch, A. J., and Rakic, P. (2011). Not(ch) just development: notch signalling in the adult brain. *Nat. Rev. Neurosci.* 12, 269–283. doi: 10.1038/nrn3024

Andersson, E. R., Sandberg, R., and Lendahl, U. (2011). Notch signaling: simplicity in design, versatility in function. *Development* 138, 3593–3612. doi: 10.1242/dev.063610

Beyer, M., Gimsa, U., Eyupoglu, I. Y., Hailer, N. P., and Nitsch, R. (2000). Phagocytosis of neuronal or glial debris by microglial cells: upregulation of MHC class II expression and multinuclear giant cell formation in vitro. *Glia* 31, 262–266. doi: 10.1002/1098-1136(200009)31:3<262::AID-GLIA70>3.0.CO;2-2

Beyer, M., Gimsa, U., Eyüpoglu, I. Y., Hailer, N. P., and Nitsch, R. (2015). Phagocytosis of neuronal or glial debris by microglial cells: upregulation of MHC class II expression and multinuclear giant cell formation in vitro. *Glia* 31, 262–266. doi: 10.1002/1098-1136(200009)31:3<262::AID-GLIA70>3.0.CO;2-2

Borgeson, E., Johnson, A. M., Lee, Y. S., Till, A., Syed, G. H., Ali-Shah, S. T., et al. (2015). Lipoxin A4 attenuates obesity-induced adipose inflammation and associated liver and kidney disease. *Cell Metab.* 22, 125–137. doi: 10.1016/j.cmet.2015.05.003

Brennan, E. P., Nolan, K. A., Borgeson, E., Gough, O. S., McEvoy, C. M., Docherty, N. G., et al. (2013). Lipoxins attenuate renal fibrosis by inducing let-7c and suppressing TGFbetaR1. *J. Am. Soc. Nephrol.* 24, 627–637. doi: 10.1681/asn.2012060550

Chen, J., Sun, Z., Jin, M., Tu, Y., Wang, S., Yang, X., et al. (2017). Inhibition of AGEs/RAGE/Rho/ROCK pathway suppresses non-specific neuroinflammation by regulating BV2 microglial M1/M2 polarization through the NF-kappaB pathway. *J. Neuroimmunol.* 305, 108–114. doi: 10.1016/j.jneuroim.2017.02.010

Chen, K., Iribarren, P., Hu, J., Chen, J., Gong, W., Cho, E. H., et al. (2006). Activation of Toll-like receptor 2 on microglia promotes cell uptake of Alzheimer disease-associated amyloid beta peptide. *J. Biol. Chem.* 281, 3651–3659. doi: 10.1074/jbc.M508125200

Chen, X. Q., Wu, S. H., Luo, Y. Y., Li, B. J., Li, S. J., Lu, H. Y., et al. (2017). Lipoxin A4 attenuates bronchopulmonary dysplasia via upregulation of let-7c and downregulation of TGF-beta1 signaling pathway. *Inflammation* 40, 2094–2108. doi: 10.1007/s10753-017-0649-7

Chen, Y., Hao, H., He, S., Cai, L., Li, Y., Hu, S., et al. (2010). Lipoxin A4 and its analogue suppress the tumor growth of transplanted H22 in mice: the role of antiangiogenesis. *Mol. Cancer Ther.* 9, 2164–2174. doi: 10.1158/1535-7163.MCT-10-0173

Colton, C. A. (2009). Heterogeneity of microglial activation in the innate immune response in the brain. *J. Neuroimmune Pharmacol.* 4, 399–418. doi: 10.1007/s11481-009-9164-4

Coric, V., van Dyck, C. H., Salloway, S., Andreasen, N., Brody, M., Richter, R. W., et al. (2012). Safety and tolerability of the gamma-secretase inhibitor avagacestat in a phase 2 study of mild to moderate Alzheimer disease. *Arch. Neurol.* 69, 1430–1440. doi: 10.1001/archneurol.2012.2194

Cuello, A. C. (2017). Early and late CNS inflammation in Alzheimer's disease: two extremes of a continuum? *Trends Pharmacol. Sci.* 38, 956–966. doi: 10.1016/j.tips.2017.07.005

Cui, Y. H., Le, Y., Zhang, X., Gong, W., Abe, K., Sun, R., et al. (2002). Up-regulation of FPR2, a chemotactic receptor for amyloid beta 1-42 (A beta 42), in murine microglial cells by TNF alpha. *Neurobiol. Dis.* 10, 366–377. doi: 10.1006/nbdi.2002.0517

Decker, Y., McBean, G., and Godson, C. (2009). Lipoxin A4 inhibits IL-1beta-induced IL-8 and ICAM-1 expression in 1321N1 human astrocytoma cells. *Am. J. Physiol. Cell Physiol.* 296, C1420–C1427. doi: 10.1152/ajpcell.00380.2008

Foldi, J., Chung, A. Y., Xu, H., Zhu, J., Outtz, H. H., Kitajewski, J., et al. (2010). Autoamplification of Notch signaling in macrophages by TLR-induced and RBP-J-dependent induction of Jagged1. *J. Immunol.* 185, 5023–5031. doi: 10.4049/jimmunol.1001544

Gazave, E., Lapebie, P., Richards, G. S., Brunet, F., Ereskovsky, A. V., Degnan, B. M., et al. (2009). Origin and evolution of the Notch signalling pathway: an overview from eukaryotic genomes. *BMC Evol. Biol.* 9:249. doi: 10.1186/1471-2148-9-249

Gewirtz, A. T., Collier-Hyams, L. S., Young, A. N., Kucharzik, T., Guilford, W. J., Parkinson, J. F., et al. (2002). Lipoxin a4 analogs attenuate induction of intestinal epithelial proinflammatory gene expression and reduce the severity of dextran sodium sulfate-induced colitis. *J. Immunol.* 168, 5260–5267. doi: 10.4049/jimmunol.168.10.5260

Ghosh, M., Xu, Y., and Pearse, D. D. (2016). Cyclic AMP is a key regulator of M1 to M2a phenotypic conversion of microglia in the presence of Th2 cytokines. *J. Neuroinflammation* 13:9. doi: 10.1186/s12974-015-0463-9

Gomez-Nicola, D., and Perry, V. H. (2015). Microglial dynamics and role in the healthy and diseased brain: a paradigm of functional plasticity. *Neuroscientist* 21, 169–184. doi: 10.1177/1073858414530512

Gordon, S. (2003). Alternative activation of macrophages. *Nat. Rev. Immunol.* 3, 23–35. doi: 10.1038/nri978

Grandbarbe, L., Michelucci, A., Heurtaux, T., Hemmer, K., Morga, E., and Heuschling, P. (2007). Notch signaling modulates the activation of microglial cells. *Glia* 55, 1519–1530. doi: 10.1002/glia.20553

Griffin, W. S. (2006). Inflammation and neurodegenerative diseases. *Am. J. Clin. Nutr.* 83, 470s–474s. doi: 10.1093/ajcn/83.2.470S

Guo, Z., Hu, Q., Xu, L., Guo, Z. N., Ou, Y., He, Y., et al. (2016). Lipoxin A4 reduces inflammation through formyl peptide receptor 2/p38 MAPK signaling pathway in subarachnoid hemorrhage rats. *Stroke* 47, 490–497. doi: 10.1161/strokeaha.115.011223

Han, X., Yao, W., Liu, Z., Li, H., Zhang, Z. J., Hei, Z., et al. (2016). Lipoxin A4 preconditioning attenuates intestinal ischemia reperfusion injury through Keap1/Nrf2 pathway in a lipoxin A4 receptor independent manner. *Oxid. Med. Cell. Longev.* 2016:9303606. doi: 10.1155/2016/9303606

Hu, X., Leak, R. K., Shi, Y., Suenaga, J., Gao, Y., Zheng, P., et al. (2014). Microglial and macrophage polarization—new prospects for brain repair. *Nat. Rev. Neurol.* 11, 56–64. doi: 10.1038/nrneurol.2014.207

Hu, X., Leak, R. K., Shi, Y., Suenaga, J., Gao, Y., Zheng, P., et al. (2015). Microglial and macrophage polarization-new prospects for brain repair. *Nat. Rev. Neurol.* 11, 56–64. doi: 10.1038/nrneurol.2014.207

Iso, T., Kedes, L., and Hamamori, Y. (2003). HES and HERP families: multiple effectors of the Notch signaling pathway. *J. Cell. Physiol.* 194, 237–255. doi: 10.1002/jcp.10208

Jin, Q., Cheng, J., Liu, Y., Wu, J., Wang, X., Wei, S., et al. (2014). Improvement of functional recovery by chronic metformin treatment is associated with enhanced alternative activation of microglia/macrophages and increased

angiogenesis and neurogenesis following experimental stroke. *Brain Behav. Immun.* 40, 131–142. doi: 10.1016/j.bbi.2014.03.003

Jin, S. W., Zhang, L., Lian, Q. Q., Liu, D., Wu, P., Yao, S. L., et al. (2007). Posttreatment with aspirin-triggered lipoxin A4 analog attenuates lipopolysaccharide-induced acute lung injury in mice: the role of heme oxygenase-1. *Anesth. Analg.* 104, 369–377. doi: 10.1213/01.ane.0000252414.00363.c4

Kanazawa, M., Miura, M., Toriyabe, M., Koyama, M., Hatakeyama, M., Ishikawa, M., et al. (2017). Microglia preconditioned by oxygen-glucose deprivation promote functional recovery in ischemic rats. *Sci. Rep.* 7:42582. doi: 10.1038/srep42582

Kantarci, A., Aytan, N., Palaska, I., Stephens, D., Crabtree, L., Benincasa, C., et al. (2018). Combined administration of resolvin E1 and lipoxin A4 resolves inflammation in a murine model of Alzheimer's disease. *Exp. Neurol.* 300, 111–120. doi: 10.1016/j.expneurol.2017.11.005

Kim, S. U., and de Vellis, J. (2005). Microglia in health and disease. *J. Neurosci. Res.* 81, 302–313. doi: 10.1002/jnr.20562

Kloss, C. U., Bohatschek, M., Kreutzberg, G. W., and Raivich, G. (2001). Effect of lipopolysaccharide on the morphology and integrin immunoreactivity of ramified microglia in the mouse brain and in cell culture. *Exp. Neurol.* 168, 32–46. doi: 10.1006/exnr.2000.7575

Kure, I., Nishiumi, S., Nishitani, Y., Tanoue, T., Ishida, T., Mizuno, M., et al. (2010). Lipoxin A(4) reduces lipopolysaccharide-induced inflammation in macrophages and intestinal epithelial cells through inhibition of nuclear factor-kappaB activation. *J. Pharmacol. Exp. Ther.* 332, 541–548. doi: 10.1124/jpet.109.159046

Lee, T. H. (1995). Lipoxin A4: a novel anti-inflammatory molecule? *Thorax* 50, 111–112. doi: 10.1136/thx.50.2.111

Levy, B. D., Lukacs, N. W., Berlin, A. A., Schmidt, B., Guilford, W. J., Serhan, C. N., et al. (2007). Lipoxin A4 stable analogs reduce allergic airway responses via mechanisms distinct from CysLT1 receptor antagonism. *FASEB J.* 21, 3877–3884. doi: 10.1096/fj.07-8653com

Liu, H. C., Zheng, M. H., Du, Y. L., Wang, L., Kuang, F., Qin, H. Y., et al. (2012). N9 microglial cells polarized by LPS and IL4 show differential responses to secondary environmental stimuli. *Cell. Immunol.* 278, 84–90. doi: 10.1016/j.cellimm.2012.06.001

Liu, R., Diao, J., He, S., Li, B., Fei, Y., Li, Y., et al. (2018). XQ-1H protects against ischemic stroke by regulating microglia polarization through PPARgamma pathway in mice. *Int. Immunopharmacol.* 57, 72–81. doi: 10.1016/j.intimp.2018.02.014

Lucas, S. M., Rothwell, N. J., and Gibson, R. M. (2006). The role of inflammation in CNS injury and disease. *Br. J. Pharmacol.* 147, S232–S240. doi: 10.1038/sj.bjp.0706400

Mantovani, A., Biswas, S. K., Galdiero, M. R., Sica, A., and Locati, M. (2013). Macrophage plasticity and polarization in tissue repair and remodelling. *J. Pathol.* 229, 176–185. doi: 10.1002/path.4133

Martin, C. R., Zaman, M. M., Gilkey, C., Salguero, M. V., Hasturk, H., Kantarci, A., et al. (2014). Resolvin D1 and lipoxin A4 improve alveolarization and normalize septal wall thickness in a neonatal murine model of hyperoxia-induced lung injury. *PLoS One* 9:e98773. doi: 10.1371/journal.pone.0098773

Martinez, F. O., Helming, L., and Gordon, S. (2009). Alternative activation of macrophages: an immunologic functional perspective. *Annu. Rev. Immunol.* 27, 451–483. doi: 10.1146/annurev.immunol.021908.132532

McColl, B. W., Allan, S. M., and Rothwell, N. J. (2009). Systemic infection, inflammation and acute ischemic stroke. *Neuroscience* 158, 1049–1061. doi: 10.1016/j.neuroscience.2008.08.019

Meng, H. L., Li, X. X., Chen, Y. T., Yu, L. J., Zhang, H., Lao, J. M., et al. (2016). Neuronal soluble Fas ligand drives M1-microglia polarization after cerebral ischemia. *CNS Neurosci. Ther.* 22, 771–781. doi: 10.1111/cns.12575

Mumm, J. S., Schroeter, E. H., Saxena, M. T., Griesemer, A., Tian, X., Pan, D. J., et al. (2000). A ligand-induced extracellular cleavage regulates gamma-secretase-like proteolytic activation of Notch1. *Mol. Cell* 5, 197–206. doi: 10.1016/S1097-2765(00)80416-5

Naegele, M., and Martin, R. (2014). The good and the bad of neuroinflammation in multiple sclerosis. *Handb. Clin. Neurol.* 122, 59–87. doi: 10.1016/b978-0-444-52001-2.00003-0

Nimmerjahn, A., Kirchhoff, F., and Helmchen, F. (2005). Resting microglial cells are highly dynamic surveillants of brain parenchyma in vivo. *Science* 308, 1314–1318. doi: 10.1126/science.1110647

Okano Kwangbo Department of Medical Science and Research of Okayama University Department of Otolaryngology (2015). [Lipoxin A4]. *Arerugi* 64, 1174–1175. doi: 10.15036/arerugi.64.1174

Oswald, F., Liptay, S., Adler, G., and Schmid, R. M. (1998). NF-kappaB2 is a putative target gene of activated Notch-1 via RBP-Jkappa. *Mol. Cell. Biol.* 18, 2077–2088. doi: 10.1128/MCB.18.4.2077

Oya, S., Yoshikawa, G., Takai, K., Tanaka, J. I., Higashiyama, S., Saito, N., et al. (2009). Attenuation of Notch signaling promotes the differentiation of neural progenitors into neurons in the hippocampal CA1 region after ischemic injury. *Neuroscience* 158, 683–692. doi: 10.1016/j.neuroscience.2008.10.043

Pacher, P., Beckman, J. S., and Liaudet, L. (2007). Nitric oxide and peroxynitrite in health and disease. *Physiol. Rev.* 87, 315–424. doi: 10.1152/physrev.00029.2006

Pan, Y., Shen, B., Gao, Q., Zhu, J., Dong, J., Zhang, L., et al. (2016). Caspase-1 inhibition attenuates activation of BV2 microglia induced by LPS-treated RAW264.7 macrophages. *J. Biomed. Res.* 30, 225–233. doi: 10.7555/jbr.30.20150141

Qi, W., Li, H., Cai, X. H., Gu, J. Q., Meng, J., Xie, H. Q., et al. (2015). Lipoxin A4 activates alveolar epithelial sodium channel gamma via the microRNA-21/PTEN/AKT pathway in lipopolysaccharide-induced inflammatory lung injury. *Lab. Invest.* 95, 1258–1268. doi: 10.1038/labinvest.2015.109

Qin, C., Fan, W. H., Liu, Q., Shang, K., Murugan, M., Wu, L. J., et al. (2017). Fingolimod protects against ischemic white matter damage by modulating microglia toward M2 polarization via STAT3 pathway. *Stroke* 48, 3336–3346. doi: 10.1161/strokeaha.117.018505

Ramirez, A. I., de Hoz, R., Salobrar-Garcia, E., Salazar, J. J., Rojas, B., Ajoy, D., et al. (2017). The role of microglia in retinal neurodegeneration: Alzheimer's disease, Parkinson, and glaucoma. *Front. Aging Neurosci.* 9:214. doi: 10.3389/fnagi.2017.00214

Real, P. J., and Ferrando, A. A. (2009). NOTCH inhibition and glucocorticoid therapy in T-cell acute lymphoblastic leukemia. *Leukemia* 23, 1374–1377. doi: 10.1038/leu.2009.75

Shang, Y., Smith, S., and Hu, X. (2016). Role of Notch signaling in regulating innate immunity and inflammation in health and disease. *Protein Cell* 7, 159–174. doi: 10.1007/s13238-016-0250-0

Streit, W. J. (2000). Microglial response to brain injury: a brief synopsis. *Toxicol. Pathol.* 28, 28–30. doi: 10.1177/019262330002800104

Streit, W. J. (2002). Microglia as neuroprotective, immunocompetent cells of the CNS. *Glia* 40, 133–139. doi: 10.1002/glia.10154

Takano, T., Fiore, S., Maddox, J. F., Brady, H. R., Petasis, N. A., and Serhan, C. N. (1997). Aspirin-triggered 15-epi-lipoxin A4 (LXA4) and LXA4 stable analogues are potent inhibitors of acute inflammation: evidence for anti-inflammatory receptors. *J. Exp. Med.* 185, 1693–1704. doi: 10.1084/jem.185.9.1693

Tang, Y., and Le, W. (2016). Differential roles of M1 and M2 microglia in neurodegenerative diseases. *Mol. Neurobiol.* 53, 1181–1194. doi: 10.1007/s12035-014-9070-5

Tanigaki, K., Nogaki, F., Takahashi, J., Tashiro, K., Kurooka, H., and Honjo, T. (2001). Notch1 and Notch3 instructively restrict bFGF-responsive multipotent neural progenitor cells to an astroglial fate. *Neuron* 29, 45–55. doi: 10.1016/S0896-6273(01)00179-9

Vital, S. A., Becker, F., Holloway, P. M., Russell, J., Perretti, M., Granger, D. N., et al. (2016). Formyl-peptide receptor 2/3/lipoxin A4 receptor regulates neutrophil-platelet aggregation and attenuates cerebral inflammation: impact for therapy in cardiovascular disease. *Circulation* 133, 2169–2179. doi: 10.1161/circulationaha.115.020633

Wada, K., Arita, M., Nakajima, A., Katayama, K., Kudo, C., Kamisaki, Y., et al. (2006). Leukotriene B4 and lipoxin A4 are regulatory signals for neural stem cell proliferation and differentiation. *FASEB J.* 20, 1785–1792. doi: 10.1096/fj.06-5809com

Wang, Q., Liu, Y., and Zhou, J. (2015). Neuroinflammation in Parkinson's disease and its potential as therapeutic target. *Transl. Neurodegener.* 4:19. doi: 10.1186/s40035-015-0042-0

Wang, Y. C., He, F., Feng, F., Liu, X. W., Dong, G. Y., Qin, H. Y., et al. (2010). Notch signaling determines the M1 versus M2 polarization of macrophages in

antitumor immune responses. *Cancer Res.* 70, 4840–4849. doi: 10.1158/0008-5472.can-10-0269

Wang, Y. P., Wu, Y., Li, L. Y., Zheng, J., Liu, R. G., Zhou, J. P., et al. (2011). Aspirin-triggered lipoxin A4 attenuates LPS-induced pro-inflammatory responses by inhibiting activation of NF-kappaB and MAPKs in BV-2 microglial cells. *J. Neuroinflammation* 8:95. doi: 10.1186/1742-2094-8-95

Wang, Z., Cheng, Q., Tang, K., Sun, Y., Zhang, K., Zhang, Y., et al. (2015). Lipid mediator lipoxin A4 inhibits tumor growth by targeting IL-10-producing regulatory B (Breg) cells. *Cancer Lett.* 364, 118–124. doi: 10.1016/j.canlet.2015.04.030

Wang, Z. F., Li, Q., Liu, S. B., Mi, W. L., Hu, S., Zhao, J., et al. (2014). Aspirin-triggered lipoxin A4 attenuates mechanical allodynia in association with inhibiting spinal JAK2/STAT3 signaling in neuropathic pain in rats. *Neuroscience* 273, 65–78. doi: 10.1016/j.neuroscience.2014.04.052

Wei, S., Luo, C., Yu, S., Gao, J., Liu, C., Wei, Z., et al. (2017). Erythropoietin ameliorates early brain injury after subarachnoid haemorrhage by modulating microglia polarization via the EPOR/JAK2-STAT3 pathway. *Exp. Cell Res.* 361, 342–352. doi: 10.1016/j.yexcr.2017.11.002

Wei, Z., Chigurupati, S., Arumugam, T. V., Jo, D. G., Li, H., and Chan, S. L. (2011). Notch activation enhances the microglia-mediated inflammatory response associated with focal cerebral ischemia. *Stroke* 42, 2589–2594. doi: 10.1161/strokeaha.111.614834

Wolf, S. A., Boddeke, H. W., and Kettenmann, H. (2017). Microglia in physiology and disease. *Annu. Rev. Physiol.* 79, 619–643. doi: 10.1146/annurev-physiol-022516-034406

Wu, F., Luo, T., Mei, Y., Liu, H., Dong, J., Fang, Y., et al. (2018). Simvastatin alters M1/M2 polarization of murine BV2 microglia via Notch signaling. *J. Neuroimmunol.* 316, 56–64. doi: 10.1016/j.jneuroim.2017.12.010

Wu, J., Wang, A., Min, Z., Xiong, Y., Yan, Q., Zhang, J., et al. (2011). Lipoxin A4 inhibits the production of proinflammatory cytokines induced by beta-amyloid in vitro and in vivo. *Biochem. Biophys. Res. Commun.* 408, 382–387. doi: 10.1016/j.bbrc.2011.04.013

Wu, L., Liu, Z. J., Miao, S., Zou, L. B., Cai, L., Wu, P., et al. (2013). Lipoxin A4 ameliorates cerebral ischaemia/reperfusion injury through upregulation of nuclear factor erythroid 2-related factor 2. *Neurol. Res.* 35, 968–975. doi: 10.1179/1743132813Y.0000000242

Wu, S. H., Liao, P. Y., Yin, P. L., Zhang, Y. M., and Dong, L. (2009). Elevated expressions of 15-lipoxygenase and lipoxin A4 in children with acute poststreptococcal glomerulonephritis. *Am. J. Pathol.* 174, 115–122. doi: 10.2353/ajpath.2009.080671

Wu, S. H., Wu, X. H., Liao, P. Y., and Dong, L. (2007). Signal transduction involved in protective effects of 15(R/S)-methyl- lipoxin A(4) on mesangioproliferative nephritis in rats. *Prostaglandins Leukot. Essent. Fatty Acids* 76, 173–180. doi: 10.1016/j.plefa.2006.12.006

Xanthos, D. N., and Sandkuhler, J. (2014). Neurogenic neuroinflammation: inflammatory CNS reactions in response to neuronal activity. *Nat. Rev. Neurosci.* 15, 43–53. doi: 10.1038/nrn3617

Xiong, X. Y., Liu, L., and Yang, Q. W. (2016). Functions and mechanisms of microglia/macrophages in neuroinflammation and neurogenesis after stroke. *Prog. Neurobiol.* 142, 23–44. doi: 10.1016/j.pneurobio.2016.05.001

Xu, F., Zhou, X., Hao, J., Dai, H., Zhang, J., He, Y., et al. (2018). Lipoxin A4 and its analog suppress hepatocarcinoma cell epithelial-mesenchymal transition, migration and metastasis via regulating integrin-linked kinase axis. *Prostaglandins Other Lipid Mediat.* 137, 9–19. doi: 10.1016/j.prostaglandins.2018.05.007

Xu, Y., Xu, Y., Wang, Y., Wang, Y., He, L., Jiang, Z., et al. (2015). Telmisartan prevention of LPS-induced microglia activation involves M2 microglia polarization via CaMKKbeta-dependent AMPK activation. *Brain Behav. Immun.* 50, 298–313. doi: 10.1016/j.bbi.2015.07.015

Xu, Z., Zhao, F., Lin, F., Chen, J., and Huang, Y. (2012). Lipoxin A4 inhibits the development of endometriosis in mice: the role of anti-inflammation and anti-angiogenesis. *Am. J. Reprod. Immunol.* 67, 491–497. doi: 10.1111/j.1600-0897.2011.01101.x

Xu, Z., Zhao, F., Xiang, H., Wang, N., Ye, D., and Huang, Y. (2014). Lipoxin A4: the double-edge sword in mice pregnancy. *Am. J. Reprod. Immunol.* 72, 57–64. doi: 10.1111/aji.12242

Yang, Y., Liu, F., Tang, M., Yuan, M., Hu, A., Zhan, Z., et al. (2016). Macrophage polarization in experimental and clinical choroidal neovascularization. *Sci. Rep.* 6:30933. doi: 10.1038/srep30933

Yao, C., Yang, D., Wan, Z., Wang, Z., Liu, R., Wu, Y., et al. (2014). Aspirin-triggered lipoxin A4 attenuates lipopolysaccharide induced inflammatory response in primary astrocytes. *Int. Immunopharmacol.* 18, 85–89. doi: 10.1016/j.intimp.2013.10.028

Ye, X. H., Wu, Y., Guo, P. P., Wang, J., Yuan, S. Y., Shang, Y., et al. (2010). Lipoxin A4 analogue protects brain and reduces inflammation in a rat model of focal cerebral ischemia reperfusion. *Brain Res.* 1323, 174–183. doi: 10.1016/j.brainres.2010.01.079

Yuan, Y., Rangarajan, P., Kan, E. M., Wu, Y., Wu, C., and Ling, E. A. (2015). Scutellarin regulates the Notch pathway and affects the migration and morphological transformation of activated microglia in experimentally induced cerebral ischemia in rats and in activated BV-2 microglia. *J. Neuroinflammation* 12:11. doi: 10.1186/s12974-014-0226-z

Zhang, H. M., Liu, P., Jiang, C., Jin, X. Q., Liu, R. N., Li, S. Q., et al. (2018). Notch signaling inhibitor DAPT provides protection against acute craniocerebral injury. *PLoS One* 13:e0193037. doi: 10.1371/journal.pone.0193037

Zhao, Q., Shao, L., Hu, X., Wu, G., Du, J., Xia, J., et al. (2013). Lipoxin a4 preconditioning and postconditioning protect myocardial ischemia/reperfusion injury in rats. *Mediators Inflamm.* 2013:231351. doi: 10.1155/2013/231351

Zhou, M., Chen, B., Sun, H., Deng, Z., Andersson, R., and Zhang, Q. (2011). The protective effects of Lipoxin A4 during the early phase of severe acute pancreatitis in rats. *Scand. J. Gastroenterol.* 46, 211–219. doi: 10.3109/00365521.2010.525715

Conflict of Interest Statement: The authors declare that the research was conducted in the absence of any commercial or financial relationships that could be construed as a potential conflict of interest.

frontiers in Cellular Neuroscience

ORIGINAL RESEARCH
published: 04 February 2019
doi: 10.3389/fncel.2019.00012

MicroRNA-155 Promotes Heat Stress-Induced Inflammation via Targeting Liver X Receptor α in Microglia

*Ping Li[1†], Gong Wang[1,2†], Xiao-Liang Zhang[1,3], Gen-Lin He[1], Xue Luo[1], Ju Yang[1], Zhen Luo[1], Ting-Ting Shen[1] and Xue-Sen Yang[1]**

[1] Laboratory of Extreme Environmental Medicine, Department of Tropical Medicine, Army Medical University, Chongqing, China, [2] Department of Neurology, Xinqiao Hospital, Army Medical University, Chongqing, China, [3] Department of Cardiology, Kunming General Hospital of Chengdu Military Command, Yunnan, China

Background: The neuroinflammatory responses of microglial cells play an important role in the process of brain dysfunction caused by heat stroke. MicroRNAs are reportedly involved in a complex signaling network and have been identified as neuroinflammatory regulators. In this study, we determined the biological roles of microRNA-155 in the inflammatory responses in heat-stressed microglia and explored the underlying mechanisms.

Methods: MicroRNA-155 mimic and inhibitor were used to separately upregulate or downregulate microRNA-155 expression. The activation state of BV-2 microglial cells (BV-2 cells) was assessed via immunoreactions using the microglial marker CD11b and CD68. Levels of induced interleukin-1β (IL-1β), interleukin-6 (IL-6) and tumor necrosis factor-α (TNF-α) were measured using real-time reverse transcription polymerase chain reaction (RT-PCR) and enzyme linked immunosorbent assays (ELISAs). The activation of nuclear factor kappa B (NF-κB) signaling proteins was evaluated by Western blotting for inhibitory kappa B alpha (IκBα) and NF-κB p65 phosphorylation and indirect immunofluorescence analysis using a p65 phosphorylation antibody. A luciferase reporter assay was used to verify liver X receptor α (LXRα) as a target gene of microRNA-155.

Results: Heat stress significantly induced IL-1β, IL-6, and TNF-α release and increased the expression of CD11b and CD68. In addition, IκBα and NF-κB p65 phosphorylation were dramatically increased by heat stress, and microRNA-155 expression was also elevated. High expression of microRNA-155 in heat-stressed microglial cells was inversely correlated with LXRα expression. We then determined the role of microRNA-155 in the heat stress-induced inflammatory responses. The results revealed that by targeting LXRα, microRNA-155 enhanced NF-κB

OPEN ACCESS

Edited by:
Yu Tang,
Central South University, China

Reviewed by:
Jing Zou,
Mayo Clinic, United States
Cintia Roodveldt,
Centro Andaluz de Biología Molecular y Medicina Regenerativa (CABIMER), Spain

***Correspondence:**
Xue-Sen Yang
xuesenyyy@aliyun.com;
xuesenyyy@hotmail.com

[†]*Co-first authors*

Received: *13 October 2018*
Accepted: *14 January 2019*
Published: *04 February 2019*

Citation:
Li P, Wang G, Zhang X-L, He G-L, Luo X, Yang J, Luo Z, Shen T-T and Yang X-S (2019) MicroRNA-155 Promotes Heat Stress-Induced Inflammation via Targeting Liver X Receptor α in Microglia. Front. Cell. Neurosci. 13:12. doi: 10.3389/fncel.2019.00012

signaling activation and facilitated immune inflammation in heat stress-treated BV-2 cells.

Conclusion: MicroRNA-155 promotes heat stress-induced inflammatory responses in microglia. The underlying mechanisms may include facilitating inflammatory factors expression by increasing NF-κB pathway activation via targeting LXRα.

Keywords: heat stress, microRNA-155, inflammation, LXRα, microglia

INTRODUCTION

Heat stroke is an overheated environment or high-intensity manual work- caused serious illness in which central nervous system (CNS) dysfunction predominates. Symptoms of CNS dysfunction, such as loss of consciousness, ataxia, coma, and delirium are also the main basis of diagnoses of heat stroke in the clinic (Bouchama, 2002; Mattis and Yates, 2011; Leon and Bouchama, 2015; Hifumi et al., 2018). The central pathophysiological mechanisms underlying CNS dysfunction during heatstroke are believed to involve the following aspects: direct damage to the CNS induced by hyperthermia; and the secondary insult resulting from the widespread process of cerebral ischaemia and hypoxia (Sharma and Hoopes, 2003; Yan et al., 2006; Chen et al., 2013). Although neuroinflammation is still not fully understood, increasing data have indicated that this process contributes to the consequences of CNS damage during heat stroke (Biedenkapp and Leon, 2013; Lin et al., 2018). An obvious neuroinflammatory response (NIR) has been clinically and experimentally verified (Guerrero et al., 2013; Lee et al., 2015; Chauhan et al., 2017). All these findings indicate that excessive activation of inflammation in the CNS may be the major pathological mechanism of heat stroke, and elucidation of the cellular mechanisms underlying the inflammatory response may provide guidelines for heat stroke prevention and therapy.

Microglia are the main immune cells in the CNS and can function as macrophages in the brain (Ginhoux et al., 2013). In serious neuropathological conditions, microglia can be activated and secrete proinflammatory cytokines and neurotoxic mediators, such as TNF-α, IL-6, IL-1β, NO and ROS, which cause additional neuroinflammation and aggravate brain disease progression (Biber et al., 2014; Brown and Vilalta, 2015; Dwyer and Ross, 2016; Beckers et al., 2018). Activated microglia have been found in the cerebral cortex, hippocampus and pituitary gland of the brain in heat stroke animal models. Interestingly, Biedenkapp and Leon (2013) revealed that expression of the activation markers of microglia was consistent with the profiles of cytokines and chemokines in heat stroke mice. These results indicated that microglia may play a pivotal immune modulatory role in the CNS during heat stroke. Microglia can be activated by various physical factors, such as electromagnetic radiation, ionizing radiation and infrasound (Hwang et al., 2006; Du et al., 2010; Yang et al., 2010). However, whether heat as another physical factor can directly active microglia is still unclear.

As a physical stress, high ambient temperature activates the proinflammatory response of microglia; this reaction may not occur through the classical adaptor- receptor signaling pathway, but it may change the expression levels of some mediators that indirectly influence inflammation. Recent studies have indicated that epigenetic mechanisms, such as microRNAs (miRNAs) and DNA methylation, participate in neuro-inflammation in neuropathological conditions (Thounaojam et al., 2013; Saika et al., 2017; Zhang et al., 2017; Cheray and Joseph, 2018; Wang X. et al., 2018). MiRNAs are an important class of epigenetic regulators that can regulate gene expression post-transcriptionally. A deep sequence data analysis revealed that compared to the negative control, miRNA-155, a well-studied inflammatory miRNA, increased 2.73-fold in peripheral blood mononuclear cells of heat-stressed cattle (Sengar et al., 2018), indicating the involvement of miR-155 in the heat stress-induced inflammatory response. Consistent evidence has indicated that miR-155 upregulation in neurological conditions is associated with enhancement of CNS inflammation and pathological changes (Lopez-Ramirez et al., 2014; Woodbury et al., 2015). Moreover, miR-155 was the first reported miRNA to be directly linked to microglial activation. Indirect evidence has shown that the inhibition of miR-155 ameliorates the pathogenesis of ischaemic stroke in mice by decreasing the production of proinflammatory mediators, and this process was proven to be mediated by the NF-κB signaling pathway in macrophages (Wen et al., 2015; Pena-Philippides et al., 2016). Further studies have indicated that miR-155 exerts proinflammatory effects by targeting different mediators of inflammatory signaling, including LXRα, SOCS-1, SHIP1 and transforming growth factor beta-activated kinase 1 and MAP3K7-binding protein 2 (TAB2) (Ceppi et al., 2009; Cardoso et al., 2012; Miller et al., 2013). Among these, LXRα, an oxysterol-activated transcription factor, is widely expressed in growing or mature neurons and glia and has also been shown to be a direct anti-inflammatory target of miR-155 (Miller et al., 2013; Skerrett et al., 2014; de Wit et al., 2017; Kurowska-Stolarska et al., 2017).

Considering the relationship between miR-155 and inflammatory-activated microglia, this study attempted to ascertain whether heat stress can directly activate microglia and induce a proinflammatory response *in vitro*. Is miR-155 involved in the heat stress-induced proinflammatory response and how does it influence the inflammation stimulated by heat stress? In this study, we employed a heat stressed-BV-2 cell model to answer

Abbreviations: 6-OHDA, 6-hydroxydopamine; COX-2, cyclooxygenase-2; IκBα, inhibitory kappa B α; IL-1β, interleukin-1β; IL-6, interleukin-6; LXRα, liver X receptor α; MPP^+, 1-methy1-4-phenylpyridinium; NF-κB, nuclear factor kappa B; NO, nitric oxide; Nur77, nerve growth factor IB; Nurr1, nuclear receptor related 1; ROS, reactive oxygen species; SHIP1, Src homology 2-containing-inositol-phosphate-1; SOCS-1, suppressor of cytokine signaling-1; TAB2, transforming growth factor beta-activated kinase 1 and MAP3K7-binding protein 2; TLR4, Toll-like receptor 4; TNF-α, tumor necrosis factor-α; VEGF, vascular endothelial growth factor.

these questions. Our preliminary data showed that miR-155 may function as a promoter in heat stress-induced inflammatory responses in BV-2 cells. The underlying mechanisms may include enhancing inflammatory factors expression by increasing NF-κB signaling pathway activation via targeting LXRα.

MATERIALS AND METHODS

Cell Culture and Treatment

The immortalized murine BV-2 microglial cell line was purchased from the American Type Culture Collection (ATCC) and was cultured in Dulbecco's modified Eagle's medium (DMEM, Gibco, NY, United States) supplemented with 10% heat-inactivated fetal bovine serum (FBS, HyClone), 2 mM glutamine, 100 U/ml penicillin, 100 μg/ml streptomycin and 50 μM 2-mercaptoethanol (Sigma-Aldrich, St. Louis, MO, United States). Cells were plated in six-well flat-bottom plates at a density of 5 × 105/ml and maintained at 37°C in a humidified atmosphere of 5% CO2. Cells were passaged every 48 h with a 1:4 split ratio and used at passages 3–10. After a 24 h incubation, miR-155 mimic, miR-155 inhibitor or their respective controls (Gene Pharma Co., Ltd.) were transfected at a final concentration of 100 nM/ml in Opi-MEM (Life Technologies GmbH, Darmstadt, Germany) using Lipofectamine® 2000 (Invitrogen, Life Technologies). Then, cells were treated with or without TO901317 for 1 h (10 nM, Sigma). Subsequently, cells were subjected to heat stress for 2 h in a prewarmed incubator at 42°C, followed by a recovery period at the normal growth temperature of 37°C. We collected the cell culture supernatant for enzyme linked immunosorbent assays (ELISAs) and extracted total RNA and protein for real-time PCR and Western blot analyses.

Cell Viability Assay

Following transfection in BV-2 cells, cell viability was evaluated using the Cell Counting Kit-8 assay (CCK-8; Dojindo, Shanghai, China) according to the manufacturer's instructions. This method is used to determine the number of metabolically active and viable cells in cell culture based on several proliferation-related elements in the cells, including dehydrogenase, NAD(H), NADP(H) and mitochondrial activity. In brief, cells were seeded in a 96-well plate at a density of 5×10^3 cells/well for 24 h and transfected with synthetic miR-155 mimic, miR-155 inhibitor or their respective controls at a final concentration of 50 nM/ml using Lipofectamine® 2000. After transfection for 24 h, 10 μl CCK-8 reagent was added to each well for 2.5 h. The absorbance at 450 nM was measured using a plate reader (Bio-tek Epoch, Winooski, VT, United States).

Real-Time PCR Analysis of mRNA Levels

Total RNA was isolated using TRIzol® reagent (Invitrogen, Carlsbad, CA, United States). Briefly, 800 ng of total RNA was reverse transcribed into cDNA using the PrimeScript™ RT reagent Kit according to the manufacturer's protocol. The synthesized cDNA was used as the template for the real-time PCR amplification that was carried out by the Bio-Rad CFX 96™ Real-Time PCR Detection System (Bio-Rad) using a KAPA SYBR® FAST qPCR kit (Kapa Biosystems, Boston, MA, United States). Specific primers were designed based on entries in the GenBank database using Primer 5.0 software (Premier Biosoft International, Palo Alto, CA, United States). Reaction conditions for real-time PCR were 3 min at 95°C, followed by 40 cycles of 3 s at 95°C and 20 s at 60°C; every cycle was followed by melt curve conditions of 65 and 95°C with increments of 0.5°C for 5 s, followed by the final plate read. HPRT served as an internal control for sample normalization, and the comparative cycle threshold method was used for data quantification. The primer sequences are shown as follows: TNF-α: Fwd 5′- GAC CCT CAC ACT CAG ATC ATC TTC T- 3′; Rev 5′-CCT CCA CTT GGT GGT TTG CT-3′. IL-6: Fwd 5′-TGG TGT GTG ACG TTC CCA TTA-3′; Rev 5′-CAG CAC GAG GCT TTT TTG TTG-3′. IL-6: Fwd 5′-ACA ACC ACG GCC TTC CCT ACT T-3′; Rev 5′-CAC GAT TTC CCA GAG AAC ATG TG-3′. iNOS: Fwd 5′-GGC AGC CTG TGA GAC CTT TG-3′; Rev 5′-GCA TTG GAA GTG AAG CGT TTC-3′. HPRT: Fwd 5′-GTT AAG CAG TAC AGC CCC AAA-3′; Rev 5′-AGG GCA TAT CCA ACA AAC TT-3′.

Real-Time PCR Analysis of miRNAs

Total RNA, including miRNA, was extracted using TRIzol® reagent (Invitrogen, Carlsbad, CA, United States). In brief, 1000 ng of total RNA was reverse transcribed into cDNA using the MicroRNA First-Strand Synthesis and MiRNA Quantitation Kits (TaKaRa, Japan) according to the manufacturer's instructions. We performed quantitative RT-PCR analyses for miRNAs using the Mir-X™ miRNA qRT-PCR SYBR® Kit (TaKaRa) in a Rotorgene 6000 Thermocycler (Corbett Life Science) using the following parameters: 95°C for 3 min, followed by 40 cycles of 95°C for 15 s, 60°C for 30 s, and 70°C for 10 s. We used U6 small nuclear RNA as an endogenous control for data normalization and calculated the relative expression using the comparative threshold cycle method $2^{-\Delta\Delta CT}$.

Enzyme-Linked Immunosorbent Assays

After the designated treatment, we evaluated the secretion levels of TNF-α, IL-6 and IL-1β in cell supernatants using enzyme immunoassay kits (eBioscience, San Diego, CA, United States) according to the manufacturer's instructions. The results of the ELISAs were read using a plate reader (Bio-tek Epoch) at 450 nm.

Luciferase Reporter Assay

The wild type LXRα-3′UTR and mut-LXRα-3′UTR dual luciferase reporter vectors (Promega, United States) were synthetized and tested by Gene Pharma Co., Ltd., and then, BV-2 cells were cotransfected with miR-155 mimic or negative control. Cells were also transfected with the pmirGLO-control vector, which is useful for monitoring the transfection efficiency. After 24 h, the firefly luciferase activity was determined using the dual luciferase reporter assay system (Promega, United States) with a GloMAX 20/20 Luminometer (Promega, United States). We obtained the relative reporter activity through normalization to the Renilla control.

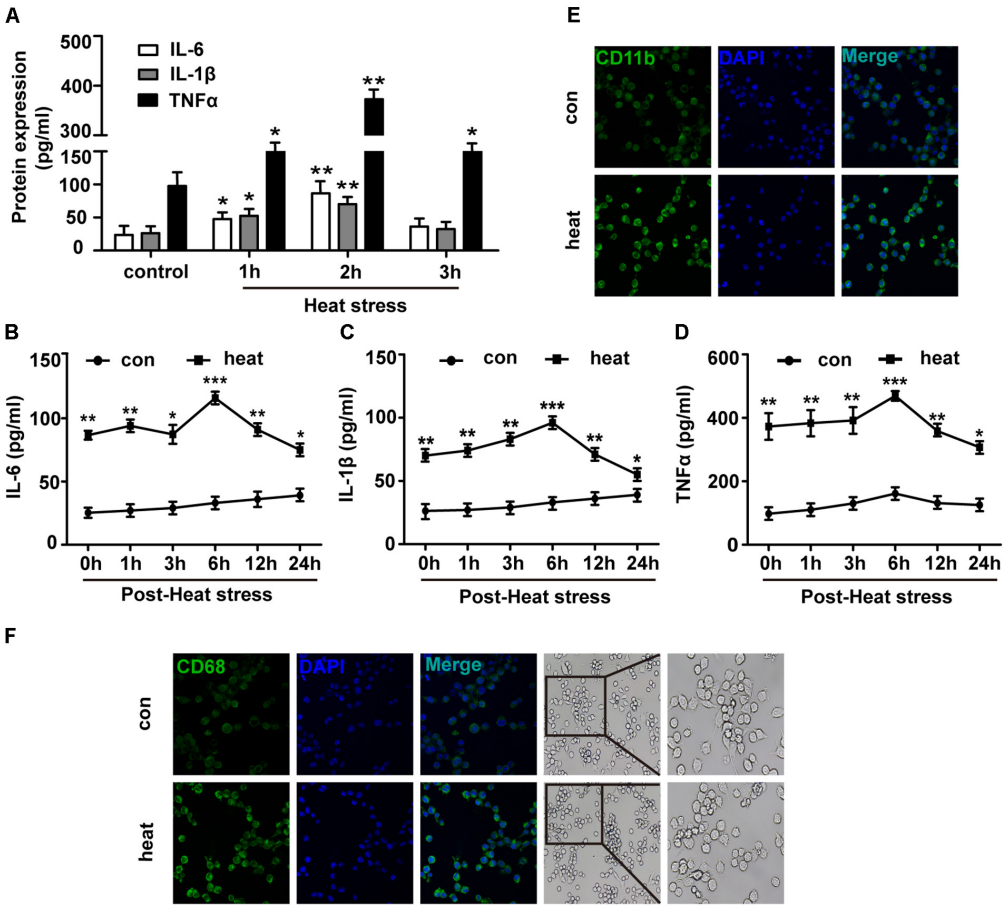

FIGURE 1 | Heat stress provokes proinflammatory responses and induces microglial activation. **(A)** BV-2 cells were incubated at 37°C (control) or were subjected to heat stress treatment at 42°C for 1, 2, or 3 h. The culture medium supernatants were collected, and the protein contents of IL-6, IL-1β, and TNF-α were assayed by ELISAs. **(B–D)** Cells were subjected to a heat stress treatment at 42°C for 2 h, followed by a recovery period at 37°C for 0, 1, 3, 6, 12, or 24 h. The protein contents of IL-6, IL-1β, and TNF-α were assayed by ELISAs. **(E,F)** Cells were subjected to a heat stress treatment at 42°C for 2 h, followed by a recovery period at 37°C for 6 h. Confocal immunofluorescence microscopy was performed on cells that were immunoreacted with antibodies against CD11b and CD68 after the treatment. The images are presented at a 400× magnification. The morphology of cells was captured by inverted microscope. The images are presented at a 100 and 200× magnification. The results are presented as the mean ± SD of three independent experiments. Statistical comparisons to the control group are indicated by $^{*}p < 0.05$, $^{**}p < 0.01$, $^{***}p < 0.001$.

Immunoblotting

Cells were lysed in RIPA-containing protease and phosphatase inhibitors (Roche, Penzberg, Germany). Nuclear protein was extracted by nuclear protein extraction kit (Beyotime Biotechnology, Shanghai, China) as per the company's protocol. Protein concentration was determined using the BCA assay (Beyotime Biotechnology, Beijing, China). The solubilized denatured protein (20 ng) was subjected to electrophoresis on polyacrylamide SDS gels and transferred to polyvinylidene difluoride (PVDF) membranes (Bio-Rad, Munich, Germany). The membranes were incubated with 5% fat-free dry milk in TBST buffer at room temperature for 1 h. We then probed the membranes with primary antibodies against Glyceraldehyde 3-phosphate dehydrogenase (GAPDH) (Santa Cruz Biotechnology, Heidelberg, Germany), IκBα, pSer32/36-IκBα, NF-κB p65, pSer536-NF-κB p65 (Cell Signaling Technology, Danvers, MA, United States), LXRα (Abcam, Santa, United States) or proliferating cell nuclear antigen (PCNA) (Santa Cruz Biotechnology, Heidelberg, Germany) overnight at 4°C. After the membranes were washed with TBST, they were incubated with horseradish peroxidase-conjugated anti-rabbit or anti-mouse secondary antibody for 1 h. The immune-reactive proteins were visualized using enhanced chemiluminescence (ECL) reagent (Bio-Rad, Munich, Germany) followed by exposure to X-ray film and quantified by using Image Lab analysis software. The data were first normalized against the internal standard GAPDH and then expressed as fold changes compared to the controls.

Immunofluorescence Staining

Cells were cultured on coverslips (10 mm × 10 mm) coated with poly-1-lysine in 24-well plates. After fixation with 4% paraformaldehyde and permeabilization with 0.3% Triton X-100, the cells were incubated in goat serum (Zhongshan Golden Bridge Biotechnology, Beijing, China) for 60 min

at room temperature to block non-specific binding sites. Cells were incubated with mouse anti-mouse cluster of differentiation molecule 11b (CD11b), pSer536-NF-κB p65 or rabbit anti-mouse cluster of differentiation 68 (CD68) (1:200; Cell Signaling Technology, Danvers, MA, United States) antibody overnight at 4°C in a humidified chamber. After being washed with PBS, cells were incubated with highly cross-adsorbed CF555-conjugated donkey anti-mouse IgG secondary antibody (1:250, Sigma-Aldrich) at 37°C for 60 min in the dark. Then, the cells were counterstained with 4′ 6-diamidino-2-phenylindole dihydrochloride (DAPI; Beyotime Biotechnology, Shanghai, China). Representative fluorescence photographs were taken by an LSM 780 confocal laser scanning microscope (400× magnification, Carl Zeiss GmbH, Jena, Germany). The photographs were analyzed by ZEN 2012 light edition software (Carl Zeiss, Jena, Germany).

Statistical Analysis

Three or more separate experiments were performed, and statistical analyses were carried out using Prism5 software (GraphPad, San Diego, CA, United States). The results are presented as the mean ± standard deviation (SD). We determined significant differences by Student's *t*-test (two groups) or one-way ANOVA (multiple comparisons). Statistical significance was established when $p < 0.05$. * denotes $p < 0.05$, ** denotes $p < 0.01$, and *** denotes $p < 0.001$.

RESULTS

Heat Stress Provokes Proinflammatory Responses and Induces Microglial Activation

To investigate the effects of heat stress on the inflammatory response of BV-2 cells, we initially examined the protein expression levels of IL-6, TNF-α and IL-1β. As presented in **Figure 1A**, the expression levels of IL-6, TNF-α, and IL-1β in the culture medium supernatants were differently increased following heat stress at 42°C for 1, 2, and 3 h and peaked at 2 h of exposure ($p < 0.01$). Thus 2-h heat stress was identified as

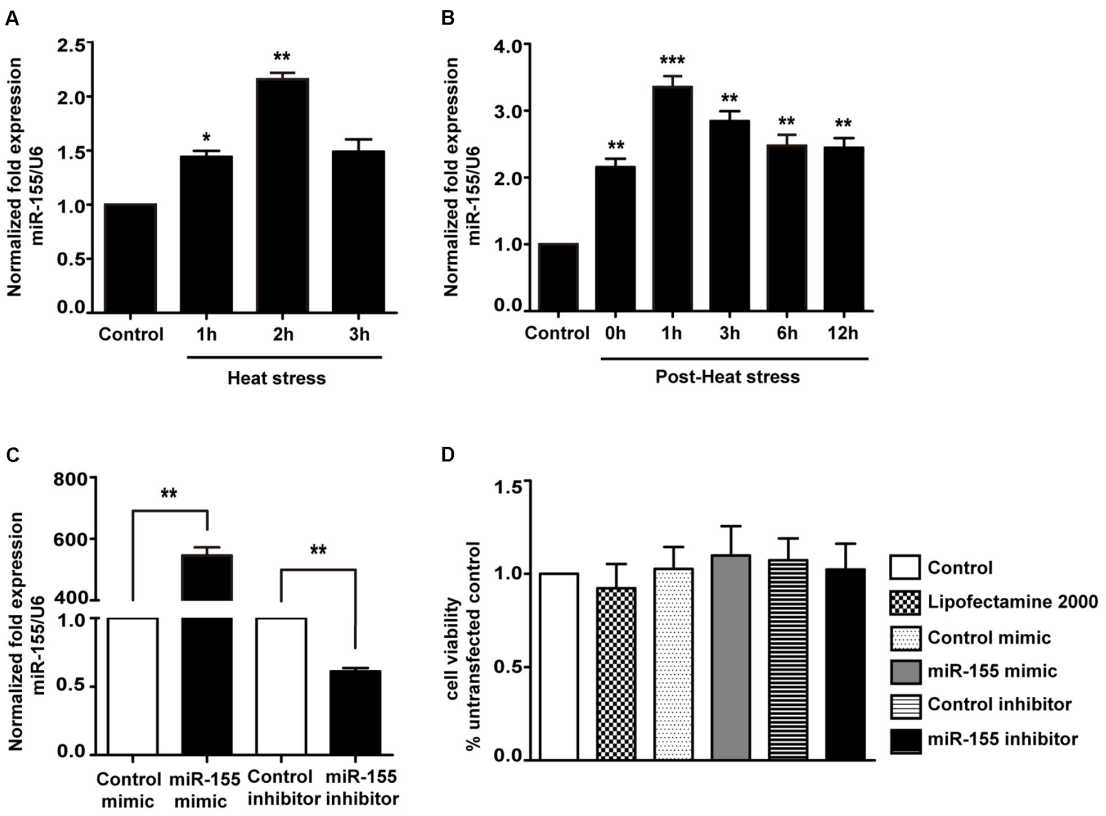

FIGURE 2 | Expression of miR-155 in BV-2 cells induced by heat stress and transfection efficacy of the miR-155 mimic and inhibitor. **(A)** BV-2 cells were incubated at 37°C (control) or were subjected to heat stress treatment at 42°C for 1, 2, or 3 h. The expression levels of miR-155 in BV-2 cells were measured by qRT-PCR and normalized to U6 expression. **(B)** Cells were subjected to a heat stress treatment at 42°C for 2 h, followed by a recovery period at 37°C for 0, 1, 3, 6, 12, or 24 h. The expression levels of miR-155 in BV-2 cells were measured by qRT-PCR and normalized to U6 expression. **(C)** After 24 h of cell transfection, miR-155 expression was measured by qRT-PCR and normalized to U6. The results are presented as the fold change with respect to the control. **(D)** Cell viability was measured using CCK-8 assays after cell transfection with miR-155 mimic (50 nM), inhibitor (50 nM) or their respective controls. The untransfected control was set to 100%. Statistical analyses were performed by using a *t*-test (two groups) or one-way ANOVA with a *post hoc* Student–Newman–Keuls test (multiple comparisons). The results are expressed as the mean ± SD of three independent experiments. Statistical comparisons to the control group are indicated by $*p < 0.05$, $**p < 0.01$, $***p < 0.001$.

a threshold condition representing the time of duration beyond which intensified alteration of growth characteristics of tested cell line occurs (data not shown). With the extension of time after 2 h of heat stress, IL-6, TNF-α, and IL-1β expression increased gradually, peaked at 6 h recovery period, and were sustained up to 24 h after heat stress, compared to that of the corresponding control group (**Figures 1B–D**; $p < 0.001$). Activated microglia were previously suggested to express different markers. Among these, CD11b and CD68 have the greatest biological significance (Hoogland et al., 2015; Yang et al., 2018). Because increased expression of CD11b and CD68 are a typical feature of microglial activation (Fernando et al., 2006; Roy et al., 2006), we examined the effect of heat exposure on the expression of CD11b and CD68 in BV-2 cells by confocal microscopy. Heat stress was found to significantly increase CD11b and CD68 expression compared with that of the control group and the morphology of BV-2 cells changed from ramified to amoeba in the heat stress group (**Figures 1E,F**). These results indicate that heat stress provoked proinflammatory responses and induced microglial activation.

Heat Stress Could Increase miR-155 Expression in Microglia

Because miR-155 is involved in peripheral inflammation and immune responses (Tili et al., 2007; Mashima, 2015), we investigated its regulation in heat stress-treated microglia. A significant increase in miR-155 expression was observed following heat stress at 42°C for 1 and 2 h (**Figure 2A**; $p < 0.05$). In contrast, heat stress did not affect miR-155 expression at 3 h of heat exposure ($p > 0.05$). With the extension of recovery time after 2 h of heat stress, miR-155 expression peaked at 1 h, and was sustained up to 24 h compared to the control group (**Figure 2B**; $p < 0.01$). Upregulation of miR-155 after heat stress

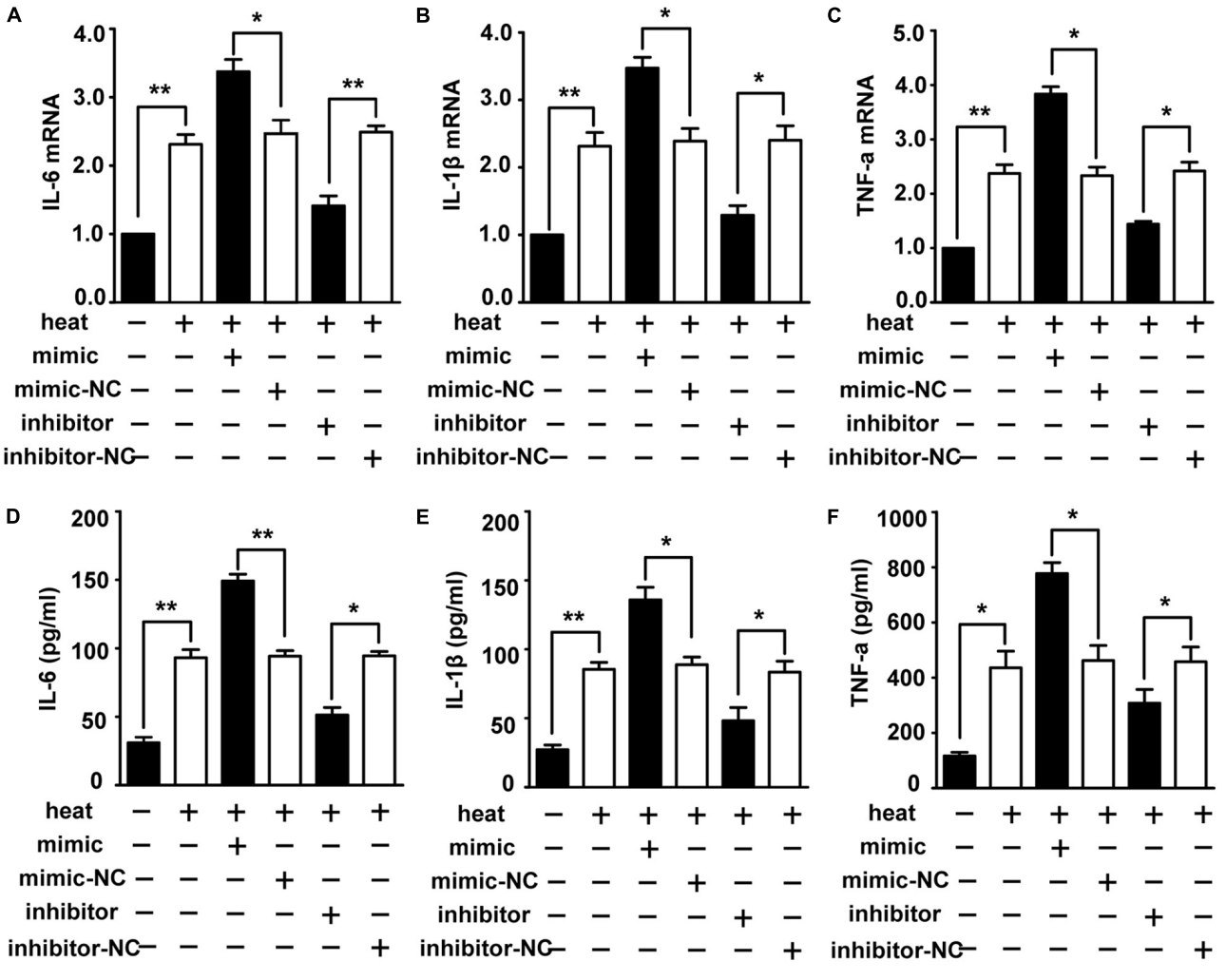

FIGURE 3 | Role of miR-155 in activating heat stress-induced inflammatory response in microglial cells. **(A–F)** BV-2 cells were transfected with miR-155 mimic, inhibitor, or their respective control for 24 h. Then, the cells were subjected to a heat stress treatment at 42°C for 2 h, followed by a recovery period at 37°C for 6 h. The mRNA and protein levels of IL-6, IL-1β, and TNF-α were assessed by qRT-PCR **(A–C)** and ELISA **(D–F)**, respectively. Statistical analyses were performed by using a *t*-test (two groups). The results are expressed as the mean ± SD of three independent experiments (*$p < 0.05$, **$p < 0.01$).

suggests that miR-155 is involved in the regulation of heat stress-triggered inflammatory responses in microglia. To address this issue, we transfected BV-2 cells with miR-155 mimic, inhibitor, or their respective controls. The transfection efficacy determined by qRT-PCR showed that transfection with the miR-155 mimic increased miR-155 expression ($p < 0.01$), whereas the miR-155 inhibitors significantly decreased its availability ($p < 0.01$) compared to those of cells transfected with negative controls, indicating effective transfection (**Figure 2C**). To exclude the possibility that transfection could affect the survival of BV-2 cells, we performed a cell viability assay. As shown in **Figure 2D**, neither miR-155 mimic nor inhibitor nor their transfection reagent Lipofectamine2000 exerted any adverse effects on cellular survival. Interestingly, cells transfected with the miR-155 mimic showed an increased trend in cell viability, although no statistical significance was achieved.

Role of miR-155 in Activating Heat Stress-Induced Inflammatory Responses in Microglia

To identify the role of miR-155 in activating the heat stress-induced inflammatory response in microglia, we examined the impacts of miR-155 on the expression of IL-6, IL-1β, and TNF-α. The results (**Figures 3A–F**) showed that overexpression of miR-155 upregulated the mRNA and protein levels of IL-6, IL-1β and TNF-α ($p < 0.05$). In contrast, inhibition of miR-155 downregulated the mRNA and protein levels of IL-6, IL-1β and TNF-α. These data suggest that miR-155 is involved in the regulation of the proinflammatory response induced by heat stress.

miR-155 Enhances NF-κB Activation in Heat-Stressed Microglia

The NF-κB pathway is considered the central regulator of inflammatory cytokines and enzymes, such as IL-6, IL-1β, and TNF-α (Lawrence, 2009; Nguyen et al., 2014). Recent studies showed that NF-κB was activated during the recovery period following heat stress in HeLa cells and human umbilical vein endothelial cells (HUVECs) (Kretz-Remy et al., 2001; Liu et al., 2015). Therefore, we investigated whether heat stress activates NF-κB in microglia. Western blot assays were performed, and the results showed that the phosphorylation levels of IκBα and p65 and the level of p65 translocation to nucleus were low at 37°C but immediately increased after heat stress treatment. The phosphorylation was further increased during the 24 h recovery time (**Figures 4A–C**). However, there were no significant IκBα changes during the recovery periods, which indicates that NF-κB activation may be accompanied by phosphorylation of IκBα and p65 but not by bulk degradation of IκBα in BV-2 cells. To further study the role of miR-155 in the activation of NF-κB, we used miR-155 mimic and inhibitor in heat-stressed BV-2 cells. Western blot results showed that the miR-155 mimic significantly increased IκBα and p65 phosphorylation and the level of p65 translocation to nucleus, but the miR-155 inhibitor downregulated this phosphorylation (**Figures 4D–F**). The IκBα changes were also not affected by miR-155 treatment. Furthermore, indirect immunofluorescence studies demonstrated that the distribution of p-p65 in the nucleus was obviously increased after 6 h of heat stress recovery at 37°C, and miR-155 aggravated these changes, while the miR-155 inhibitor restrained the changes (**Figures 4G,H**). Taken together, these results suggest that heat stress induces the activation and translocation of NF-κB during the recovery period in BV-2 cells and that miR-155 enhances NF-κB activation and translocation. These findings indicated that miR-155 can regulate the inflammatory response induced by heat stress through the NF-κB signaling pathway in microglia.

Liver X Receptor α Is a Functional Target of miR-155

LXRα has been shown to inhibit the expression of lipopolysaccharide (LPS)-induced IL-1β, IL-6, and TNF-α and thus has a critical role in the regulation of inflammation (Wang J. et al., 2018). Two different online database searchers, TargetScan[1] and miRanda[2], predicted that the 3′UTR of the LXRα mRNA transcript in mice contains putative binding sites for miR-155, and the binding site appears to be highly conserved in humans (**Figure 5A**). Next, we performed luciferase reporter assays in the cells to determine whether LXRα is a direct target of miR-155. Cotransfection of agomir-155 with the luciferase reporter gene linked to the wild-type (WT) segment of the LXRα 3′UTR strongly repressed luciferase activity ($p < 0.05$), and the luciferase activity of the mutant was significantly rescued (**Figure 5B**). These findings demonstrate that miR-155 can directly target the 3′UTR of LXRα mRNA through this binding site. To identify whether the miR-155-LXRα pathway is active in heat-exposed BV-2 cells, we separately transfected cells with miR-155 mimic, miR-155 inhibitor or their respective negative controls. As shown in **Figures 5C,D**, qPCR and Western blot analyses indicated that overexpression of miR-155 inhibited LXRα expression at both the mRNA and protein levels, while inhibition of miR-155 resulted in a significant increase in LXRα mRNA and protein levels ($p < 0.05$) in heat-stressed BV-2 cells. Thus, miR-155 can directly target LXRα in BV-2 cells. Next, we examined the role of LXRα in BV-2 cells during various periods of recovery time. Western blotting showed that LXRα expression was rapidly inhibited and was maintained at low levels for more than 6 h before increasing to baseline levels after a 12 h recovery period (**Figure 5E**). These results indicated the threshold 6 h recovery time of heat stress with prominent proinflammatory activity.

Exogenous LXRα Agonist Ameliorates the Effects of miR-155 and Heat Stress on the Inflammatory Responses and NF-κB Activation in Microglia

To test whether LXRα is involved in mediating the effects of miR-155 on inflammatory responses and NF-κB activation, we used the LXRα agonist TO901317 to elevate the LXRα

[1]http://www.targetscan.org/

[2]http://www.microrna.org/microrna/home.do

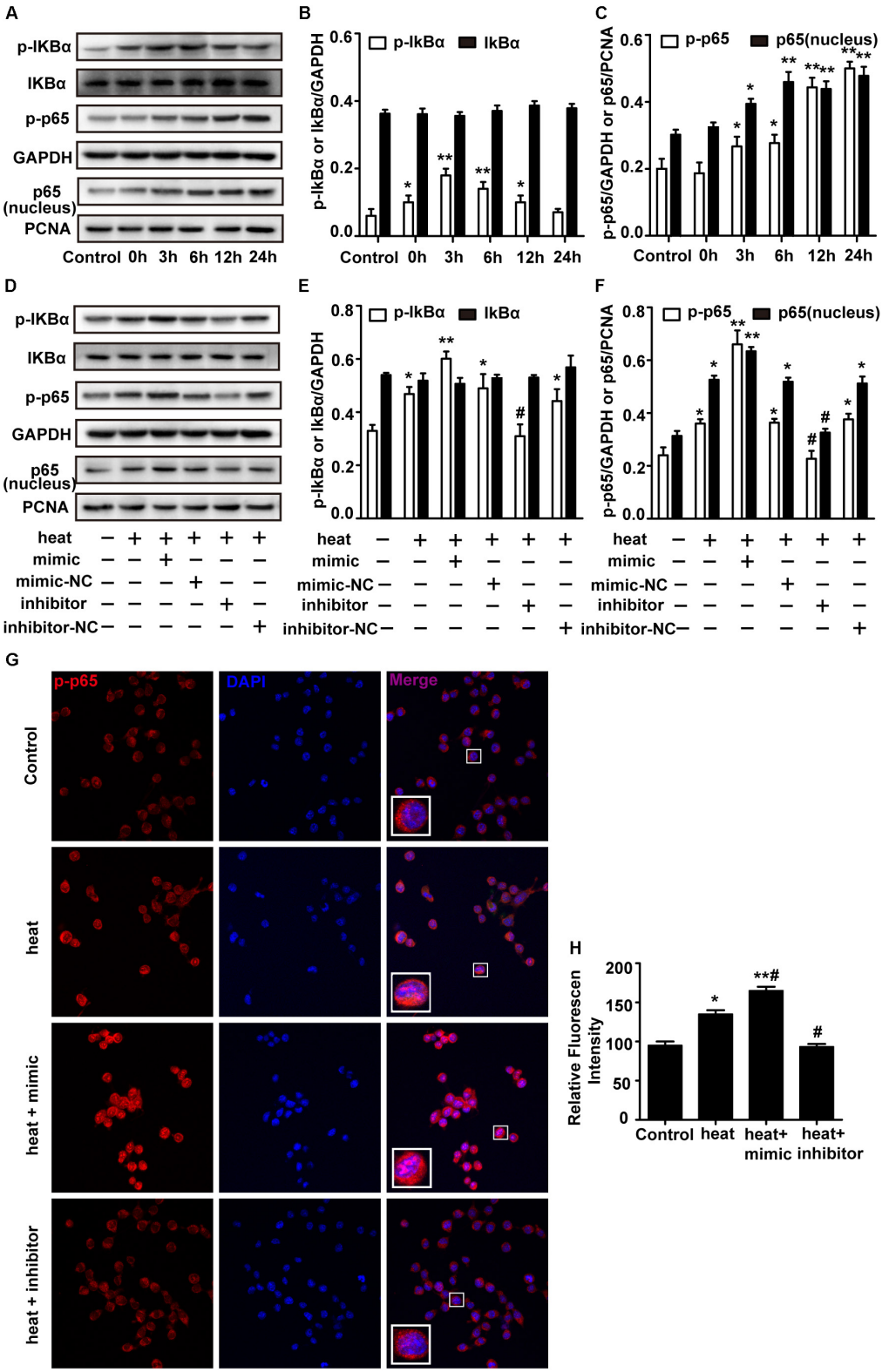

FIGURE 4 | miR-155 enhances NF-κB activation in heat-stressed microglia. **(A–C)** Cells were subjected to a heat stress treatment at 42°C for 2 h, followed by a recovery period at 37°C for 0, 3, 6, 12, or 24 h. Total protein expression levels of IκBα, p-IκBα, p-p65, GAPDH and nucleus protein expression levels of p65 and PCNA were determined by Western blotting. Densitometric analysis was performed. **(D–F)** BV-2 cells were transfected with miR-155 mimic, inhibitor, or their

(Continued)

FIGURE 4 | Continued
respective controls for 24 h. Then, the cells were subjected to a heat stress treatment at 42°C for 2 h, followed by a recovery period at 37°C for 6 h. Total protein expression levels of IκBα, p-IκBα, p-p65, GAPDH and nucleus protein expression levels of p65 and PCNA were determined by Western blotting. Densitometric analysis was performed. **(G,H)** After the treatment, the cells were fixed and processed for indirect immunofluorescence analysis using the antibody against p-p65. Representative images and the analysis are shown. Statistical analyses were performed by using a *t*-test (two groups) or one-way ANOVA with a *post hoc* Student–Newman–Keuls test (multiple comparisons). The results are expressed as the mean ± SD of three independent experiments. Statistical comparisons to control group are indicated by $^{*}p < 0.05$, $^{**}p < 0.01$. Statistical comparisons to the heat stress group are indicated by $\#p < 0.05$.

expression downregulated by miR-155 mimic and heat stress. The addition of TO901317 significantly reversed the decreased LXRα expression induced by miR-155 mimic and heat stress, indicating effective treatment of LXRα agonist (**Figures 6A,B**). Meanwhile, the elevated phosphorylation of IκBα and p65 and the level of p65 translocation to nucleus induced by the miR-155 mimic and heat stress was also reversed by TO901317 (**Figures 6A,C,D**). Furthermore, indirect immunofluorescence studies demonstrated that the distribution changes of p65 in the nucleus were reversed by TO901317 (**Figures 6H,I**). Moreover, TO901317 blocked the upregulated protein levels of IL-6, IL-1β, and TNF-α induced by miR-155 and heat stress (**Figures 6E–G**). Taken together, these observations suggest that the effects of miR-155 on inflammatory responses and NF-κB activation are dependent on the LXRα pathway.

DISCUSSION

The inflammatory response plays a critical role in the injury process following hyperthermia in the CNS. In the present study, we observed a significant increase in miR-155 and proinflammatory cytokines after 2 h of heat stress at 42°C in BV-2 microglial cells. Moreover, inhibition of miR-155 significantly reduced the levels of proinflammatory cytokines, such as IL-6, IL-1β, and TNF-α. Overexpression of miR-155 augmented the release of these cytokines. These results indicated that miR-155 is involved in the heat stress-induced inflammatory response in BV-2 cells. Mechanistically, the NF-κB signaling pathway was found to be activated in heat-stressed BV-2 cells, and miR-155 overexpression could promote the NF-κB signaling pathway by inhibiting LXRα translation. In contrast, this enhanced inflammatory response could be alleviated by a specific agonist of LXRα, TO901317. Our results demonstrated that miR-155 overexpression controls LXRα activity, with subsequent NF-κB activation, thereby causing a robust promotion of the proinflammatory response in heat-stressed BV-2 cells.

Microglia are the inherent immune effector cells of the CNS and play a significant role in the inflammatory response of the CNS. Many stimuli, such as surface structures of bacteria, abnormal endogenous proteins, cytokines and physical stress, have been reported to trigger the transformation of resting microglia to activated states (Hwang et al., 2006; Du et al., 2010; Yang et al., 2010; Radler et al., 2014; Jin et al., 2016; Hoogland et al., 2018). Recently, accumulating evidence has demonstrated that heat stress as a physical stimulus can induce microglial activation in the brain (Biedenkapp and Leon, 2013; Kim et al., 2015; Lee et al., 2015). However, whether such activation is induced directly by heat stress or results from central nervous injury is still unknown. In this study, we observed a dramatic increase in CD11b expression in an *in vitro* model by exposing BV-2 cells to heat stress conditions. Our results confirmed that heat stress could directly induce microglial activation *in vitro*. Several studies have indicated that following activation, microglia can produce a range of inflammatory mediators, including cytokines, chemokines, prostaglandins, and NO (Herber et al., 2006; Fismen et al., 2012; Kim et al., 2018), which subsequently aggravate neuronal injury (Block et al., 2007). In addition, a number of studies showed that the expression of cytokines, such as IL-6, IL-1β, and TNF-α, was elevated in the CNS of heat-exposed mice (Biedenkapp and Leon, 2013; Lee et al., 2015; King et al., 2017). Consistently, our results showed significantly increased release of the proinflammatory factors IL-6, IL-1β, and TNF-α in BV-2 cells after heat exposure. These results suggest that heat stress, as an external physical factor, could facilitate microglial proinflammatory responses through the secretion of proinflammatory factors. Thus, this microglial reactivity may ultimately contribute to brain inflammation and related neurotoxicity under heat stress conditions.

The inflammatory response is characterized by coordinated activation of inflammatory mediators and various signaling pathways. NF-κB has long been considered an essential transcription factor for the induction of inflammatory mediators, such as COX-2, IL-6, IL-1β and TNF-α (Lawrence, 2009). When NF-κB is associated with inhibitory molecules of the IκB family in the cytosol, it is inactive. Correspondingly, the activation of NF-κB involves IκB phosphorylation and the translocation of the NF-κB dimer from the cytoplasm to the nucleus (Lawrence, 2009). Here, our experiments showed that heat stress immediately increased the phosphorylation levels of IκBα and p65; moreover, the phosphorylation was further increased during the recovery time. However, the expression of IκBα was not significantly changed in this study. These results indicate that NF-κB pathway activation induced by heat stress may be accompanied by phosphorylation of IκBα and p65 but not by bulk degradation of IκBα in microglia. Furthermore, other studies demonstrated that NF-κB signaling was activated by heat stress and contributed to the inflammatory responses in macrophages or apoptosis in HUVECs (Kretz-Remy et al., 2001; Lee et al., 2015; Liu et al., 2015; Hop et al., 2018). These observations suggest that heat exposure likely affects microglial activation and cytokine release through the activation of the NF-κB pathway.

Inflammation-related gene expression in the brain can be regulated not only by transcription factors at the transcriptional level but also by miRNAs at the post-transcriptional level. Many miRNAs play an important role in heat-related disease

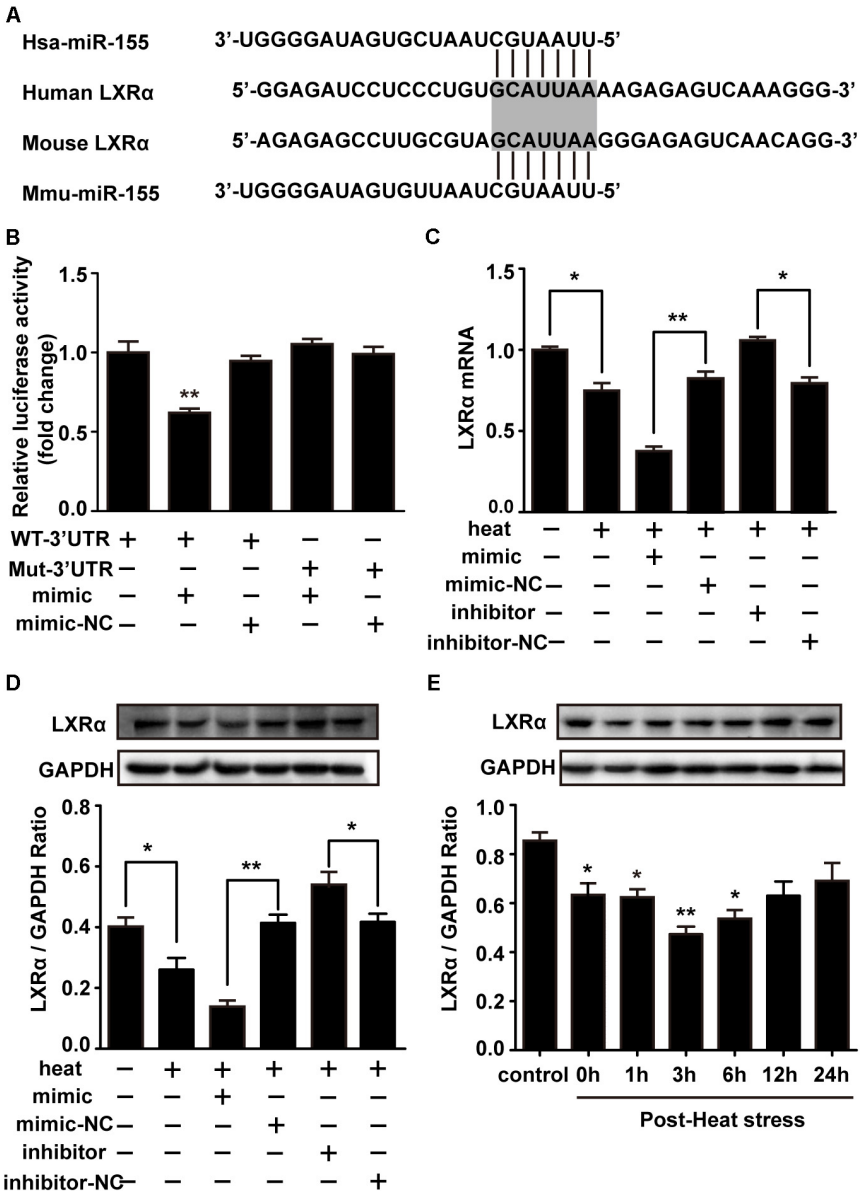

FIGURE 5 | Liver X receptor α is a functional target of miR-155. **(A)** A potential target site for human and mouse miR-155 in the 3′UTR of the LXRα mRNA. The seed region is highlighted. **(B)** Luciferase reporter assays were used to validate miR-155 binding of the LXRα 3′UTR in BV-2 cells. The luciferase reporter plasmids carrying the WT or Mut 3′UTR of LXRα and miR-155 mimic or mimic-NC were cotransfected into BV-2 cells for 24 h, and then, luciferase activity was detected. $^{*}p < 0.01$, relative to the mimic group. **(C,D)** BV-2 cells were transfected with miR-155 mimic, inhibitor, or their respective controls for 24 h. Then, the cells were subjected to a heat stress treatment at 42°C for 2 h, followed by a recovery period at 37°C for 6 h. Western blot and qRT-PCR were used to assess the protein and mRNA expression of LXRα. **(E)** Cells were subjected to a heat stress treatment at 42°C for 2 h, followed by a recovery period at 37°C for 0, 1, 3, 6, 12, or 24 h. The protein contents of LXRα were assayed by Western blot. Statistical analyses were performed by using a *t*-test (two groups) or one-way ANOVA with a *post hoc* Student–Newman-Keuls test (multiple comparisons). The results are expressed as the mean ± SD of three independent experiments. Statistical comparisons to the control group are indicated by $^{*}p < 0.05$, $^{**}p < 0.01$.

(Roufayel et al., 2014; Liu et al., 2017). Given that miR-155 is upregulated by heat stress in peripheral blood mononuclear cells, as shown by deep sequence data analysis (Sengar et al., 2018), and participates in the proinflammatory responses (Faraoni et al., 2009), we hypothesized that miR-155 was deeply involved in regulating heat stress-induced microglial activation and inflammation. The present results showed that the expression of miR-155 was elevated following heat exposure. In addition, ectopic high levels of miR-155 could increase, and blocking miR-155 could decrease, the production of IL-6, IL-1β, and TNF-α induced by heat stress. Meanwhile, miR-155 enhanced NF-κB activation in heat-stressed microglia. These results were consistent with those of other reports, which showed that miR-155 enhanced NF-κB signaling and cytokine release in oxidized

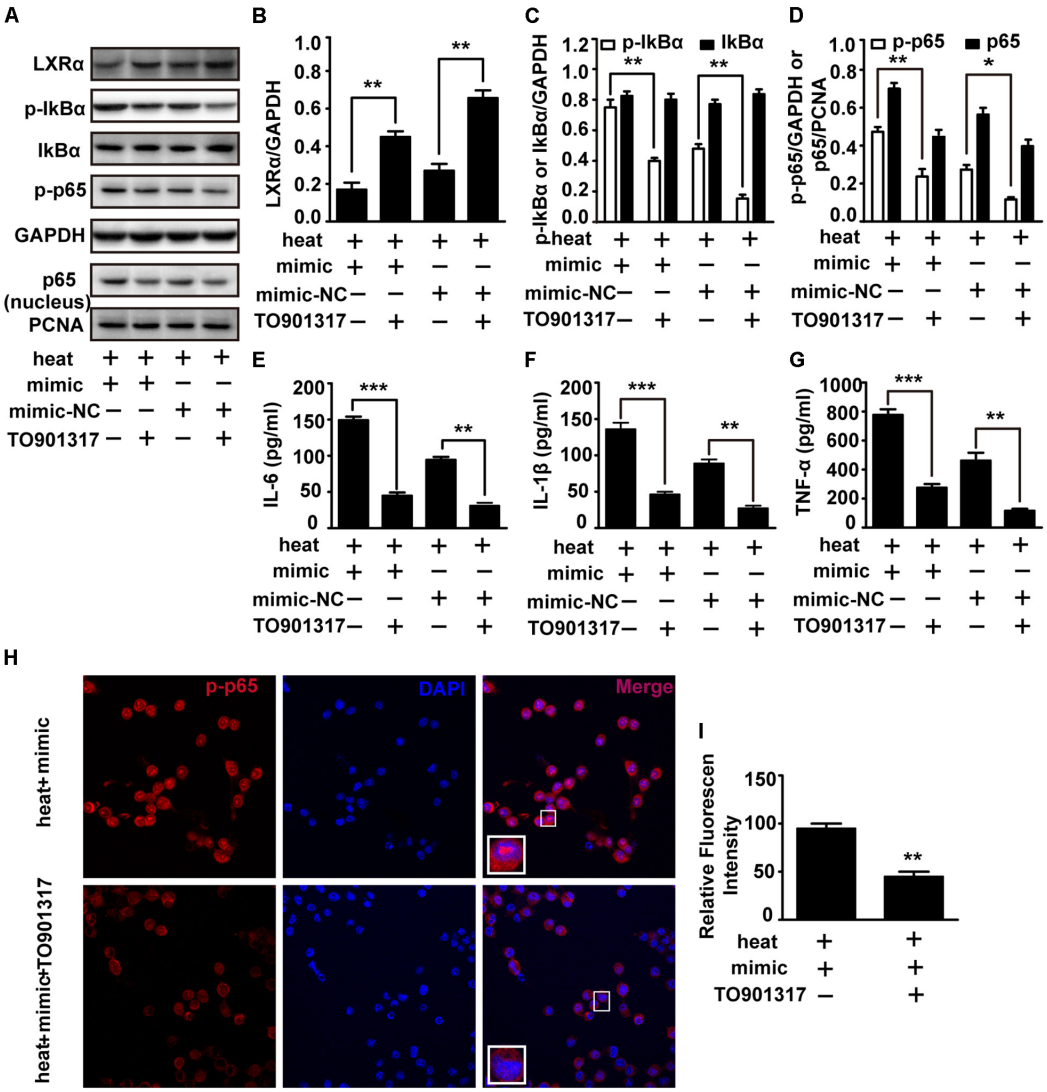

FIGURE 6 | An exogenous LXRα agonist ameliorates the effects of miR-155 and heat stress on the inflammatory responses and NF-κB activation in microglia. BV-2 cells were pretreated with or without 10 nM/ml TO901317 1 h before being transfected with miR-155 mimic or mimic control. Then, the cells were subjected to a heat stress treatment at 42°C for 2 h, followed by a recovery period at 37°C for 6 h. **(A)** Total protein expression levels of LXRα, IκBα, p-IκBα, p-p65, GAPDH and nucleus protein expression levels of p65 and PCNA were determined by Western blotting. **(B–D)** Densitometric analysis was performed. **(E–G)** The protein expression levels of IL-6, IL-1β, and TNF-α were assessed by ELISAs. **(H,I)** Indirect immunofluorescence analysis using the antibody against p-p65. Representative images and the analysis are shown. Statistical analyses were performed by using a *t*-test. The results are expressed as the mean ± SD of three independent experiments (*$p < 0.05$, **$p < 0.01$, ***$p < 0.001$).

low density lipoprotein (oxLDL)-stimulated macrophages (Yang et al., 2015; Ye et al., 2016). These results indicated that miR-155 acts as a promoter of inflammatory responses in heat-stressed microglia via the NF-κB pathway.

Among the miR-155 targets, LXRα attracted our attention. LXRs are oxysterol-activated nuclear receptors that play a pivotal role in cholesterol homeostasis, glycolipid metabolism and the inflammatory response (Zelcer, 2006; Yoon et al., 2013). In the CNS, LXRs are widespread in growing or mature neurons and glial cells (Mandrekar-Colucci and Landreth, 2011). Recent studies showed that LXRα could disrupt NF-κB activation by a process called *trans*-repression and thus has an anti-inflammatory function (Zhang-Gandhi and Drew, 2007; Mandrekar-Colucci and Landreth, 2011; Cui et al., 2012; Canavan et al., 2013). Therefore, we investigated the role of miR-155-LXRα in regulating the heat stress-induced inflammatory response to elucidate the underlying mechanism. First, we observed a significant inverse correlation between miR-155 and LXRα expression after heat exposure in microglia. Using a luciferase reporter assay, we verified LXRα as a target of miR-155 in heat-induced microglia. To test whether LXRα is involved in mediating the effects of miR-155 on inflammatory responses and NF-κB activation, we used the LXRα agonist TO901317 (Wu et al., 2016; Paterniti et al., 2017) to elevate the LXRα expression

downregulated by the miR-155 mimic and heat stress. The results showed that the elevated activation of NF-κB by the miR-155 mimic and heat stress was reversed by TO901317. Moreover, TO901317 blocked the upregulated protein levels of IL-6, IL-1β, and TNF-α induced by miR-155 and heat stress. Taken together, these observations suggest that the effects of miR-155 on inflammatory responses and NF-κB activation are dependent on the LXRα pathway. Furthermore, we found that TO901317 only partially reversed the changes evoked by the miR-155 mimic, suggesting that other targets might be involved in miR-155's function in heat stress-induced microglia.

Chronic inflammation has long been hypothesized to be a driving force in various diseases. Exploring the mechanism of inflammation in different cell types can provide support to the treatment of inflammation-related diseases. It has been demonstrated klotho can suppress inflammation by inactivating NF-κB activation in cardiomyocytes, which make it to be a potential therapeutic agent to treat diabetic cardiomyopathy (Guo et al., 2018). Wei et al. (2016) and Zou et al. (2017) proved that memantine and Cystain C can promote the cell survival of 6 -hydroxydopamine (6-OHDA)-lesioned PC12 cells by regulating Nurr77 or VEGF, indicating a new approach for the treatment of Parkinson's disease (PD). MPP^+-induced inflammatory activation of BV-2 microglia may be mediated by TLR4/NF-κB inflammatory signaling, involving the further discovery of PD pathophysiology (Zhou et al., 2016). In the present study, we validated that miR-155 aggravated the inflammatory response following heat stress in BV-2 cells. Given the different patterns of inflammatory responses in various diseases, the discovery of miR-155-NF-κB pathway in heat stressed-microglia may be a new breakthrough in the treatment of CNS inflammation in heat stroke. Although we preliminary revealed this inflammatory mechanism in BV-2 cells, serial verified researches toward this issue should be concerned, especially the employment of primary microglia cultures and animal experiments.

CONCLUSION

In this study, we investigated the effect of miR-155 on the heat stress-induced inflammatory response in BV-2 microglial cells. We found that excessive heat stress is a physical stimulus that can activate microglia and provoke inflammatory cytokines release. In this process, miR-155, as a regulator, enhanced inflammatory factors expression by increasing NF-κB signaling pathway activation via targeting LXRα. Regardless of the detailed mechanism, the data presented in this study may provide new insight into the mechanism of heat-related diseases.

AUTHOR CONTRIBUTIONS

X-SY, PL, and GW designed the research. PL, GW, X-LZ, XL, JY, ZL, and T-TS performed the experiments. PL, GW, X-SY, X-LZ, and G-LH analyzed the data. PL and X-SY wrote the manuscript. All authors reviewed the manuscript.

FUNDING

This work was funded by the National Natural Science Foundation of China (No. 81773396) and Major Project of the "Twelfth Five-year Plan" for Logistic Scientific Research of PLA (No. AWS17J014).

ACKNOWLEDGMENTS

We thank Li-Ting Wang for help with confocal microscopy.

REFERENCES

Beckers, L., Stroobants, S., D'Hooge, R., and Baes, M. (2018). Neuronal dysfunction and behavioral abnormalities are evoked by neural cells and aggravated by inflammatory microglia in peroxisomal β-oxidation deficiency. *Front. Cell. Neurosci.* 12:136 doi: 10.3389/fncel.2018.00136

Biber, K., Owens, T., and Boddeke, H. (2014). What is microglia neurotoxicity (Not)? *Glia* 62, 841-854. doi: 10.1002/glia.22654

Biedenkapp, J. C., and Leon, L. R. (2013). Increased cytokine and chemokine gene expression in the CNS of mice during heat stroke recovery. *Am. J. Phys. Regul. Integr. Comp. Physiol.* 305, R978–R986. doi: 10.1152/ajpregu.00011.2013

Block, M. L., Zecca, L., and Hong, J. (2007). Microglia-mediated neurotoxicity: uncovering the molecular mechanisms. *Nat. Rev. Neurosci.* 8, 57–69. doi: 10.1038/nrn2038

Bouchama, A K. J. (2002). Heat stroke. *N. Engl. J. Med.* 25, 1978–1988. doi: 10.1056/NEJMra011089

Brown, G. C., and Vilalta, A. (2015). How microglia kill neurons. *Brain Res.* 1628, 288–297. doi: 10.1016/j.brainres.2015.08.031

Canavan, M., McCarthy, C., Larbi, N. B., Dowling, J. K., Collins, L., O'Sullivan, F., et al. (2013). Activation of liver X receptor suppresses the production of the IL-12 family of cytokines by blocking nuclear translocation of NF-κBp50. *Innate Immun. Lond.* 20, 675–687. doi: 10.1177/1753425913501915

Cardoso, A. L., Guedes, J. R., Pereira, D. A. L., and Pedroso, D. L. M. (2012). miR-155 modulates microglia-mediated immune response by down-regulating SOCS-1 and promoting cytokine and nitric oxide production. *Immunology* 135, 73–88. doi: 10.1111/j.1365-2567.2011.03514x

Ceppi, M., Pereira, P. M., Dunand-Sauthier, I., Barras, E., Reith, W., Santos, M. A., et al. (2009). MicroRNA-155 modulates the interleukin-1 signaling pathway in activated human monocyte-derived dendritic cells. *Proc. Natl. Acad. Sci. U.S.A.* 106, 2735–2740. doi: 10.1073/pnas.0811073106

Chauhan, N. R., Kapoor, M., Prabha Singh, L., Gupta, R. K., Chand Meena, R., Tulsawani, R., et al. (2017). Heat stress-induced neuroinflammation and aberration in monoamine levels in hypothalamus are associated with temperature dysregulation. *Neuroscience* 358, 79–92. doi: 10.1016/j.neuroscience.2017.06.023

Chen, S. H., Lin, M. T., and Chang, C. P. (2013). Ischemic and oxidative damage to the hypothalamus may be responsible for heat stroke. *Curr. Neuropharmacol.* 11, 129–140. doi: 10.2174/1570159X11311020001

Cheray, M., and Joseph, B. (2018). Epigenetics Control Microglia Plasticity. *Front. Cell. Neurosci.* 12:243. doi: 10.3389/fncel.2018.00243

Cui, W., Sun, Y., Wang, Z., Xu, C., Peng, Y., and Li, R. (2012). Liver X receptor activation attenuates inflammatory response and protects cholinergic neurons in APP/PS1 transgenic mice. *Neuroscience* 210, 200–210. doi: 10.1016/j.neuroscience.2012.02.047

de Wit, N. M., Vanmol, J., Kamermans, A., Hendriks, J., and de Vries, H. E. (2017). Inflammation at the blood-brain barrier: the role of liver X receptors. *Neurobiol. Dis.* 107, 57–65. doi: 10.1016/j.nbd.2016.09.015

Du, F., Yin, L., Shi, M., Cheng, H., Xu, X., Liu, Z., et al. (2010). Involvement of microglial cells in infrasonic noise-induced stress via upregulated expression of corticotrophin releasing hormone type 1 receptor. *Neuroscience* 167, 909–919. doi: 10.1016/j.neuroscience.2010.02.060

Dwyer, J. B., and Ross, D. A. (2016). Modern microglia: novel targets in psychiatric neuroscience. *Biol. Psychiat.* 80, e47–e49. doi: 10.1016/j.biopsych.2016.08.006

Faraoni, I., Antonetti, F. R., Cardone, J., and Bonmassar, E. (2009). miR-155 gene: a typical multifunctional microRNA. *Biochimica Biophys. Acta* 1792, 497-505. doi: 10.1016/j.bbadis.2009.02.013

Fernando, M. S., Simpson, J. E., Matthews, F., Brayne, C., Lewis, C. E., Barber, R., et al. (2006). White matter lesions in an unselected cohort of the elderly. *Stroke* 37, 1391–1398. doi: 10.1161/01.STR.0000221308.94473.14

Fismen, L., Hjelde, A., Svardal, A. M., and Djurhuus, R. (2012). Differential effects on nitric oxide synthase, heat shock proteins and glutathione in human endothelial cells exposed to heat stress and simulated diving. *Eur. J. Appl. Physiol.* 112, 2717–2725. doi: 10.1007/s00421-011-2241-4

Ginhoux, F., Lim, S., Hoeffel, G., Low, D., and Huber, T. (2013). Origin and differentiation of microglia. *Front. Cell. Neurosci.* 7:45 doi: 10.3389/fncel.2013.00045

Guerrero, W. R., Varghese, S., Savitz, S., and Wu, T. C. (2013). Heat stress presenting with encephalopathy and MRI findings of diffuse cerebral injury and hemorrhage. *BMC Neurol.* 13, 63–66. doi: 10.1186/1471-2377-13-63

Guo, Y., Zhuang, X., Huang, Z., Zou, J., Yang, D., Hu, X., et al. (2018). Klotho protects the heart from hyperglycemia-induced injury by inactivating ROS and NF-κB-mediated inflammation both in vitro and in vivo. *Biochim. Biophys. Acta* 1864, 238–251. doi: 10.1016/j.bbadis.2017.09.029

Herber, D. L., Maloney, J. L., Roth, L. M., Freeman, M. J., Morgan, D., and Gordon, M. N. (2006). Diverse microglial responses after intrahippocampal administration of lipopolysaccharide. *Glia* 53, 382–391. doi: 10.1002/glia.20272

Hifumi, T., Kondo, Y., Shimizu, K., and Miyake, Y. (2018). Heat stroke. *J. Inten. Care* 6:30. doi: 10.1186/s40560-018-0298-4

Hoogland, I. C. M., Houbolt, C., van Westerloo, D. J., van Gool, W. A., and van de Beek, D. (2015). Systemic inflammation and microglial activation: systematic review of animal experiments. *J. Neuroinflamm.* 12:114. doi: 10.1186/s12974-015-0332-6

Hoogland, I. C. M., Westhoff, D., Engelen-Lee, J., Melief, J., Valls Serón, M., Houben-Weerts, J. H. M. P., et al. (2018). Microglial Activation After Systemic Stimulation with Lipopolysaccharide and *Escherichia coli*. *Front. Cell. Neurosci.* 12:110 doi: 10.3389/fncel.2018.00110

Hop, H. T., Arayan, L. T., Reyes, A. W. B., Huy, T. X. N., Min, W. G., Lee, H. J., et al. (2018). Heat-stress-modulated induction of NF-κB leads to brucellacidal pro-inflammatory defense against Brucella abortus infection in murine macrophages and in a mouse model. *BMC Microbiol.* 18, 44–56. doi: 10.1186/s12866-018-1185-9

Hwang, S., Jung, J., Kim, T., Lim, S., Oh, E., Kim, J., et al. (2006). Ionizing radiation induces astrocyte gliosis through microglia activation. *Neurobiol. Dis.* 21, 457–467. doi: 10.1016/j.nbd.2005.08.006

Jin, S., Kim, J. G., Park, J. W., Koch, M., Horvath, T. L., and Lee, B. J. (2016). Hypothalamic TLR2 triggers sickness behavior via a microglia-neuronal axis. *Sci. Rep.* 6:29424. doi: 10.1038/srep29424

Kim, M. E., Park, P. R., Na, J. Y., Jung, I., Cho, J. H., and Lee, J. S. (2018). Anti-neuroinflammatory effects of galangin in LPS-stimulated BV-2 microglia through regulation of IL-1beta production and the NF-kappaB signaling pathways. *Mol. Cell. Biochem.* doi: 10.1007/s11010-018-3401-1 [Epub ahead of print].

Kim, M. J., Cho, J. H., Cho, J., Park, J. H., Ahn, J. H., Tae, H., et al. (2015). Impact of hyperthermia before and during ischemia–reperfusion on neuronal damage and gliosis in the gerbil hippocampus induced by transient cerebral ischemia. *J. Neurol. Sci.* 348, 101–110. doi: 10.1016/j.jns.2014.11.015

King, M. A., Leon, L. R., Morse, D. A., and Clanton, T. L. (2017). Unique cytokine and chemokine responses to exertional heat stroke in mice. *J. Appl. Physiol.* 122, 296–306. doi: 10.1152/japplphysiol.00667.2016

Kretz-Remy, C., Munsch, B., and Arrigo, A. (2001). NFκB-dependent transcriptional activation during heat shock recovery. *J. Biol. Chem.* 276, 43723–43733. doi: 10.1074/jbc.M010821200

Kurowska-Stolarska, M., Hasoo, M. K., Welsh, D. J., Stewart, L., McIntyre, D., Morton, B. E., et al. (2017). The role of microRNA-155/liver X receptor pathway in experimental and idiopathic pulmonary fibrosis. *J. Allergy Clin. Immun.* 139, 1946–1956. doi: 10.1016/j.jaci.2016.09.021

The nuclear factor NF- kappaB pathway in inflammation. *Csh. Perspect. Biol. 1*, a001651-a001651. doi: 10.1101/cshperspect.a001651

Lee, W., Moon, M., Kim, H. G., Lee, T. H., and Oh, M. S. (2015). Heat stress-induced memory impairment is associated with neuroinflammation in mice. *J. Neuroinflamm.* 12:102. doi: 10.1186/s12974-015-0324-6

Leon, L. R., and Bouchama, A. (2015). Heat stroke. *Compr. Physiol.* 2, 611–647. doi: 10.1002/cphy.c140017

Lin, Y., Liu, T., Hu, C., Chen, C., and Wang, J. (2018). Expressions of chemokines and their receptors in the brain after heat stroke-induced cortical damage. *J. Neuroimmunol.* 318, 15–20. doi: 10.1016/j.jneuroim.2018.01.014

Liu, Y., Zhou, G., Wang, Z., Guo, X., Xu, Q., Huang, Q., et al. (2015). NF-κB signaling is essential for resistance to heat stress-induced early stage apoptosis in human umbilical vein endothelial cells. *Sci. Rep.* 5:13547. doi: 10.1038/srep13547

Liu, J., Zhu, G., Xu, S., Liu, S., Lu, Q., and Tang, Z. (2017). Analysis of miRNA expression profiling in human umbilical vein endothelial cells affected by heat stress. *Int. J. Mol. Med.* 40, 1719–1730. doi: 10.3892/ijmm.2017.3174

Lopez-Ramirez, M. A., Wu, D., Pryce, G., Simpson, J. E., Reijerkerk, A., King-Robson, J., et al. (2014). MicroRNA-155 negatively affects blood–brain barrier function during neuroinflammation. *FASEB J.* 28, 2551–2565. doi: 10.1096/fj.13-248880

Mandrekar-Colucci, S., and Landreth, G. E. (2011). Nuclear receptors as therapeutic targets for Alzheimer's disease. *Expert Opin. Ther. Tar.* 15, 1085–1097. doi: 10.1517/14728222.2011.594043

Mashima, R. (2015). Physiological roles of miR-155. *Immunology* 145, 323–333. doi: 10.1111/imm.12468

Mattis, J. G., and Yates, A. M. (2011). Heat stroke: helping patients keep their cool. *Nurse Pract.* 36, 48–52. doi: 10.1097/01.NPR.0000396476.99238.39

Miller, A. M., Gilchrist, D. S., Nijjar, J., Araldi, E., Ramirez, C. M., Lavery, C. A., et al. (2013). MiR-155 has a protective role in the development of non-alcoholic hepatosteatosis in mice. *PLoS One* 8:e72324. doi: 10.1371/journal.pone.0072324

Nguyen, D. P., Li, J., Yadav, S. S., and Tewari, A. K. (2014). Recent insights into NF-κB signalling pathways and the link between inflammation and prostate cancer. *BJU Int.* 114, 168–176. doi: 10.1111/bju.12488

Paterniti, I., Campolo, M., Siracusa, R., Cordaro, M., Di Paola, R., Calabrese, V., et al. (2017). Liver X receptors activation, through TO901317 binding, reduces neuroinflammation in Parkinson's disease. *PLoS One* 12:e0174470. doi: 10.1371/journal.pone.0174470

Pena-Philippides, J.C., Caballero-Garrido, E., Lordkipanidze, T., and Roitbak, T. (2016). *In vivo* inhibition of miR-155 significantly alters post-stroke inflammatory response. *J. Neuroinflamm.* 13:287. doi: 10.1186/s12974-016-0753-x

Radler, M. E., Hale, M. W., and Kent, S. (2014). Calorie restriction attenuates lipopolysaccharide (LPS)-induced microglial activation in discrete regions of the hypothalamus and the subfornical organ. *Brain Behav. Immun.* 38, 13–24. doi: 10.1016/j.bbi.2013.11.014

Roufayel, R., Johnston, D. S., and Mosser, D. D. (2014). The elimination of miR-23a in heat-stressed cells promotes NOXA-induced cell death and is prevented by HSP70. *Cell Death Dis.* 5:e1546. doi: 10.1038/cddis.2014.484

Roy, A., Fung, Y. K., Liu, X., and Pahan, K. (2006). Up-regulation of Microglial CD11b Expression by Nitric Oxide. *J. Biol. Chem.* 281, 14971–14980. doi: 10.1074/jbc.M600236200

Saika, R., Sakuma, H., Noto, D., Yamaguchi, S., Yamamura, T., and Miyake, S. (2017). MicroRNA-101a regulates microglial morphology and inflammation. *J. Neuroinflamm.* 14:109. doi: 10.1186/s12974-017-0884-8

Sengar, G. S., Deb, R., Singh, U., Raja, T. V., Kant, R., Sajjanar, B., et al. (2018). Differential expression of microRNAs associated with thermal stress in Frieswal (*Bos taurus* x Bos indicus) crossbred dairy cattle. *Cell Stress Chaperones* 23, 155–170. doi: 10.1007/s12192-017-0833-6

Sharma, H. S., and Hoopes, P. J. (2003). Hyperthermia induced pathophysiology of the central nervous system. *Int. J. Hyperthermia* 19, 325–354. doi: 10.1080/0265673021000054621

Skerrett, R., Malm, T., and Landreth, G. (2014). Nuclear receptors in neurodegenerative diseases. *Neurobiol. Dis.* 72, 104–116. doi: 10.1016/j.nbd.2014.05.019

Thounaojam, M. C., Kaushik, D. K., and Basu, A. (2013). MicroRNAs in the brain: it's regulatory role in neuroinflammation. *Mol. Neurobiol.* 47, 1034–1044. doi: 10.1007/s12035-013-8400-3

Tili, E., Michaille, J. J., Cimino, A., Costinean, S., Dumitru, C. D., Adair, B., et al. (2007). Modulation of miR-155 and miR-125b levels following lipopolysaccharide/TNF-alpha stimulation and their possible roles in regulating the response to endotoxin shock. *J. Immunol.* 179, 5082–5089. doi: 10.4049/jimmunol.179.8.5082

Wang, J., Xiao, C., Wei, Z., Wang, Y., Zhang, X., and Fu, Y. (2018). Activation of liver X receptors inhibit LPS-induced inflammatory response in primary bovine mammary epithelial cells. *Vet. Immunol. Immunop.* 197, 87–92. doi: 10.1016/j.vetimm.2018.02.002

Wang, X., Chen, S., Ni, J., Cheng, J., Jia, J., and Zhen, X. (2018). miRNA-3473b contributes to neuroinflammation following cerebral ischemia. *Cell Death Dis.* 9, 11–24. doi: 10.1038/s41419-017-0014-7

Wei, X., Gao, H., Zou, J., Liu, X., Chen, D., Liao, J., et al. (2016). Contra-directional coupling of Nur77 and Nurr1 in Neurodegeneration: a novel mechanism for memantine-induced anti-inflammation and anti-mitochondrial impairment. *Mol. Neurobiol.* 53, 5876–5892. doi: 10.1007/s12035-015-9477-7

Wen, Y., Zhang, X., Dong, L., Zhao, J., Zhang, C., and Zhu, C. (2015). Acetylbritannilactone modulates MicroRNA-155-mediated inflammatory response in ischemic cerebral tissues. *Mol. Med.* 21, 197–209. doi: 10.2119/molmed.2014.00199

Woodbury, M. E., Freilich, R. W., Cheng, C. J., Asai, H., Ikezu, S., Boucher, J. D., et al. (2015). miR-155 is essential for inflammation-induced hippocampal neurogenic dysfunction. *J. Neurosci.* 35, 9764–9781. doi: 10.1523/JNEUROSCI.4790-14.2015

Wu, C., Chen, C., Lai, C., Hung, T., Lin, C., Chao, M., et al. (2016). Treatment with TO901317, a synthetic liver X receptor agonist, reduces brain damage and attenuates neuroinflammation in experimental intracerebral hemorrhage. *J. Neuroinflamm.* 13:62. doi: 10.1186/s12974-016-0524-8

Yan, Y., Zhao, Y., Wang, H., and Fan, M. (2006). Pathophysiological factors underlying heatstroke. *Med. Hypotheses* 67, 609–617. doi: 10.1016/j.mehy.2005.12.048

Yang, X., He, G., Hao, Y., Chen, C., Li, M., Wang, Y., et al. (2010). The role of the JAK2-STAT3 pathway in pro-inflammatory responses of EMF-stimulated N9 microglial cells. *J. Neuroinflamm.* 7, 54–67. doi: 10.1186/1742-2094-7-54

Yang, X., Wang, L., Wu, H., and Jiao, L. (2018). Effects of prebiotic galacto-oligosaccharide on postoperative cognitive dysfunction and neuroinflammation through targeting of the gut-brain axis. *BMC Anesthesiol.* 18:177. doi: 10.1186/s12871-018-0642-1

Yang, Y., Yang, L., Liang, X., and Zhu, G. (2015). MicroRNA-155 Promotes Atherosclerosis Inflammation via Targeting SOCS1. *Cell. Physiol. Biochem.* 36, 1371-1381. doi: 10.1159/000430303

Ye, J., Guo, R., Shi, Y., Qi, F., Guo, C., and Yang, L. (2016). miR-155 regulated inflammation response by the SOCS1-STAT3-PDCD4 axis in atherogenesis. *Mediat. Inflamm.* 2016, 1–14. doi: 10.1155/2016/8060182

Yoon, C. H., Kwon, Y. J., Lee, S. W., Park, Y. B., Lee, S. K., and Park, M. C. (2013). Activation of liver X receptors suppresses inflammatory gene expressions and transcriptional corepressor clearance in rheumatoid arthritis fibroblast like synoviocytes. *J. Clin. Immunol.* 33, 190–199. doi: 10.1007/s10875-012-9799-4

Zelcer, N. (2006). Liver X receptors as integrators of metabolic and inflammatory signaling. *J. Clin. Invest.* 116, 607–614. doi: 10.1172/JCI27883

Zhang, X., Yang, R., Hu, B., Lu, P., Zhou, L., He, Z., et al. (2017). Reduced circulating levels of miR-433 and miR-133b are potential biomarkers for Parkinson's disease. *Front. Cell. Neurosci.* 11:170. doi: 10.3389/fncel.2017.00170

Zhang-Gandhi, C. X., and Drew, P. D. (2007). Liver X receptor and retinoid X receptor agonists inhibit inflammatory responses of microglia and astrocytes. *J. Neuroimmunol.* 183, 50–59. doi: 10.1016/j.jneuroim.2006.11.007

Zhou, P., Weng, R., Chen, Z., Wang, R., Zou, J., Liu, X., et al. (2016). TLR4 signaling in MPP+ -induced activation of BV-2 Cells. *Neural Plast.* 2016, 1–9. doi: 10.1155/2016/5076740

Zou, J., Chen, Z., Wei, X., Chen, Z., Fu, Y., Yang, X., et al. (2017). Cystatin C as a potential therapeutic mediator against Parkinson's disease via VEGF-induced angiogenesis and enhanced neuronal autophagy in neurovascular units. *Cell Death Dis.* 8:e2854. doi: 10.1038/cddis.2017.240

Conflict of Interest Statement: The authors declare that the research was conducted in the absence of any commercial or financial relationships that could be construed as a potential conflict of interest.

frontiers in Cellular Neuroscience

ORIGINAL RESEARCH
published: 06 June 2019
doi: 10.3389/fncel.2019.00258

Deletion of CD38 Suppresses Glial Activation and Neuroinflammation in a Mouse Model of Demyelination

Jureepon Roboon[1], Tsuyoshi Hattori[1], Hiroshi Ishii[1], Mika Takarada-Iemata[1], Thuong Manh Le[1], Yoshitake Shiraishi[2], Noriyuki Ozaki[2], Yasuhiko Yamamoto[3], Akira Sugawara[4], Hiroshi Okamoto[3,5], Haruhiro Higashida[6], Yasuko Kitao[1] and Osamu Hori[1]*

[1] Department of Neuroanatomy, Graduate School of Medical Sciences, Kanazawa University, Kanazawa, Japan, [2] Department of Functional Anatomy, Graduate School of Medical Sciences, Kanazawa University, Kanazawa, Japan, [3] Department of Biochemistry and Molecular Vascular Biology, Graduate School of Medical Sciences, Kanazawa University, Kanazawa, Japan, [4] Department of Molecular Endocrinology, Tohoku University Graduate School of Medicine, Sendai, Japan, [5] Department of Biochemistry, Tohoku University Graduate School of Medicine, Sendai, Japan, [6] Research Center for Child Mental Development, Kanazawa University, Kanazawa, Japan

OPEN ACCESS

Edited by:
Xiaobo Mao, Johns Hopkins University, United States

Reviewed by:
Robert Weissert, University of Regensburg, Germany
Jorge Matias-Guiu, Complutense University of Madrid, Spain

***Correspondence:**
Tsuyoshi Hattori
thattori@staff.kanazawa-u.ac.jp

Specialty section:
This article was submitted to Non-Neuronal Cells, a section of the journal Frontiers in Cellular Neuroscience

Received: *11 March 2019*
Accepted: *23 May 2019*
Published: *06 June 2019*

Citation:
Roboon J, Hattori T, Ishii H, Takarada-Iemata M, Le TM, Shiraishi Y, Ozaki N, Yamamoto Y, Sugawara A, Okamoto H, Higashida H, Kitao Y and Hori O (2019) Deletion of CD38 Suppresses Glial Activation and Neuroinflammation in a Mouse Model of Demyelination. Front. Cell. Neurosci. 13:258. doi: 10.3389/fncel.2019.00258

CD38 is an enzyme that catalyzes the synthesis of cyclic adenosine diphosphate-ribose from nicotinamide adenine dinucleotide (NAD^+). We recently reported that this molecule regulates the maturation and differentiation of glial cells such as astrocytes and oligodendrocytes (OLs) in the developing brain. To analyze its role in the demyelinating situation, we employed cuprizone (CPZ)-induced demyelination model in mice, which is characterized by oligodendrocyte-specific apoptosis, followed by the strong glial activation, demyelination, and repopulation of OLs. By using this model, we found that CD38 was upregulated in both astrocytes and microglia after CPZ administration. Experiments using wild-type and CD38 knockout (KO) mice, together with those using cultured glial cells, revealed that CD38 deficiency did not affect the initial decrease of the number of OLs, while it attenuated CPZ-induced demyelination, and neurodegeneration. Importantly, the clearance of the degraded myelin and oligodendrocyte repopulation were also reduced in CD38 KO mice. Further experiments revealed that these observations were associated with reduced levels of glial activation and inflammatory responses including phagocytosis, most likely through the enhanced level of NAD^+ in CD38-deleted condition. Our results suggest that CD38 and NAD^+ in the glial cells play a critical role in the demyelination and subsequent oligodendrocyte remodeling through the modulation of glial activity and neuroinflammation.

Keywords: demyelination, gliosis, cuprizone, neuroinflammation, NAD^+

INTRODUCTION

Multiple sclerosis (MS) is a chronic inflammatory, demyelinating, and degenerative disease of the central nervous system (CNS), and has been one of the leading causes of neurological disability among young adults. Although MS is generally considered an autoimmune disorder (Compston and Coles, 2008), evidence suggests that the activation of glial cells is also a prominent feature of the

demyelinating lesions (Cao and He, 2013; Bond et al., 2014), and that progressive MS is associated with chronic activation of glial cells in the CNS (Lassmann et al., 2012).

Cuprizone (CPZ)-induced experimental demyelination is a suitable rodent model to study the mechanisms leading to demyelination and subsequent remyelination in the CNS without a significant autoimmune lymphocytic response (Remington et al., 2007). In this model, the first pathological event is the selective apoptotic death of mature oligodendrocytes (OLs) in particular brain regions such as the corpus callosum (CC), which results in primary demyelination (Blakemore, 1972). However, the pathology of CPZ-induced demyelination also includes prominent astrocytic reactions and microglial invasion (Praet et al., 2014). In this model, astrocytes were suggested to exert an immune response through the expression of cytokines and recruitment of microglia to demyelinating lesions (Williams et al., 2007; Gudi et al., 2014). Recent studies demonstrated that ablation of astrocytes or astrocyte-targeted production of interleukin-6 led to a reduction in the activation and invasion of microglia into demyelinating lesions, which resulted in delayed demyelination and subsequently delayed oligodendrocyte precursor cell (OPC) proliferation, and remyelination (Skripuletz et al., 2013; Petkovic et al., 2016). Regarding microglial activation, some *in vitro* data suggest that CPZ-induced OL apoptosis requires the presence of microglia-derived proinflammatory mediators such as TNFα and inducible nitric oxide synthase (iNOS) (Pasquini et al., 2007; Raposo et al., 2013).

CD38 is an enzyme that catalyzes the synthesis of cyclic adenosine diphosphate-ribose (cADPR) from nicotinamide adenine dinucleotide (NAD^+) (Lee, 2001; Malavasi et al., 2008). CD38 has been shown to promote the secretion of oxytocin from hypothalamic neurons and insulin from pancreatic beta cells (Takasawa et al., 1993; Jin et al., 2007). In the brain, however, CD38 expression has been observed not only in oxytocin neurons, but also in glial cells, including astrocytes and microglia (Yamada et al., 1997; Akimoto et al., 2013). We have demonstrated that astrocytic CD38 regulates maturation of astrocytes and differentiation of OPCs into OLs by consuming NAD^+ in the brain under physiological conditions (Hattori et al., 2017). In pathological conditions, CD38 has been reported to be involved in the activation of microglia and astrocytes in mouse models of glioma and traumatic brain injury, and human HIV-infected brains (Kou et al., 2009; Levy et al., 2009, 2012). However, the role of CD38 in demyelination is still unclear, although its involvement in the modulation of T-cell activation was reported in the experimental autoimmune encephalomyelitis (EAE), another widely used animal model of MS (Herrmann et al., 2016).

In this study, we investigated the role of CD38 in CPZ-induced demyelination model. We found that CD38 was upregulated in both astrocytes and microglia in the demyelinating area after CPZ administration. CD38 deficiency attenuated glial activation and demyelination, most likely through the enhanced level of NAD^+, while it suppressed myelin clearance, and OL repopulation. These observations suggest critical roles of CD38 and NAD^+ in the glial cells in the processes of demyelination and neuroinflammation.

MATERIALS AND METHODS

Chemicals

The chemicals used in this study are as follows: bis-cyclohexanone oxaldihydrazone (CPZ) (C9012, Sigma-Aldrich, St. Louis, MO, United States), LPS (20389-04, Nacalai Tesque, Kyoto, Japan), β-NAD^+ (24334-97, Nacalai Tesque), 8-bromo-cADPR (8-Br-cADPR) (151898-26-9, Santa Cruz Biotechnology), 3-(4,5-dimethyl-2-thiazolyl)-2,5-diphenyltetrazolium bromide (MTT) (29893-1, Nacalai Tesque), and phenazine methosulfate (PMS) (26712-51, Nacalai Tesque).

Animals

Wild-type (WT) and CD38 knockout (KO) male ICR mice were used for the experiments (body weight; 30–35 g). CD38 KO mice were generated as described previously, and backcrossed for more than eight times (Kato et al., 1999). All mice were housed at mouse cage (345 mm × 168 mm × 140 mm) in a temperature-controlled room (24°C) with a 12 :12 light-dark cycle. The animals were killed at various time points as described in Section "Results." All animal experiments were performed in accordance with the guidelines and approved by the Animal Care and Use Committee of Kanazawa University (AP-143305).

Cuprizone Administration

To induce demyelination in 10-week-old ICR male mice, they were administered a diet containing 0.4% CPZ mixed into standard rodent chow ground into a fine powder, as previously described (Song et al., 2007). The powder was served in small ceramic bowls placed into the cages, which were cleaned twice weekly. The mice were fed CPZ for 1, 2, 3, or 5 weeks. Control mice were fed standard rodent chow.

Quantitative Real-Time Polymerase Chain Reaction

RNA was extracted from brain tissue or cultured cells using RNeasy® Mini Kit (74106, Qiagen, Hilden, Germany). Total RNA was reverse-transcribed using the High-Capacity cDNA Reverse Transcription Kit (4368814, Applied Biosystems, Warrington, United Kingdom) and analyzed by quantitative real-time polymerase chain reaction (RT-qPCR). RT-qPCR was performed as previously described (Hattori et al., 2010). Individual cDNA sequences were amplified using the Thunderbird™ SYBR qPCR® Mix (QPS-201, Toyobo Co., Ltd.) using specific primers. The comparative Ct method was used for data analyses in MxPro 4.10 (Agilent Technologies). Specific ratio comparisons (gene of interest/*Gapdh*) were used to evaluate differences in transcript expression between groups. The primer sequences are listed in **Supplementary Table 1**.

Western Blot Analyses

Samples from brains or cultured cells were homogenized in a buffer containing 1% NP-40, 0.1% sodium dodecyl sulfate (SDS), and 0.2% deoxycholate. Denatured lysates were electrophoretically separated using SDS-polyacrylamide gel electrophoresis, and proteins were transferred onto

polyvinylidene fluoride membranes. The membranes were then blocked in 5% skimmed milk for 30 min, incubated with anti-CD38 (AF4947, R&D systems, MN, United States, 1:500), anti-glial fibrillary acidic protein (GFAP) (G9269, Sigma, MO, United States, 1:5,000), anti-ionized calcium binding adaptor molecule 1 (Iba1) (019-19741, Wako, Osaka, Japan, 1:500), or anti-myelin basic protein (MBP) (MAB396, Merck Millipore, Darmstadt, Germany, 1:1,000) antibodies for 12 h at 4°C. The primary and secondary antibodies (for details see **Supplementary Table 2**) were used according the manufactures' instructions. The membranes were then incubated with anti-rabbit (SC-2004, 1:5,000), anti-mouse (SC-516102, 1:5,000), anti-goat (SC-2354, 1:1,000) or anti-rat (NA9350, Amersham Pharmacia biotech, 1:1000), horseradish peroxidase-linked immunoglobulin G (Cell Signaling Technology, Tokyo, Japan) for 2 h at room temperature. Immunoreactivity was detected using an enhanced chemiluminescence system (GE Healthcare Bio-Sciences, PA, United States). Densitometric quantification was performed using ImageJ software (https://imagej.nih.gov/ij/).

Immunohistochemistry

After perfusion with 4% paraformaldehyde (PFA), brains were removed from mice and subjected to post-fixation in 4% PFA, followed by dehydration in 30% sucrose. Twenty micrometer-thick sections from bregma +1.2 mm to bregma −1.4 mm were obtained using a cryostat (CM1950, Leica, Nussloch, Germany). To evaluate demyelination, endogenous peroxidase activity was blocked with 0.3% H_2O_2 in 70% methanol for 30 min. After blocking with normal goat serum, the sections were incubated with anti-MBP (MAB396, Merck Millipore, 1:100), anti-degraded MBP (dMBP) (AB5864, Merck Millipre, 1:2000), or anti-Amyloid Precursor Protein (APP) (MAB348, Millipore, 1:200) antibodies for overnight at 4°C. After washing in phosphate-buffered saline (PBS), the sections were incubated for 30 min at room temperature with the secondary antibody (MP-7444, MP7402, MP7401, ImmPRESS reagent, Vector Laboratories, Peterborough, United Kingdom), followed by further incubation in a peroxidase substrate solution [SK-4105, ImmPACT 3′-diaminobenzidine (DAB), Vector Laboratories). Demyelination areas in the CC were analyzed by light microscopy at 20× magnification (BZ-X710, Keyence) and quantified using ImageJ software. To determine the percentage of demyelination, the demyelinating area was divided by the total area.

For the detection of GFAP, Iba1, SMI-32, Platelet-derived growth factor receptor alpha (PDGFRα), adenomatous polyposis coli (APC), the sections were processed for immunostaining with antibodies against GFAP (1:2000), Iba1 (1:500), SMI-32 (801701, Biolegend, CA, United States 1:500), PDGFRα (sc-338, Santa Cruz Biotechnology, 1:500) and APC (OP80, Calbiochem, CA, United States, 1:100). Alexa488- or Cy3-conjugated secondary antibodies were used to visualize immunolabeling. Immunofluorescent staining of primary cultures was performed as previously described (Hattori et al., 2007). Imaging was performed on a laser scanning confocal microscope (Eclipse TE2000U, Nikon, Tokyo, Japan) using Nikon EZ-C1 software or a fluorescence microscope (BZ-X710). The numbers of APC-, GFAP-, and Iba1-positive cells with identified nuclei [4′,6-diamidino-2-phenylindole (DAPI)-stained] in the medial part of the CC from 2 sections per mouse were determined at a magnification of 20× (BZ-X710). The results are presented as the number of cells per mm^2.

In situ Hybridization-Immunohistochemistry

In situ hybridization was performed as previously described (Hattori et al., 2014). cDNA fragments of mouse CD38 were amplified by reverse transcription-PCR using the sense/antisense primer set of 5′-ATGCAGGGCGGGGGTCCCCGG- 3′/5′ -TCAGGCCTCGGTTTCCTGAG- 3′, and used as templates for probe synthesis. In brief, brains were removed from mice after perfusion with PBS and immediately placed at -80°C. Serial 14 μm-thick coronal sections were obtained using a cryostat and hybridized with digoxigenin-labeled *Cd38* RNA probes. After development and thorough washing, the brain sections were subjected to immunohistochemistry using primary antibodies such as polyclonal rabbit anti-GFAP (1:2,000), polyclonal rabbit anti-Iba1 (1:200), and mouse anti-APC (1:100). The sections were incubated with primary antibodies overnight at 4°C, and, after washing, were incubated with the secondary antibody (ImmPRESS reagent, Vector Laboratories) for 30 min at room temperature. After washing with PBS, the sections were incubated in a peroxidase substrate solution (ImmPACT DAB, Vector Laboratories). The numbers of GFAP- and Iba1-positive cells with CD38 mRNA expression in two sections per mouse were determined using a light microscope at a magnification of 40× (BZ-X710). Data are presented as the number of cells per mm^2.

Electron Microscopy

Mice were perfused with heparinized ringer solution followed by a fixative consisting of 2% paraformaldehyde and 2.5% glutaraldehyde in 30 mM HEPES-NaOH buffer (pH 7.4). The CC was cut from brains removed 2 h after perfusion and then fixed with the same fixative by immersion at 4*circ*C overnight. After washing with 30 mM HEPES-NaOH buffer (pH 7.4), the tissue blocks were post-fixed with 1% OsO4 for 2 h, dehydrated in increasing concentrations of ethanol, and embedded in Quetol 812 resin (NISSIN EM Co., Tokyo, Japan) at 65°C for 24 h. Sagittal-Vertical ultrathin sections were cut at about 80 nm thickness using an ultramicrotome (LKB-8800, LKB produkter, Bromma, Sweden) and collected on nickel grids (NISSIN EM Co.). The sections were stained with uranyl acetate and lead citrate, and analyzed in a transmission electron microscope (EM; JOEL, Tokyo, Japan) using an accelerating voltage of 80 kV. The photographs were analyzed using Image J Software to calculate the g-ratio. The g-ratio was calculated as previously described (Goebbels et al., 2010). To study the demyelinated axons of the CC, serial 1 μm-thick semi-thin sections were cut with a glass knife, stained with 1% toluidine blue, and examined by light microscopy at a magnification of 60× (BZ-X710). The number of myelinated axons was calculated as previously described (Fan et al., 2017). Eight sections, with an area of 650 μm^2 per section, were evaluated from 4 animals for each group. 100 axons from 2 mice in each group were analyzed to determine the g-ratio.

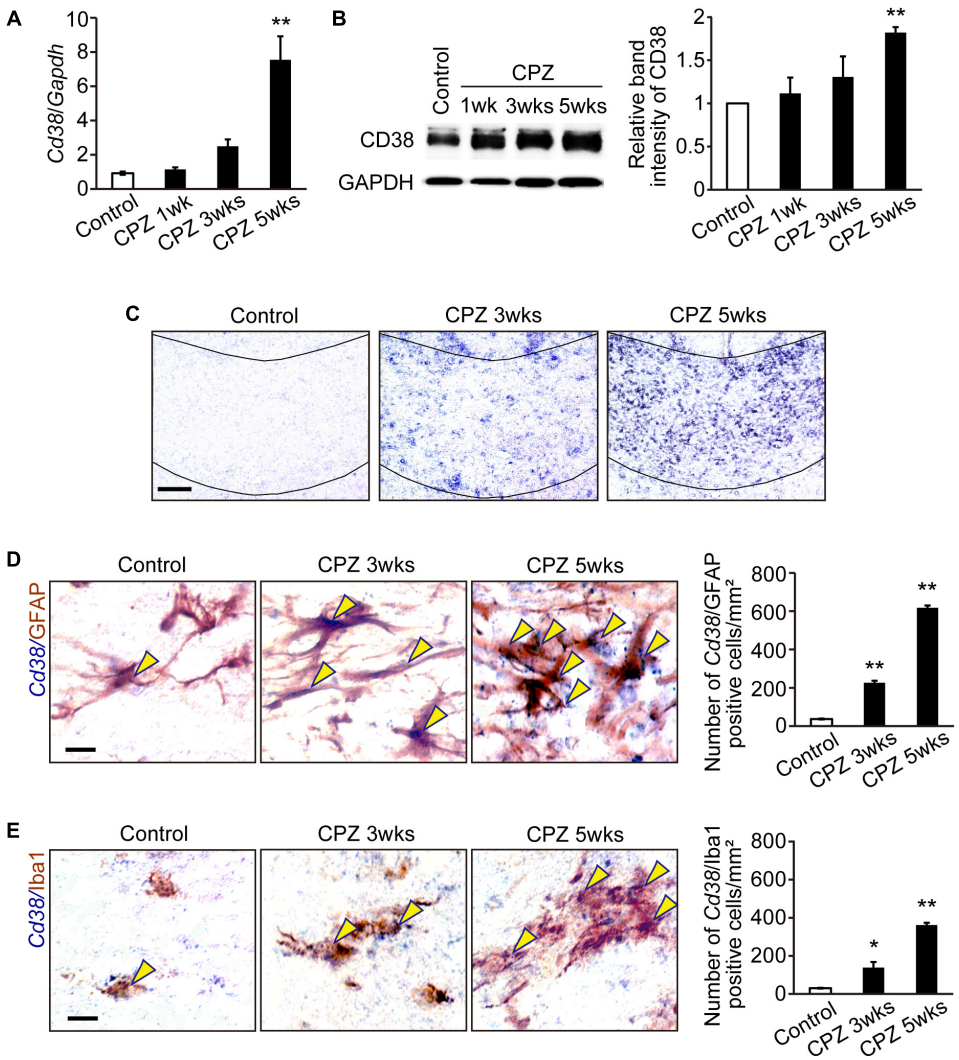

FIGURE 1 | CD38 expression was increased in demyelinating lesions. **(A)** RT-qPCR analysis for *Cd38* mRNA expression in the CC after administration of CPZ for 1, 3, and 5 weeks $n = 5$. **(B)** Western blotting analyses of CD38 in the CC after different periods of CPZ administration. The graph depicts the relative optical density of CD38 normalized to the loading control glyceraldehyde 3-phosphate dehydrogenase (GAPDH) $n = 5$. **(C)** *In situ* hybridization analyses in the CC after administration of CPZ for different period using an antisense RNA probe to *Cd38*. Scale bar: 100 μm. **(D,E)** Double *in situ* hybridization-immunohistochemistry analyses in the CC after CPZ administration for 3 and 5 weeks with an antisense RNA probe to *Cd38* and antibodies against GFAP (upper) and Iba1 (lower). Yellow arrowheads indicate *Cd38*-expressing astrocytes or microglia. The graph depict the numbers of *Cd38*/GFAP- or *Cd38*/Iba1-positive cells in the CC after CPZ administration for 3 and 5 weeks, $n = 4$. Data are expressed as mean ± SEM. Scale bars: 20 μm. *P* values are determined by one-way ANOVA followed by Tukey-kramer test. $^{*}p < 0.05$ and $^{**}p < 0.01$ vs. control.

Analysis of NAD Levels in the CC

Nicotinamide adenine dinucleotide (NAD^+ + NADH) levels were determined as previously described (Shibata and Murata, 1986). In brief, the CC was harvested from WT and CD38 KO mice after administration of CPZ for 5 weeks. The tissue was weighed and homogenized in an extraction buffer or 50 mM potassium phosphate buffer (pH 6.0) containing 100 mM nicotinamide using hand-held homogenizers. The samples were centrifuged at 8000 × *g* for 3 min following incubation at 90°C for 1.5 min. The supernatant (50 μl) was incubated at 37°C for 10 min in 32.5 mM glycylglycine-NaOH buffer, 50 mM nicotinamide, 0.25 M EtOH, 0.083 mg/ml MTT, and 0.27 mg/ml PMS (pH 7.4). After the addition of alcohol dehydrogenase (12.5 IU/ml), the increase in absorbance at 570 nm was monitored using a Multiskan GO Microplate Spectrophotometer (Thermo Fischer Scientific, MA, United States). The values were normalized to milligrams of tissue or protein.

Glial Cell Cultures

Cerebral cortices from WT and CD38 KO neonatal mice (P1 to P3) were harvested and digested at 37°C by Dispase II (383-02281, 2 mg/mL, Wako). The Cells were plated in 75-cm^2 culture flasks (Corning) in Dulbecco's Modified Eagle Medium (DMEM) supplemented with 10% fetal bovine serum (FBS)

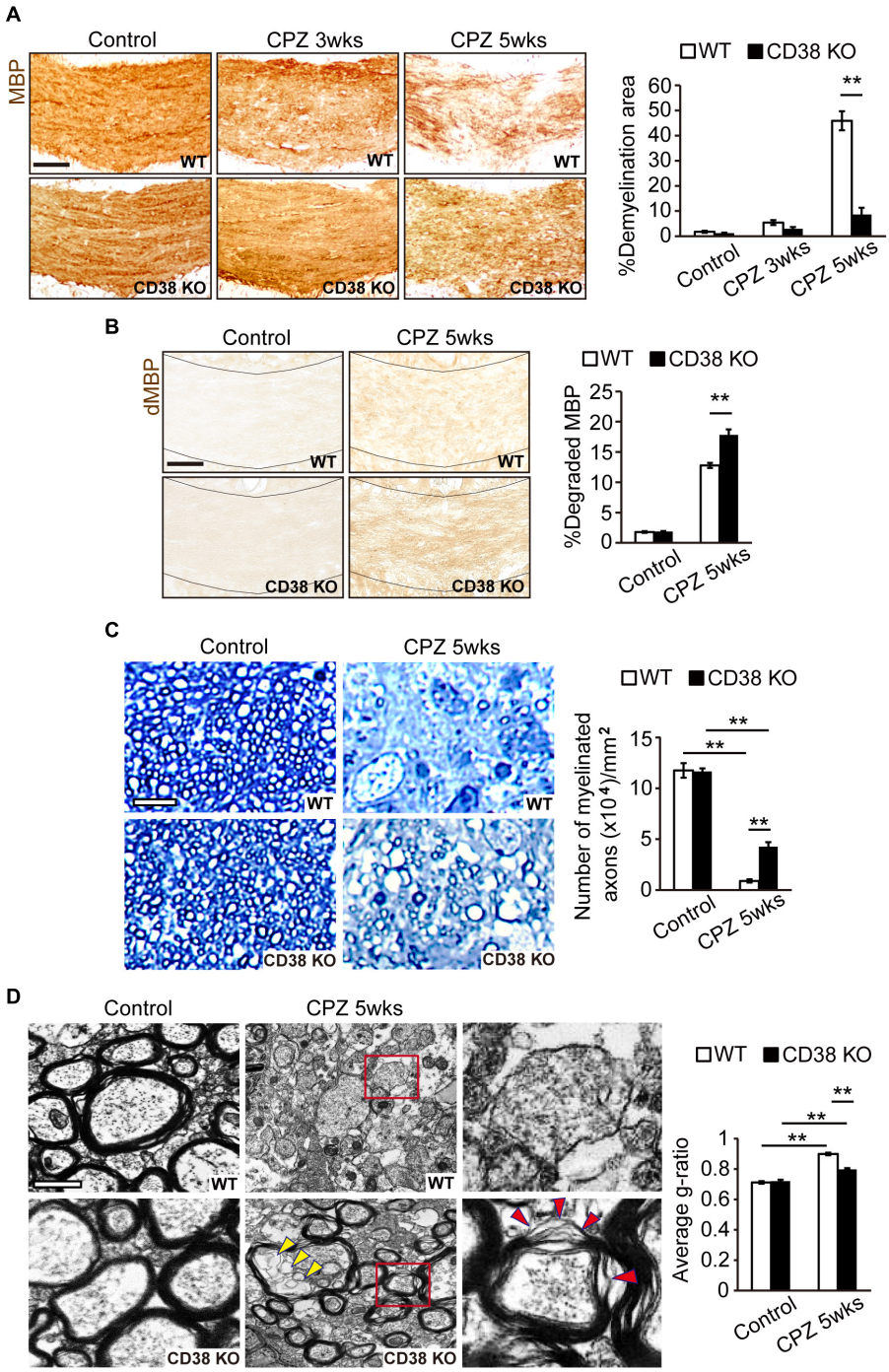

FIGURE 2 | Demyelination was attenuated in CD38 KO mice. **(A)** Representative images of MBP immunohistochemistry in the CC of control and CPZ-administered (3 and 5 weeks) WT and CD38 KO mice. Scale bar: 200 μm. The graph shows densitometric analysis of the demyelinating areas in the CC of control and CPZ-administered (3 and 5 weeks) WT and CD38 KO mice, $n = 4$. **(B)** Representative images of dMBP immunohistochemistry in the CC of control and CPZ-administered (5 weeks) WT and CD38 KO mice. Scale bar: 200 μm. The graph shows densitometric analysis of the demyelinating areas in the CC of control and CPZ-administered (5 weeks) WT and CD38 KO mice, $n = 4$. **(C)** Toluidine blue staining of semi-thin resin sections of the CC of control and CPZ-administered (5 weeks) WT and CD38 KO mice. The graph shows the number of myelinated axons in the CC ($n = 4$ in each group). Scale bar: 5 μm. **(D)** Representative electron microscopic images of sagittal-sections of the CC of control and CPZ-administered (5 weeks) WT and CD38 KO mice. Right panels show higher magnification of the boxed areas in the middle panels. Yellow and red arrowheads in the lower panels indicate vacuoles and sheath breakdown in the myelinated axons, respectively. The graph shows g-ratio (axon diameter/fiber diameter) of the myelin sheath ($n = 100$ axons in each group). Scale bar: 1 μm. Data are expressed as mean ± SEM. *P* values are determined by two-way ANOVA followed by Scheffe's *F* test. $^{**}p < 0.01$ between two conditions.

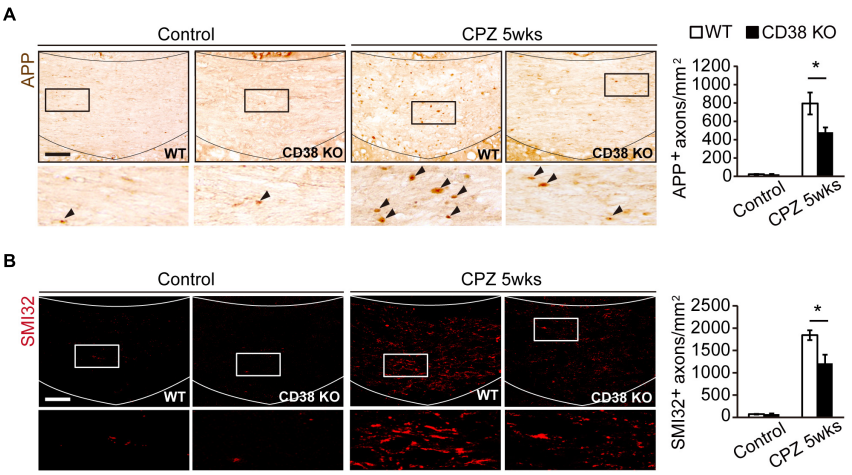

FIGURE 3 | Axonal damage was attenuated in CD38 KO mice. **(A)** Representative images of APP immunohistochemistry in the CC of control and CPZ-administered (5 weeks) WT and CD38 KO mice. Lower panels show higher magnification of the boxed areas in the upper panels. Arrowheads indicate APP-positive cells. The graph represents the number of APP-positive axons in the CC of control and CPZ-administered (5 weeks) WT and CD38 KO mice, $n = 4$. **(B)** Representative images of SMI-32 immunohistochemistry in the CC of control and CPZ-administered (5 weeks) WT and CD38 KO mice. The graph represents the number of SMI-32-positive axons in the CC of control and CPZ-administered (5 weeks) WT and CD38 KO mice, $n = 4$. Data are expressed as mean ± SEM. *P* values are determined by two-way ANOVA followed by Scheffe's *F* test. $^*p < 0.05$ between two conditions. Scale bars: 100 μm.

(172012, Sigma-Aldrich) and penicillin and streptomycin (26239-42, 32204-92, Nacalai Tesque). The cells were collected after 14 days of cultivation. They were then incubated with CD11b (microglia) MicroBeads (130-093-634, microbeads conjugated to monoclonal anti-human/mouse CD11b antibody, Miltenyi Biotec, Bergisch Gladbach, Germany) for 15 min at 4°C. The cells were then washed in separation buffer and centrifuged at 300 × *g* for 10 min. They were resuspended in the same buffer and applied to a magnetic column fitted into a QuadroMACS™ cell separator (Miltenyi Biotec). The cells were separated into CD11b-positive or CD11b-negative fractions and plated onto poly-L-lysine-coated plastic culture dishes. The CD11b-positive fraction, which contained microglia (>97% of the cells were Iba1 positive), was used for the experiments 24 h after plating. The CD11b-negative fraction, which contained astrocytes (>92% of the cells were GFAP positive), was plated and used for experiments after reaching confluence.

Small Interference RNA

Silencing of CD38 was performed by transfecting the cells with small interference RNAs (siRNAs), as previously described (Hattori et al., 2017). The targeted sequence of the mouse CD38 was as follows: 5′ -GGACCCAAATAAGGTTCA- 3′. We used Stealth RNAi™ siRNA negative control Med GC from Thermo Fisher Scientific as a control siRNA (12935-300). Microglia were transfected with siRNA 1 day after plating, while astrocytes were transfected with siRNA 4 and 6 days after plating. Two days later, the cells were treated with LPS (100 ng/ml) for 6 h, and total RNA was isolated for qRT-PCR.

Phagocytosis Assays

The microglia phagocytosis assay was performed using myelin debris with or without LPS at the concentration of 100 ng/ml, as previously described (Clarner et al., 2015). In brief, the CC was harvested under sterile conditions from adult ICR mice, and the cerebral cortices were carefully removed. The samples were homogenized in PBS using an ultrasonic converter and centrifuged at 1,000 × *g* for 10 min. The supernatant was used as myelin debris. Myelin debris at the concentration of 15 μg/ml was used to assess the phagocytic activity of cells. After 24 h of LPS stimulation, immunocytochemistry was performed using anti-Iba1 (1:200) and anti-MBP (1:200) antibodies overnight at 4°C. Five independent microglia cultures were evaluated using a light microscope at a magnification of 20× (BZ-X710, Keyence). Phagocytic activity is presented as the percentage of myelin-containing microglia in the total number of microglia.

Statistical Analysis

The experimental results are expressed as mean ± standard error of the mean (SEM), with the number of experiments indicated by (n). No statistical evaluations were performed to predetermine sample sizes, but our sample sizes are similar to those generally used in the field. One-way ANOVA followed by Tukey-kramer test or two-way ANOVA followed by Scheffe's *F* test was used for the statistical analysis. *P* values <0.05 were considered statistically significant.

RESULTS

CD38 Expression Was Increased During CPZ Administration

We first investigated the expression of CD38 in the CC in WT mice at different time points after CPZ administration. RT-qPCR revealed that the expression of CD38 mRNA was significantly increased 5 weeks after CPZ administration (**Figure 1A**). Western

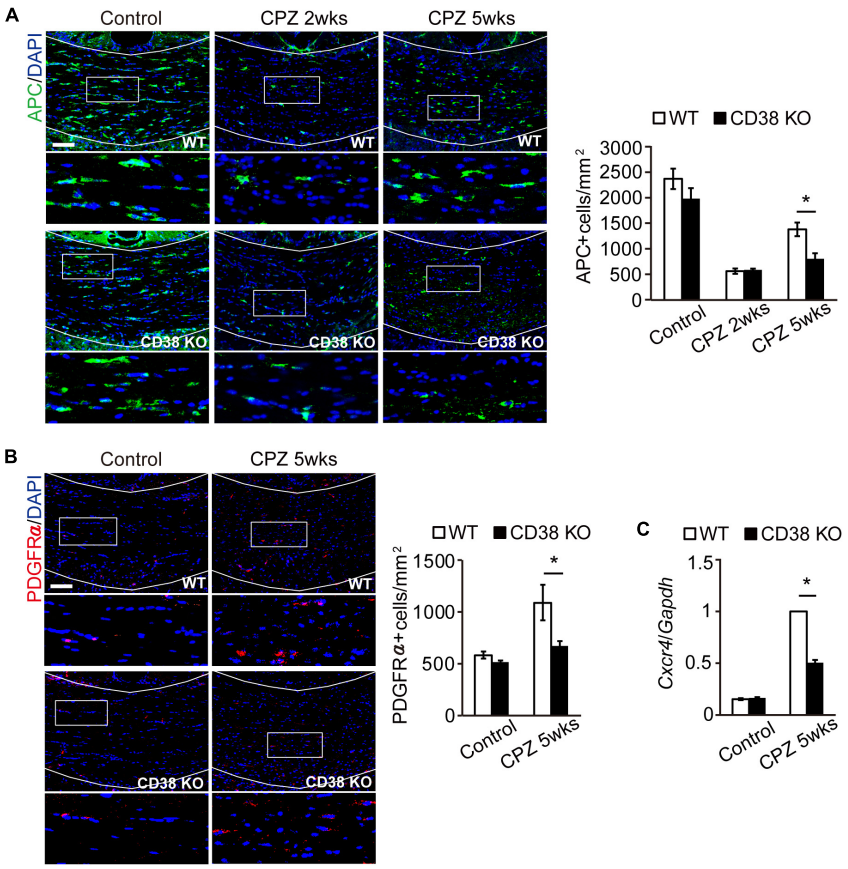

FIGURE 4 | OL repopulation was impaired in CD38 KO mice. **(A,B)** Representative images of APC **(A)** and PDGFRα **(B)** immunohistochemistry in the CC of control and CPZ-administered WT and CD38 KO mice. Nuclei were counterstained with DAPI. Lower panels show higher magnification of the boxed areas in the upper panels. The graph represents the number of APC- or PDGFRα-positive cells in the CC of control and CPZ-administered (2 and 5 weeks) WT and CD38 KO mice, $n = 4$. **(C)** RT-qPCR analysis for *Cxcr4* expression in the CC of control and CPZ-administered (5 weeks) WT and CD38 KO mice, $n = 4$. Data are expressed as mean ± SEM. *P* values are determined by two-way ANOVA followed by Scheffe's *F* test. $^*p < 0.05$ between two conditions. Scale bars: 100 μm.

blotting also revealed that the expression of CD38 protein was gradually increased and reached a significantly higher level 5 weeks after CPZ administration when compared to that in the normal condition (**Figure 1B**). *In situ* hybridization confirmed the induction of CD38 mRNA in the CC 3–5 weeks after CPZ administration (**Figure 1C**). Furthermore, *in situ* hybridization-immunohistochemistry using cell type-specific antibodies revealed that the levels of CD38 transcripts were significantly increased both in GFAP-positive astrocytes and in Iba1-positive microglia (**Figures 1D,E**) 3–5 weeks after CPZ administration. Consistent with our recent report (Hattori et al., 2017), the number of CD38-positive cells among APC-positive OLs was much lower than that of GFAP-positive astrocytes (**Supplementary Figure 1**).

Demyelination Was Attenuated, but Myelin Clearance Was Reduced in CD38 KO Mice

To investigate the role of CD38 in the process of demyelination, CPZ was administered to both WT, and CD38 KO mice for 5 weeks. Demyelination was analyzed by immunohistochemistry for MBP. The normal myelin pattern was observed in the CC of mice from both genotypes under physiological conditions (**Figure 2A**). In contrast, demyelination was observed 3 weeks and then strongly increased 5 weeks after CPZ administration in WT mice (upper panels in **Figure 2A**). Interestingly, demyelination was significantly decreased in CD38 KO mice 5 weeks after CPZ administration (lower panels in **Figure 2A**). To evaluate whether preserved myelin in CD38 KO mice was functionally intact or degraded, we performed immunohistochemistry for dMBP (**Figure 2B**). The degraded myelin was increased in both genotypes, but the level was higher in CD38 KO mice than in WT mice 5 weeks after CPZ administration, suggesting that the preserved myelin in CD38 KO mice includes the degraded one. Toluidine Blue staining of semi-thin sections of the CC confirmed a strong reduction in the number of myelinated axons in both genotypes 5 weeks after CPZ administration, but the level was milder in CD38 KO mice than in WT mice (**Figure 2C**). Furthermore, ultrastructure analyses using electron microscopy revealed nearly complete demyelination in WT mice (Upper panels in **Figure 2D**),

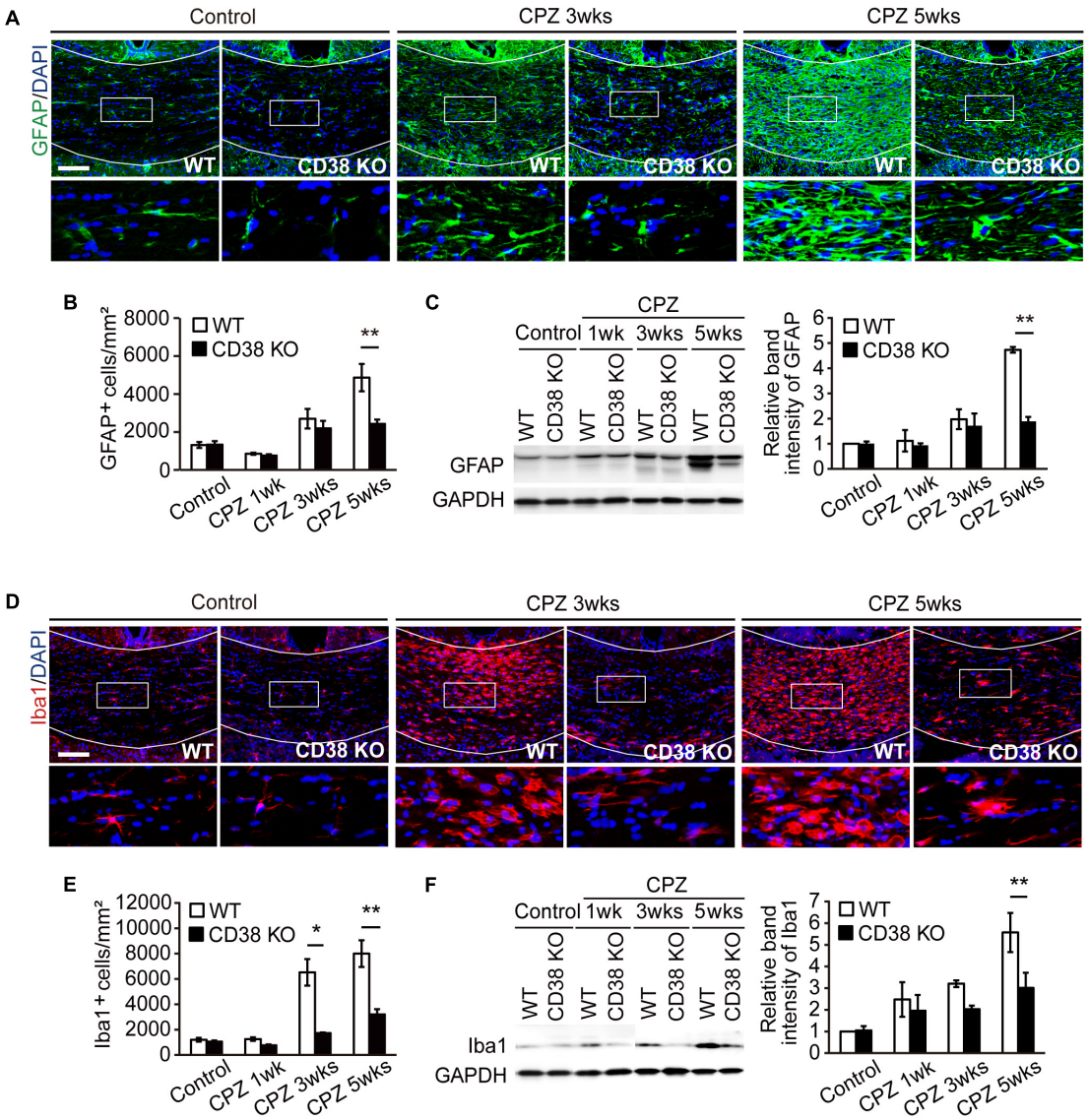

FIGURE 5 | Glial activation was attenuated in CD38 KO mice. **(A)** Representative images of GFAP immunohistochemistry in the CC of control and CPZ-administered (3 and 5 weeks) WT and CD38 KO mice. Nuclei were counterstained with DAPI. Lower panels show higher magnification of the boxed areas in the upper panels. **(B)** The Graph represents the number of GFAP-positive astrocytes in the CC of control and CPZ-administered (1, 3, and 5 weeks) WT and CD38 KO mice, $n = 4$. **(C)** Western blotting analyses of GFAP in the CC of WT and CD38 KO mice after different periods of CPZ administration. The graph depicts the relative optical density of GFAP normalized to the loading control GAPDH $n = 5$. **(D)** Representative images of Iba1 immunohistochemistry in the CC of control and CPZ-administered (3 and 5 weeks) WT and CD38 KO mice. Nuclei were counterstained with DAPI. Lower panels show higher magnification of the boxed areas in the upper panels. **(E)** The graph represents the number of Iba1-positive microglia in the CC of control and CPZ-administered (1, 3, and 5 weeks) WT and CD38 KO mice $n = 5$. **(F)** Western blotting analyses of Iba1 in the CC of WT and CD38 KO mice after different periods of CPZ administration. The graph depicts the relative optical density of Iba1 normalized to the loading control GAPDH $n = 5$. Data are expressed as mean ± SEM. *P* values are determined by two-way ANOVA followed by Scheffe's *F* test. $^{*}p < 0.05$ and $^{**}p < 0.01$ between two conditions. Scale bars: 100 μm.

while relatively preserved myelin, and improved g-ratio in CD38 KO mice (lower panels in **Figure 2D** and the graph) 5 weeks after CPZ administration. However, the majority of the remaining myelin in CD38 KO mice showed an altered myelin structure. The myelin sheaths in CD38 KO mice displayed splits/breakdown and vacuoles (red and yellow arrowheads, respectively, in **Figure 2D**). Additionally, activated microglia with many phagocytozed materials, probably degraded myelin, were often observed in WT mice, but not in CD38 KO mice, after CPZ administration (**Supplementary Figure 2**).

Axonal Damage Was Attenuated in CD38 KO Mice

It has been reported that, together with extensive demyelination, CPZ administration causes axonal damage which is characterized

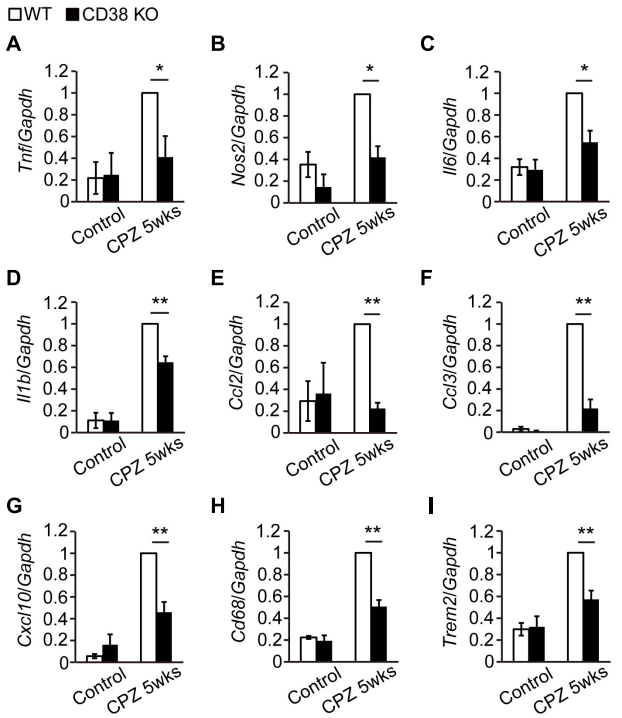

FIGURE 6 | Expression levels of inflammatory genes were decreased in CD38 KO mice. **(A–I)** RT-qPCR analysis for the expression of inflammatory genes in the CC of control and CPZ-administered (5 weeks) WT and CD38 KO mice $n = 5$. Data are expressed as mean ± SEM. *P* values are determined by two-way ANOVA followed by Scheffe's *F* test. $*p < 0.05$ and $**p < 0.01$ between two conditions.

by axonal swelling and bulb-like formation (Piaton et al., 2010). These structures include deposits of APP (Petkovic et al., 2016) and dephosphorylated neurofilament (Herrero-Herranz et al., 2008; Havranek et al., 2017). To analyze the extent of axonal damage after CPZ administration, we performed immunohistochemistry using anti-APP antibody (**Figure 3A**) and anti-SMI-32 antibody (**Figure 3B**), the latter recognizes non-phosphorylated forms of neurofilament H. More APP- and SMI-32-positive deposits were observed in WT mice than in CD38 KO mice after CPZ administration. These results suggest that CPZ-induced axonal damage was attenuated in CD38 KO mice.

OL Repopulation Was Impaired in CD38 KO Mice

CPZ administration induces selective apoptosis in the mature OLs early on (first 2 weeks), followed by the accumulation of OPCs to the demyelinating lesion, and differentiation into the new mature OLs, which is a critical step for remyelination (Praet et al., 2014). We thus analyzed the status of APC-expressing mature OLs and PDGFR-expressing OPCs during CPZ administration. Immunohistochemistry revealed that, although the initial loss of mature OLs 2 weeks after CPZ administration was observed to a similar level in both genotypes (**Figures 4A,B**), the number of OPCs (**Figure 4B**), and mature OLs (**Figure 4A**) were significantly lower in CD38 KO mice than in WT mice 5 weeks after CPZ administration. Consistent with these results, RT-qPCR analysis revealed that the expression of CXCR4, which is induced in the OPCs and promote their maturation and remyelination after CPZ administration (Patel et al., 2010), was significantly lower in CD38 KO mice 5 weeks after CPZ administration (**Figure 4C**). These results suggest suppression of the OL repopulation in CD38 KO mice after CPZ administration.

Glial Activation Was Attenuated in CD38 KO Mice

As demyelination is accompanied by extensive astroglial and microglial responses that greatly influence the extent of further demyelination and remyelination (Gudi et al., 2014), the status of glial cells was analyzed by immunohistochemistry, and western blot for GFAP and Iba1. The numbers of GFAP-positive cells and the expression levels of GFAP protein were increased after CPZ administration in WT mice, but were significantly lower in CD38 KO mice (**Figures 5A–C**). Similarly, the numbers of Iba1-positive cells and the expression levels of Iba1 protein were increased after CPZ administration, but were significantly lower in CD38 KO mice (**Figures 5D–F**). These data indicate that deletion of CD38 suppresses CPZ-induced glial activation.

Inflammatory Responses Were Reduced in CD38 KO Mice

Activated astrocytes and microglia produce a battery of inflammatory cytokines/chemokines (Gudi et al., 2014) and subsequently harm OLs and axons. RT-qPCR analysis revealed that the expressions of genes such as *Tnf, Il1b, Nos2, Ccl2, Ccl3,* and *Cxcl10* were increased after CPZ administration (**Figures 6A–G**), but their levels were lower in CD38 KO mice, suggesting that deletion of CD38 suppresses the induction of inflammatory genes. Similarly, the expression levels of phagocytosis-associated genes such as *Trem2* (Triggering Receptor Expressed on Myeloid cells) and *Cd68* genes were significantly lower in CD38 KO mice after CPZ administration (**Figures 6H,I**).

Silencing/Deletion of *Cd38* Gene Suppressed the Activation of Astrocytes and Microglia *in vitro*

To determine whether CD38 regulates glial activation cell-autonomously, we analyzed the expression of glial markers and cytokines/chemokines in both cultured astrocytes (**Figures 7A–F**) and microglia (**Figures 7G–L**) after transfecting them with CD38 siRNA or control RNA. In astrocytes, the expression levels of *Cd38* and *Gfap* were significantly reduced following the silencing of *Cd38* gene, both in the absence and presence of lipopolysaccharide (LPS), as we recently described (Hattori et al., 2017). Although LPS strongly induced astrocyte-related chemokines such as *Cxcl10, Cxcl12, Ccl2,* and *Ccl3* in both genotypes, the levels were significantly lower in CD38 siRNA-transfected cells (**Figures 7B–F**). These results indicate that CD38 regulates the activation of astrocytes cell-autonomously.

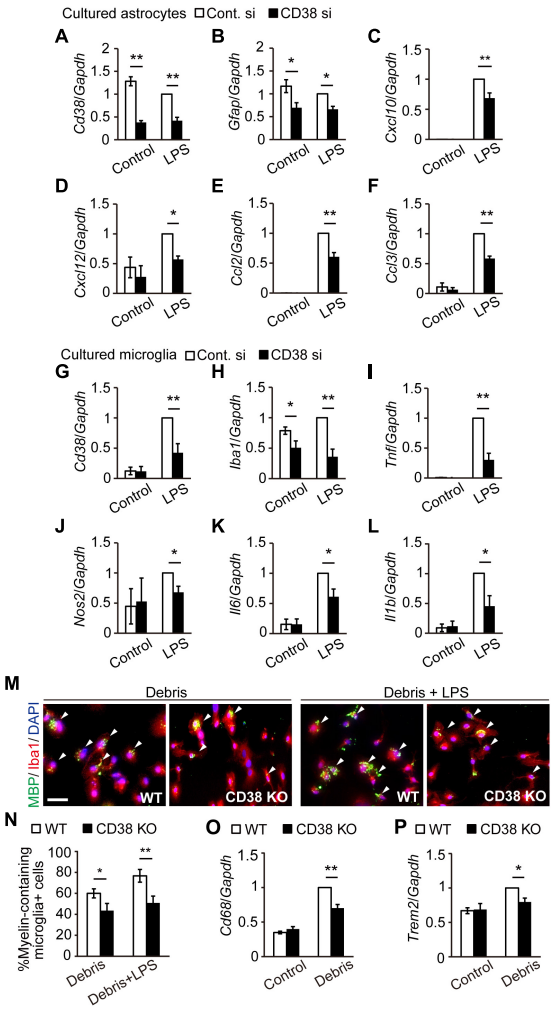

FIGURE 7 | Silencing/deletion of *Cd38* gene reduced the activation of astrocytes and microglia *in vitro*. **(A–F)** Primary astrocyte cultures were transfected with CD38 siRNA or control siRNA at 4 and 6 days *in vitro* (DIV) and stimulated with LPS at 8 DIV. Total RNA was prepared from cells 6 h after treatment with LPS. The expression levels of *Cd38, Gfap, Cxcl10, Cxcl12*, *Ccl2,* and *Ccl3* transcripts were determined using RT-qPCR $n = 7$. **(G–L)** Primary microglia cultures were transfected with CD38 siRNA or control siRNA at 1 DIV and treated with LPS at 2 DIV. Total RNA was prepared from cells 6 h after treatment with LPS. The expression levels of *Cd38, Iba1, Tnf, Nos2, Il6,* and *Il1*β transcripts were determined using RT-qPCR $n = 5$. **(M–P)** Evaluation of phagocytois. Primary microglia cultures of WT and CD38 KO mice were treated with LPS and myelin debris for 24 h. **(M)** Cells were stained with anti-Iba1 and -MBP antibodies. Arrowheads indicate phagocytic microglial containing MBP inside the cell body. Scale bar: 20 μm. **(N)** The graph depicts percentage of myelin-containing microglia $n = 5$. **(O,P)** The expression levels of *Cd68* and *Trem2* transcripts were determined by RT-qPCR $n = 5$. All data are expressed as mean ± SEM. All *P* values are determined by two-way ANOVA followed by Scheffe's *F* test. $^*p < 0.05$ and $^{**}p < 0.01$ between two conditions.

In microglia, LPS also induced *Cd38* and glia-related inflammatory genes, such as *Nos2* and those coding for cytokines in both genotypes, while the levels were significantly lower in CD38 siRNA-transfected microglia (**Figures 7G,I–L**). The expression of *Iba1* was also reduced by silencing CD38 both in the absence and presence of LPS (**Figure 7H**). CD38 KO microglia had a similar phenotype to microglia subjected to CD38 silencing (**Supplementary Figures 3A–F**). Furthermore, CD38 KO microglia exhibited lower phagocytic activity (**Figures 7M,N**) and lower levels of expressions of phagocytosis-associated molecules (**Figures 7O,P**). These results indicate that CD38 also regulates the activation of microglia cell-autonomously.

NAD^+ Suppressed the Activation of Astrocytes and Microglia

Since we and other groups have reported that CD38 KO mice exhibit increased NAD^+ levels in the brain (Jin et al., 2007; Hattori et al., 2017), we measured NAD (NAD^+ + NADH) concentrations in the CC of WT and CD38 KO mice administered CPZ as well as those not administered CPZ. Consistent with the results of our recent study, NAD levels were significantly higher in CD38 KO mice than in WT mice in the normal condition (control). Although CPZ administration for 5 weeks slightly increased the NAD level in mice of both genotypes, CD38 KO mice still exhibited significantly higher levels of NAD than WT mice (**Figure 8A**). We also investigated the effects of NAD^+ and cADPR, which are the substrate and product of CD38, respectively, on the activation of astrocytes and microglia. Pretreatment of cultured astrocytes or microglia with NAD^+, but not with 8Br-cADPR (a cADPR antagonist), reduced the expression levels of *Gfap, Cxcl10, Cxcl12,* and *Ccl2* in astrocytes (**Figures 8B–F**), and those of *Iba1* and some inflammatory genes such as *Tnf* and *Nos2* in microglia (**Figures 8G–K**) after LPS stimulation. These results suggest that deletion of the *Cd38 gene* suppresses the activation of astrocytes and microglia by increasing NAD^+ levels.

DISCUSSION

In the current study, we examined the role of CD38 in CPZ-induced demyelination model in mice. CD38 expression was enhanced in both astrocytes and microglia after CPZ administration. The deletion of CD38 ameliorated demyelination and neurodegeneration, while it suppressed myelin clearance and subsequent OL repopulation. CD38 deficiency, or addition of NAD^+ suppressed activation of both astrocytes and microglia, and inflammatory responses in those cells. These results suggest that CD38 in the glial cells regulates neuroinflammation by controlling NAD^+ level in the brain, and affects both of CPZ-induced demyelination and subsequent OL remodeling.

In a recent report, Herrmann et al. (2016) demonstrated that CD38 was crucially involved in the pathology of EAE. CD38 expression was strongly elevated both in the encephalitogenic lymph node (LN) cells and in the CNS-infiltrating cells after induction of EAE. Furthermore, deletion of CD38 ameliorated clinical symptoms, and its effect was associated with reduced levels of both antibody production and T-cell response in CD38 KO cells after administration of myelin oligodendrocyte glycoprotein (MOG) 1-125. In contrast to their report, our study demonstrated both beneficial and detrimental effects

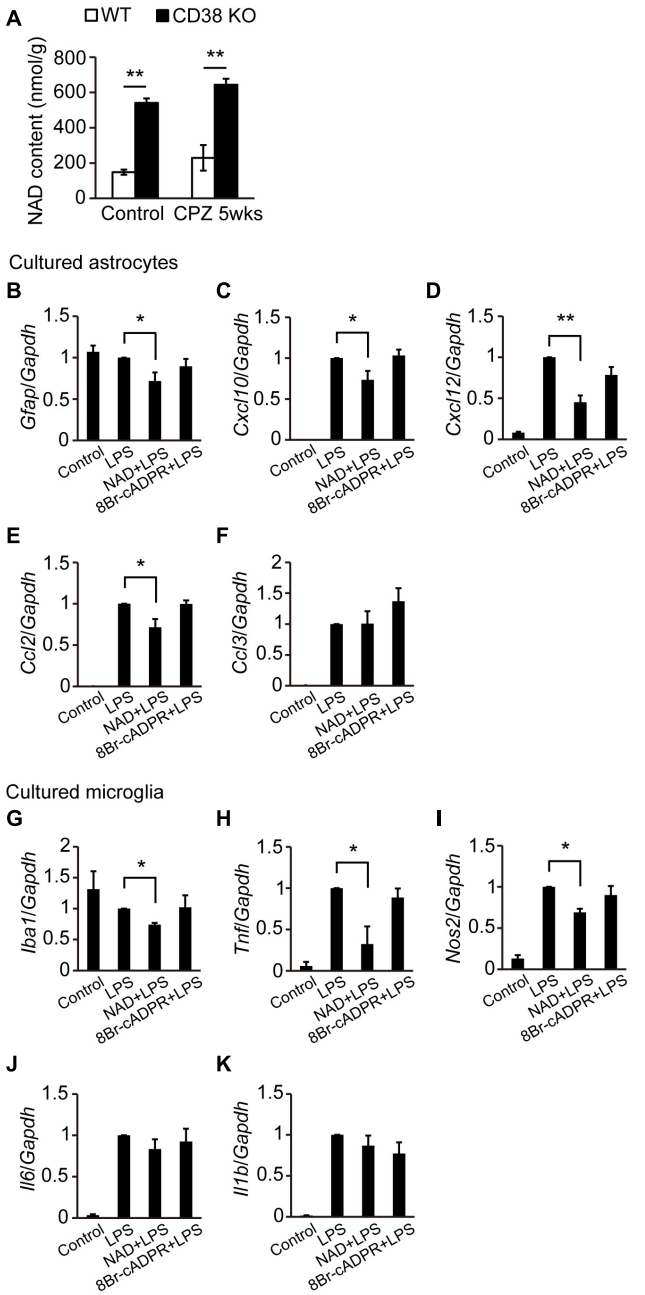

FIGURE 8 | NAD^+ suppressed the activation of astrocytes and microglia. **(A)** Determination of NAD levels in the CC of control and CPZ-administered (5 weeks) WT and CD38 KO mice, $n = 4$. P values are determined by two-way ANOVA followed by Scheffe's F test. $^{**}p < 0.01$ between two conditions. **(B–F)** Primary astrocyte cultures were treated with NAD^+ (200 μM) or 8Br-cADPR (20 μM) for 5 days (4–9 DIV) and then stimulated with LPS at 9 DIV $n = 6$. P values are determined by one-way ANOVA followed by Tukey-kramer test. $^*p < 0.05$ and $^{**}p < 0.01$ between two conditions. **(G–K)** Microglia cultures were treated with NAD^+ (200 μM) or 8Br-cADPR (20 μM) for 1 day (1–2 DIV), and then stimulated with LPS at 2 DIV $n = 6$. P values are determined by one-way ANOVA followed by Tukey-kramer test. $^*p < 0.05$ between two conditions. In **(B–K)**, total RNA was prepared from cells 6 h after treatment with LPS. The expression levels of *Gfap, Iba1,* and proinflammatory molecule transcripts were determined by RT-qPCR. All data are expressed as mean ± SEM.

of CD38 deletion in a different MS model, CPZ-induced demyelination model in mice, which lacks an autoimmune lymphocytic response in its pathology. The expression of CD38 was also increased in the CPZ-induced demyelinating region (**Figures 1A–C**), and consistent with the observations in EAE, deletion of CD38 ameliorated both demyelination (**Figures 2A,C**) and neurodegeneration (**Figures 3A,B**), while underlying mechanisms may be different. In our model, CD38 played critical roles in the glial activation and subsequent neuroinflammation both in mice (**Figures 5**, **6A–G**) and in cultured astroglial and microglial cells (**Figures 7A–L** and **Supplementary Figure 3**), which caused secondary damages to OLs and neurons through the production of toxic cytokines and chemokines such as TNF-α, IL-1β, iNOS, CCL2, CCL3, and CXCL10 (Selmaj and Raine, 1988; Merrill et al., 1993; McMahon et al., 2001; Skripuletz et al., 2013). We speculate that it will be quite interesting and important to study more detail of the role of glial CD38 in the settings of EAE and MS.

In the present study, we also observed the reduced levels of the clearance of degraded myelin (**Figures 2B,D**) and oligodendrocyte repopulation (**Figures 4A–C**) in CD38 KO mice 5 weeks after CPZ administration. Consistent with these results, the phagocytic activity (**Figures 7M,N** and **Supplementary Figures 2A,B**) and the expression of phagocytosis-associated genes such as *Cd68* and *Trem2* (**Figures 6H,I**, **7O,P**) were reduced in CD38 KO mice and in CD38 KO mice-derived microglia. As microglial phagocytosis of the degraded myelin is essential for the proper OPC maturation into OLs after demyelination (Petkovic et al., 2016), our findings suggest that CD38-mediated glial activation, and phagocytosis may also play a critical role in the process of remyelination. However, it is not clear yet how the numbers of both OPCs and OLs were reduced in CD38 KO mice 5 weeks after CPZ administration (**Figures 4A–C**). Our previous report demonstrated that astrocytic CD38 facilitated the maturation of OPCs, but not their own proliferation in the postnatal developing periods (Hattori et al., 2017). Further studies are required to clarify this point.

Herrmann et al. (2016) also demonstrated in their report that Sphingosine 1-phosphate (S1P)-receptor modulator FTY720 (fingolimod), which is the first oral therapeutic agent for MS and exerts its function, at least in part, by inhibiting lymphocyte trafficking from secondary lymphoid organs, effectively suppressed EAE severity and reduced the level of CD38 expression in the lymph nodes. Interestingly, S1P receptors are also highly expressed in the brain cells including astrocytes (Van Doorn et al., 2010; Choi et al., 2011). It was previously reported that FTY720 ameliorated demyelination and neurodegeneration in CPZ-induced demyelination model, while it failed to enhance remyelination *in vivo* (Kim et al., 2011; Slowik et al., 2015). Although our preliminary results have revealed no significant differences between WT and CD38 KO mice in the expression levels of S1P and AKT2, a downstream molecule in SIP signaling, 5 weeks after CPZ administration, further analysis may clarify the possible link between S1P and CD38 pathways in the glia-mediated regulation of demyelination and neurodegeneration.

It was also reported that nicotinamide, which is a precursor of CD38 substrate NAD^+, reduced demyelination, axonal degeneration, and infiltration of $CD4^+$ T-cells in EAE (Kaneko et al., 2006). Furthermore, NAD^+ has been shown to reverse the progression of EAE by regulating $CD4^+$ T-cell differentiation and apoptosis (Tullius et al., 2014). These studies indicate that NAD^+ has beneficial effects on MS pathology. In the current study, we demonstrated the suppressing effect of NAD^+ on the glial activation, as well as inflammatory responses *in vitro*, and the higher level of NAD in the CD38 KO brains in both of the control and CPZ-administrated conditions. We speculate that NAD^+ also has both beneficial and detrimental effects in the process of demyelination, depending on the situations such as acute inflammatory phase and chronic neurodegenerating phase. Although the molecular mechanism of NAD^+-mediated regulation of glial activity is still unclear, a NAD^+-dependent deacetylase sirtuin2 (SIRT2) in microglia may be involved in this process, as previously described (Pais et al., 2013). Furthermore, since brain NAD^+ level can be increased by administration of NAD^+ precursors such as nicotinamide riboside and nicotinamide mononucleotide (Gong et al., 2013), it will be intriguing to test these molecules in CPZ-induced demyelination model.

In conclusion, we identified novel effects of CD38 and NAD^+ on demyelination and neuroinflammation using CPZ-induced demyelination model. CD38 and NAD^+ in glial cells may have both beneficial and detrimental effects, and further studies to regulate the balance of these effects will make them potential targets for therapeutic intervention of MS and other demyelinating diseases.

DATA AVAILABILITY

All datasets generated for this study are included in the manuscript and/or the **Supplementary Files**.

ETHICS STATEMENT

All animal experiments were performed in accordance with the guideline and approved by the Animal Care and Use Committee of Kanazawa University (AP-143305).

AUTHOR CONTRIBUTIONS

TH and OH designed the experiments. JR, TH, and YS conducted the studies. HI, MT-I, NO, and TL assisted with the experiments and provided the intellectual input. YY, AS, HO, and HH supervised the study. JR, TH, HO, HH, YK, and OH interpreted the data and wrote the manuscript.

FUNDING

This work was supported by Grants-in Aid for Scientific Research (18K06501 to TH, 18K06500 to OH, 17K10821 to HI, and 18K06463 to MT-I) from the Ministry of Education, Science, Technology, Sports and Culture of Japan, and by Kanazawa University SAKIGAKE project 2018 and CHOZEN project.

ACKNOWLEDGMENTS

We thank Mr. Takashi Tamatani for providing technical assistance and Dr. Shigeru Yokoyama for providing a mouse *Cd38* cloning vector.

SUPPLEMENTARY MATERIAL

The Supplementary Material for this article can be found online at: https://www.frontiersin.org/articles/10.3389/fncel.2019.00258/full#supplementary-material

REFERENCES

Akimoto, N., Kamiyama, Y., Yamafuji, M., Fujita, K., Seike, T., Kido, M., et al. (2013). Immunohistochemistry of CD38 in different cell types in the hypothalamus and pituitary of male mice. *Am. Sci. Pub.* 2, 54–61. doi: 10.1166/msr.2013.1021

Blakemore, W. F. (1972). Observations on oligodendrocyte degeneration, the resolution of status spongiosus and remyelination in cuprizone intoxication in mice. *J. Neurocytol.* 1, 413–426. doi: 10.1007/bf01102943

Bond, L., Lusher, D., Williams, I., and Butler, H. (2014). Friends or foes? Relational dissonance and adolescent psychological wellbeing. *PLoS One* 9:e83388. doi: 10.1371/journal.pone.0083388

Cao, L., and He, C. (2013). Polarization of macrophages and microglia in inflammatory demyelination. *Neurosci. Bull.* 29, 189–198. doi: 10.1007/s12264-013-1324-1320

Choi, J. W., Gardell, S. E., Herr, D. R., Rivera, R., Lee, C. W., Noguchi, K., et al. (2011). FTY720 (fingolimod) efficacy in an animal model of multiple sclerosis requires astrocyte sphingosine 1-phosphate receptor 1 (S1P1) modulation. *Proc. Natl. Acad. Sci. U.S.A.* 108, 751–756. doi: 10.1073/pnas.1014154108

Clarner, T., Janssen, K., Nellessen, L., Stangel, M., Skripuletz, T., Krauspe, B., et al. (2015). CXCL10 triggers early microglial activation in the cuprizone model. *J. Immunol.* 194, 3400–3413. doi: 10.4049/jimmunol.1401459

Compston, A., and Coles, A. (2008). Multiple sclerosis. *Lancet* 372, 1502–1517. doi: 10.1016/S0140-6736(08)61620-61627

Fan, H. B., Chen, L. X., Qu, X. B., Ren, C. L., Wu, X. X., Dong, F. X., et al. (2017). Transplanted miR-219-overexpressing oligodendrocyte precursor cells promoted remyelination and improved functional recovery in a chronic demyelinated model. *Sci. Rep.* 7:41407. doi: 10.1038/srep41407

Goebbels, S., Oltrogge, J. H., Kemper, R., Heilmann, I., Bormuth, I., Wolfer, S., et al. (2010). Elevated phosphatidylinositol 3,4,5-trisphosphate in glia triggers cell-autonomous membrane wrapping and myelination. *J. Neurosci.* 30, 8953–8964. doi: 10.1523/JNEUROSCI.0219-10.2010

Gong, B., Pan, Y., Vempati, P., Zhao, W., Knable, L., Ho, L., et al. (2013). Nicotinamide riboside restores cognition through an upregulation of proliferator-activated receptor-gamma coactivator 1alpha regulated beta-secretase 1 degradation and mitochondrial gene expression in Alzheimer's mouse models. *Neurobiol. Aging* 34, 1581–1588. doi: 10.1016/j.neurobiolaging.2012.12.005

Gudi, V., Gingele, S., Skripuletz, T., and Stangel, M. (2014). Glial response during cuprizone-induced de- and remyelination in the CNS: lessons learned. *Front. Cell Neurosci.* 8:73. doi: 10.3389/fncel.2014.00073

Hattori, T., Baba, K., Matsuzaki, S., Honda, A., Miyoshi, K., Inoue, K., et al. (2007). A novel DISC1-interacting partner DISC1-binding zinc-finger protein:

implication in the modulation of DISC1-dependent neurite outgrowth. *Mol. Psychiatry* 12, 398–407. doi: 10.1038/sj.mp.4001945

Hattori, T., Kaji, M., Ishii, H., Jureepon, R., Takarada-Iemata, M., Minh Ta, H., et al. (2017). CD38 positively regulates postnatal development of astrocytes cell-autonomously and oligodendrocytes non-cell-autonomously. *Glia* 65, 974–989. doi: 10.1002/glia.23139

Hattori, T., Shimizu, S., Koyama, Y., Emoto, H., Matsumoto, Y., Kumamoto, N., et al. (2014). DISC1 (disrupted-in-schizophrenia-1) regulates differentiation of oligodendrocytes. *PLoS One* 9:e88506. doi: 10.1371/journal.pone.0088506

Hattori, T., Shimizu, S., Koyama, Y., Yamada, K., Kuwahara, R., Kumamoto, N., et al. (2010). DISC1 regulates cell-cell adhesion, cell-matrix adhesion and neurite outgrowth. *Mol. Psychiatry* 15, 798–809. doi: 10.1038/mp.2010.60

Havranek, T., Lestanova, Z., Mravec, B., Strbak, V., Bakos, J., and Bacova, Z. (2017). Oxytocin modulates expression of neuron and glial markers in the Rat hippocampus. *Folia Biol.* 63, 91–97.

Herrero-Herranz, E., Pardo, L. A., Gold, R., and Linker, R. A. (2008). Pattern of axonal injury in murine myelin oligodendrocyte glycoprotein induced experimental autoimmune encephalomyelitis: implications for multiple sclerosis. *Neurobiol. Dis.* 30, 162–173. doi: 10.1016/j.nbd.2008.01.001

Herrmann, M. M., Barth, S., Greve, B., Schumann, K. M., Bartels, A., and Weissert, R. (2016). Identification of gene expression patterns crucially involved in experimental autoimmune encephalomyelitis and multiple sclerosis. *Dis. Model. Mech.* 9, 1211–1220. doi: 10.1242/dmm.025536

Jin, D., Liu, H. X., Hirai, H., Torashima, T., Nagai, T., Lopatina, O., et al. (2007). CD38 is critical for social behaviour by regulating oxytocin secretion. *Nature* 446, 41–45. doi: 10.1038/nature05526

Kaneko, S., Wang, J., Kaneko, M., Yiu, G., Hurrell, J. M., Chitnis, T., et al. (2006). Protecting axonal degeneration by increasing nicotinamide adenine dinucleotide levels in experimental autoimmune encephalomyelitis models. *J. Neurosci.* 26, 9794–9804. doi: 10.1523/JNEUROSCI.2116-06.2006

Kato, I., Yamamoto, Y., Fujimura, M., Noguchi, N., Takasawa, S., and Okamoto, H. (1999). CD38 disruption impairs glucose-induced increases in cyclic ADP-ribose, [Ca2+]i, and insulin secretion. *J. Biol. Chem.* 274, 1869–1872. doi: 10.1074/jbc.274.4.1869

Kim, H. J., Miron, V. E., Dukala, D., Proia, R. L., Ludwin, S. K., Traka, M., et al. (2011). Neurobiological effects of sphingosine 1-phosphate receptor modulation in the cuprizone model. *FASEB J.* 25, 1509–1518. doi: 10.1096/fj.10-173203

Kou, W., Banerjee, S., Eudy, J., Smith, L. M., Persidsky, R., Borgmann, K., et al. (2009). CD38 regulation in activated astrocytes: implications for neuroinflammation and HIV-1 brain infection. *J. Neurosci. Res.* 87, 2326–2339. doi: 10.1002/jnr.22060

Lassmann, H., Van Horssen, J., and Mahad, D. (2012). Progressive multiple sclerosis: pathology and pathogenesis. *Nat. Rev. Neurol.* 8, 647–656. doi: 10.1038/nrneurol.2012.168

Lee, H. C. (2001). Physiological functions of cyclic ADP-ribose and NAADP as calcium messengers. *Annu. Rev. Pharmacol. Toxicol.* 41, 317–345. doi: 10.1146/annurev.pharmtox.41.1.317

Levy, A., Bercovich-Kinori, A., Alexandrovich, A. G., Tsenter, J., Trembovler, V., Lund, F. E., et al. (2009). CD38 facilitates recovery from traumatic brain injury. *J. Neurotrauma* 26, 1521–1533. doi: 10.1089/neu.2008.0746

Levy, A., Blacher, E., Vaknine, H., Lund, F. E., Stein, R., and Mayo, L. (2012). CD38 deficiency in the tumor microenvironment attenuates glioma progression and modulates features of tumor-associated microglia/macrophages. *Neuro. Oncol.* 14, 1037–1049. doi: 10.1093/neuonc/nos121

Malavasi, F., Deaglio, S., Funaro, A., Ferrero, E., Horenstein, A. L., Ortolan, E., et al. (2008). Evolution and function of the ADP ribosyl cyclase/CD38 gene family in physiology and pathology. *Physiol. Rev.* 88, 841–886. doi: 10.1152/physrev.00035.2007

McMahon, E. J., Cook, D. N., Suzuki, K., and Matsushima, G. K. (2001). Absence of macrophage-inflammatory protein-1alpha delays central nervous system demyelination in the presence of an intact blood-brain barrier. *J. Immunol.* 167, 2964–2971. doi: 10.4049/jimmunol.167.5.2964

Merrill, J. E., Ignarro, L. J., Sherman, M. P., Melinek, J., and Lane, T. E. (1993). Microglial cell cytotoxicity of oligodendrocytes is mediated through nitric oxide. *J. Immunol.* 151, 2132–2141.

Pais, T. F., Szego, E. M., Marques, O., Miller-Fleming, L., Antas, P., Guerreiro, P., et al. (2013). The NAD-dependent deacetylase sirtuin 2 is a suppressor of microglial activation and brain inflammation. *EMBO J.* 32, 2603–2616. doi: 10.1038/emboj.2013.200

Pasquini, L. A., Calatayud, C. A., Bertone Una, A. L., Millet, V., Pasquini, J. M., and Soto, E. F. (2007). The neurotoxic effect of cuprizone on oligodendrocytes depends on the presence of pro-inflammatory cytokines secreted by microglia. *Neurochem. Res.* 32, 279–292. doi: 10.1007/s11064-006-9165-9160

Patel, J. R., Mccandless, E. E., Dorsey, D., and Klein, R. S. (2010). CXCR4 promotes differentiation of oligodendrocyte progenitors and remyelination. *Proc. Natl. Acad. Sci. U.S.A.* 107, 11062–11067. doi: 10.1073/pnas.1006301107

Petkovic, F., Campbell, I. L., Gonzalez, B., and Castellano, B. (2016). Astrocyte-targeted production of interleukin-6 reduces astroglial and microglial activation in the cuprizone demyelination model: implications for myelin clearance and oligodendrocyte maturation. *Glia* 64, 2104–2119. doi: 10.1002/glia.23043

Piaton, G., Gould, R. M., and Lubetzki, C. (2010). Axon-oligodendrocyte interactions during developmental myelination, demyelination and repair. *J. Neurochem.* 114, 1243–1260. doi: 10.1111/j.1471-4159.2010.06831.x

Praet, J., Guglielmetti, C., Berneman, Z., Van Der Linden, A., and Ponsaerts, P. (2014). Cellular and molecular neuropathology of the cuprizone mouse model: clinical relevance for multiple sclerosis. *Neurosci. Biobehav. Rev.* 47, 485–505. doi: 10.1016/j.neubiorev.2014.10.004

Raposo, C., Nunes, A. K., Luna, R. L., Araujo, S. M., Da Cruz-Hofling, M. A., and Peixoto, C. A. (2013). Sildenafil (Viagra) protective effects on neuroinflammation: the role of iNOS/NO system in an inflammatory demyelination model. *Mediators Inflamm.* 2013:321460. doi: 10.1155/2013/321460

Remington, L. T., Babcock, A. A., Zehntner, S. P., and Owens, T. (2007). Microglial recruitment, activation, and proliferation in response to primary demyelination. *Am. J. Pathol.* 170, 1713–1724. doi: 10.2353/ajpath.2007.060783

Selmaj, K. W., and Raine, C. S. (1988). Tumor necrosis factor mediates myelin and oligodendrocyte damage in vitro. *Ann. Neurol.* 23, 339–346. doi: 10.1002/ana.410230405

Shibata, K., and Murata, K. (1986). Blood NAD as an index of niacin nutrition. *Nutr. Int.* 2, 177–181.

Skripuletz, T., Hackstette, D., Bauer, K., Gudi, V., Pul, R., Voss, E., et al. (2013). Astrocytes regulate myelin clearance through recruitment of microglia during cuprizone-induced demyelination. *Brain* 136, 147–167. doi: 10.1093/brain/aws262

Slowik, A., Schmidt, T., Beyer, C., Amor, S., Clarner, T., and Kipp, M. (2015). The sphingosine 1-phosphate receptor agonist FTY720 is neuroprotective after cuprizone-induced CNS demyelination. *Br. J. Pharmacol.* 172, 80–92. doi: 10.1111/bph.12938

Song, S. Y., Kato, C., Adachi, E., Moriya-Sato, A., Inagawa-Ogashiwa, M., Umeda, R., et al. (2007). Expression of an acyl-CoA synthetase, lipidosin, in astrocytes of the murine brain and its up-regulation during remyelination following cuprizone-induced demyelination. *J. Neurosci. Res.* 85, 3586–3597. doi: 10.1002/jnr.21456

Takasawa, S., Nata, K., Yonekura, H., and Okamoto, H. (1993). Cyclic ADP-ribose in insulin secretion from pancreatic beta cells. *Science* 259, 370–373. doi: 10.1126/science.8420005

Tullius, S. G., Biefer, H. R., Li, S., Trachtenberg, A. J., Edtinger, K., Quante, M., et al. (2014). NAD^+ protects against EAE by regulating $CD4^+$ T-cell differentiation. *Nat. Commun.* 5:5101. doi: 10.1038/ncomms6101

Van Doorn, R., Van Horssen, J., Verzijl, D., Witte, M., Ronken, E., Van Het Hof, B., et al. (2010). Sphingosine 1-phosphate receptor 1 and 3 are upregulated in multiple sclerosis lesions. *Glia* 58, 1465–1476. doi: 10.1002/glia.21021

Williams, A., Piaton, G., and Lubetzki, C. (2007). Astrocytes–friends or foes in multiple sclerosis? *Glia* 55, 1300–1312. doi: 10.1002/glia.20546

Yamada, M., Mizuguchi, M., Otsuka, N., Ikeda, K., and Takahashi, H. (1997). Ultrastructural localization of CD38 immunoreactivity in rat brain. *Brain Res.* 756, 52–60. doi: 10.1016/s0006-8993(97)00117-0

Conflict of Interest Statement: The authors declare that the research was conducted in the absence of any commercial or financial relationships that could be construed as a potential conflict of interest.

frontiers in Cellular Neuroscience

REVIEW
published: 13 June 2019
doi: 10.3389/fncel.2019.00263

Neuroinflammation and Glial Phenotypic Changes in Alpha-Synucleinopathies

*Violetta Refolo and Nadia Stefanova**

Division of Neurobiology, Department of Neurology, Medical University of Innsbruck, Innsbruck, Austria

The role of neuroinflammation has been increasingly recognized in the field of neurodegenerative diseases. Many studies focusing on the glial cells involved in the inflammatory responses of the brain, namely microglia and astroglia, have over the years pointed out the dynamic and changing behavior of these cells, accompanied by different morphologies and activation forms. This is particularly evident in diseased conditions, where glia react to any shift from homeostasis, acquiring different phenotypes. Particularly for microglia, it has soon become clear that such phenotypes are multiple, as multiple are the functions related to them. Several approaches have over time revealed different facets of microglial phenotypic diversity, and advanced genetic analyses, in recent years, have added new insights into microglial heterogeneity, opening novel scenarios that researchers have just started to explore. Among neurodegenerative diseases, an important section is represented by alpha-synucleinopathies. Here alpha-synuclein accumulates abnormally in the brain and, depending on its pattern of distribution, leads to the development of different clinical conditions. Also for these proteinopathies, neuroinflammation and glial activation have been identified as constant and crucial factors during disease development. In the present review we will address the current literature about glial phenotypic changes with respect to alpha-synucleinopathies, as well as consider the pathophysiological and therapeutic implications of such a dynamic cellular behavior.

Keywords: microglia, astroglia, alpha-synuclein, neuroinflammation, Parkinson's disease, multiple system atrophy

OPEN ACCESS

Edited by:
Xiaobo Mao,
Johns Hopkins University,
United States

Reviewed by:
Andrew MacLean,
Tulane University School of Medicine,
United States
Veronica Ghiglieri,
University of Perugia, Italy
Enquan Xu,
Duke University, United States

***Correspondence:**
Nadia Stefanova
Nadia.Stefanova@i-med.ac.at

Specialty section:
This article was submitted to Non-Neuronal Cells, a section of the journal Frontiers in Cellular Neuroscience

Received: *28 February 2019*
Accepted: *28 May 2019*
Published: *13 June 2019*

Citation:
Refolo V and Stefanova N (2019) Neuroinflammation and Glial Phenotypic Changes in Alpha-Synucleinopathies. Front. Cell. Neurosci. 13:263. doi: 10.3389/fncel.2019.00263

INTRODUCTION

Alpha-synucleinopathies are a family of neurodegenerative disorders characterized by the misfolding and accumulation in the brain of alpha-synuclein, a 140-amino-acid protein, encoded by the *SNCA* gene. The physiological form of alpha-synuclein is known to be normally present in neurons, and particularly enriched at pre-synaptic terminals. Its function is still partially unclear, but it seems to be associated with synaptic vesicles' trafficking during neurotransmitter release (Bellani et al., 2010). The major diseases belonging to the group of alpha-synucleinopathies are Parkinson's disease (PD), multiple system atrophy (MSA) and dementia with Lewi bodies (DLB) (Spillantini and Goedert, 2000; Goedert et al., 2017). Whereas in PD and DLB alpha-synuclein forms filamentous aggregates in neurons, in form of Lewy bodies and Lewy neurites (Spillantini et al., 1997, 1998a), MSA is mainly characterized by oligodendrocytic inclusions of the protein, called glial cytoplasmic inclusions (GCIs), representing the hallmark of the disease (Papp et al., 1989; Spillantini et al., 1998b; Wakabayashi et al., 1998; Wenning and Jellinger, 2005;

Jellinger and Lantos, 2010). PD is one of the most common neurodegenerative diseases, with clinical presentations including bradykinesia, rigidity, resting tremor and gait instability (Gelb et al., 1999). Its main pathological features are loss of dopaminergic neurons in the substantia nigra pars compacta (SNc) and widespread distribution of Lewy bodies and neurites at post-mortem analysis (Forno, 1996; Gelb et al., 1999). Such alpha-synuclein pathology is hypothesized to slowly spread from medulla oblongata and olfactory system to brainstem, limbic system and finally neocortex (Halliday et al., 2011). On the other hand, MSA is mainly characterized by parkinsonism, autonomic failure and cerebellar ataxia in various combinations. GCIs are distributed throughout the brain, and the disease can be subdivided into a parkinsonian (MSA-P) and a cerebellar variant (MSA-C), depending on its main clinical and pathological presentation (striatonigral degeneration (SND) or olivopontocerebellar atrophy (OPCA), respectively) (Fanciulli and Wenning, 2015; Krismer and Wenning, 2017). Finally, DLB is, after Alzheimer disease (AD), the second most frequent cause of dementia in elderly people. It is characterized by visual hallucinations, fluctuating consciousness and parkinsonism (McKeith et al., 2005), with abundant cortical Lewy bodies and various levels of AD-related pathology (Trojanowski and Lee, 1998; Spillantini and Goedert, 2000). Beyond the details that distinguish the single alpha-synucleinopathies, the common picture of alpha-synuclein pathology, neurodegeneration and atrophy, in various degrees, is accompanied by neuroinflammation and glial reactivity, which represent another constant finding in these conditions. In line with findings in other neurodegenerative diseases (Akiyama et al., 2000; Henkel et al., 2004; Mrak and Griffin, 2005; Liu and Wang, 2017), there is cumulative evidence of the participation of neuroinflammatory processes in the development and progression of the pathology for PD and MSA (Gerhard et al., 2003; Wang Q. et al., 2015). As far as DLB is concerned, reports of neuroinflammation and gliosis exist (Mackenzie, 2000; Terada et al., 2000; Surendranathan et al., 2018), but are much less numerous and detailed than the ones addressing other diseases, leaving room for much progress in the field. An increasing number of studies points toward different forms of neuroinflammatory responses, linked to multiple glial phenotypes. From a starting idea of cells broadly acting in a positive or detrimental way on the diseased brain (Cherry et al., 2014), a far more multifaceted picture has emerged over the years. Not only the specific pathology, but also other variables, such as disease stage, brain region and aging process, can indeed influence the glial response to the surrounding stimuli (Grabert et al., 2016; Refolo et al., 2018). Thereby, we will here review the glial phenotypic changes related to neuroinflammatory responses and neurodegeneration in alpha-synucleinopathies, with a particular focus on PD and MSA.

GLIAL CELLS INVOLVED IN NEUROINFLAMMATION

The term neuroinflammation (that is, inflammation taking place in the central nervous system (CNS)) comprises a number of events meant to tackle possible or actual threats for the brain. In other words, every time the CNS is faced with infectious agents, traumatic injuries or other unknown elements that might cause a disruption of its homeostasis, it will protect itself by initiation of a series of actions aiming at the elimination of the pathogenic factor. Main actors in this scenario are astroglia and microglia (Kreutzberg, 1995; O'Callaghan and Sriram, 2005). Upon activation, also called "gliosis," these cells get involved in the production of (and, at the same time, response to) inflammatory cytokines and chemokines, which maintain and enhance the inflammatory condition.

Microglia, in particular, get increasingly highlighted as key players in these processes. Nevertheless, the spectrum of their tasks extends beyond this. Franz Nissl was the first to describe these cells in the end of the nineteenth century, defining them as rod cells (originally "Stabchenzellen"), capable of proliferation, motility and phagocytosis. In 1846, Rudolf Virchow first talked about neuroglia as a kind of glue keeping neurons together, and it became clear only later that these neuroglia were in fact composed of three different cell types, namely oligodendroglia, astroglia and microglia. It was only in 1919 that Pio del Rio-Hortega, a student of the Spanish neuroanatomist Santiago Ramon y Cajal, could distinguish microglia from the other glial cells based on their morphological and functional characteristics (for the English translation of del Rio-Hortega's four papers where microglia's description can be found, published in 1919, please refer to Sierra et al., 2016). Firstly believed to have a neuroectodermal origin, it took quite a long time before it was accepted that microglia have a myeloid origin, like macrophages (Perry et al., 1985; Akiyama and McGeer, 1990; Mckercher et al., 1996; Beers et al., 2006). After this finding, new debates opened about the exact origin of their progenitors. Indeed, it was first believed that microglia could be derived from blood-circulating monocytes, hence having a bone marrow origin. However, increasing evidence emerged over time about a separated embryonic origin of microglia. Nowadays it is accepted that microglia originate in the yolk sac and seed the rudimental brain during early phases of fetal development (Takahashi et al., 1989; Takahashi and Naito, 1993; Alliot et al., 1999; Rezaie et al., 2005; Monier et al., 2007; Prinz et al., 2017). Microglia are extremely dynamic cells. Besides their inflammatory action, it has been shown that they are very important in the maintenance of the homeostasis of the brain in healthy conditions, and play significant roles in neural development and plasticity. Microglia represent between 5 and 20% of all glial cells, and 10% of all the cells populating the mammal brain (Lawson et al., 1990; Katsumoto et al., 2014). Interestingly, it seems that the density of microglia differs between brain regions, with highest levels found in the SN (Yang et al., 2013). One of the main features these cells present in homeostatic conditions is their surveillance activity in the brain. It has been shown, also by *in vivo* imaging, that they stretch out and retract continuously their processes in a highly dynamic way, in order to scan the surrounding microenvironment (Nimmerjahn et al., 2005). If, during their surveillance activity, they come across any kind of risk factor, they get activated and start a series of actions meant to get rid of it, as we will discuss later in more detail.

Furthermore, they express specific surface molecules and release soluble factors that influence neuronal and astrocytic function (Kettenmann et al., 2011), and are able to clear debris and aggregated proteins (Lee et al., 2010c). In an earlier phase, during fetal development, they assist neurogenesis guiding the formation of prenatal circuits (Squarzoni et al., 2015) and phagocytosing apoptotic cells (Fourgeaud et al., 2016). In post-natal life, microglia continue helping the maintenance of functional neuronal circuits by synaptic pruning. For instance, studies using *in vivo* imaging and high-resolution electron microscopy in mice have shown that microglia get in contact with dendritic spines through their processes, suggesting an active role of these cells in synaptic remodeling (Wake et al., 2009; Tremblay et al., 2010). The awareness of such a role for microglia in the regulation of neuronal networks, in particular during pre-natal and early post-natal phases, has soon prompted the possibility of their involvement in autism spectrum disorders and other neurodevelopmental disorders, such as schizophrenia, and increasing evidence is supporting this idea (Morgan et al., 2010; Tetreault et al., 2012; Sekar et al., 2016; Howes and McCutcheon, 2017). Interestingly, it has been proposed that early synaptic alterations might take place also in alpha-synucleinopathies, as recently shown in the striatum of a PD mouse model (Giordano et al., 2018). These and other observations raise the possibility for glial involvement also in such alpha-synuclein-related events (Aono et al., 2017). This is, for instance, suggested by a study showing restoration of striatal synaptic plasticity in PD rats in association with the reduction of micro- and astrogliosis (Cacace et al., 2017; Ghiglieri et al., 2018). Finally, work by Hagemeyer et al. (2017) suggests that microglia might also contribute to development and homeostasis of oligodendrocyte precursor cells and to myelinogenesis in adulthood.

Also astroglia give an important contribution to neuro-inflammation, besides performing many other fundamental functions for the maintenance and homeostasis of the CNS. After Virchow's proposed concept of neuroglia, the first description of an astrocyte came from Deiters (1865), even though the term "astrocyte" was introduced only later on by Lenhossék (1895) to describe a star-shaped subtype of parenchymal glia. More details about astrocytic morphology and diversity started to be unraveled by Ramon y Cajal and del Rio-Hortega between the end of the nineteenth and the beginning of the twentieth century (Sierra et al., 2016), and, since then, a crescendo of knowledge about these cells has been accumulated. Astrocytes represent the most abundant cell type in the brain. They derive from neuroepithelial radial glia (Kriegstein and Alvarez-Buylla, 2009), although only a portion of astrocytes originates from these precursors during embryonic development; the remaining mature astroglia form during post-natal life by symmetric division of already existing ones (Ge et al., 2012). The actions of astrocytes in the healthy brain are very diverse and key to its proper function. For instance, these cells, and in particular their "endfeet," are part of the so called neurovascular unit of the blood brain barrier (BBB), thus representing the link between neurons and blood vessels in the brain, and contributing to the great selectivity of this interface between CNS and peripheral tissues (Abbott et al., 2006; Noell et al., 2011). In relation to this, they have also been shown to be involved in the recently discovered "glymphatic system" of the brain. This, comparably to what the lymphatic system does in the rest of the body, allows the elimination of the brain's waste from the CNS. The astrocytic aquaporin-4 (AQP4), in particular, enables the movement of subarachnoid CSF into the interstitial space, so that CSF can be exchanged with interstitial fluid, and the latter gets eventually driven toward the lymphatic nodes (Iliff et al., 2012; Nedergaard, 2013; Xie et al., 2013). This mechanism might be important also for the clearance of potentially pathogenic proteins, as shown for amyloid-β (Xie et al., 2013). Beside this, astrocytes are fundamental regulators of homeostasis in the brain's parenchyma. They control ion concentrations in the extracellular space (in particular K^+), in order to maintain ideal conditions for neuronal excitability and signaling (Song and Gunnarson, 2012; Bellot-Saez et al., 2017). They as well monitor the levels of several neurotransmitters (such as glutamate), which is of paramount importance for their turnover, and to prevent excitotoxicity (Rothstein et al., 1996). Furthermore, they provide an important metabolic support to neurons, for instance through glycogen storage and lactate production (Brown and Ransom, 2007; Stobart and Anderson, 2013). Astrocytes have also been shown to play a role in synaptogenesis and in supporting neuronal connectivity (Eroglu and Barres, 2010; Allen and Eroglu, 2017).

NEUROINFLAMMATION IN ALPHA-SYNUCLEINOPATHIES

As emerges from the last paragraph, microglia and astroglia are gaining more and more attention from different research fields, alongside with the awareness of the plethora of functions they carry out already in the healthy brain. Nevertheless, as the focus of this review is their role in neuroinflammation in alpha-synucleinopathies, we will now concentrate on this aspect of their activity.

Microglia are indeed known for representing the primary defense line of the CNS. They are surveilling the brain's parenchyma and constantly monitoring it with their highly motile processes (Nimmerjahn et al., 2005). Every even slight shift from homeostasis leads these very sensitive cells to react and take on a reactive form; this, however, rather than being a simple passage from one state to the other, is a more complex and dynamic process, in which microglia go through different forms of activation, with changes of their morphological and functional characteristics. The main actions that can be undertaken by activated microglia are the production and release of cytokines, chemokines and reactive oxygen (ROS) and nitrogen species (NOS), contributing to the development of the inflammatory event, as well as the phagocytosis of potentially harmful agents and cellular debris. Antigen presentation is also reported in several cases (Lynch, 2009). All of these activities are theoretically beneficial, as long as they are self-limiting, directed against the proper target and quickly resolving after removal of the threat. Functions such as production of anti-inflammatory cytokines, wound healing and debris clearance then allow microglia to restore a normal, homeostatic condition (Cherry et al., 2014).

Problems arise, however, when the pro-inflammatory event gets out of control, for instance because of persistence of the hazardous factor, as happens in alpha-synucleinopathies, and in neurodegenerative diseases in general. The ensuing vicious circle, involving the continuous and progressively amplified release of pro-inflammatory molecules and recruitment of further immune mediators, builds up a chronic inflammatory state, leading to toxicity and damage of the surrounding cellular environment. This seems to happen at the cost of the anti-inflammatory, protective functions of microglia, which are at this point not able to keep up with their detrimental effects anymore. It is still a matter of debate whether microglia and neuroinflammation are cause or consequence of the pathological events taking place in neurodegenerative diseases, but there is by now little doubt that they play a role during their progression. As of alpha-synucleinopathies, PET imaging studies have shown the presence of activated microglia in the brains of both PD (Gerhard et al., 2006) and MSA patients (Gerhard et al., 2003), despite some controversies (Ghadery et al., 2017), and increased microglial numbers have been detected by immunohistochemistry in post-mortem PD (McGeer et al., 1988; Imamura et al., 2003; Doorn et al., 2014) and MSA brain tissue (Ishizawa et al., 2004; Salvesen et al., 2015, 2017; Nykjaer et al., 2017). Genetic studies have identified several loci connected to neuroinflammation and microglial activation as risk factors for PD (Hamza et al., 2010; Holmans et al., 2013) and MSA (Nishimura et al., 2002; Infante et al., 2005; Ogaki et al., 2018). In experimental settings, it has been shown that the injection of alpha-synuclein into the SN of rats and mice leads to microgliosis, suggesting that this protein might represent a direct initiator of neuroinflammation (Wilms et al., 2009; Couch et al., 2011). The triggered neuroinflammation, in turn, seems to play a major part in neurodegeneration. It has been shown, for example, that alpha-synuclein-activated microglia enhance neuronal loss *in vitro* (Zhang et al., 2005). Furthermore, through anti-inflammatory agents such as minocycline it has been observed that such interventions have a neuroprotective effect in animal models (Du et al., 2001; Wu et al., 2002), at least if carried out before full-blown pathology is reached (Stefanova et al., 2007), thus suggesting a crucial role for microglial activation, particularly during early stages of the disease.

Astrocytes provide an important contribution during neuroinflammatory responses as well. These cells are able, besides their other multiple functions, to become reactive and work as immune mediators in the brain when elicited by proper stimuli. This includes the recognition of hazard signals, the production and release of cytokines and chemokines and the setting up of a so called glial scar (Sofroniew and Vinters, 2010). The latter is a formation principally made of reactive astrocytes, but also microglia and extracellular matrix, which has the main role of limiting the damage caused by a brain's lesion, through a sort of sealing effect. If on the one hand this represents the main beneficial effect of the scar, on the other hand there is also production of pro-inflammatory and neurotoxic mediators at its level. Furthermore, until recently it was common belief that glial scars inhibit axon regrowth beyond the scar itself, hampering regeneration (Windle et al., 1952; Silver and Miller, 2004). However, it has been highlighted that positive and detrimental effects might be time dependent, with the first ones appearing immediately after injury and the latter following later on (Rolls et al., 2009), and that glial scar formation might be even crucial for axon regeneration (Anderson et al., 2016). This again points toward the versatility of glial cells and their functions. Astrogliosis has long been described in MSA (Schwarz et al., 1996; Song et al., 2009), with reactive astrocytes observed in striatonigral and olivopontocerebellar structures, the degree of astrogliosis paralleling the neurodegenerative process (Ozawa et al., 2004) and increasing astrogliosis in proximity to GCIs (Radford et al., 2015). In PD this neuropathological feature has often been reported as being less prominent than in MSA (Mirza et al., 2000; Tong et al., 2015), until a role for astrocytes has been recognized in PD pathogenesis too (Durrenberger et al., 2009; Halliday and Stevens, 2011; Booth et al., 2017). Also for MSA there are actually some controversies in this regard, or at least indications for regional differences in astroglial responses. Whereas Salvesen et al. (2015, 2017), for instance, found increased astrocytic numbers in several brain regions, Nykjaer et al. (2017) did not see any significant difference in the number of astroglia within the white matter of MSA cases, with respect to healthy controls. As a side note, one should always be cautious when comparing studies using different parameters to assess microglial or astroglial activation, since increases or decreases in cell counts do not always parallel phenotypic or genotypic changes, which might be better indicators of these cells' reactivity. Several genetic risk factors for PD, such as DJ-1, parkin and PINK-1, have been implicated in astrocytic function (Hayashi et al., 2000; Bandopadhyay et al., 2004; Neumann et al., 2004; Solano et al., 2008; Choi et al., 2013, 2016; Kim et al., 2016), suggesting a role for astrocytes in PD pathogenesis. Alpha-synuclein, besides accumulating in neurons, has been found in astrocytes in PD as well. It is hypothesized that the protein might be released by the neurons and taken up by astroglial cells (Braak et al., 2007; Halliday and Stevens, 2011). Such a transfer has been indeed observed in *in vitro* and *in vivo* experimental settings, accompanied by the induction of a pro-inflammatory environment (Lee et al., 2010b). Furthermore, it has been shown that cultured astrocytes take up oligomeric alpha-synuclein, however, an excess of it can lead to mitochondrial damage and impaired lysosomal degradation, with consequent accumulation of the protein (Lindström et al., 2017). As of MSA, whereas Song et al. (2009) did not observe any major alpha-synuclein accumulation in astroglial cells, phosphorylated alpha-synuclein aggregates were described in astrocytes located at subpial and periventricular level in another study (Nakamura et al., 2016). Moreover, a mouse model with A53T alpha-synuclein overexpression in astrocytes showed impaired astroglial physiological activity, together with astrogliosis and consequent microgliosis and neurodegeneration (Gu et al., 2010). This study highlighted, among other things, the importance of the crosstalk between microglia and astroglia in pathological settings, pointing, in this case, toward the astrocyte-induced, secondary microglial activation as the main culprit for the neuronal loss observed in the mouse model. Nevertheless, it has also been recently

shown that activated microglia are able to induce reactivity of astrocytes, especially toward a pro-inflammatory, neurotoxic phenotype (Liddelow et al., 2017). Altogether, these data seem to indicate that the interaction between glial cells might be more complex and diverse than previously thought, and absolutely worth further in-depth studies.

SNAPSHOTS OF GLIAL NEUROINFLAMMATORY RESPONSES TO ALPHA-SYNUCLEIN

As introduced in the last paragraph, alpha-synuclein definitely exerts an effect on the innate immune system, eliciting the reactivity of glial cells in the brain. Different mechanisms and pathways have started to be unraveled, showing distinct cellular responses. For instance, through binding to CD36, monomeric alpha-synuclein can lead to the production of TNF-alpha and other pro-inflammatory mediators, as well as oxidative stress, by a cascade involving Erk phosphorylation (Su et al., 2008). The same was shown also for mutant alpha-synuclein (Su et al., 2009). A pro-inflammatory microglial response has been shown to be elicited also through FcγR-mediated phagocytosis of aggregated alpha-synuclein (Cao et al., 2012). Further, oligomeric alpha-synuclein interaction with CD11b has been reported to induce activation of the NADPH oxidase NOX2 and consequent toxic effects through production of ROS (Zhang et al., 2005; Wang S. et al., 2015). Similarly, induction of oxidative stress was observed after interaction of oligomeric alpha-synuclein with the purinergic receptor P2X7 (Jiang et al., 2015). Toll-like receptors (TLRs) represent another important class of mediators of microglial reactivity. Among the different existing types of these pattern-recognition receptors (PRR), TLR4 and TLR2 are the ones reported to be most prominently involved in the response to alpha-synuclein. Specifically, TLR4 has been shown to play an important role in the clearance of different forms of alpha-synuclein by microglia, thus providing a neuroprotective effect, as demonstrated in a mouse model of MSA and in *in vitro* settings (Stefanova et al., 2011; Fellner et al., 2013; Venezia et al., 2017). On the other hand, it has been demonstrated by different approaches that TLR2 specifically responds to oligomeric alpha-synuclein with a pro-inflammatory, neurotoxic cascade of events (Kim et al., 2013; **Figure 1**).

The role of these TLRs has been investigated also in astrocytes. In contrast to what had been observed for microglia, Rannikko et al. (2015) reported that absence of TLR4 did not have any effect on alpha-synuclein uptake by astroglial cells, whereas it decreased their pro-inflammatory responses. Similar findings had been previously reported by Fellner et al., who had also found c-terminally truncated alpha-synuclein as the most potent inducer of glial neurotoxic behavior (Fellner et al., 2013). As to TLR2, Kim et al. (2018) showed that exposure to an anti-TLR2 treatment led to amelioration of pathology and symptoms, with reduced accumulation of alpha-synuclein in neurons and astroglia, in an alpha-synucleinopathy transgenic mouse model (**Figure 1**). Such effects were reported to be mediated by blockage of alpha-synuclein transmission among neurons, and from neurons to astrocytes (Kim et al., 2018). Such a neuron-to-astrocyte alpha-synuclein transfer had already been previously observed, together with a shift toward an astroglial pro-inflammatory profile (Lee et al., 2010b). In this context, also the idea of astroglia as intermediate players in the activation of microglia during alpha-synuclein pathology arose; astrocytes can indeed release microglia-attractant chemokines, and directly influence their reactivity state through the cytokines they produce (Lee et al., 2010a).

These and other non-reported mechanisms indicate a complexity in glial neuroinflammatory responses (in alpha-synucleinopathies, but not only) which is still mostly unexplored. The tools available until recently allowed us to catch mainly separate processes, like in single snapshots, with little chance of putting the pieces together and looking at the complete picture, in a scenario suggesting multiple functions and ways of action for diverse cellular subtypes. Nevertheless, different methods have helped us over time to discover more about the different facets of glial reactivity and the role of their interplay.

MICROGLIAL HETEROGENEITY AND PHENOTYPIC CHANGES

Microglia, the innate immune defenders of the CNS, are among the most resourceful cells of our body, being able to perform a myriad of different tasks in health and disease. By doing so they not only contribute to shaping brain architecture and support the development and maintenance of a robust cerebral environment, but they also directly take on and lead the response to homeostasis dysregulations, pathogen attacks and every kind of pathological changes that might occur in the brain. This diversity in functions suggests a great versatility of microglial cells. Already del Rio-Hortega, when first describing microglia, had noticed that they were characterized by a significant degree of heterogeneity even in their normal state, differentiating, for example, between monopolar and bipolar microglia, as well as different types of multipolar microglia, based on the appearance of their processes, such as multipolar cells with branched expansions and multipolar with spiny appendages. He was able to recognize changes in microglial morphology in pathological conditions as well, with increases in dendritic and somatic volume, and sometimes also in cell numbers. He also thoroughly described another type of microglia, the so called "rod cells," named after their peculiar elongated shape. The characterization of each type of cell was also accompanied by incredibly precise drawings, which del Rio-Hortega was used to make by exactly reproducing what he observed at the microscope. Furthermore, he first recognized microglial functions such as their phagocytic capacity and high motility during pathology (Sierra et al., 2016). Del Rio-Hortega's meticulous study of microglial features and differences might nowadays surprise for its accuracy and the way it presented, and almost anticipated, details that we are today able to visualize and appreciate with far more advanced techniques than the ones used at his time. Nonetheless, these precious notions remained long neglected, in line with the rejection, by the majority of the academic world of that time, of his idea of the

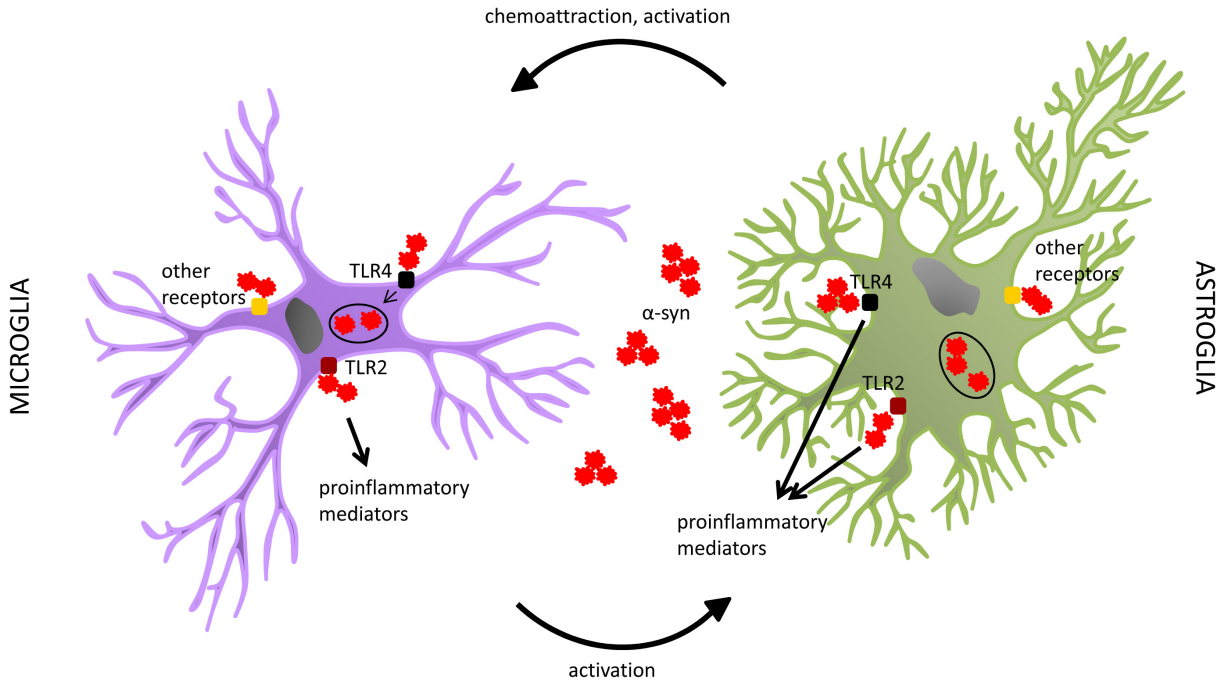

FIGURE 1 | Both microglia and astrocytes have been shown to interact with alpha-synuclein. Among the different receptors suggested to play a role in such interaction, a special focus has been put on TLR4 and TLR2. In microglia, TLR4 seems to be involved in alpha-synuclein clearance, whereas TLR2 rather participates in the production of pro-inflammatory mediators. In astroglia, both receptors have been reported to play a role in the pro-inflammatory response to alpha-synuclein, with no proof of an involvement of TLR4 in the uptake of the protein by this cell type. Both microglia and astroglia can internalize alpha-synuclein. It seems however that, despite their capability to also degrade it in normal conditions, this process might get impaired in alpha-synucleinopathies, probably due to the overload of pathogenic alpha-synuclein, with consequent accumulation of the protein in glial cells. This might lead to their dysfunction and an enhanced neurotoxic profile. Other receptors, and related pathways, have also been associated with glial responses to alpha-synuclein. Further studies are warranted to highlight alternative mechanisms involved in these processes. The interplay between glial cells seems to be relevant as well. Astrocytes, through the release of specific sets of chemokines and cytokines, are able to attract microglia and influence their activation state. On the other hand, recent evidence indicates that also microglia can induce specific astroglial profiles, which can actively affect the pathology progression.

existence of different glial cell types. It took many decades before microglia started again to attract the attention of researchers (Blinzinger and Kreutzberg, 1968; Sierra et al., 2016).

In more recent years, many studies have been undertaken to better understand the diverse physiological and functional characteristics of these very intriguing cells. As one of the most straightforward parameters to assess, **microglial morphology and morphological changes** have been extensively analyzed as measures of microglial activation. It was long shown that microglia tend to adopt a more amoeboid shape, starting from a ramified structure, upon activation (Kreutzberg, 1996; Sierra et al., 2016). Based on the awareness of the plastic and dynamic nature of these cells, different methods have been then established in order to better appreciate the gradual activation process and the involved intermediate phenotypes. For instance, Sanchez-Guajardo et al. (2010) have introduced a morphological classification for microglial activation, which distinguishes these cells in four activation subtypes (called A, B, C, and D), in a rat PD model. Through this classification they have been able to differentiate between microglia going from a resting to a completely activated state based on the appearance of cell body, nucleus and processes (namely, from microglia with thin, long processes and small nucleus and cell body, passing through a state with more abundant secondary ramifications, to one with increased volume of soma and nucleus, together with shortening and thickening of the processes, till the final, amoeboid stage of completely activated cells) (Sanchez-Guajardo et al., 2010). The same method was adapted also to a non-human primate model of PD (Barkholt et al., 2012) and to a mouse model of MSA (Refolo et al., 2018), and proved useful to identify time- and region-dependent differences in the distribution of different microglial subtypes in these models of alpha-synucleinopathies. Several other methods were meanwhile developed in order to make the process more objective and, in some cases, automated. Another subdivision in four types of microglia was obtained through a system of hierarchical cluster analysis of 3D morphometric parameters of the cells (Yamada and Jinno, 2013). Other methods to morphologically distinguish microglial subsets, based on mathematical and computational approaches, include fractal analysis (Karperien et al., 2013; Morrison et al., 2017), Sholl analysis (Morrison and Filosa, 2013; Heindl et al., 2018), as well as combinations of statistics and clustering analyses, as described by Davis et al. (2017). Moreover, Verdonk et al. (2016) developed a system for automated assessment of several parameters related to microglial morphology in CX3CR1$^{GFP/+}$ mice, which present with fluorescent microglia. Beyond the practical differences

among the applied approaches, all these methodologies share the ability to show the extreme variability of microglia in normal, but even more in pathologic conditions. Deviations from the classical morphologies, and thus further phenotypic changes, have additionally been observed with aging. For instance, in aged human brains dystrophic microglia have been described, showing fragmented cytoplasm, deramified processes and bulbous swellings (Streit, 2004), whereas reduced complexity (Sierra et al., 2007; Damani et al., 2011) and size (Damani et al., 2011; Hefendehl et al., 2014) of processes have been observed in old rodents. This may represent an important matter of future research in the field of neurodegenerative diseases, since the changes microglia undergo with aging might be an additional, significant factor to be taken into account when considering their role and way of contributing to these diseases. Studies showing phagocytosis deficits in aged microglia support this hypothesis (Njie et al., 2012; Solito and Sastre, 2012; Bliederhaeuser et al., 2016), and recent transcriptomic data suggest the existence of an aging-related phenotype of these cells (Olah et al., 2018), with possible differences between mouse and human aged microglia (Galatro et al., 2017). A separate morphological category of microglial cells, already described, as mentioned before, by del Rio-Hortega, is that of rod-shaped microglia. The existence of these particular cells was actually already reported in 1899 by Franz Nissl, who defined "*Stäbchenzellen*" cells with an elongated cell body, generally located close to neighboring neurons (Nissl, 1899) and often forming "trains" of aligned cells. Described in different neurological conditions (Wierzba-Bobrowicz et al., 2002; Lambertsen et al., 2011; Ziebell et al., 2012), they have been shown to be induced also by alpha-synuclein (Zhang et al., 2005). Although rod-type microglia have been suggested to play a role in synaptic reorganization after injury (Ziebell et al., 2012; Au and Ma, 2017), their exact properties remain elusive, both in alpha-synucleinopathies and in other diseases. Finally, a very recently defined new phenotype of microglia is the "dark microglia," so called because of their electron-dense cytoplasm and nucleoplasm when analyzed through transmission electron microscopy. These cells are mainly associated with pathological conditions and have been shown to be actively phagocytic, engulfing in particular synaptic elements (Bisht et al., 2016). So far, studies assessing the presence of dark microglia in alpha-synucleinopathies are still lacking.

Even though these and other morphological analyses have been and continue proving fundamental for the understanding of microglial multiple facets, they are generally *per se* lacking substantial information about the **functional correlates** to the described cell subsets. The easiest ways to address this issue generally include the additional use of microglial markers associated with specific functions (such as CD68 for phagocytic activity or MHCII for antigen presentation) or a detailed description of their effects on the surrounding microenvironment, with consequent assumption of the role they might play in such a context. As these approaches are limited and somewhat speculative, a need emerged quite soon for more robust ways to characterize microglial functional phenotypes. The most popular functional classification of microglia is the M1/M2 activation profile, which has been dominating the literature for several years. This classification originally relied on the need for a conceptual simplification of microglia's spectrum of actions in neuroinflammatory conditions, as well as on the observation of their ability to broadly act either in a beneficial or a detrimental way in the diseased brain. From here the idea to divide microglia in a pro-inflammatory, "classically" activated subset (M1) and in an anti-inflammatory, "alternatively" activated one (M2). This nomenclature was adopted from the M1/M2 distinction originally introduced for macrophages, based on the differential profile they developed under Th1 or Th2 cell specific cytokine stimulation (Nathan et al., 1983; Stein et al., 1992; Doyle et al., 1994; Mills et al., 2000). M1 microglia are generally described as active producers of pro-inflammatory mediators, such as TNFα, IL-1β, IL-6, MIP-1α, ROS and NOS, through which they exert their detrimental effects over prolonged inflammatory periods. On the other hand, M2 microglia are reported to release anti-inflammatory mediators, such as IL-10 and IL-4, and upregulate markers like Arg1 and CD206, being involved in downregulation of the inflammatory process and restoration of a homeostatic condition (Boche et al., 2013; Cherry et al., 2014). However, the availability of more advanced technologies, and their implementation for the study of microglia, has in recent years further broadened our understanding of these cells' changeable nature and multiple functional subsets, as we will shortly discuss. Even though the M1/M2 classification is still often used or referred to by many studies, there is meanwhile consensus among microglia experts that this is an excessive oversimplification of their varied character, not appropriate anymore to reflect their complexity, and that it should therefore be replaced by more modern concepts (Ransohoff, 2016; Ajami et al., 2018).

Novel, selective **genetic analyses** do indeed represent the new gold standard to get insights into glial multiplicity; these very modern technologies allow in-depth analysis of the cells' genetic identity and thus clustering in genetic/functional groups that would have never been possible before. In the last few years, several studies have taken advantage of such analyses to unravel new facets of microglial heterogeneous behavior in different conditions. Grabert et al. (2016) were able to confirm regional microglial differences through RNA extraction of microglia isolated from different mouse brain regions. Furthermore, by doing so in mice sacrificed at different ages, they also showed differential changes along the aging process in the analyzed brain regions, which might represent an underlying mechanism for region-specific vulnerability in some brain areas involved in neurodegenerative processes (Grabert et al., 2016). A similar rationale was used by De Biase et al. (2017) to analyze microglial differences among basal ganglia nuclei, which are affected in PD and MSA. Even among these nuclei they found microglial heterogeneity through transcriptome analysis, further showing that the differences started to appear around the second post-natal week of the mice, apparently induced, and later maintained, by specific local cues (De Biase et al., 2017). Tay et al. (2017) observed transcriptional changes between microglia isolated from the ipsi- and contralateral facial nuclei of mice which had undergone unilateral facial nerve axotomy, and differences were evident also at different time points after the lesion. In the same

study they also established a new fluorescence fate mapping system, which allowed them to analyze microglial dynamics in living animals through intravital microscopy via a cranial window (Tay et al., 2017). Finally, transcriptional profiling of microglia isolated from the spinal cord of a mouse model of amyotrophic lateral sclerosis (ALS) aided the identification of a protective type of these cells, which seems to be fundamental for the clearance of the pathogenic protein TDP-43 and the regeneration of the affected motor neurons (Spiller et al., 2018). Interestingly, in most of these studies the authors followed also the morphological variations accompanying microglial genetic changes, showing the willingness to link the newly addressed transcriptomic data with the classic morphological profiles.

Even though these analyses on discrete microglial groups had already represented a huge step further in the comprehension of the genetic background of their heterogeneity, the advent of **single-cell technologies** has led the research in the field to the next level. Considering the repeatedly proven changes that microglia undergo, it was not pointless to expect an even greater variability, which single-cell analyses would be even more sensitive to. To begin with, Mathys et al. (2017) applied single-cell RNA sequencing to microglia isolated from the hippocampus of an AD-like neurodegeneration mouse model, and found distinct subsets, changing with disease stage and degree of neurodegeneration. Using a slightly different approach, that is single-cell mass cytometry, Ajami et al. (2018) demonstrated the presence of different myeloid cell profiles among mouse models of different diseases, whereas Bottcher et al. (2019) confirmed region-specific heterogeneity also for human microglia. Very interestingly, in a work of 2017, Keren-Shaul and colleagues performed single-cell transcriptome analysis of microglia isolated from an AD mouse model and discovered a new microglia type, which they called "DAM" (disease-associated microglia), completely absent in healthy wild-type animals. These cells were reported to be activated in two sequential steps (the first one being Trem2-independent while the second one Trem2-dependent), to be mostly concentrated around amyloid-β (Aβ) plaques and to have phagocytic activity toward Aβ, overall described as having a beneficial effect on AD pathology. Furthermore, they found DAM also in an ALS mouse model (Keren-Shaul et al., 2017). Through the same technology, in a subsequent study Tay et al. (2018) identified a unique microglia population, ensuing specifically in the beginning of the recovery phase in a neurodegeneration model, and these cells showed high transcriptional similarity with the DAM described by Keren-Shaul et al. (2017). Moreover, also in the previously cited work by Mathys et al., one of the microglial subpopulations detected by the authors, mainly appearing in an advanced stage of the disease, shared many genes with DAM (Mathys et al., 2017). In a recent study, Masuda et al. further found disease-specific microglial subsets, in addition to age- and region-specific ones, after analysis of single microglial cells isolated from mouse and human brains (Masuda et al., 2019). These studies show the relevance of such analyses, not only for a more in-depth appreciation of the multiple microglial phenotypes, but, even more importantly, for the discovery of subsets of these cells directly involved in specific mechanisms/disease stages/functions during pathologic processes. The possibility of identifying selected targets, and knowing their exact genetic signature, indeed opens concrete chances for tailored therapeutic interventions. DAM might represent one of microglial subpopulations to be modulated for this purpose. As they have been detected already in AD and ALS models, it is possible that they might play a role also in other neurodegenerative conditions. Both for this and for other candidate microglial subgroups, this kind of studies represents the future also in the field of alpha-synucleinopathies, and, once addressed, will for sure lead to enormous progress in the understanding of microglial contribution to these pathologies.

ASTROGLIAL HETEROGENEITY AND PHENOTYPIC CHANGES

When looking at what is known about astroglial phenotypic heterogeneity and changes, the situation is quite different if compared to microglia. That the term astrocyte comprises a varied population of cells already in the healthy brain is actually nothing new, as different morphologies, markers, functions and cerebral locations have been long reported. The first distinction that has been made was the one between protoplasmic astrocytes, residing in the gray matter and presenting with a ramified morphology, and fibrous ones, which can be found in the white matter and have long, scarcely ramified processes (Ramon y Cajal, 1909; Sofroniew and Vinters, 2010). In PD, accumulation of alpha-synuclein was observed in protoplasmic astrocytes but not fibrous ones, whereas in MSA fibrous astrocytes where the ones shown to be the most reactive to the concomitant pathology (Song et al., 2009). Specialized astroglia have then been detected, such as Müller glia in the retina and Bergmann glia in the cerebellum, but also velate astrocytes, tanycytes, ependymal glia, marginal glia, perivascular glia (Emsley and Macklis, 2006) and further categories that can be found throughout the literature (Verkhratsky and Nedergaard, 2018). Both inter-regional and intra-regional differences have been highlighted, not only morphologically, but also in terms of functions and protein expression (Garcia-Abreu et al., 1995; Oberheim et al., 2012). In recent years, more advanced technologies have been implemented in the field. For instance, five different astrocytic subpopulations were identified through an intersectional fluorescence-activated cell sorting (FACS)-based method, and subsequent RNA sequencing, in different mouse brain regions (John Lin et al., 2017), whereas an extensive study on the mouse brain at the single-cell level revealed the presence of seven transcriptionally distinct types of astrocytes (Zeisel et al., 2018).

However, phenotypic changes upon astrogliosis are far less known than the ones occurring in microglia, as this research field is still in its infancy. Also for astrocytes, pathological changes in the CNS lead to their activation. Reactive astrocytes are generally recognized for being hypertrophic, upregulating glial fibrillary acidic protein (GFAP, one of the most used astroglial markers) and often for the formation of a glial scar, as already previously discussed in the text (Sofroniew and Vinters, 2010). This view of reactive astrogliosis has however evolved in the last years, driven by new studies focusing on this

process. In 2012, by transcriptome analysis of astrocytes isolated from an ischemia and an inflammation mouse model, it was shown that both pathologic conditions elicited reactivity of these cells, but in different ways; whereas the differentially expressed genes after stroke suggested a rather protective phenotype, the ones upregulated upon neuroinflammation indicated potentially detrimental effects (Zamanian et al., 2012). Similarly, "pro-" and "anti-inflammatory" astroglial polarization states were observed also in another work, through *in vitro* and *in vivo* approaches (Jang et al., 2013). Thus, the dichotomy long used for macrophages and microglia started to be considered also for astrocytes. Indeed, in 2017 Liddelow and coworkers introduced the distinction between "A1" and "A2" astrocytes; they defined as A1 those with a detrimental function, showing upregulation of genes involved in the classical complement cascade, and A2 those with a beneficial effect, mainly upregulating genes encoding for neurotrophic factors. This was done in the context of a study where they showed that activated microglia, by production and release of mediators such as TNF, Il-1α and C1q, were the direct initiators of astroglial polarization toward the A1 phenotype. These astrocytes, in turn, took on a neurotoxic profile and caused degeneration of neurons and oligodendrocytes (Liddelow et al., 2017). This, among other findings, confirmed the importance of the crosstalk between microglia and astrocytes, and opened new exciting possibilities for the understanding of glial involvement in pathological processes. In their work, Liddelow et al. (2017) further showed that post-mortem PD brains (as well as those of patients with other neurodegenerative conditions) were positive for A1 markers in regions affected by the disease, thus postulating that these astrocytes might play a role in neurodegeneration. Soon after, Yun et al. demonstrated that, by preventing microglial activation through administration of a glucagon-like peptide-1 receptor (GLP1R) agonist, they were able to hinder astroglial transition toward an A1 phenotype, and this resulted in neuroprotection and preservation of motor functions in two mouse models of PD (Yun et al., 2018). On the other hand, another study showed that microglia can lead to the induction of an astrocytic neuroprotective profile via a pathway involving the $P2Y_1$ receptor (Shinozaki et al., 2017). On the basis of what has happened in the microglia field, it remains to be seen whether this A1/A2 classification will prove appropriate for astrocytes, or whether it will need to be further revised. Nevertheless, these studies have been fundamental for offering a new angle to look at astrocytes and glial interactions, and have paved the way for new research targets in the field. Another type of change that has been associated with astroglial involvement in disease is that coming along with aging and cellular senescence. In 2018, Chinta and colleagues demonstrated that paraquat (a neurotoxin which has been associated with increased risk of developing PD) induces astrocytic senescence in PD brains, as well as in experimental models, suggesting that this factor might contribute to PD pathology (Chinta et al., 2018). In line with this, a study analyzing the transcriptome of aging astrocytes, isolated from different mouse brain regions, showed differential age- and region-specific changes, possibly related to specific pathologic mechanisms taking place in aging-associated diseases (Boisvert et al., 2018). Furthermore, Clarke et al. (2018) observed, through a similar approach, the induction of the astrocytic A1 phenotype with aging. Also in this case, microglia were found to be the promoting agent for this shift. Altogether, it is clear that big advances have been made, especially in very recent years, in the understanding of astroglial reactivity and contribution to neurodegenerative processes, such those taking place in alpha-synucleinopathies. The dialog with microglia seems to be of critical importance in this context, and will for sure represent the focus of further exciting research in the near future. Nevertheless, as suggested by the finding of different, molecularly defined astroglial subpopulations already in the healthy brain (John Lin et al., 2017; Zeisel et al., 2018), there is probably still much more to be uncovered about the fine changes that their profiles can undergo in distress conditions, and population and single-cell molecular analyses will also in this case open up many new possibilities.

IMPLICATIONS FOR THERAPEUTIC APPROACHES

To date, PD and MSA are still lacking a cure. Researchers are struggling in the attempt to uncover pathogenic mechanisms and significant contributing factors, in order to find exact targets to address for effective therapeutic options, but every effort so far has failed, particularly when coming to clinical trials. Among the pathogenic candidates, neuroinflammation has gained a relevant position over time, along with the increasing recognition of the role it plays in alpha-synucleinopathies (Zhang et al., 2005; Stefanova et al., 2007; Wilms et al., 2009; Couch et al., 2011). Several treatments, targeting this process at different levels, have been experimented, and in most cases they have proven successful when tested in animal models. One example for this is minocycline, a tetracycline antibiotic showing anti-inflammatory effects, apparently through interference with the release of pro-inflammatory mediators by microglia (Tikka and Koistinaho, 2001; Wu et al., 2002). Although conflicting results emerged from different studies (Chen et al., 2000; Zhu et al., 2002; Smith et al., 2003; Diguet et al., 2004), it is generally accepted that minocycline has the potential for being neuroprotective in various neurological conditions, as has been demonstrated in several occasions (Zhu et al., 2002; Wang et al., 2003; Hunter et al., 2004). It has been tested in PD and MSA animal models as well, showing positive effects in terms of neuroinflammatory responses and neuropathology (Du et al., 2001; He et al., 2001; Wu et al., 2002; Tomás-Camardiel et al., 2004; Stefanova et al., 2007). However, when going into clinical trials, in none of the two diseases minocycline exerted the hoped beneficial effect (NINDS NET-PD Investigators, 2008; Dodel et al., 2010). In MSA patients, it even lowered the levels of activated microglia with respect to the placebo-treated group, but this was not sufficient to ensure also an amelioration of the motor symptoms (Dodel et al., 2010). This is a good example to point out the limitations of most of the treatments targeting neuroinflammation so far. One of the major issues is the timing of treatment initiation. As demonstrated in the experimental models getting minocycline, it seems to be of critical importance to start the administration before onset of

the clinical symptoms. When neurodegeneration has already abundantly taken place, which is the case in clinically diagnosed patients, it is apparently too late to target microglial activation, at least with the compounds tested up to now. This is also in line with the demonstrated early onset of neuroinflammatory responses during the development of alpha-synucleinopathies (Stefanova et al., 2007; Marinova-Mutafchieva et al., 2009; Refolo et al., 2018). Early treatment seems to be essential for success.

However, another problem might be the specificity of such drugs. Next-generation population and single-cell molecular analyses have opened our eyes on a much higher variability in microglial responses than ever thought. Various subpopulations of microglia have already been described, with region-, age- and disease-specific differences, and the study of this variegation is only in its beginnings (De Biase et al., 2017; Mathys et al., 2017; Ajami et al., 2018; Bottcher et al., 2019; Masuda et al., 2019). In particular, the discovery of DAM, a type of microglia found in association with diseased conditions (Keren-Shaul et al., 2017), has introduced the possibility of specific profiles having specialized functions during pathological processes. In the light of this, it is clear that targeting discrete microglial subpopulations will represent the future for new therapeutic approaches. Indeed, aiming at general microglial pathways, which may be common to different types

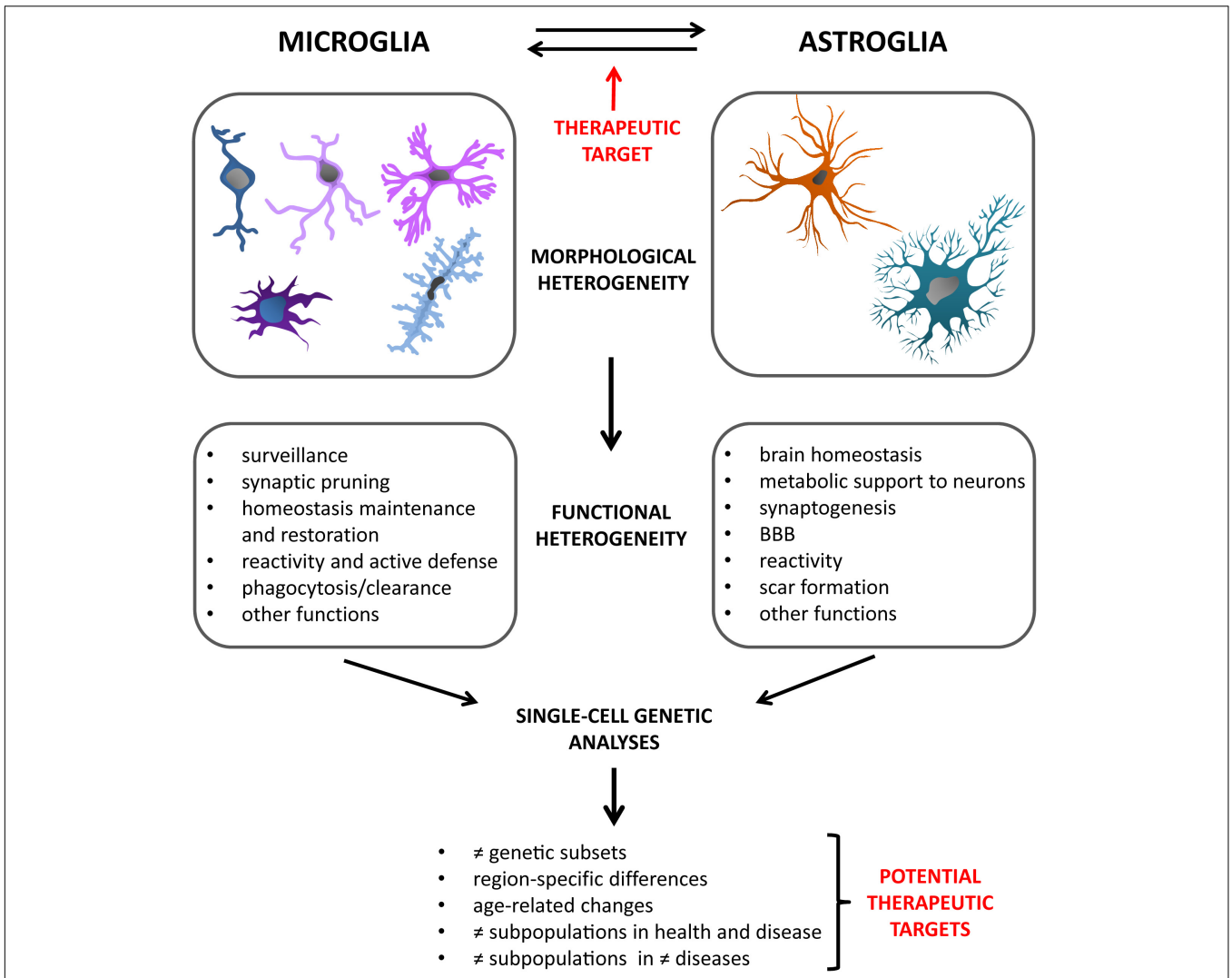

FIGURE 2 | Glial cells are characterized by great heterogeneity. Besides their multiple morphological phenotypes, they present with an impressive variety of functions, both in health and disease. New technologies are progressively allowing us to acquire increasingly in-depth insights into these varied glial profiles. In particular, single-cell genetic analyses have in recent years opened up a new range of possibilities in this regard. They have indeed revealed the existence of different glial subsets, defined on a genetic basis. Moreover, studies carried out considering different variables, such as age, brain regions, healthy or diseased state, have added further facets to the already intricate picture of the diverse glial subtypes. The field of alpha-synucleinopathies will also greatly benefit from studies of this kind in the near future, creating the possibility for novel, targeted therapeutic approaches. Also the microglia-astroglia crosstalk has been recently confirmed as an important way by which glial cells can mutually influence the respective activation profiles and responses to pathology. This might offer another therapeutic target to assess in future studies.

of them, risks to be counterproductive and even deleterious in the long term. For instance, in case of infection, or any other type of acute event for which a pro-inflammatory intervention by microglia would be of vital importance, such generalized inflammation suppressants could do more harm than good. Knowing exactly which subtypes of cells exert the real, maybe pure detrimental effects, via specialized pathways, will enable us to detect the proper targets to silence, and get a step closer to our goal. Moreover, not only the "bad microglia" can be exploited to improve a pathological state. The DAM described by Keren-Shaul et al. (2017), as well as microglial subpopulations observed in other studies (Spiller et al., 2018; Tay et al., 2018), were recognized as acting in a beneficial way on certain aspects of the pathology, and to ensue during defined stages of the disease. Specifically boosting cells with such a protective profile has therefore the potential to represent another powerful strategy to steer the disease course in a tailored way, for instance by enhancing regenerative effects or the clearance of pathogenic proteins. Combination of such "customized" treatments, precisely dampening or promoting exact, molecularly defined, microglial subtypes, might be the winning move for successful modulation of what is comprised in the broad concept of "microglial activation." Furthermore, based on the observation of different microglial molecular profiles among models of distinct pathologies (Ajami et al., 2018; Masuda et al., 2019), it is possible that also the subpopulations to be pharmacologically targeted may differ from disease to disease. Further research will be needed to discover such pathology-specific microglial niches and, where appropriate, adjust therapeutic interventions accordingly (**Figure 2**).

In the regard of treatments targeting neuroinflammation, it has to be recognized that microglial activation is generally meant as the main focus of such approaches. However, several studies have started to highlight the relevant and often neglected role that also astroglial reactivity plays during neuroinflammatory responses, such as those taking place during alpha-synucleinopathies (Durrenberger et al., 2009; Song et al., 2009; Booth et al., 2017). Particularly, in recent years, it has emerged that also astrocytes possess at least a dichotomous behavior, with polarization states showing pro- or anti-inflammatory actions (Liddelow et al., 2017) and apparently offering further chances for therapeutic interventions. As discussed before, also for astrocytes molecular analyses at the single-cell level will help to find out more about their variable nature in response to diseased conditions, and will thus increase the selection of targets for single and combined treatments. Nevertheless, even with a greater awareness of astroglial importance *per se*, microglia are far from being out of the scene. Indeed, many of the most recent studies addressing astrocytic differential involvement in neuroinflammation and pathology have as well shown that microglia are able, through specific cues, to guide astrocytes toward different functional profiles (Liddelow et al., 2017; Shinozaki et al., 2017; Yun et al., 2018). This shows that also the crosstalk between microglia and astrocytes should not be underestimated, but rather further analyzed, in particular in the context of neurodegeneration (**Figure 2**). A better understanding of the way glial cells interact, also in the light of their multiple phenotypes, specific pathology and disease stage, will be key to the development of proper therapeutic strategies.

CONCLUSION

There is by now little doubt that neuroinflammation is a factor at least heavily influencing the pathology development in alpha-synucleinopathies like PD and MSA. Being the big protagonists in this context, microglia, and over time also astrocytes, have been recognized as important elements to be modulated for therapeutic interventions in these diseases, as well as in neurodegenerative conditions in general. Even though the idea of these cells being able to acquire different phenotypes, accompanied by different morphologies and functions, was not new, the advent of modern imaging techniques, followed by advanced molecular analyses, has greatly widened our knowledge about their multiple ways to act in health and react in disease. Even more recently, RNA sequencing and other technologies, carried out at the single-cell level, have shed additional light on glial heterogeneity; they are enabling us to identify various glial subpopulations, differing in a region-, age-, disease- and disease stage-specific way, that we are just starting to appreciate. Further studying glial subpopulations in a context-dependent manner, and at the level of single cells, will be crucial for future identification of specific therapeutic targets; it will indeed allow for therapies aiming at neuroinflammation in an intelligent way. Furthermore, the microglia-astroglia crosstalk, long overlooked and just recently gaining new attention, has also lately demonstrated to be significant for the regulation of neuroinflammatory responses. This might represent an additional target for disease modifying strategies, and will thus need to be further addressed in the future. Glial variability and multiple phenotypes might seem confusing. Nevertheless, this heterogeneity is an invaluable tool for targeted interventions in diseases characterized by prominent neuroinflammatory events, and its understanding will open a whole range of new possibilities for these conditions.

AUTHOR CONTRIBUTIONS

VR conceived and wrote the manuscript. NS gave feedback and edited the manuscript.

FUNDING

This work was supported by grants from the Austrian Science Fund (FWF) W1206-08 to NS, F4414 to NS, and grant of the Province of Tirol "Fit for Science" to VR.

REFERENCES

Abbott, N. J., Ronnback, L., and Hansson, E. (2006). Astrocyte-endothelial interactions at the blood-brain barrier. *Nat. Rev. Neurosci.* 7, 41–53. doi: 10.1038/nrn1824

Ajami, B., Samusik, N., Wieghofer, P., Ho, P. P., Crotti, A., Bjornson, Z., et al. (2018). Single-cell mass cytometry reveals distinct populations of brain myeloid cells in mouse neuroinflammation and neurodegeneration models. *Nat. Neurosci.* 21, 541–551. doi: 10.1038/s41593-018-0100-x

Akiyama, H., Barger, S., Barnum, S., Bradt, B., Bauer, J., Cole, G. M., et al. (2000). Inflammation and Alzheimer's disease. *Neurobiol. Aging* 21, 383–421.

Akiyama, H., and McGeer, P. L. (1990). Brain microglia constitutively express beta-2 integrins. *J. Neuroimmunol.* 30, 81–93.

Allen, N. J., and Eroglu, C. (2017). Cell biology of astrocyte-synapse interactions. *Neuron* 96, 697–708. doi: 10.1016/j.neuron.2017.09.056

Alliot, F., Godin, I., and Pessac, B. (1999). Microglia derive from progenitors, originating from the yolk sac, and which proliferate in the brain. *Brain Res. Dev. Brain Res.* 117, 145–152.

Anderson, M. A., Burda, J. E., Ren, Y., Ao, Y., O'shea, T. M., Kawaguchi, R., et al. (2016). Astrocyte scar formation aids central nervous system axon regeneration. *Nature* 532, 195–200. doi: 10.1038/nature17623

Aono, H., Choudhury, M. E., Higaki, H., Miyanishi, K., Kigami, Y., Fujita, K., et al. (2017). Microglia may compensate for dopaminergic neuron loss in experimental Parkinsonism through selective elimination of glutamatergic synapses from the subthalamic nucleus. *Glia* 65, 1833–1847. doi: 10.1002/glia.23199

Au, N. P. B., and Ma, C. H. E. (2017). Recent advances in the study of bipolar/rod-shaped microglia and their roles in neurodegeneration. *Front. Aging Neurosci.* 9:128. doi: 10.3389/fnagi.2017.00128

Bandopadhyay, R., Kingsbury, A. E., Cookson, M. R., Reid, A. R., Evans, I. M., Hope, A. D., et al. (2004). The expression of DJ-1 (PARK7) in normal human CNS and idiopathic Parkinson's disease. *Brain* 127, 420–430. doi: 10.1093/brain/awh054

Barkholt, P., Sanchez-Guajardo, V., Kirik, D., and Romero-Ramos, M. (2012). Long-term polarization of microglia upon alpha-synuclein overexpression in nonhuman primates. *Neuroscience* 208, 85–96. doi: 10.1016/j.neuroscience.2012.02.004

Beers, D. R., Henkel, J. S., Xiao, Q., Zhao, W., Wang, J., Yen, A. A., et al. (2006). Wild-type microglia extend survival in PU.1 knockout mice with familial amyotrophic lateral sclerosis. *Proc. Natl. Acad. Sci. U.S.A.* 103, 16021–16026. doi: 10.1073/pnas.0607423103

Bellani, S., Sousa, V. L., Ronzitti, G., Valtorta, F., Meldolesi, J., and Chieregatti, E. (2010). The regulation of synaptic function by alpha-synuclein. *Commun. Integr. Biol.* 3, 106–109.

Bellot-Saez, A., Kekesi, O., Morley, J. W., and Buskila, Y. (2017). Astrocytic modulation of neuronal excitability through K(+) spatial buffering. *Neurosci. Biobehav. Rev.* 77, 87–97. doi: 10.1016/j.neubiorev.2017.03.002

Bisht, K., Sharma, K. P., Lecours, C., Sanchez, M. G., El Hajj, H., Milior, G., et al. (2016). Dark microglia: a new phenotype predominantly associated with pathological states. *Glia* 64, 826–839. doi: 10.1002/glia.22966

Bliederhaeuser, C., Grozdanov, V., Speidel, A., Zondler, L., Ruf, W. P., Bayer, H., et al. (2016). Age-dependent defects of alpha-synuclein oligomer uptake in microglia and monocytes. *Acta Neuropathol.* 131, 379–391. doi: 10.1007/s00401-015-1504-2

Blinzinger, K., and Kreutzberg, G. (1968). Displacement of synaptic terminals from regenerating motoneurons by microglial cells. *Z. Zellforsch. Mikrosk. Anat.* 85, 145–157.

Boche, D., Perry, V. H., and Nicoll, J. A. (2013). Review: activation patterns of microglia and their identification in the human brain. *Neuropathol. Appl. Neurobiol.* 39, 3–18. doi: 10.1111/nan.12011

Boisvert, M. M., Erikson, G. A., Shokhirev, M. N., and Allen, N. J. (2018). The aging astrocyte transcriptome from multiple regions of the mouse brain. *Cell Rep.* 22, 269–285. doi: 10.1016/j.celrep.2017.12.039

Booth, H. D. E., Hirst, W. D., and Wade-Martins, R. (2017). The role of astrocyte dysfunction in Parkinson's disease pathogenesis. *Trends Neurosci.* 40, 358–370. doi: 10.1016/j.tins.2017.04.001

Bottcher, C., Schlickeiser, S., Sneeboer, M. A. M., Kunkel, D., Knop, A., Paza, E., et al. (2019). Human microglia regional heterogeneity and phenotypes determined by multiplexed single-cell mass cytometry. *Nat. Neurosci.* 22, 78–90. doi: 10.1038/s41593-018-0290-2

Braak, H., Sastre, M., and Del Tredici, K. (2007). Development of alpha-synuclein immunoreactive astrocytes in the forebrain parallels stages of intraneuronal pathology in sporadic Parkinson's disease. *Acta Neuropathol.* 114, 231–241.

Brown, A. M., and Ransom, B. R. (2007). Astrocyte glycogen and brain energy metabolism. *Glia* 55, 1263–1271. doi: 10.1002/glia.20557

Cacace, F., Mineo, D., Viscomi, M. T., Latagliata, E. C., Mancini, M., Sasso, V., et al. (2017). Intermittent theta-burst stimulation rescues dopamine-dependent corticostriatal synaptic plasticity and motor behavior in experimental parkinsonism: possible role of glial activity. *Mov. Disord.* 32, 1035–1046. doi: 10.1002/mds.26982

Cao, S., Standaert, D. G., and Harms, A. S. (2012). The gamma chain subunit of Fc receptors is required for alpha-synuclein-induced pro-inflammatory signaling in microglia. *J. Neuroinflammation* 9:259. doi: 10.1186/1742-2094-9-259

Chen, M., Ona, V. O., Li, M., Ferrante, R. J., Fink, K. B., Zhu, S., et al. (2000). Minocycline inhibits caspase-1 and caspase-3 expression and delays mortality in a transgenic mouse model of Huntington disease. *Nat. Med.* 6, 797–801. doi: 10.1038/77528

Cherry, J. D., Olschowka, J. A., and O'banion, M. K. (2014). Neuroinflammation and M2 microglia: the good, the bad, and the inflamed. *J. Neuroinflammation* 11:98. doi: 10.1186/1742-2094-11-98

Chinta, S. J., Woods, G., Demaria, M., Rane, A., Zou, Y., Mcquade, A., et al. (2018). Cellular senescence is induced by the environmental neurotoxin paraquat and contributes to neuropathology linked to Parkinson's disease. *Cell Rep.* 22, 930–940. doi: 10.1016/j.celrep.2017.12.092

Choi, I., Choi, D. J., Yang, H., Woo, J. H., Chang, M. Y., Kim, J. Y., et al. (2016). PINK1 expression increases during brain development and stem cell differentiation, and affects the development of GFAP-positive astrocytes. *Mol. Brain* 9:5. doi: 10.1186/s13041-016-0186-6

Choi, I., Kim, J., Jeong, H. K., Kim, B., Jou, I., Park, S. M., et al. (2013). PINK1 deficiency attenuates astrocyte proliferation through mitochondrial dysfunction, reduced AKT and increased p38 MAPK activation, and downregulation of EGFR. *Glia* 61, 800–812. doi: 10.1002/glia.22475

Clarke, L. E., Liddelow, S. A., Chakraborty, C., Munch, A. E., Heiman, M., and Barres, B. A. (2018). Normal aging induces A1-like astrocyte reactivity. *Proc. Natl. Acad. Sci. U.S.A.* 115, E1896–E1905. doi: 10.1073/pnas.1800165115

Couch, Y., Alvarez-Erviti, L., Sibson, N. R., Wood, M. J., and Anthony, D. C. (2011). The acute inflammatory response to intranigral alpha-synuclein differs significantly from intranigral lipopolysaccharide and is exacerbated by peripheral inflammation. *J. Neuroinflammation* 8:166. doi: 10.1186/1742-2094-8-166

Damani, M. R., Zhao, L., Fontainhas, A. M., Amaral, J., Fariss, R. N., and Wong, W. T. (2011). Age-related alterations in the dynamic behavior of microglia. *Aging Cell* 10, 263–276. doi: 10.1111/j.1474-9726.2010.00660.x

Davis, B. M., Salinas-Navarro, M., Cordeiro, M. F., Moons, L., and De Groef, L. (2017). Characterizing microglia activation: a spatial statistics approach to maximize information extraction. *Sci. Rep.* 7:1576. doi: 10.1038/s41598-017-01747-8

De Biase, L. M., Schuebel, K. E., Fusfeld, Z. H., Jair, K., Hawes, I. A., Cimbro, R., et al. (2017). Local cues establish and maintain region-specific phenotypes of basal ganglia microglia. *Neuron* 95, 341–356.e6. doi: 10.1016/j.neuron.2017.06.020

Deiters, O. (1865). *Untersuchungen über Gehirn und Rückenmark des Menschen und der Säugethiere* (Braunschweig: Vieweg).

Diguet, E., Fernagut, P. O., Wei, X., Du, Y., Rouland, R., Gross, C., et al. (2004). Deleterious effects of minocycline in animal models of Parkinson's disease and Huntington's disease. *Eur. J. Neurosci.* 19, 3266–3276. doi: 10.1111/j.0953-816X.2004.03372.x

Dodel, R., Spottke, A., Gerhard, A., Reuss, A., Reinecker, S., Schimke, N., et al. (2010). Minocycline 1-year therapy in multiple-system-atrophy: effect on clinical symptoms and [(11)C] (R)-PK11195 PET (MEMSA-trial). *Mov. Disord.* 25, 97–107. doi: 10.1002/mds.22732

Doorn, K. J., Moors, T., Drukarch, B., Van De Berg, W., Lucassen, P. J., and Van Dam, A. M. (2014). Microglial phenotypes and toll-like receptor 2 in the substantia nigra and hippocampus of incidental Lewy body disease cases and

Parkinson's disease patients. *Acta Neuropathol. Commun.* 2:90. doi: 10.1186/s40478-014-0090-1

Doyle, A. G., Herbein, G., Montaner, L. J., Minty, A. J., Caput, D., Ferrara, P., et al. (1994). Interleukin-13 alters the activation state of murine macrophages in vitro: comparison with interleukin-4 and interferon-gamma. *Eur. J. Immunol.* 24, 1441–1445. doi: 10.1002/eji.1830240630

Du, Y., Ma, Z., Lin, S., Dodel, R. C., Gao, F., Bales, K. R., et al. (2001). Minocycline prevents nigrostriatal dopaminergic neurodegeneration in the MPTP model of Parkinson's disease. *Proc. Natl. Acad. Sci. U.S.A.* 98, 14669–14674. doi: 10.1073/pnas.251341998

Durrenberger, P. F., Filiou, M. D., Moran, L. B., Michael, G. J., Novoselov, S., Cheetham, M. E., et al. (2009). DNAJB6 is present in the core of Lewy bodies and is highly up-regulated in Parkinsonian astrocytes. *J. Neurosci. Res.* 87, 238–245. doi: 10.1002/jnr.21819

Emsley, J. G., and Macklis, J. D. (2006). Astroglial heterogeneity closely reflects the neuronal-defined anatomy of the adult murine CNS. *Neuron Glia Biol.* 2, 175–186. doi: 10.1017/S1740925X06000202

Eroglu, C., and Barres, B. A. (2010). Regulation of synaptic connectivity by glia. *Nature* 468, 223–231. doi: 10.1038/nature09612

Fanciulli, A., and Wenning, G. K. (2015). Multiple-system atrophy. *N. Engl. J. Med.* 372, 249–263. doi: 10.1056/NEJMra1311488

Fellner, L., Irschick, R., Schanda, K., Reindl, M., Klimaschewski, L., Poewe, W., et al. (2013). Toll-like receptor 4 is required for alpha-synuclein dependent activation of microglia and astroglia. *Glia* 61, 349–360. doi: 10.1002/glia.22437

Forno, L. S. (1996). Neuropathology of Parkinson's disease. *J. Neuropathol. Exp. Neurol.* 55, 259–272.

Fourgeaud, L., Traves, P. G., Tufail, Y., Leal-Bailey, H., Lew, E. D., Burrola, P. G., et al. (2016). TAM receptors regulate multiple features of microglial physiology. *Nature* 532, 240–244. doi: 10.1038/nature17630

Galatro, T. F., Holtman, I. R., Lerario, A. M., Vainchtein, I. D., Brouwer, N., Sola, P. R., et al. (2017). Transcriptomic analysis of purified human cortical microglia reveals age-associated changes. *Nat. Neurosci.* 20, 1162–1171. doi: 10.1038/nn.4597

Garcia-Abreu, J., Moura Neto, V., Carvalho, S. L., and Cavalcante, L. A. (1995). Regionally specific properties of midbrain glia: I. Interactions with midbrain neurons. *J. Neurosci. Res.* 40, 471–477. doi: 10.1002/jnr.490400406

Ge, W. P., Miyawaki, A., Gage, F. H., Jan, Y. N., and Jan, L. Y. (2012). Local generation of glia is a major astrocyte source in postnatal cortex. *Nature* 484, 376–380. doi: 10.1038/nature10959

Gelb, D. J., Oliver, E., and Gilman, S. (1999). Diagnostic criteria for Parkinson disease. *Arch. Neurol.* 56, 33–39.

Gerhard, A., Banati, R. B., Goerres, G. B., Cagnin, A., Myers, R., Gunn, R. N., et al. (2003). [11C](R)-PK11195 PET imaging of microglial activation in multiple system atrophy. *Neurology* 61, 686–689.

Gerhard, A., Pavese, N., Hotton, G., Turkheimer, F., Es, M., Hammers, A., et al. (2006). In vivo imaging of microglial activation with [11C](R)-PK11195 PET in idiopathic Parkinson's disease. *Neurobiol. Dis.* 21, 404–412. doi: 10.1016/j.nbd.2005.08.002

Ghadery, C., Koshimori, Y., Coakeley, S., Harris, M., Rusjan, P., Kim, J., et al. (2017). Microglial activation in Parkinson's disease using [(18)F]-FEPPA. *J. Neuroinflammation* 14:8.

Ghiglieri, V., Calabrese, V., and Calabresi, P. (2018). Alpha-synuclein: from early synaptic dysfunction to neurodegeneration. *Front. Neurol.* 9:295. doi: 10.3389/fneur.2018.00295

Giordano, N., Iemolo, A., Mancini, M., Cacace, F., De Risi, M., Latagliata, E. C., et al. (2018). Motor learning and metaplasticity in striatal neurons: relevance for Parkinson's disease. *Brain* 141, 505–520. doi: 10.1093/brain/awx351

Goedert, M., Jakes, R., and Spillantini, M. G. (2017). The synucleinopathies: twenty years on. *J. Parkinsons Dis.* 7, S51–S69. doi: 10.3233/JPD-179005

Grabert, K., Michoel, T., Karavolos, M. H., Clohisey, S., Baillie, J. K., Stevens, M. P., et al. (2016). Microglial brain region-dependent diversity and selective regional sensitivities to aging. *Nat. Neurosci.* 19, 504–516. doi: 10.1038/nn.4222

Gu, X. L., Long, C. X., Sun, L., Xie, C., Lin, X., and Cai, H. (2010). Astrocytic expression of Parkinson's disease-related A53T alpha-synuclein causes neurodegeneration in mice. *Mol. Brain* 3:12. doi: 10.1186/1756-6606-3-12

Hagemeyer, N., Hanft, K. M., Akriditou, M. A., Unger, N., Park, E. S., Stanley, E. R., et al. (2017). Microglia contribute to normal myelinogenesis and to oligodendrocyte progenitor maintenance during adulthood. *Acta Neuropathol.* 134, 441–458. doi: 10.1007/s00401-017-1747-1

Halliday, G. M., Holton, J. L., Revesz, T., and Dickson, D. W. (2011). Neuropathology underlying clinical variability in patients with synucleinopathies. *Acta Neuropathol.* 122, 187–204. doi: 10.1007/s00401-011-0852-9

Halliday, G. M., and Stevens, C. H. (2011). Glia: initiators and progressors of pathology in Parkinson's disease. *Mov. Disord.* 26, 6–17. doi: 10.1002/mds.23455

Hamza, T. H., Zabetian, C. P., Tenesa, A., Laederach, A., Montimurro, J., Yearout, D., et al. (2010). Common genetic variation in the HLA region is associated with late-onset sporadic Parkinson's disease. *Nat. Genet.* 42, 781–785. doi: 10.1038/ng.642

Hayashi, S., Wakabayashi, K., Ishikawa, A., Nagai, H., Saito, M., Maruyama, M., et al. (2000). An autopsy case of autosomal-recessive juvenile Parkinsonism with a homozygous exon 4 deletion in the parkin gene. *Mov. Disord.* 15, 884–888.

He, Y., Appel, S., and Le, W. (2001). Minocycline inhibits microglial activation and protects nigral cells after 6-hydroxydopamine injection into mouse striatum. *Brain Res.* 909, 187–193.

Hefendehl, J. K., Neher, J. J., Suhs, R. B., Kohsaka, S., Skodras, A., and Jucker, M. (2014). Homeostatic and injury-induced microglia behavior in the aging brain. *Aging Cell* 13, 60–69. doi: 10.1111/acel.12149

Heindl, S., Gesierich, B., Benakis, C., Llovera, G., Duering, M., and Liesz, A. (2018). Automated morphological analysis of microglia after stroke. *Front. Cell. Neurosci.* 12:106. doi: 10.3389/fncel.2018.00106

Henkel, J. S., Engelhardt, J. I., Siklós, L., Simpson, E. P., Kim, S. H., Pan, T., et al. (2004). Presence of dendritic cells, MCP-1, and activated microglia/macrophages in amyotrophic lateral sclerosis spinal cord tissue. *Ann. Neurol.* 55, 221–235. doi: 10.1002/ana.10805

Holmans, P., Moskvina, V., Jones, L., Sharma, M., International Parkinson's Disease Genomics Consortium, Vedernikov, A., et al. (2013). A pathway-based analysis provides additional support for an immune-related genetic susceptibility to Parkinson's disease. *Hum. Mol. Genet.* 22, 1039–1049. doi: 10.1093/hmg/dds492

Howes, O. D., and McCutcheon, R. (2017). Inflammation and the neural diathesis-stress hypothesis of schizophrenia: a reconceptualization. *Transl. Psychiatry* 7:e1024. doi: 10.1038/tp.2016.278

Hunter, C. L., Bachman, D., and Granholm, A. C. (2004). Minocycline prevents cholinergic loss in a mouse model of Down's syndrome. *Ann. Neurol.* 56, 675–688. doi: 10.1002/ana.20250

Iliff, J. J., Wang, M., Liao, Y., Plogg, B. A., Peng, W., Gundersen, G. A., et al. (2012). A paravascular pathway facilitates CSF flow through the brain parenchyma and the clearance of interstitial solutes, including amyloid beta. *Sci. Transl. Med.* 4:147ra111. doi: 10.1126/scitranslmed.3003748

Imamura, K., Hishikawa, N., Sawada, M., Nagatsu, T., Yoshida, M., and Hashizume, Y. (2003). Distribution of major histocompatibility complex class II-positive microglia and cytokine profile of Parkinson's disease brains. *Acta Neuropathol.* 106, 518–526.

Infante, J., Llorca, J., Berciano, J., and Combarros, O. (2005). Interleukin-8, intercellular adhesion molecule-1 and tumour necrosis factor-alpha gene polymorphisms and the risk for multiple system atrophy. *J. Neurol. Sci.* 228, 11–13. doi: 10.1016/j.jns.2004.09.023

Ishizawa, K., Komori, T., Sasaki, S., Arai, N., Mizutani, T., and Hirose, T. (2004). Microglial activation parallels system degeneration in multiple system atrophy. *J. Neuropathol. Exp. Neurol.* 63, 43–52.

Jang, E., Kim, J. H., Lee, S., Kim, J. H., Seo, J. W., Jin, M., et al. (2013). Phenotypic polarization of activated astrocytes: the critical role of lipocalin-2 in the classical inflammatory activation of astrocytes. *J. Immunol.* 191, 5204–5219. doi: 10.4049/jimmunol.1301637

Jellinger, K. A., and Lantos, P. L. (2010). Papp-Lantos inclusions and the pathogenesis of multiple system atrophy: an update. *Acta Neuropathol.* 119, 657–667. doi: 10.1007/s00401-010-0672-3

Jiang, T., Hoekstra, J., Heng, X., Kang, W., Ding, J., Liu, J., et al. (2015). P2X7 receptor is critical in alpha-synuclein–mediated microglial NADPH oxidase

activation. *Neurobiol. Aging* 36, 2304–2318. doi: 10.1016/j.neurobiolaging.2015.03.015

John Lin, C. C., Yu, K., Hatcher, A., Huang, T. W., Lee, H. K., Carlson, J., et al. (2017). Identification of diverse astrocyte populations and their malignant analogs. *Nat. Neurosci.* 20, 396–405. doi: 10.1038/nn.4493

Karperien, A., Ahammer, H., and Jelinek, H. F. (2013). Quantitating the subtleties of microglial morphology with fractal analysis. *Front. Cell. Neurosci.* 7:3. doi: 10.3389/fncel.2013.00003

Katsumoto, A., Lu, H., Miranda, A. S., and Ransohoff, R. M. (2014). Ontogeny and functions of central nervous system macrophages. *J. Immunol.* 193, 2615–2621. doi: 10.4049/jimmunol.1400716

Keren-Shaul, H., Spinrad, A., Weiner, A., Matcovitch-Natan, O., Dvir-Szternfeld, R., Ulland, T. K., et al. (2017). A unique microglia type associated with restricting development of Alzheimer's disease. *Cell* 169, 1276–1290.e17. doi: 10.1016/j.cell.2017.05.018

Kettenmann, H., Hanisch, U. K., Noda, M., and Verkhratsky, A. (2011). Physiology of microglia. *Physiol. Rev.* 91, 461–553. doi: 10.1152/physrev.00011.2010

Kim, C., Ho, D. H., Suk, J. E., You, S., Michael, S., Kang, J., et al. (2013). Neuron-released oligomeric alpha-synuclein is an endogenous agonist of TLR2 for paracrine activation of microglia. *Nat. Commun.* 4:1562. doi: 10.1038/ncomms2534

Kim, C., Spencer, B., Rockenstein, E., Yamakado, H., Mante, M., Adame, A., et al. (2018). Immunotherapy targeting toll-like receptor 2 alleviates neurodegeneration in models of synucleinopathy by modulating alpha-synuclein transmission and neuroinflammation. *Mol. Neurodegener.* 13:43. doi: 10.1186/s13024-018-0276-2

Kim, J. M., Cha, S. H., Choi, Y. R., Jou, I., Joe, E. H., and Park, S. M. (2016). DJ-1 deficiency impairs glutamate uptake into astrocytes via the regulation of flotillin-1 and caveolin-1 expression. *Sci. Rep.* 6:28823. doi: 10.1038/srep28823

Kreutzberg, G. W. (1995). Microglia, the first line of defence in brain pathologies. *Arzneimittelforschung* 45, 357–360.

Kreutzberg, G. W. (1996). Microglia: a sensor for pathological events in the CNS. *Trends Neurosci.* 19, 312–318.

Kriegstein, A., and Alvarez-Buylla, A. (2009). The glial nature of embryonic and adult neural stem cells. *Annu. Rev. Neurosci.* 32, 149–184. doi: 10.1146/annurev.neuro.051508.135600

Krismer, F., and Wenning, G. K. (2017). Multiple system atrophy: insights into a rare and debilitating movement disorder. *Nat. Rev. Neurol.* 13, 232–243. doi: 10.1038/nrneurol.2017.26

Lambertsen, K. L., Deierborg, T., Gregersen, R., Clausen, B. H., Wirenfeldt, M., Nielsen, H. H., et al. (2011). Differences in origin of reactive microglia in bone marrow chimeric mouse and rat after transient global ischemia. *J. Neuropathol. Exp. Neurol.* 70, 481–494. doi: 10.1097/NEN.0b013e31821db3aa

Lawson, L. J., Perry, V. H., Dri, P., and Gordon, S. (1990). Heterogeneity in the distribution and morphology of microglia in the normal adult mouse brain. *Neuroscience* 39, 151–170.

Lee, H. J., Kim, C., and Lee, S. J. (2010a). Alpha-synuclein stimulation of astrocytes: potential role for neuroinflammation and neuroprotection. *Oxid. Med. Cell. Longev.* 3, 283–287. doi: 10.4161/oxim.3.4.12809

Lee, H. J., Suk, J. E., Patrick, C., Bae, E. J., Cho, J. H., Rho, S., et al. (2010b). Direct transfer of alpha-synuclein from neuron to astroglia causes inflammatory responses in synucleinopathies. *J. Biol. Chem.* 285, 9262–9272. doi: 10.1074/jbc.M109.081125

Lee, S., Varvel, N. H., Konerth, M. E., Xu, G., Cardona, A. E., Ransohoff, R. M., et al. (2010c). CX3CR1 deficiency alters microglial activation and reduces beta-amyloid deposition in two Alzheimer's disease mouse models. *Am. J. Pathol.* 177, 2549–2562. doi: 10.2353/ajpath.2010.100265

Lenhossék, M. (1895). *Der Feinere Bau des Nervensystems im Lichte Neuester Forschung*, 2nd Edn. Berlin: Fischer's Medicinische Buchhandlung H. Kornfield.

Liddelow, S. A., Guttenplan, K. A., Clarke, L. E., Bennett, F. C., Bohlen, C. J., Schirmer, L., et al. (2017). Neurotoxic reactive astrocytes are induced by activated microglia. *Nature* 541, 481–487. doi: 10.1038/nature21029

Lindström, V., Gustafsson, G., Sanders, L. H., Howlett, E. H., Sigvardson, J., Kasrayan, A., et al. (2017). Extensive uptake of alpha-synuclein oligomers in astrocytes results in sustained intracellular deposits and mitochondrial damage. *Mol. Cell. Neurosci.* 82, 143–156. doi: 10.1016/j.mcn.2017.04.009

Liu, J., and Wang, F. (2017). Role of neuroinflammation in amyotrophic lateral sclerosis: cellular mechanisms and therapeutic implications. *Front. Immunol.* 8:1005. doi: 10.3389/fimmu.2017.01005

Lynch, M. A. (2009). The multifaceted profile of activated microglia. *Mol. Neurobiol.* 40, 139–156. doi: 10.1007/s12035-009-8077-9

Mackenzie, I. R. (2000). Activated microglia in dementia with Lewy bodies. *Neurology* 55, 132–134.

Marinova-Mutafchieva, L., Sadeghian, M., Broom, L., Davis, J. B., Medhurst, A. D., and Dexter, D. T. (2009). Relationship between microglial activation and dopaminergic neuronal loss in the substantia nigra: a time course study in a 6-hydroxydopamine model of Parkinson's disease. *J. Neurochem.* 110, 966–975. doi: 10.1111/j.1471-4159.2009.06189.x

Masuda, T., Sankowski, R., Staszewski, O., Bottcher, C., Amann, L., Scheiwe, C., et al. (2019). Spatial and temporal heterogeneity of mouse and human microglia at single-cell resolution. *Nature* 566, 388–392. doi: 10.1038/s41586-019-0924-x

Mathys, H., Adaikkan, C., Gao, F., Young, J. Z., Manet, E., Hemberg, M., et al. (2017). Temporal tracking of microglia activation in neurodegeneration at single-cell resolution. *Cell Rep.* 21, 366–380. doi: 10.1016/j.celrep.2017.09.039

McGeer, P. L., Itagaki, S., Boyes, B. E., and Mcgeer, E. G. (1988). Reactive microglia are positive for HLA-DR in the substantia nigra of Parkinson's and Alzheimer's disease brains. *Neurology* 38, 1285–1291.

McKeith, I. G., Dickson, D. W., Lowe, J., Emre, M., O'brien, J. T., Feldman, H., et al. (2005). Diagnosis and management of dementia with Lewy bodies: third report of the DLB Consortium. *Neurology* 65, 1863–1872. doi: 10.1212/01.wnl.0000187889.17253.b1

Mckercher, S. R., Torbett, B. E., Anderson, K. L., Henkel, G. W., Vestal, D. J., Baribault, H., et al. (1996). Targeted disruption of the PU.1 gene results in multiple hematopoietic abnormalities. *EMBO J.* 15, 5647–5658.

Mills, C. D., Kincaid, K., Alt, J. M., Heilman, M. J., and Hill, A. M. (2000). M-1/M-2 macrophages and the Th1/Th2 paradigm. *J. Immunol.* 164, 6166–6173.

Mirza, B., Hadberg, H., Thomsen, P., and Moos, T. (2000). The absence of reactive astrocytosis is indicative of a unique inflammatory process in Parkinson's disease. *Neuroscience* 95, 425–432.

Monier, A., Adle-Biassette, H., Delezoide, A. L., Evrard, P., Gressens, P., and Verney, C. (2007). Entry and distribution of microglial cells in human embryonic and fetal cerebral cortex. *J. Neuropathol. Exp. Neurol.* 66, 372–382. doi: 10.1097/nen.0b013e3180517b46

Morgan, J. T., Chana, G., Pardo, C. A., Achim, C., Semendeferi, K., Buckwalter, J., et al. (2010). Microglial activation and increased microglial density observed in the dorsolateral prefrontal cortex in autism. *Biol. Psychiatry* 68, 368–376. doi: 10.1016/j.biopsych.2010.05.024

Morrison, H., Young, K., Qureshi, M., Rowe, R. K., and Lifshitz, J. (2017). Quantitative microglia analyses reveal diverse morphologic responses in the rat cortex after diffuse brain injury. *Sci. Rep.* 7:13211. doi: 10.1038/s41598-017-13581-z

Morrison, H. W., and Filosa, J. A. (2013). A quantitative spatiotemporal analysis of microglia morphology during ischemic stroke and reperfusion. *J. Neuroinflammation* 10:4. doi: 10.1186/1742-2094-10-4

Mrak, R. E., and Griffin, W. S. (2005). Glia and their cytokines in progression of neurodegeneration. *Neurobiol. Aging* 26, 349–354. doi: 10.1016/j.neurobiolaging.2004.05.010

Nakamura, K., Mori, F., Kon, T., Tanji, K., Miki, Y., Tomiyama, M., et al. (2016). Accumulation of phosphorylated alpha-synuclein in subpial and periventricular astrocytes in multiple system atrophy of long duration. *Neuropathology* 36, 157–167. doi: 10.1111/neup.12243

Nathan, C. F., Murray, H. W., Wiebe, M. E., and Rubin, B. Y. (1983). Identification of interferon-gamma as the lymphokine that activates human macrophage oxidative metabolism and antimicrobial activity. *J. Exp. Med.* 158, 670–689.

Nedergaard, M. (2013). Neuroscience. Garbage truck of the brain. *Science* 340, 1529–1530. doi: 10.1126/science.1240514

Neumann, M., Muller, V., Gorner, K., Kretzschmar, H. A., Haass, C., and Kahle, P. J. (2004). Pathological properties of the Parkinson's disease-associated protein DJ-1 in alpha-synucleinopathies and tauopathies: relevance for multiple system atrophy and Pick's disease. *Acta Neuropathol.* 107, 489–496.

Nimmerjahn, A., Kirchhoff, F., and Helmchen, F. (2005). Resting microglial cells are highly dynamic surveillants of brain parenchyma in vivo. *Science* 308, 1314–1318. doi: 10.1126/science.1110647

NINDS NET-PD Investigators (2008). A pilot clinical trial of creatine and minocycline in early Parkinson disease: 18-month results. *Clin. Neuropharmacol.* 31, 141–150. doi: 10.1097/WNF.0b013e3181342f32

Nishimura, M., Kawakami, H., Komure, O., Maruyama, H., Morino, H., Izumi, Y., et al. (2002). Contribution of the interleukin-1beta gene polymorphism in multiple system atrophy. *Mov. Disord.* 17, 808–811. doi: 10.1002/mds.10124

Nissl, F. (1899). Ueber einige Beziehungen zwishcen Nerven zellerkrankungen und gliosen Erscheinnungen bei verschiedenen Psychosen. *Arch. Psychiatry* 32, 1–21.

Njie, E. G., Boelen, E., Stassen, F. R., Steinbusch, H. W., Borchelt, D. R., and Streit, W. J. (2012). Ex vivo cultures of microglia from young and aged rodent brain reveal age-related changes in microglial function. *Neurobiol. Aging* 33, 195.e1–195.e12. doi: 10.1016/j.neurobiolaging.2010.05.008

Noell, S., Wolburg-Buchholz, K., Mack, A. F., Beedle, A. M., Satz, J. S., Campbell, K. P., et al. (2011). Evidence for a role of dystroglycan regulating the membrane architecture of astroglial endfeet. *Eur. J. Neurosci.* 33, 2179–2186. doi: 10.1111/j.1460-9568.2011.07688.x

Nykjaer, C. H., Brudek, T., Salvesen, L., and Pakkenberg, B. (2017). Changes in the cell population in brain white matter in multiple system atrophy. *Mov. Disord.* 32, 1074–1082. doi: 10.1002/mds.26979

Oberheim, N. A., Goldman, S. A., and Nedergaard, M. (2012). Heterogeneity of astrocytic form and function. *Methods Mol. Biol.* 814, 23–45. doi: 10.1007/978-1-61779-452-0_3

O'Callaghan, J. P., and Sriram, K. (2005). Glial fibrillary acidic protein and related glial proteins as biomarkers of neurotoxicity. *Expert Opin. Drug Saf.* 4, 433–442. doi: 10.1517/14740338.4.3.433

Ogaki, K., Heckman, M. G., Koga, S., Martens, Y. A., Labbe, C., Lorenzo-Betancor, O., et al. (2018). Association study between multiple system atrophy and TREM2 p.R47H. *Neurol. Genet.* 4:e257. doi: 10.1212/NXG.0000000000000257

Olah, M., Patrick, E., Villani, A. C., Xu, J., White, C. C., Ryan, K. J., et al. (2018). A transcriptomic atlas of aged human microglia. *Nat. Commun.* 9:539. doi: 10.1038/s41467-018-02926-5

Ozawa, T., Paviour, D., Quinn, N. P., Josephs, K. A., Sangha, H., Kilford, L., et al. (2004). The spectrum of pathological involvement of the striatonigral and olivopontocerebellar systems in multiple system atrophy: clinicopathological correlations. *Brain* 127, 2657–2671. doi: 10.1093/brain/awh303

Papp, M. I., Kahn, J. E., and Lantos, P. L. (1989). Glial cytoplasmic inclusions in the CNS of patients with multiple system atrophy (striatonigral degeneration, olivopontocerebellar atrophy and Shy-Drager syndrome). *J. Neurol. Sci.* 94, 79–100.

Perry, V. H., Hume, D. A., and Gordon, S. (1985). Immunohistochemical localization of macrophages and microglia in the adult and developing mouse brain. *Neuroscience* 15, 313–326.

Prinz, M., Erny, D., and Hagemeyer, N. (2017). Ontogeny and homeostasis of CNS myeloid cells. *Nat. Immunol.* 18, 385–392. doi: 10.1038/ni.3703

Radford, R., Rcom-H'cheo-Gauthier, A., Wong, M. B., Eaton, E. D., Quilty, M., Blizzard, C., et al. (2015). The degree of astrocyte activation in multiple system atrophy is inversely proportional to the distance to alpha-synuclein inclusions. *Mol. Cell. Neurosci.* 65, 68–81. doi: 10.1016/j.mcn.2015.02.015

Ramon y Cajal, S. (1909). *Histologie du Systeme Nerveux de l'homme et des Vertebres*. Paris: Maloine.

Rannikko, E. H., Weber, S. S., and Kahle, P. J. (2015). Exogenous alpha-synuclein induces toll-like receptor 4 dependent inflammatory responses in astrocytes. *BMC Neurosci.* 16:57. doi: 10.1186/s12868-015-0192-0

Ransohoff, R. M. (2016). A polarizing question: do M1 and M2 microglia exist? *Nat. Neurosci.* 19, 987–991. doi: 10.1038/nn.4338

Refolo, V., Bez, F., Polissidis, A., Kuzdas-Wood, D., Sturm, E., Kamaratou, M., et al. (2018). Progressive striatonigral degeneration in a transgenic mouse model of multiple system atrophy: translational implications for interventional therapies. *Acta Neuropathol. Commun.* 6:2. doi: 10.1186/s40478-017-0504-y

Rezaie, P., Dean, A., Male, D., and Ulfig, N. (2005). Microglia in the cerebral wall of the human telencephalon at second trimester. *Cereb. Cortex* 15, 938–949. doi: 10.1093/cercor/bhh194

Rolls, A., Shechter, R., and Schwartz, M. (2009). The bright side of the glial scar in CNS repair. *Nat. Rev. Neurosci.* 10, 235–241. doi: 10.1038/nrn2591

Rothstein, J. D., Dykes-Hoberg, M., Pardo, C. A., Bristol, L. A., Jin, L., Kuncl, R. W., et al. (1996). Knockout of glutamate transporters reveals a major role for astroglial transport in excitotoxicity and clearance of glutamate. *Neuron* 16, 675–686.

Salvesen, L., Ullerup, B. H., Sunay, F. B., Brudek, T., Lokkegaard, A., Agander, T. K., et al. (2015). Changes in total cell numbers of the basal ganglia in patients with multiple system atrophy - A stereological study. *Neurobiol. Dis.* 74, 104–113. doi: 10.1016/j.nbd.2014.11.008

Salvesen, L., Winge, K., Brudek, T., Agander, T. K., Lokkegaard, A., and Pakkenberg, B. (2017). Neocortical neuronal loss in patients with multiple system atrophy: a stereological study. *Cereb. Cortex* 27, 400–410. doi: 10.1093/cercor/bhv228

Sanchez-Guajardo, V., Febbraro, F., Kirik, D., and Romero-Ramos, M. (2010). Microglia acquire distinct activation profiles depending on the degree of alpha-synuclein neuropathology in a rAAV based model of Parkinson's disease. *PLoS One* 5:e8784. doi: 10.1371/journal.pone.0008784

Schwarz, J., Weis, S., Kraft, E., Tatsch, K., Bandmann, O., Mehraein, P., et al. (1996). Signal changes on MRI and increases in reactive microgliosis, astrogliosis, and iron in the putamen of two patients with multiple system atrophy. *J. Neurol. Neurosurg. Psychiatry* 60, 98–101.

Sekar, A., Bialas, A. R., De Rivera, H., Davis, A., Hammond, T. R., Kamitaki, N., et al. (2016). Schizophrenia risk from complex variation of complement component 4. *Nature* 530, 177–183. doi: 10.1038/nature16549

Shinozaki, Y., Shibata, K., Yoshida, K., Shigetomi, E., Gachet, C., Ikenaka, K., et al. (2017). Transformation of astrocytes to a neuroprotective phenotype by microglia via P2Y1 receptor downregulation. *Cell Rep.* 19, 1151–1164. doi: 10.1016/j.celrep.2017.04.047

Sierra, A., De Castro, F., Del Rio-Hortega, J., Rafael Iglesias-Rozas, J., Garrosa, M., and Kettenmann, H. (2016). The "Big-Bang" for modern glial biology: translation and comments on Pio del Rio-Hortega 1919 series of papers on microglia. *Glia* 64, 1801–1840. doi: 10.1002/glia.23046

Sierra, A., Gottfried-Blackmore, A. C., Mcewen, B. S., and Bulloch, K. (2007). Microglia derived from aging mice exhibit an altered inflammatory profile. *Glia* 55, 412–424. doi: 10.1002/glia.20468

Silver, J., and Miller, J. H. (2004). Regeneration beyond the glial scar. *Nat. Rev. Neurosci.* 5, 146–156. doi: 10.1038/nrn1326

Smith, D. L., Woodman, B., Mahal, A., Sathasivam, K., Ghazi-Noori, S., Lowden, P. A., et al. (2003). Minocycline and doxycycline are not beneficial in a model of Huntington's disease. *Ann. Neurol.* 54, 186–196. doi: 10.1002/ana.10614

Sofroniew, M. V., and Vinters, H. V. (2010). Astrocytes: biology and pathology. *Acta Neuropathol.* 119, 7–35.

Solano, R. M., Casarejos, M. J., Menendez-Cuervo, J., Rodriguez-Navarro, J. A., Garcia De Yebenes, J., and Mena, M. A. (2008). Glial dysfunction in parkin null mice: effects of aging. *J. Neurosci.* 28, 598–611. doi: 10.1523/JNEUROSCI.4609-07.2008

Solito, E., and Sastre, M. (2012). Microglia function in Alzheimer's disease. *Front. Pharmacol.* 3:14. doi: 10.3389/fphar.2012.00014

Song, Y., and Gunnarson, E. (2012). Potassium dependent regulation of astrocyte water permeability is mediated by cAMP signaling. *PLoS One* 7:e34936. doi: 10.1371/journal.pone.0034936

Song, Y. J., Halliday, G. M., Holton, J. L., Lashley, T., O'sullivan, S. S., Mccann, H., et al. (2009). Degeneration in different Parkinsonian syndromes relates to astrocyte type and astrocyte protein expression. *J. Neuropathol. Exp. Neurol.* 68, 1073–1083. doi: 10.1097/NEN.0b013e3181b66f1b

Spillantini, M. G., Crowther, R. A., Jakes, R., Cairns, N. J., Lantos, P. L., and Goedert, M. (1998a). Filamentous alpha-synuclein inclusions link multiple system atrophy with Parkinson's disease and dementia with Lewy bodies. *Neurosci. Lett.* 251, 205–208.

Spillantini, M. G., Crowther, R. A., Jakes, R., Hasegawa, M., and Goedert, M. (1998b). alpha-Synuclein in filamentous inclusions of Lewy bodies from Parkinson's disease and dementia with Lewy bodies. *Proc. Natl. Acad. Sci. U.S.A.* 95, 6469–6473.

Spillantini, M. G., and Goedert, M. (2000). The alpha-synucleinopathies: Parkinson's disease, dementia with Lewy bodies, and multiple system atrophy. *Ann. N. Y. Acad. Sci.* 920, 16–27.

Spillantini, M. G., Schmidt, M. L., Lee, V. M., Trojanowski, J. Q., Jakes, R., and Goedert, M. (1997). Alpha-synuclein in Lewy bodies. *Nature* 388, 839–840. doi: 10.1038/42166

Spiller, K. J., Restrepo, C. R., Khan, T., Dominique, M. A., Fang, T. C., Canter, R. G., et al. (2018). Microglia-mediated recovery from ALS-relevant motor neuron degeneration in a mouse model of TDP-43 proteinopathy. *Nat. Neurosci.* 21, 329–340. doi: 10.1038/s41593-018-0083-7

Squarzoni, P., Thion, M. S., and Garel, S. (2015). Neuronal and microglial regulators of cortical wiring: usual and novel guideposts. *Front. Neurosci.* 9:248. doi: 10.3389/fnins.2015.00248

Stefanova, N., Fellner, L., Reindl, M., Masliah, E., Poewe, W., and Wenning, G. K. (2011). Toll-like receptor 4 promotes alpha-synuclein clearance and survival of nigral dopaminergic neurons. *Am. J. Pathol.* 179, 954–963. doi: 10.1016/j.ajpath.2011.04.013

Stefanova, N., Reindl, M., Neumann, M., Kahle, P. J., Poewe, W., and Wenning, G. K. (2007). Microglial activation mediates neurodegeneration related to oligodendroglial alpha-synucleinopathy: implications for multiple system atrophy. *Mov. Disord.* 22, 2196–2203. doi: 10.1002/mds.21671

Stein, M., Keshav, S., Harris, N., and Gordon, S. (1992). Interleukin 4 potently enhances murine macrophage mannose receptor activity: a marker of alternative immunologic macrophage activation. *J. Exp. Med.* 176, 287–292.

Stobart, J. L., and Anderson, C. M. (2013). Multifunctional role of astrocytes as gatekeepers of neuronal energy supply. *Front. Cell. Neurosci.* 7:38. doi: 10.3389/fncel.2013.00038

Streit, W. J. (2004). Microglia and Alzheimer's disease pathogenesis. *J. Neurosci. Res.* 77, 1–8. doi: 10.1002/jnr.20093

Su, X., Federoff, H. J., and Maguire-Zeiss, K. A. (2009). Mutant alpha-synuclein overexpression mediates early proinflammatory activity. *Neurotox. Res.* 16, 238–254. doi: 10.1007/s12640-009-9053-x

Su, X., Maguire-Zeiss, K. A., Giuliano, R., Prifti, L., Venkatesh, K., and Federoff, H. J. (2008). Synuclein activates microglia in a model of Parkinson's disease. *Neurobiol. Aging* 29, 1690–1701. doi: 10.1016/j.neurobiolaging.2007.04.006

Surendranathan, A., Su, L., Mak, E., Passamonti, L., Hong, Y. T., Arnold, R., et al. (2018). Early microglial activation and peripheral inflammation in dementia with Lewy bodies. *Brain* 141, 3415–3427. doi: 10.1093/brain/awy265

Takahashi, K., and Naito, M. (1993). Development, differentiation, and proliferation of macrophages in the rat yolk sac. *Tissue Cell* 25, 351–362.

Takahashi, K., Yamamura, F., and Naito, M. (1989). Differentiation, maturation, and proliferation of macrophages in the mouse yolk sac: a light-microscopic, enzyme-cytochemical, immunohistochemical, and ultrastructural study. *J. Leukoc. Biol.* 45, 87–96.

Tay, T. L., Mai, D., Dautzenberg, J., Fernandez-Klett, F., Lin, G., Sagar, et al. (2017). A new fate mapping system reveals context-dependent random or clonal expansion of microglia. *Nat. Neurosci.* 20, 793–803. doi: 10.1038/nn.4547

Tay, T. L., Sagar, Dautzenberg, J., Grun, D., and Prinz, M. (2018). Unique microglia recovery population revealed by single-cell RNAseq following neurodegeneration. *Acta Neuropathol. Commun.* 6:87. doi: 10.1186/s40478-018-0584-3

Terada, S., Ishizu, H., Haraguchi, T., Takehisa, Y., Tanabe, Y., Kawai, K., et al. (2000). Tau-negative astrocytic star-like inclusions and coiled bodies in dementia with Lewy bodies. *Acta Neuropathol.* 100, 464–468.

Tetreault, N. A., Hakeem, A. Y., Jiang, S., Williams, B. A., Allman, E., Wold, B. J., et al. (2012). Microglia in the cerebral cortex in autism. *J. Autism Dev. Disord.* 42, 2569–2584. doi: 10.1007/s10803-012-1513-0

Tikka, T. M., and Koistinaho, J. E. (2001). Minocycline provides neuroprotection against N-methyl-D-aspartate neurotoxicity by inhibiting microglia. *J. Immunol.* 166, 7527–7533.

Tomás-Camardiel, M., Rite, I., Herrera, A. J., De Pablos, R. M., Cano, J., Machado, A., et al. (2004). Minocycline reduces the lipopolysaccharide-induced inflammatory reaction, peroxynitrite-mediated nitration of proteins, disruption of the blood-brain barrier, and damage in the nigral dopaminergic system. *Neurobiol. Dis.* 16, 190–201. doi: 10.1016/j.nbd.2004.01.010

Tong, J., Ang, L. C., Williams, B., Furukawa, Y., Fitzmaurice, P., Guttman, M., et al. (2015). Low levels of astroglial markers in Parkinson's disease: relationship to alpha-synuclein accumulation. *Neurobiol. Dis.* 82, 243–253. doi: 10.1016/j.nbd.2015.06.010

Tremblay, M. E., Lowery, R. L., and Majewska, A. K. (2010). Microglial interactions with synapses are modulated by visual experience. *PLoS Biol.* 8:e1000527. doi: 10.1371/journal.pbio.1000527

Trojanowski, J. Q., and Lee, V. M. (1998). Aggregation of neurofilament and alpha-synuclein proteins in Lewy bodies: implications for the pathogenesis of Parkinson disease and Lewy body dementia. *Arch. Neurol.* 55, 151–152.

Venezia, S., Refolo, V., Polissidis, A., Stefanis, L., Wenning, G. K., and Stefanova, N. (2017). Toll-like receptor 4 stimulation with monophosphoryl lipid A ameliorates motor deficits and nigral neurodegeneration triggered by extraneuronal alpha-synucleinopathy. *Mol. Neurodegener.* 12:52. doi: 10.1186/s13024-017-0195-7

Verdonk, F., Roux, P., Flamant, P., Fiette, L., Bozza, F. A., Simard, S., et al. (2016). Phenotypic clustering: a novel method for microglial morphology analysis. *J. Neuroinflammation* 13:153. doi: 10.1186/s12974-016-0614-7

Verkhratsky, A., and Nedergaard, M. (2018). Physiology of astroglia. *Physiol. Rev.* 98, 239–389. doi: 10.1152/physrev.00042.2016

Wakabayashi, K., Yoshimoto, M., Tsuji, S., and Takahashi, H. (1998). Alpha-synuclein immunoreactivity in glial cytoplasmic inclusions in multiple system atrophy. *Neurosci. Lett.* 249, 180–182.

Wake, H., Moorhouse, A. J., Jinno, S., Kohsaka, S., and Nabekura, J. (2009). Resting microglia directly monitor the functional state of synapses in vivo and determine the fate of ischemic terminals. *J. Neurosci.* 29, 3974–3980. doi: 10.1523/JNEUROSCI.4363-08.2009

Wang, Q., Liu, Y., and Zhou, J. (2015). Neuroinflammation in Parkinson's disease and its potential as therapeutic target. *Transl. Neurodegener.* 4:19.

Wang, S., Chu, C. H., Stewart, T., Ginghina, C., Wang, Y., Nie, H., et al. (2015). alpha-Synuclein, a chemoattractant, directs microglial migration via H_2O_2-dependent Lyn phosphorylation. *Proc. Natl. Acad. Sci. U.S.A.* 112, E1926–E1935. doi: 10.1073/pnas.1417883112

Wang, X., Zhu, S., Drozda, M., Zhang, W., Stavrovskaya, I. G., Cattaneo, E., et al. (2003). Minocycline inhibits caspase-independent and -dependent mitochondrial cell death pathways in models of Huntington's disease. *Proc. Natl. Acad. Sci. U.S.A.* 100, 10483–10487. doi: 10.1073/pnas.1832501100

Wenning, G. K., and Jellinger, K. A. (2005). The role of alpha-synuclein in the pathogenesis of multiple system atrophy. *Acta Neuropathol.* 109, 129–140. doi: 10.1007/s00401-004-0935-y

Wierzba-Bobrowicz, T., Gwiazda, E., Kosno-Kruszewska, E., Lewandowska, E., Lechowicz, W., Bertrand, E., et al. (2002). Morphological analysis of active microglia–rod and ramified microglia in human brains affected by some neurological diseases (SSPE, Alzheimer's disease and Wilson's disease). *Folia Neuropathol.* 40, 125–131.

Wilms, H., Rosenstiel, P., Romero-Ramos, M., Arlt, A., Schafer, H., Seegert, D., et al. (2009). Suppression of MAP kinases inhibits microglial activation and attenuates neuronal cell death induced by alpha-synuclein protofibrils. *Int. J. Immunopathol. Pharmacol.* 22, 897–909. doi: 10.1177/039463200902200405

Windle, W. F., Clemente, C. D., and Chambers, W. W. (1952). Inhibition of formation of a glial barrier as a means of permitting a peripheral nerve to grow into the brain. *J. Comp. Neurol.* 96, 359–369.

Wu, D. C., Jackson-Lewis, V., Vila, M., Tieu, K., Teismann, P., Vadseth, C., et al. (2002). Blockade of microglial activation is neuroprotective in the 1-methyl-4-phenyl-1,2,3,6-tetrahydropyridine mouse model of Parkinson disease. *J. Neurosci.* 22, 1763–1771.

Xie, L., Kang, H., Xu, Q., Chen, M. J., Liao, Y., Thiyagarajan, M., et al. (2013). Sleep drives metabolite clearance from the adult brain. *Science* 342, 373–377. doi: 10.1126/science.1241224

Yamada, J., and Jinno, S. (2013). Novel objective classification of reactive microglia following hypoglossal axotomy using hierarchical cluster analysis. *J. Comp. Neurol.* 521, 1184–1201. doi: 10.1002/cne.23228

Yang, T. T., Lin, C., Hsu, C. T., Wang, T. F., Ke, F. Y., and Kuo, Y. M. (2013). Differential distribution and activation of microglia in the brain of male C57BL/6J mice. *Brain Struct. Funct.* 218, 1051–1060. doi: 10.1007/s00429-012-0446-x

Yun, S. P., Kam, T. I., Panicker, N., Kim, S., Oh, Y., Park, J. S., et al. (2018). Block of A1 astrocyte conversion by microglia is neuroprotective in models of Parkinson's disease. *Nat. Med.* 24, 931–938. doi: 10.1038/s41591-018-0051-5

Zamanian, J. L., Xu, L., Foo, L. C., Nouri, N., Zhou, L., Giffard, R. G., et al. (2012). Genomic analysis of reactive astrogliosis. *J. Neurosci.* 32, 6391–6410. doi: 10.1523/JNEUROSCI.6221-11.2012

Zeisel, A., Hochgerner, H., Lonnerberg, P., Johnsson, A., Memic, F., Van Der Zwan, J., et al. (2018). Molecular architecture of the mouse nervous system. *Cell* 174, 999–1014.e22. doi: 10.1016/j.cell.2018.06.021

Zhang, W., Wang, T., Pei, Z., Miller, D. S., Wu, X., Block, M. L., et al. (2005). Aggregated alpha-synuclein activates microglia: a process leading to disease

progression in Parkinson's disease. *FASEB J.* 19, 533–542. doi: 10.1096/fj.04-2751com

Zhu, S., Stavrovskaya, I. G., Drozda, M., Kim, B. Y., Ona, V., Li, M., et al. (2002). Minocycline inhibits cytochrome c release and delays progression of amyotrophic lateral sclerosis in mice. *Nature* 417, 74–78. doi: 10.1038/417074a

Ziebell, J. M., Taylor, S. E., Cao, T., Harrison, J. L., and Lifshitz, J. (2012). Rod microglia: elongation, alignment, and coupling to form trains across the somatosensory cortex after experimental diffuse brain injury. *J. Neuroinflammation* 9:247. doi: 10.1186/1742-2094-9-247

Conflict of Interest Statement: The authors declare that the research was conducted in the absence of any commercial or financial relationships that could be construed as a potential conflict of interest.

frontiers in Cellular Neuroscience

ORIGINAL RESEARCH
published: 28 June 2019
doi: 10.3389/fncel.2019.00264

Glutaminase C Regulates Microglial Activation and Pro-inflammatory Exosome Release: Relevance to the Pathogenesis of Alzheimer's Disease

Ge Gao[1†], Shu Zhao[1†], Xiaohuan Xia[1†], Chunhong Li[1], Congcong Li[1], Chenhui Ji[1,2], Shiyang Sheng[1], Yalin Tang[1], Jie Zhu[1], Yi Wang[1], Yunlong Huang[1,2]* and Jialin C. Zheng[1,2,3]**

[1] Center for Translational Neurodegeneration and Regenerative Therapy, Shanghai Tenth People's Hospital Affiliated to Tongji University School of Medicine, Shanghai, China, [2] Department of Pharmacology and Experimental Neuroscience, University of Nebraska Medical Center, Omaha, NE, United States, [3] Collaborative Innovation Center for Brain Science, Tongji University, Shanghai, China

OPEN ACCESS

Edited by:
Yu Tang,
Central South University, China

Reviewed by:
Fatah Kashanchi,
George Mason University, United States
Douglas Gordon Walker,
Arizona State University, United States

***Correspondence:**
Yi Wang
yiwang87@tongji.edu.cn
Yunlong Huang
yhuan1@unmc.edu
Jialin C. Zheng
jialinzheng@tongji.edu.cn

[†]These authors have contributed equally to this work

Specialty section:
This article was submitted to Non-Neuronal Cells, a section of the journal Frontiers in Cellular Neuroscience

Received: 05 March 2019
Accepted: 28 May 2019
Published: 28 June 2019

Citation:
Gao G, Zhao S, Xia X, Li C, Li C, Ji C, Sheng S, Tang Y, Zhu J, Wang Y, Huang Y and Zheng JC (2019) Glutaminase C Regulates Microglial Activation and Pro-inflammatory Exosome Release: Relevance to the Pathogenesis of Alzheimer's Disease. Front. Cell. Neurosci. 13:264. doi: 10.3389/fncel.2019.00264

Microglial activation is a key pathogenic process at the onset of Alzheimer's disease (AD). Identifying regulators of microglial activation bears great potential in elucidating causes and mechanisms of AD and determining candidates for early intervention. Previous studies demonstrate abnormal elevation of glutaminase C (GAC) in HIV-infected or immune-activated microglia. However, whether GAC elevation causes microglial activation remains unknown. In this study, we found heightened expression levels of GAC in early AD mouse brain tissues compared with those in control littermates. Investigations on an *in vitro* neuroinflammation model revealed that GAC is increased in primary mouse microglia following pro-inflammatory stimulation. To model GAC elevation we overexpressed GAC by plasmid transfection and observed that GAC-overexpression shift the microglial phenotype to a pro-inflammatory state. Treatment with BPTES, a glutaminase inhibitor, reversed LPS-induced microglial activation and inflammation. Furthermore, we discovered that GAC overexpression in mouse microglia increased exosome release and changed exosome content, which includes specific packaging of pro-inflammatory miRNAs that activate microglia. Together, our results demonstrate a causal effect of GAC elevation on microglial activation and exosome release, both of which promote the establishment of a pro-inflammatory microenvironment. Therefore, GAC may have important relevance to the pathogenesis of AD.

Keywords: Alzheimer's disease, glutaminase C, microglia activation, brain inflammation, glutaminase inhibitor, exosome

INTRODUCTION

Alzheimer's disease (AD) is currently the most common neurodegenerative disease worldwide, with an incidence of approximate 6% among population over 65, and around 20% over 80 (Danborg et al., 2014; Reitz and Mayeux, 2014). It is the number one cause for dementia in the aged population, imposing significant personal, societal, and economic tolls (WHO 2018 Annual Report). Chronic inflammation and neuronal damage are key processes of AD

Abbreviations: AD, Alzheimer's disease; CNS, central nervous system; GAC, glutaminase C; GLS1, glutaminase 1; KGA, kidney-type glutaminase; LPS, lipopolysaccharides; NTA, nanoparticle tracking analysis.

(Sardi et al., 2011). Microglia are the resident immune cells in the CNS and form the first line of defense during brain injury or disease (Block and Hong, 2005; Glass et al., 2010). The activation of microglia plays a central role in neuroinflammation during AD. Pathogenesis of AD is known to involve accumulation of amyloid peptides (Aβ) that leads to microglial activation and release of pro-inflammatory mediators such as cytokines, reactive oxygen species, and toxic chemicals. These mediators include several neurotoxic secretory products that may ultimately cause severe neurotoxicity and loss of synaptic connections (Tan et al., 1999; Sastre et al., 2006).

Our previous studies demonstrated that the expression of GLS1 is up-regulated in HIV-1-infected macrophages and microglia, which causes neurotoxicity and serves as a key pathogenic process in HIV-1-associated neurocognitive disorders (Huang et al., 2011). GLS1 is the enzyme catalyzing the hydrolysis of glutamine to produce glutamate in the CNS (Curthoys and Watford, 1995). It has two variants due to alternative splicing, including KGA and GAC (Elgadi et al., 1999; Porter et al., 2002). GAC is the variant that is elevated in HIV-1-infected macrophages and microglia (Huang et al., 2011). Interestingly, transgenic mice with GAC overexpression in neural stem/progenitor cells (NPC) and neural cells-derived from NPC (Nestin-GAC mice) exhibited microglial activation, brain inflammation, and memory deficits (Wang et al., 2017) similar to those key pathogenic processes as seen in AD. However, whether GAC is altered in AD-related neuroinflammation and whether GAC alteration directly instigates microglial activation and brain inflammation remain unknown.

In this study, we found that the expression levels of GAC, but not KGA, were elevated in AD transgenic mouse brain tissues compared with those in control littermates. Notably, GAC elevation was in concurrence with increased expression levels of pro-inflammatory markers. GAC overexpression in resting microglia polarized microglia into an active and pro-inflammatory state. Furthermore, GAC overexpression increased the release of exosomes that contain specific packaging of pro-inflammatory miRNAs, which may promote a pro-inflammatory circumstance for microglial activation.

MATERIALS AND METHODS

Mice and Microglia Culture

APP/PS1 mice and C57 mice (purchased from Shanghai Model Organisms Center) are housed and bred in the Comparative Medicine animal facilities of Tongji University School of Medicine (TUSM). All procedures were conducted according to protocols approved by the Institutional Animal Care and Use Committee of TUSM. Mouse genotype was validated by PCR. Mouse primary microglia was isolated from whole brains of C57 mice at postnatal day 1 (P1). Mouse brains were dissected out after removing peripheral blood vessels and washed twice with HBSS. Next, mouse brains were digested at 37°C for 30 min in 0.25% trypsin solution supplemented with 0.05% DNase I. Digestion was stopped by FBS (Invitrogen). The tissue sediment was centrifuged at 1500 rpm for 5 min at 4°C and washed twice with HBSS. After trituration, cells were plated and cultured in DMEM with 10 ng/mL GM-CSF and 10% FBS, 50 U penicillin and 50 mg/mL streptomycin at 37°C. Culture dishes or plates were coated with 100 μg/mL Poly-D-Lysine (Sigma) and 5 μg/mL Fibronectin (Sigma). The culture medium was replaced every 3 days. Cells were subjected to three passages for purification purpose. Microglia purity was confirmed by immunostaining with antibodies against Iba1 (cat# 019-19741, WAKO).

Plasmid Transfection for GAC Overexpression

Plasmids expressing human KGA and GAC were commercially purchased (Jikai, Inc.). Cultured mouse microglia were transfected by plasmids with KGA or GAC expression with Lipofectmine2000 (Life Technologies, Inc.) according to the manufacture's instruction for 48 h before collected for further analyses.

Protein Extraction and Western Blot

Mice were euthanized and brains were removed and homogenized by a homogenizer in the M-PER Protein Extraction Buffer (Pierce) containing a protease inhibitor cocktail (Sigma). Protein concentrations were determined with a BCA Protein Assay Kit (Pierce). Proteins (5—10 μg) from tissue lysates or proteins (20–30 μg) from cell lysates were separated by sodium dodecyl sulfate polyacrylamide gel electrophoresis (SDS-PAGE) and electrophoretic transferred to polyvinylidene fluoride membranes (Millipore and Bio-Rad). Membranes were incubated with primary antibodies for CD86 (rabbit, cat#ab86392, Abcam, 1:1000), GLS1 (rabbit, cat#ab156876, Abcam, 1:1000), CD206 (mouse, cat#AF2535, R&D Systems, 1:500), neuron-specific Class III β-tubulin (Tuj1) (rabbit, cat#T2200, Sigma-Aldrich, 1:1000), Flotillin-1 (mouse, cat#610821, BD Biosciences, 1:1000), or β-actin (Sigma-Aldrich) overnight at 4°C followed by a horseradish peroxidase-linked secondary anti-rabbit or anti-mouse antibody (Cell Signaling Technologies, 1:10,000) incubation. Antigen-antibody complexes were visualized by Pierce ECL Western Blotting Substrate (Thermo Fisher Scientific, Waltham, MA, United States). For data quantification, films were scanned with a CanonScan 9950F scanner; the acquired images were analyzed using the free public domain NIH ImageJ program[1].

Enzyme-Linked Immunosorbent Assay (ELISA)

Serum of cultured primary mouse microglia with/without GAC overexpression was collected and pro-inflammatory cytokine TNF-α was measured with commercially available ELISA kits (cat# 50349-MNAE, Sino Biological) according to manufacturer's protocols.

Immunochemistry

Immunochemistry was done as previously described (Ma et al., 2019). Briefly, cells or tissue sections were fixed in 4%

[1]http://rsb.info.nih.gov/nih-image/

paraformaldehyde (Sigma) for 15 min at room temperature (RT), washed 3 times with PBS (Thermo Fisher Scientific), and incubated with permeabilizing and blocking buffer containing 5% goat serum (Vector Laboratories) and 0.2% Triton X-100 (Bio-Rad) in PBS for 1 h at RT. Fixed cells or tissue sections were incubated with primary antibody for Iba1 (goat, cat# ab5076, Abcam, 1:500), GLS1 (rabbit, cat# ab156876, Abcam, 1:2000), GFAP (rabbit, cat# Z0334, DAKO, 1:500), or neuron-specific Class III β-tubulin (Tuj1, rabbit, cat# T2200, Sigma-Aldrich, 1:500) overnight at 4°C. The next day, cells or tissue sections were washed with PBS and incubated with secondary antibodies (Molecular Probes) for 1 h at RT. Cells were counterstained with DAPI (Sigma-Aldrich). Images were taken using a Nikon Eclipse E800 microscope equipped with a digital imaging system and imported into Image-Pro Plus, version 7.0 (Media Cybernetics) for quantification. 600–1,000 immunostained cells from 15 randomly picked fields per group were counted.

RNA Isolation and qPCR Analysis

Total RNA was isolated by Purification Kit (Fermentas) with DNase I digestion (Qiagen) to remove genomic DNA. Messenger RNA – derived cDNA was generated using Oligo-dT priming with Transcriptor First Strand cDNA Synthesis Kit (Roche). RNase inhibitor was used to prevent degradation. Amplification was performed using SYBR Green PCR Master Mix (Applied Biosystems) and specific primer sets (**Supplementary Table S1**). GAPDH was used for the normalization of all mRNA expression levels.

Analyses of Glutamate by Amplex Red Glutamic Acid/Glutamate Oxidase Assay Kit

Intracellular and extracellular glutamate levels in microglia culture were determined by Amplex Red Glutamic Acid/Glutamate Oxidase Assay Kit (Invitrogen, A12221) based on the manufacture's instruction. For intracellular glutamate assay, cellular protein lysates were diluted to the same protein concentration before entering the assay. For extracellular glutamate assay, culture media was changed to a phenol red-free media 24 h before the assay, and same volumes of supernatant were entered into the assay.

Isolation of Exosomes

Exosomes were isolated from the serum-free microglia culture as previously described (Wu et al., 2018). Gradient ultracentrifugation was utilized for exosomes isolation. Briefly, cells were planted on poly-L-Ornithine/laminin-coated 10 cm dish and cultured in for 12 h. First, supernatants were centrifuged at 300 × *g* for 10 min to remove free cells, then at 3000 × *g* for 20 min to remove debris, and 10,000 × *g* for 30 min to remove organelles. Exosomes were collected through ultracentrifugation at 100,000 × *g* for 2 h. All centrifugation steps were performed at 4°C.

Nanoparticle Tracking Analysis (NTA)

The size and number of exosomes were determined as previously described (Wu et al., 2018). Briefly, microglial cells were planted on poly-L-Ornithine/laminin-coated 10 cm dish and cultured. The supernatants of cultured cells were collected after 12 h, and the collected exosomes were resuspended in 150 μl PBS and diluted at 1:100 in PBS. One milliliter solution was used for NanoSight analysis. NTA was done on NanoSight NS300 system (Malvern Instruments, United Kingdom) with a sCMOS camera. The conditions of the measurements were set at 25°C, 1 cP viscosity, 25 s per capture frame and 60 s for measurement time. Three individual measurements were performed for the measurement of sizes and concentrations of exosomes.

Statistical Analyses

Data from two groups were evaluated statistically by two-tailed, paired or unpaired student *t*-test. Data were shown as mean ± SD, and significance was determined as $P < 0.05$.

RESULTS

GAC Expression Is Elevated in Early AD Mouse Brain Tissues

In order to determine whether GLS1 expression was altered in the pathogenic process of AD, we investigated the protein expression levels of both KGA and GAC in APP/PS1 mouse brains. We found that the protein expression levels of KGA, GAC, and the pro-inflammatory marker CD86 were not changed in 1 month (1 M) APP/PS1 mouse brain compared with those in 1 M control mouse brains (**Figure 1A**). Interestingly, in 3 months (3 M) mouse brain, the expression levels of GAC and CD86 were higher in APP/PS1 mice than those in control littermates. In contrast, KGA expression levels did not show significant difference between the two groups (**Figure 1B**). In 6 months (6 M) mouse brain, protein expression levels of KGA, GAC, and CD86 were higher in APP/PS1 mice than those in control littermates (**Figure 1C**). However, at 9 months (9 M), the protein expression levels of KGA, GAC, or CD86 no longer displayed significant difference compared with those in control littermates (**Figure 1D**). The increase of GAC at 3 M was in concurrence with an increase of microglial activation in 3 M AD mouse brain as evidenced by more $Iba1^+$ activated microglia in 3 M AD mouse hippocampus, compared to healthy controls (**Figure 1E**). More importantly, GLS1 co-localized with Iba1 in 3 M AD mouse hippocampus (**Figure 1F**). The co-localization of GLS1 and Iba1 could also be observed in 18 M AD mouse hippocampus (**Supplementary Figure S1**). Together, these data demonstrate an elevation of GLS1 isoforms at early stages of AD (3–6 M in APP/PS1 mouse) mouse brains in concurrence with the activation of microglia.

GAC Is Specifically Up-Regulated in Pro-inflammatory Microglia

To study whether GAC expression was altered under pro-inflammatory and anti-inflammatory states, we treated cultured

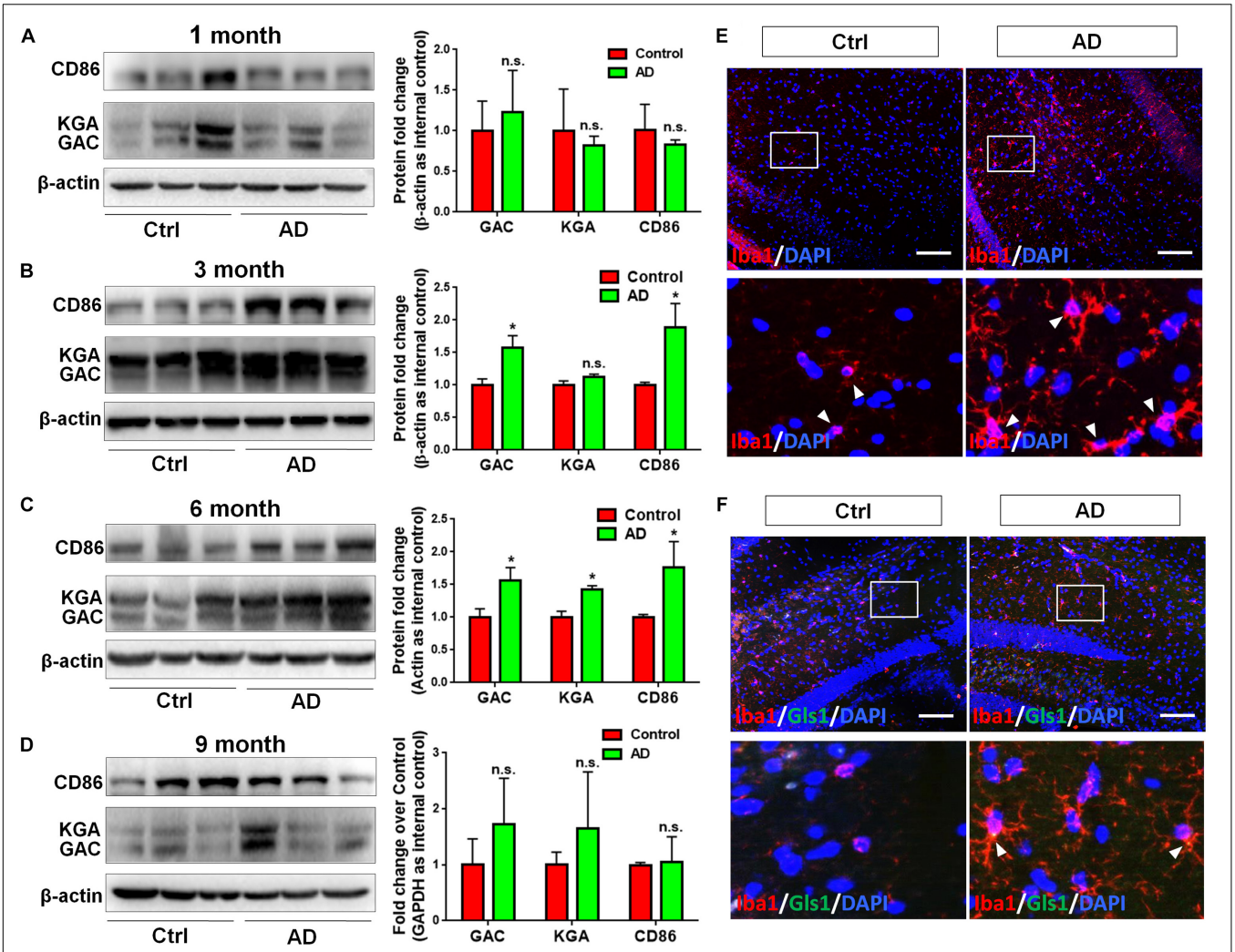

FIGURE 1 | Upregulation of GAC in early stage AD mouse brain tissues. **(A–D)** Brains of 1, 3, 6, and 9 months APP/PS1 mice and their control littermates were removed and homogenized for protein analyses. Representative Western blots were shown and CD86, KGA, and GAC protein expression levels in 1 month APP/PS1 and control mouse brains **(A)**, 3 month APP/PS1 and control mouse brains **(B)**, 6 month APP/PS1 and control mouse brains **(C)**, 9 month APP/PS1 and control mouse brains **(D)** were normalized to β-actin and presented as fold change compared with those in control mouse brains. Error bars denote s.d. from triplicate measurements. $^*P < 0.05$, by two-tailed *t*-test ($n = 3$). **(E,F)** Brains of 3 and 6 month APP/PS1 mice and their control littermates were removed after intracranial perfusion and prepared for immunofluorescence staining. Representative pictures of Iba1 expression in 3 month APP/PS1 and control mouse brain **(E)**, GLS1 and Iba1 expressions in 6 month APP/PS1 and control mouse brain **(F)** were shown. Images at the lower panels were high-magnification images of the corresponding small box area from the upper panels. Scale bar: 10 μm.

mouse microglia with LPS (100 ng/mL), IL-4 (50 ng/mL), or IL-10 (50 ng/mL) to induce the pro-inflammatory, anti-inflammatory, and de-activated phenotypes of microglia, respectively. The enrichment of mouse microglia was validated by co-immunostaining of Iba1 with glia marker GFAP and neuronal marker Tuj1. Almost all cells expressed immunoreactivity corresponding to Iba1 but not GFAP or Tuj1 (**Supplementary Figure S2**). Total RNA was collected at 6 h and protein lysates were collected at 24 h after LPS, IL-4, or IL-10 treatment. The mRNA levels of pro-inflammatory markers, tumor necrosis factor–α (*TNF*-α) and inducible nitric oxide synthase (*iNOS*) were significantly elevated after LPS treatment, but either remained the same (*TNF*-α) or decreased (*iNOS*) after IL-4 or IL-10 treatment (**Figure 2A**). Anti-inflammatory markers *CD206* and *Ym1* were decreased in LPS-treated microglia but increased in IL-4-treated microglia (**Figure 2A**). Importantly, the mRNA levels of *GAC*, but not those of *KGA*, were significantly elevated in LPS-treated microglia and decreased in IL-10-treated microglia (**Figure 2B**). In accordance with mRNA results, protein analyses revealed increase of GAC (but not KGA) and CD86 in LPS-treated microglia (**Figures 2C,D**). IL-10 treatment increased CD206 protein expression, but decreased CD86, KGA, and GAC protein expressions levels in microglia (**Figures 2C–E**). These data demonstrate a strong association between GAC expression and the pro-inflammatory phenotype of microglia, suggesting that GAC may involve in the activation of microglia.

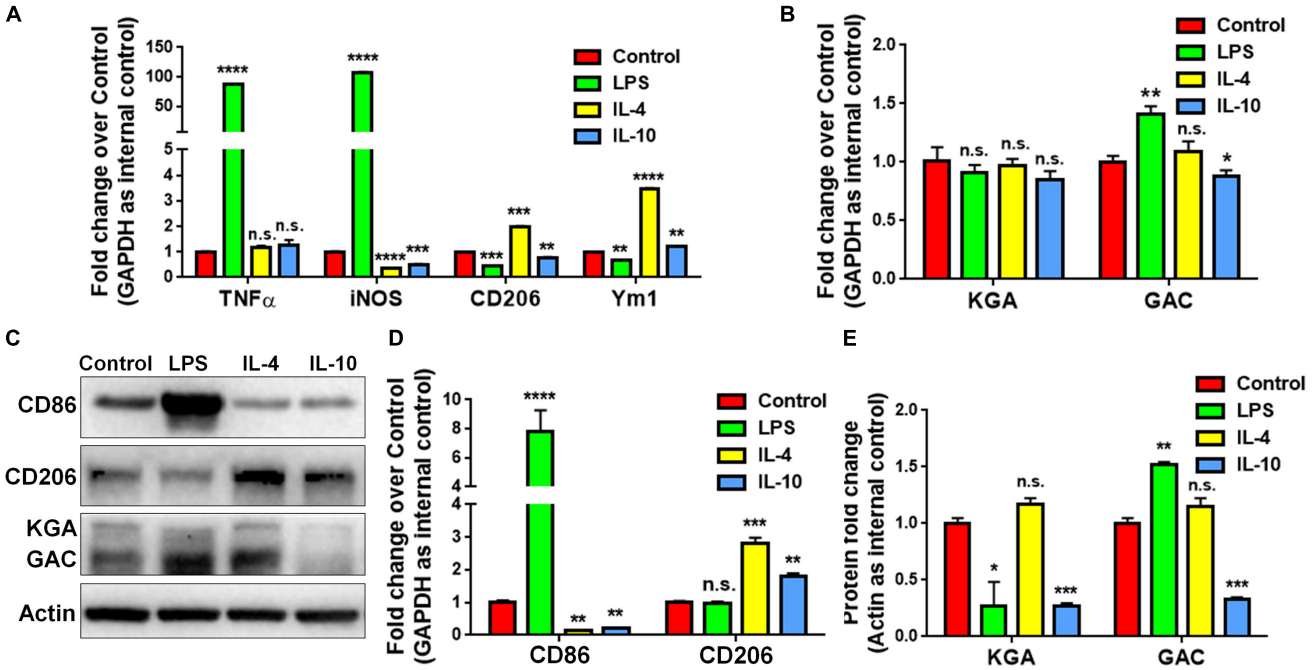

FIGURE 2 | Upregulation of GAC in pro-inflammatory mouse microglia. **(A–E)** Primary mouse microglia were treated with LPS (100 ng/mL), IL-4 (50 ng/mL), and IL-10 (50 ng/mL). Total RNA was collected after the treatment for 6 h **(A,B)**. Protein lysates were collected after 24 h **(C–E)**. mRNA levels of *TNF*-α, *iNOS*, *CD206,* and *Ym1* **(A)** and *KGA* and *GAC* **(B)** were determined by qPCR analyses. Data were normalized to *GAPDH* and presented as fold change compared to control microglia. Error bars denote s.d. from triplicate measurements. Representative immunoblots of CD86, CD206, KGA, and GAC protein levels **(C)** were shown and CD86, CD206 **(D)**, KGA, and GAC **(E)** protein expression levels were normalized to β-actin and presented as fold change compared to control microglia. Error bars denote s.d. from triplicate measurements. $^{*}P < 0.05$, $^{**}P < 0.01$, $^{***}P < 0.001$, $^{****}P < 0.0001$, by two-tailed *t*-test ($n = 3$). Experiments were carried out three times in triplicates with 5–7 P1 mice per group.

GAC Overexpression Induces Microglial Activation

To test our premise that GAC is sufficient to induce microglial activation, we overexpressed GAC in primary mouse microglia by plasmid transfection. We first confirmed that GAC was indeed overexpressed in cultured cells by qPCR (60-fold increase, **Figure 3A**) and Western blots (2-fold increase, **Figures 3D,E**). Next, we examined the expression of pro-inflammatory and anti-inflammatory genes and found that the mRNA levels of pro-inflammatory genes *TNF*-α and *iNOS* were elevated in GAC-overexpressed microglia (**Figure 3B**). Protein analysis revealed an increased release of TNF-α and increased expression of CD86 in GAC-overexpressed microglia (**Figures 3C–E**). On contrary to the elevation of pro-inflammatory molecules, mRNA levels of anti-inflammatory molecules *CD206* and *Ym1* were found to be decreased after GAC overexpression (**Figure 3B**). Consistent with the mRNA decrease, protein analysis revealed a decrease of CD206 protein levels in microglia after GAC overexpression (**Figures 3D,E**). Interestingly, KGA overexpression in microglia did not activate microglia or cause neuroinflammation (**Supplementary Figure S3**). Therefore, these data demonstrate that elevated levels of GAC, but not KGA, are sufficient to activate microglia and induce microglia into a pro-inflammatory phenotype.

GAC Mediates LPS-Induced Microglial Activation

To further determine whether GAC activity is critical for pro-inflammatory transformation of microglia during LPS activation, we used BPTES, a glutaminase inhibitor, to suppress GAC activity when microglia were treated with LPS. BPTES (10 μM) was added to microglia cultures for 1 h before treatment with LPS (50 ng/mL) for 6 h. As expected, LPS treatment dramatically increased the mRNA levels of pro-inflammatory markers *TNF*-α and *iNOS*, and BPTES abolished such increases (**Figures 4A,B**). In comparison, LPS treatment significantly decreased the mRNA levels of anti-inflammatory markers *CD206* and *Ym1*. However, BPTES failed to reverse such decreases (**Figures 4C,D**). These results demonstrate that LPS-induced microglial activation through elevation of GAC activities.

GAC-Induced Microglial Activation Is Not Through Autocrine Secretion of Glutamate

To identify whether GAC overexpression induced microglial activation via an autocrine secretion of glutamate, we first measured both intracellular and extracellular glutamate levels in microglial cultures after KGA or GAC overexpression.

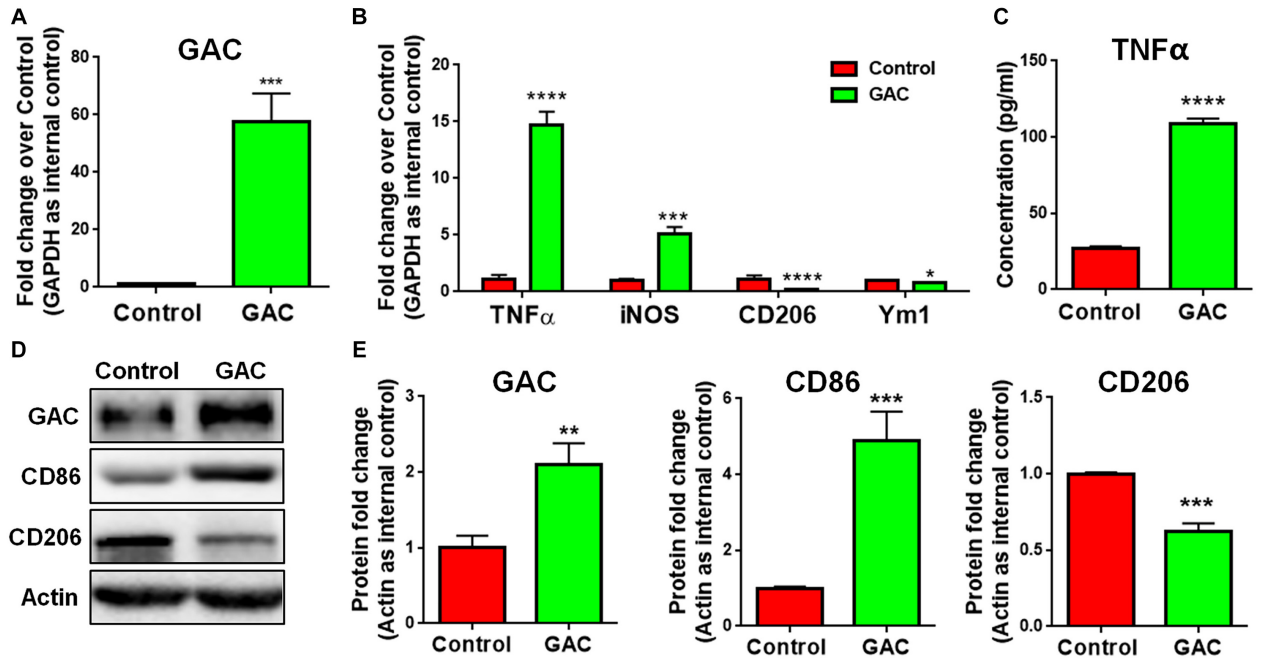

FIGURE 3 | GAC overexpression induces microglial activation. **(A–E)** Primary mouse microglia were transfected with GAC overexpressing plasmid for 48 h. Total RNA and protein lysates were collected. mRNA levels of *GAC* **(A)**, *TNF-α*, *iNOS*, *CD206,* and *Ym1* **(B)** were determined by qPCR analyses. Data were normalized to *GAPDH* and presented as fold change compared to control microglia. Error bars denote s.d. from triplicate measurements. Concentrations of released TNF-α from microglia mere determined by ELISA **(C)**. Error bars denote s.d. from triplicate measurements. Representative immunoblots of GAC, CD86, and CD206 **(D)** were shown along with quantifications of GAC, CD86, and CD206 protein expression levels **(E)**. Data were normalized to β-actin and presented as fold change compared to control microglia. Error bars denote s.d. from triplicate measurements. $^{*}P < 0.05$, $^{**}P < 0.01$, $^{***}P < 0.001$, $^{****}P < 0.0001$, by two-tailed *t*-test ($n = 3$). Experiments were carried out three times in triplicates with 5–7 P1 mice per group for *in vitro* perturbation.

Intracellular glutamate was found increased in KGA- and GAC-overexpressed microglia culture (**Figure 5A**), but extracellular glutamate was not significantly changed in microglia culture with either KGA or GAC overexpression, indicating GAC did not regulate microglial activation through elevating extracellular glutamate (**Figure 5B**). To further exclude the effect of extracellular glutamate, we directly added different doses of glutamate to microglia cultures for 24 h and found that extra glutamate did not promote microglial activation but instead decreased mRNA levels of *TNF-α*, *iNOS*, *CD206*, and *Ym1* at 100 or 300 μM concentration (**Figure 5C**). Protein analysis revealed no change of CD86 or CD206 expression levels after addition of glutamate into microglia cultures (**Figure 5D**). These results suggest that although GAC overexpression is sufficient to induce microglial activation, the activation is independent of autocrine secretion of glutamate.

GAC Overexpression Accelerates Exosome Release From Microglia

To determine the mechanism(s) of GAC-mediated microglial activation, we investigated exosome secretion by microglia after GAC overexpression. Our previous studies revealed that GLS1 regulated exosome release in HIV-1-infected macrophages and BV2 microglia cell lines (Wu et al., 2018). To investigate whether GAC had similar regulatory role on exosome release of primary microglia, we examined the concentrations of exosomes released from equal number of microglia with or without GAC overexpression. First we validated exosomes isolated from GAC-overexpressed microglia and control microglia by examining the expression of exosome markers CD-9 and Flotillin-2 (**Figure 6A**). The protein lysate from both groups generated specific bands for CD-9 and Flotillin-2, confirming the successful isolation of exosomes through ultra-centrifugation. Quantitative analyses of CD-9 and Flotillin-2 revealed higher levels of CD-9 and Flotillin-2 in GAC overexpression group, compared to control, suggesting a positive effect of GAC on microglia exosome release (**Figure 6B**). Consistent with the data on exosome markers, NTA revealed that although the exosome sizes were similar between GAC overexpression and control groups (**Figure 6C**), exosome concentrations were significantly higher in GAC overexpression group compared to the control group (**Figure 6D**). Calculation on the number of exosomes released per cell through dividing the number of exosomes by the number of plated microglia revealed that control microglia released about 100 exosomes while microglia with GAC overexpression released 120 exosomes in 48 h (**Figure 6E**). We assumed that numbers of microglia in the culture did not change since no significant difference was observed when microglia were transfected with control or GAC overexpression plasmid at 0 h and 48 h (**Supplementary Figure S4**). Together, our results

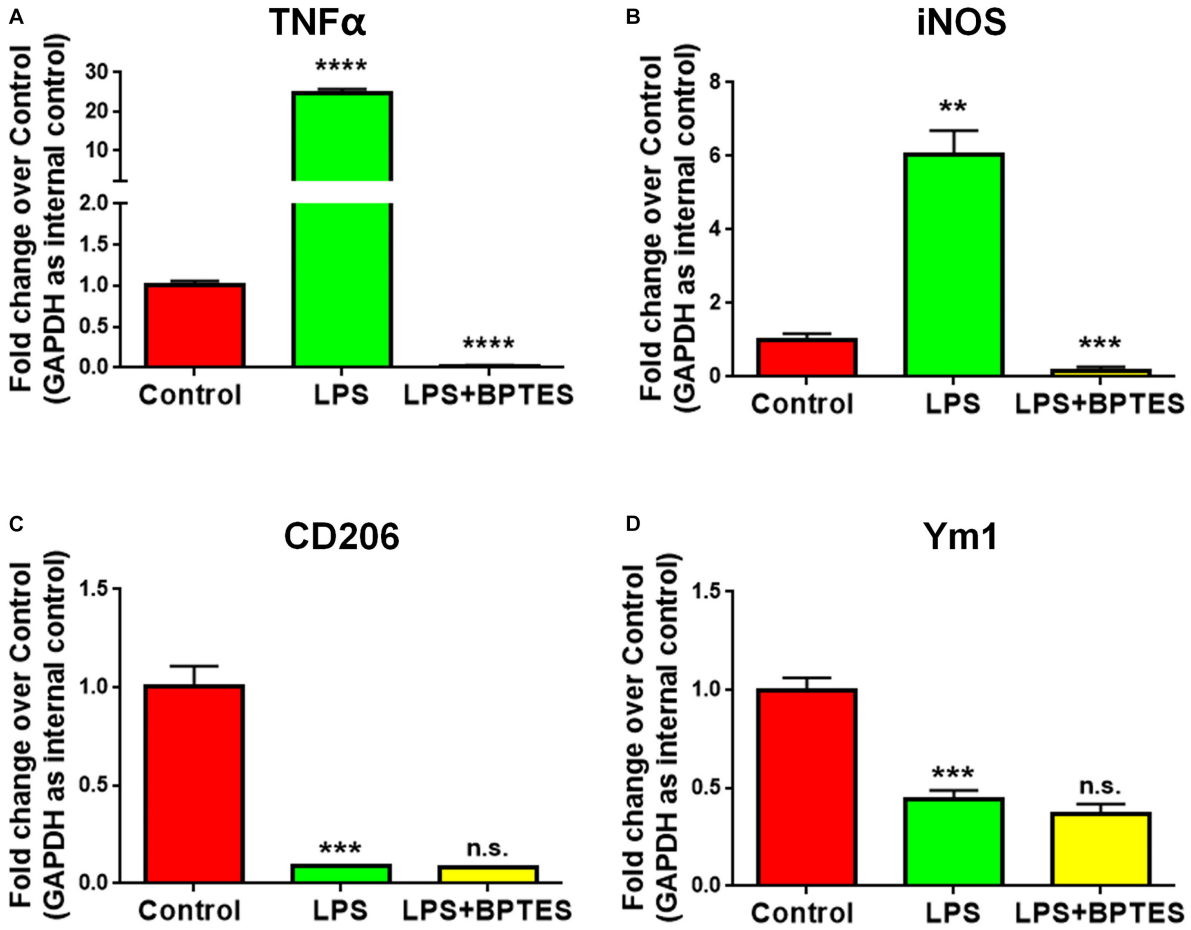

FIGURE 4 | Treatment with glutaminase inhibitor reverses LPS-induced microglial activation. **(A–D)** Mouse microglia were treated with or without BPTES (10 μM) for 1 h before being exposed to LPS (50 ng/mL) for 6 h. Total RNA was collected for qPCR analyses. mRNA levels of *TNF*-α **(A)**, *iNOS* **(B)**, *CD206* **(C)**, *Ym1* **(D)** were determined by qPCR analyses. Data were normalized to *GAPDH* and presented as fold change compared to control microglia. Error bars denote s.d. from triplicate measurements. $^{**}P < 0.01$, $^{***}P < 0.001$, $^{****}P < 0.0001$, as compared to control microglia, by two-tailed *t*-test ($n = 3$); Experiments were carried out three times in triplicates with 5–7 P1 mice per group.

demonstrate that GAC overexpression increases exosome release from primary microglia.

GAC Overexpression Alters the Function and Content of Microglia-Derived Exosomes

To study the functional impacts of exosomes derived from GAC-overexpressed microglia, we added exosomes (15 μg exosome protein/mL medium) derived from control or GAC-overexpressed microglia to mouse microglia for 24 h. qPCR analyses revealed significant increase of transcripts corresponding to pro-inflammatory molecules, including *TNF*-α and *iNOS*, indicating that exosomes from GAC-activated microglia are sufficient to induce the inflammatory phenotype in quiescent/resting microglia (**Figure 7A**). Interestingly, *GAC* mRNA levels were substantially increased in microglia treated with exosomes derived from GAC-activated microglia (**Figure 7B**), which indicates a positive feedback loop of GAC transcription through exosomes. Because exosome mainly functions through small non-coding RNAs, we investigated the miRNA content and found significant upregulations of classic pro-inflammatory miRNAs (such as *miR-130*, *miR-145a*, *miR-23b*, and *miR-146a*, etc.) and downregulations of anti-inflammatory miRNAs (such as *miR-124* and *let-7b*) in exosomes from GAC-activated microglia (**Figure 7C**). These concerted alterations of exosome content suggest that activation of microglia by GAC overexpression is closely associated with microglia-derived exosomes that favor pro-inflammatory microenvironment (**Figure 7D**).

DISCUSSION

Brain inflammation, neuronal, and synaptic injury are key pathological features of AD (Sardi et al., 2011). The degree of these pathological features is often in line with the severity of AD (Kashani et al., 2008). Microglia are the residential macrophages of the CNS, regulating brain inflammation as well as neural and synaptic activity in defense against pathogens,

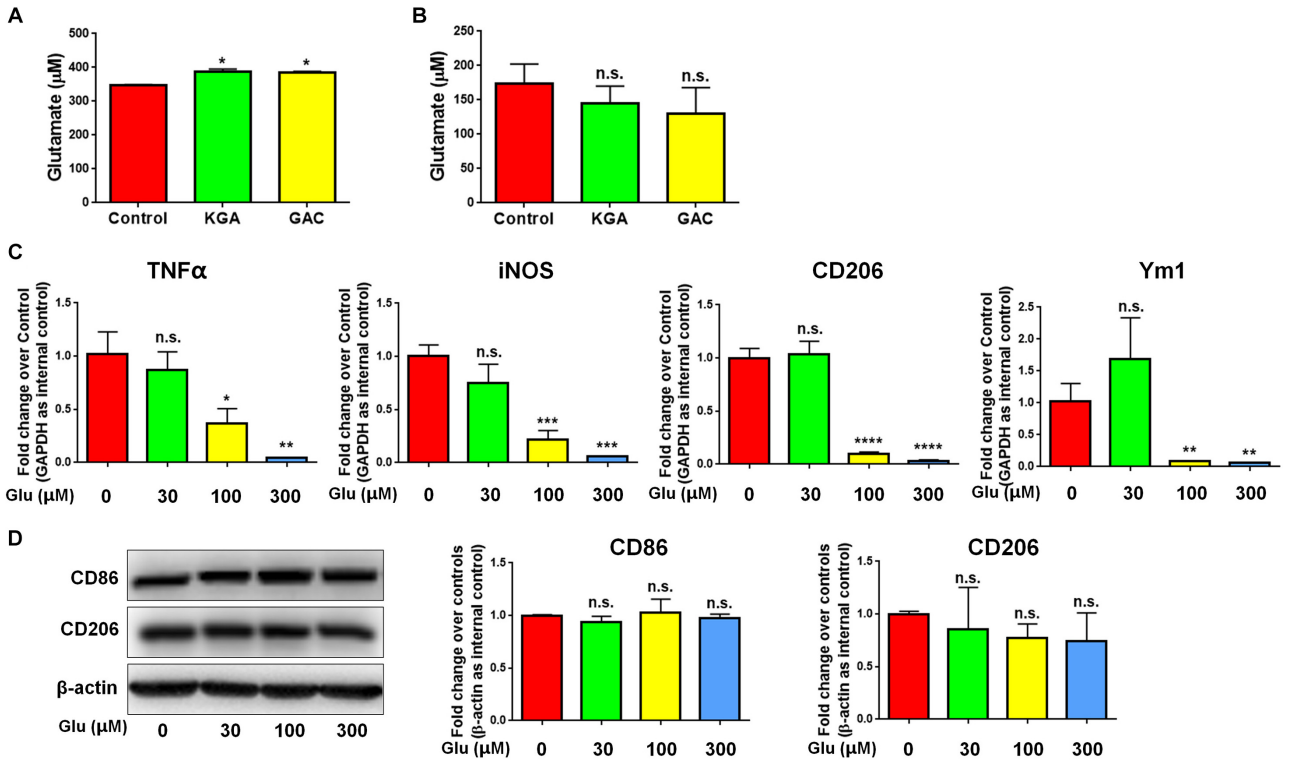

FIGURE 5 | GAC overexpression induces neuroinflammation in a glutamate-independent manner. **(A,B)** Intracellular glutamate levels **(A)** and extracellular glutamate levels **(B)** in control, KGA-, and GAC-overexpressed microglia cultures were determined through the Glutamate Assay Kit. **(C)** mRNA levels of *TNF-α*, *iNOS*, *CD206,* and *Ym1* in microglia treated with different doses of glutamate were determined by qPCR analyses. Data were normalized to *GAPDH* and presented as fold change compared to control microglia. **(D)** Representative blots and quantification of protein levels of CD86 and CD206 in microglia treated with different doses of glutamate. Western blot data were normalized to β-actin and presented as fold change compared to control microglia. Error bars denote s.d. from triplicate measurements. $^{*}P < 0.05$, $^{**}P < 0.01$, $^{***}P < 0.001$, $^{****}P < 0.0001$, as compared to control microglia, by two-tailed *t*-test ($n = 3$); Experiments were carried out three times in triplicates with 5–7 P1 mice per group.

wounds, and injuries (Block and Hong, 2005; Glass et al., 2010). Recent studies support a central role of microglia that not only instigates immune activation but also sustains elevated expression and release of pro-inflammatory mediators for AD etiopathology (Tan et al., 1999; Sastre et al., 2006). In this paradigm, investigations on regulators and mechanism(s) of microglial activation show great promise to unmask causes for AD and identify potential therapeutic targets for early AD interventions.

In the current study, we investigated whether GAC alteration had a causal effect on microglial activation. We demonstrated a significantly heightened expression of GAC in early stages of AD mouse brain tissues (**Figure 1**) and in mouse microglia after pro-inflammatory activation (**Figure 2**). Overexpression of GAC, but not KGA, led to microglial activation and inflammation (**Figure 3**). Importantly, glutaminase inhibitor BPTES was able to abolish LPS-induced microglial activation (**Figure 4**). Furthermore, GAC overexpression induced a large increase in exosome release (**Figure 5**), and exosomes released from GAC-overexpressed microglia activated resting microglia, which is associated with drastic upregulations of pro-inflammatory miRNAs and downregulations of anti-inflammatory miRNA in exosomes (**Figure 6**). Together, these results demonstrate a causal effect of GAC overexpression on microglial activation and inflammatory exosome release that are relevant to early AD pathogenesis.

The causal effect of heightened GAC expression on microglial activation has important clinical implications. One of the characteristics of AD is that there is often a long lag (10 to 20 years) for the first sign of symptoms (memory decline, disorientation, motivation loss, etc.) to occur in patients after the onset of pathological alterations in the CNS. This lag may serve as a promising therapeutic window that could be researched for novel approaches to stop or at least slow down AD progress. In the clinics, the majority of AD patients are diagnosed after symptoms occur. Therefore, therapeutic interventions often have little effects to alleviate clinical symptoms. Through current investigations, we found elevated levels of GAC expressions specifically in the 3 and 6 months APP/PS1 mouse brains. With the progression of AD, GAC levels halted their increases in 9 months APP/PS1 mouse brain, likely due to neural damage and loss in the later stages of AD. The elevation of GAC expression closely associated with the temporal pattern of plaque formation, which, starts to occur around at 3 months in mice (López-González et al., 2015). The correlation indicates the strong association of GAC deregulation and neuroinflammation

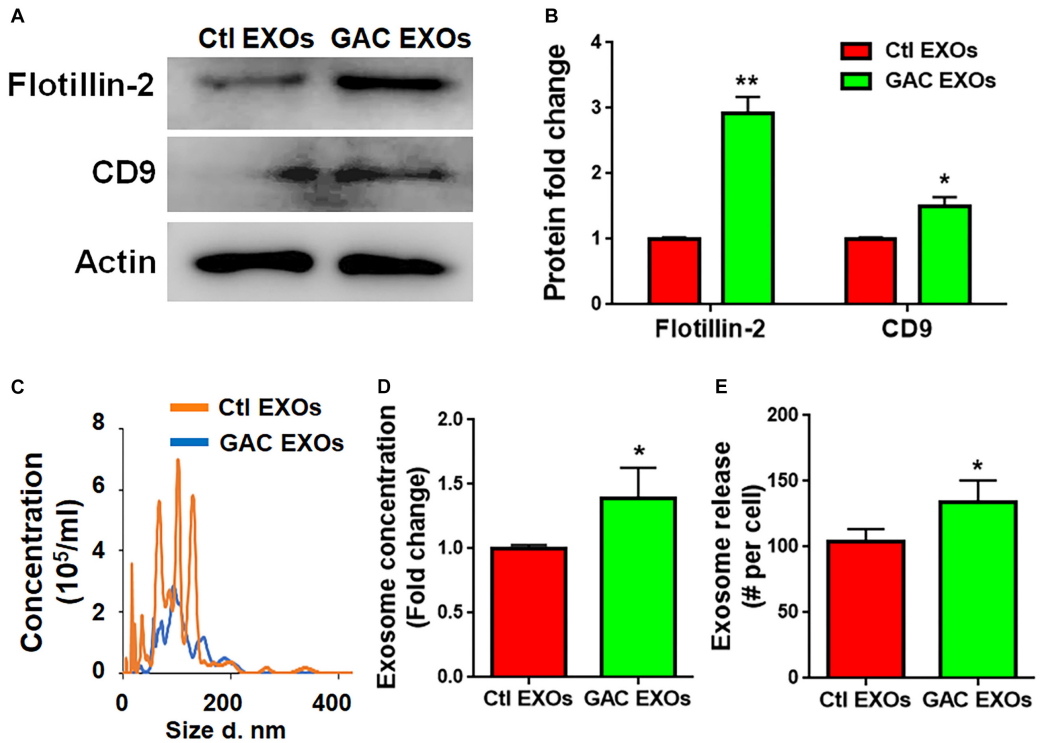

FIGURE 6 | GAC overexpression increases exosome release. Exosomes released from microglia with and without GAC overexpression were collected through gradient ultracentrifugation. **(A,B)** Representative blot and quantification of CD-9 and Flotillin-2 protein expressions. **(C–E)** Size and concentration of exosomes released from microglia with and without GAC overexpression were isolated from culture supernatants and visualized through NTA **(C)**. Quantification of exosome concentration **(D)** and number of exosomes released per cell **(E)** were performed through NTA. Error bars denote s.d. from triplicate measurements. $^*P < 0.05$, $^{**}P < 0.01$, by two-tailed *t*-test ($n = 3$). Experiments were carried out three times in triplicates with 5–7 P1 mice per group for *in vitro* experiments.

with the appearance of classical AD pathological attributes such as Aβ plaque formation. Thus, our results suggest that GAC expression changes occur very early and could implicate pathological progression of AD.

It is interesting to note that only GAC, but not KGA (the other splice variant of GLS1), is significantly heightened in both early stage AD mouse brain tissues and LPS-induced pro-inflammatory microglia (**Figures 1**, **2**). These data are consistent with the specific upregulation of GAC in HIV-infected microglia in our previous finding (Huang et al., 2011). GAC and KGA share the same DNA sequence on mitochondrial localization signal and core catalytic domain, but possess unique C-terminals due to alternative splicing at post-transcriptional modification of mRNAs (Elgadi et al., 1999; Aledo et al., 2000; de la Rosa et al., 2009). Cellular location of KGA and GAC differ in cancer cells (Cassago et al., 2012). Literatures suggest that because of the shortened 3′ UTR of GAC mRNA, miRNAs capable of targeting KGA mRNA, such as *miR-23*, are unable to bind to GAC mRNA (Gao et al., 2009; Xia et al., 2014; Masamha et al., 2016; Liu et al., 2018). In our study, we observed a dynamic complimentary upregulation of the above miRNAs in LPS-activated microglia to reverse the ongoing and toxic upregulation of KGA and GAC (data not shown). Thus, elevated KGA mRNAs are likely targeted by miRNAs, but GAC mRNAs may be more difficult to be targeted compared to KGA.

GAC is one of the splice variants of GLS1. In the CNS, GLS1 expression mainly follows a neuron-specific pattern under physiological circumstance (Ye et al., 2013). Normally, GLS1 activity and expression are mainly found in neuron-rich regions such as cortex but at lower levels in myelin-rich areas (Najlerahim et al., 1990; Botman et al., 2014). However, GLS1 activity and expression are also detected in astrocytes with lower levels than that in neurons (Kvamme et al., 2001). As the rate-limiting enzyme for glutaminolysis, GLS1 asserts control over the metabolic conditions of CNS cells. Our previous studies revealed the involvement of GLS1 deregulation in neuroinflammation and toxic effect of various cultured CNS cells, including macrophages, microglia (Zhao et al., 2004; Huang et al., 2011; Tian et al., 2012), and neurons (Ye et al., 2013; Hoffman et al., 2016). Moreover, GLS1 deregulation has been implicated in various neurodegenerative and neuropsychiatric disorders (Werner et al., 2001; Gluck et al., 2002; D'Alessandro et al., 2011; Huang et al., 2011; Zhao et al., 2012; Burbaeva et al., 2014). The current study demonstrates a causal role of heightened GAC expression on microglial activation (**Figure 3**), shedding new insights into neuroinflammation mechanisms along with our previous finding that mice with GAC overexpression in the CNS exhibited neuroinflammation and memory deficits (Wang et al., 2017). GAC as a mitochondrial enzyme has a key role in cellular bioenergetics and metabolism. Cellular metabolism has recently

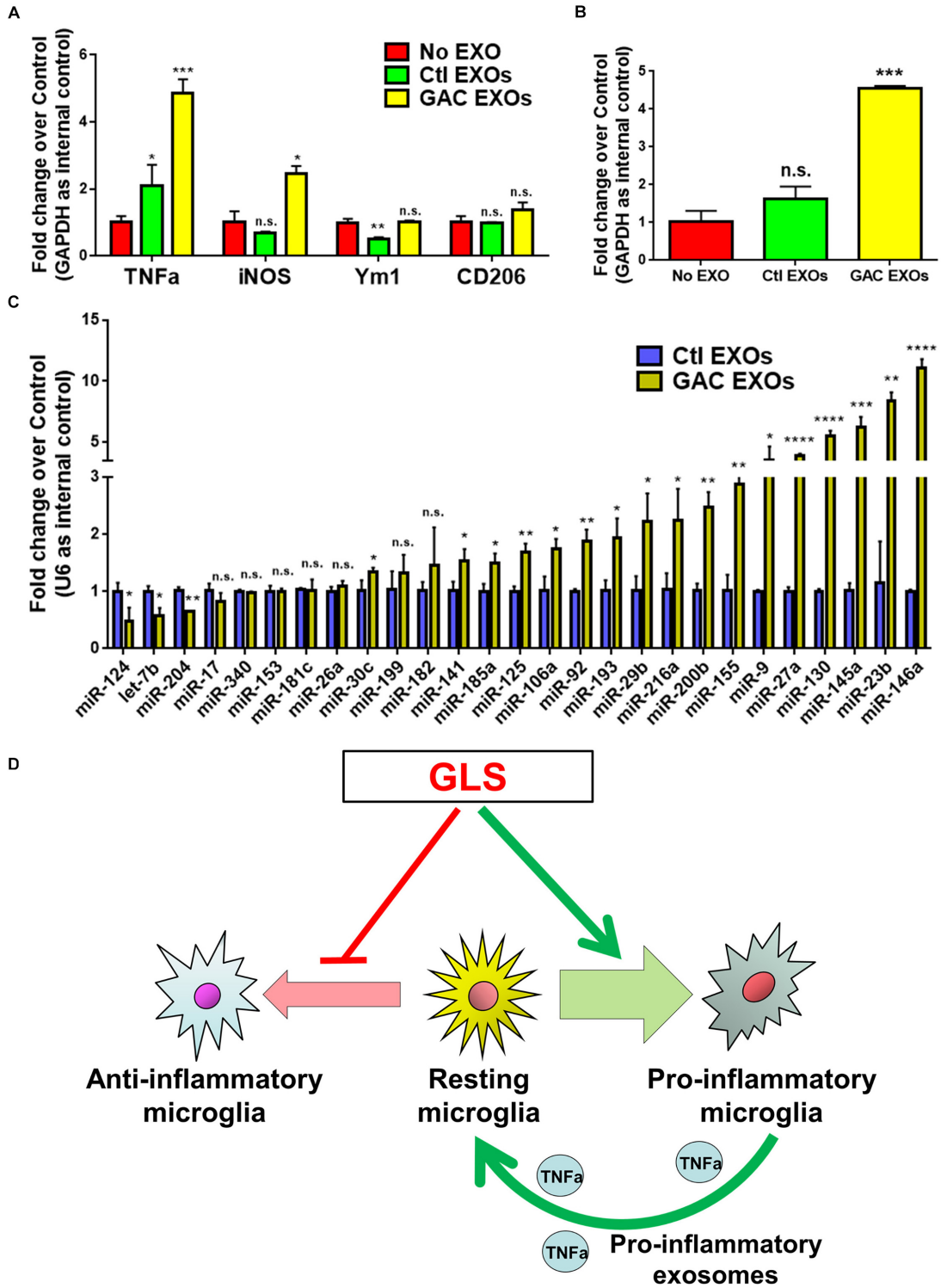

FIGURE 7 | Functional and content analyses of exosomes released from GAC-activated microglia. **(A,B)** Primary mouse microglia were treated with exosomes released from GAC-overexpressed microglia or control microglia. Total RNA was collected from microglia after co-cultured with exosomes for 24 h. mRNA levels of *TNF-α, iNOS*, *Ym1*, and *CD206* **(A)** and *GAC* **(B)** were determined by qPCR. Data were normalized to *GAPDH* and presented as fold change compared to control microglia. Error bars denote s.d. from triplicate measurements. **(C)** Levels of pro-inflammatory miRNAs and anti-inflammatory miRNAs in exosomes were determined from control microglia and GAC-activated microglia through qPCR analyses. Data were normalized to U6 snRNA and presented as fold change compared to exosomes from control microglia. Error bars denote s.d. from triplicate measurements. $^{*}P < 0.05$, $^{**}P < 0.01$, $^{***}P < 0.001$, $^{****}P < 0.0001$, by two-tailed *t*-test ($n = 3$). Experiments were carried out three times in triplicates with 5–7 P1 mice per group. **(D)** A schematic representation of GAC-induced microglial activation.

gained increasing attention as mediators of inflammatory responses of immune cells as indicated by the shifting of resting microglia and macrophages to pro-inflammatory states through glutamine synthetase inhibition (Palmieri et al., 2017a,b). Findings of the current study are in accordance with these previous reports that GAC overexpression led to microglial activation to the pro-inflammatory state. Interestingly, our results showed that GAC overexpression-induced microglial activation is not due to an increased in extracellular glutamate as evidenced by the data showing that addition of glutamate to culture media caused neither microglial activation (**Figure 5C**) nor apoptosis (**Supplementary Figure S5**). Microglia did not express inotropic glutamate receptors and metabotropic glutamate receptors except mGluR2/3 (data not shown). These data indicated that GAC-induced microglial activation is in a glutamate-independent mechanism, which is likely to be closely associated with changes in cellular metabolism. Unlike GAC, we did not observe any effects of KGA on the inflammatory responses of microglia *in vitro*. One possible explanation is that KGA may be less involved in cellular bioenergetics and metabolism due to its cytoplasmic localization, reported in cancer cells, which needs to be further clarified in microglia (Cassago et al., 2012).

Our previous studies demonstrate an increase in exosome release from activated macrophages (Wu et al., 2018). The current study revealed that GAC overexpression promoted exosome release from primary microglia. Furthermore, a substantially altered pro-inflammatory (as evidenced by increase in pro-inflammatory miRNAs and decrease in anti-inflammatory miRNAs) miRNA expression profile was observed in exosomes released from GAC overexpressed microglia (**Figure 7**), indicating that exosomal miRNAs from AD patients' cerebral spinal fluid or plasma might be promising candidates of biomarkers for early AD diagnosis.

In summary, the current study revealed a heightened expression of GAC in early stage AD mouse brain tissues and pro-inflammatory mouse primary microglia. This heightened expression is sufficient to induce microglial activation and make functional changes to exosomes and exosome content in microglia. These results strongly implicate the role of GAC-mediated gene expression and exosome release on microglial activation in the early pathogenesis of AD.

DATA AVAILABILITY

The raw data supporting the conclusions of this manuscript will be made available by the authors, without undue reservation, to any qualified researcher.

ETHICS STATEMENT

All work involving animals was approved by the Institutional Animal Care and Use Committee of the Tongji University School of Medicine.

AUTHOR CONTRIBUTIONS

XX, YW, YH, and JCZ conceived and designed the experiments. GG, SZ, XX, CHL, CCL, CJ, YT, SS, and JZ performed the experiments. GG, SZ, XX, and YW analyzed the data. GG, SZ, XX, YW, YH, and JCZ contributed to the reagents, materials, and analysis tools. XX, YW, YH, and JCZ wrote the manuscript.

FUNDING

This work was supported in part by research grants from the National Basic Research Program of China (973 Program Grant No. 2014CB965001 to JZ), the State Key Program of the National Natural Science Foundation of China (#81830037), Joint Research Fund for Overseas Chinese, Hong Kong and Macao Young Scientists of the National Natural Science Foundation of China (#81329002 to JZ), and Research Fund for Young Scientists of the National Natural Science Foundation of China (#81801063 to YW); The project was also supported in part by the NIH, National Institute of Neurological Disorders and Stroke, 1R01NS097195 (JZ), and the National Institute of Mental Health, 2P30MH062261, Developmental (YH). The content is solely the responsibility of the authors and does not necessarily represent the official views of the National Institutes of Health.

ACKNOWLEDGMENTS

We are grateful to Ms. Li Wu, Yuju Li, Yanyan Zhang, and Dr. Ling Ye for their valuable technical support, comments and suggestions regarding the content of the manuscript.

SUPPLEMENTARY MATERIAL

The Supplementary Material for this article can be found online at: https://www.frontiersin.org/articles/10.3389/fncel.2019.00264/full#supplementary-material

REFERENCES

Aledo, J. C., Gómez-Fabre, P. M., Olalla, L., and Márquez, J. (2000). Identification of two human glutaminase loci and tissue-specific expression of the two related genes. *Mamm. Genome* 11, 1107–1110.

Block, M. L., and Hong, J. S. (2005). Microglia and inflammation-mediated neurodegeneration: multiple triggers with a common mechanism. *Prog. Neurobiol.* 76, 77–98.

Botman, D., Tigchelaar, W., and Van Noorden, C. J. (2014). Determination of phosphate-activated glutaminase activity and its kinetics in mouse tissues using metabolic mapping (quantitative enzyme histochemistry). *J. Histochem. Cytochem.* 62, 813–826. doi: 10.1369/0022155414551177

Burbaeva, G., Boksha, I. S., Tereshkina, E. B., Savushkina, O. K., Prokhorova, T. A., and Vorobyeva, E. A. (2014). Glutamate and GABA-metabolizing enzymes in post-mortem cerebellum in Alzheimer's disease: phosphate-activated

glutaminase and glutamic acid decarboxylase. *Cerebellum* 13, 607–615. doi: 10.1007/s12311-014-0573-4

Cassago, A., Ferreira, A. P., Ferreira, I. M., Fornezari, C., Gomes, E. R., Greene, K. S., et al. (2012). Mitochondrial localization and structure-based phosphate activation mechanism of Glutaminase C with implications for cancer metabolism. *Proc. Natl. Acad. Sci. U.S.A.* 109, 1092–1097. doi: 10.1073/pnas.1112495109

Curthoys, N. P., and Watford, M. (1995). Regulation of glutaminase activity and glutamine metabolism. *Annu. Rev. Nutr.* 15, 133–159.

D'Alessandro, G., Calcagno, E., Tartari, S., Rizzardini, M., Invernizzi, R. W., and Cantoni, L. (2011). Glutamate and glutathione interplay in a motor neuronal model of amyotrophic lateral sclerosis reveals altered energy metabolism. *Neurobiol. Dis.* 43, 346–355. doi: 10.1016/j.nbd.2011.04.003

Danborg, P. B., Simonsen, A. H., Waldemar, G., and Heegaard, N. H. (2014). The potential of microRNAs as biofluid markers of neurodegenerative diseases–a systematic review. *Biomarkers* 19, 259–268. doi: 10.3109/1354750X.2014.904001

de la Rosa, V., Campos-Sandoval, J. A., Martín-Rufián, M., Cardona, C., Matés, J. M., Segura, J. A., et al. (2009). A novel glutaminase isoform in mammalian tissues. *Neurochem. Int.* 55, 76–84. doi: 10.1016/j.neuint.2009.02.021

Elgadi, K. M., Meguid, R. A., Qian, M., Souba, W. W., and Abcouwer, S. F. (1999). Cloning and analysis of unique human glutaminase isoforms generated by tissue-specific alternative splicing. *Physiol. Genomics* 1, 51–62.

Gao, P., Tchernyshyov, I., Chang, T. C., Lee, Y. S., Kita, K., Ochi, T., et al. (2009). c-Myc suppression of miR-23a/b enhances mitochondrial glutaminase expression and glutamine metabolism. *Nature* 458, 762–765. doi: 10.1038/nature07823

Glass, C. K., Saijo, K., Winner, B., Marchetto, M. C., and Gage, F. H. (2010). Mechanisms underlying inflammation in neurodegeneration. *Cell* 140, 918–934. doi: 10.1016/j.cell.2010.02.016

Gluck, M. R., Thomas, R. G., Davis, K. L., and Haroutunian, V. (2002). Implications for altered glutamate and GABA metabolism in the dorsolateral prefrontal cortex of aged schizophrenic patients. *Am. J. Psychiatry* 159, 1165–1173.

Hoffman, E. M., Zhang, Z., Schechter, R., and Miller, K. E. (2016). Glutaminase increases in rat dorsal root ganglion neurons after unilateral adjuvant-induced hind paw inflammation. *Biomolecules* 6:10. doi: 10.3390/biom6010010

Huang, Y., Zhao, L., Jia, B., Wu, L., Li, Y., Curthoys, N., et al. (2011). Glutaminase dysregulation in HIV-1-infected human microglia mediates neurotoxicity: relevant to HIV-1-associated neurocognitive disorders. *J. Neurosci.* 31, 15195–15204. doi: 10.1523/JNEUROSCI.2051-11.2011

Kashani, A., Lepicard, E., Poirel, O., Videau, C., David, J. P., Fallet-Bianco, C., et al. (2008). Loss of VGLUT1 and VGLUT2 in the prefrontal cortex is correlated with cognitive decline in Alzheimer disease. *Neurobiol. Aging* 29, 1619–1630.

Kvamme, E., Torgner, I. A., and Roberg, B. (2001). Kinetics and localization of brain phosphate activated glutaminase. *J. Neurosci. Res.* 66, 951–958.

Liu, L., Cui, S., Wan, T., Li, X., Tian, W., Zhang, R., et al. (2018). Long non-coding RNA HOTAIR acts as a competing endogenous RNA to promote glioma progression by sponging miR-126-5p. *J. Cell Physiol.* 233, 6822–6831. doi: 10.1002/jcp.26432

López-González, I., Schlüter, A., Aso, E., Garcia-Esparcia, P., Ansoleaga, B., LLorens, F., et al. (2015). Neuroinflammatory signals in Alzheimer disease and APP/PS1 transgenic mice: correlations with plaques, tangles, and oligomeric species. *J. Neuropathol. Exp. Neurol.* 74, 319–344. doi: 10.1097/NEN.0000000000000176

Ma, Y., Wang, K., Pan, J., Fan, Z., Tian, C., Deng, X., et al. (2019). Induced neural progenitor cells abundantly secrete extracellular vesicles and promote the proliferation of neural progenitors via extracellular signal-regulated kinase pathways. *Neurobiol. Dis.* 124, 322–334. doi: 10.1016/j.nbd.2018.12.003

Masamha, C. P., Xia, Z., Peart, N., Collum, S., Li, W., Wagner, E. J., et al. (2016). CFIm25 regulates glutaminase alternative terminal exon definition to modulate miR-23 function. *RNA* 22, 830–838. doi: 10.1261/rna.055939.116

Najlerahim, A., Harrison, P. J., Barton, A. J., Heffernan, J., and Pearson, R. C. (1990). Distribution of messenger RNAs encoding the enzymes glutaminase, aspartate aminotransferase and glutamic acid decarboxylase in rat brain. *Brain Res. Mol. Brain Res.* 7, 317–333.

Palmieri, E. M., Menga, A., Lebrun, A., Hooper, D. C., Butterfield, D. A., Mazzone, M., et al. (2017a). Blockade of glutamine synthetase enhances inflammatory response in microglial cells. *Antioxid. Redox Signal.* 26, 351–363. doi: 10.1089/ars.2016.6715

Palmieri, E. M., Menga, A., Martín-Pérez, R., Quinto, A., Riera-Domingo, C., De Tullio, G., et al. (2017b). Pharmacologic or genetic targeting of glutamine synthetase skews macrophages toward an m1-like phenotype and inhibits tumor metastasis. *Cell Rep.* 20, 1654–1666.

Porter, L. D., Ibrahim, H., Taylor, L., and Curthoys, N. P. (2002). Complexity and species variation of the kidney-type glutaminase gene. *Physiol. Genomics* 9, 157–166.

Reitz, C., and Mayeux, R. (2014). Alzheimer disease: epidemiology, diagnostic criteria, risk factors and biomarkers. *Biochem. Pharmacol.* 88, 640–651.

Sardi, F., Fassina, L., Venturini, L., Inguscio, M., Guerriero, F., Rolfo, E., et al. (2011). Alzheimer's disease, autoimmunity and inflammation. The good, the bad and the ugly. *Autoimmun. Rev.* 11, 149–153. doi: 10.1016/j.autrev.2011.09.005

Sastre, M., Klockgether, T., and Heneka, M. T. (2006). Contribution of inflammatory processes to Alzheimer's disease: molecular mechanisms. *Int. J. Dev. Neurosci.* 24, 167–176.

Tan, J., Town, T., Paris, D., Mori, T., Suo, Z., Crawford, F., et al. (1999). Microglial activation resulting from CD40-CD40L interaction after beta-amyloid stimulation. *Science* 286, 2352–2355.

Tian, C., Liu, T., Fang, S., Du, X., and Jia, C. (2012). Association of C47T polymorphism in SOD2 gene with coronary artery disease: a case-control study and a meta-analysis. *Mol. Biol. Rep.* 39, 5269–5276. doi: 10.1007/s11033-011-1324-y

Wang, Y., Li, Y., Zhao, R., Wu, B., Lanoha, B., Tong, Z., et al. (2017). Glutaminase C overexpression in the brain induces learning deficits, synaptic dysfunctions, and neuroinflammation in mice. *Brain Behav. Immun.* 66, 135–145. doi: 10.1016/j.bbi.2017.06.007

Werner, P., Pitt, D., and Raine, C. S. (2001). Multiple sclerosis: altered glutamate homeostasis in lesions correlates with oligodendrocyte and axonal damage. *Ann. Neurol.* 50, 169–180.

Wu, B., Liu, J., Zhao, R., Li, Y., Peer, J., Braun, A. L., et al. (2018). Glutaminase 1 regulates the release of extracellular vesicles during neuroinflammation through key metabolic intermediate alpha-ketoglutarate. *J. Neuroinflam.* 15:79. doi: 10.1186/s12974-018-1120-x

Xia, Z., Donehower, L. A., Cooper, T. A., Neilson, J. R., Wheeler, D. A., Wagner, E. J., et al. (2014). Dynamic analyses of alternative polyadenylation from RNA-seq reveal a 3′-UTR landscape across seven tumour types. *Nat. Commun.* 5:5274. doi: 10.1038/ncomms6274

Ye, L., Huang, Y., Zhao, L., Li, Y., Sun, L., Zhou, Y., et al. (2013). IL-1beta and TNF-alpha induce neurotoxicity through glutamate production: a potential role for neuronal glutaminase. *J. Neurochem.* 125, 897–908. doi: 10.1111/jnc.12263

Zhao, J., Lopez, A. L., Erichsen, D., Herek, S., Cotter, R. L., Curthoys, N. P., et al. (2004). Mitochondrial glutaminase enhances extracellular glutamate production in HIV-1-infected macrophages: linkage to HIV-1 associated dementia. *J. Neurochem.* 88, 169–180.

Zhao, L., Huang, Y., Tian, C., Taylor, L., Curthoys, N., Wang, Y., et al. (2012). Interferon-alpha regulates glutaminase 1 promoter through STAT1 phosphorylation: relevance to HIV-1 associated neurocognitive disorders. *PLoS One* 7:e32995. doi: 10.1371/journal.pone.0032995

Conflict of Interest Statement: The authors declare that the research was conducted in the absence of any commercial or financial relationships that could be construed as a potential conflict of interest.

frontiers in Cellular Neuroscience

ORIGINAL RESEARCH
published: 16 July 2019
doi: 10.3389/fncel.2019.00320

Astrogliosis Associated With Behavioral Abnormality in a Non-anaphylactic Mouse Model of Cow's Milk Allergy

Nicholas A. Smith[1], *Danielle L. Germundson*[1], *Colin K. Combs*[2], *Lane P. Vendsel*[1] *and Kumi Nagamoto-Combs*[1]*

[1] *Department of Pathology, University of North Dakota School of Medicine and Health Sciences, Grand Forks, ND, United States,* [2] *Department of Biomedical Sciences, University of North Dakota School of Medicine and Health Sciences, Grand Forks, ND, United States*

Etiology of neuropsychiatric disorders is complex, involving multiple factors that can affect the type and severity of symptoms. Although precise causes are far from being identified, allergy or other forms of hypersensitivity to dietary ingredients have been implicated in triggering or worsening of behavioral and emotional symptoms, especially in patients suffering from depression, anxiety, attention-deficit hyperactivity, and/or autism. Among such ingredients, cow's milk, along with wheat gluten, is commonly suspected. However, the contributory role of cow's milk in these disorders has not been elucidated due to insufficient pathophysiological evidence. In the present study, we therefore investigated neuroinflammatory changes that are associated with behavioral abnormality using a non-anaphylactic mouse model of cow's milk allergy (CMA). Male and female C57BL/6J mice were subjected to a 5-week oral sensitization procedure without or with a major milk allergen, beta-lactoglobulin (BLG). All mice were then later challenged with BLG, and their anxiety- and depression-associated behaviors were subsequently assessed during the 6th and 7th weeks. We found that BLG-sensitized male mice exhibited significantly increased anxiety- and depression-like behavior, although they did not display anaphylactic reactions when challenged with BLG. Female behavior was not noticeably affected by BLG sensitization. Upon examination of the small intestines, reduced immunoreactivity to occludin was detected in the ileal mucosa of BLG-sensitized mice although the transcriptional expression of this tight-junction protein was not significantly altered when measured by quantitative RT-PCR. On the other hand, the expression of tumor necrosis factor alpha (TNFα) in the ileal mucosa was significantly elevated in BLG-sensitized mice, suggesting the sensitization had resulted in intestinal inflammation. Inflammatory responses were also detected in the brain of BLG-sensitized mice, determined by the hypertrophic morphology of GFAP-immunoreactive astrocytes. These reactive astrocytes were particularly evident near the blood vessels in the midbrain region, resembling the perivascular barrier previously reported by others in experimental autoimmune encephalitis (EAE) mouse models. Interestingly, increased levels of COX-2

OPEN ACCESS

Edited by:
Yu Tang,
Xiangya Hospital, Central South University, China

Reviewed by:
Takumi Takizawa,
Gunma University, Japan
Jiro Kasahara,
Tokushima University, Japan

***Correspondence:**
Kumi Nagamoto-Combs
kumi.combs@UND.edu

Specialty section:
This article was submitted to Non-Neuronal Cells, a section of the journal Frontiers in Cellular Neuroscience

Received: *15 March 2019*
Accepted: *28 June 2019*
Published: *16 July 2019*

Citation:
Smith NA, Germundson DL, Combs CK, Vendsel LP and Nagamoto-Combs K (2019) Astrogliosis Associated With Behavioral Abnormality in a Non-anaphylactic Mouse Model of Cow's Milk Allergy. Front. Cell. Neurosci. 13:320. doi: 10.3389/fncel.2019.00320

and TNFα were also found in this region. Taken together, our results demonstrated that BLG sensitization elicits inflammatory responses in the intestine and brain without overt anaphylactic signs of milk allergy, signifying food allergy as a potential pathogenic factor of neuropsychiatric disorders.

Keywords: food allergy, astrocyte, anxiety, depression, intestine, occludin, tumor necrosis factor, neuroinflammation

INTRODUCTION

Behavioral and emotional disorders, such as anxiety, depression, attention-deficit hyperactivity disorder (ADHD), obsessive-compulsive disorder, and autism, are major mental health problems that could severely affect quality of life. In the United States alone, ∼20% of adolescents and adults are reported to have experienced mental disorders in 2016[1]. The actual number of people who suffer from these conditions is expected to be greater than reported, considering that these disorders often go undiagnosed due to unwillingness of patients to disclose their conditions or failure of their caregivers to recognize the symptoms (Glazier et al., 2015; Hirschtritt et al., 2017; Klik et al., 2018). Even among diagnosed patients who seek treatments, some are resistant to conventional pharmacological and psychotherapeutic interventions, requiring increased dosage of medications and/or more aggressive treatments such as electroconvulsive therapy and neurostimulation (Al-Harbi, 2012; Hirschtritt et al., 2017). Nonetheless, not all patients benefit from these treatments, signifying the need for alternative intervention approaches for these debilitating conditions.

Interestingly, certain dietary items have been long suspected to trigger or exacerbate emotional and behavioral symptoms (Crayton, 1986), suggesting a potential role of food allergy/hypersensitivity (FAH) in the etiology of neuropsychiatric conditions. While many clinical cohort studies have reported that significant behavioral comorbidities exist among individuals with FAH (Addolorato et al., 1998; Parker and Watkins, 2002; Costa-Pinto and Basso, 2012; Shanahan et al., 2014; Ferro et al., 2016), the contributory role of diet in neuropsychiatric disorders has been controversial due to insufficient pathophysiological evidence and inconsistent results across studies. In order to determine the causative role of FAH in behavioral changes without genetic, dietary, and environmental variables commonly associated with human cohorts, we utilized a mouse model of cow's milk allergy (CMA) and examined behavioral changes and pathophysiology in the gut and brain mediated by FAH.

To observe CMA-mediated changes in typical innate activities of mice, a non-anaphylactic mouse model of CMA was previously established by orally sensitizing the C57BL/6J strain of mice with a whey protein (WP) mixture and cholera toxin (CT) as an adjuvant (Germundson et al., 2018). These sensitized mice generally exhibited mild to no anaphylaxis upon WP challenge, allowing a series of behavioral assessments to be performed the next day. In this study, we limited the allergen to β-lactoglobulin (BLG; Bos d 5), in order to isolate the effect of this major whey allergen, which is absent in human breast milk (Malacarne et al., 2002). We report that BLG-sensitized male mice displayed anxiety- and depression-like behavior similar to the mice sensitized with the WP mixture. Moreover, we found astrocytic hypertrophy in the ventral midbrain of the BLG-sensitized brain, particularly near the blood vessels, resembling the perivascular "barriers" or "cuffs" described in mouse models of experimental autoimmune encephalitis (EAE) (Voskuhl et al., 2009; Sofroniew and Vinters, 2010). These results indicated that oral BLG sensitization of otherwise healthy mice results in region-specific perivascular astrogliosis, likely modifying the functional property of the blood brain barrier.

MATERIALS AND METHODS

Mice

C57BL/6J mice were purchased from The Jackson Laboratories (Bar Harbor, ME, USA) and housed in a pathogen-free room at the University of North Dakota animal facility under 12-h light/12-h dark cycle. Male and female pups were weaned at 3 weeks old and placed on a whey-free rodent diet (Teklad 2018, Envigo, Indianapolis, IN, USA) with *ad libitum* access to ultra-filtered water. Mice were weighed weekly and their health and growth were monitored throughout the experiment. All procedures involving mice were approved by the University of North Dakota Institutional Animal Care and Use Committee.

BLG Sensitization Procedure

At 3-weeks of age, mice were randomly divided into sex-matched sham and BLG-treatment groups. One week later, sensitization was carried out for 5 weeks as described previously with modifications (Germundson et al., 2018). In brief, BLG-sensitized mice were given a weekly oral gavage dose of 1 mg BLG (#L0130, MilliporeSigma, Burlington, MA, U.S.A.) in 200 μL of a sodium carbonate/bicarbonate-buffered vehicle [pH 9.6] containing 10 μg per dose of cholera toxin (CT; #100B, List biological Laboratories, Inc., Campbell, CA, USA) as the adjuvant. The sham mice received the CT-containing vehicle without BLG. On the 6th week, all mice were orally challenged with 50 mg BLG in 200 μL carbonate/bicarbonate buffer. Thirty minutes after the challenge, presence or absence of hypersensitivity reactions, such as scratching of face and ears, perioral swelling, decreased mobility, respiratory distress, and/or lethargy, were noted. Behavioral tests were subsequently performed during the next 2 days. Mice were challenged one more time with 50 mg of BLG on the 7th week followed by two more days of behavioral

[1]National Institute of Mental Health. Center for Behavioral Health Statistics and Quality (2017). Retrieved from https://www.nimh.nih.gov/health/statistics/mental-illness.shtml.

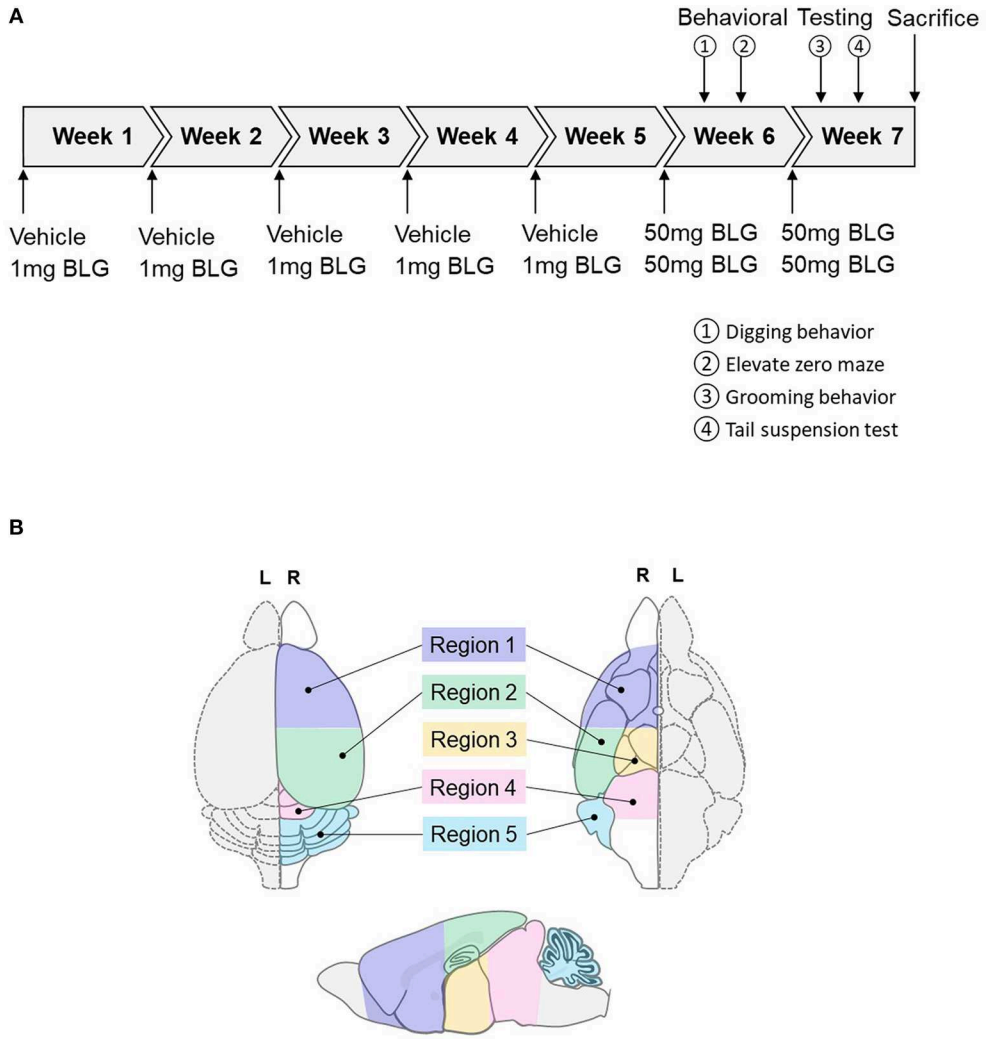

FIGURE 1 | Schematics of the experimental timeline and the regions of the brain analyzed in the study. **(A)** Starting at 4-weeks of age, mice were given a weekly oral administration of 200 μL vehicle (carbonate/bicarbonate buffer containing 10 μg CT, pH 9.6) with or without 1 mg BLG for 5 weeks. In the 6th and 7th weeks, all mice were challenged with 50 mg BLG in carbonate/bicarbonate buffer (without CT), and their behavior was subsequently tested at 1- and 2-day post-challenge. One day after the last behavior test in Week 7, mice were sacrificed, and blood and tissue samples were harvested. **(B)** Diagrams depicting the dorsal (left), ventral (right), and sagittal (bottom) views of a mouse brain. Upon collection of brain samples, the left hemisphere (L, dotted outline) was immersion-fixed in 4% PFA while the right hemisphere (R, solid outline) was subdivided into the following five regions: Region 1, rostral brain including prefrontal and frontal cortices and underlying subcortical structures (e.g., striatum); Region 2, parietotemporal cortices and the hippocampus; Region 3, the thalamus and hypothalamus, Region 4, the midbrain; and Region 5, the cerebellum.

tests and sacrificed the following day. A schematic depicting the sensitization and challenge schedule is shown in **Figure 1A**.

Behavioral Testing

Behavior of mice was evaluated over the course of 2 days after each of the two BLG challenges in Week 6 and 7 (**Figure 1A**). One day after the first challenge in Week 6, innate digging behavior was assessed by placing each mouse in an enclosure (24.8-cm width × 38.7-cm depth × 29.2-cm height containing 5-cm thickness of clean corncob bedding. Mice were acclimated for 5 min and allowed to freely explore the cage for 15 min thereafter. Their activities were recorded on a digital camera and the occurrence of digging activity was counted from the video recordings by two observers who were blinded to the experimental conditions of the mice. On the second day after the challenge in Week 6, anxiety-like behavior was observed using an elevated zero maze (EZM; Stoelting Co., Wood Dale, IL, USA). Activity of each mouse on the EZM was recorded for 5 min and the amount of time mice spent in the open and closed zones of the maze and the number of entries to each of the zones were recorded.

One day after the second BLG challenge in Week 7, mice were individually placed in empty cages and their grooming behavior was video-recorded for 10 min after 5 min of acclimation. As

with the scoring of digging behavior, the frequency of grooming behavior was counted by two blinded observers from the video recordings. The presence or absence of grooming activity was monitored by giving 1 or 0 point, respectively, during each of 60 × 10-s intervals and the sum of the points for the testing period (10 min) was considered the grooming frequency of the mice. On the second day after the second challenge, a tail suspension test (TST) was performed based on a previously described protocol (Can et al., 2012). Briefly, mice were suspended by their tail from a horizontal bar with a piece of laboratory tape so that their nose was ∼30 cm above the base of the bar support. Because the C57BL/6 strain is known for their tendency to climb their tail (Mayorga and Lucki, 2001), a piece of plastic tubing was used to maintain the mice in the suspended position. Their attempts to escape from the position were video-recorded for 6 min, and the frequency and length of immobility as well as the latency to the first immobile episode were compared between groups as indications of depression-like behavior.

All behavior testing was performed at the University of North Dakota Behavioral Research Core Facility. The ANY-maze software (Stoelting, Co.) was used to establish all test parameters, to control video recordings, and to compute the results.

Tissue Collection

Mice were sacrificed 1 day after the behavioral tests in Week 7 via CO_2 asphyxiation followed by cardiac puncture and exsanguination. Terminal blood was collected before transcardiac perfusion with phosphate-buffered saline (PBS). The brain from each mouse was carefully removed and bisected sagitally. The left hemisphere was immersion fixed in 4% paraformaldehyde for histological analysis and the right hemisphere further dissected into 5 regions. Region 1 contained the prefrontal and frontal cortices and underlying subcortical structures including the striatum; Region 2 comprised the parietotemporal cortices and underlying hippocampus; Region 3 contained the thalamus and hypothalamus; Region 4 included the midbrain and rostral brainstem; and Region 5 was the cerebellum (**Figure 1B**). Each of these regional samples was immediately frozen and stored at −80°C until used for western blot and ELISA analyses. The ileum portion of the small intestine was also dissected and fixed for immunohistological staining or frozen stored for RNA isolation for RT-qPCR analysis.

Enzyme-Linked Immunosorbent Assay (ELISA) for the Detection of BLG-Specific IgE/IgG1 and TNFα

The amount of antigen-specific immunoglobulin E (IgE) and G1 (IgG1) antibodies present in sera was quantified using ELISA as described previously with modifications (Germundson et al., 2018). Briefly, the wells of the ELISA plate were coated with 20 μg/mL BLG in a 100 mM sodium carbonate/bicarbonate buffer overnight at 4°C, washed thoroughly and blocked with PBS containing 0.05% Tween-20 and fetal bovine serum (Assay Buffer, eBioscience ELISA Support Pack Plus # BMS414, Thermo Fisher Scientific, Waltham, MA, USA). Sera isolated from the terminal blood of mice were diluted 1:1 for IgE or 1:50 for IgG1 detection with Assay Buffer before adding to the antigen-coated wells. The plate was incubated for 12 h at 4°C and BLG-specific IgE was detected with biotinylated anti-mouse IgE (used at 1:1,000, #13-5992-81, ThermoFisher Scientific) or anti-mouse IgG1 (used at 1:1,000, #13-4015-82, ThermoFisher Scientific) followed by avidin-HRP and TMB (3,3′,5,5′-tetramethylbenzidine) according to the manufacturer's instructions. The plate was read at 450 nm on a Biotek ELx 800 microplate reader using Gen5 v3.02 software (Biotek Instruments, Winooski, VT, USA).

The amount of tumor necrosis factor alpha (TNFα) in the midbrain samples (Region 4) was quantified using TNFα DuoSet® ELISA (#DY410, R&D Systems, Minneapolis, MN, USA) according to the manufacturer's protocol. Briefly, an ELISA plate (#2580, Corning EIA/RIA 8-Well Strips) was coated with TNFα capture antibody overnight at room temperature. After washing and blocking the wells, each protein extract from Region 4 (200 ng/100 μL/well) was placed in duplicates and incubated for 2 h at room temperature. TNFα in the samples were visualized by sequentially incubating the wells with the detection antibody and streptavidin-HRP. The substrate reaction was allowed to occur for 20 min before termination, and the plate was read as described above. The duplicate values from each sample were averaged and TNFα concentration was calculated from the standard curve.

Immunohistochemistry

Tissues collected for histology were immediately immersion-fixed in 4% paraformaldehyde. Fixed ileal and brain tissues were embedded in gelatin and frozen sectioned at 14 and 40 μm, respectively. For immunostaining, tissue sections were treated with 0.3% peroxidase and blocked in PBS containing 0.5% bovine serum albumin and 5% normal goat serum (#16210072, ThermoFisher Scientific), and incubated with a primary antibody against rabbit anti-mouse occludin (used at 1:100, #711500, ThermoFisher Scientific), glial fibrillary acidic protein (GFAP; used at 1:1,000, #12389S, Cell Signaling Technology, Boston, MA, USA) or Iba1 (used at 1:1000, #019-19741, Wako Chemicals, Richmond, VA) for 24–48 h at 4°C. Tissues were subsequently incubated in anti-rabbit IgG (used at 1:2,000, #PK-6101, Vector Laboratories, Burlingame, CA, USA) or mouse-adsorbed rabbit anti-rat IgG (used at 1:100, #BA-4001, Vector Labs) antibody. Immunoreactivity was visualized with Vector Elite ABC kit (#PK-6101, Vector Labs) with VIP as the chromogen (#SK-4600, Vector Labs).

Reverse Transcriptase Quantitative Polymerase Chain Reaction (RT-qPCR)

Ileal tissue samples were homogenized in TRIzol solution (#15596018, Thermo Fisher Scientific) using 5-mm stainless steel beads in a Bullet Blender Storm 24 (Next Advance, Troy, NY, USA) set to speed 6 for 3 min with 30-s intervals. Total RNA was extracted and purified by ethanol precipitation according to the manufacturer's instructions. The amount of RNA was quantified using Nanodrop One (Thermo Fisher Scientific), and 1 μg of total RNA was used to synthesize cDNA libraries with an iScript™ cDNA Synthesis Kit (#1708891,

Bio-Rad Laboratories, Hercules, CA, USA) by priming at 25°C for 5 min, reverse transcription at 46°C for 20 min, and inactivation at 95°C for 1 min. Quantitative PCR reactions were performed with 100 ng cDNA and specific primer sets for murine TNFα (*Tnfα;* qMmuCED0004141, Bio-Rad), occludin (*Ocln*; fwd: 5′-AAAGCAAGTTAAGGGATCTG-3′; Rev: 5′-TGGCATCTCTCTAAGGTTTC-3′, MilliporeSigma), or glyceraldehyde 3-phosphate dehydrogenase (*Gapdh*; qMmuCED0027497, Bio-Rad) using iTaq™ Universal SYBR® Green Supermix (#1725120, Bio-Rad) on a C1000 Touch Thermo Cycler (Bio-Rad) for 40 cycles (denaturing at 95°C for 15 s, annealing at 60°C for 30 s, and extension at 72°C for 30 s). Resulting Cq values were calculated using Bio-Rad CFX Manager Software version 3.1.

Western Blot Analysis

Total proteins from each isolated region of the right brain hemisphere were extracted in RIPA buffer (20 mM Tris, pH 7.4, 150 mM NaCl, 1 mM Na_3VO_4 10 mM sodium fluoride, 1 mM EDTA, 1 mM EGTA, 0.2 mM phenylmethylsulfonyl fluoride, 1% Triton X-100, 0.1% SDS, and 0.5% deoxycholate) and quantified using the Bradford method (Bradford, 1976). Western blotting was carried out as described previously (Nagamoto-Combs et al., 2014) with 25 μg of protein samples resolved on 15% SDS-polyacrylamide gels. Resolved proteins were transferred onto PVDF membranes and detected with a primary antibody against GFAP (used at 1:1,000, #12389S, Cell Signaling Technology), cyclooxygenase 2 (COX-2; used at 1:1,000, #sc-1745, Santa Cruz Biotechnology, Santa Cruz, CA, USA) or GAPDH (used at 1:1,000, sc-32233, Santa Cruz Biotechnology) overnight at 4°C or 2 h at room temperature with gentle rocking. The membranes were subsequently incubated in an appropriate HRP-conjugated secondary antibody (Santa Cruz Biotechnology). Target proteins were visualized using Amersham ECL Prime Western Blotting Detection Reagent (#RPN2232, GE Healthcare, Pittsburgh, PA, USA) on an Aplegen Omega Lum G Gel Documentation System (Gel Company, Inc., San Francisco, CA, USA). After the detection of chemiluminescence signal, PVDF membranes were treated with 0.2 N sodium hydroxide for 10 min at room temperature with gentle agitation to remove the antibodies and re-probed for another target protein. The levels of proteins were quantitated from the captured image using LI-COR Image Studio Lite Software 5.0 (LI-COR Biosciences, Lincoln, NE, USA) and normalized to the amount of GAPDH detected from the same PVDF membrane.

Statistical Analysis

For quantitative results, the average value of each experimental group was calculated and compared using GraphPad Prism software version 8.01 (GraphPad Software, Inc., La Jolla, CA, USA). Statistical significance of the differences between sham and BLG groups was independently analyzed for male and female groups using unpaired *t*-tests. Welch's correction was used when sample sizes varied, and Mann-Whitney test was employed where normal distribution of data values was not observed. A *p*-value less than 0.05 ($p < 0.05$) was considered statistically significant.

RESULTS

BLG Sensitization of C57BL/6J Mice Results in Increased Serum Levels of Allergen-Specific IgE and IgG1 in Male Mice Without Eliciting Obvious Signs of Anaphylaxis After BLG Challenge

To monitor the overall health and steady growth of the experimental mice, their body weights were recorded during the sensitization protocol. The average body weights of mice in each group before the initiation of sensitization (Week 1) and at the time of allergen challenges (Week 6 and 7) were compared between the sex-matched treatment groups (**Figure 2A**). No significant differences were found in the body weights between the groups at any of the time points examined, suggesting that BLG-sensitized mice had comparable growth to the sham mice.

A week after the 5 weekly sensitization procedures, all mice underwent a BLG challenge in Week 6 for the assessment of their physical responses to allergen re-exposure. No obvious signs of anaphylaxis were exhibited by male or female mice from both of the treatment groups at 30 min post-challenge. This lack of physical reactions to the allergen was observed again after the second challenge in Week 7.

In order to ensure that the BLG-sensitization protocol successfully induced acquired immunity in our mouse model, we next determined the levels of serum BLG-specific IgE and IgG1 using ELISA (**Figures 2B,C**, respectively). While the serum levels of BLG-specific IgE were comparable among the male and female sham groups, both of the BLG sensitized groups showed wider ranges of BLG-specific IgE levels. The serum samples from a few mice in each group contained much greater BLG-specific IgE than the others within the group (**Figure 2B**). There were modest but significant increases in the average levels of BLG-specific IgE in both sensitized male and female mice compared to their respective sham groups (male sham: 0.14 ± 0.04; male BLG: 0.5 ± 0.3; female sham: 0.10 ± 0.01; female BLG: 0.9 ± 0.5; $n = 8$ in all groups, $p < 0.05$, Mann-Whitney test). When the extreme values were identified as outliers by GraphPad Prism software and removed from the analysis, the statistical significance of the BLG-induced IgE levels increased to $p < 0.01$ for male mice (male sham: 0.10 ± 0.02, $n = 7$; male BLG: 0.23 ± 0.05, $n = 7$; one outlier from each group was removed from the analysis [sham, 0.40; BLG, 2.37]). In contrast, removal of outliers from the female groups resulted in the loss of statistical significance for female groups [female sham: 0.10 ± 0.01, $n = 8$; female BLG: 0.17 ± 0.06, $n = 6$; two outliers removed from the analysis of the BLG group [3.58, 2.32]. The analysis excluding the outliers is shown in **Supplementary Figure 1**. Similarly, BLG-specific IgG1 levels were also elevated in the sensitized mice for both sexes with less variability than IgE (**Figure 2C**). These results indicated that the BLG-sensitization procedure elicited acquired immunity toward BLG with elevated antigen-specific IgE and IgG1 in both male and female mice. Although a subset of sensitized mice showed greater degrees of antibody productions, their apparent physical health was

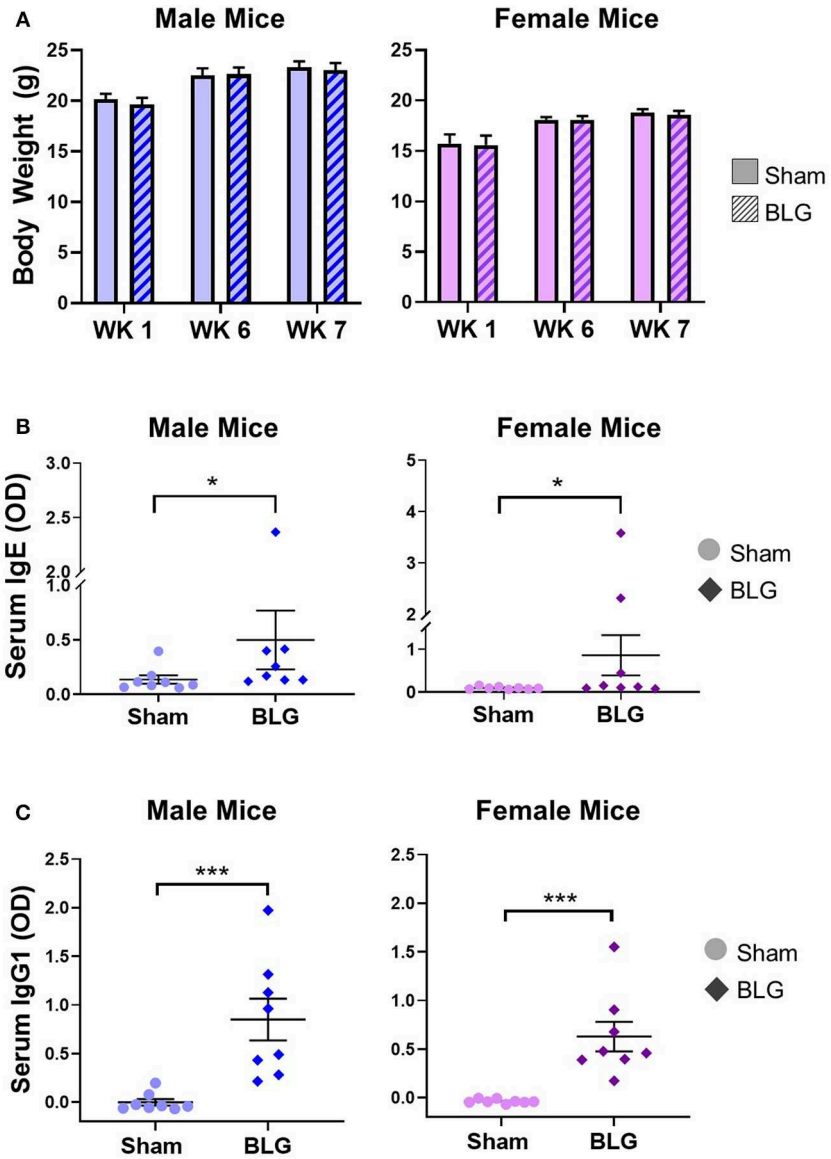

FIGURE 2 | Physical growth and adaptive immunity development during BLG sensitization. **(A)** Weights of mice were recorded during Weeks 1, 6, and 7 of sensitization to assess potential impact of the sensitization regime on overall health and growth. **(B,C)** Serum isolated from the terminal blood was used to quantify the levels of BLG-specific IgE **(B)** or IgG1 **(C)** using ELISA. Values shown in the graphs indicate the group average ± SEM, $^{*}p < 0.05$; $^{***}p < 0.001$. (Mann-Whitney test), male sham: $n = 8$; male BLG: $n = 8$; female sham: $n = 8$; female BLG: $n = 8$.

not visibly affected, and the allergen challenge did not result in anaphylaxis.

BLG Sensitization Resulted in Anxiety- and Depression-Like Behavioral Changes in Male C57BL/6J Mice

BLG-mediated changes in mouse behaviors were examined using 4 different behavioral tests. The digging behavior observation and EZM were performed after the first challenge while grooming behavior observation and TST were carried out after the second challenge (see the Methods section). The frequency of digging activity within the 10-min observation period was 15 ± 3 in male sham, 21 ± 2 in male BLG-sensitized, 13 ± 3 in female sham, and 16 ± 5 in female BLG-sensitized mice ($n = 8$ per group, **Figure 3A**). Although there was a trend toward increased digging activity in male BLG-mice compared to their sex-matched sham, the difference did not reach a statistical significance ($p = 0.1$). However, the EZM showed a significant decrease in the average duration of visit to open zone in male mice (sham: 5.7 ± 0.6, $n = 6$; BLG: 4.1 ± 0.3; $n = 7$; $p < 0.05$) and not in female (sham 4.2 ± 0.3, $n = 8$; BLG: 4.6 ± 0.3; $n = 7$; **Figure 3B**). Further surveillance of the test recordings revealed that the mice with a shorter duration of visit to open zones often did

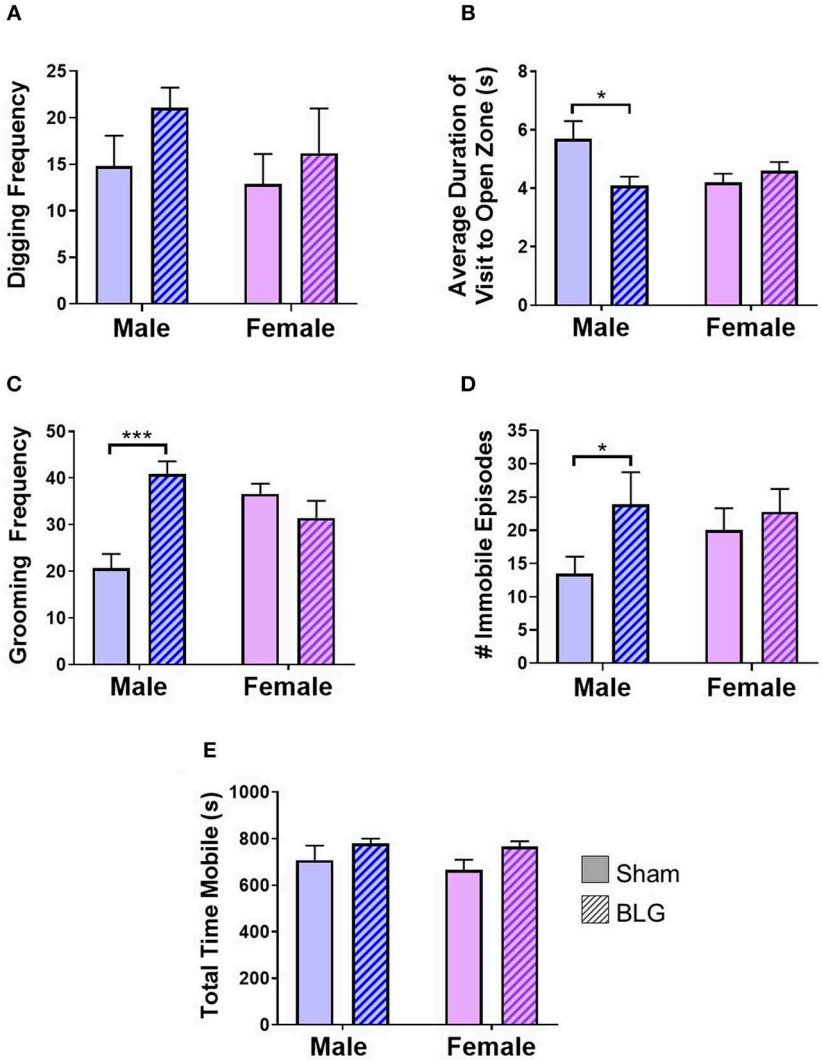

FIGURE 3 | Assessments of anxiety- or depression-like behavior after BLG challenge. Behavioral tests were performed at 1- and 2-day post-challenge. **(A)** Digging frequency was quantified by two observers who were unaware of the experimental conditions. Either the presence (1 point) or absence (0 points) of digging behavior was recorded in every 10-s interval during the 10-min test period. The total points scored by the two observers were averaged and used as the final score for each mouse. **(B)** For EZM test, the average duration each mouse spent within the open zone per visit was computed by ANYmaze software and later validated by an observer. **(C)** Grooming frequency was quantified by two observers for scoring either the presence (1 point) or absence (0 points) of grooming behavior as described for the digging frequency scoring. **(D)** For TST, the number of immobility episodes was used as the measure of the mice's helpless behavior that reflected their depression-like state. **(E)** Total time mobile was also computed from the recordings during the digging behavior to verify their motility to distinguish their immobility from lethargy. Values shown in the bar graphs indicate the group average ± SEM, $^{*}p < 0.05$, $^{***}p < 0.001$ (unpaired *t*-tests) $n = 7$–8.

not walk through the open zone to the other closed zone, but they briefly surveyed the entry to the open zone and returned to the original closed zone (see **Supplementary Material**). In addition, the analysis of grooming behavior after the second BLG challenge indicated that BLG-sensitized male mice groomed themselves more often than their sham counterpart (sham: 20 ± 3, $n = 8$; BLG: 41 ± 3; $n = 8$; $p < 0.001$) while no sensitization-dependent differences were observed between the female groups (sham: 36 ± 2, $n = 8$; BLG: 31 ± 4; $n = 8$), indicating that only male BLG-sensitized mice displayed more anxiety-like behavior than sham mice (**Figure 3C**). Similarly with the TST (**Figure 3D**), only male BLG-mice exhibited more depression-like behavior than the sham with greater numbers of immobile episodes during the 6-min testing period (sham: 14 ± 3, $n = 8$; BLG: 24 ± 5; $n = 8$; $p < 0.05$) while female sensitized mice did not (sham: 20 ± 3, $n = 8$; BLG: 23 ± 3; $n = 8$). To assure that the observed behavioral differences in the sensitized mice were not due to lethargy-related immobility, the total time in seconds mice were mobile during their digging tests were compared between the groups (**Figure 3E**). There were no obvious differences in the total time mobile among male and female sham and BLG mice, indicating that the changes

in the behavioral parameters observed with the male BLG-sensitized mice did not result from physical or ambulatory difficulties. These results demonstrated that the male mice were susceptible to behavioral alterations upon BLG sensitization, even though they did not exhibit apparent anaphylactic reactions when challenged with the allergen.

BLG Sensitization Altered the Levels of Tight Junction Protein and the Expression of Proinflammatory Cytokine in the Small Intestine

Next, we sought to identify changes in different brain regions that might contribute to the observed sex-dependent behavioral abnormality. Since BLG-mediated behavioral changes were only observed in male mice, we focused our further analyses on male animals. Allergens that paracellularly enter intestinal mucosa through compromised epithelial tight junction barriers may be recognized as pathogens by antigen presenting cells (APCs) and initiate immune responses. To examine whether BLG sensitization resulted in decreased barrier integrity, the levels of a tight junction protein, occludin, were examined in the intestinal tissue. Immunohistochemical assessment of the ileum from the male sham (**Figures 4A,a**) and BLG-sensitized mice (**Figures 4B,b**) showed that there was decreased staining in the villi of the latter group. This decreased immunoreactivity for occludin was likely a result of post-translational regulation since the amount of occludin transcripts in the ileal tissue from BLG-sensitized mice did not differ from the sham mice when determined using RT-qPCR (**Figure 4C**).

Aberrant paracellular infiltration of allergens could trigger inflammatory responses by intestinal immune cells. Thus, we also investigated the inflammatory status of the gut mucosa by determining the amount of a proinflammatory cytokine, TNFα. An RT-qPCR assay indicated that there was a modest but significant increase in TNFα mRNA in the ileum (**Figure 4D**), signifying the presence of proinflammatory events at the site of allergen insult.

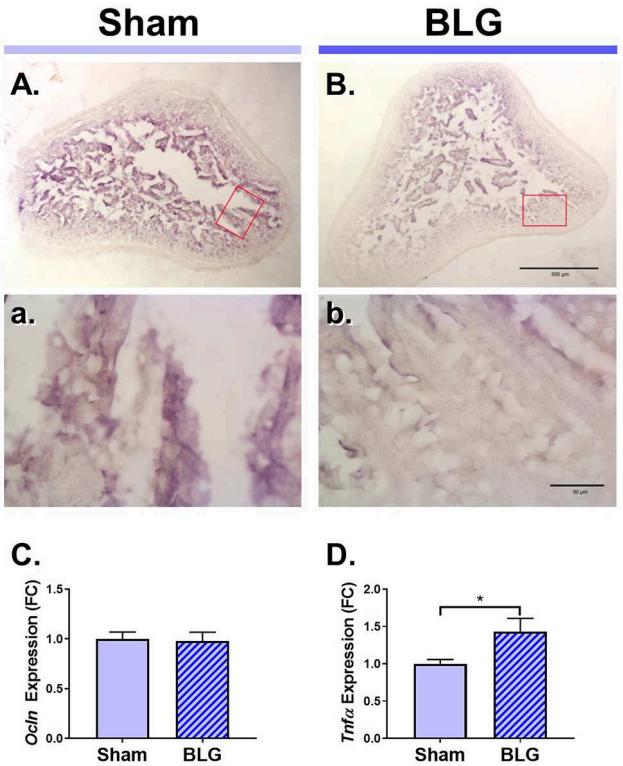

FIGURE 4 | Immunohistochemical detection of occludin and the RT-qPCR assays for *Ocln* and *TNFα* expression in the ileum of male sham and BLG mice. Ileal sections (14 μm) from male sham **(A,a)** and BLG **(B,b)** mice were immunostained for occludin. The red rectangles in panels **(A,B)** indicate where the respective higher magnification images, **(a)** and **(b)**, were taken. The low-magnification **(A,B)** and high-magnification **(a,b)** images were taken with a 4X and 40X objectives, respectively. Scale bars: 500 μm for **(A)** and **(B)**; 50 μm for **(a)** and **(b)**. The expression levels of *Ocln* **(C)** and *Tnfα* **(D)** in the ileal tissue samples were also quantitated using RT-qPCR assay. The Cq values for *Ocln* and *Tnfα* were normalized to the Cq values of *Gapdh* (ΔCq) to calculate the expression values ($\Delta Cq = 2^{-\Delta Cq}$). Values shown in the bar graphs are expressed as the fold change (ΔΔCq) ± SEM. *$p < 0.05$ (unpaired *t*-test with Welch's correction), $n = 6$–8.

GFAP-Immunoreactive Astrocytes Were Hypertrophic in the Midbrain Region of the BLG-Sensitized Mice

Under the hypothesis that glia cells could respond to inflammatory mediators from the intestine and elicit neuroinflammation that would ultimately result in altered behavior, brain tissues from sham and BLG-sensitized male mice were immunostained for astrocyte and microglia markers, GFAP and Iba1, respectively. Iba1-immunopositive cells were observed throughout the brain sections although we did not observe noticeable differences between sham and BLG-sensitized mice (not shown). GFAP-stained astrocytes were also found ubiquitously in the brain, but they were more localized to specific regions such as within the white matter. In midbrain sections, the majority of astrocytes were found within the substantia nigra pars reticulata (**Figure 5**). GFAP-positive cells were abundantly present in both sham (**Figure 5A**) and BLG-sensitized (**Figure 5B**) mice. Interestingly, astrocytes in this area of BLG-sensitized mouse brain appeared darker and their processes seemed greater in number and thickness (**Figures 5b',b"**). Perivascular astrocytes were notably different, with apparently increased density of GFAP-positive end-feet contacting the vascular wall (arrowheads in **Figure 5b'**). These observations provided evidence for glial response, at least by astrocytes in the midbrain regions, in the central nervous system of BLG-sensitized mice.

In order to verify our immunohistological observations, western blot analysis was performed using protein extracts from different brain regions (**Figure 6**, see **Figure 1B** for the division of the regions). The level of GFAP was slightly elevated in the Region 2 (parietotemporal cortices and hippocampus) and Region 3 (thalamus and hypothalamus) of the BLG-sensitized mice, although the difference was not statistically significant (Region 2: 1.4 ± 0.2-fold, $p = 0.1$; Region 3: 1.5 ± 0.3-fold, $p = 0.1$). However, in Region 4 containing the midbrain and

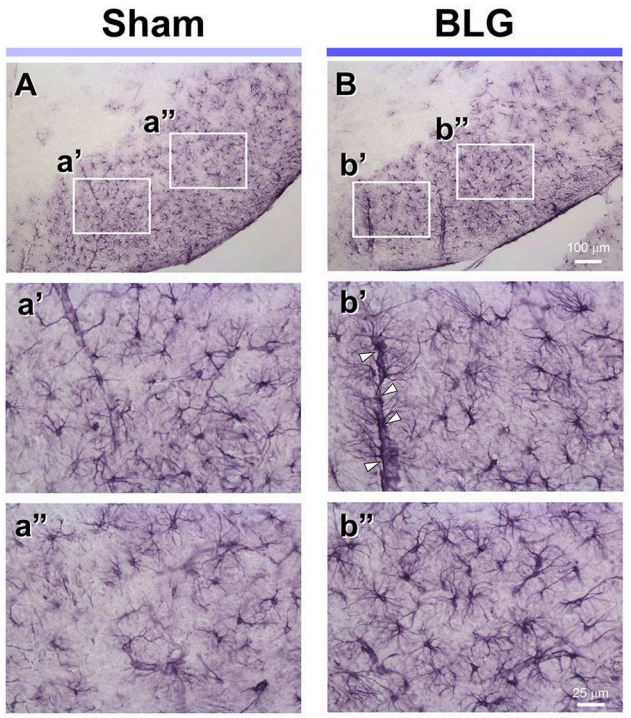

FIGURE 5 | GFAP immunoreactivity in the midbrain of sham and BLG-sensitized mice. GFAP-positive astrocytes were identified by immunohistochemically staining brain sections (40 μm). Representative midbrain sections from sham **(A,a',a")** and BLG-sensitized **(B,b',b")** male mice are shown. The white rectangles in **(A,B)** indicate where the respective higher magnification images **a'–b"** were taken. The open arrowheads indicate dense GFAP-immunoreactive astrocyte end-feet along the blood vessel. The low-magnification **(A,B)** and high-magnification **(a',a", b',b")** images taken with a 10X and 40X objectives, respectively. Scale bars: 100 μm for **(A)** and **(B)**; 25 μm for **a'–b"**.

rostral brainstem, the difference in GFAP levels between the two groups of mice was significant with a 1.6 ± 0.2-fold increase in the sensitized mice ($p < 0.001$). This result indicated that BLG sensitization resulted in upregulation of GFAP in this region, corroborating our immunohistological observation of hypertrophic astrocytes in the same region. As an additional marker of proinflammatory change, we next examined protein levels of COX-2 in the various brain regions (**Figure 7**). Exactly as observed when examining GFAP levels, a significant increase in COX-2 protein levels in sensitized mouse brains was noted only in the midbrain and rostral brainstem samples (Region 4).

The Proinflammatory Cytokine, TNFα, Was Elevated in the Midbrain Region

Based on our observation of astrogliosis and elevated COX-2 protein levels in the midbrain regions, we hypothesized that the GFAP-positive reactive astrocytes might be responding to and/or producing inflammatory mediator(s). Since astrocytes are capable of producing and responding to TNFα (Eddleston and Mucke, 1993), we measured the levels of this proinflammatory cytokine in the midbrain region (Region 4) using ELISA (**Figure 8**). As predicted, the amount of TNFα was significantly elevated in this region of BLG-sensitized mice by ∼2.7-fold (sham: 1,273 ± 384 pg/mL; BLG: 3,469 ± 194 pg/mL, $n = 8$). This result demonstrated that proinflammatory events are present at least in this region of the brain of BLG-sensitized mice and provided the evidence that sensitization to a milk allergen results in neuroinflammation associated with behavioral abnormality.

DISCUSSION

For several decades, the association of FAH with behavioral, emotional and cognitive impairments has been suggested, often referred to as "cerebral allergy" (Davison, 1949) or "allergic tension-fatigue syndrome" (Speer, 1954, 1958). More recently, a growing number of reports have more specifically described FAH comorbidities with depression (Patten and Williams, 2007; Garg and Silverberg, 2015; Ferro et al., 2016), anxiety (Lyons and Forde, 2004; Patten and Williams, 2007; Garg and Silverberg, 2014; Shanahan et al., 2014; Ferro et al., 2016), ADHD (Garg and Silverberg, 2014; Shanahan et al., 2014; Ferro et al., 2016; Topal et al., 2016), and autism (Lyall et al., 2015; Xu et al., 2018). However, the evidence that FAH in fact modifies physiological functions of the brain is still insufficient, and the mechanism remains to be elucidated.

One of the major obstacles in the assessment of brain pathophysiology in FAH-associated neuropsychiatric conditions is controlling the variables associated with the study subjects, such as genetic background, diet, socioeconomic status, local environment, and culture, all of which may contribute to differences in behavior as well as FAH development. In addition, experimental parameters for quantitative assessments are often limited to evaluation scores on questionnaires for neuropsychiatric conditions and blood IgE levels and/or skin tests for FAH. While it is undeniably challenging to evaluate mood- and emotion-elicited behavior in animal models, performing a series of behavioral tests helps to validate the results. Furthermore, animal models provide many advantages in an experimental study by allowing to control genetic, environmental, and dietary variables and to directly evaluate pathophysiology of the brain and other organs. Indeed, a mouse model of CMA with the C3H/HeOuJ strain has been utilized to demonstrate autistic-like deficit in social behavior and neurochemical changes in the brain (de Theije et al., 2014).

In the present study, we produced non-anaphylactic CMA in C57BL/6J mice using BLG as the allergen and assessed the cellular and molecular changes in the intestine and brain to identify CMA-induced pathology that might have contributed to their abnormal behavioral outcomes. During the 7 weeks of the sensitization/challenge period, both male and female mice showed no differences in their growth rate (**Figure 2A**). Importantly, we did not observe overt anaphylaxis symptoms in any of the groups after each of the two challenges at Week 6 and 7, although significant increases in BLG-specific IgE and IgG1 levels were observed in both male and female sensitized mice

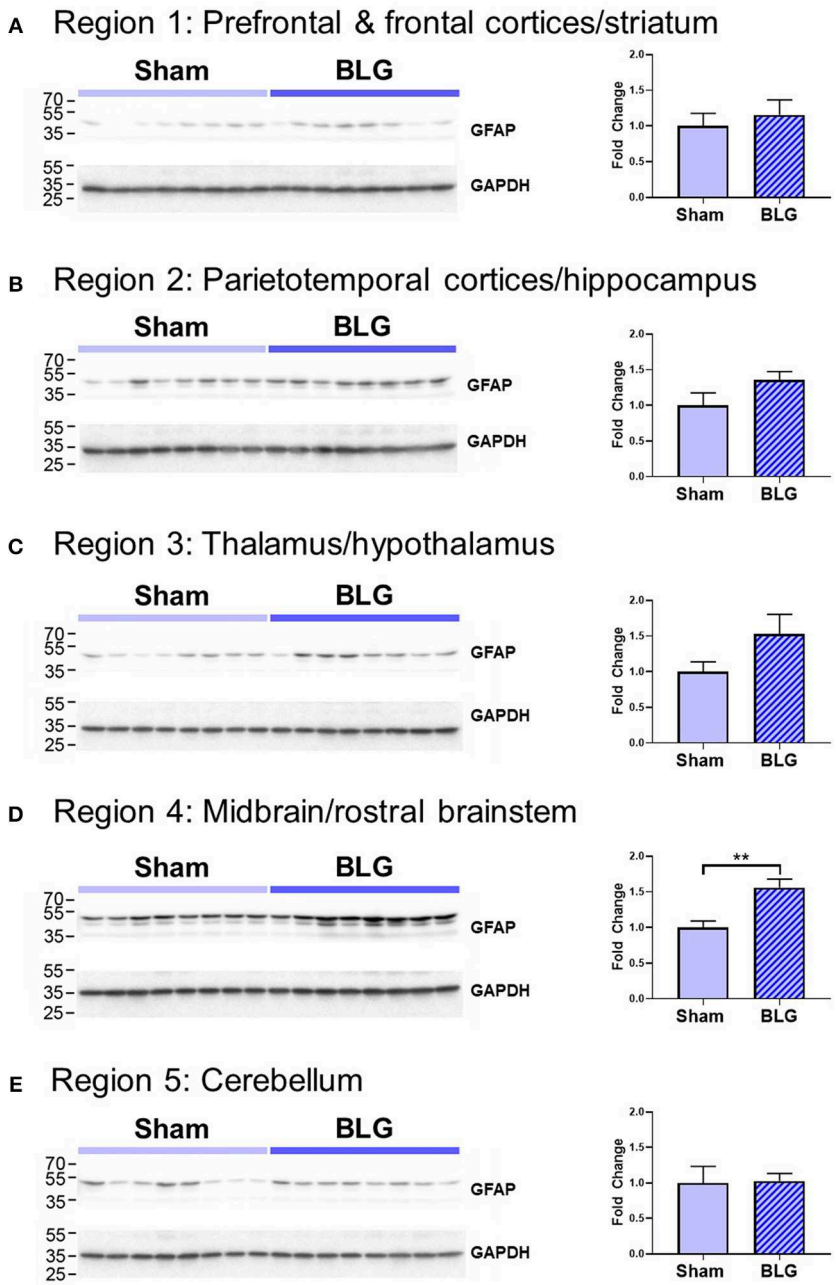

FIGURE 6 | Western blot analysis of GFAP in the isolated five brain regions. Soluble proteins isolated from the 5 regions were resolved on discontinuous 15% SDS-polyacrylamide gels for western blot detection of GFAP (upper panels). **(A)** Region 1, **(B)** Region 2, **(C)** Region 3, **(D)** Region 4, and **(E)** Region 5 as described in **Figure 1B**. Chemiluminescence signals for GFAP were digitally captured and shown in the upper panels. GAPDH was also detected from the same blots and used as a reference for loading variability (lower panels). The captured GFAP signals were quantified using LI-COR Image Studio Lite software and normalized to GAPDH signals. Values shown in the bar graphs indicate the group average ± SEM. $^{**}p < 0.01$ (unpaired *t*-test), $n = 8$.

(**Figures 2B,C**). This result indicated that acquired immunity to BLG can be established without observable physical reactions.

Our behavioral assessments of sham and BLG-sensitized mice included digging and grooming frequencies, EZM, and TST (**Figure 3**). Digging behavior in rodents is an innate burrowing behavior, and the test is often performed by placing the animal in a cage with a thick layer of bedding without or with marbles (Deacon, 2006). Unlike the WP-sensitized mice we previously described (Germundson et al., 2018), BLG-sensitized mice did not exhibit decreased digging behavior. Instead, there was an increased trend in male sensitized mice, suggesting that the behavioral effect of BLG sensitization appears to be distinct from

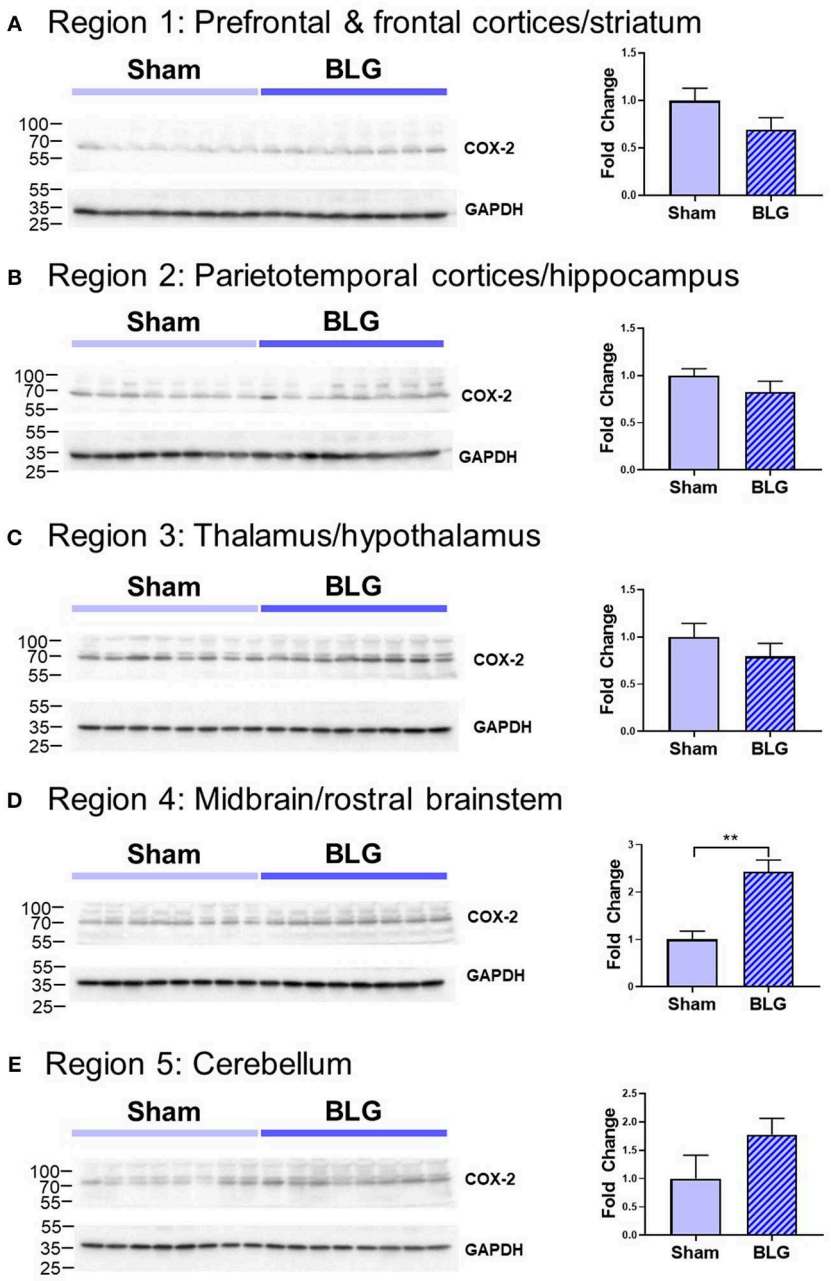

FIGURE 7 | Western blot analysis of COX-2 in the isolated five brain regions. Soluble proteins isolated from the five regions were resolved on discontinuous 15% SDS-polyacrylamide gels for western blot detection of COX-2 (upper panels). **(A)** Region 1, **(B)** Region 2, **(C)** Region 3, **(D)** Region 4, and **(E)** Region 5 as described in **Figure 1B**. Chemiluminescence signals for COX-2 were digitally captured and shown in the upper panels. GAPDH was also detected from the same blots and used as a reference for loading variability (lower panels). The captured COX-2 signals were quantified using LI-COR Image Studio Lite software and normalized to GAPDH signals. Values shown in the bar graphs indicate the group average ± SEM. $^{**}p < 0.001$ (unpaired *t*-test), $n = 8$.

that of the WP mixture. Although the reason for the discrepancy between the two mouse models of CMA in this behavioral outcome is not clear, it may be postulated that other constituents in the WP mixture, such as α-lactalbumin, immunoglobulins, and lactoferrin (Farrell et al., 2004), had a more diverse effect than BLG alone.

Grooming is another intrinsic rodent behavior consisting of a complex series of movements, and the frequency, total time spent, and sequence of grooming can be affected by extrinsic factors such as stress (Kalueff et al., 2016). We observed that female sham mice groomed more frequently than their male counterpart (**Figure 3C**), and the frequency of female

grooming behavior was not affected by BLG sensitization. On the contrary, BLG-sensitized male mice showed significantly elevated grooming behavior, indicative of their stressed or anxious state (Kalueff et al., 2016). This observation was corroborated by their performance in the EZM test, in which male BLG-sensitized mice spent significantly less time than the sham mice in the open zones when entered (**Figure 3B**). These results together support the notion that BLG-sensitized male mice exhibited anxiety-like behavior.

Because anxiety and depression are often comorbid (Johansson et al., 2013; Tiller, 2013), we also examined whether the BLG-sensitized mice would exhibit depression-like behavior. In the TST, depression-like behavior is quantified by the animal's immobility, which reflects decreased attempts to escape from the helpless position (Cryan et al., 2005). Our results demonstrated that male BLG-sensitized mice indeed displayed depression-like behavior, although no difference was observed between sham and BLG-sensitized female mice (**Figure 3D**). From our observation that the overall activity of male and female mice did not differ between sham and BLG-sensitized groups, it is unlikely that the immobility resulted from inability to move or lethargy (**Figure 3E**). Taken together, our behavioral tests indicated that BLG sensitization elicited anxiety- and depression-like behavior in male-specific manner. This sex-dependent behavior manifestation was also observed with WP-sensitized mice and have been discussed previously (Germundson et al., 2018).

Interestingly, similar sex differences in behavioral observations have been reported with human patients with neuropsychiatric disorders, including ADHD, obsessive-compulsive disorder (OCD), and autism spectrum disorder (ASD). Several meta-analysis studies have indeed found greater prevalence in male population (Hanna, 1995; Gaub and Carlson, 1997; Gershon, 2002; de Mathis et al., 2011; Russell et al., 2011). This male dominance in these conditions seem to arise from the fact that male patients exhibit more noticeable behavioral phenotypes than female patients. For example, boys with ADHD display more externalized and/or disruptive behavior than girls, who in contrast tend to show more internalized, inattentive behavior (Gaub and Carlson, 1997; Gershon, 2002). Similarly, some studies on sexual dimorphism in ASD symptomatology reported that boys have more severe autistic traits and therefore are more likely to be diagnosed with ASD than girls (Russell et al., 2011; Mandy et al., 2012). Biological factors, such as sex hormone-dependent structural development of the prefrontal and orbitofrontal cortices, thalamus, and basal ganglia (Maia et al., 2008), the volume of the pituitary gland (MacMaster et al., 2006), and polymorphisms in the serotonergic system (de Mathis et al., 2011; Verma et al., 2014; Shuffrey et al., 2017), have been suggested to underlie the sex differences in behavioral manifestations.

In addition to behavioral differences, sexual dimorphism of the immune systems has been well-recognized. Gene regulation by gonadal hormones and the expression of X-chromosome genes are known to differentially affect the immune system in males and females, including immunoglobulin productions, T-lymphocyte functions and allergic/atopic disease susceptibility and symptom severity [see reviews by DunnGalvin et al., 2006; Pennell et al., 2012; Klein and Flanagan, 2016]. However, male dominance of food allergy appears to be inconsistent across studies, depending on allergen types and patient age groups, as well as on the study method used and year examined (Jarvis and Burney, 1998; Becklake and Kauffmann, 1999; Kelly and Gangur, 2009; Acker et al., 2017). Therefore, the roles of these biological and immune dimorphisms in the sex-specific behavioral response to BLG sensitization and challenge are complex and require further scrutiny in humans as well as in our animal models of CMA.

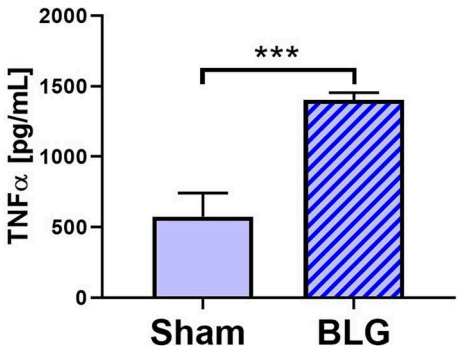

FIGURE 8 | Quantification of TNFα levels in the midbrain region of sham and BLG male mice using ELISA. The levels of TNFα in the midbrain region were quantified by ELISA. Values indicate the group average ± SEM. ***$p < 0.001$ (unpaired t-test), $n = 8$.

Moving forward, we focused our pathophysiological investigation on male mice to assess histological and biochemical changes that might reflect the behavioral changes that deviated from the sham control. In orally-sensitized mice, the site of allergen insult is the gastrointestinal (GI) tract. Decreased mucosal occludin immunoreactivity and increased proinflammatory cytokine expression in the BLG-sensitized ileum suggested that the immune responses to the allergen during sensitization had impaired intestinal barrier (**Figure 4**). In addition, it is possible that dysbiosis had occurred during the sensitization and elicited these changes in intestinal physiology, since gut microbe compositions can be influenced by diet and shifts in compositions can result in inflammation (Round and Mazmanian, 2009; Clements and Carding, 2018). These changes in the gut physiology and microbiota are likely to be produced gradually during the sensitization period, rather than immediately after the BLG challenge, since immune activation status in food-allergen sensitized mice has been reported to be heightened as evidenced by greater proliferative capacity of splenocytes compared to naïve mice without restimulation with the allergen (Li et al., 2000). However, time course of pathophysiology development and potential involvement of gut microbiota are yet to be determined in our mouse

model. Loss of intestinal barrier and intestinal dysbiosis have been reported in autistic patients (de Magistris et al., 2010; Fiorentino et al., 2016) and their implication in pathogenesis of neuropsychiatric conditions has been reviewed in recent literature (Karakula-Juchnowicz et al., 2016; Grochowska et al., 2018).

Inflammatory responses were also found in the brain of BLG-sensitized mice. Although we did not detect apparent microgliosis by Iba1 immunostaining (not shown), we observed notable differences in GFAP-positive astrocyte morphology in certain areas of the brain, especially perivascular regions of the midbrain (**Figure 5**). Interestingly, similar observations of hypertrophic perivascular astrocytes have been observed in our WP-sensitized aged mice (Germundson et al., 2018) and also reported in the spinal cord of EAE mice (Voskuhl et al., 2009). These astrocytes resemble scar forming astrocytes often described in central nervous system injuries and are thought to establish barriers to control infiltration of leukocytes from the blood circulation (Voskuhl et al., 2009; Sofroniew and Vinters, 2010). Importantly, increased expression of GFAP plays a crucial role in this barrier formation since ablation of GFAP-expressing astrocytes results in profound increases in the number of leukocyte infiltrates in the spinal cord of EAE mice (Voskuhl et al., 2009). Thus, it is feasible to postulate that BLG sensitization stimulated peripheral immune cells and increased their circulating levels, and the perivascular astrocytes had become activated to regulate the amount of inflammatory influence from the periphery. To provide evidence for this notion, juxtaposition of leukocytes with GFAP-immunoreactive astrocyte end-feet across the blood vessel walls need to be demonstrated in our mouse model of CMA as shown in the EAE mice (Voskuhl et al., 2009). Nonetheless, semi-quantitative analysis with western blotting showed that the GFAP levels in the midbrain regions were significantly elevated in BLG-sensitized mice when compared to sham mice (**Figure 6**), supporting our immunohistochemical observations.

Astrocytes are multifaceted glia cells in the central nervous system, and they play essential roles in metabolic support, intercellular signaling, blood flow regulation, myelination, and synaptic pruning [reviewed by Sofroniew and Vinters, 2010]. It is of interest to examine whether these functions of astrocytes become dysregulated in BLG-sensitized mice and influence their behavior. Astrocytes are also important mediators of neuroinflammation with the ability to produce and secrete pro- as well as anti-inflammatory molecules (Eddleston and Mucke, 1993; John et al., 2003). The fact that the levels of TNFα were significantly elevated in the midbrain regions of the BLG-sensitized mice suggested that the astrocytes were acting as proinflammatory mediators (**Figure 7**). However, it seems counterintuitive that microglia did not show reactive morphology in response to the elevated proinflammatory cytokine levels. One possible explanation is that TNFα detected in our samples had derived from the intestines or circulating leukocytes and was not produced by astrocytes, which had successfully prevented the cytokine and cytokine-producing cells from activating microglia. An alternative explanation may be that our experimental paradigm was too transient, and BLG-sensitized mice needed to be repetitively challenged to elicit more chronic inflammation in order for microglia to become activated. These hypotheses, along with the possible involvement of other proinflammatory cytokines, such as IL-1β and IL-6, need to be tested in future studies.

In conclusion, we have demonstrated that sensitization of C57BL/6J mice with BLG induces anxiety- and depression-like behaviors in male mice that are associated with decreases in tight junction proteins in the intestines and astrogliosis in the brain. Elevated TNFα levels in both of these locations suggest that this proinflammatory cytokine plays a role, at least in part, in mediating immune responses to the cow's milk allergen in sensitized mice. Whether these pathophysiological findings directly influence the behavior of sensitized mice is yet to be determined. However, clinical reports of symptom improvements in patients with treatment-resistant depression and other psychiatric conditions after elimination diet (Parker and Watkins, 2002) and plasmapheresis (Barzman et al., 2018) support the involvement of FAH-triggered immune responses in pathogenesis of behavioral disorders. Treatments with antihistamines and/or steroidal/non-steroidal anti-inflammatory reagents to, respectively, inhibit the effects of hypersensitivity-mediated immediate immune reactions (e.g., mast cell degranulation) and subsequent inflammation in our mouse model will be useful in clarifying the involvement of proinflammatory cytokines in the development of observed brain pathophysiology and behavioral changes. Elucidating the mechanisms by which immune responses to a dietary component manifest as brain and behavioral dysfunction may therefore provide potential therapeutic approaches beyond the use of neuromodulatory drugs.

DATA AVAILABILITY

All datasets generated for this study are included in the manuscript and/or the **Supplementary Files**.

ETHICS STATEMENT

This study was carried out in accordance with the recommendations of University of North Dakota Institutional Animal Care and Use Committee. The protocol was approved by the University of North Dakota Institutional Animal Care and Use Committee.

AUTHOR CONTRIBUTIONS

NS performed the experiments, data collection and analyses, and drafted the manuscript. DG and CC assisted with the experiments, data and tissue collection and analyses, and critically reviewed and edited the manuscript. LV assisted with

the experiments and data collection. KN-C designed, planned, and performed the experiments and analyses, drafted and edited the manuscript, and obtained the funding for the study.

FUNDING

This work, including the purchases of the animals and reagents, was supported by an Institutional Development Award (IDeA) from the National Institute of General Medical Sciences of the National Institutes of Health (P20GM103442), University of North Dakota Epigenomics of Development and Disease Center of Biomedical Research Excellence Pilot Grant (5P20GM104360-05).

ACKNOWLEDGMENTS

The authors would like to thank Patricia Doyle, Lillie Meduna, Angela Floden, and Dr. Gunjan Manocha for their technical assistance.

SUPPLEMENTARY MATERIAL

The Supplementary Material for this article can be found online at: https://www.frontiersin.org/articles/10.3389/fncel.2019.00320/full#supplementary-material

Video S1 | Male Sham mouse carefully walking across the open zone of the EZM.

Video S2 | Male BLG mouse briefly surveying the open zone of the EZM and returning to the closed zone.

Supplementary Figure 1 | An alternative analysis for the post-sensitization serum levels of BLG-specific IgE shown in **Figure 2B**. Serum isolated from the terminal blood was used to quantify the levels of BLG-specific IgE using ELISA. A group analysis including all sample values are shown in **Figure 2B**. As an alternative analysis of the results, outliers within each group were identified using GraphPad Prism software (ROUT, Q = 1%), and Mann-Whitney test was performed excluding the outlier values from the statistical analysis. For male groups, statistical significance of $^{**}p < 0.01$ was found between sham and BLG mice (male sham: 0.10 ± 0.02, $n = 7$; male BLG: 0.23 ± 0.05, $n = 7$; one outlier from each group was removed from the analysis [sham, 0.40; BLG, 2.37]). Statistically significant difference between female sham and BLG groups was not found using this method of analysis [female sham: 0.10 ± 0.01, $n = 8$; female BLG: 0.17 ± 0.06, $n = 6$; two outliers removed from the analysis of the BLG group [3.58, 2.32].

REFERENCES

Acker, W. W., Plasek, J. M., Blumenthal, K. G., Lai, K. H., Topaz, M., Seger, D. L., et al. (2017). Prevalence of food allergies and intolerances documented in electronic health records. *J. Allergy Clin. Immunol.* 140, 1587–1591.e1. doi: 10.1016/j.jaci.2017.04.006

Addolorato, G., Marsigli, L., Capristo, E., Caputo, F., Dall'Aglio, C., and Baudanza, P. (1998). Anxiety and depression: a common feature of health care seeking patients with irritable bowel syndrome and food allergy. *Hepatogastroenterology* 45, 1559–1564.

Al-Harbi, K. S. (2012). Treatment-resistant depression: therapeutic trends, challenges, and future directions. *Patient Prefer. Adherence* 6, 369–388. doi: 10.2147/PPA.S29716

Barzman, D. H., Jackson, H., Singh, U., Griffey, M., Sorter, M., and Bernstein, J. A. (2018). An atypical presentation of pediatric acute neuropsychiatric syndrome responding to plasmapheresis treatment. *Case Rep. Psychiatry* 2018:8189067. doi: 10.1155/2018/8189067

Becklake, M. R., and Kauffmann, F. (1999). Gender differences in airway behaviour over the human life span. *Thorax* 54, 1119–1138. doi: 10.1136/thx.54.12.1119

Bradford, M. M. (1976). A rapid and sensitive method for the quantitation of microgram quantities of protein utilizing the principle of protein-dye binding. *Anal. Biochem.* 72, 248–254. doi: 10.1016/0003-2697(76)90527-3

Can, A., Dao, D. T., Terrillion, C. E., Piantadosi, S. C., Bhat, S., and Gould, T. D. (2012). The tail suspension test. *J. Vis. Exp.* 59:e3769. doi: 10.3791/3769

Center for Behavioral Health Statistics and Quality (2017). *2016 National Survey on Drug Use and Health: Methodological Summary and Definitions*. Rockville, MD: Substance Abuse and Mental Health Services Administration.

Clements, S. J., and Carding, S. (2018). Diet, the intestinal microbiota, and immune health in aging. *Crit. Rev. Food Sci. Nutr.* 58, 651–661. doi: 10.1080/10408398.2016.1211086

Costa-Pinto, F. A., and Basso, A. S. (2012). Neural and behavioral correlates of food allergy. *Chem. Immunol. Allergy* 98, 222–239. doi: 10.1159/000336525

Crayton, J. W. (1986). Adverse reactions to foods: relevance to psychiatric disorders. *J. Allergy Clin. Immunol.* 78(1 Pt 2), 243–250. doi: 10.1016/0091-6749(86)90018-7

Cryan, J. F., Mombereau, C., and Vassout, A. (2005). The tail suspension test as a model for assessing antidepressant activity: review of pharmacological and genetic studies in mice. *Neurosci. Biobehav. Rev.* 29, 571–625. doi: 10.1016/j.neubiorev.2005.03.009

Davison, H. M. (1949). Cerebral allergy. *South. Med. J.* 42, 712–716. doi: 10.1097/00007611-194908000-00017

de Magistris, L., Familiari, V., Pascotto, A., Sapone, A., Frolli, A., Iardino, P., et al. (2010). Alterations of the intestinal barrier in patients with autism spectrum disorders and in their first-degree relatives. *J. Pediatr. Gastroenterol. Nutr.* 51, 418–424. doi: 10.1097/MPG.0b013e3181dcc4a5

de Mathis, M. A., Alvarenga, P.d, Funaro, G., Torresan, R. C., Moraes, I., Torres, A. R., et al. (2011). Gender differences in obsessive-compulsive disorder: a literature review. *Braz. J. Psychiatry* 33, 390–399. doi: 10.1590/S1516-44462011000400014

de Theije, C. G., Wu, J., Koelink, P. J., Korte-Bouws, G. A., Borre, Y., Kas, M. J., et al. (2014). Autistic-like behavioural and neurochemical changes in a mouse model of food allergy. *Behav. Brain Res.* 261, 265–274. doi: 10.1016/j.bbr.2013.12.008

Deacon, R. M. (2006). Digging and marble burying in mice: simple methods for *in vivo* identification of biological impacts. *Nat. Protoc.* 1, 122–124. doi: 10.1038/nprot.2006.20

DunnGalvin, A., Hourihane, J. O. B., Frewer, L., Knibb, R. C., Oude Elberink, J. N. G., and Klinge, I. (2006). Incorporating a gender dimension in food allergy research: a review. *Allergy* 61, 1336–1343. doi: 10.1111/j.1398-9995.2006.01181.x

Eddleston, M., and Mucke, L. (1993). Molecular profile of reactive astrocytes–implications for their role in neurologic disease. *Neuroscience* 54, 15–36. doi: 10.1016/0306-4522(93)90380-X

Farrell, H. M., Jimenez-Flores, R., Bleck, G. T., Brown, E. M., Butler, J. E., Creamer, L. K., et al. (2004). Nomenclature of the proteins of cows' milk—sixth revision. *J. Dairy Sci.* 87, 1641–1674. doi: 10.3168/jds.S0022-0302(04)73319-6

Ferro, M. A., Van Lieshout, R. J., Ohayon, J., and Scott, J. G. (2016). Emotional and behavioral problems in adolescents and young adults with food allergy. *Allergy* 71, 532–540. doi: 10.1111/all.12829

Fiorentino, M., Sapone, A., Senger, S., Camhi, S. S., Kadzielski, S. M., Buie, T. M., et al. (2016). Blood-brain barrier and intestinal epithelial barrier alterations in autism spectrum disorders. *Mol. Autism* 7:49. doi: 10.1186/s13229-016-0110-z

Garg, N., and Silverberg, J. I. (2014). Association between childhood allergic disease, psychological comorbidity, and injury requiring medical attention. *Ann. Allergy Asthma Immunol.* 112, 525–532. doi: 10.1016/j.anai.2014.03.006

Garg, N., and Silverberg, J. I. (2015). Epidemiology of childhood atopic dermatitis. *Clin. Dermatol.* 33, 281–288. doi: 10.1016/j.clindermatol.2014.12.004

Gaub, M., and Carlson, C. L. (1997). Gender differences in ADHD: a meta-analysis and critical review. *J. Am. Acad. Child Adolesc. Psychiatry* 36, 1036–1045. doi: 10.1097/00004583-199708000-00011

Germundson, D. L., Smith, N. A., Vendsel, L. P., Kelsch, A. V., Combs, C. K., and Nagamoto-Combs, K. (2018). Oral sensitization to whey proteins induces age- and sex-dependent behavioral abnormality and neuroinflammatory responses

in a mouse model of food allergy: a potential role of mast cells. *J. Neuroinflamm.* 15:120. doi: 10.1186/s12974-018-1146-0

Gershon, J. (2002). A meta-analytic review of gender differences in ADHD. *J. Atten. Disord.* 5, 143–154. doi: 10.1177/108705470200500302

Glazier, K., Swing, M., and McGinn, L. K. (2015). Half of obsessive-compulsive disorder cases misdiagnosed: vignette-based survey of primary care physicians. *J. Clin. Psychiatry.* 76, e761–e767. doi: 10.4088/JCP.14m09110

Grochowska, M., Wojnar, M., and Radkowski, M. (2018). The gut microbiota in neuropsychiatric disorders. *Acta Neurobiol. Exp.* 78, 69–81. doi: 10.21307/ane-2018-008

Hanna, G. L. (1995). Demographic and clinical features of obsessive-compulsive disorder in children and adolescents. *J. Am. Acad. Child Adolesc. Psychiatry* 34, 19–27. doi: 10.1097/00004583-199501000-00009

Hirschtritt, M. E., Bloch, M. H., and Mathews, C. A. (2017). Obsessive-compulsive disorder: advances in diagnosis and treatment. *JAMA* 317, 1358–1367. doi: 10.1001/jama.2017.2200

Jarvis, D., and Burney, P. (1998). ABC of allergies. The epidemiology of allergic disease. *BMJ* 316, 607–610. doi: 10.1136/bmj.316.7131.607

Johansson, R., Carlbring, P., Heedman, A., Paxling, B., and Andersson, G. (2013). Depression, anxiety and their comorbidity in the Swedish general population: point prevalence and the effect on health-related quality of life. *PeerJ.* 1:e98. doi: 10.7717/peerj.98

John, G. R., Lee, S. C., and Brosnan, C. F. (2003). Cytokines: powerful regulators of glial cell activation. *Neuroscientist* 9, 10–22. doi: 10.1177/1073858402239587

Kalueff, A. V., Stewart, A. M., Song, C., Berridge, K. C., Graybiel, A. M., and Fentress, J. C. (2016). Neurobiology of rodent self-grooming and its value for translational neuroscience. *Nat. Rev. Neurosci.* 17, 45–59. doi: 10.1038/nrn.2015.8

Karakula-Juchnowicz, H., Dzikowski, M., Pelczarska, A., Dzikowska, I., and Juchnowicz, D. (2016). The brain-gut axis dysfunctions and hypersensitivity to food antigens in the etiopathogenesis of schizophrenia. *Psychiatr. Pol.* 50, 747–760. doi: 10.12740/PP/OnlineFirst/45053

Kelly, C., and Gangur, V. (2009). Sex disparity in food allergy: evidence from the PubMed database. *J. Allergy* 2009:159845. doi: 10.1155/2009/159845

Klein, S. L., and Flanagan, K. L. (2016). Sex differences in immune responses. *Nat. Rev. Immunol.* 16, 626–638. doi: 10.1038/nri.2016.90

Klik, K. A., Williams, S. L., and Reynolds, K. J. (2018). Toward understanding mental illness stigma and help-seeking: a social identity perspective. *Soc. Sci. Med.* 222, 35–43. doi: 10.1016/j.socscimed.2018.12.001

Li, X. M., Serebrisky, D., Lee, S. Y., Huang, C. K., Bardina, L., Schofield, B. H., et al. (2000). A murine model of peanut anaphylaxis: T- and B-cell responses to a major peanut allergen mimic human responses. *J. Allergy Clin. Immunol.* 106(1 Pt 1), 150–158. doi: 10.1067/mai.2000.107395

Lyall, K., Van de Water, J., Ashwood, P., and Hertz-Picciotto, I. (2015). Asthma and allergies in children with autism spectrum disorders: results from the CHARGE Study. *Autism Res.* 8, 567–574. doi: 10.1002/aur.1471

Lyons, A. C., and Forde, E. M. (2004). Food allergy in young adults: perceptions and psychological effects. *J. Health Psychol.* 9, 497–504. doi: 10.1177/1359105304044032

MacMaster, F. P., Russell, A., Mirza, Y., Keshavan, M. S., Banerjee, S. P., Bhandari, R., et al. (2006). Pituitary volume in pediatric obsessive-compulsive disorder. *Biol. Psychiatry* 59, 252–257. doi: 10.1016/j.biopsych.2005.06.028

Maia, T. V., Cooney, R. E., and Peterson, B. S. (2008). The neural bases of obsessive-compulsive disorder in children and adults. *Dev. Psychopathol.* 20, 1251–1283. doi: 10.1017/S0954579408000606

Malacarne, M., Martuzzi, F., Summer, A., and Mariani, P. (2002). Protein and fat composition of mare's milk: some nutritional remarks with reference to human and cow's milk. *Int. Dairy J.* 12, 869–877. doi: 10.1016/S0958-6946(02)00120-6

Mandy, W., Chilvers, R., Chowdhury, U., Salter, G., Seigal, A., and Skuse, D. (2012). Sex differences in autism spectrum disorder: evidence from a large sample of children and adolescents. *J. Autism Dev. Disord.* 42, 1304–1313. doi: 10.1007/s10803-011-1356-0

Mayorga, A. J., and Lucki, I. (2001). Limitations on the use of the C57BL/6 mouse in the tail suspension test. *Psychopharmacology* 155, 110–112. doi: 10.1007/s002130100687

Nagamoto-Combs, K., Kulas, J., and Combs, C. K. (2014). A novel cell line from spontaneously immortalized murine microglia. *J. Neurosci. Methods* 233, 187–198. doi: 10.1016/j.jneumeth.2014.05.021

Parker, G., and Watkins, T. (2002). Treatment-resistant depression: when antidepressant drug intolerance may indicate food intolerance. *Aust. N. Z. J. Psychiatry* 36, 263–265. doi: 10.1046/j.1440-1614.2002.00978.x

Patten, S. B., and Williams, J. V. (2007). Self-reported allergies and their relationship to several Axis I disorders in a community sample. *Int. J. Psychiatry Med.* 37, 11–22. doi: 10.2190/L811-0738-10NG-7157

Pennell, L. M., Galligan, C. L., and Fish, E. N. (2012). Sex affects immunity. *J. Autoimmun.* 38, J282–J291. doi: 10.1016/j.jaut.2011.11.013

Round, J. L., and Mazmanian, S. K. (2009). The gut microbiota shapes intestinal immune responses during health and disease. *Nat. Rev. Immunol.* 9, 313–323. doi: 10.1038/nri2515

Russell, G., Steer, C., and Golding, J. (2011). Social and demographic factors that influence the diagnosis of autistic spectrum disorders. *Soc. Psychiatry Psychiatr. Epidemiol.* 46, 1283–1293. doi: 10.1007/s00127-010-0294-z

Shanahan, L., Zucker, N., Copeland, W. E., Costello, E. J., and Angold, A. (2014). Are children and adolescents with food allergies at increased risk for psychopathology? *J. Psychosom. Res.* 77, 468–473. doi: 10.1016/j.jpsychores.2014.10.005

Shuffrey, L. C., Guter, S. J., Delaney, S., Jacob, S., Anderson, G. M., Sutcliffe, J. S., et al. (2017). Is there sexual dimorphism of hyperserotonemia in autism spectrum disorder? *Autism Res.* 10, 1417–1423. doi: 10.1002/aur.1791

Sofroniew, M. V., and Vinters, H. V. (2010). Astrocytes: biology and pathology. *Acta Neuropathol.* 119, 7–35. doi: 10.1007/s00401-009-0619-8

Speer, F. (1954). The allergic tension-fatigue syndrome. *Pediatr. Clin. North Am.* 1029–1037. doi: 10.1016/S0031-3955(16)30167-5

Speer, F. (1958). The allergic tension-fatigue syndrome in children. *Int. Arch. Allergy Appl. Immunol.* 12, 207–214. doi: 10.1159/000228455

Tiller, J. W. (2013). Depression and anxiety. *Med. J. Aust.* 199, S28–S31. doi: 10.5694/mjao12.10628

Topal, E., Catal, F., Soylu, N., Ozcan, O. O., Celiksoy, M. H., Babayigit, A., et al. (2016). Psychiatric disorders and symptoms severity in pre-school children with cow's milk allergy. *Allergol. Immunopathol.* 44, 445–449. doi: 10.1016/j.aller.2016.03.001

Verma, D., Chakraborti, B., Karmakar, A., Bandyopadhyay, T., Singh, A. S., Sinha, S., et al. (2014). Sexual dimorphic effect in the genetic association of monoamine oxidase A (MAOA) markers with autism spectrum disorder. *Prog. Neuropsychopharmacol. Biol. Psychiatry* 50, 11–20. doi: 10.1016/j.pnpbp.2013.11.010

Voskuhl, R. R., Peterson, R. S., Song, B., Ao, Y., Morales, L. B., Tiwari-Woodruff, S., et al. (2009). Reactive astrocytes form scar-like perivascular barriers to leukocytes during adaptive immune inflammation of the CNS. *J. Neurosci.* 29, 11511–11522. doi: 10.1523/JNEUROSCI.1514-09.2009

Xu, G., Snetselaar, L. G., Jing, J., Liu, B., Strathearn, L., and Bao, W. (2018). Association of food allergy and other allergic conditions with autism spectrum disorder in children. *JAMA Netw. Open* 1:e180279. doi: 10.1001/jamanetworkopen.2018.0279

Conflict of Interest Statement: The authors declare that the research was conducted in the absence of any commercial or financial relationships that could be construed as a potential conflict of interest.

frontiers in Cellular Neuroscience

ORIGINAL RESEARCH
published: 08 August 2019
doi: 10.3389/fncel.2019.00307

Time-Dependent Changes in Microglia Transcriptional Networks Following Traumatic Brain Injury

Saef Izzy[1,2,3,4†], Qiong Liu[5,6†], Zhou Fang[4,7,8,9], Sevda Lule[3,10], Limin Wu[3,10], Joon Yong Chung[3,10], Aliyah Sarro-Schwartz[1,4], Alexander Brown-Whalen[2,3], Caroline Perner[2,3,4], Suzanne E. Hickman[2,3,4], David L. Kaplan[11], Nikolaos A. Patsopoulos[4,7,8,9], Joseph El Khoury[2,3,4] and Michael J. Whalen[3,4,10]**

[1] Department of Neurology, Brigham and Women's Hospital, Harvard Medical School, Boston, MA, United States, [2] Center for Immunology and Inflammatory Diseases, Massachusetts General Hospital, Harvard Medical School, Boston, MA, United States, [3] Massachusetts General Hospital, Harvard Medical School, Charlestown, MA, United States, [4] Harvard Medical School, Boston, MA, United States, [5] Department of Anatomy, Histology and Embryology, School of Basic Medical Sciences, Fudan University, Shanghai, China, [6] Shanghai Key Laboratory of Medical Imaging Computing and Computer Assisted Intervention, Shanghai, China, [7] Systems Biology and Computer Science Program, Ann Romney Center for Neurological Diseases, Department of Neurology, Brigham and Women's Hospital, Boston, MA, United States, [8] Division of Genetics, Department of Medicine, Brigham and Women's Hospital, Harvard Medical School, Boston, MA, United States, [9] Broad Institute of Harvard and Massachusetts Institute of Technology, Cambridge, MA, United States, [10] Department of Pediatrics, Massachusetts General Hospital, Harvard Medical School, Boston, MA, United States, [11] Department of Biomedical Engineering, Tufts University, Medford, MA, United States

OPEN ACCESS

Edited by:
Yu Tang,
Xiangya Hospital Central South University, China

Reviewed by:
Susanna Rosi,
University of California, San Francisco, United States
Adam Bachstetter,
University of Kentucky, United States

***Correspondence:**
Joseph El Khoury
jelkhoury@mgh.harvard.edu
Michael J. Whalen
MWHALEN@mgh.harvard.edu

[†] These authors have contributed equally to this work

Specialty section:
This article was submitted to Non-Neuronal Cells, a section of the journal Frontiers in Cellular Neuroscience

Received: *05 March 2019*
Accepted: *24 June 2019*
Published: *08 August 2019*

Citation:
Izzy S, Liu Q, Fang Z, Lule S, Wu L, Chung JY, Sarro-Schwartz A, Brown-Whalen A, Perner C, Hickman SE, Kaplan DL, Patsopoulos NA, El Khoury J and Whalen MJ (2019) Time-Dependent Changes in Microglia Transcriptional Networks Following Traumatic Brain Injury. Front. Cell. Neurosci. 13:307. doi: 10.3389/fncel.2019.00307

The neuroinflammatory response to traumatic brain injury (TBI) is critical to both neurotoxicity and neuroprotection, and has been proposed as a potentially modifiable driver of secondary injury in animal and human studies. Attempts to broadly target immune activation have been unsuccessful in improving outcomes, in part because the precise cellular and molecular mechanisms driving injury and outcome at acute, subacute, and chronic time points after TBI remain poorly defined. Microglia play a critical role in neuroinflammation and their persistent activation may contribute to long-term functional deficits. Activated microglia are characterized by morphological transformation and transcriptomic changes associated with specific inflammatory states. We analyzed the temporal course of changes in inflammatory genes of microglia isolated from injured brains at 2, 14, and 60 days after controlled cortical impact (CCI) in mice, a well-established model of focal cerebral contusion. We identified a time dependent, injury-associated change in the microglial gene expression profile toward a reduced ability to sense tissue damage, perform housekeeping, and maintain homeostasis in the early stages following CCI, with recovery and transition to a specialized inflammatory state over time. This later state starts at 14 days post-injury and is characterized by a biphasic pattern of IFNγ, IL-4, and IL-10 gene expression changes, with concurrent proinflammatory and anti-inflammatory gene changes. Our transcriptomic data sets are an important step to understand microglial role in TBI pathogenesis at the molecular level and identify common pathways that affect outcome. More studies to evaluate gene expression at the single cell level and focusing on subacute and chronic timepoint are warranted.

Keywords: traumatic brain injury, microglia, transcriptome, neurodegeneration, mice, neuroimmunology, neuroinflammation

INTRODUCTION

Traumatic brain injury (TBI) is a leading cause of mortality, morbidity, and disability in children and adults, with an economic burden of over $60 billion per year in the United States (Langlois et al., 2006; McKinlay et al., 2008). No specific therapy is proven to reduce long-term cognitive sequelae of TBI and only limited options exist for rehabilitation (Gordon et al., 2006; McCrory et al., 2009; Helmick and Members of Consensus Conference, 2010), in part because mechanisms driving injury and outcome remain poorly defined. One mechanism thought to be important in long-term outcome after TBI is neuroinflammation (Ramlackhansingh et al., 2011; Loane et al., 2014; Jassam et al., 2017; Simon et al., 2017a). TBI activates resident microglia, induces cytokines production in the brain, and causes influx of peripheral immune cells, followed by a chronic activation of resident microglia and astrocytes (Das et al., 2012; Sofroniew, 2015; Simon et al., 2017a). Neuroinflammation can participate in repair mechanisms and has also been proposed as a potentially modifiable driver of secondary injury in animal and human studies (Jassam et al., 2017; Simon et al., 2017b). However, the precise cellular and molecular mechanisms of neuroinflammation leading to neurological deficits at acute, subacute, and chronic time points after TBI remain to be defined (Jassam et al., 2017; Simon et al., 2017a).

Microglia are macrophage-like cells that reside in the central nervous system (CNS) and play a critical role in neuroinflammation (Ransohoff and El Khoury, 2015; Hickman et al., 2018). They are among the first responders to brain injury and their persistent activation in TBI animal models and in humans with TBI may contribute to long-term functional deficits (Gentleman et al., 2004; Coughlin et al., 2015; Witcher et al., 2015; Muccigrosso et al., 2016; Jassam et al., 2017). Activated microglia may be characterized based on morphological transformation from ramified (resting state) to amoeboid (activated state) (Donat et al., 2017; Hickman et al., 2018). Alternatively, transcriptomics can be used to describe specific inflammatory states (Hickman et al., 2018). Transcriptomic analyses of microglia in aged mice and human macrophages showed that these cell types undergo disease and stimulus-specific gene expression changes (Hickman et al., 2013; Xue et al., 2014). Our understanding of microglia-specific gene functions, pathways, and networks in Alzheimer disease (AD), amyotrophic lateral sclerosis, and other neurodegenerative diseases has been rapidly evolving and now offers a road map to study gene expression in other complex diseases like TBI (Chiu et al., 2013; Hickman et al., 2013, 2018).

Despite the evidence for a significant role for microglia in the pathogenesis of TBI, few studies to date have examined microglia-specific gene expression as a function of time in a preclinical TBI model. Almost all prior studies in preclinical TBI models used whole brain tissue to infer inflammatory responses to injury of microglia and other brain cell types (Kobori et al., 2002; Matzilevich et al., 2002; Almeida-Suhett et al., 2014; Lipponen et al., 2016); however, this approach does not necessarily reflect microglia-specific gene expression changes (Hickman et al., 2013). Moreover, most of these prior studies were limited to acute post-injury time points (Redell et al., 2013; Samal et al., 2015; White et al., 2016; Wong et al., 2016). A recent single-cell RNA sequencing study of cells isolated by fluorescence activated cell sorting (FACS) from mouse TBI brain samples at 24 h after fluid percussion injury provided unique information, based on only 249 cells from sham and 293 cells from injured animals, about how TBI impacts diverse gene expression changes in hippocampal cell types (Arneson et al., 2018). However, to our knowledge, no study has characterized temporal expression patterns, including the chronic period, of microglia-specific inflammatory gene expression in a preclinical TBI model.

Here, we analyzed the temporal course of changes in inflammatory gene transcription of microglia isolated from injured brain by FACS up to 60 days after controlled cortical impact (CCI) in mice, a well-established model of focal cerebral contusion (Jassam et al., 2017), using the Nanostring gene expression analysis platform. We identified a time-dependent, injury-associated change in the microglial phenotype toward a reduced ability to sense tissue damage, perform housekeeping, and maintain homeostasis in the early stages following CCI, with recovery and transition to a pro-inflammatory state over time.

MATERIALS AND METHODS

Experimental Animals

Studies were performed using 3-month-old male C57BL6J mice (Stock #000664, Jackson Laboratories, Bar Harbor, ME, United States). All procedures were performed in accordance with the NIH Guide for Care and Use of Laboratory Animals and followed protocols approved by the MGH Institutional Animal Care and Use Committee. Mice had access to food and water *ad libitum* and were housed on a 12-h day–night cycle in laminar flow racks in a temperature-controlled room (25°C). Investigators were blinded to study groups in all experiments. Mice were randomized to sham and injured at 2 days post-injury (dpi). Shams and CCI mice were housed in the same cage. Subsequent groups were injured at 14 and 60 dpi without any specific randomization scheme since the mice were genetically identical and compared to 2 day shams.

Controlled Cortical Impact (CCI)

A CCI model was used as previously described (Bermpohl et al., 2007). Mice were anesthetized with 4.5% isoflurane (Anaquest) in 70% nitrous oxide and 30% oxygen using a Fluotec 3 vaporizer (Colonial Medical). The mice were placed in a stereotaxic frame and a 5-mm craniotomy was made over the parieto-temporal cortex using a drill and a trephine. The bone flap was removed and discarded, and a pneumatic cylinder with a 3-mm flat tip impounder with velocity 6 m/s, depth 0.6 mm, and duration 100 ms was used to induce CCI. The scalp was sutured closed and the mice were returned to their cages to recover.

Preparation of Brain Tissue for CD11b Immunohistochemistry

The mice were anesthetized with avertin and transcardially perfused with PBS. The brains were extracted and postfixed in 4%

paraformaldehyde overnight, cryoprotected in 15% followed by 30% sucrose overnight, frozen at −80°C, prior to making coronal sections (12 μm) on poly-L-lysine-coated slide (Thermo Fisher Scientific) using the cryostat. The brains were cut at 0.5 mm intervals from the anterior to the posterior of the brain, starting at 1.56 mm from the bregma position.

CD11b Immunohistochemistry

Brain sections were washed twice with Dulbecco's phosphate-buffered saline (DPBS) (without calcium and magnesium) before undergoing fixation with 95% ethanol (pre-cooled to 4°C) for 10 min. Antigen retrieval was performed with a 15-min incubation of pre-warmed (37°C) trypsin (0.25%) before blocking endogenous peroxidase activity with a 5-min incubation of 0.3% hydrogen peroxide and 0.3% normal rabbit serum in DPBS. Sections were blocked in DPBS with 1.5% normal rabbit serum for 20 min before primary antibody incubation with 1:100 CD11B (Serotec MCA711G; Serotec, Oxford, United Kingdom) in DPBS with 2.5% normal rabbit serum. The primary antibody was visualized with the avidin–biotin horseradish peroxidase technique in accordance with manufacturer's instructions [Vector Laboratories, Vectastain Elite Kit PK6104, NovaRED Peroxidase (HRP) Substrate Kit SK-4800, Burlingame, CA, United States]. Sections were then counterstained with hematoxylin in accordance with the manufacturer's instructions (Vector Laboratories, H-3401, Burlingame, CA, United States), and mounted with Vectamount Permanent Mounting Medium (Vector Laboratories, H-5000, Burlingame, CA, United States). Brightfield images were subsequently obtained using a Zeiss Axio Scan.Z1 slide scanner with the ZenBlue software (Carl Zeiss, Jena, Germany).

CD11b+ Surface Area Quantification

The presence of microglia was determined by quantifying CD11B+ cell surface area in the cortex of coronal brain sections stained slides. Analysis of percent microglia-positive surface area was performed on 10 photomicrographs per animal ($n = 3$ mice for each time point). Each scanned photomicrograph was used to produce four images: two from the ipsilateral hemisphere and two from the contralateral hemisphere. Within the ipsilateral hemisphere, one image was taken in the cortex, peripheral to the site of injury, while one image was taken far from the site of injury. The two contralateral hemisphere images mirrored the locations of the ipsilateral images. Together, these images were taken as representative of each hemisphere (**Figure 1E**). Each of the four images was analyzed using ImageJ software (National Institute of Health[1]). Images were split by color channel, and the channel of interest was thresholded using the Yen setting. ImageJ was used to analyze the percent of surface area occupied by CD11B+ cells in each image. CD11b quantification data are shown as mean ± SEM and analyzed using R studio with statistical significance assigned when $p < 0.05$. Differences in CD11b surface area between 2 and 14 dpi vs. sham were analyzed using a one-way analysis of variance (ANOVA) followed by a Tukey's honest significant difference test.

[1]https://imagej.nih.gov/ij/

Isolation of Brain Microglia by Fluorescence Activated Cell Sorting (FACS)

Microglia were isolated by FACS as previously described (Hickman et al., 2013). The mice were anesthetized with avertin and transcardially perfused with PBS. The brains were extracted and placed in PBS on ice. The brains were dissociated using collagenase and dispase and gentleMACS dissociator (Miltenyi Biotech). The cells were separated using physiologic Percoll and were blocked with donkey serum and fetal bovine serum and incubated with APC anti-mouse CD11b and PerCP anti-mouse CD45 antibodies for 30 min. Microglia were sorted based on CD45 low to intermediate/CD11b high expression using BD FACSAria II (Becton Dickinson, Inc.) (**Supplementary Figure S1**).

Nanostring Gene Expression Analysis

Microglia isolated by FACS were stored in RNAlater Stabilization Solution (AM7020, Invitrogen) at −80°C until further processing. Total RNA from the sorted cells was extracted using miRNeasy Micro Kit from Qiagen (Redwood City, CA, United States) for purification of total RNA from small amounts of cells according to the manufacturer's instructions. Microglia RNA integrity number (RIN) was between 8 and 9. mRNA expression analysis with the NanoString nCounter® Mouse Inflammation v2 Panel was performed according to the manufacturer's protocol (NanoString Technologies Inc., Seattle, WA, United States).

Quantitative Real-Time Polymerase Chain Reaction

Relative expressions of selected microglia genes for sham vs. 2 dpi were verified by real-time qPCR. First-strand complementary DNA (cDNA) was synthesized using RT2 First Strand Kit (Qiagen, Redwood City, CA, United States) according to manufacturer's instructions. RT^2 qPCR Primer Assay for Mouse IL-1β, IL-6, and TNF (Qiagen, Redwood City, CA, United States) were used according to manufacturer's protocol to validate the gene expression changes shown by Nanostring. Data normalization was performed by quantification of the endogenous 18S ribosomal RNA.

Bioinformatics

Data Normalization

The raw Nanostring nCounter genes were normalized using NanoStringDiff (Wang et al., 2016), adjusting for positive controls, housekeeping genes, and background level. The NanoStringNorm (Waggott et al., 2012) packages was used to generate normalized gene expression, for plotting and clustering purposes.

Differential Gene Expression Analysis

We use a generalized linear model (GLM) with negative binomial family as implemented in the NanoStringDiff (Wang et al., 2016) to examine differential gene expressions for the following

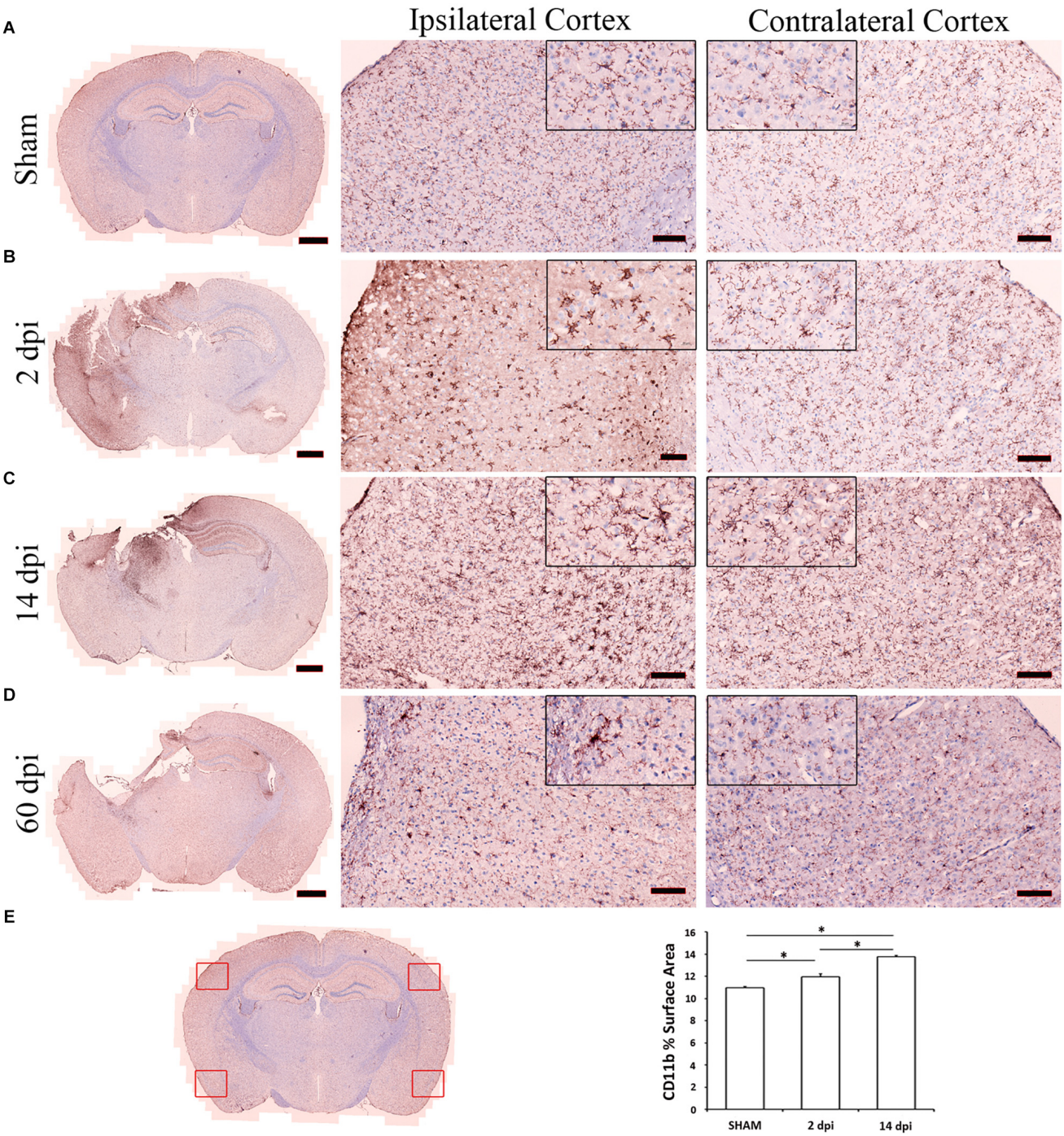

FIGURE 1 | Microglia activation after controlled cortical impact (CCI). Microglia were labeled with anti-CD11b antibody. This figure shows representative photomicrographs of cortical microglia taken from contralateral and ipsilateral hemispheres from sham **(A)**, 2 **(B)**, 14 **(C)**, 60 **(D)** days post-injury (dpi). The left column illustrates the distribution of microglia activation at low magnification. Compared to the uninjured sham **(A)**, increased CD11b staining is observed across the cortex at 2 **(B)** and 14 dpi **(C)**. Highly ramified microglia with spherical cell bodies in sham animals become less ramified with swollen or stretched cell bodies by 2 and 14 dpi (see magnified 20 μm corner views). Images are representative of three animals per time point. Scale bars are 1 mm, 100 μm, and 20 μm for photomicrographs on increasing magnification. **(E)** Scanned photomicrograph was used to produce four images as representative of each hemisphere and two from the contralateral hemisphere. CD11b surface area was analyzed using ImageJ software and quantification data are shown as mean ± SEM differences in CD11b surface area between region and time post-injury. Compared to the uninjured sham, there is significant increase in CD11b surface area across the cortex at 2 ($p = 0.0006$) and 14 dpi ($p < 2e{-}16$).

comparisons: acute (2 dpi vs. sham), subacute (14 dpi vs. sham), and chronic (60 dpi vs. sham).

Pattern-Oriented Time-Series Clustering

To better model and discover genes that follow time-series patterns that are of potential biological interest, we developed a framework named pattern-oriented time-series clustering. Firstly, the gene expressions normalized by NanoStringNorm were filtered by 25% quantile in terms of mean and standard deviation. The rest of the genes were standardized between 0 and 1. Secondly, we calculated the differences in the standardized gene expression for the following pairwise comparisons: 2 dpi vs. sham, 14 dpi vs. 2 dpi, and 60 dpi vs. 14 dpi, and named the differences standardized linear changes (SLCs). We used one group of sham (n = 4) as a baseline for comparison with the three other time points including 2 (n = 4), 14 (n = 4), and 60 dpi (n = 3). We used SLC to depict the temporal patterns that could not be captured by either p-value or log2 (fold-changes) alone. We defined four sub-patterns, namely up, down, stable, and noisy, to compose the time-series pattern for a certain gene. Up and down are the trends with relatively large up or downward SLCs, signaling the genes and intervals with the most changes, while stable are the trends with the lowest absolute value of SLCs, representing the genes that are most stable during such intervals. The trends are categorized as noisy otherwise.

To decide the sub-pattern of each time interval, for each gene, the time interval with the largest absolute SLC, $|SLC_{max}|$, was named up/down by the sign of SLC. Then we calculated absolute relative SLC, $|SLC_i/SLC_{max}|$, where i is the index to one of the other two intervals. To determine those sub-patterns, we defined two parameters, $cutoff_{up}$ and $cutoff_{low}$. If the absolute relative SLC was greater than $cutoff_{high}$, the corresponding sub-pattern was categorized as up/down according to the sign of SLC; if less than $cutoff_{low}$, it was categorized as stable; otherwise, it was categorized as noisy. From this analysis there were 4^4 = 64 possible patterns, i.e., clusters of genes. We performed sensitivity analyses for the two cutoff parameters, tuning $cutoff_{high}$ from 0.3 to 0.75, by 0.05, and $cutoff_{low}$ from 0.05 to 0.275, by 0.025, and accept parameter based on p-measurement, defined as $p\_measurement = w/c \times K_1 \times K_2$, where c is a constant, w is the weight defined as $w = 1/(cutoff_{high} \times cutoff_{low})$ to penalize on selecting loose cutoffs (**Supplementary Figure S2**). K_1 and K_2 are the number of clusters with no noisy sub-patterns, and number of clusters with no opposite-directed sub-patterns, respectively. The latter was used to select patterns that are only biologically meaningful to our subjects.

Gene Set Enrichment and Pathway Analyses

We performed gene set enrichment analysis (GSEA) (Subramanian et al., 2005) on the normalized gene expression dataset with REACTOME and KEGG datasets from c2.all.v6.2.cymbols.gmt curated gene sets using 1,000 permutations. Pathways with false discovery rate (FDR) < 0.05 were selected as significant. We plotted heatmap for the gene sets from cytokine regulated genes as defined by Xue et al. (2014). The genes in heatmap were clustered by k-means clustering methods with k selected using the gap-statistics.

Protein–Protein Interaction Networks

To identify the top regulators in a certain cluster of genes, we performed network analysis using STRING database (Szklarczyk et al., 2017) with all default settings. The top regulators were selected by ranking the sum of confident scores greater than 0.4 (by default) of each gene.

RESULTS

We subjected 2-month-old male C57BL6J mice (Jackson Laboratories, N = 3–4/group) to either CCI or to sham injury using established protocols (Bermpohl et al., 2007). CCI produced a cavitary lesion and overt hippocampal damage associated with morphological changes in microglia indicative of activation (Fox et al., 1998). **Figure 1** shows representative photomicrographs of cortical microglia taken from contralateral and ipsilateral hemispheres at 2–60 dpi. CCI caused a significant increase in microglia numbers at 2 and 14 dpi vs. sham, and clear morphological changes consistent with microglia activation at 2, 14, and 60 dpi in ipsilateral cortex including shorter, thicker, and less ramified processes and swollen or stretched cell bodies. Similar changes in microglia morphology were also observed in some contralateral regions (**Figures 1A–D**). Microglia were isolated from brain tissue by enzymatic digestion as previously described (Hickman et al., 2013). Cells were stained with fluorescent antibodies to CD11b and CD45, two well-established microglia and macrophage markers (Sedgwick et al., 1991) and subsequently isolated using FACS at 2, 14, and 60 dpi as previously described (Sedgwick et al., 1991). RNA was then isolated from microglia and subjected to Nanostring analysis, a quantitative gene expression analysis platform with qPCR sensitivity using a probe set of 550 genes involved in inflammation and immunity (O'Neil et al., 2018; Zhang et al., 2018). We found more genes upregulated significantly at 60 dpi than 2 or 14 dpi (**Figure 2A**).

Microglia Gene Expression at 2 Days Post-injury

Using the Nanostring™ gene expression platform, we identified 152 genes with significant changes in expression at 2 dpi compared to sham, including 51 upregulated and 101 downregulated genes (**Figures 2A,B** and **Supplementary Table S1**). Genes associated with chemotaxis (CXCL1, CXCL3, CCL19, CXCR1, CXCR2, CXCR4, CCR2) as well as cytokine signaling (IL1b, IL1R2, IL23a, IL6, TNF, and IFNB1) were significantly upregulated, suggesting a role for microglia in recruitment of microglia from neighboring areas of the brain as well as recruitment of peripheral leukocytes to injured brain (Liu et al., 2018). Genes involved in the anti-inflammatory transforming growth factor-beta (TGF-β) cytokine signaling pathway (TGFB1, TGFBR1, TGFBR2, SMAD3, SKI) were significantly downregulated at 2 dpi (**Figure 3B**). Likewise,

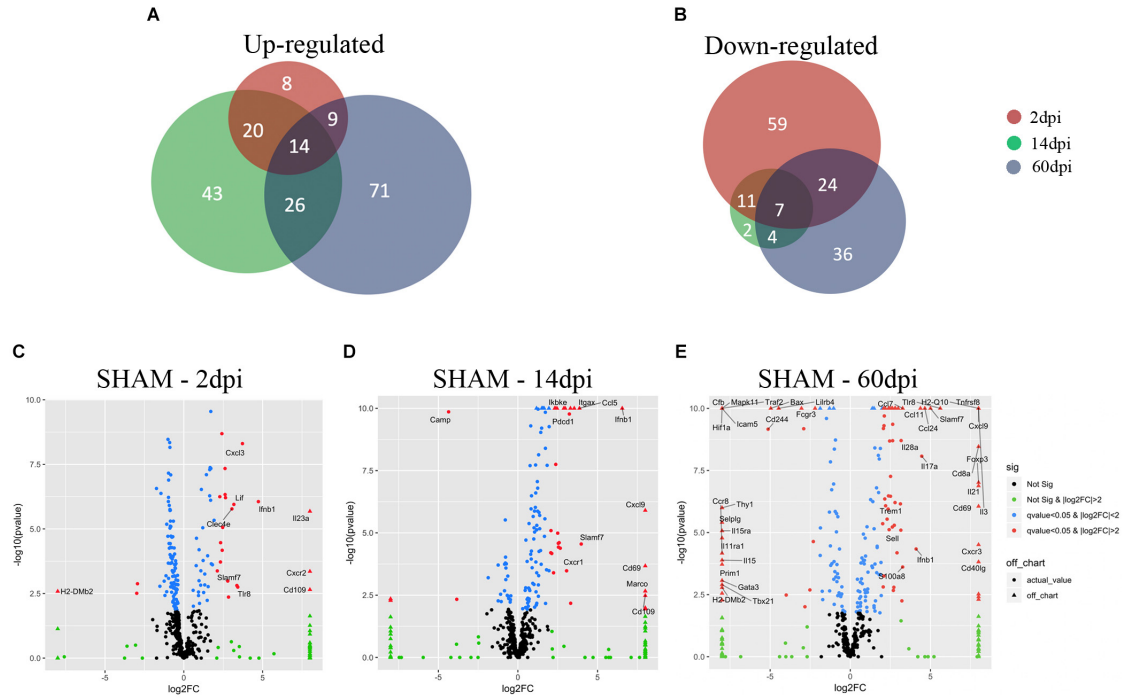

FIGURE 2 | Microglial gene expression after CCI. **(A,B)** Venn diagrams showing the overlap between 2, 14, and 60 dpi, vs. sham of **(A)** up-regulated genes (adjusted p-value < 0.05) and **(b)** down-regulated genes (adjusted p-value < 0.05). **(C–E)** Volcano plot showing the microglia gene expression of **(C)** 2 dpi vs. sham, **(D)** 14 dpi vs. sham, and **(E)** 60 dpi vs. sham. On the x-axis are the log2-fold changes and the y-axis is the –log10(p-value). Genes in black: False discovery rate (FDR) ≥ 0.05, $|\log2(FC)| \leq 2$; genes in green: FDR ≥ 0.05, $|\log2(FC)| > 2$; genes in blue: FDR < 0.05, $|\log2(FC)| \leq 2$; and genes in red: FDR < 0.05, $|\log2(FC)| > 2$. Genes in red with FDR ≤ 0.05, $|\log2(FC)| > 3$ are named.

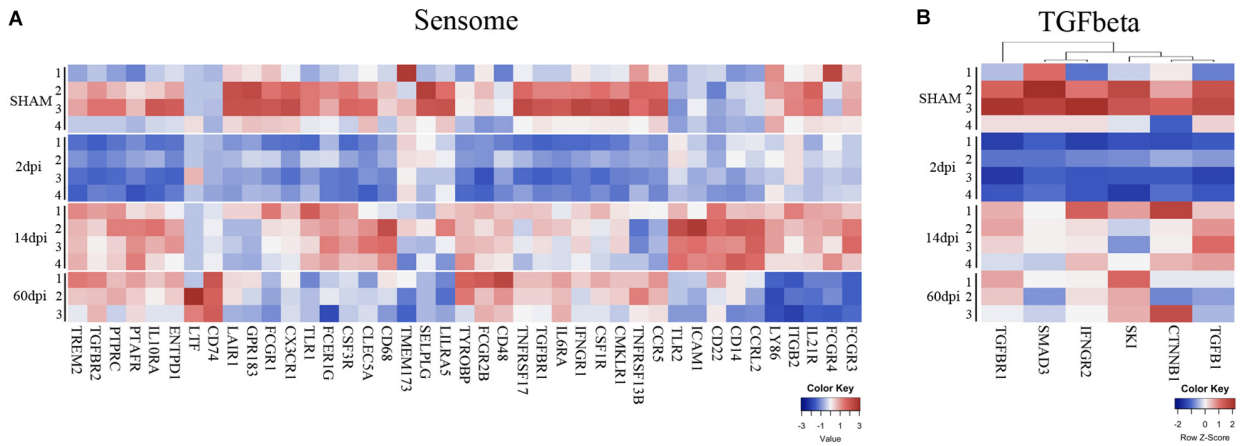

FIGURE 3 | Time-dependent changes of microglial sensome genes and TGF-beta pathway after TBI. Heatmap of normalized gene expressions profiles for **(A)** microglia sensome and **(B)** TGF beta signaling pathway.

subset of genes from the Interferon gamma (IFNγ) pathways (HFE, TAP1, JAK2, STAT1, CD86, FCGR1, PSMB9, IRF8, IRF1, CXCL9) were also downregulated at 2 dpi (**Figure 4**).

IL23a was one of the most significantly upregulated genes in 2 dpi (**Figure 2C** and **Supplementary Table S1**). IL23a is a cytokine required for the expansion and survival of TH17 cells that also drives a pathogenic T cell population that induces inflammation (Aggarwal et al., 2003). The exact impact of IL23a upregulation is not clear. We also observed significant upregulation in CXCR2 gene expression, a chemokine that regulates neutrophil migration in a closed head injury model that may also play a role in secondary brain damage (Semple et al., 2010) (**Figure 2C** and **Supplementary Table S1**). The third most induced gene was CD109, which is known

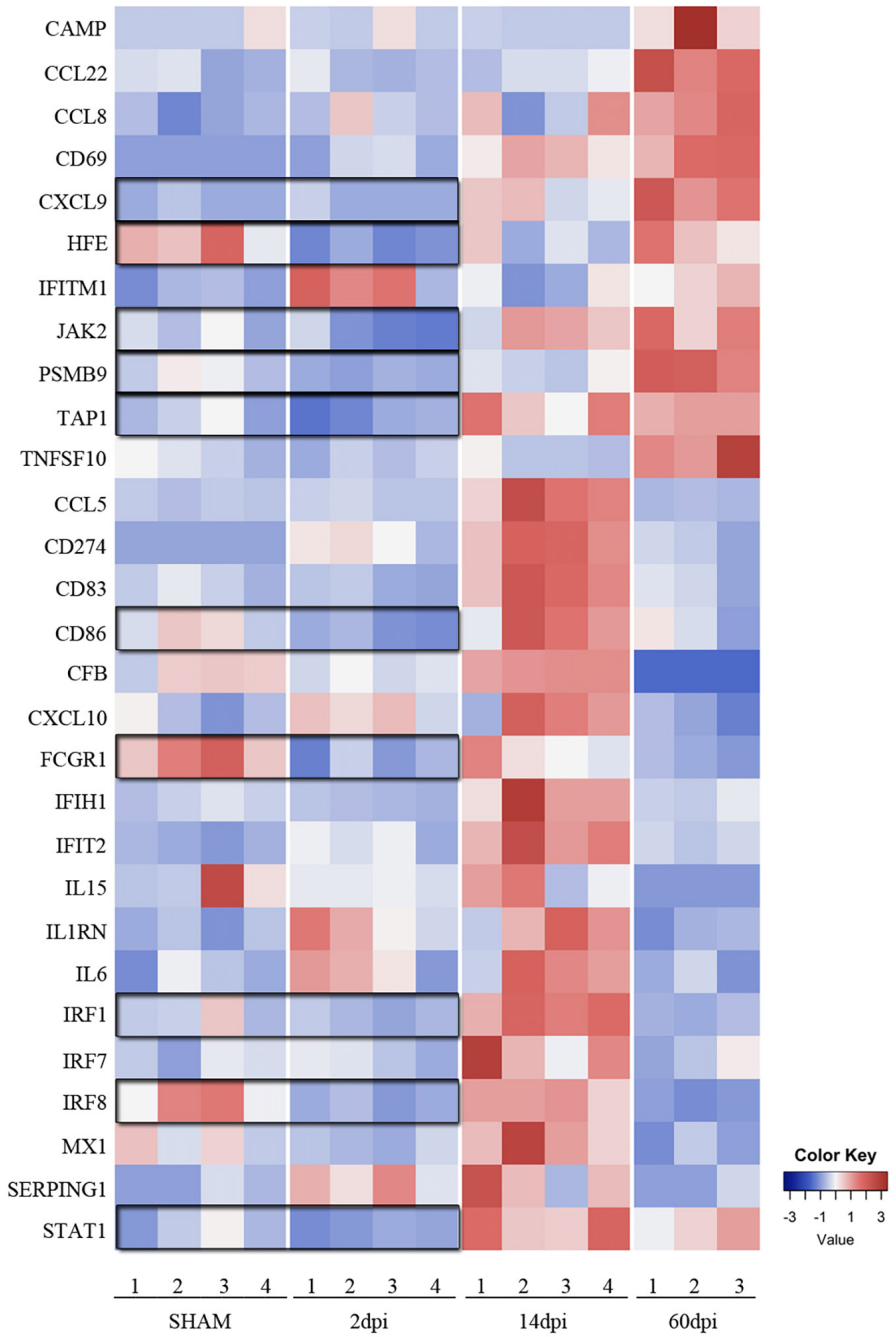

FIGURE 4 | Time-dependent changes of interferon gamma signaling pathway after TBI. Heatmap of genes in the interferon gamma signaling pathway at 2, 14, and 60 dpi vs. sham.

to modulate TGF-β receptor endocytosis and degradation and thereby play a critical role in inhibiting TGF-β signaling (Bizet et al., 2011; **Figure 2C** and **Supplementary Table S1**). We also found increased pro-inflammatory IL1 beta as well as CXC chemokine ligand 1 (CXCL1), a chemoattractant for neutrophils (Szmydynger-Chodobska et al., 2016; Arneson et al., 2018; **Supplementary Table S1**). Our findings at 2 dpi are consistent with a recently published single-cell RNA sequencing study which evaluated the impact of acute (1 dpi) fluid percussion injury on cell type-specific genes and found a significant increase in IL-1 beta and CXCL1, and Cebpb (Arneson et al., 2018). Together, the downregulation of IFNγ

and TGF-β cytokine pathways and concomitant upregulation of pro-inflammatory genes suggest a heterogenous inflammatory, stimulus-specific microglial activation state rather than a predominant proinflammatory "M1" or anti-inflammatory "M2" state as previously described for classical macrophage activation (Mills et al., 2000; Morganti et al., 2016b).

Microglia Gene Expression at 14 Days Post-injury

We identified 127 genes with statistically significantly altered expression in the subacute phase, including 103 upregulated and 24 downregulated vs. sham (**Figures 2A,B** and **Supplementary Table S2**). Similar to the 2 dpi findings, many upregulated genes were involved in chemokine signaling (CCL3, CCL4, CCL5, CCL8, CCL19, CXCL1, CXCL9, CXCL10, CXCL13, CXCR1, CXCR4) and proinflammatory cytokine signaling. Interferon gamma pathway genes including IRF1, IRF7, JAK2, MX1, STAT1, TAP1, CCL5, CCL8, CD274, CD69, CD86, CD83, CXCL10, CXCL9, lFIH1, LFIT2, IL1RN were significantly upregulated at 14 dpi compared to sham. Expression of TGF-β signaling genes, which were significantly downregulated vs. sham at 2 dpi, appeared to increase at 14 dpi compared to 2 dpi. In addition, CD109 continued to be one of the highest upregulated genes at this subacute timepoint (Bizet et al., 2011) even though TGFβ pathway genes were down (**Figure 2D** and **Supplementary Table S2**).

At 14 dpi, macrophage receptor with collagenous structure (Marco), a scavenger receptor on macrophages that regulates phagocyte innate immune responses, was one of the most significantly upregulated genes (Jing et al., 2013; **Figure 2D** and **Supplementary Table S2**). The complement system is another key mediator of the systemic innate inflammatory response which participates in many functions, including opsonization, phagocytosis, immune cell chemotaxis, and cell lysis, among others (Hammad et al., 2018). We found significant increases in gene expression of complement components C1s, C3, and C4a, which is consistent with an important role for complement at the subacute time point (Yager et al., 2008; Alawieh et al., 2018; Hammad et al., 2018). These data suggest increased capacity for phagocytosis at 14 dpi, possibly to promote debris clearance caused by injury. Interestingly, we also found significant upregulation of CD69, which is an immunomodulatory molecule induced during lymphocyte activation, deficiency of which has been recent found to associate with poor outcome after ischemic stroke (Brait et al., 2019; **Figure 2D** and **Supplementary Table S2**).

DNA Primase Subunit 1 (Prim1) and Cxcl3 were among the most downregulated genes at 14 dpi (**Supplementary Table S2**). Cxcl3 plays a key role in promoting neutrophil migration across epithelial barriers (Szmydynger-Chodobska et al., 2009; Liu et al., 2018). The finding that Cxcl3 is downregulated by 14 dpi is consistent with reduction of neutrophil infiltration at 7 days after CCI in rodents (Clark et al., 1994). Downregulation of a cyclic AMP (cAMP) pathway in the acute stages post-injury also persisted to 14 dpi (Atkins et al., 2007; **Figure 2D**). Restoration of cAMP levels in a fluid-percussion injury and other models of CNS injury was associated with improved functional outcome (Block et al., 1997; Nikulina et al., 2004; Atkins et al., 2007). Together, our findings suggest a dynamic gene expression response to CCI in microglia that is apparent at 14 dpi and includes reinstating TGF beta and IFNγ pathway gene expression as well as induction of phagocytosis pathways including complement.

Microglia Gene Expression in the Chronic Phase Post-injury (60 Dpi)

In the chronic phase post-injury, we observed 191 genes significantly changed, including 120 genes that were upregulated and 71 downregulated compared to sham (**Figures 2A,B** and **Supplementary Table S3**). Upregulated genes in the chronic phase were involved in adaptive and innate immune pathways as well as cytokine and chemokine signaling, suggesting an evolution toward a pro-inflammatory state in the chronic period (**Supplementary Table S3**). For instance, compared to sham, many genes in the IFNγ cytokine signaling pathway were significantly upregulated compared to sham at 60 dpi (**Figure 4**).

Il-3, a cytokine which stimulates proliferation of myeloid lineage cells was one of the most induced genes at 60 dpi (**Figure 2E**). Interestingly, injection of Il-3 and granulocyte macrophage colony stimulating factor together from 2 to 7 days after stab wound injury in rats attenuates brain tissue loss and improves motor function at 2 months, suggesting a reparative function for increased IL-3 (Nishihara et al., 2011). Tumor necrosis factor receptor superfamily member 8 (Tnfrsf8) was also one of the most significantly upregulated genes at 60 dpi, and is known to regulate the proliferative potential of autoreactive CD8 effector T cells and protect the body against autoimmunity (Oflazoglu et al., 2009; **Figure 2E**). We also found significant upregulation of IL-21 (**Figure 2E**). IL-21 is known to regulate immune responses by promoting antibody production, T cell-mediated immunity, and NK cell and $CD8^+$ T cell cytotoxicity; inhibiting IL-21 in experimental stroke correlated with improved behavioral outcome (Clarkson et al., 2014).

Several TBI studies observed significant upregulation of hypoxia-inducible transcription factor-1α (HIF-1α) acutely post-injury (Ding et al., 2009; Huang et al., 2010), we found significant downregulation of HIF-1α at 60 dpi (**Figure 2E** and **Supplementary Table S3**). HIF-1α upregulates genes involved with blood–brain barrier (BBB) disruption (Yan et al., 2011), edema formation (Higashida et al., 2011), and apoptosis (Bruick, 2000). A recent study in a closed head injury model showed that the inhibition of HIF-1α was associated with worse motor deficit, hypothermia, and increased lesion size, suggesting a role for HIF-1α in recovery after TBI (Umschweif et al., 2013). The correlation between HIF-1α downregulation at 60 dpi and long-term outcome cognitive deficits after CCI may suggest a functional role for HIF-1α in the chronic period.

Microglial Gene Expression Over the Course of CCI

In order to identify genes that follow a specific pattern over the three study time points, we performed pattern-oriented time-series modeling and clustering. According to

pairwise comparisons, there were 191 genes with significant time-dependent changes when we compared sham vs. 60 dpi (FDR < 0.05). Focusing on genes that were changed at 60 dpi, we built a clustering model to study their expression patterns over time (e.g., compared to 2 and 14 dpi). We found 13 meaningful clusters; 10 clusters had less than 5 genes, and 3 clusters with more than 5 genes are described below (**Supplementary Table S4** and **Supplementary Figure S3**).

The first cluster included 52 genes which were stable at 2 and 14 dpi and significantly upregulated at 60 dpi. Genes in this cluster were involved in secondary injury mechanisms including cytokine receptor and cytokines interactions, chemokine receptors, and immune, adaptive immune system, and cell-mediated toxicity. The second cluster included eight genes which were stable during acute but became significantly upregulated over the subacute and chronic time points post-injury. Two genes were involved in INF gamma signaling including (IRF3 and VCAM) and two other genes in hemostasis including (CLU, CD48). TNFSF12 and CD5 were also upregulated in this manner. The third cluster included five genes which were stable during acute and subacute time points and became significantly downregulated at chronic stages post-injury. Three genes involved in apoptosis were FADD, BAX, PSMB7, and two others involved in complement activation including ITGB2 (integrin, beta 2) (a complement component 3 receptor 3 and 4 subunit) as well as C1QBP (complement component 1, q subcomponent binding protein) (**Supplementary Figure S3**).

Changes in Microglia Sensome Genes After CCI

One of the major functions of microglia is sensing changes in the brain environment including injury signals (Hickman et al., 2018). Our group has previously identified 100 genes involved in this process that constitute what we termed the microglia "sensome" (Hickman et al., 2013). To determine the effects of CCI on the microglial sensome, we analyzed the pattern of changes of the sensome genes in response to CCI. Sensome genes that were significantly changed by CCI in a unique and time-dependent pattern (**Figure 3A**). Of the 46 sensome genes examined, we found the majority of sensome genes downregulated at 2 dpi with statistically significant downregulation of 21 of these genes and only 2 genes (Clec5a and Tlr2) that were significantly upregulated. Sensome gene expression began to normalize at 14 dpi with only some sensome genes that were upregulated (Tlr2, Cd86, Tyrobp, Ptafr, Icam1, Icam4, Ccrl2, Cd14, CD22, CD48, CD74) and five genes were significantly downregulated (Selplg, Gpr183, Ccr5, Lair1, Tnfrsf13b). The trend continued at 60 dpi, where only five sensome genes remained upregulated (Tyrobp, Cd74, Ltf, CD22, CD48) (**Figure 3A**). Sensome genes, like TREM2, (triggering receptor expressed on myeloid cells 2), which play a key role in transforming microglia from a homeostatic to a neural disease-associated state was also found to be downregulated at 2 dpi followed by upregulation at later time points (Hickman and El Khoury, 2014; **Figure 3A**).

Together, the data suggest a biphasic pattern of changes in the sensome genes represented by initial downregulation at 2 dpi followed by return to baseline of the majority of these genes at 14 and 60 days (**Figure 3A**). These changes suggest that there may be dysregulation in ability of microglia to sense tissue damage, perform housekeeping, and maintain hemostasis in the early stages after CCI with possible subsequent recovery over time.

Cytokine Gene Expression Signatures After CCI

To determine the time-dependent effect of TBI on the microglia cytokine pathways, we mined our gene set for cytokine regulated genes as defined by Xue et al. (2014). As we observed with sensome genes, we also found a time-dependent change in genes involved in cytokine pathways following TBI. Interestingly, in parallel to changes in the sensome changes, we found downregulation of genes involved in the TGFβ pathway at 2 dpi (**Figure 3B**) TGF-β is required for maintaining the microglial homeostatic state (Butovsky et al., 2014) and is likely needed for maintaining expression of sensome genes. Our data suggest that downregulation of sensome genes at 2 dpi is possibly linked to downregulation of the TGFβ pathway at this early time point post-injury.

In contrast to sensome and TGFβ pathway genes, genes from various cytokine pathways were mostly upregulated at 14 dpi. These include genes from pro- and anti-inflammatory pathways such as IL-6, Interferon-gamma (proinflammatory), and IL-4 and IL-10 (anti-inflammatory) indicating a mixed pattern of gene regulation (**Figures 4**, **5**) that participate in injury and repair mechanisms. Our data are consistent with other TBI studies which suggest that the role of microglia in the CCI model is more complex than the oversimplified prior classification of M1 vs. M2 (Kumar et al., 2016; Morganti et al., 2016b). This mixed state appears to persist at 14 and 60 dpi.

Interestingly, a pattern of regulation of cytokine pathways genes including IL-10, IL-4, interferon gamma, and IL-1 emerged. Genes upregulated at 14 dpi returned to baseline at 60 dpi, whereas genes that remained stable at 14 dpi were upregulated at 60 dpi (**Figures 4**, **5**). Such pattern suggests a defined sequence of gene expression changes post-TBI.

Potential Regulators of Gene Networks in TBI

To identify known and predicted functional protein–protein interactions relevant to the microglia transcriptome after CCI, we used the STRING v11.0 database (von Mering et al., 2003). STRING quantitatively integrates protein interaction data from multiple sources for a large number of organisms.

At 14 dpi, TNF (direct association of 82 out of 102 genes), IL6 (direct association of 78 out of 102 genes), and Toll-like receptor-2 (direct association of 62 out of 102) were among the top most confident centers of microglial upregulated gene networks. These findings are consistent with studies showing a critical role for IL 6 (Poulsen et al., 2005), TNF (Longhi et al., 2013), and TLR-mediated signaling (Hua et al., 2011) pathways in induction and regulation of inflammatory responses in the acute stages following injury. Our study provides evidence of a role in the subacute stages post-injury, consistent with a prior study

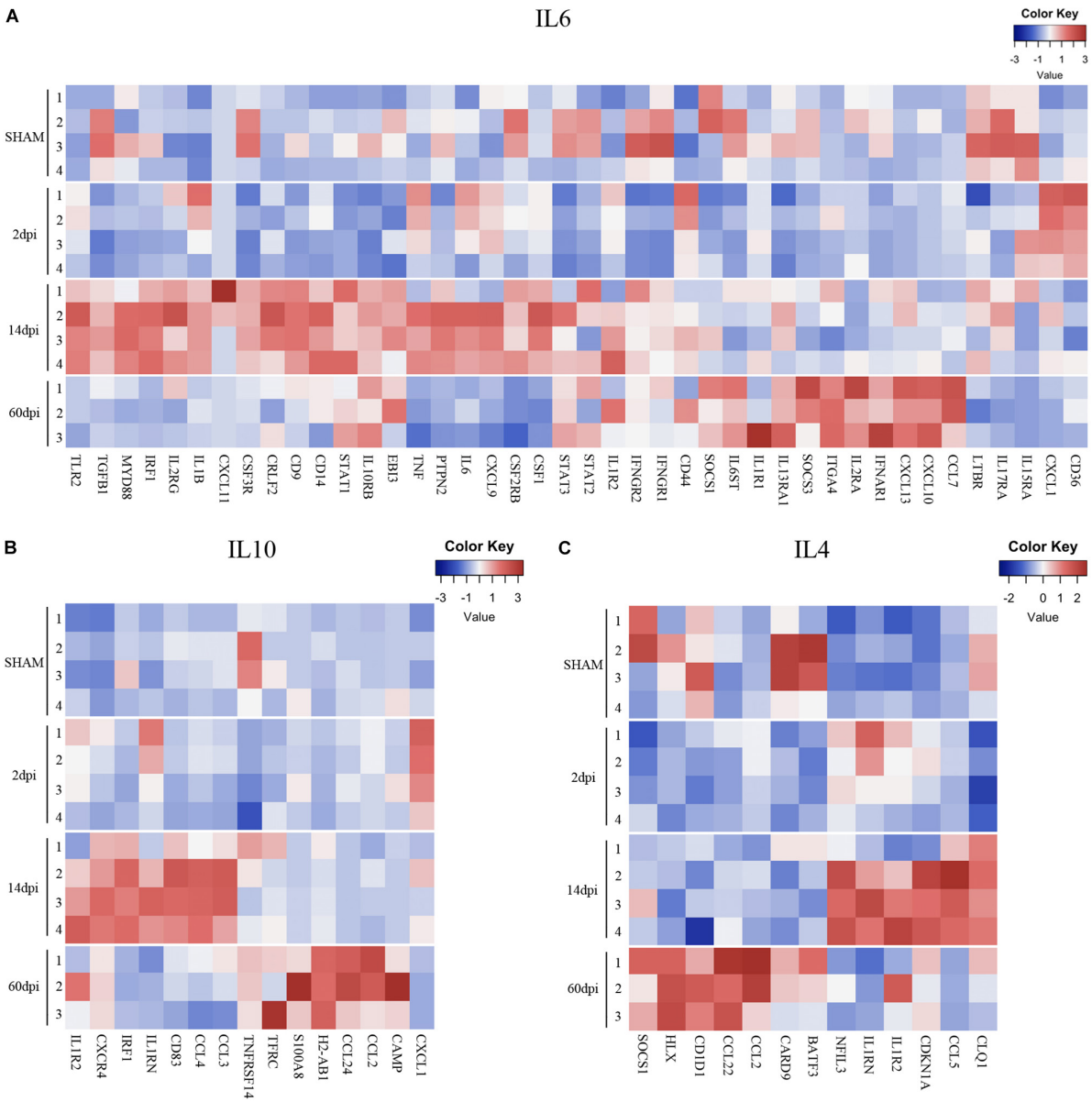

FIGURE 5 | Pro- and anti-inflammatory cytokine gene expression profiles after TBI. Heatmap of normalized gene expressions profiles for **(A)** IL6, **(B)** IL10, and **(C)** IL4 signaling pathways.

showing differential effects of TNF knockout on motor function early vs. late after CCI (Bermpohl et al., 2007; **Figure 6A**).

One of the top downregulated genes with the highest confidence in microglial gene networks at 14 dpi was CCR5. CCR5 is a cysteine–cysteine chemokine receptor which is highly expressed in microglia and is important for chemotaxis, *in vitro* and *in vivo* (Bajetto et al., 2002). Pharmacological blockade of CCR5 reduced migration velocity and the number of perilesional migratory microglia in a model of focal brain injury (Carbonell et al., 2005). Downregulation of CCR5 might impact microglia migration to injured brain regions at a subacute phase post insult. In addition, previous work used CCR2/5 inhibitor in aged animals following TBI showed significant reduction in the recruitment of peripheral macrophages to the injured site and decrease in their pro-inflammatory response (Morganti et al., 2016a). Another recent study used CCR5 knockdown showed improved cognitive recovery in a pre-clinical closed head injury TBI model and also associated with enhanced motor recovery after stroke in patients with mutated CCR5 gene (Joy et al., 2019).

At 60 dpi, CD40 is one of the upregulated genes with the highest confidence in the microglial gene networks with direct association of 59 of 112 genes. CD40 is a member of the tumor necrosis factor (TNF) receptor superfamily.

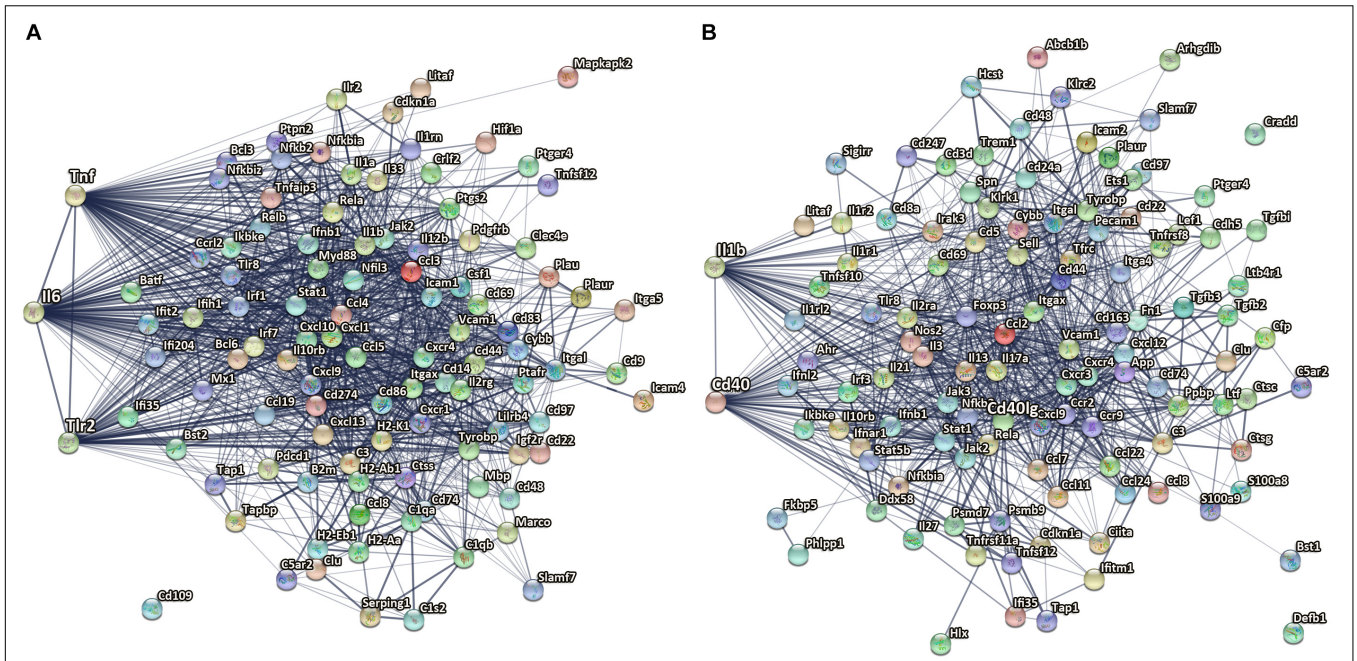

FIGURE 6 | Microglial genes with highest confidence in gene networks after TBI. **(A)** TNF, IL6, and Tlr2 are among the top most confident centers of microglial upregulated genes network at 14 dpi. **(B)** IL-1β and CD40 are among the top 10 upregulated genes with the highest confidence in microglial gene networks at 60 dpi. The edge thickness indicates the strength of data support by STRING analysis, from thin, medium to thick corresponds to confident score 0.4, 0.7, and 0.9. The nodes are colored in alphabetical order of protein name, graphs in each node are known or predicted 3D structure.

CD40 is a receptor on antigen-presenting cells (including macrophages and microglia) and an essential mediator of various inflammatory responses (Elgueta et al., 2009). Abnormal expression of CD40 has been associated with autoimmune inflammatory diseases such as multiple sclerosis (Aarts et al., 2017), as well as AD pathology in experimental animals (Calingasan et al., 2002; Laporte et al., 2006). Furthermore, antagonizing CD40L and genetic disruption of CD40 signaling improved cognitive function and AD-related pathology in AD animal models (Tan et al., 2002; Laporte et al., 2006; **Figure 6B**).

In addition, IL-1β was also found to be among the top 10 upregulated genes with the highest confidence in microglial gene networks at 60 dpi. IL-1β is a pro-inflammatory cytokine that is upregulated as part of the acute inflammatory innate host response to trauma, infection, and other types of injury (Garlanda et al., 2013; **Figure 6B**). IL-1β is also known to be a key mediator of neuronal function (Smith et al., 2009), glial activation, and immune cell recruitment as well as neurodegeneration in CNS injury models and neurodegenerative diseases (Wang et al., 2015). IL-1β is acutely increased after TBI in humans and experimental TBI models, and blocking its activity has been shown to be beneficial in experimental models of TBI (Clausen et al., 2009, 2011; McKee and Lukens, 2016). The genetic antagonism of IL-1R1 had divergent effects on neurological function in focal vs. diffuse injury TBI models (Chung et al., 2019). In line with the literature we identified IL-1β to be a key regulator not only at acute and subacute time points but also at chronic stages (60 dpi) after CCI. The association between IL-1β chronic inflammatory profiles and long-term outcome post-injury should be further evaluated.

Effects of Injury on the Microglial Biological Pathways

We performed GSEA (Online Methods) to identify pathways that are differentially changed in microglia post-injury. GSEA pathway analyses showed upregulation of multiple mechanisms in chronic time points post-injury including immune system, cytokine–cytokine receptor interaction, KEGG chemokine signaling, adaptive immune system, KEGG cell adhesion CAMs, JAK-STAT signaling pathways, and cytotoxicity. Interferon signaling, Toll receptor cascades, NOD-like receptor signaling, and IFN alfa and beta pathways were more upregulated at 14 dpi. These data constitute further evidence of a time-dependent injury-associated change in the microglial phenotype toward a pro-inflammatory state (**Supplementary Figure S4**).

Relative Expressions of Selected Microglia Genes for Sham vs. 2 Dpi Were Measured by Real-Time qPCR

To validate our Nanostring gene expression analysis, RT^2 qPCR was used to measure the relative expression of three upregulated genes including (TNF, IL1b, and IL6). Similar to the 2 dpi Nanostring data, there was significant upregulation of these three genes at 2 dpi when compared sham vs. injured mice ($n = 3$) (**Supplementary Figure S5**).

DISCUSSION

To our knowledge this is the first study to define the temporal course of microglial inflammation-related gene expression at acute, subacute, and chronic time points in a pre-clinical TBI model. We identified gene expression changes suggesting dysregulation of the ability of microglia to sense tissue damage, perform housekeeping functions, and maintain homeostasis in the early stages post-CCI, with subsequent recovery of these pathways over time. We also identified injury-associated changes in the microglial phenotype toward a chronic pro-inflammatory state post-TBI.

Microglia have extensive processes that allow them to detect changes in their environment. For this purpose, microglia also have an armamentarium of cellular receptors and proteins previously defined by our group as the "microglia sensome" (Hickman et al., 2013). In this dataset, we found downregulation of microglia sensome genes at 2 dpi followed by upregulation at later time points. Dysregulation of microglial sensome early after TBI has not been previously reported in a TBI model. Further studies are needed to assess the functional impact of sensome gene downregulation after CCI.

Our data also suggest that TGF-β cytokine signaling behaved in a pattern similar to sensome genes at 2 dpi. TGF-β is essential for maintaining a microglial homeostatic phenotype (Butovsky et al., 2014). The downregulation of TGF-β may in part regulate the reduced expression of microglial sensome genes at 2 dpi. TGFβ signaling is involved in regulating microglial activation and its disruption could potential lead to neuroinflammatory response dysregulation, increased cytotoxicity (Brionne et al., 2003), and it also has to be associated with many neurodegenerative diseases including AD (Town et al., 2008; von Bernhardi et al., 2015). The cross talk between TGF-β and microglia sensome post-injury has not been fully evaluated in TBI and given the key regulatory role of this signaling pathway, further studies are needed to evaluate the TGFβ-mediated effects on microglial functions and long-term outcome in TBI.

Of note, triggering receptor expressed on myeloid cells 2 (TREM2), an innate immune receptor expressed on the surface of microglia, was also significantly downregulated at 2 dpi compared to sham then returned to baseline expression by 14 dpi. TREM2 is also part of the microglial sensome and is expressed on dendritic cells, osteoclasts, and macrophages (Hickman et al., 2013). TREM2 forms a signaling complex with the adaptor tyrosine kinase-binding protein (TyroBP or DAP12) which in turn plays critical roles in regulating microglia activation, enhance their sensing functions, survival, phagocytosis, and cytokine production (Hickman and El Khoury, 2014). In addition, TREM2–DAP12 signaling plays a central role in the pathogenesis of several diseases (beneficial for some diseases and harmful for others) including frontotemporal dementia, AD, and multiple sclerosis (Hickman and El Khoury, 2014; Hickman et al., 2018). However, the role of TREM2–DAP12 signaling in TBI is still not yet known. Trem2 knockout mice had reduced macrophage infiltration at 3 dpi, and reduced hippocampal atrophy, and improved behavioral outcome at 120 dpi in a lateral fluid percussion model, suggesting a role for TREM2 in outcome after cerebral contusion (Saber et al., 2017). Further studies are warranted to further investigating the role of this key microglial regulator post-injury.

The proinflammatory IFNγ genes had a more complex response post-TBI. A large number of genes in this pathway were upregulated at 14 dpi. Interestingly, those genes returned to baseline at 60 dpi. Interestingly, genes in this pathway that remained unchanged at 14 dpi were upregulated at 60 dpi. IFNγ upregulates the neurotoxic pathways in microglia including reactive oxygen species (ROS) production and others, as well as genes involved in antigen presentation and proinflammatory T-lymphocyte-related chemokines (Takeuchi et al., 2006; Moran et al., 2007; Spencer et al., 2016). Similarly, CCI upregulated the anti-inflammatory cytokine pathways of IL-4 and IL-10 response genes at 14 and 60 dpi. Our data suggest there is a biphasic pattern of IFNγ, IL-4, and IL-10 gene expression changes, with concurrent proinflammatory and anti-inflammatory states at subacute and chronic timepoints post-TBI. This mixed inflammatory profile indicates that the oversimplified pro-inflammatory "M1"and anti-inflammatory "M2" polarization states do not necessarily reflect the diversity of microglia functions and their related signaling pathways during complex diseases such as TBI (Morganti et al., 2016b; Hirbec et al., 2017; Jassam et al., 2017).

Our study has some limitations; first, our sampling method using the entire brain to interrogate microglia gene expression is limited by inclusion of microglia that may not undergo significant morphological changes but may still perhaps undergo transcriptional changes even though distant from contusion. We think our methodology is the most non-biased, but we do recognize that we may lose some signal with this approach. Further single cell studies to evaluate the regional differences in microglia activation after injury are warranted. Second, sex-specific transcriptomic profiles were found when comparing adult female and male mice (Hanamsagar et al., 2017); however, we used only male mice in our study, and future studies in addressing the impact of gender on microglial gene expression at acute and chronic timepoints.

The generation of our transcriptomic data sets is an important step forward to understand microglia biology and functional diversity and their role in TBI pathogenesis at the molecular level and identify common pathways that affect outcome. However, because of the mixed picture noted in the subacute and chronic stage, we need to better understand cellular cross talk post-injury at the single cell level, taking into consideration age, gender, and anatomical proximity to the injury to establish definitive profiles for microglia during different stages of TBI. Recent, single-cell RNA-Seq to study the impact of concussive injury on single cell hippocampal cell types in the acute stage is a step in the right direction (Arneson et al., 2018). More studies to evaluate gene expression at the single cell level and

in focusing on subacute and chronic timepoint are warranted. Establishing a definitive quantitative time-dependent microglia transcriptome post focal head injury will open the door for more precise experimentation using targeted gene deletion with Cre–Lox approach and inducible microglia promoter-specific gene manipulation to identify potential novel targets for treatment of TBI.

DATA AVAILABILITY

The gene expression data have been uploaded to the GEO repository. Following is the associated link https://www.ncbi.nlm.nih.gov/geo/query/acc.cgi?acc=GSE132809.

ETHICS STATEMENT

Experiments were performed and animals were treated humanely according to ARRIVE guidelines. All procedures were performed in accordance with the NIH Guide for Care and Use of Laboratory Animals and followed protocols approved by the MGH Institutional Animal Care and Use Committee.

AUTHOR CONTRIBUTIONS

SI, ZF, SL, SH, NP, DK, JK, and MW: manuscript conception and design. QL: equal contribution to the manuscript concept and design, acquisition of data, analysis and interpretation, and critical revision of the manuscript for important intellectual content. CP: acquisition and analysis of the data. SI, SL, LW, JC, AS-S, AB-W, SH, JK, and MW: acquisition of the data, and analysis and interpretation. QL, ZF, SL, JC, AS-S, NP, and DK: critical revision of the manuscript for important intellectual content. SI, LW, SH, JK, and MW: critical revision of the manuscript for important intellectual content and study supervision.

FUNDING

This work was supported by the National Institute on Aging (NIA) Grant 1RF1AG051506 (to JK), the R01NS092847-01 (to DK), and National Natural Science Fund of China 31871029 (to QL).

SUPPLEMENTARY MATERIAL

The Supplementary Material for this article can be found online at: https://www.frontiersin.org/articles/10.3389/fncel.2019.00307/full#supplementary-material

FIGURE S1 | Gating strategy for flow cytometry. Gates for sorting population of microglia (CD11b high and CD45 low to intermediate) are shown.

FIGURE S2 | Sensitivity analysis of *p*-measurement by cutoff$_{high}$ and cutoff$_{low}$ in pattern-oriented time-series clustering. Higher *p*-measurement corresponds to less noise in clusters of genes.

FIGURE S3 | REACTOM pathways of three clusters that follow a specific pattern over the three study time points. Pathway analysis of level of significance by –log10(FDR) of up-regulated genes in the three comparisons from left to right: stable-stable-up, stable-up-up, and stable-stable-down. Genes in the stable-stable-up cluster were involved in secondary injury mechanisms including cytokine receptor and cytokines interactions, chemokine receptors, and immune, adaptive immune system, and cell-mediated toxicity.

FIGURE S4 | REACTOM pathways. Pathway analysis of level of significance by –log10(FDR) of up-regulated genes in the three comparisons from left to right: 2 dpi vs. sham, 14 dpi vs. sham, and 60 dpi vs. sham. This showed that the pathways are most significantly altered in 14 and 60 dpi.

FIGURE S5 | Relative expressions of selected microglia genes for sham vs. 2 dpi were verified by real-time qPCR. Relative RNA expression of selected genes including TNF, IL1b, and IL6 RNA measured by PCR in sham vs. injured groups ($n = 3$) at 2 dpi. Consistent with the Nanostring data, there is significant upregulation of TNF, IL1b, and IL6 at 2 dpi in CCI injured vs. sham mice. Error bars indicate standard errors of the mean. $^*p < 0.05$.

TABLE S1 | List of significantly changed genes at 2 dpi vs. sham.

TABLE S2 | List of significantly changed genes at 14 dpi vs. sham.

TABLE S3 | List of significantly changed genes at 60 dpi vs. sham.

TABLE S4 | List of clusters and genes per cluster that follow a specific pattern over the three study time points.

REFERENCES

Aarts, S., Seijkens, T. T. P., van Dorst, K. J. F., Dijkstra, C. D., Kooij, G., and Lutgens, E. (2017). The CD40-CD40L dyad in experimental autoimmune encephalomyelitis and multiple sclerosis. *Front. Immunol.* 8:1791. doi: 10.3389/fimmu.2017.01791

Aggarwal, S., Ghilardi, N., Xie, M. H., de Sauvage, F. J., and Gurney, A. L. (2003). Interleukin-23 promotes a distinct CD4 T cell activation state characterized by the production of interleukin-17. *J. Biol. Chem.* 278, 1910–1914. doi: 10.1074/jbc.M207577200

Alawieh, A., Langley, E. F., Weber, S., Adkins, D., and Tomlinson, S. (2018). Identifying the role of complement in triggering neuroinflammation after traumatic brain injury. *J. Neurosci.* 38, 2519–2532. doi: 10.1523/JNEUROSCI.2197-17.2018

Almeida-Suhett, C. P., Li, Z., Marini, A. M., Braga, M. F., and Eiden, L. E. (2014). Temporal course of changes in gene expression suggests a cytokine-related mechanism for long-term hippocampal alteration after controlled cortical impact. *J. Neurotrauma* 31, 683–690. doi: 10.1089/neu.2013.3029

Arneson, D., Zhang, G., Ying, Z., Zhuang, Y., Byun, H. R., Ahn, I. S., et al. (2018). Single cell molecular alterations reveal target cells and pathways of concussive brain injury. *Nat. Commun.* 9:3894. doi: 10.1038/s41467-018-06222-0

Atkins, C. M., Oliva, A. A. Jr., Alonso, O. F., Pearse, D. D., Bramlett, H. M., and Dietrich, W. D. (2007). Modulation of the cAMP signaling pathway after traumatic brain injury. *Exp. Neurol.* 208, 145–158. doi: 10.1016/j.expneurol.2007.08.011

Bajetto, A., Bonavia, R., Barbero, S., and Schettini, G. (2002). Characterization of chemokines and their receptors in the central nervous system: physiopathological implications. *J. Neurochem.* 82, 1311–1329. doi: 10.1046/j.1471-4159.2002.01091.x

Bermpohl, D., You, Z., Lo, E. H., Kim, H. H., and Whalen, M. J. (2007). TNF alpha and Fas mediate tissue damage and functional outcome after traumatic brain

injury in mice. *J. Cereb. Blood Flow Metab.* 27, 1806–1818. doi: 10.1038/sj.jcbfm.9600487

Bizet, A. A., Liu, K., Tran-Khanh, N., Saksena, A., Vorstenbosch, J., Finnson, K. W., et al. (2011). The TGF-beta co-receptor, CD109, promotes internalization and degradation of TGF-beta receptors. *Biochim. Biophys. Acta* 1813, 742–753. doi: 10.1016/j.bbamcr.2011.01.028

Block, F., Tondar, A., Schmidt, W., and Schwarz, M. (1997). Delayed treatment with rolipram protects against neuronal damage following global ischemia in rats. *Neuroreport* 8, 3829–3832. doi: 10.1097/00001756-199712010-00033

Brait, V. H., Miro-Mur, F., Perez-de-Puig, I., Notario, L., Hurtado, B., Pedragosa, J., et al. (2019). CD69 plays a beneficial role in ischemic stroke by dampening endothelial activation. *Circ. Res.* 124, 279–291. doi: 10.1161/CIRCRESAHA.118.313818

Brionne, T. C., Tesseur, I., Masliah, E., and Wyss-Coray, T. (2003). Loss of TGF-beta 1 leads to increased neuronal cell death and microgliosis in mouse brain. *Neuron* 40, 1133–1145. doi: 10.1016/s0896-6273(03)00766-9

Bruick, R. K. (2000). Expression of the gene encoding the proapoptotic Nip3 protein is induced by hypoxia. *Proc. Natl. Acad. Sci. U.S.A.* 97, 9082–9087. doi: 10.1073/pnas.97.16.9082

Butovsky, O., Jedrychowski, M. P., Moore, C. S., Cialic, R., Lanser, A. J., Gabriely, G., et al. (2014). Identification of a unique TGF-beta-dependent molecular and functional signature in microglia. *Nat. Neurosci.* 17, 131–143. doi: 10.1038/nn.3599

Calingasan, N. Y., Erdely, H. A., and Altar, C. A. (2002). Identification of CD40 ligand in Alzheimer's disease and in animal models of Alzheimer's disease and brain injury. *Neurobiol. Aging* 23, 31–39. doi: 10.1016/s0197-4580(01)00246-9

Carbonell, W. S., Murase, S., Horwitz, A. F., and Mandell, J. W. (2005). Migration of perilesional microglia after focal brain injury and modulation by CC chemokine receptor 5: an in situ time-lapse confocal imaging study. *J. Neurosci.* 25, 7040–7047. doi: 10.1523/JNEUROSCI.5171-04.2005

Chiu, I. M., Morimoto, E. T., Goodarzi, H., Liao, J. T., O'Keeffe, S., Phatnani, H. P., et al. (2013). A neurodegeneration-specific gene-expression signature of acutely isolated microglia from an amyotrophic lateral sclerosis mouse model. *Cell Rep.* 4, 385–401. doi: 10.1016/j.celrep.2013.06.018

Chung, J. Y., Krapp, N., Wu, L., Lule, S., McAllister, L. M., Edmiston, W. J., et al. (2019). Interleukin-1 receptor 1 deletion in focal and diffuse experimental traumatic brain injury in mice. *J. Neurotrauma* 36, 370–379. doi: 10.1089/neu.2018.5659

Clark, R. S., Schiding, J. K., Kaczorowski, S. L., Marion, D. W., and Kochanek, P. M. (1994). Neutrophil accumulation after traumatic brain injury in rats: comparison of weight drop and controlled cortical impact models. *J. Neurotrauma* 11, 499–506. doi: 10.1089/neu.1994.11.499

Clarkson, B. D., Ling, C., Shi, Y., Harris, M. G., Rayasam, A., Sun, D., et al. (2014). T cell-derived interleukin (IL)-21 promotes brain injury following stroke in mice. *J. Exp. Med.* 211, 595–604. doi: 10.1084/jem.20131377

Clausen, F., Hanell, A., Bjork, M., Hillered, L., Mir, A. K., Gram, H., et al. (2009). Neutralization of interleukin-1beta modifies the inflammatory response and improves histological and cognitive outcome following traumatic brain injury in mice. *Eur. J. Neurosci.* 30, 385–396. doi: 10.1111/j.1460-9568.2009.06820.x

Clausen, F., Hanell, A., Israelsson, C., Hedin, J., Ebendal, T., Mir, A. K., et al. (2011). Neutralization of interleukin-1beta reduces cerebral edema and tissue loss and improves late cognitive outcome following traumatic brain injury in mice. *Eur. J. Neurosci.* 34, 110–123. doi: 10.1111/j.1460-9568.2011.07723.x

Coughlin, J. M., Wang, Y., Munro, C. A., Ma, S., Yue, C., Chen, S., et al. (2015). Neuroinflammation and brain atrophy in former NFL players: an in vivo multimodal imaging pilot study. *Neurobiol. Dis.* 74, 58–65. doi: 10.1016/j.nbd.2014.10.019

Das, M., Mohapatra, S., and Mohapatra, S. S. (2012). New perspectives on central and peripheral immune responses to acute traumatic brain injury. *J. Neuroinflammation* 9:236. doi: 10.1186/1742-2094-9-236

Ding, J. Y., Kreipke, C. W., Speirs, S. L., Schafer, P., Schafer, S., and Rafols, J. A. (2009). Hypoxia-inducible factor-1alpha signaling in aquaporin upregulation after traumatic brain injury. *Neurosci. Lett.* 453, 68–72. doi: 10.1016/j.neulet.2009.01.077

Donat, C. K., Scott, G., Gentleman, S. M., and Sastre, M. (2017). Microglial activation in traumatic brain injury. *Front. Aging Neurosci.* 9:208. doi: 10.3389/fnagi.2017.00208

Hirbec, H. E., Noristani, H. N., and Perrin, F. E. (2017). Microglia responses in acute and chronic neurological diseases: what microglia-specific transcriptomic studies taught (and did Not Teach) Us. *Front. Aging Neurosci.* 9:227. doi: 10.3389/fnagi.2017.00227

Elgueta, R., Benson, M. J., de Vries, V. C., Wasiuk, A., Guo, Y., and Noelle, R. J. (2009). Molecular mechanism and function of CD40/CD40L engagement in the immune system. *Immunol. Rev.* 229, 152–172. doi: 10.1111/j.1600-065X.2009.00782.x

Fox, G. B., Fan, L., Levasseur, R. A., and Faden, A. I. (1998). Sustained sensory/motor and cognitive deficits with neuronal apoptosis following controlled cortical impact brain injury in the mouse. *J. Neurotrauma* 15, 599–614. doi: 10.1089/neu.1998.15.599

Garlanda, C., Dinarello, C. A., and Mantovani, A. (2013). The interleukin-1 family: back to the future. *Immunity* 39, 1003–1018. doi: 10.1016/j.immuni.2013.11.010

Gentleman, S. M., Leclercq, P. D., Moyes, L., Graham, D. I., Smith, C., Griffin, W. S., et al. (2004). Long-term intracerebral inflammatory response after traumatic brain injury. *Forensic Sci. Int.* 146, 97–104. doi: 10.1016/j.forsciint.2004.06.027

Gordon, W. A., Zafonte, R., Cicerone, K., Cantor, J., Brown, M., Lombard, L., et al. (2006). Traumatic brain injury rehabilitation: state of the science. *Am. J. Phys. Med. Rehabil.* 85, 343–382. doi: 10.1097/01.phm.0000202106.01654.61

Hammad, A., Westacott, L., and Zaben, M. (2018). The role of the complement system in traumatic brain injury: a review. *J. Neuroinflammation* 15:24. doi: 10.1186/s12974-018-1066-z

Hanamsagar, R., Alter, M. D., Block, C. S., Sullivan, H., Bolton, J. L., and Bilbo, S. D. (2017). Generation of a microglial developmental index in mice and in humans reveals a sex difference in maturation and immune reactivity. *Glia* 65, 1504–1520. doi: 10.1002/glia.23176

Helmick, K., and Members of Consensus Conference (2010). Cognitive rehabilitation for military personnel with mild traumatic brain injury and chronic post-concussional disorder: results of April 2009 consensus conference. *NeuroRehabilitation* 26, 239–255. doi: 10.3233/NRE-2010-0560

Hickman, S., Izzy, S., Sen, P., Morsett, L., and El Khoury, J. (2018). Microglia in neurodegeneration. *Nat. Neurosci.* 21, 1359–1369. doi: 10.1038/s41593-018-0242-x

Hickman, S. E., and El Khoury, J. (2014). TREM2 and the neuroimmunology of Alzheimer's disease. *Biochem. Pharmacol.* 88, 495–498. doi: 10.1016/j.bcp.2013.11.021

Hickman, S. E., Kingery, N. D., Ohsumi, T. K., Borowsky, M. L., Wang, L. C., Means, T. K., et al. (2013). The microglial sensome revealed by direct RNA sequencing. *Nat. Neurosci.* 16, 1896–1905. doi: 10.1038/nn.3554

Higashida, T., Peng, C., Li, J., Dornbos, D. III, Teng, K., Li, X., et al. (2011). Hypoxia-inducible factor-1alpha contributes to brain edema after stroke by regulating aquaporins and glycerol distribution in brain. *Curr. Neurovasc. Res.* 8, 44–51. doi: 10.2174/156720211794520251

Hua, F., Wang, J., Ishrat, T., Wei, W., Atif, F., Sayeed, I., et al. (2011). Genomic profile of Toll-like receptor pathways in traumatically brain-injured mice: effect of exogenous progesterone. *J. Neuroinflammation* 8:42. doi: 10.1186/1742-2094-8-42

Huang, R. Q., Cheng, H. L., Zhao, X. D., Dai, W., Zhuang, Z., Wu, Y., et al. (2010). Preliminary study on the effect of trauma-induced secondary cellular hypoxia in brain injury. *Neurosci. Lett.* 473, 22–27. doi: 10.1016/j.neulet.2010.02.011

Jassam, Y. N., Izzy, S., Whalen, M., McGavern, D. B., and El Khoury, J. (2017). Neuroimmunology of traumatic brain injury: time for a paradigm shift. *Neuron* 95, 1246–1265. doi: 10.1016/j.neuron.2017.07.010

Jing, J., Yang, I. V., Hui, L., Patel, J. A., Evans, C. M., Prikeris, R., et al. (2013). Role of macrophage receptor with collagenous structure in innate immune tolerance. *J. Immunol.* 190, 6360–6367. doi: 10.4049/jimmunol.1202942

Joy, M. T., Ben Assayag, E., Shabashov-Stone, D., Liraz-Zaltsman, S., Mazzitelli, J., Arenas, M., et al. (2019). CCR5 is a therapeutic target for recovery after stroke and traumatic brain injury. *Cell* 176, 1143–1157.e13. doi: 10.1016/j.cell.2019.01.044

Kobori, N., Clifton, G. L., and Dash, P. (2002). Altered expression of novel genes in the cerebral cortex following experimental brain injury. *Brain Res. Mol. Brain Res.* 104, 148–158. doi: 10.1016/s0169-328x(02)00331-5

Kumar, A., Alvarez-Croda, D. M., Stoica, B. A., Faden, A. I., and Loane, D. J. (2016). Microglial/macrophage polarization dynamics following traumatic brain injury. *J. Neurotrauma* 33, 1732–1750. doi: 10.1089/neu.2015.4268

Langlois, J. A., Rutland-Brown, W., and Wald, M. M. (2006). The epidemiology and impact of traumatic brain injury: a brief overview. *J. Head Trauma Rehabil.* 21, 375–378. doi: 10.1097/00001199-200609000-00001

Laporte, V., Ait-Ghezala, G., Volmar, C. H., and Mullan, M. (2006). CD40 deficiency mitigates Alzheimer's disease pathology in transgenic mouse models. *J. Neuroinflammation* 3:3. doi: 10.1186/1742-2094-3-3

Lipponen, A., Paananen, J., Puhakka, N., and Pitkanen, A. (2016). Analysis of post-traumatic brain injury gene expression signature reveals tubulins, Nfe2l2, Nfkb, Cd44, and S100a4 as treatment targets. *Sci. Rep.* 6:31570. doi: 10.1038/srep31570

Liu, Y. W., Li, S., and Dai, S. S. (2018). Neutrophils in traumatic brain injury (TBI): friend or foe? *J. Neuroinflammation* 15:146. doi: 10.1186/s12974-018-1173-x

Loane, D. J., Kumar, A., Stoica, B. A., Cabatbat, R., and Faden, A. I. (2014). Progressive neurodegeneration after experimental brain trauma: association with chronic microglial activation. *J. Neuropathol. Exp. Neurol.* 73, 14–29. doi: 10.1097/NEN.0000000000000021

Longhi, L., Perego, C., Ortolano, F., Aresi, S., Fumagalli, S., Zanier, E. R., et al. (2013). Tumor necrosis factor in traumatic brain injury: effects of genetic deletion of p55 or p75 receptor. *J. Cereb. Blood Flow Metab.* 33, 1182–1189. doi: 10.1038/jcbfm.2013.65

Matzilevich, D. A., Rall, J. M., Moore, A. N., Grill, R. J., and Dash, P. K. (2002). High-density microarray analysis of hippocampal gene expression following experimental brain injury. *J. Neurosci. Res.* 67, 646–663. doi: 10.1002/jnr.10157

McCrory, P., Meeuwisse, W., Johnston, K., Dvorak, J., Aubry, M., Molloy, M., et al. (2009). Consensus statement on concussion in sport: the 3rd international conference on concussion in sport held in Zurich, November 2008. *J. Athl. Train* 44, 434–448. doi: 10.4085/1062-6050-44.4.434

McKee, C. A., and Lukens, J. R. (2016). Emerging roles for the immune system in traumatic brain injury. *Front. Immunol.* 7:556. doi: 10.3389/fimmu.2016.00556

McKinlay, A., Grace, R. C., Horwood, L. J., Fergusson, D. M., Ridder, E. M., and MacFarlane, M. R. (2008). Prevalence of traumatic brain injury among children, adolescents and young adults: prospective evidence from a birth cohort. *Brain Inj.* 22, 175–181. doi: 10.1080/02699050801888824

Mills, C. D., Kincaid, K., Alt, J. M., Heilman, M. J., and Hill, A. M. (2000). M-1/M-2 macrophages and the Th1/Th2 paradigm. *J. Immunol.* 164, 6166–6173. doi: 10.4049/jimmunol.164.12.6166

Moran, L. B., Duke, D. C., and Graeber, M. B. (2007). The microglial gene regulatory network activated by interferon-gamma. *J. Neuroimmunol.* 183, 1–6. doi: 10.1016/j.jneuroim.2006.10.023

Morganti, J. M., Riparip, L. K., Chou, A., Liu, S., Gupta, N., and Rosi, S. (2016a). Age exacerbates the CCR2/5-mediated neuroinflammatory response to traumatic brain injury. *J. Neuroinflammation* 13:80. doi: 10.1186/s12974-016-0547-1

Morganti, J. M., Riparip, L. K., and Rosi, S. (2016b). Call off the Dog(ma): M1/M2 polarization is concurrent following traumatic brain injury. *PLoS One* 11:e0148001. doi: 10.1371/journal.pone.0148001

Muccigrosso, M. M., Ford, J., Benner, B., Moussa, D., Burnsides, C., Fenn, A. M., et al. (2016). Cognitive deficits develop 1month after diffuse brain injury and are exaggerated by microglia-associated reactivity to peripheral immune challenge. *Brain Behav. Immun.* 54, 95–109. doi: 10.1016/j.bbi.2016.01.009

Nikulina, E., Tidwell, J. L., Dai, H. N., Bregman, B. S., and Filbin, M. T. (2004). The phosphodiesterase inhibitor rolipram delivered after a spinal cord lesion promotes axonal regeneration and functional recovery. *Proc. Natl. Acad. Sci. U.S.A.* 101, 8786–8790. doi: 10.1073/pnas.0402595101

Nishihara, T., Ochi, M., Sugimoto, K., Takahashi, H., Yano, H., Kumon, Y., et al. (2011). Subcutaneous injection containing IL-3 and GM-CSF ameliorates stab wound-induced brain injury in rats. *Exp. Neurol.* 229, 507–516. doi: 10.1016/j.expneurol.2011.04.006

Oflazoglu, E., Grewal, I. S., and Gerber, H. (2009). Targeting CD30/CD30L in oncology and autoimmune and inflammatory diseases. *Adv. Exp. Med. Biol.* 647, 174–185. doi: 10.1007/978-0-387-89520-8_12

O'Neil, S. M., Witcher, K. G., McKim, D. B., and Godbout, J. P. (2018). Forced turnover of aged microglia induces an intermediate phenotype but does not rebalance CNS environmental cues driving priming to immune challenge. *Acta Neuropathol. Commun.* 6:129. doi: 10.1186/s40478-018-0636-8

Poulsen, C. B., Penkowa, M., Borup, R., Nielsen, F. C., Caceres, M., Quintana, A., et al. (2005). Brain response to traumatic brain injury in wild-type and interleukin-6 knockout mice: a microarray analysis. *J. Neurochem.* 92, 417–432. doi: 10.1111/j.1471-4159.2004.02877.x

Ramlackhansingh, A. F., Brooks, D. J., Greenwood, R. J., Bose, S. K., Turkheimer, F. E., Kinnunen, K. M., et al. (2011). Inflammation after trauma: microglial activation and traumatic brain injury. *Ann. Neurol.* 70, 374–383. doi: 10.1002/ana.22455

Ransohoff, R. M., and El Khoury, J. (2015). Microglia in health and disease. *Cold Spring Harb. Perspect. Biol.* 8:a020560. doi: 10.1101/cshperspect.a020560

Redell, J. B., Moore, A. N., Grill, R. J., Johnson, D., Zhao, J., Liu, Y., et al. (2013). Analysis of functional pathways altered after mild traumatic brain injury. *J. Neurotrauma* 30, 752–764. doi: 10.1089/neu.2012.2437

Saber, M., Kokiko-Cochran, O., Puntambekar, S. S., Lathia, J. D., and Lamb, B. T. (2017). Triggering receptor expressed on myeloid cells 2 deficiency alters acute macrophage distribution and improves recovery after traumatic brain injury. *J. Neurotrauma* 34, 423–435. doi: 10.1089/neu.2016.4401

Samal, B. B., Waites, C. K., Almeida-Suhett, C., Li, Z., Marini, A. M., Samal, N. R., et al. (2015). Acute response of the hippocampal transcriptome following mild traumatic brain injury after controlled cortical impact in the rat. *J. Mol. Neurosci.* 57, 282–303. doi: 10.1007/s12031-015-0626-2

Sedgwick, J. D., Schwender, S., Imrich, H., Dorries, R., Butcher, G. W., and ter Meulen, V. (1991). Isolation and direct characterization of resident microglial cells from the normal and inflamed central nervous system. *Proc. Natl. Acad. Sci. U.S.A.* 88, 7438–7442. doi: 10.1073/pnas.88.16.7438

Semple, B. D., Bye, N., Ziebell, J. M., and Morganti-Kossmann, M. C. (2010). Deficiency of the chemokine receptor CXCR2 attenuates neutrophil infiltration and cortical damage following closed head injury. *Neurobiol. Dis.* 40, 394–403. doi: 10.1016/j.nbd.2010.06.015

Simon, D. W., McGeachy, M. J., Bayir, H., Clark, R. S., Loane, D. J., and Kochanek, P. M. (2017a). The far-reaching scope of neuroinflammation after traumatic brain injury. *Nat. Rev. Neurol.* 13, 171–191. doi: 10.1038/nrneurol.2017.13

Simon, D. W., McGeachy, M. J., Bayir, H., Clark, R. S. B., Loane, D. J., and Kochanek, P. M. (2017b). The far-reaching scope of neuroinflammation after traumatic brain injury. *Nat. Rev. Neurol.* 13:572. doi: 10.1038/nrneurol.2017.116

Smith, D. E., Lipsky, B. P., Russell, C., Ketchem, R. R., Kirchner, J., Hensley, K., et al. (2009). A central nervous system-restricted isoform of the interleukin-1 receptor accessory protein modulates neuronal responses to interleukin-1. *Immunity* 30, 817–831. doi: 10.1016/j.immuni.2009.03.020

Sofroniew, M. V. (2015). Astrocyte barriers to neurotoxic inflammation. *Nat. Rev. Neurosci.* 16, 249–263. doi: 10.1038/nrn3898

Spencer, N. G., Schilling, T., Miralles, F., and Eder, C. (2016). Mechanisms underlying interferon-gamma-induced priming of microglial reactive oxygen species production. *PLoS One* 11:e0162497. doi: 10.1371/journal.pone.0162497

Subramanian, A., Tamayo, P., Mootha, V. K., Mukherjee, S., Ebert, B. L., Gillette, M. A., et al. (2005). Gene set enrichment analysis: a knowledge-based approach for interpreting genome-wide expression profiles. *Proc. Natl. Acad. Sci. U.S.A.* 102, 15545–15550. doi: 10.1073/pnas.0506580102

Szklarczyk, D., Morris, J. H., Cook, H., Kuhn, M., Wyder, S., Simonovic, M., et al. (2017). The STRING database in 2017: quality-controlled protein-protein association networks, made broadly accessible. *Nucleic Acids Res.* 45, D362–D368. doi: 10.1093/nar/gkw937

Szmydynger-Chodobska, J., Shan, R., Thomasian, N., and Chodobski, A. (2016). The involvement of pial microvessels in leukocyte invasion after mild traumatic brain injury. *PLoS One* 11:e0167677. doi: 10.1371/journal.pone.0167677

Szmydynger-Chodobska, J., Strazielle, N., Zink, B. J., Ghersi-Egea, J. F., and Chodobski, A. (2009). The role of the choroid plexus in neutrophil invasion after traumatic brain injury. *J. Cereb. Blood Flow Metab.* 29, 1503–1516. doi: 10.1038/jcbfm.2009.71

Takeuchi, H., Wang, J., Kawanokuchi, J., Mitsuma, N., Mizuno, T., and Suzumura, A. (2006). Interferon-gamma induces microglial-activation-induced cell death: a hypothetical mechanism of relapse and remission in multiple sclerosis. *Neurobiol. Dis.* 22, 33–39. doi: 10.1016/j.nbd.2005.09.014

Tan, J., Town, T., Crawford, F., Mori, T., DelleDonne, A., Crescentini, R., et al. (2002). Role of CD40 ligand in amyloidosis in transgenic Alzheimer's mice. *Nat. Neurosci.* 5, 1288–1293. doi: 10.1038/nn968

Town, T., Laouar, Y., Pittenger, C., Mori, T., Szekely, C. A., Tan, J., et al. (2008). Blocking TGF-beta-Smad2/3 innate immune signaling mitigates

Alzheimer-like pathology. *Nat. Med.* 14, 681–687. doi: 10.1038/nm1781

Umschweif, G., Alexandrovich, A. G., Trembovler, V., Horowitz, M., and Shohami, E. (2013). Hypoxia-inducible factor 1 is essential for spontaneous recovery from traumatic brain injury and is a key mediator of heat acclimation induced neuroprotection. *J. Cereb. Blood Flow Metab.* 33, 524–531. doi: 10.1038/jcbfm.2012.193

von Bernhardi, R., Cornejo, F., Parada, G. E., and Eugenin, J. (2015). Role of TGFbeta signaling in the pathogenesis of Alzheimer's disease. *Front. Cell Neurosci.* 9:426. doi: 10.3389/fncel.2015.00426

von Mering, C., Huynen, M., Jaeggi, D., Schmidt, S., Bork, P., and Snel, B. (2003). STRING: a database of predicted functional associations between proteins. *Nucleic Acids Res.* 31, 258–261. doi: 10.1093/nar/gkg034

Waggott, D., Chu, K., Yin, S., Wouters, B. G., Liu, F. F., and Boutros, P. C. (2012). NanoStringNorm: an extensible R package for the pre-processing of NanoString mRNA and miRNA data. *Bioinformatics* 28, 1546–1548. doi: 10.1093/bioinformatics/bts188

Wang, H., Horbinski, C., Wu, H., Liu, Y., Sheng, S., Liu, J., et al. (2016). NanoStringDiff: a novel statistical method for differential expression analysis based on NanoString nCounter data. *Nucleic Acids Res.* 44:e151. doi: 10.1093/nar/gkw677

Wang, W. Y., Tan, M. S., Yu, J. T., and Tan, L. (2015). Role of pro-inflammatory cytokines released from microglia in Alzheimer's disease. *Ann. Transl. Med.* 3:136. doi: 10.3978/j.issn.2305-5839.2015.03.49

White, T. E., Surles-Zeigler, M. C., Ford, G. D., Gates, A. S., Davids, B., Distel, T., et al. (2016). Bilateral gene interaction hierarchy analysis of the cell death gene response emphasizes the significance of cell cycle genes following unilateral traumatic brain injury. *BMC Genomics* 17:130. doi: 10.1186/s12864-016-2412-0

Witcher, K. G., Eiferman, D. S., and Godbout, J. P. (2015). Priming the inflammatory pump of the CNS after traumatic brain injury. *Trends Neurosci.* 38, 609–620. doi: 10.1016/j.tins.2015.08.002

Wong, Y. H., Wu, C. C., Wu, J. C., Lai, H. Y., Chen, K. Y., Jheng, B. R., et al. (2016). Temporal genetic modifications after controlled cortical impact–understanding traumatic brain injury through a systematic network approach. *Int. J. Mol. Sci.* 17:216. doi: 10.3390/ijms17020216

Xue, J., Schmidt, S. V., Sander, J., Draffehn, A., Krebs, W., Quester, I., et al. (2014). Transcriptome-based network analysis reveals a spectrum model of human macrophage activation. *Immunity* 40, 274–288. doi: 10.1016/j.immuni.2014.01.006

Yager, P. H., You, Z., Qin, T., Kim, H. H., Takahashi, K., Ezekowitz, A. B., et al. (2008). Mannose binding lectin gene deficiency increases susceptibility to traumatic brain injury in mice. *J. Cereb. Blood Flow Metab.* 28, 1030–1039. doi: 10.1038/sj.jcbfm.9600605

Yan, J., Zhou, B., Taheri, S., and Shi, H. (2011). Differential effects of HIF-1 inhibition by YC-1 on the overall outcome and blood-brain barrier damage in a rat model of ischemic stroke. *PLoS One* 6:e27798. doi: 10.1371/journal.pone.0027798

Zhang, M., Gillaspy, A. F., Gipson, J. R., Cassidy, B. R., Nave, J. L., Brewer, M. F., et al. (2018). Neuroinvasive listeria monocytogenes infection triggers IFN-activation of microglia and upregulates microglial miR-155. *Front. Immunol.* 9:2751. doi: 10.3389/fimmu.2018.02751

Conflict of Interest Statement: The authors declare that the research was conducted in the absence of any commercial or financial relationships that could be construed as a potential conflict of interest.

frontiers in Cellular Neuroscience

ORIGINAL RESEARCH
published: 10 September 2019
doi: 10.3389/fncel.2019.00411

Discrimination of Prion Strain Targeting in the Central Nervous System via Reactive Astrocyte Heterogeneity in CD44 Expression

Barry M. Bradford, Christianus A. W. Wijaya and Neil A. Mabbott**

The Roslin Institute and R(D)SVS, The University of Edinburgh, Edinburgh, United Kingdom

OPEN ACCESS

Edited by:
Xiaobo Mao,
Johns Hopkins University,
United States

Reviewed by:
Enquan Xu,
Duke University, United States
Alessio Cardinale,
Bambino Gesu' Children's Research Hospital (IRCCS), Italy
Chan Chen,
West China Hospital, Sichuan University, China

***Correspondence:**
Barry M. Bradford
barry.bradford@roslin.ed.ac.uk
Neil A. Mabbott
neil.mabbot@roslin.ed.ac.uk

Specialty section:
This article was submitted to Cellular Neuropathology, a section of the journal Frontiers in Cellular Neuroscience

Received: *14 June 2019*
Accepted: *26 August 2019*
Published: *10 September 2019*

Citation:
Bradford BM, Wijaya CAW and Mabbott NA (2019) Discrimination of Prion Strain Targeting in the Central Nervous System via Reactive Astrocyte Heterogeneity in CD44 Expression. Front. Cell. Neurosci. 13:411. doi: 10.3389/fncel.2019.00411

Prion diseases or transmissible spongiform encephalopathies are fatal, progressive, neurodegenerative, protein-misfolding disorders. Prion diseases may arise spontaneously, be inherited genetically or be acquired by infection and affect a variety of mammalian species including humans. Prion infections in the central nervous system (CNS) cause extensive neuropathology, including abnormal accumulations of misfolded host prion protein, vacuolar change resulting in sponge-like (spongiform) appearance of CNS tissue, neurodegeneration and reactive glial responses. Many different prion agent strains exist and these can differ based on disease duration, clinical signs and the targeting and distribution of the neuropathology in distinct brain areas. Reactive astrocytes are a prominent feature in the prion disease affected CNS as revealed by distinct morphological changes and upregulation of glial fibrillary acidic protein (GFAP). The CD44 antigen is a transmembrane glycoprotein involved in cell-cell interactions, cell adhesion and migration. Here we show that CD44 is also highly expressed in a subset of reactive astrocytes in regions of the CNS targeted by prions. Astrocyte heterogeneity revealed by differential CD44 upregulation occurs coincident with the earliest neuropathological changes during the pre-clinical phase of disease, and is not affected by the route of infection. The expression and distribution of CD44 was compared in brains from a large collection of 15 distinct prion agent strains transmitted to mice of different prion protein (*Prnp*) genotype backgrounds. Our data show that the pattern of CD44 upregulation observed in the hippocampus in each prion agent strain and host *Prnp* genotype combination was unique. Many mouse-adapted prion strains and hosts have previously been characterized based on the pattern of the distribution of the spongiform pathology or the misfolded PrP deposition within the brain. Our data show that CD44 expression also provides a reliable discriminatory marker of prion infection with a greater dynamic range than misfolded prion protein deposition, aiding strain identification. Together, our data reveal CD44 as a novel marker to detect reactive astrocyte heterogeneity during CNS prion disease and for enhanced identification of distinct prion agent strains.

Keywords: prion, transmissible spongiform encephalopathy, neurodegeneration, neuroinflammation, astrocyte, CD44

INTRODUCTION

Prion diseases, or transmissible spongiform encephalopathies, are a unique group of infectious, sub-acute, neurodegenerative disorders. These disease have been identified in several mammalian species and include scrapie in sheep and goats, bovine spongiform encephalopathy (BSE) in cattle, chronic wasting disease (CWD) in cervids and Creutzfeldt-Jakob disease (CJD) in humans. During prion disease, abnormally folded isoforms (PrP^{Sc}) of the host-encoded cellular prion protein (PrP^{C}) accumulate and aggregate in affected tissues (Prusiner, 1982). The infectious prion is considered to constitute almost entirely of PrP^{Sc} implying that prions are infectious proteins. Prion disease within the central nervous system (CNS) causes extensive neuropathology and neurodegeneration. This characteristically includes neuronal vacuolation resulting in a spongiform (sponge-like) appearance of brain tissue in histopathological specimens (Fraser and Dickinson, 1967) and progressive loss of dendritic spines (Fang et al., 2016), synapses (Jeffrey et al., 2000), axons (Jeffrey et al., 1995) and neuronal cell bodies (Giese et al., 1995). These histopathological signs are also accompanied by activation of the astrocytes and microglia (Kercher et al., 2007).

Many distinct prion agent strains have been identified and characterized by transmission into laboratory mice (Boyle et al., 2017). Once adapted to their new host environment, these prion strains can be stably maintained by passage within that same host species, resulting in reproducible disease incubation periods, clinical presentation and targeting of prion neuropathology (Dickinson and Fraser, 1977). As well as conservation of biological properties, prion strains also have preserved biochemical properties, which has led to the hypothesis that the distinct conformational state of the misfolded prion protein encodes this diversity (Safar et al., 1998; Peretz et al., 2001, 2002; Arima et al., 2005). The diversity in the targeting of neuropathological changes within the CNS resulting from different prion strains has been key to facilitating strain identification (Fraser and Dickinson, 1967, 1968, 1973; Bruce et al., 1989, 1991; Fraser, 1993; van Keulen et al., 2015; Boyle et al., 2017).

Reactive astrocytes are a prominent feature in the prion disease affected brain but whether they play a role in the development of, or protection from, the neurodegeneration during prion disease is uncertain. Both neurons and astrocytes can facilitate prion agent replication (Diedrich et al., 1991; Race et al., 1995; Raeber et al., 1997; Kovács et al., 2005; Sarasa et al., 2012; Krejciova et al., 2017) and induce microglial recruitment (Marella and Chabry, 2004) at early stages of prion disease neuropathogenesis. Indeed expression of the prion protein gene (*Prnp*) in astrocytes alone is sufficient to support prion infection in the brains of infected mice (Raeber et al., 1997). Data from an *in vitro* study have suggested that the reactive astrocytes may also play a role in the recruitment of microglia toward regions of the brain affected by prions (Marella and Chabry, 2004). To-date, analyses of the astrocytic response during prion infection have predominantly focused on the immunohistochemical detection of upregulated expression of the intermediate filament glial fibrillary acidic protein (GFAP) and morphological changes to the astrocyte cytoskeleton (Georgsson et al., 1993; Monzon et al., 2018). However, independent studies have shown that the activation status of the reactive astrocytes is highly heterogeneous (Zamanian et al., 2012), and can be broadly categorized into neurotoxic 'A1' or neuroprotective 'A2' phenotypes based on functional and transcriptional characteristics (Liddelow et al., 2017). Whether CNS prion infections also lead to the development of neurotoxic or neuroprotective phenotypes in astrocytes, and whether this differs amongst different prion agent strains is not known.

Transcriptional analyses have shown that expression of the adhesion molecule CD44 is significantly elevated in reactive astrocytes induced by a range of pro-inflammatory stimuli (Liddelow et al., 2017). Furthermore, the expression of CD44 expression was significantly elevated in neurotoxic A1 astrocytes when compared to the A2 astrocytes with a neuroprotective phenotype. Therefore, in the current study we used the immunohistochemical analysis of CD44 expression to characterize the heterogeneity of the reactive astrocyte response in the brains of mice infected with a large range of distinct prion agent strains. We show that in the brains of mice infected with prions, strong astrocyte-associated CD44 expression was detected as early as halfway through the disease incubation period and concurrent with some of the earliest neuropathological changes. Data from prion disease transmission to mice have revealed the discriminatory properties and limitations of disease-specific vacuolation or PrP^{d} in identifying prion disease strain and host differences. Furthermore, not all prion diseases are transmissible to laboratory mice, and for novel natural prion disease cases the incubation period of disease is often unknown. The identification of a novel marker of prion disease that can discriminate prion strains in different host *Prnp* genotypes irrespective of survival time or route of infection could prove useful in understanding the variety of strains in natural prion disease cases both in humans and animals. Our data from the analysis of a large collection brains from mice infected with 15 distinct prion agent strains suggest CD44 expression fulfils these criteria and can be used as a novel marker to detect reactive astrocyte heterogeneity during CNS prion disease.

MATERIALS AND METHODS

Animals

C57BL/Dk and VM/Dk mice were bred and housed under specific pathogen-free conditions with a 12:12 h light:dark cycle. Food and water were provided *ad libitum*. Necessary approvals for the mouse experiments described in this study were obtained from the Institute for Animal Health Neuropathogenesis Unit Ethical Review Committee, the University of Edinburgh Ethical Review Committee, and the UK Home Office.

Prion Infection

Groups of C57BL/Dk, VM/Dk and F1 cross offspring termed "CVF1" mice were injected intracerebrally (IC) with 20 μl of a 1% (weight/volume) brain homogenate prepared from mice

terminally infected with prions. For intraperitoneal (IP) or intravenous (IV) infection the mice were injected with the same dose and volume of prions into the peritoneal cavity or tail vein, respectively. For oral infection mice were individually housed overnight in bedding-free cages with a single food pellet dosed with 50 μl of a 1% (weight/volume) brain homogenate. The mice were maintained in these cages until the food pellet was fully consumed, upon which they were then returned to standard group caging. All mice were coded and assessed by independent technicians at weekly intervals for the clinical signs of prion disease. Mice were scored as "unaffected," "possibly affected" and "definitely affected" using standard criteria (Brown et al., 2012) and culled at a standard clinical end-point (maximally on their 3rd clinical assessment of definitely affected). Mean disease survival times were calculated as the interval between infection with prions and the detection of positive clinical signs of terminal prion disease.

Neuropathological Analysis

Clinical prion disease diagnoses were confirmed by histopathological assessment of vacuolation (spongiform pathology) in the brain. Brains were codified at post-mortem and fixed in 10% formal saline, trimmed into 5 routine coronal slices based on external features, processed and embedded in paraffin wax. Sections were cut at 6 μm thickness, stained with hematoxylin & eosin and scored for spongiform vacuolar degeneration by blinded assessment as described previously (Fraser and Dickinson, 1967). Sections were scored by an independent scientist for the presence and severity (scale 0–5) of prion-disease-specific vacuolation in nine gray matter and three white matter brain areas: G1, dorsal medulla; G2, cerebellar cortex; G3, superior colliculus; G4, hypothalamus; G5, medial thalamus; G6, hippocampus; G7, septum; G8, cerebral cortex; G9, forebrain cerebral cortex; W1, cerebellar white matter; W2, midbrain white matter; W3, cerebral peduncle.

Immunohistochemistry (IHC)

Sections (6 μm) were cut on a HM325 Rotary Microtome (Thermo Fisher Scientific, Runcorn, United Kingdom) and mounted on Superfrost Plus slides (Menzel-Glaser GmbH, Braunschweig, Germany). Before immunostaining the sections were deparaffinised using an XL Autostainer (Leica Biosystems, Newcastle upon Tyne, United Kingdom) and pre-treated by autoclaving (15 min at 121°C) in Target Retrieval Solution pH 6.0 (DAKO UK Ltd., Ely, United Kingdom). For the detection of PrP sections were then immersed in formic acid (98%) for 5 min, and subsequently immunostained with anti-PrP-specific mAb [Clone BH1] (Morales et al., 2007). To detect astrocytes the sections were immunostained with rabbit anti-GFAP (DAKO), biotinylated anti-mouse/human CD44 [Clone: IM7] (Biolegend, London, United Kingdom) or anti CD44var6 [Clone 9A4] (eBioscience, Ltd., Hatfield, United Kingdom). To detect microglia the sections were immunostained with anti-Iba1 polyclonal antibody (AIF1; Wako Chemicals GmbH, Neuss, Germany). Following the addition of primary antibodies, biotin-conjugated species-specific secondary antibodies (Jackson ImmunoResearch Europe Ltd., Ely, United Kingdom) were applied. Biotinylated antibidies were detected using horse radish peroxidase-conjugated to the avidin-biotin complex [HRP-ABC] kit (Vector Laboratories, Peterborough, United Kingdom) and visualized with 3,3'-diaminobenzidine [DAB] (Merck KGaA, Darmstadt, Germany) and counterstained with hematoxylin. For dual CD44/GFAP staining, CD44 was detected using the HRP substrate Vector NovaRed (Vector Laboratories, Peterborough, United Kingdom) and GFAP detected with alkaline phosphatase conjugated anti-rabbit antibody (Jackson Immunoresearch) and 5-bromo-4-chloro-3-indolyl phosphate/nitro blue tetrazolium (BCIP/NBT) substrate (Merck). Sections were viewed using an Eclipse Ni-E microscope (Nikon Instruments Europe BV, Amsterdam, Netherlands) with Zen software (Carl Zeiss Ltd. Cambridge, United Kingdom).

Immunofluorescence

For immunofluorescence analysis, goat anti-rabbit iFluora594 (AAT Bioquest, Sunnyvale, United States) was applied following anti-GFAP immunostaining, and goat anti-mouse Alexaflluor647^{TM} (Life Technologies Ltd., Inchinnan, United Kingdom) was applied following anti-PrP (clone BH1) immunostaining. For CD44 and CD44v6 staining procedures were performed as above and visualized using the HRP substrate Tyramide iFluora488 (AAT Bioquest). Sections were mounted using fluorescent mounting medium (DAKO) before analysis. Images were captured using a confocal laser scanning LSM710 microscope with Zen software (Zeiss).

Thioflavin Staining of Amyloid

Paraffin-embedded sections as above were dewaxed and rehydrated, incubated in 1% thioflavin-S (Merck KGaA) for 5 min, differentiated in 70% industrial denatured alcohol for 3 × 1 min and washed in distilled water. Slides were mounted using fluorescent mounting medium (DAKO) and images captured using a confocal laser scanning LSM710 microscope with Zen software (Zeiss).

Image Analysis

For morphometric analysis, coded IHC sections and images were analyzed using ImageJ software[1] by blinded assessment as described (Inman et al., 2005). Images were captured from a minimum of $N = 6$ mice/group. To visualize staining intensity the deconvoluted DAB channel was false-colored using an inverted 16 color lookup table [LUT] representing variance in pixel intensity (see calibration bar in each figure). Thus, each image was color deconvoluted using the vector H-DAB and the percentage area coverage of each IHC marker in each of the 9 gray matter areas was then measured. Data are expressed as mean ± SEM from a minimum of 72 images/profile.

Statistical Analysis

Survival periods, vacuolation scores and percentage area coverage of IHC staining are presented as mean ± SEM from $N = 4$–31 mice/group. Pearson correlation coefficients were

[1] http://rsb.info.nih.gov/ij/

calculated from $N = 6$ mice/group. Survival time and image analysis quantification data were compared using paired T-tests. Statistical analyses were performed using Minitab 17 software (Minitab Ltd., Coventry, United Kingdom).

RESULTS

Comparison of Survival Times and Neuropathology in a Large Collection of Distinct Mouse-Adapted Prion Agent Strains

The identification or definition of distinct prion strains from various sources has been well characterized by their transmission into laboratory mice (Boyle et al., 2017). These analyses show that distinct prion agent strains can differ significantly in the duration of the survival times and the targeting of the neuropathology (spongiform pathology) in the brain. Therefore, in the current study we compiled a large collection of brains from mice infected with 15 distinct and defined mouse-adapted strains and used it to compare glial cell responses during CNS prion disease. Full details of all the prion agent strains used and the recipient mouse strain backgrounds are provided in **Table 1**.

Prion agent strain characteristics can also be significantly influenced by host *Prnp* genotype (Dickinson and Meikle, 1971). Therefore, in this study we studied brains from C57Bl/Dk mice that have the *Prnp*-a (108L, 189T) genotype, and VM/Dk mice that have a *Prnp*-b (108F, 189V) genotype (Westaway et al., 1987). All mice were injected IC with a 1% dose of brain homogenate and brains were analyzed at the terminal stage of disease. The relative prion disease survival times in the recipient mice are shown in **Figure 1**. These data show that the order of the relative survival times, particularly in CVF1 mice, can be used to distinguish similar strains such as 79A from 139A for example.

The distribution and magnitude of the prion disease-specific spongiform pathology (vacuolation) in nine gray matter regions and three white matter regions of the brains from mice in each group are shown in **Figure 2**. These data, in combination with the survival time data in **Figure 1** have enabled each of these distinct strains to be identified and distinguished from each other in the brains of laboratory mice (Bruce et al., 1997). These data were used here to confirm the nature and identity of these distinct prion agent strains used for the further investigations below.

PrP^{Sc} Deposition

The abnormal accumulation of misfolded prion disease-specific PrP (PrP^d) is a characteristic feature in the brain during CNS prion disease. The pattern of the PrP^d deposition within the brains of infected mice has previously been used to help discriminate some prion agent strains, although this was not possible for all strains analyzed (van Keulen et al., 2015). Here, to compare the pattern of PrP^d deposition between distinct prion agent strains, terminal brain sections were immunostained using anti-PrP antibody BH1. The resulting images were then false-colored to compare the signal intensities of the immunostaining between strains (**Figure 3**). In the brains of C57Bl/Dk mice most prion strains could be distinguished by PrP^d deposition pattern as shown previously (van Keulen et al., 2015). However, the dynamic range was low due to the diffuse and widespread nature of the PrP^d deposition observed for some prion agent strains including 22A, 22C, 22F, 79A, 80A, and 139A (**Figures 3C,E**). Variance was also minimal between the hippocampal CA2-focussed 87A (**Figure 3B**) and 79V (**Figure 3E**) strains, and the intense PrP deposits observed throughout the hippocampus of mice infected with the ME7 (**Figure 3B**) and 22L prion agent strains (**Figure 3C**). However, the PrP deposition observed in the brains of mice infected with BSE (**Figure 3D**) and CWD (**Figure 3F**) derived prion strains was readily distinguishable from those of scrapie origin (**Figures 3B,C,E**).

TABLE 1 | Prion agent strains analyzed in this study.

Strain	Disease	Origin	Passage	Passage/line	References
ME7	Natural sheep scrapie	Suffolk sheep	9^{th}	C57Bl/Dk	Zlotnik and Rennie, 1963
22A	Experimental sheep scrapie SSBP1	Cheviot sheep	10^{th}	VM/Dk	Dickinson and Meikle, 1969
22C	Experimental sheep scrapie SSBP1	Cheviot Sheep	8^{th}	C57Bl/Dk	Dickinson, 1976
22F	Experimental sheep scrapie SSBP1	Cheviot Sheep	9^{th}	C57Bl/Dk	Dickinson, 1976
22L	Experimental sheep scrapie SSBP1	Cheviot Sheep	13^{th}	C57Bl/Dk	Dickinson, 1976
79A	Experimental sheep scrapie SSBP1	'Drowsy' goat	12^{th}	C57Bl/Dk	Dickinson, 1976; Pattison and Millson, 1961
79V	Experimental sheep scrapie SSBP1	'Drowsy' goat	5^{th}	VM/Dk	Dickinson, 1976; Pattison and Millson, 1961
80A	Experimental sheep scrapie SSBP1	'Scratching' goat	5^{th}	C57Bl/Dk	Pattison and Millson, 1961
87A	Natural sheep scrapie	Cheviot × Border Leicester sheep	9^{th}	C57Bl/Dk	Bruce et al., 1976
87V	Natural sheep scrapie	Cheviot x Border Leicester sheep	9^{th}	VM/Dk	Bruce et al., 1976
139A	Experimental sheep scrapie SSBP1	'Drowsy' goat Chandler isolate	9^{th}	C57Bl/Dk	Chandler, 1961; Pattison and Millson, 1961
221C	Natural sheep scrapie	Halfbreed sheep	4^{th}	C57Bl/Dk	Bruce et al., 2002
301C	BSE	Holstein-Fresian cow	7^{th}	C57Bl/Dk	Bruce et al., 1994
301V	BSE	Holstein-Fresian cow	7^{th}	VM/Dk	Bruce et al., 1994
409V	CWD	Mule deer	5^{th}	VM/Dk	Bruce et al., 2002*

**Confirmed US CWD case material identified circa 1980 provided by Stuart Young and Beth Williams, Wild Animal Disease Center and Department of Pathology, College of Veterinary Medicine and Biomedical Sciences, Colorado State University, Fort Collins, CO, United States (Williams and Young, 1980).*

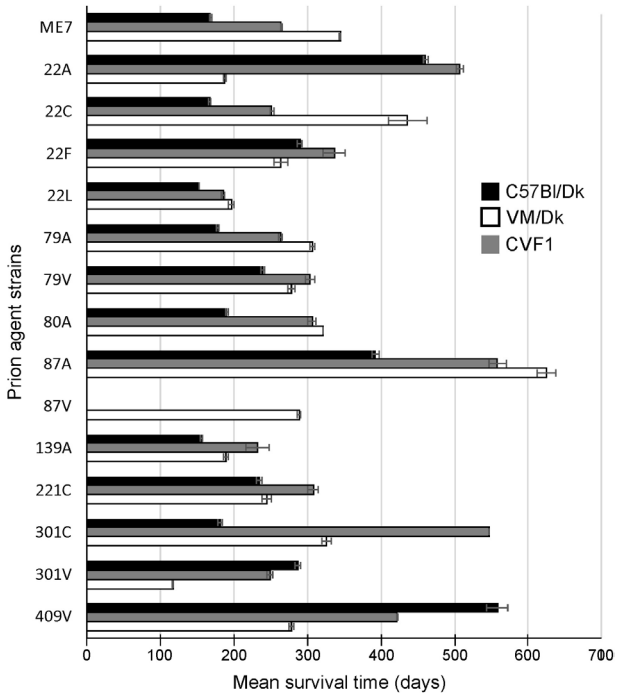

FIGURE 1 | Mean prion disease survival times in laboratory mice infected with a variety of distinct prion agent strains. Groups of C57Bl/Dk (*Prnp*-a), CVF1 (*Prnp*-a/b) or VM/Dk (*Prnp*-b) mice were injected intracerebrally with a variety of distinct prion agent strains (**Table 1**) and survival times recorded from mice confirmed to have clinical and pathological signs of prion disease. Mean survival times in days ± SEM are displayed for each mouse-passaged prion strain group (N = 4–31 mice/group, total = 446 mice). Attempted transmissions of the 87 V strain to C57Bl/Dk or CVF1 mice have not produced positive clinical or pathological signs of prion disease in recipient mice up to at least 600 days post injection.

Next, the percentage area coverage of PrP^d+ immunostaining was measured across nine distinct brain gray matter areas (**Figure 4**). The intensity of the PrP^d+ immunostaining across these areas was then compared between each prion agent strain by paired *T*-test (**Supplementary Table 1**). This analysis showed the highly discriminatory nature of PrP^d detection in prion agent strain typing and revealed statistically significant differences in 55% (84/153) of comparisons. For example 22A-C57Bl/Dk was almost completely distinguishable by PrP^d profile against all other strains, except when compared against 80A-C57Bl/Dk (P = 0.052, **Supplementary Table 1**). Similarly the PrP^d profiles for BSE (301C & 301V) and CWD (409V) derived prion agent strains were readily discriminated from most natural and experimental scrapie strains with high levels of significance. However as noted above, this analysis showed that several strains were indistinguishable across many brain regions due to similarities in the amount of PrP^d present, as reported previously (van Keulen et al., 2015).

In addition to data from the analysis of a range of natural sheep scrapie, experimental sheep scrapie, experimental goat scrapie and BSE, derived agent strains, we also present data from the serial passage of CWD prions (derived from Mule Deer) in VM/Dk mice (prion agent strain 409V). Staining with thioflavin-S showed that amyloid PrP^d accumulations were a characteristic feature in the brain after infection with 409V prions (**Figure 5A**). In terminally affected VM mice these florid amyloid PrP plaques were mostly observed in the corpus callosum dorsal to the hippocampus and occasionally in the thalamus. In the brains of C57Bl/Dk mice large florid and multicentric plaques were observed in the corpus callosum and throughout the thalamus and hippocampus (**Figure 5A**). Comparison of the pattern of the PrP^d accumulation across all the prion agent strains used in this study suggested that the features of the amyloid accumulations could be reliably used to distinguish the CWD-derived 409V prion agent strain following experimental transmission to mice (**Figures 3F**, **5A**).

Glial Activation

Microglia are the phagocytic cells of the brain and their activation during CNS prion disease is also a prominent histopathological characteristic (Aguzzi and Zhu, 2017). Microglia are critical in host defence against prion disease and appear to phagocytose prions and delay disease pathogenesis (Carroll et al., 2018). Microglia proliferate and infiltrate prion-affected brain areas and display activated morphology as identified by immunostaining for allograft inflammatory factor 1 (AIF1; **Figure 5B**, upper row).

Next, the percentage area coverage of AIF1 + immunostaining was measured across nine distinct brain gray matter areas (**Figure 6**). As above, the intensity of the AIF1 + immunostaining across these areas was then compared between each prion agent strain by paired *T*-test (**Supplementary Table 2**). This analysis showed the discriminatory extent of AIF1+ immunostaining in prion agent strain discrimination in the brain revealing statistically significant differences in 48% (73/153) of comparisons (**Supplementary Table 2**). Of note, prion agent strains with the highest levels (e.g., 22C-C57Bl/Dk and 87A-C57/Dk) and lowest levels (e.g., 409V-C57Bl/Dk) of AIF1+ immunostaining generated some of the highest statistically significant differences when compared to most other strains.

Astrocytes contribute to the maintenance of health and function of the CNS and are considered important in neurodegenerative diseases (Phatnani and Maniatis, 2015) including prion disease (Aguzzi and Liu, 2017). Reactive astrocytes were identified by immunostaining for the intermediate filament GFAP and their altered morphology (**Figure 5B**, lower row). The precise role and function of astrocytes in prion disease is not known beyond regional variance in their activation dependent upon prion strain (Monzon et al., 2018) and ability to replicate prions (Sarasa et al., 2012; Krejciova et al., 2017), hence their selection for further investigation in this study.

Next, the percentage area coverage of GFAP+ immunostaining was measured across nine distinct brain gray matter areas (**Figure 6**). The intensity of the GFAP+ immunostaining across these areas was then compared between each prion agent strain by paired *T*-test (**Supplementary Table 3**). This analysis suggested that GFAP+ immunostaining had the least discriminatory properties revealing statistically significant

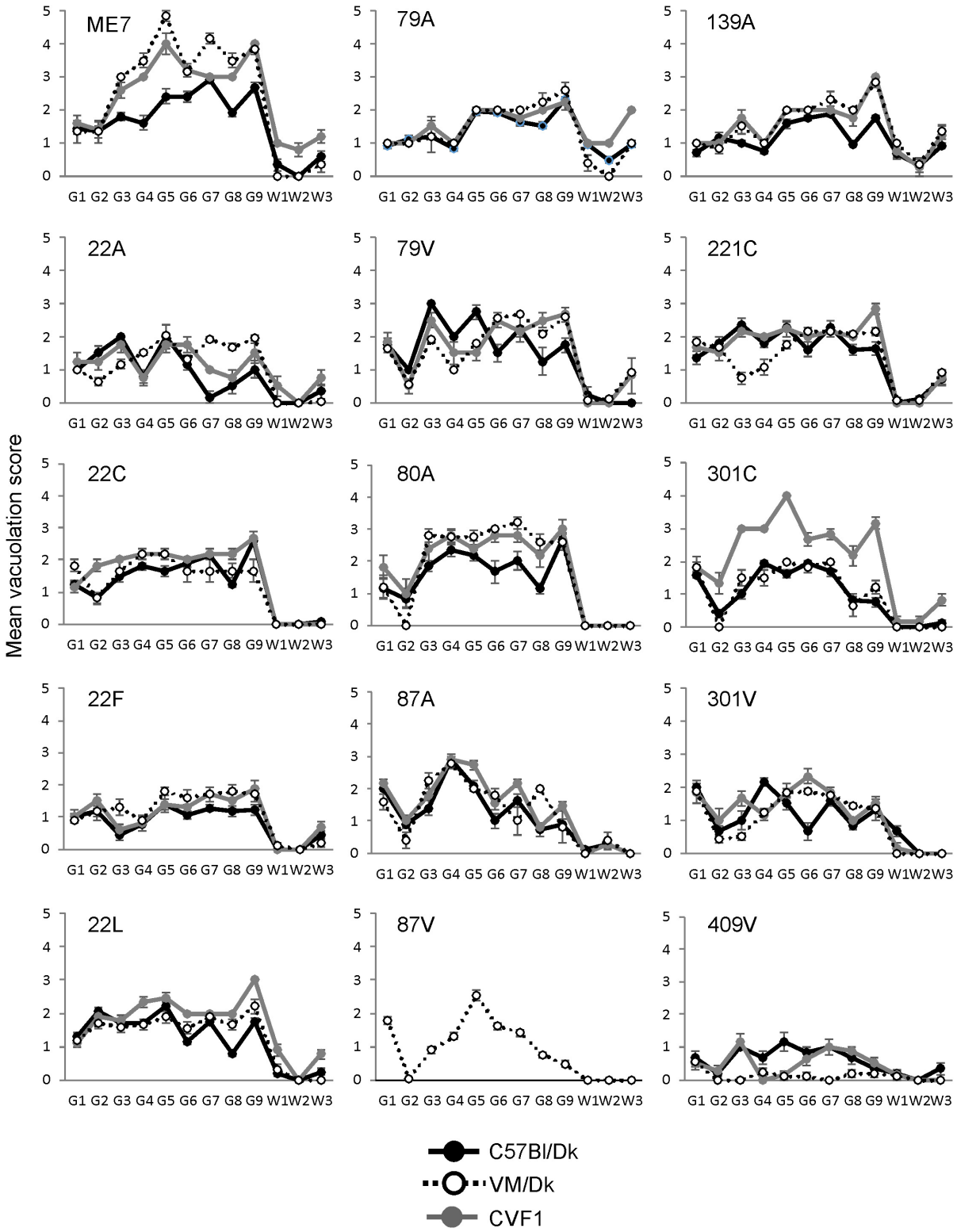

FIGURE 2 | Comparison of the magnitude and distribution of the spongiform pathology in the brains of mice infected with a variety of distinct prion agent strains. Groups of C57Bl/Dk or VM/Dk mice were injected intracerebrally with a variety of distinct prion agent strains (**Table 1**). Brains were collected at the terminal stage of disease and the magnitude and distribution of the spongiform pathology (vacuolation) scored for each of the following brain regions G1, dorsal medulla; G2, cerebellar cortex; G3, superior colliculus; G4, hypothalamus; G5, medial thalamus; G6, hippocampus; G7, septum; G8, cerebral cortex; G9, forebrain cerebral cortex; W1, cerebellar white matter; W2, midbrain white matter; W3, cerebral peduncle. Data represent mean vacuolation severity scores ± SEM.

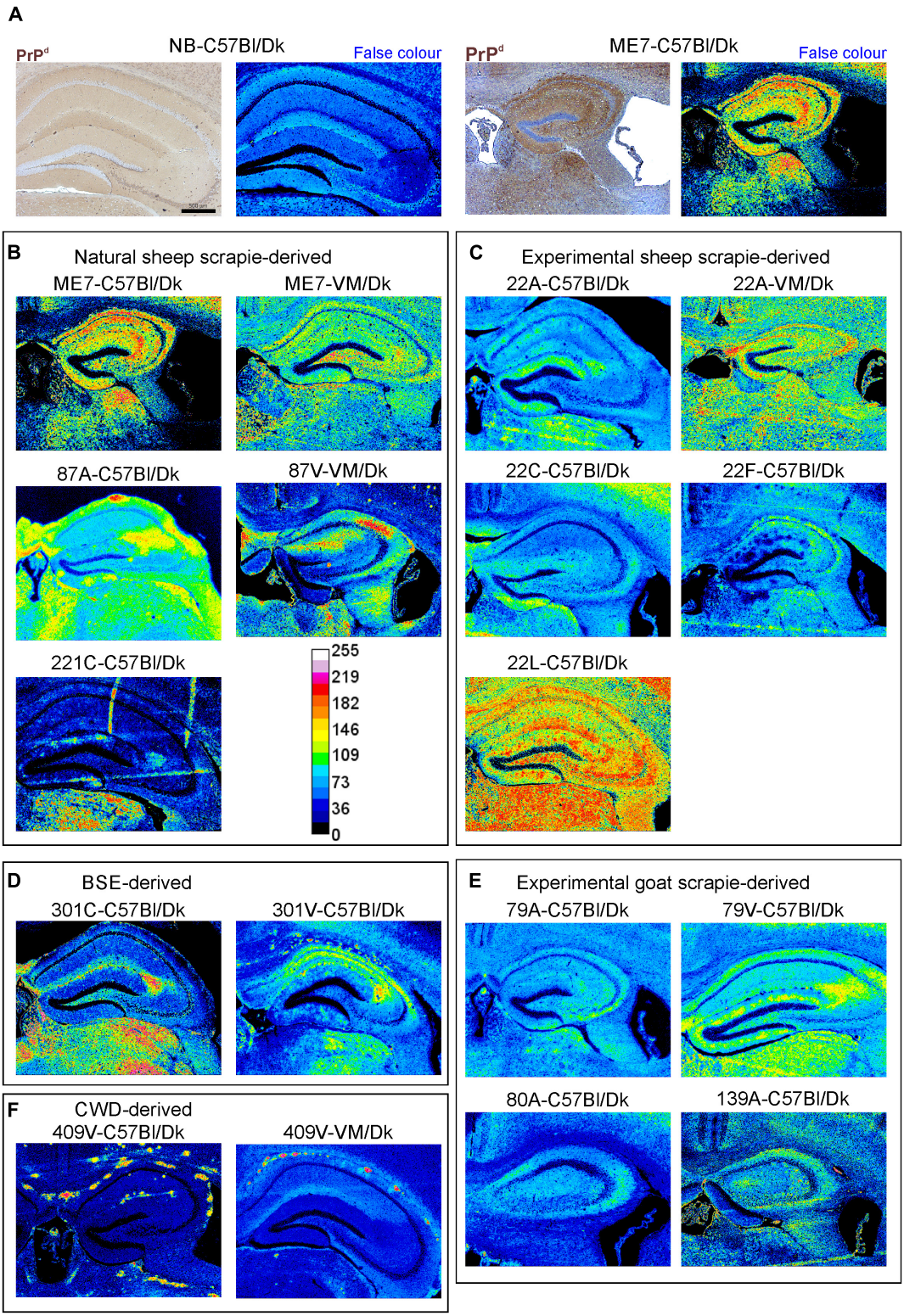

FIGURE 3 | Immunohistopathological comparison of the PrP^d immunostaining in the brains of mice infected with a variety of distinct prion agent strains. Groups of C57Bl/Dk or VM/Dk mice were injected intracerebrally with a variety of distinct prion agent strains (**Table 1**). Brains were collected at the terminal stage of disease and immunostained to detect PrP^d. Images were then false-colored to compare the signal intensities of the immunostaining between each group. **(A)** Normal brain infected mice display no PrP^d compared to mice terminally affected with ME7 scrapie prions. **(B–F)** Comparison of false colored images to show the variation in PrP^d+ immunostaining between diverse prion strains isolated from a variety of sources. Representative images from 6 mice/group are shown. Scale bars = 500 μm.

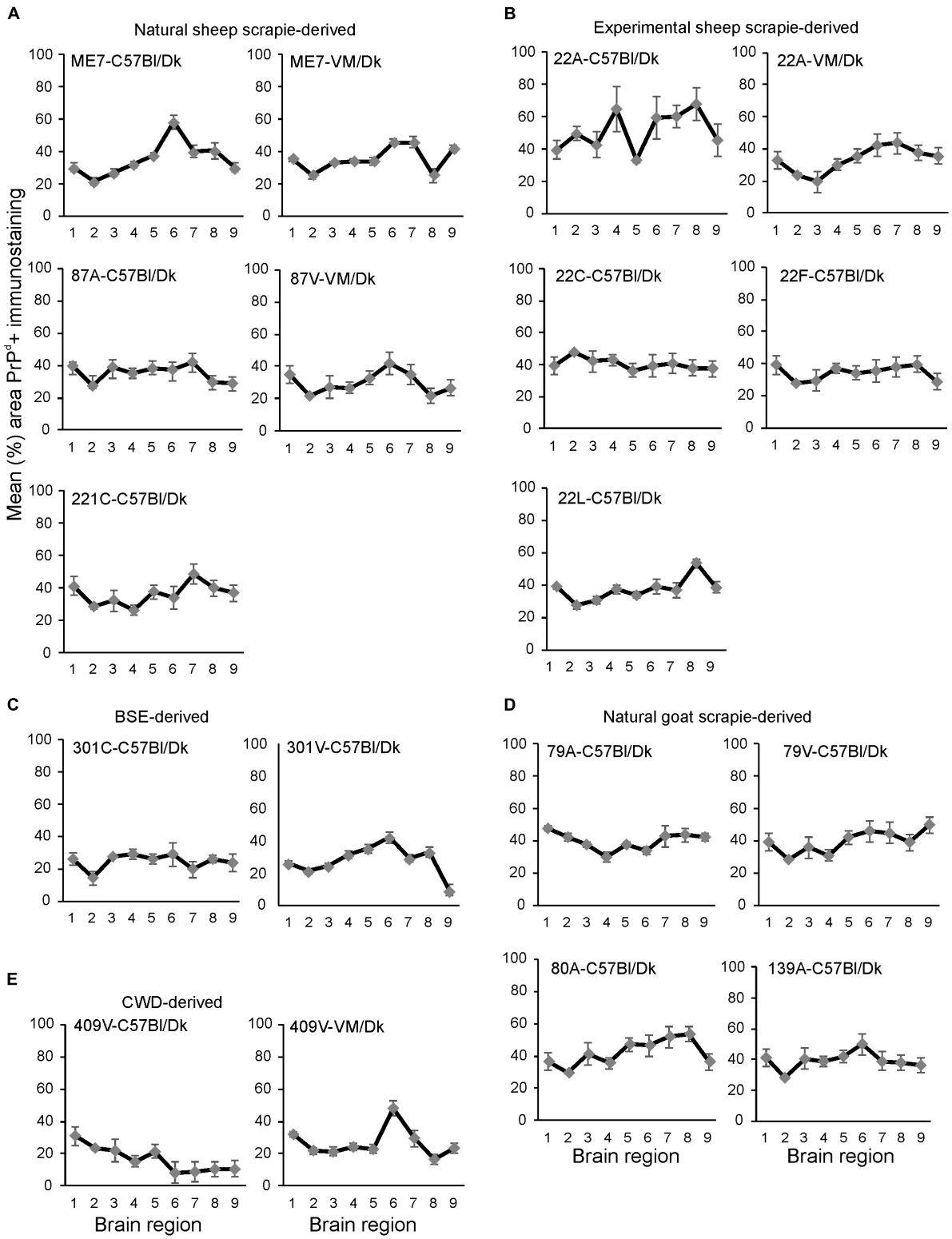

FIGURE 4 | (A–E) Comparison of the magnitude and distribution of the PrPd+ immunostaining in the brains of mice infected with a variety of distinct prion agent strains. Groups of C57Bl/Dk or VM/Dk mice were injected intracerebrally with a variety of distinct prion agent strains (**Table 1**). Brains were collected at the terminal stage of disease and immunostained to detect PrP^{d} and the percentage area coverage compared in each of the following gray matter brain regions G1, dorsal medulla; G2, cerebellar cortex; G3, superior colliculus; G4, hypothalamus; G5, medial thalamus; G6, hippocampus; G7, septum; G8, cerebral cortex; G9, forebrain cerebral cortex. *N* = 6 mice/group. Data represent mean ± SEM, from a minimum of 54 images/group.

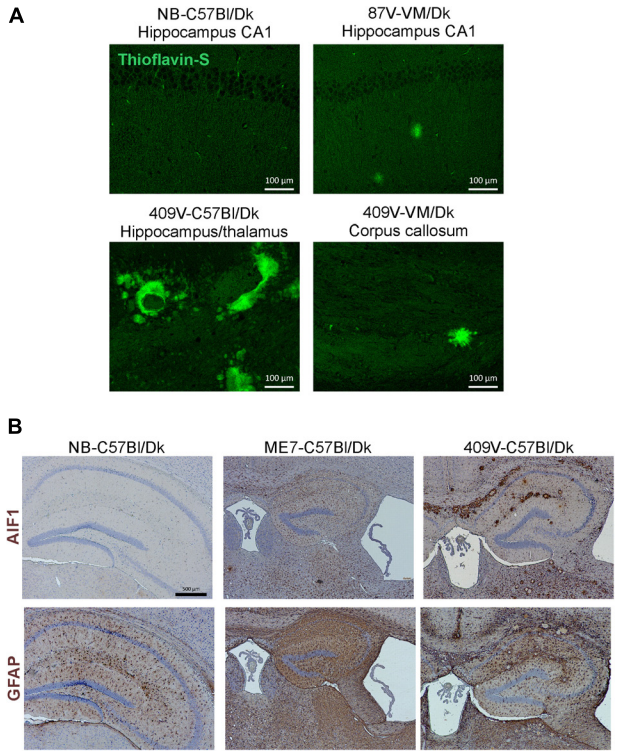

FIGURE 5 | Histopathological detection of amyloid and activated glial cells in the brain following prion infection. **(A)** Thioflavin-S staining of normal brain C57Bl/Dk, 87V-VM/Dk, 409V-C57Bl/Dk and 409V-VM/Dk prion agent strain and host combinations revealed characteristic amyloid deposits in the brains of mice with amyloidal PrP accumulations. Images are representative of $N = 4$ mice/group. Scale bars = 100 µm. **(B)** Immunohistochemical detection of microglia (AIF1+ cells, upper row) and astrocytes (GFAP+ cells, lower row). This analysis showed minimal AIF1+ and GFAP+ immunostaining in the brains of uninfected control mice, whereas expression of these markers was strongly upregulated in brains of mice with terminal prion disease. Representative images $N = 6$ mice/group are shown. Scale bars = 500 µm.

differences in only 34% (52/153) of prion agent strain comparisons. Of note, prion agent strains with low levels of GFAP+ immunostaining (e.g., CWD-derived 409V-C57Bl/Dk and 409V-VM/Dk) or large regional diversity (e.g., 22L-C57Bl/Dk and to a lesser extent 22F-C57Bl/Dk and 87V-VM/Dk) generated some of the highest statistically significant differences when compared to most other strains.

CD44 Expression Is Upregulated During CNS Prion Disease

Molecular profiling of reactive astrocytes has identified CD44 as a pan-activation marker (Liddelow et al., 2017). In the brains of mice with terminal ME7 prion disease CD44 immunostaining was observed in a wide range of areas and sub-regions (**Figure 7A**). Furthermore, immunostaining for CD44 and GFAP suggested that CD44 was associated with astrocytes (**Figure 7B**).

Next, mice were injected IC with ME7 scrapie prions and the expression of CD44 in the brain compared throughout the pre-clinical phase. At 45 day post-injection (dpi) with prions, upregulated CD44 expression was only detected in association with the damage caused by the injection needle-track (**Figure 7C**, upper row). However, by 80 dpi CD44 expression was elevated in the thalamus on the same side of the brain as the injection site. This coincided with early signs of PrP^d accumulation, and evidence of astrocyte and microglia activation (**Figure 7C**, middle row). By 118 dpi CD44 upregulation was also observed in the contralateral thalamus and mirrored the distribution of the astrocyte activation (**Figure 7C**, bottom row). When *Cd44* mRNA is expressed alternative splicing can encode different CD44 isoforms. For example, CD44 variant 6 isoform (CD44v6) containing exon 11 is upregulated by and interacts with the chemotactic and phagocytosis inducing microglial expressed protein osteopontin (Weber et al., 1996; Katagiri et al., 1999; Gao et al., 2003; Marroquin et al., 2004; Khan et al., 2005; Morisaki et al., 2016). Our data suggest that the CD44 expressed during these early pre-clinical stages appeared to be predominantly of the CD44v6 isoform (**Figure 7C**).

We next determined whether the route of prion exposure influenced the expression of CD44 in the brain. Our analysis showed a similar upregulation of CD44 expression in the brain at the terminal stage of disease after exposure to prions via intraperitoneal injection, IV injection or oral infection (**Figure 7D**). These data show that for the ME7 prion agent strain the specified pattern of CD44 upregulation in the CNS during prion disease is unaffected by the route of infection.

Distinct Patterns of CD44 Expression in the Brains of Mice Infected With Different Prion Agent Strains

Little if any CD44 expression was detected by IHC in the brains of uninfected control mice, whereas abundant CD44 expression was detected in the brains of C57Bl/Dk mice infected with ME7 scrapie prions (**Figure 8A**). We next compared the distribution and abundance of CD44 expression in the brains of mice infected with distinct prion agent strains. To specifically compare the abundance and variance of the CD44 upregulation between prion agent strains, immunostained images were false-colored in respect to pixel intensity. This analysis revealed patterns of CD44 upregulation in the brain that were specific for each prion agent strain (**Figures 8B–E**). Furthermore, by comparing the CD44 expression profile specifically within the hippocampus, it was possible to discriminate each prion agent strain/host combination based solely on CD44 localization (**Table 2** and **Figure 8**). CD44 heterogeneity within activated astrocytes has been previously identified in mouse models of Alexander disease (Sosunov et al., 2013). Our data suggest that CD44 upregulation within the hippocampus is also a useful marker to discriminate the neuropathological changes during CNS prion disease.

This analysis also revealed that the abundance of the CD44 expression in the brains of mice with terminal prion disease appeared to mirror the magnitude and distribution of the PrP^d. For example, in prion agent strain/recipient mouse genotype combinations that displayed diffuse PrP^d accumulation e.g., ME7, experimental sheep scrapie 22A, 22C, 22F, and 22L and

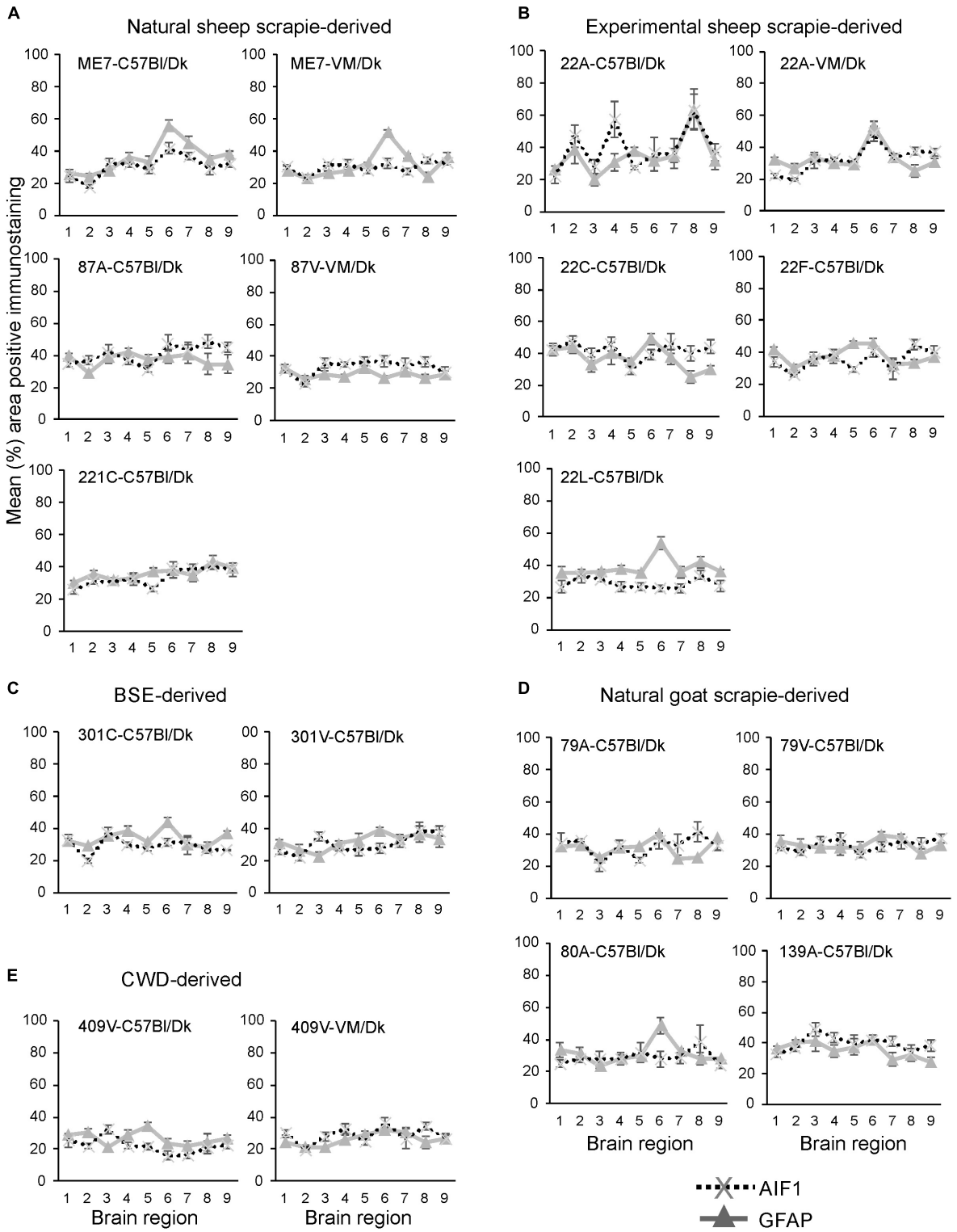

FIGURE 6 | (A–E) Comparison of the magnitude and distribution of the GFAP+ and AIF1+ immunostaining in the brains of mice infected with a variety of distinct prion agent strains. Groups of C57Bl/Dk or VM/Dk mice were injected intracerebrally with a variety of distinct prion agent strains (**Table 1**). Brains were collected at the terminal stage of disease and immunostained to detect GFAP+ cells (astrocytes) and AIF1+ cells (microglia). The percentage area coverage of each marker was then compared in each of the following gray matter brain regions G1, dorsal medulla; G2, cerebellar cortex; G3, superior colliculus; G4, hypothalamus; G5, medial thalamus; G6, hippocampus; G7, septum; G8, cerebral cortex; G9, forebrain cerebral cortex. *N* = 6 mice/group. Data represent mean ± SE, from a minimum of 54 images/group.

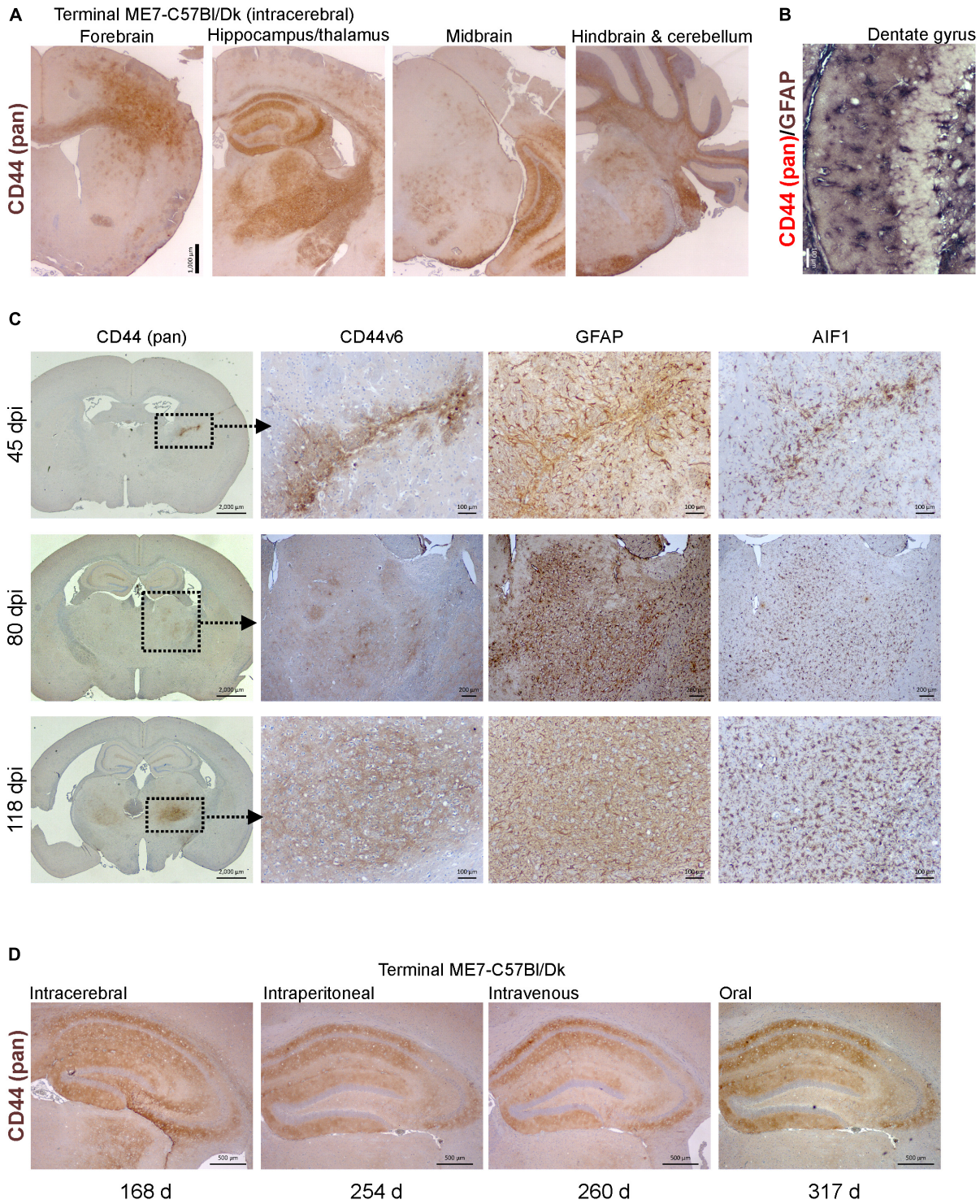

FIGURE 7 | CD44 expression is upregulation in the brain during prion disease. **(A)** C57Bl/Dk mice were injected intracerebrally with ME7 scrapie prions and brains collected at the terminal stage of disease and immunostained to detect CD44. Scale bar = 1,000 μm. **(B)** Dual immunostaining for CD44 and GFAP suggested a correlation in their patterns implying an astrocyte origin. Scale bar = 100 μm. **(C)** C57Bl/Dk mice were injected intracerebrally with ME7 scrapie prions, brains were collected at intervals after infection and immunostained to detect CD44, CD44v6, GFAP and IBA1. Analysis of brains from 45, 80, and 118 days post injection (dpi) shows the progressive increase in expression from the needle-track, injection side thalamus and bilateral spread, respectively. Images are representative of $N = 4$ mice/group. Scale bars = 2,000, 100, or 200 μm as indicated. Upregulation of CD44 coincided with astrocyte (GFAP) and microglial (AIF1) responses. **(D)** CD44 pattern in terminal mouse brain following intracerebral, intraperitoneal, intravenous or oral ME7 infection reveals similar distribution of immunostaining irrespective of the route of exposure. Survival times (days) indicated. Images representative of $N = 6$ mice/group. Scale bars = 500 μm.

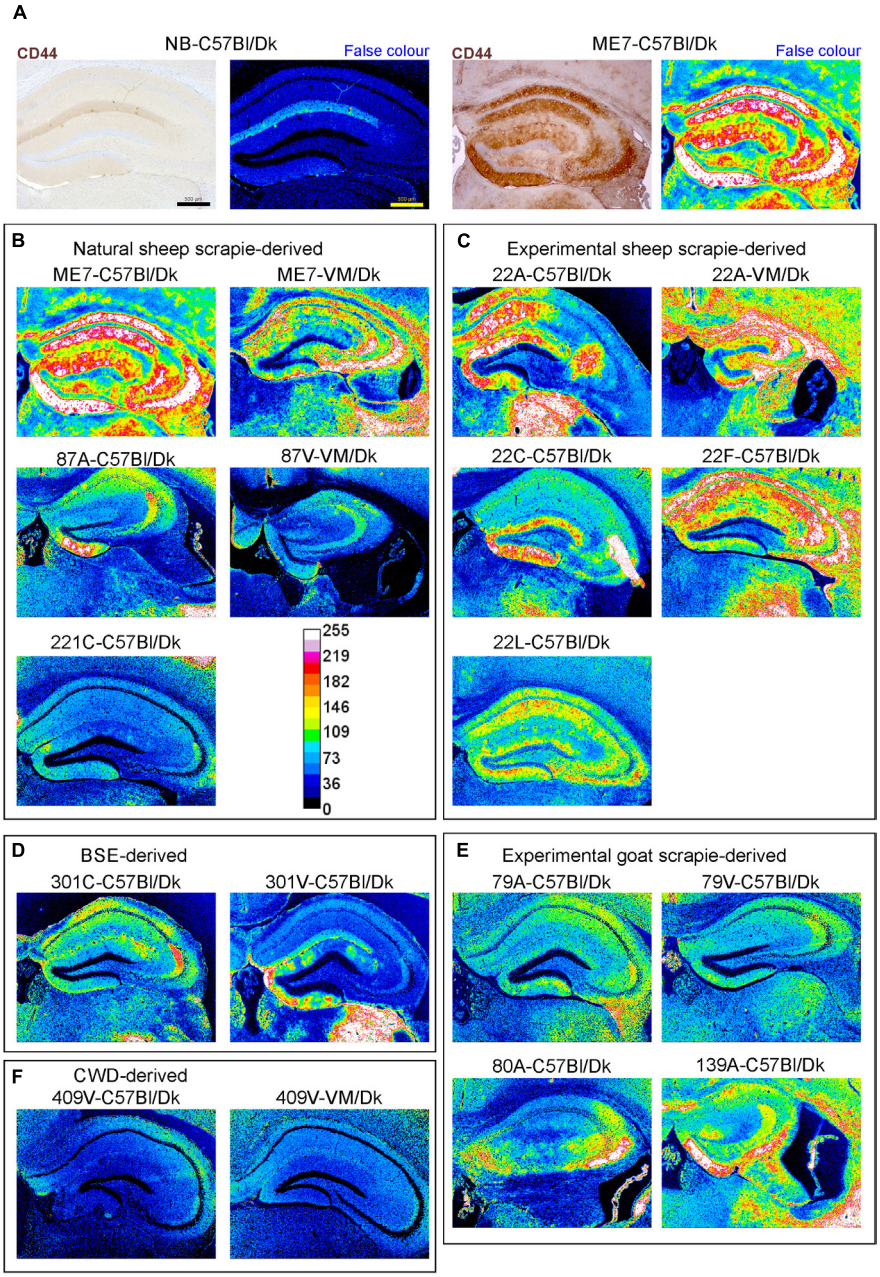

FIGURE 8 | Distinct patterns of CD44+ immunostaining in the hippocampus region of the brains of mice infected with a variety of distinct prion agent strains. Groups of C57Bl/Dk or VM/Dk mice were injected intracerebrally with a variety of distinct prion agent strains (**Table 1**). Brains were collected at the terminal stage of disease and immunostained to detect CD44. Images were then false-colored to compare the signal intensities of the immunostaining between each group. **(A)** Normal brain infected mice display little CD44+ immunostaining when compared to mice terminally affected with ME7 scrapie prions. **(B–F)** Comparison of false colored images to show the variation in CD44+ immunostaining between diverse prion strains isolated from a variety of sources. Representative images from 6 mice/group are shown. Scale bars = 500 μm.

experimental goat scrapie derived strains 79A, 79V, 80A and 139A, the abundance of the CD44 expression was similarly diffuse (**Figures 3B,C,E**, **8B,C,E**). However, in mice infected with 409V prions, the CD44 expression almost exclusively associated with regions containing amyloid PrP^d accumulations.

Since host *Prnp* genotype can significantly affect prion disease survival times and the characteristics of the neuropathology (Dickinson and Fraser, 1977; van Keulen et al., 2015), we next compared CD44 expression in the brains of C57Bl/Dk mice or VM/Dk mice infected with the ME7 or 22A scrapie prion agent strains. This analysis showed infection of C57Bl/Dk mice or VM/Dk mice with the same prion agent strain gave rise to distinct patterns of CD44 expression in the hippocampus (**Figures 8B,C**). This analysis suggests that host *Prnp* genotype

TABLE 2 | Prion agent strain typing based on hippocampal CD44 expression pattern.

Strain-Host	CA1	CA2	CA3	DG
ME7-C57/Dk	+++ so +++ sr + slm	+ so + sr	+++ so + sp ++ slu +++ sr	++ po ++ superior mo +++ inferior mo
22A-C57/Dk	+++ so* +++ sr* +++ slm*	–	+++ sr*	+++ superior mo* ++ inferior mo*
22C-C57/Dk	+ so	+ so	++ sr* ++ so*	++ superior mo* +++ inferior mo*
22F-C57/Dk	+++ so* ++ sp +++ sr* +++ slm*	++ so* ++ sp ++ sr*	++ so* ++ sr*	++ superior mo + inferior mo *mo apex
4 22L-C57/Dk	+ so* ++ sr*	+ so* + sr*	++ so* + slu + sr	+ superior mo ++ inferior mo
79A-C57/Dk	+ so + sr	+ so + sr	++ so ++ slu	+ mo 'astrocytic'
79V-C57/Dk	–	+ so + sr	+++so ++ slu + sr + slm	+ inferior mo
80A-C57/Dk	–	+ so	+slu +++ so	+++ inferior mo
87A-C57/Dk	+ so + sr	+ so +++ sr	+ slu	++ inferior mo*
139A-C57/Dk	++ so ++ sr	+ so + sr	+++ so ++ slu	+++ inferior mo
221C-C57/Dk	–	–	++ so + slu	+ 'astrocytic'/inferior mo
409V-C57/Dk	–	–	–	+ peri plaque DG/Thalamus
301C-C57/Dk	+ so*	+ so* + sr ++ slm*	+ slu	–
301V-C57/Dk	+ slm	–	+ slu	+++ mo 'astrocytic'
ME7-VM/Dk	++ so* ++ sp ++ sr* ++ slm	++ so ++ sr ++ slm	+++ so* +++ sr* + slm	+ mo 'astrocytic' + po
22A-VM/Dk	+++ so* ++ sp +++ sr* +++ slm*	++ so* ++ sr* +++ slm*	++ so* +++ sr* +++ slm	++ mo* ++ po*
87V-VM/Dk	+ so + sr ++ slm	+ so + sr	+ so ++ slu	++ apex mo
409V-VM/Dk	+ peri plaque so/cc	–	–	–

**Regions also stain positive for CD44v6. cc, corpus callosum; mo, molecular layer; po, polymorph layer; slm, stratum lacunosum moleculare; slu, stratum lucidum; so, stratum oriens; sp, stratum pyrimidale; sr, stratum radiatum.*

may also influences the expression pattern of CD44 in the CNS during prion disease.

Next, the magnitude of the CD44+ immunostaining was compared for each strain/host combination investigated by calculating the mean percentage area coverage across nine distinct gray matter areas (**Figures 9A–E**). The intensity of the CD44+ immunostaining across these areas was then compared between each prion agent strain by paired *T*-test (**Supplementary Table 4**). This analysis highlighted the discriminatory nature of reactive astrocyte heterogeneity in CD44 in the brains of mice infected with distinct prion agent strains. Furthermore, this analysis suggested that CD44 + immunostaining had the most discriminatory properties revealing statistically significant differences in 70% (107/153) of comparisons. Of note BSE (301C and 301V) and CWD (409V) derived strains and ME7-C57Bl/Dk were highly statistically significantly different from other scrapie derived strains. Furthermore the same prion strain, e.g., ME7 or 22A produced statistically significantly different profiles when in different *Prnp* genotype hosts.

Representative images of AIF1+; CD44+, CD44v6+, GFAP+ and PrP^d+ immunostaining on serial sections from brains from all the prion agent strain/recipient mouse combinations studied are provided in **Supplementary Figure 1**. Analysis of the correlation of these neuropathological markers of CNS prions disease (AIF1 + microglia; CD44+ and GFAP+ astrocytes; PrP^d) showed the variance across all the prion agent strain/recipient mouse combinations studied (**Supplementary Table 5**). This analysis suggested that the strongest and most significant correlate was CD44 with GFAP amongst most strain-host combinations. Also of note was the lack of correlation with AIF1+ microglia when comparing the neuropathology of ME7 prion agent strain in the brains of C57Bl/Dk mice and VM/Dk mice.

CD44 Upregulation Is Astrocytic and Correlates With Prion Accumulation

In the brains of mice infected with several prion agent strains, astrocytic patterns of PrP^d deposition can be detected (**Figure 10A**). Our analysis suggested that the regions of the brain with astrocytic prion accumulation mirrored those displaying high levels of CD44. Immunostaining with the N-terminal pan-CD44 antibody showed diffuse neuropil staining with un- or lightly stained astrocytes in relief (**Figure 10B**). Co-staining with the pan-CD44 antibody and GFAP similarly showed minimal direct co-localisation between these two proteins in astrocytes (**Figure 10C**). This observation is consistent with the demonstration that the pan-CD44 antibody recognizes an N-terminal epitope in the cleavable and soluble ectodomain of the CD44 protein (Nagano and Saya, 2004).

Activation of CD44v6 isoform on endothelial cells requires association of the CD44 carboxy-terminus with ezrin that couples the CD44v6 isoform to the cytoskeleton (Tremmel et al., 2009). At the terminal stage prion disease our IHC analysis showed that the CD44v6 isoform displayed either an intense staining pattern throughout the astrocyte, or mixed pattern including strong staining throughout the astrocyte and a surrounding diffuse staining pattern (**Figure 10D**). The pattern of CD44v6 immunostaining appeared to be more distinctly localized when compared to the widespread and diffuse pattern obtained with pan-CD44 staining. It is plausible that the pan-CD44 upregulation observed at the terminal stage also includes standard CD44 and/or splice variants other than CD44v6.

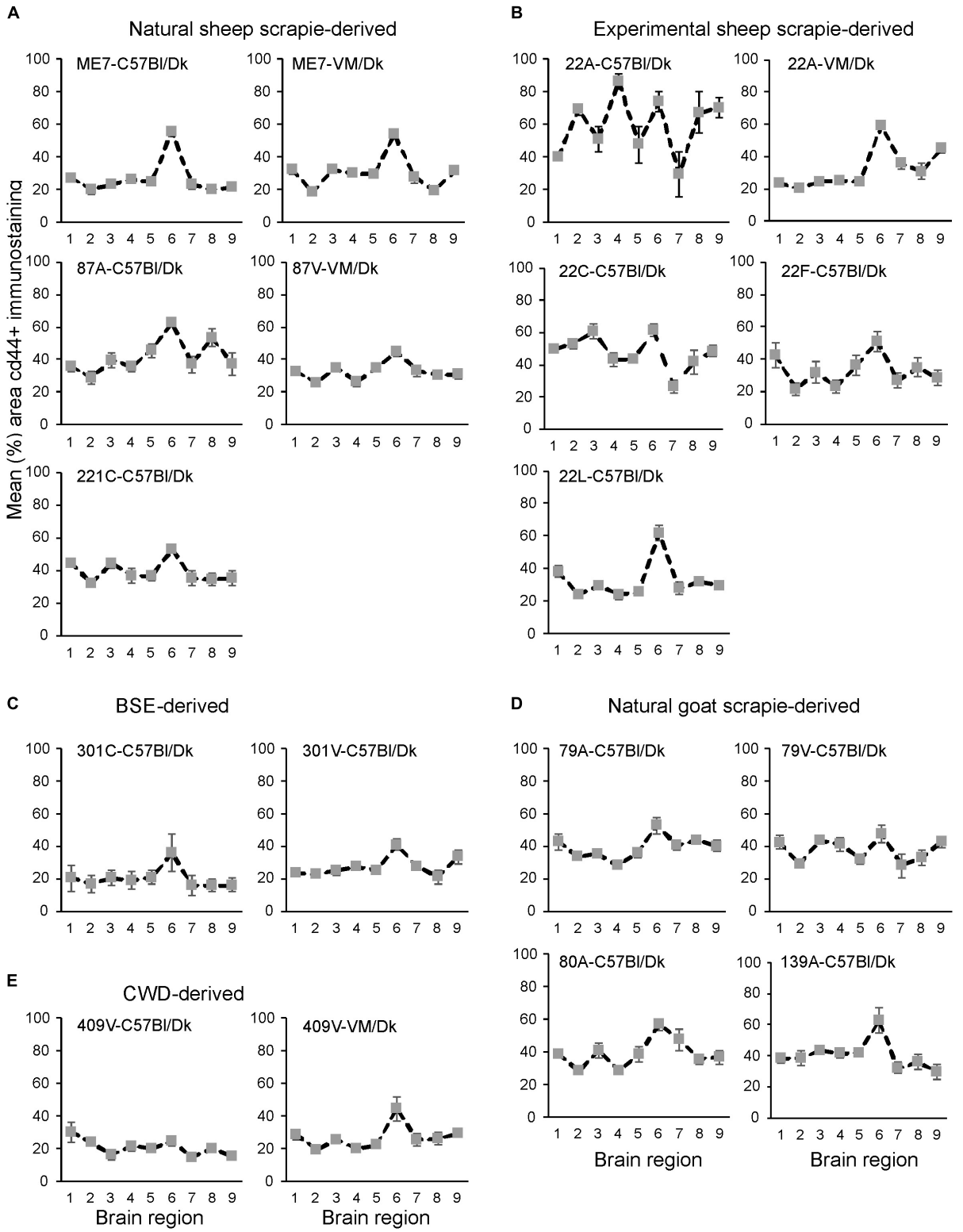

FIGURE 9 | (A–E) Comparison of the magnitude and distribution of the CD44+ immunostaining in the brains of mice infected with a variety of distinct prion agent strains. Groups of C57Bl/Dk or VM/Dk mice were injected intracerebrally with a variety of distinct prion agent strains (**Table 1**). Brains were collected at the terminal stage of disease and immunostained to detect CD44. The percentage area coverage of CD44+ immunostaining was then compared in each of the following gray matter brain regions G1, dorsal medulla; G2, cerebellar cortex; G3, superior colliculus; G4, hypothalamus; G5, medial thalamus; G6, hippocampus; G7, septum; G8, cerebral cortex; G9, forebrain cerebral cortex. *N* = 6 mice/group. Data represent mean ± SEM, from a minimum of 54 images/group.

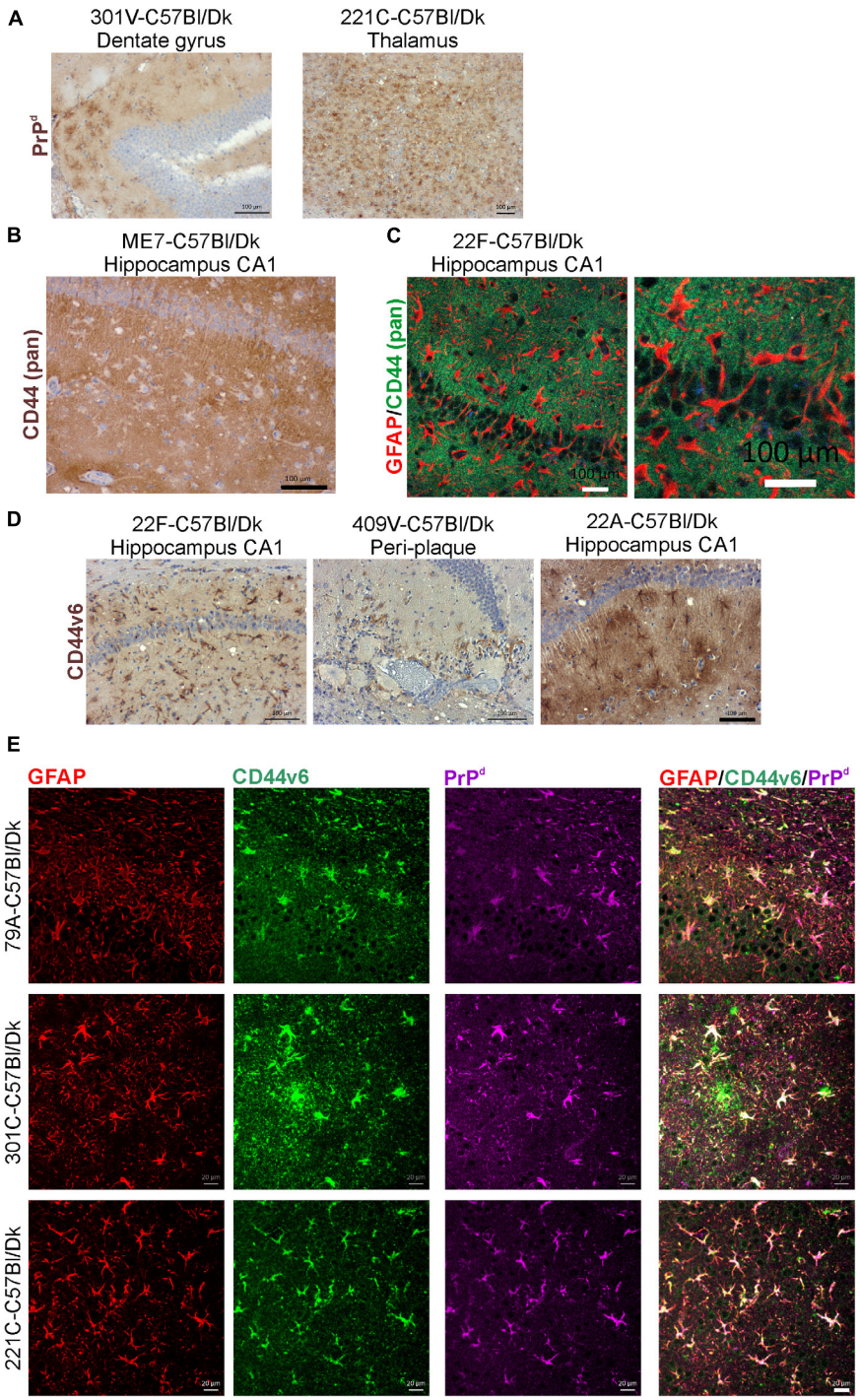

FIGURE 10 | CD44v6 expression and PrP^d colocalize with GFAP + astrocytes in the brains during prion disease. **(A)** Immunohistochemical demonstration of astrocytic PrP^d immunostaining patterns in brains of mice infected with certain prion agent strains. **(B,C)** Immunohistochemical analysis shows pan-CD44 expression surrounds but does not co-localize with GFAP in astrocytes. **(D)** Immunostaining for CD44v6 shows astrocytic staining pattern suggesting that astrocytes are the predominant cellular source of CD44 upregulation during prion disease. **A–C** scale bars = 100 µm. **(E)** Immunofluorescent analysis of CD44, GFAP and PrP^d in the brains of mice with prion disease shows that CD44+ /GFAP+ astrocytes accumulate PrP^d. Scale bars = 20 µm.

For example, in the brains of human Alzheimer's disease patients upregulation of splice variants CD44v3 and CD44v10 as well as CD44v6 has also been observed (Pinner et al., 2017). This combination of staining patterns also suggests that CD44v6 may have undergone extracellular cleavage and binding to the cytoskeleton in specific astrocyte subpopulations

(**Figures 10D,E**). IHC for GFAP, CD44v6 and PrP^{d} revealed colocalization in specific astrocyte populations (**Figure 10E**).

DISCUSSION

Prion diseases are a diverse group of infectious neurodegenerative disorders that are considered to be caused by abnormally folded prion protein. The observation of different clinical syndromes following the transmission of experimental scrapie prions in goats led to the suggestion of variation in prion strains (Pattison and Millson, 1961). Transmissions into laboratory mice proved that prion disease isolates may be resolved into individual strains of infectious agent, that retain specific properties including the duration of the survival time and the targeting of the neuropathology to defined brain areas (Bruce, 2003). Of course, one of the major contentious issues in the prion hypothesis is how a misfolded host protein (PrP^{Sc}) can encode such diverse strain-specific properties. Plausibly, the prion agent diversity may be encoded partly or in combination through variation in primary structure, N-linked glycosylation and folding confirmation (Morales et al., 2007). The exact mechanisms that control prion agent strain targeting within the CNS are unknown, despite the neuroinflammatory nature of prion neurodegeneration being identified (Burwinkel et al., 2004; Riemer et al., 2009; Crespo et al., 2012).

In this study, we set out to characterize astrocyte responses to prion infection and uncovered a host response to infection that defines prion strain targeting within the CNS. Until now prion strain typing has typically involved lengthy and expensive transmission experiments in panels of laboratory mice (Boyle et al., 2017). However, this detailed prion strain-typing is necessary for the identification and characterization of novel and emerging prion diseases, especially those with zoonotic potential. Here we show that prion agent strains can be readily discriminated via profiling of astrocyte CD44 expression within the CNS. In the current study, astrocyte responses to prion infection were characterized using anti-pan-CD44 and the splice variant specific anti-CD44v6 antibodies on a wide-range of mouse-adapted prion disease strains derived from sheep scrapie, BSE and CWD. We show that the upregulation of CD44 expression occurs in sub-region specific brain areas revealing an undiscovered level of heterogeneity in astrocyte populations following prion infection. Further analysis showed that the variety in the presentation of the CD44+ immunostaining between each prion stain/host combination revealed unique and distinguishable patterns, especially within the hippocampus. Indeed even in the brains of mice infected with the amyloidogenic mouse-adapted CWD strain 409V, the astrocytes surrounding the PrP plaques responded via upregulating both GFAP and CD44. Furthermore, the expression profile of the CD44+ immunostaining in mice infected with the ME7 scrapie agent strain was unaltered by the route of infection. CD44 was upregulated as early as halfway through the incubation period and occurred concurrently with some of the earliest neuropathological changes. CD44 positive astrocytes also displayed accumulation of PrP^{Sc}, suggesting they may act as reservoirs for prion production within the CNS during infection.

Following on from our analysis of prion agent strain-specific CD44 patterns in brains of experimentally infected mice, further work is now required to investigate the variation in CD44 expression patterns in natural prion disease in both human and animal hosts. Such analysis is essential to determine whether this the pattern of the CD44+ immunostaining in the brain can similarly be used to discriminate distinct prion diseases in these natural host species.

The pattern and morphology of the pan-CD44 labeling in prion-infected brain indicated an astrocytic source, as observed previously in Alzheimer's disease (Akiyama et al., 1993). Immunostaining of prion disease-affected brains with an antibody against the common (pan) extracellular N-terminus of CD44 surrounded, but did not co-localize, with cytoplasmic and cytoskeletal GFAP. To provide additional confirmation that the source of the CD44 was astrocytic in nature we investigated further the expression of splice variant CD44v6, since independent studies have shown that when this variant is upregulated in certain cell populations it is coupled to the cytoskeleton when activated (Tremmel et al., 2009). Our data suggested that the distribution of splice variant CD44v6 expression was mostly associated with the GFAP+ compartment of relevant reactive astrocytes following prion infection. In some strain/host combinations, additional diffuse immunostaining was also apparent in association with the cell membrane. Furthermore, the lack of labeling with the N-terminal pan-CD44 antibody in that same GFAP+ compartment implies that the v6 epitope in the extracellular stem region of the CD44 protein is retained whereas the panCD44 N-terminal epitope is not. Thus it is plausible that during CNS prion disease intracellular and potentially activated CD44v6 has been N-terminally cleaved by extracellular proteases, rather than intracellular γ-secretase cleavage (Nagano and Saya, 2004; Pelletier et al., 2006; Anderegg et al., 2009). Data from Alzheimer's disease patients has also revealed increases in other CD44 splice variants, in particular CD44v3 and CD44v10 (Pinner et al., 2017). Whether the expression of other CD44 splice variants is similarly induced in astrocytes during prion disease remains to be determined.

Together, our data show that during CNS prion disease specific reactive astrocytes express high levels of CD44 and the splice variant form, CD44v6. Analysis of CD44 expression in distinct regions throughout the brain also suggested that CD44 was not universally upregulated in GFAP+ activated astrocytes. The precise role of the CD44+ astrocytes during CNS prion disease remains to be determined. CD44 is a multifunctional single-chain transmembrane glycoprotein, which mediates cellular responses to the extracellular environment (Ponta et al., 2003; Dzwonek and Wilczynski, 2015). Within the CNS CD44 has been shown to regulate the functional and structural plasticity and integrity of dendritic spines and synapses (Skupien et al., 2014; Roszkowska et al., 2016), as well as regulating astrocyte morphology (Konopka et al., 2016). Since these features are adversely affected during CNS prion disease (Jeffrey et al., 1995, 2000) it is plausible that the altered CD44 expression described here may contribute to the

development of the neuropathology. Transcriptomic analyses of the reactive astrocytes induced by various pro-inflammatory stimuli have shown that CD44 expression is significantly elevated in neurotoxic A1 astrocytes when compared to A2 astrocytes (Liddelow et al., 2017). Thus is it plausible that the enhanced expression of CD44 or CD44v6 during CNS prion disease may also be indicative of a neurotoxic phenotype in the reactive astrocytes. Specific blockade of the ability of microglia to stimulate A1 astrocyte conversion can provide neuroprotection in a mouse model of α-synucleinopathy-induced neurodegeneration (Yun et al., 2018). Further studies are required to determine whether the modulation of astrocyte activation may likewise be beneficial during CNS prion disease.

DATA AVAILABILITY

All datasets generated for this study are included in the manuscript and/or the **Supplementary Files**.

ETHICS STATEMENT

The animal studies were reviewed and approved by the Institute for Animal Health Neuropathogenesis Unit Ethical Review Committee, the University of Edinburgh Ethical Review Committee, and the UK Home Office.

AUTHOR CONTRIBUTIONS

BB and NM contributed to the conception and design of the study, and wrote the manuscript. BB and CW acquired the data and performed the statistical analysis. All authors interpreted the data and contributed to the final version of the manuscript revision.

FUNDING

This work was supported by The Roslin Institute Strategic Programme Grant funding from the Biotechnological and Biological Sciences Research Council (grant number BBS/E/D/20002173) and Infectious Diseases One Health Masters Studentship funding to CW co-funded by the Erasmus+ Programme of the European Union.

ACKNOWLEDGMENTS

The majority of the mouse transmissions described in this study were originally undertaken by former colleagues at the Neuropathogenesis Unit (Institute for Animal Health, Edinburgh, United Kingdom) including: Moira Bruce, Simon Cumming, Alan Dickinson, Hugh Fraser, James Hope, Richard Kimberlin, Irene McConnell, George Outram, and Robert Somerville. We thank Aileen Boyle, Gillian McGregor, and the Easter Bush Pathology Services Group (University of Edinburgh) for technical support.

SUPPLEMENTARY MATERIAL

The Supplementary Material for this article can be found online at: https://www.frontiersin.org/articles/10.3389/fncel.2019.00411/full#supplementary-material

REFERENCES

Aguzzi, A., and Liu, Y. (2017). role for astroglia in prion diseases. *J. Exp. Med.* 214, 3477–3479. doi: 10.1084/jem.20172045

Aguzzi, A., and Zhu, C. (2017). Microglia in prion diseases. *J. Clin. Invest.* 127, 3230–3239. doi: 10.1172/JCI90605

Akiyama, H., Tooyama, I., Kawamata, T., Ikeda, K., and McGeer, P. L. (1993). Morphological diversities of CD44 positive astrocytes in the cerebral cortex of normal subjects and patients with Alzheimer's disease. *Brain Res.* 632, 249–259. doi: 10.1016/0006-8993(93)91160-t

Anderegg, U., Eichenberg, T., Parthaune, T., Haiduk, C., Saalbach, A., Milkova, L., et al. (2009). ADAM10 is the constitutive functional sheddase of CD44 in human melanoma cells. *J. Invest. Dermatol.* 129, 1471–1482. doi: 10.1038/jid.2008.323

Arima, K., Nishida, N., Sakaguchi, S., Shigematsu, K., Atarashi, R., Yamaguchi, N., et al. (2005). Biological and biochemical characteristics of prion strains conserved in persistently infected cell cultures. *J. Virol.* 79, 7104–7112. doi: 10.1128/jvi.79.11.7104-7112.2005

Boyle, A., Hogan, K., Manson, J. C., and Diack, A. B. (2017). "Typing of prion diseases using in vivo mouse models," in *Prions: Methods and Protocols*, ed. V. A. Lawson, (New York, NY: Springer), 263–283. doi: 10.1007/978-1-4939-7244-9_18

Brown, K. L., Gossner, A., Mok, S., and Mabbott, N. A. (2012). The effects of host age on the transport of complement-bound complexes to the spleen and the pathogenesis of intravenous scrapie infection. *J. Virol.* 86, 25–35. doi: 10.1128/JVI.05581-11

Bruce, M., Chree, A., McConnell, I., Foster, J., Pearson, G., and Fraser, H. (1994). Transmission of bovine spongiform encephalopathy and scrapie to mice: strain variation and the species barrier. *philos. Trans. R. Soc. Lond Ser. B Biol. Sci.* 343, 405–411. doi: 10.1098/rstb.1994.0036

Bruce, M. E. (2003). TSE strain variation. *Br. Med. Bull.* 66, 99–108. doi: 10.1093/bmb/66.1.99

Bruce, M. E., Boyle, A., Cousens, S., McConnell, I., Foster, J., Goldmann, W., et al. (2002). Strain characterization of natural sheep scrapie and comparison with BSE. *J. Gen. Virol.* 83(Pt 3), 695–704. doi: 10.1099/0022-1317-83-3-695

Bruce, M. E., Dickinson, A. G., and Fraser, H. (1976). Cerebral amyloidosis in scrapie in the mouse: effect of agent strain and mouse genotype. *Neuropathol. Appl. Neurobiol.* 2, 471–478. doi: 10.1111/j.1365-2990.1976.tb00521.x

Bruce, M. E., McBride, P. A., and Farquhar, C. F. (1989). Precise targeting of the pathology of the sialoglycoprotein, PrP, and vacuolar degeneration in mouse scrapie. *Neurosci. Lett.* 102, 1–6. doi: 10.1016/0304-3940(89)90298-x

Bruce, M. E., McConnell, I., Fraser, H., and Dickinson, A. G. (1991). The disease characteristics of different strains of scrapie in sinc congenic mouse lines: implications for the nature of the agent and host control of pathogenesis. *J. Gen. Virol.* 72(Pt 3), 595–603. doi: 10.1099/0022-1317-72-3-595

Bruce, M. E., Will, R. G., Ironside, J. W., McConnell, I., Drummond, D., Suttie, A., et al. (1997). Transmissions to mice indicate that 'new variant' CJD is caused by the BSE agent. *Nature* 389, 498–501. doi: 10.1038/39057

Burwinkel, M., Riemer, C., Schwarz, A., Schultz, J., Neidhold, S., Bamme, T., et al. (2004). Role of cytokines and chemokines in prion infections of the central nervous system. *Int. J. Dev. Neurosci.* 22, 497–505. doi: 10.1016/j.ijdevneu.2004.07.017

Carroll, J. A., Race, B., Williams, K., Striebel, J., and Chesebro, B. (2018). Microglia are critical in host defense against prion disease. *J. Virol.* 92, e549–e518. doi: 10.1128/JVI.00549-18

Chandler, R. L. (1961). Encephalopathy in mice produced by inoculation with Scrapie brain material. *Lancet* 277, 1378–1379. doi: 10.1016/s0140-6736(61)92008-6

Crespo, I., Roomp, K., Jurkowski, W., Kitano, H., and del Sol, A. (2012). Gene regulatory network analysis supports inflammation as a key neurodegeneration process in prion disease. *BMC Syst. Biol.* 6:132. doi: 10.1186/1752-0509-6-132

Dickinson, A. G. (1976). Scrapie in sheep and goats. *Front. Biol.* 44:209–241.

Dickinson, A. G., and Fraser, H. (1977). Scrapie: pathogenesis in inbred mice: an assessment of host control and response involving many strains of agent. in *Slow Virus Infections of the Central Nervous System* eds V. ter Meulen, and M. Katz, (New York, NY: Springer).

Dickinson, A. G., and Meikle, V. M. H. (1969). A comparison of some biological characteristics of the mouse-passaged scrapie agents, 22A and ME7. *Gene. Res.* 13, 213–225. doi: 10.1017/s0016672300002895

Dickinson, A. G., and Meikle, V. M. H. (1971). Host-genotype and agent effects in scrapie incubation: change in allelic interaction with different strains of agent. *Mol. Gen. Gene.* 112, 73–79. doi: 10.1007/bf00266934

Diedrich, J. F., Bendheim, P. E., Kim, Y. S., Carp, R. I., and Haase, A. T. (1991). Scrapie-associated prion protein accumulates in astrocytes during scrapie infection. *Proc. Natl. Acad. Sci. U.S.A.* 88, 375–379. doi: 10.1073/pnas.88.2.375

Dzwonek, J., and Wilczynski, G. M. (2015). CD44: molecular interactions, signaling and functions in the nervous system. *Front. Cell. Neurosci.* 9:175. doi: 3389/fncel.2015.00175

Fang, C., Imberdis, T., Garza, M. C., Wille, H., and Harris, D. A. (2016). A neuronal culture system to detect prion synaptotoxicity. *PLoS Pathogens.* 12:e1005623. doi: 10.1371/journal.ppat.1005623

Fraser, H. (1993). Diversity in the neuropathology of scrapie-like diseases in animals. *Br. Med. Bull.* 49, 792–809. doi: 10.1093/oxfordjournals.bmb.a072647

Fraser, H., and Dickinson, A. G. (1967). Distribution of experimentally induced scrapie lesions in the brain. *Nature* 216, 1310–1311. doi: 10.1038/2161310a0

Fraser, H., and Dickinson, A. G. (1968). The sequential development of the brain lesions of scrapie in three strains of mice. *J. Comp. Pathol.* 78, 301–311. doi: 10.1016/0021-9975(68)90006-6

Fraser, H., and Dickinson, A. G. (1973). Scrapie in mice. *J. Comp. Pathol.* 83, 29–40.

Gao, C., Guo, H., Downey, L., Marroquin, C., Wei, J., and Kuo, P. C. (2003). Osteopontin-dependent CD44v6 expression and cell adhesion in HepG2 cells. *Carcinogenesis* 24, 1871–1878. doi: 10.1093/carcin/bgg139

Georgsson, G., Gísladóttir, E., and Árnadóttir, S. (1993). Quantitative assessment of the astrocytic response in natural scrapie of sheep. *J. Comp. Pathol.* 108, 229–240. doi: 10.1016/s0021-9975(08)80287-3

Giese, A., Groschup, M. H., Hess, B., and Kretzschmar, H. A. (1995). Neuronal cell death in scrapie-infected mice is due to apoptosis. *Brain Pathol.* 5, 213–221. doi: 10.1111/j.1750-3639.1995.tb00597.x

Inman, C. F., Rees, L. E. N., Barker, E., Haverson, K., Stokes, C. R., and Bailey, M. (2005). Validation of computer-assisted, pixel-based analysis of multiple-colour immunofluorescence histology. *J. Immunol. Methods* 302, 156–167. doi: 10.1016/j.jim.2005.05.005

Jeffrey, M., Fraser, J. R., Halliday, W. G., Fowler, N., Goodsir, C. M., and Brown, D. A. (1995). Early unsuspected neuron and axon terminal loss in scra pie-infected mice revealed by morphometry and immunocytochemistry. *Neuropathol. Appl. Neurobiol.* 21, 41–49. doi: 10.1111/j.1365-2990.1995.tb01027.x

Jeffrey, M., Halliday, W. G., Bell, J., Johnston, A. R., MacLeod, N. K., Ingham, C., et al. (2000). Synapse loss associated with abnormal PrP precedes neuronal degeneration in th.e scrapie-infected murine hippocampus. *Neuropathol. Appl. Neurobiol.* 26, 41–54. doi: 10.1046/j.1365-2990.2000.00216.x

Katagiri, Y. U., Sleeman, J., Fujii, H., Herrlich, P., Hotta, H., Tanaka, K., et al. (1999). Variants but not CD44s cooperate with β1-containing integrins to permit cells to bind to osteopontin independently of arginine-glycine-aspartic acid, thereby stimulating cell motility and chemotaxis. *Cancer Res.* 59, 219–226.

Kercher, L., Favara, C., Striebel, J. F., LaCasse, R., and Chesebro, B. (2007). Prion protein expression differences in microglia and astroglia influence scrapie-induced neurodegeneration in the retina and brain of transgenic mice. *J. Virol.* 81, 10340–10351. doi: 10.1128/jvi.00865-07

Khan, S. A., Cook, A. C., Kappil, M., Günthert, U., Chambers, A. F., Tuck, A. B., et al. (2005). Enhanced cell surface CD44 variant (v6, v9) expression by osteopontin in breast cancer epithelial cells facilitates tumor cell migration: Novel post-transcriptional, post-translational regulation. *Clin. Exp. Meta.* 22, 663–673. doi: 10.1007/s10585-006-9007-0

Konopka, A., Zeug, A., Skupien, A., Kaza, B., Mueller, F., Chwedorowicz, A., et al. (2016). Cleavage of hyaluronan and CD44 adhesion molecule regulate astrocyte morphology via Rac1 signalling. *PloS one* 11:e0155053. doi: 10.1371/journal.pone.0155053

Kovács, G. G., Preusser, M., Strohschneider, M., and Budka, H. (2005). Subcellular localization of disease-associated prion protein in the human brain. *Am. J. Pathol.* 166, 287–294. doi: 10.1016/s0002-9440(10)62252-3

Krejciova, Z., Alibhai, J., Zhao, C., Krencik, R., Rzechorzek, N. M., Ullian, E. M., et al. (2017). Human stem cell–derived astrocytes replicate human prions in a PRNP genotype–dependent manner. *J. Exp. Med.* 214, 3481–3495. doi: 10.1084/jem.20161547

Liddelow, S. A., Guttenplan, K. A., Clarke, L. E., Bennett, F. C., Bohlen, C. J., Schirmer, L., et al. (2017). Neurotoxic reactive astrocytes are induced by activated microglia. *Nature* 541:481. doi: 10.1038/nature21029

Marella, M., and Chabry, J. (2004). Neurons and astrocytes respond to prion infection by inducing microglia recruitment. *J. Neurosci.* 24, 620–627. doi: 10.1523/jneurosci.4303-03.2004

Marroquin, C. E., Downey, L., Guo, H., and Kuo, P. C. (2004). Osteopontin increases CD44 expression and cell adhesion in RAW 264.7 murine leukemia cells. *Immunol. Lett.* 95, 109–112. doi: 10.1016/j.imlet.2004.06.001

Monzon, M., Hernandez, R. S., Garces, M., Sarasa, R., and Badiola, J. J. (2018). Glial alterations in human prion diseases: a correlative study of astroglia, reactive microglia, protein deposition, and neuropathological lesions. *Medicine* 97:e0320. doi: 10.1097/MD.0000000000010320

Morales, R., Abid, K., and Soto, C. (2007). The prion strain phenomenon: molecular basis and unprecedented features. *Biochim. Biophys. Acta* 1772, 681–691. doi: 10.1016/j.bbadis.2006.12.006

Morisaki, Y., Niikura, M., Watanabe, M., Onishi, K., Tanabe, S., Moriwaki, Y., et al. (2016). Selective expression of osteopontin in ALS-resistant motor neurons is a critical determinant of late phase neurodegeneration mediated by matrix metalloproteinase-9. *Sci. Rep.* 6:27354. doi: 10.1038/srep27354

Nagano, O., and Saya, H. (2004). Mechanism and biological significance of CD44 cleavage. *Cancer Sci.* 95, 930–935. doi: 10.1111/j.1349-7006.2004.tb03179.x

Pattison, I. H., and Millson, G. C. (1961). Scrapie produced experimentally in goats with special reference to the clinical syndrome. *J. Comp. Pathol. Ther.* 71, 101–108.

Pelletier, L., Guillaumot, P., Frêche, B., Luquain, C., Christiansen, D., Brugière, S., et al. (2006). γ-secretase-dependent proteolysis of CD44 promotes neoplastic transformation of rat fibroblastic cells. *Cancer Res.* 66, 3681–3687. doi: 10.1158/0008-5472.can-05-3870

Peretz, D., Scott, M. R., Groth, D., Williamson, R. A., Burton, D. R., Cohen, F. E., et al. (2001). Strain-specified relative conformational stability of the scrapie prion protein. *Protein Sci.* 10, 854–863. doi: 10.1110/ps.39201

Peretz, D., Williamson, R. A., Legname, G., Matsunaga, Y., Vergara, J., Burton, D. R., et al. (2002). A change in the conformation of prions accompanies the emergence of a new prion strain. *Neuron* 34, 921–932. doi: 10.1016/s0896-6273(02)00726-2

Phatnani, H., and Maniatis, T. (2015). Astrocytes in neurodegenerative disease. *Cold Spring Harbor Pers. Biol.* 7:a020628. doi: 10.1101/cshperspect.a020628

Pinner, E., Gruper, Y., Ben Zimra, M., Kristt, D., Laudon, M., Naor, D., et al. (2017). CD44 splice variants as potential players in alzheimer's disease pathology. *J. Alzheimers Dis.* 58, 1137–1149. doi: 10.3233/JAD-161245

Ponta, H., Sherman, L., and Herrlich, P. A. (2003). CD44: From adhesion molecules to signalling regulators. *Nat. Rev. Mol. Cell Biol.* 4, 33–45. doi: 10.1038/nrm1004

Prusiner, S. B. (1982). Novel proteinaceous infectious particles cause scrapie. *Science* 216, 136–144. doi: 10.1126/science.6801762

Race, R. E., Priola, S. A., Bessen, R. A., Ernst, D., Dockter, J., Rall, G. F., et al. (1995). Neuron-specific expression of a hamster prion protein minigene in transgenic mice induces susceptibility to hamster scrapie agent. *Neuron* 15, 1183–1191. doi: 10.1016/0896-6273(95)90105-1

Raeber, A. J., Race, R. E., Brandner, S., Priola, S. A., Sailer, A., Bessen, R. A., et al. (1997). Astrocyte-specific expression of hamster prion protein (PrP) renders

PrP knockout mice susceptible to hamster scrapie. *EMBO J.* 16, 6057–6065. doi: 10.1093/emboj/16.20.6057

Riemer, C., Gultner, S., Heise, I., Holtkamp, N., and Baier, M. (2009). Neuroinflammation in prion diseases: concepts and targets for therapeutic intervention. *CNS Neurol. Disord. Drug Targets* 8, 329–341. doi: 10.2174/187152709789542014

Roszkowska, M., Skupien, A., Wójtowicz, T., Konopka, A., Gorlewicz, A., Kisiel, M., et al. (2016). CD44: a novel synaptic cell adhesion molecule regulating structural and functional plasticity of dendritic spines. *Mol. Biol. Cell.* 27, 4055–4066. doi: 10.1091/mbc.e16-06-0423

Safar, J., Wille, H., Itri, V., Groth, D., Serban, H., Torchia, M., et al. (1998). Eight prion strains have PrP(Sc) molecules with different conformations. *Nat. Med.* 4, 1157–1165. doi: 10.1038/2654

Sarasa, R., Martinez, A., Monleon, E., Bolea, R., Vargas, A., Badiola, J. J., et al. (2012). Involvement of astrocytes in transmissible spongiform encephalopathies: a confocal microscopy study. *Cell Tissue Res.* 350, 127–134. doi: 10.1007/s00441-012-1461-1

Skupien, A., Konopka, A., Trzaskoma, P., Labus, J., Gorlewicz, A., Swiech, L., et al. (2014). CD44 regulates dendrite morphogenesis through Src tyrosine kinase-dependent positioning of the Golgi. *J. Cell Sci.* 127, 5038–5051. doi: 10.1242/jcs.154542

Sosunov, A. A., Guilfoyle, E., Wu, X., McKhann, G. M., and Goldman, J. E. (2013). Phenotypic conversions of "Protoplasmic" to "Reactive" astrocytes in alexander disease. *J. Neurosci.* 33, 7439–7450. doi: 10.1523/JNEUROSCI.4506-12.2013

Tremmel, M., Matzke, A., Albrecht, I., Laib, A. M., Olaku, V., Ballmer-Hofer, K., et al. (2009). A CD44v6 peptide reveals a role of CD44 in VEGFR-2 signaling and angiogenesis. *Blood.* 114, 5236–5244. doi: 10.1182/blood-2009-04-219204

van Keulen, L. J. M., Langeveld, J. P. M., Dolstra, C. H., Jacobs, J., Bossers, A., and van Zijderveld, F. G. (2015). TSE strain differentiation in mice by immunohistochemical PrPSc profiles and triplex Western blot. *Neuropathol. Appl. Neurobiol.* 41, 756–779. doi: 10.1111/nan.12181

Weber, G. F., Ashkar, S., Glimcher, M. J., and Cantor, H. (1996). Receptor-ligand interaction between CD44 and osteopontin (Eta-1). *Science* 271, 509–512. doi: 10.1126/science.271.5248.509

Westaway, D., Goodman, P. A., Mirenda, C. A., McKinley, M. P., Carlson, G. A., and Prusiner, S. B. (1987). Distinct prion proteins in short and long scrapie incubation period mice. *Cell* 51, 651–662. doi: 10.1016/0092-8674(87)90134-6

Williams, E. S., and Young, S. (1980). Chronic wasting disease of captive mule deer: a spongiform encephalopathy. *J. Wildl. Dis.* 16, 89–98. doi: 10.7589/0090-3558-16.1.89

Yun, S. P., Kam, T.-I., Panicker, N., Kim, S., Oh, Y., Park, J.-S., et al. (2018). Block of A1 astrocyte conversion by microglia is neuroprotective in models of Parkinson's disease. *Nat. Med.* 24, 931–938. doi: 10.1038/s41591-018-0051-5

Zamanian, J. L., Xu, L., Foo, L. C., Nouri, N., Zhou, L., Giffard, R. G., et al. (2012). Genomic analysis of reactive astrogliosis. *J. Neurosci.* 32, 6391–6410. doi: 10.1523/jneurosci.6221-11.2012

Zlotnik, I., and Rennie, J. C. (1963). Further observations on experimental transmission of scrapie from sheep and goats to laboratory mice. *J. Comp. Pathol.* 73, 150–162.

Conflict of Interest Statement: The authors declare that the research was conducted in the absence of any commercial or financial relationships that could be construed as a potential conflict of interest.

frontiers in Cellular Neuroscience

MINI REVIEW
published: 18 September 2019
doi: 10.3389/fncel.2019.00424

The Endocannabinoid System as a Window Into Microglial Biology and Its Relationship to Autism

*Daniel John Araujo[1], Karensa Tjoa[1] and Kaoru Saijo[1,2]**

[1] Department of Molecular & Cell Biology, University of California, Berkeley, Berkeley, CA, United States, [2] Helen Wills Neuroscience Institute, University of California, Berkeley, Berkeley, CA, United States

Microglia are the resident, innate immune cells of the central nervous system (CNS) and are critical in managing CNS injuries and infections. Microglia also maintain CNS homeostasis by influencing neuronal development, viability, and function. However, aberrant microglial activity and phenotypes are associated with CNS pathology, including autism spectrum disorder (ASD). Thus, improving our knowledge of microglial regulation could provide insights into the maintenance of CNS homeostasis as well as the prevention and treatment of ASD. Control of microglial activity is in part overseen by small, lipid-derived molecules known as endogenous cannabinoids (endocannabinoids). Endocannabinoids are one component of the endocannabinoid system (ECS), which also includes the enzymes that metabolize these ligands, in addition to cannabinoid receptor 1 (CB_1) and 2 (CB_2). Interestingly, increased ECS signaling leads to an anti-inflammatory, neuroprotective phenotype in microglia. Here, we review the literature and propose that ECS signaling represents a largely untapped area for understanding microglial biology and its relationship to ASD, with special attention paid to issues surrounding the use of recreational cannabis (marijuana). We also discuss major questions within the field and suggest directions for future research.

Keywords: microglia, endocannabinoids, autism, neuroinflammation, neurodevelopment

OPEN ACCESS

Edited by:
Yu Tang,
Central South University, China

Reviewed by:
Carmen Guaza,
Cajal Institute (CSIC), Spain
Nagarkatti Prakash,
University of South Carolina, United States
Raphael Mechoulam,
The Hebrew University of Jerusalem, Israel

***Correspondence:**
Kaoru Saijo
ksaijo@berkeley.edu

Specialty section:
This article was submitted to Cellular Neurophysiology, a section of the journal Frontiers in Cellular Neuroscience

Received: *13 June 2019*
Accepted: *03 September 2019*
Published: *18 September 2019*

Citation:
Araujo DJ, Tjoa K and Saijo K (2019) The Endocannabinoid System as a Window Into Microglial Biology and Its Relationship to Autism. Front. Cell. Neurosci. 13:424. doi: 10.3389/fncel.2019.00424

INTRODUCTION

Microglia represent a self-sustaining population of cells that originates from the yolk sac and colonizes the brain *in utero* (Alliot et al., 1999; Ginhoux et al., 2010; Bruttger et al., 2015; Askew et al., 2017; Huang et al., 2018). Microglia are the resident immune cells of the central nervous system (CNS) and thus are the first line of defense against CNS infection and injury. For example, they phagocytize debris and pathogens as well as initiate neuroinflammatory responses through release of cytokines such as interleukin-1 (IL-1), IL-6, and tumor necrosis factor alpha (TNF-α) (Yang et al., 2010; Janda et al., 2018). They also recruit natural killer cells, macrophages, and lymphocytes to sites of infection and injury (Yang et al., 2010). Moreover, microglia influence the health of their local environment through release of neurotrophic and neurotoxic factors (Nakajima et al., 2001; Srinivasan et al., 2004; Parkhurst et al., 2013).

In addition to the aforementioned roles, microglia carry out other functions essential for CNS homeostasis (Saijo and Glass, 2011; Butovsky and Weiner, 2018; Lenz and Nelson, 2018). Specifically, these cells oversee neurogenesis by both phagocytizing and directing the migration

of newborn neurons (Sierra et al., 2010; Ribeiro Xavier et al., 2015). Microglia also regulate neuronal connections by engulfing excessive synaptic structures through use of the classical complement cascade (Stevens et al., 2007). Lastly, microglia modulate neuronal plasticity via release of neurotrophins such as brain-derived neurotrophic factor (BDNF) (Parkhurst et al., 2013). Early wiring of the brain requires tight control of these processes and therefore microglia critically impact CNS development (Paolicelli et al., 2011; Bialas and Stevens, 2013; Shigemoto-Mogami et al., 2014).

Due to their wide-ranging contributions to CNS homeostasis and development, microglia displaying irregular activity and/or phenotypes can lead to disorders of the CNS (Salter and Stevens, 2017; Butovsky and Weiner, 2018). In this review, we focus on microglial dysfunction as it relates to autism spectrum disorder and associated conditions. We also discuss the role of the endogenous cannabinoid system in modulating microglial involvement in these disorders.

MICROGLIA AND AUTISM SPECTRUM DISORDER

The Autism and Developmental Disabilities Monitoring Network estimates the current prevalence of autism spectrum disorder (ASD) to be 1 in 59 among children in the United States (Baio et al., 2018). ASD denotes a collection of heterogeneous neurodevelopmental disorders defined by (1) repetitive, restricted behaviors and interests and (2) abnormalities in socio-communication (American Psychiatry Association, 2013). Thus, ASD is an umbrella term and it encompasses several disorders including autism, Asperger's syndrome, pervasive developmental disorder not otherwise specified, and childhood disintegrative disorder (American Psychiatry Association, 2013). Conditions frequently comorbid with ASD include intellectual disability, attention-deficit/hyperactivity disorder, epilepsy, perturbed sleep patterns, aggression, anxiety, and altered sensory perception (Leitner, 2014; Srivastava and Schwartz, 2014; Fakhoury, 2015; Park et al., 2016; Postorino et al., 2016). These associated conditions can vary in severity and be more or less common within patient subsets. Finally, due to the lack of available therapeutics for ASD, there is a continuous, pressing need for investigation into the causes and progression of the disorder.

Given their role in CNS development and neuroinflammation, microglia are poised to influence the pathogenesis of ASD (Edmonson et al., 2016; Salter and Stevens, 2017; Lenz and Nelson, 2018). Evidence for microglial involvement in ASD comes from both post-mortem- and positron-emission tomography (PET)-imaging studies which show increased neuroinflammation and numbers of activated microglia in brains of ASD patients (Vargas et al., 2005; Morgan et al., 2010; Suzuki et al., 2013). More recently, a large-scale analysis of transcriptomic datasets from post-mortem cerebral cortex has revealed a distinct microglial signature in ASD brains (Gandal et al., 2018). This is concordant with previous observations of microglial activation-related gene enrichment in ASD brain-derived gene networks (Voineagu et al., 2011).

Altered synaptic density is observed in post-mortem ASD brain tissue (Hutsler and Zhang, 2010) and ASD mouse models (Comery et al., 1997; Tang et al., 2014; Wang et al., 2017). These alterations are presumably due to deficits in developmental synaptic pruning (Hansel, 2019). Indeed, current thinking posits that microglia can exert control over the progression of ASD through synaptic pruning dysregulation (Di Marco et al., 2016; Lenz and Nelson, 2018). This hypothesis is supported by the finding that inhibiting microglial autophagy leads to increased synaptic density and reduced sociability in mice (Kim et al., 2017). Moreover, mice with loss of microglia-enriched fractalkine receptor CX3C-chemokine receptor 1 (CX3CR1) display impaired synaptic pruning and reduced social interactions (Zhan et al., 2014). Additional support for the involvement of microglia in ASD pathogenesis comes from studies on mouse models of Rett syndrome (RTT), a syndromic form of ASD caused by mutations in the gene encoding methyl-CpG binding protein 2 (MECP2) (Lombardi et al., 2015). In one model of RTT, neuronal, but not microglial, loss of *Mecp2* leads to excessive synaptic engulfment by microglia in later stages of the disease (Schafer et al., 2016). This suggests that neuronal loss of MECP2 is sufficient to induce aberrant microglial activity and it is consistent with the observation that deletion of *Mecp2* using a *Cx3cr1*-Cre line does not produce RTT-like symptoms (Wolf et al., 2017). Furthermore, *Mecp2*-null microglia produce toxic levels of glutamate that damage post-synaptic structures *in vitro* (Maezawa and Jin, 2010). Still, due to the phenotypic and genetic heterogeneity of ASD, it remains to be seen if these findings in RTT models are representative of autism etiology in general.

Finally, children born to mothers who experience infections or autoimmune disease during their pregnancies are more likely to develop ASD (Jiang et al., 2016; Careaga et al., 2017). This phenomenon, known as maternal immune activation (MIA), has been phenocopied in rodent models (Shi et al., 2003; Patterson, 2011; Careaga et al., 2017; Salter and Stevens, 2017). While embryonic microglia may mediate the neuroinflammatory consequences of MIA (Salter and Stevens, 2017), how this underlies ASD remains unclear.

Considered together, the aforementioned findings implicate microglia as targets for the treatment of ASD. Due to its anti-inflammatory effects, the endogenous cannabinoid (endocannabinoid) system represents a promising tool for modulating microglial involvement in ASD. We next provide a brief overview of the endocannabinoid system and then summarize the evidence linking microglial-endocannabinoid signaling to ASD, with attention paid to issues surrounding the use of recreational cannabis.

THE ARCHITECTURE OF THE ENDOCANNABINOID SYSTEM

The endocannabinoid system (ECS) exerts control over microglial activity and therefore shows promise for treating

CNS dysfunction (Benito et al., 2008; Stella, 2009; Lisboa et al., 2016). The ECS consists of three major components: (1) small, lipid-derived endocannabinoids (eCBs), (2) the enzymes responsible for synthesizing and degrading eCBs, and (3) the metabotropic receptors that recognize eCBs (Lutz et al., 2015). The most well-known eCBs in the brain are *N*-arachidonoylethanolamine (AEA or anandamide) and 2-arachidonoylglycerol (2-AG) (Lutz et al., 2015; Parsons and Hurd, 2015). In response to increased cytoplasmic calcium, 2-AG and AEA are synthesized on demand from lipid precursors by the enzymes diacylglycerol lipase (DAGL) and *N*-acyl-phosphatidylethanolamine phospholipase D (NAPE-PLD), respectively (Alger and Kim, 2011; Lutz et al., 2015; Parsons and Hurd, 2015). The enzyme primarily responsible for degrading 2-AG is monoacylglycerol lipase (MAGL), whereas AEA is catabolized by fatty acid amide hydrolase (FAAH). In the CNS, these components are expressed in neurons, microglia, astrocytes, and oligodendrocytes (**Figure 1**; Stella, 2009; Lutz et al., 2015; Ilyasov et al., 2018). The two main receptors for eCBs include cannabinoid receptors 1 (CB_1) and 2 (CB_2), both of which are G protein-coupled (Parsons and Hurd, 2015). Finally, while CB_1 is enriched in neurons, CB_2 expression is primarily restricted to microglia (Stella, 2009).

Acute consumption of *Cannabis sativa* (marijuana) yields wide-ranging effects on memory, cognition, appetite, and mood in both humans and rodents (Curran et al., 2016; Kendall and Yudowski, 2016). These effects result from action of the phytocannabinoid (or plant-derived cannabinoid) Δ^9-tetrahydrocannabinol (THC) on CB_1 within the brain (Panagis et al., 2014; Curran et al., 2016; Kendall and Yudowski, 2016). Yet, long-term consequences of cannabis use have been poorly studied, especially with regards to microglia and their impact on neuronal circuitry. Notably, increased eCB signaling is associated with an anti-inflammatory, protective phenotype in microglia (Benito et al., 2008; Stella, 2009; Lisboa et al., 2016). For example, pharmacological inhibition of FAAH decreases microglial activation marker expression,

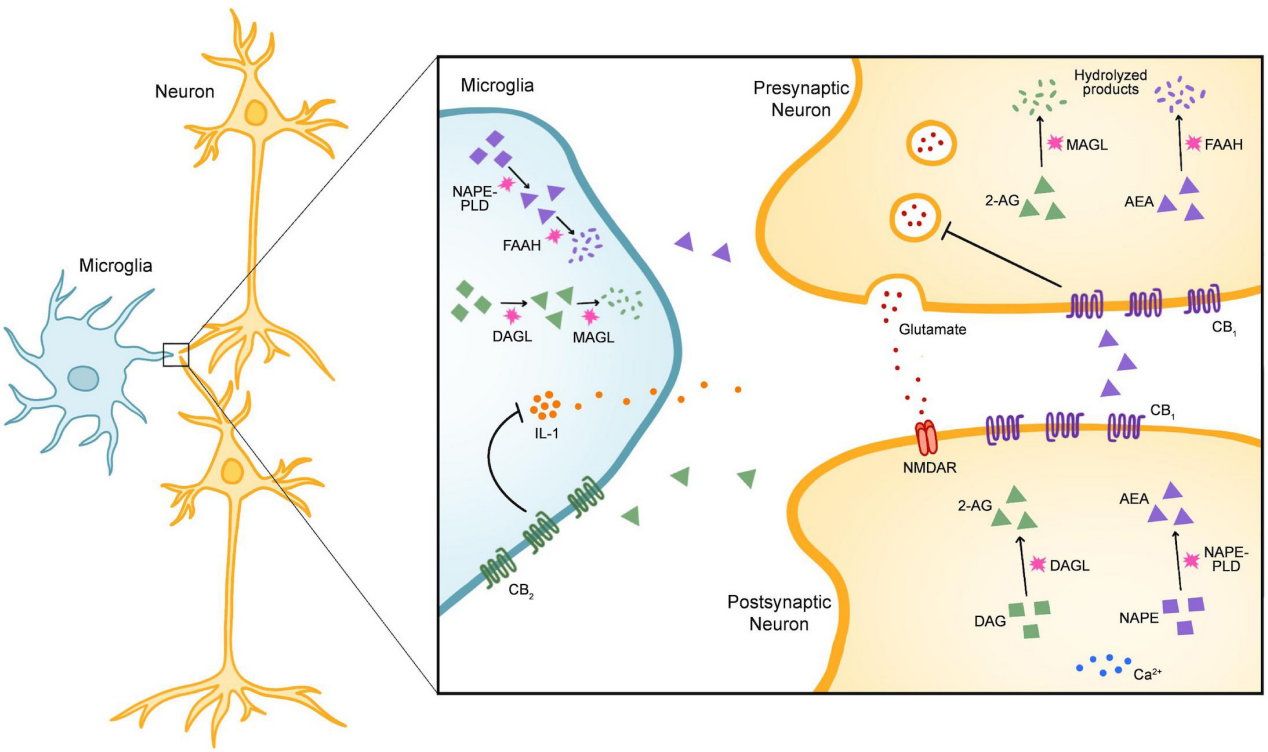

FIGURE 1 | The Components of the Endogenous Cannabinoid System in Microglia and Neurons. In the central nervous system (CNS), the endogenous cannabinoids (eCBs) *N*-arachidonoylethanolamine (AEA) and 2-arachidonoylglycerol (2-AG) are the most widely-recognized ligands of the endogenous cannabinoid (endocannabinoid) system (ECS). The two main receptors for eCBs are cannabinoid receptor 1 (CB_1) and cannabinoid receptor 2 (CB_2), both of which are G-protein coupled. Within the CNS, eCB signaling is classically understood to modulate synaptic activity. In the example given here, release of glutamate from presynaptic neurons activates *N*-methyl-D-aspartate receptors (NMDARs) in postsynaptic neurons. In response to increased cytoplasmic calcium, the enzyme diacylglycerol lipase (DAGL) catalyzes the synthesis of 2-AG from diacylglycerol (DAG) and *N*-acyl-phosphatidylethanolamine phospholipase D (NAPE-PLD) catalyzes the synthesis of AEA from the precursor *N*-acylphosphatidylethanolamine (NAPE). After 2-AG and AEA are released into the synaptic cleft, they stimulate CB_1 receptors on presynaptic neurons and inhibit further neurotransmitter release. 2-AG is mainly degraded by the enzyme monoacylglycerol lipase (MAGL) whereas AEA is degraded by fatty-acid amide hydrolase (FAAH). While DAGL, NAPE-PLD, MAGL, and FAAH are expressed broadly throughout the CNS, CB_1 is enriched in neurons and CB_2 is enriched in microglia. Stimulation of CB_2 leads to a protective phenotype in microglia that is characterized by a reduction in the release of pro-inflammatory cytokines such as interleukin-1 (IL-1).

cytokine production, and synaptic plasticity deficits, in the hippocampi of aged rats (Murphy et al., 2012). Additionally, stimulation of CB_2 inhibits microglial activation and increases striatal neuron survival and motor coordination in a model of Huntington's disease excitotoxicity (Palazuelos et al., 2009). Moreover, exposure to anti-inflammatory cytokines increases eCB production and CB_2 expression in microglia (Mecha et al., 2015). These findings cast the ECS as an attractive target for influencing microglial activity (Dhopeshwarkar and Mackie, 2014; Lisboa et al., 2016; Cassano et al., 2017; Donvito et al., 2018). However, the consequences of manipulating eCB signaling on ASD risk and pathogenesis are largely uncharacterized. The increasing legality and use of cannabis currently seen throughout the world therefore requires a better understanding of eCB signaling in microglia as it relates to ASD.

MICROGLIAL-ENDOCANNABINOID SIGNALING AND ASD

Cannabis Use and ASD Risk

Approximately 2.5–5% of people between the ages of 15–64 years old consume cannabis, making it the most popular illicit drug in the world (Gunn et al., 2016). THC readily crosses the fetal-placental barrier (Wu et al., 2011) and is also secreted in breast milk (Perez-Reyes and Wall, 1982). As of now, there is no strong link between prenatal cannabis use and an increased risk of ASD in offspring. Prenatal exposure to cannabis does correlate with negative outcomes in child development, including growth restriction (Zuckerman et al., 1989; El Marroun et al., 2009; Gunn et al., 2016) and decreased cognitive performance (Richardson et al., 2002; Goldschmidt et al., 2004; Gunn et al., 2016). Still, few studies have been carried out on this topic and these observations are not always reproducible (Wu et al., 2011; El Marroun et al., 2018). Since rates of cannabis use in both pregnant and non-pregnant women are steadily increasing (Brown et al., 2017), there is an unmet need for clarifying the relationship between prenatal cannabis exposure and CNS development. Thus, future clinical and pre-clinical investigations should focus on elucidating the long-lasting effects of prenatal cannabis exposure and if these effects are linked to ASD pathogenesis. Such studies should be paired with efforts to determine if prenatal cannabis exposure impacts microglial synaptic pruning and thereby neurodevelopment in general. These experiments could also take place in the context of pathogen-induced MIA to better recapitulate environmental risks for ASD.

Cannabinoid Signaling as a Target for ASD Treatment

Pre-clinical evidence supporting the role of ECS signaling in ASD comes from research on rodent models of MIA and neuroinflammation. For instance, in response to the innate immunostimulant polyinosinic:polycytidylic acid [poly(I:C)], MIA-based production of IL-17 induces abnormal cortical development and ASD-like sociability deficits in mouse offspring (Choi et al., 2016). Interestingly, administration of AEA decreases IL-17 production and increases expression of the anti-inflammatory cytokine IL-10 in a mouse model of immune hypersensitivity (Jackson et al., 2014). Treatment with the innate immunostimulant lipopolysaccharide (LPS) during adolescence leads to increased AEA tone and FAAH activity in the amygdala, as well as decreased sociability, in mice (Doenni et al., 2016). These alterations are attenuated with administration of an FAAH inhibitor (Doenni et al., 2016). Still, the contribution of microglia to either the initiation or resolution of these neuroinflammatory effects is unknown and should be the focus of future endeavors.

Cannabidiol (CBD), the second major phytocannabinoid in cannabis (Atakan, 2012), has gained attention as a possible treatment for ASD (Salgado and Castellanos, 2018). Indeed, three clinical reports have recently established that CBD alleviates major symptoms associated with ASD, including seizures, sleeplessness, and anxiety, in children (Barchel et al., 2018; Aran et al., 2019; Bar-Lev Schleider et al., 2019). In addition, because CBD possess a weak affinity for CB_1 and CB_2, it has no psychoactive effects and may even prevent some of the harmful consequences of THC (Zuardi et al., 2012; Morales et al., 2017; Mouro et al., 2019). Lastly, a commercially available, oral CBD extract (Epidiolex) has recently gained FDA-approval for treatment of drug-resistant epilepsy (Sekar and Pack, 2019), which can be an additional burden faced by ASD patients (Sansa et al., 2011; Kokoszka et al., 2017; Long et al., 2019). Nevertheless, because exposure to other cannabinoids negatively affects the development of the adolescent brain in rats (Cha et al., 2006; Schneider and Koch, 2007; Quinn et al., 2008), parents and physicians should practice extreme caution when recommending the use of cannabinoids to treat ASD (Atakan, 2012).

Subsequent work in this field must emphasize replicating the usefulness of ECS signaling in ASD via paradigms that include larger and more diverse populations. If these results hold, it will be important to establish if abatement of ASD symptoms is due to eCB signaling in microglia. For example, CBD blocks microglial activation (Martin-Moreno et al., 2011) and neuroinflammation (Elliott et al., 2018; Maroon and Bost, 2018), both of which are linked to seizure susceptibility (Rana and Musto, 2018; Zhao et al., 2018). Consequently, it will be beneficial to establish if CBD-based reduction of epilepsy in ASD patients is reliant on microglial-based mechanisms. Utilizing mice with microglia-specific loss of ECS components in combination with ASD-relevant mouse models could shed light on this area.

CONCLUSION

Microglia are indispensable orchestrators of CNS development and homeostasis and are therefore likely involved in the pathogenesis of ASD. Microglial activity can be modulated by eCB signaling, which makes the ECS a potentially forceful tool in the prevention and management of CNS dysfunction.

Future work must focus on detailing the mechanisms by which altered eCB signaling in microglia yields protective and detrimental effects in the CNS, particularly as it relates to the effects of chronic cannabis use. Answering these questions could provide improved therapeutics for ASD and its associated conditions.

AUTHOR CONTRIBUTIONS

All authors wrote the manuscript. KT and DA designed the figure.

FUNDING

This work was supported by a National Institutes of Health (NIH) postdoctoral training grant (T32AI100829-06A1 to DA) and an NIH research project grant (1R01HD092093 to KS).

ACKNOWLEDGMENTS

The authors would like to thank Dr. Marissa Co for providing invaluable comments in this manuscript.

REFERENCES

Alger, B. E., and Kim, J. (2011). Supply and demand for endocannabinoids. *Trends Neurosci.* 34, 304–315. doi: 10.1016/j.tins.2011.03.003

Alliot, F., Godin, I., and Pessac, B. (1999). Microglia derive from progenitors, originating from the yolk sac, and which proliferate in the brain. *Brain Res. Dev. Brain Res.* 117, 145–152. doi: 10.1016/s0165-3806(99)00113-3

American Psychiatry Association, (2013). *Diagnostic and Statistical Manual of Mental Disorders: DSM-5*, 5th Edn. Arlington, VA: American Psychiatry Association.

Aran, A., Cassuto, H., Lubotzky, A., Wattad, N., and Hazan, E. (2019). Brief report: cannabidiol-rich cannabis in children with autism spectrum disorder and severe behavioral problems-a retrospective feasibility study. *J. Autism Dev. Disord.* 49, 1284–1288. doi: 10.1007/s10803-018-3808-2

Askew, K., Li, K., Olmos-Alonso, A., Garcia-Moreno, F., Liang, Y., Richardson, P., et al. (2017). Coupled proliferation and apoptosis maintain the rapid turnover of microglia in the adult brain. *Cell Rep.* 18, 391–405. doi: 10.1016/j.celrep.2016.12.041

Atakan, Z. (2012). Cannabis, a complex plant: different compounds and different effects on individuals. *Ther. Adv. Psychopharmacol.* 2, 241–254. doi: 10.1177/2045125312457586

Baio, J., Wiggins, L., Christensen, D. L., Maenner, M. J., Daniels, J., Warren, Z., et al. (2018). Prevalence of autism spectrum disorder among children aged 8 years - autism and developmental disabilities monitoring network, 11 sites, United States, 2014. *MMWR Surveill. Summ.* 67, 1–23. doi: 10.15585/mmwr.ss6706a1

Barchel, D., Stolar, O., De-Haan, T., Ziv-Baran, T., Saban, N., Fuchs, D. O., et al. (2018). Oral cannabidiol use in children with autism spectrum disorder to treat related symptoms and Co-morbidities. *Front. Pharmacol.* 9:1521. doi: 10.3389/fphar.2018.01521

Bar-Lev Schleider, L., Mechoulam, R., Saban, N., Meiri, G., and Novack, V. (2019). Real life experience of medical cannabis treatment in autism: analysis of safety and efficacy. *Sci. Rep.* 9:200. doi: 10.1038/s41598-018-37570-y

Benito, C., Tolon, R. M., Pazos, M. R., Nunez, E., Castillo, A. I., and Romero, J. (2008). Cannabinoid CB2 receptors in human brain inflammation. *Br. J. Pharmacol.* 153, 277–285.

Bialas, A. R., and Stevens, B. (2013). TGF-beta signaling regulates neuronal C1q expression and developmental synaptic refinement. *Nat. Neurosci.* 16, 1773–1782. doi: 10.1038/nn.3560

Brown, Q. L., Sarvet, A. L., Shmulewitz, D., Martins, S. S., Wall, M. M., and Hasin, D. S. (2017). Trends in marijuana use among pregnant and nonpregnant reproductive-aged women, 2002-2014. *JAMA* 317, 207–209.

Bruttger, J., Karram, K., Wortge, S., Regen, T., Marini, F., Hoppmann, N., et al. (2015). Genetic cell ablation reveals clusters of local self-renewing microglia in the mammalian central nervous system. *Immunity* 43, 92–106. doi: 10.1016/j.immuni.2015.06.012

Butovsky, O., and Weiner, H. L. (2018). Microglial signatures and their role in health and disease. *Nat. Rev. Neurosci.* 19, 622–635. doi: 10.1038/s41583-018-0057-5

Careaga, M., Murai, T., and Bauman, M. D. (2017). Maternal immune activation and autism spectrum disorder: from rodents to nonhuman and human primates. *Biol. Psychiatry* 81, 391–401. doi: 10.1016/j.biopsych.2016.10.020

Cassano, T., Calcagnini, S., Pace, L., De Marco, F., Romano, A., and Gaetani, S. (2017). Cannabinoid receptor 2 signaling in neurodegenerative disorders: from pathogenesis to a promising therapeutic target. *Front. Neurosci.* 11:30. doi: 10.3389/fnins.2017.00030

Cha, Y. M., White, A. M., Kuhn, C. M., Wilson, W. A., and Swartzwelder, H. S. (2006). Differential effects of delta9-THC on learning in adolescent and adult rats. *Pharmacol. Biochem. Behav.* 83, 448–455. doi: 10.1016/j.pbb.2006.03.006

Choi, G. B., Yim, Y. S., Wong, H., Kim, S., Kim, H., Kim, S. V., et al. (2016). The maternal interleukin-17a pathway in mice promotes autism-like phenotypes in offspring. *Science* 351, 933–939. doi: 10.1126/science.aad0314

Comery, T. A., Harris, J. B., Willems, P. J., Oostra, B. A., Irwin, S. A., Weiler, I. J., et al. (1997). Abnormal dendritic spines in fragile X knockout mice: maturation and pruning deficits. *Proc. Natl. Acad. Sci. U.S.A.* 94, 5401–5404. doi: 10.1073/pnas.94.10.5401

Curran, H. V., Freeman, T. P., Mokrysz, C., Lewis, D. A., Morgan, C. J., and Parsons, L. H. (2016). Keep off the grass? Cannabis, cognition and addiction. *Nat. Rev. Neurosci.* 17, 293–306. doi: 10.1038/nrn.2016.28

Dhopeshwarkar, A., and Mackie, K. (2014). CB2 Cannabinoid receptors as a therapeutic target-what does the future hold? *Mol. Pharmacol.* 86, 430–437. doi: 10.1124/mol.114.094649

Di Marco, B., Bonaccorso, C. M., Aloisi, E., D'Antoni, S., and Catania, M. V. (2016). Neuro-Inflammatory mechanisms in developmental disorders associated with intellectual disability and autism spectrum disorder: a neuro- immune perspective. *CNS Neurol. Disord. Drug Targets* 15, 448–463. doi: 10.2174/1871527315666160321105039

Doenni, V. M., Gray, J. M., Song, C. M., Patel, S., Hill, M. N., and Pittman, Q. J. (2016). Deficient adolescent social behavior following early-life inflammation is ameliorated by augmentation of anandamide signaling. *Brain Behav. Immun.* 58, 237–247. doi: 10.1016/j.bbi.2016.07.152

Donvito, G., Nass, S. R., Wilkerson, J. L., Curry, Z. A., Schurman, L. D., Kinsey, S. G., et al. (2018). The endogenous cannabinoid system: a budding source of targets for treating inflammatory and neuropathic pain. *Neuropsychopharmacology* 43, 52–79. doi: 10.1038/npp.2017.204

Edmonson, C. A., Ziats, M. N., and Rennert, O. M. (2016). A non-inflammatory role for microglia in autism spectrum disorders. *Front. Neurol.* 7:9. doi: 10.3389/fneur.2016.00009

El Marroun, H., Brown, Q. L., Lund, I. O., Coleman-Cowger, V. H., Loree, A. M., Chawla, D., et al. (2018). An epidemiological, developmental and clinical overview of cannabis use during pregnancy. *Prev. Med.* 116, 1–5. doi: 10.1016/j.ypmed.2018.08.036

El Marroun, H., Tiemeier, H., Steegers, E. A., Jaddoe, V. W., Hofman, A., Verhulst, F. C., et al. (2009). Intrauterine cannabis exposure affects fetal growth trajectories: the generation R study. *J. Am. Acad. Child Adolesc. Psychiatry* 48, 1173–1181. doi: 10.1097/CHI.0b013e3181bfa8ee

Elliott, D. M., Singh, N., Nagarkatti, M., and Nagarkatti, P. S. (2018). Cannabidiol attenuates experimental autoimmune encephalomyelitis model of multiple sclerosis through induction of myeloid-derived suppressor cells. *Front. Immunol.* 9:1782. doi: 10.3389/fimmu.2018.01782

Fakhoury, M. (2015). Autistic spectrum disorders: a review of clinical features, theories and diagnosis. *Int. J. Dev. Neurosci.* 43, 70–77. doi: 10.1016/j.ijdevneu.2015.04.003

Gandal, M. J., Haney, J. R., Parikshak, N. N., Leppa, V., Ramaswami, G., Hartl, C., et al. (2018). Shared molecular neuropathology across major psychiatric disorders parallels polygenic overlap. *Science* 359, 693–697. doi: 10.1126/science.aad6469

Ginhoux, F., Greter, M., Leboeuf, M., Nandi, S., See, P., Gokhan, S., et al. (2010). Fate mapping analysis reveals that adult microglia derive from primitive macrophages. *Science* 330, 841–845. doi: 10.1126/science.1194637

Goldschmidt, L., Richardson, G. A., Cornelius, M. D., and Day, N. L. (2004). Prenatal marijuana and alcohol exposure and academic achievement at age 10. *Neurotoxicol. Teratol.* 26, 521–532. doi: 10.1016/j.ntt.2004.04.003

Gunn, J. K., Rosales, C. B., Center, K. E., Nunez, A., Gibson, S. J., Christ, C., et al. (2016). Prenatal exposure to cannabis and maternal and child health outcomes: a systematic review and meta-analysis. *BMJ Open* 6:e009986. doi: 10.1136/bmjopen-2015-009986

Hansel, C. (2019). Deregulation of synaptic plasticity in autism. *Neurosci. Lett.* 688, 58–61. doi: 10.1016/j.neulet.2018.02.003

Huang, Y., Xu, Z., Xiong, S., Sun, F., Qin, G., Hu, G., et al. (2018). Repopulated microglia are solely derived from the proliferation of residual microglia after acute depletion. *Nat. Neurosci.* 21, 530–540. doi: 10.1038/s41593-018-0090-8

Hutsler, J. J., and Zhang, H. (2010). Increased dendritic spine densities on cortical projection neurons in autism spectrum disorders. *Brain Res.* 1309, 83–94. doi: 10.1016/j.brainres.2009.09.120

Ilyasov, A. A., Milligan, C. E., Pharr, E. P., and Howlett, A. C. (2018). The endocannabinoid system and oligodendrocytes in health and disease. *Front. Neurosci.* 12:733. doi: 10.3389/fnins.2018.00733

Jackson, A. R., Nagarkatti, P., and Nagarkatti, M. (2014). Anandamide attenuates Th-17 cell-mediated delayed-type hypersensitivity response by triggering IL-10 production and consequent microRNA induction. *PLoS One* 9:e93954. doi: 10.1371/journal.pone.0093954

Janda, E., Boi, L., and Carta, A. R. (2018). Microglial phagocytosis and its regulation: a therapeutic target in Parkinson's disease? *Front. Mol. Neurosci.* 11:144. doi: 10.3389/fnmol.2018.00144

Jiang, H. Y., Xu, L. L., Shao, L., Xia, R. M., Yu, Z. H., Ling, Z. X., et al. (2016). Maternal infection during pregnancy and risk of autism spectrum disorders: a systematic review and meta-analysis. *Brain Behav. Immun.* 58, 165–172. doi: 10.1016/j.bbi.2016.06.005

Kendall, D. A., and Yudowski, G. A. (2016). Cannabinoid receptors in the central nervous system: their signaling and roles in disease. *Front. Cell Neurosci.* 10:294. doi: 10.3389/fncel.2016.00294

Kim, H. J., Cho, M. H., Shim, W. H., Kim, J. K., Jeon, E. Y., Kim, D. H., et al. (2017). Deficient autophagy in microglia impairs synaptic pruning and causes social behavioral defects. *Mol. Psychiatry* 22, 1576–1584. doi: 10.1038/mp.2016.103

Kokoszka, M. A., McGoldrick, P. E., La Vega-Talbott, M., Raynes, H., Palmese, C. A., Wolf, S. M., et al. (2017). Epilepsy surgery in patients with autism. *J. Neurosurg. Pediatr.* 19, 196–207. doi: 10.3171/2016.7.PEDS1651

Leitner, Y. (2014). The co-occurrence of autism and attention deficit hyperactivity disorder in children - what do we know? *Front. Hum. Neurosci.* 8:268. doi: 10.3389/fnhum.2014.00268

Lenz, K. M., and Nelson, L. H. (2018). Microglia and beyond: innate immune cells as regulators of brain development and behavioral function. *Front. Immunol.* 9:698. doi: 10.3389/fimmu.2018.00698

Lisboa, S. F., Gomes, F. V., Guimaraes, F. S., and Campos, A. C. (2016). Microglial cells as a link between cannabinoids and the immune hypothesis of psychiatric disorders. *Front. Neurol.* 7:5. doi: 10.3389/fneur.2016.00005

Lombardi, L. M., Baker, S. A., and Zoghbi, H. Y. (2015). MECP2 disorders: from the clinic to mice and back. *J. Clin. Invest.* 125, 2914–2923. doi: 10.1172/JCI78167

Long, S., Zhou, H., Li, S., Wang, T., Ma, Y., Li, C., et al. (2019). The clinical and genetic features of co-occurring epilepsy and autism spectrum disorder in chinese children. *Front. Neurol.* 10:505. doi: 10.3389/fneur.2019.00505

Lutz, B., Marsicano, G., Maldonado, R., and Hillard, C. J. (2015). The endocannabinoid system in guarding against fear, anxiety and stress. *Nat. Rev. Neurosci.* 16, 705–718. doi: 10.1038/nrn4036

Maezawa, I., and Jin, L. W. (2010). Rett syndrome microglia damage dendrites and synapses by the elevated release of glutamate. *J. Neurosci.* 30, 5346–5356. doi: 10.1523/JNEUROSCI.5966-09.2010

Maroon, J., and Bost, J. (2018). Review of the neurological benefits of phytocannabinoids. *Surg. Neurol. Int.* 9:91. doi: 10.4103/sni.sni_45_18

Martin-Moreno, A. M., Reigada, D., Ramirez, B. G., Mechoulam, R., Innamorato, N., Cuadrado, A., et al. (2011). Cannabidiol and other cannabinoids reduce microglial activation in vitro and in vivo: relevance to Alzheimer's disease. *Mol. Pharmacol.* 79, 964–973. doi: 10.1124/mol.111.071290

Mecha, M., Feliu, A., Carrillo-Salinas, F. J., Rueda-Zubiaurre, A., Ortega-Gutierrez, S., de Sola, R. G., et al. (2015). Endocannabinoids drive the acquisition of an alternative phenotype in microglia. *Brain Behav. Immun.* 49, 233–245. doi: 10.1016/j.bbi.2015.06.002

Morales, P., Hurst, D. P., and Reggio, P. H. (2017). Molecular targets of the phytocannabinoids: a complex picture. *Prog. Chem. Org. Nat. Prod.* 103, 103–131. doi: 10.1007/978-3-319-45541-9_4

Morgan, J. T., Chana, G., Pardo, C. A., Achim, C., Semendeferi, K., Buckwalter, J., et al. (2010). Microglial activation and increased microglial density observed in the dorsolateral prefrontal cortex in autism. *Biol. Psychiatry* 68, 368–376. doi: 10.1016/j.biopsych.2010.05.024

Mouro, F. M., Miranda-Lourenco, C., Sebastiao, A. M., and Diogenes, M. J. (2019). From cannabinoids and neurosteroids to statins and the ketogenic diet: new therapeutic avenues in rett syndrome? *Front. Neurosci.* 13:680. doi: 10.3389/fnins.2019.00680

Murphy, N., Cowley, T. R., Blau, C. W., Dempsey, C. N., Noonan, J., Gowran, A., et al. (2012). The fatty acid amide hydrolase inhibitor URB597 exerts anti-inflammatory effects in hippocampus of aged rats and restores an age-related deficit in long-term potentiation. *J. Neuroinflammation* 9:79. doi: 10.1186/1742-2094-9-79

Nakajima, K., Honda, S., Tohyama, Y., Imai, Y., Kohsaka, S., and Kurihara, T. (2001). Neurotrophin secretion from cultured microglia. *J. Neurosci. Res.* 65, 322–331. doi: 10.1002/jnr.1157

Palazuelos, J., Aguado, T., Pazos, M. R., Julien, B., Carrasco, C., Resel, E., et al. (2009). Microglial CB2 cannabinoid receptors are neuroprotective in Huntington's disease excitotoxicity. *Brain* 132, 3152–3164. doi: 10.1093/brain/awp239

Panagis, G., Mackey, B., and Vlachou, S. (2014). Cannabinoid regulation of brain reward processing with an emphasis on the role of CB1 receptors: a step back into the future. *Front. Psychiatry* 5:92. doi: 10.3389/fpsyt.2014.00092

Paolicelli, R. C., Bolasco, G., Pagani, F., Maggi, L., Scianni, M., Panzanelli, P., et al. (2011). Synaptic pruning by microglia is necessary for normal brain development. *Science* 333, 1456–1458. doi: 10.1126/science.1202529

Park, H. R., Lee, J. M., Moon, H. E., Lee, D. S., Kim, B. N., Kim, J., et al. (2016). A short review on the current understanding of autism spectrum disorders. *Exp. Neurobiol.* 25, 1–13. doi: 10.5607/en.2016.25.1.1

Parkhurst, C. N., Yang, G., Ninan, I., Savas, J. N., Yates, J. R. III, Lafaille, J. J., et al. (2013). Microglia promote learning-dependent synapse formation through brain-derived neurotrophic factor. *Cell* 155, 1596–1609. doi: 10.1016/j.cell.2013.11.030

Parsons, L. H., and Hurd, Y. L. (2015). Endocannabinoid signalling in reward and addiction. *Nat. Rev. Neurosci.* 16, 579–594. doi: 10.1038/nrn4004

Patterson, P. H. (2011). Maternal infection and immune involvement in autism. *Trends Mol. Med.* 17, 389–394. doi: 10.1016/j.molmed.2011.03.001

Perez-Reyes, M., and Wall, M. E. (1982). Presence of delta9-tetrahydrocannabinol in human milk. *N. Engl. J. Med.* 307, 819–820. doi: 10.1056/nejm198209233071311

Postorino, V., Fatta, L. M., Sanges, V., Giovagnoli, G., De Peppo, L., Vicari, S., et al. (2016). Intellectual disability in autism spectrum disorder: investigation of prevalence in an italian sample of children and adolescents. *Res. Dev. Disabil.* 48, 193–201. doi: 10.1016/j.ridd.2015.10.020

Quinn, H. R., Matsumoto, I., Callaghan, P. D., Long, L. E., Arnold, J. C., Gunasekaran, N., et al. (2008). Adolescent rats find repeated Delta(9)-THC less aversive than adult rats but display greater residual cognitive deficits and changes in hippocampal protein expression following exposure. *Neuropsychopharmacology* 33, 1113–1126. doi: 10.1038/sj.npp.1301475

Rana, A., and Musto, A. E. (2018). The role of inflammation in the development of epilepsy. *J. Neuroinflammation* 15:144. doi: 10.1186/s12974-018-1192-7

Ribeiro Xavier, A. L., Kress, B. T., Goldman, S. A., Lacerda de Menezes, J. R., and Nedergaard, M. (2015). A distinct population of microglia supports adult neurogenesis in the subventricular zone. *J. Neurosci.* 35, 11848–11861. doi: 10.1523/JNEUROSCI.1217-15.2015

Richardson, G. A., Ryan, C., Willford, J., Day, N. L., and Goldschmidt, L. (2002). Prenatal alcohol and marijuana exposure: effects on neuropsychological outcomes at 10 years. *Neurotoxicol. Teratol.* 24, 309–320. doi: 10.1016/s0892-0362(02)00193-9

Saijo, K., and Glass, C. K. (2011). Microglial cell origin and phenotypes in health and disease. *Nat. Rev. Immunol.* 11, 775–787. doi: 10.1038/nri3086

Salgado, C. A., and Castellanos, D. (2018). Autism spectrum disorder and cannabidiol: have we seen this movie before? *Glob. Pediatr. Health* 5:2333794X18815412.

Salter, M. W., and Stevens, B. (2017). Microglia emerge as central players in brain disease. *Nat. Med.* 23, 1018–1027. doi: 10.1038/nm.4397

Sansa, G., Carlson, C., Doyle, W., Weiner, H. L., Bluvstein, J., Barr, W., et al. (2011). Medically refractory epilepsy in autism. *Epilepsia* 52, 1071–1075. doi: 10.1111/j.1528-1167.2011.03069.x

Schafer, D. P., Heller, C. T., Gunner, G., Heller, M., Gordon, C., Hammond, T., et al. (2016). Microglia contribute to circuit defects in Mecp2 null mice independent of microglia-specific loss of Mecp2 expression. *eLife* 5:e15224. doi: 10.7554/eLife.15224

Schneider, M., and Koch, M. (2007). The effect of chronic peripubertal cannabinoid treatment on deficient object recognition memory in rats after neonatal mPFC lesion. *Eur. Neuropsychopharmacol.* 17, 180–186. doi: 10.1016/j.euroneuro.2006.03.009

Sekar, K., and Pack, A. (2019). Epidiolex as adjunct therapy for treatment of refractory epilepsy: a comprehensive review with a focus on adverse effects. *F1000Res* 8:234. doi: 10.12688/f1000research.16515.1

Shi, L., Fatemi, S. H., Sidwell, R. W., and Patterson, P. H. (2003). Maternal influenza infection causes marked behavioral and pharmacological changes in the offspring. *J. Neurosci.* 23, 297–302. doi: 10.1523/jneurosci.23-01-00297.2003

Shigemoto-Mogami, Y., Hoshikawa, K., Goldman, J. E., Sekino, Y., and Sato, K. (2014). Microglia enhance neurogenesis and oligodendrogenesis in the early postnatal subventricular zone. *J. Neurosci.* 34, 2231–2243. doi: 10.1523/JNEUROSCI.1619-13.2014

Sierra, A., Encinas, J. M., Deudero, J. J., Chancey, J. H., Enikolopov, G., Overstreet-Wadiche, L. S., et al. (2010). Microglia shape adult hippocampal neurogenesis through apoptosis-coupled phagocytosis. *Cell Stem Cell* 7, 483–495. doi: 10.1016/j.stem.2010.08.014

Srinivasan, B., Roque, C. H., Hempstead, B. L., Al-Ubaidi, M. R., and Roque, R. S. (2004). Microglia-derived pronerve growth factor promotes photoreceptor cell death via p75 neurotrophin receptor. *J. Biol. Chem.* 279, 41839–41845. doi: 10.1074/jbc.m402872200

Srivastava, A. K., and Schwartz, C. E. (2014). Intellectual disability and autism spectrum disorders: causal genes and molecular mechanisms. *Neurosci. Biobehav. Rev.* 46(Pt 2), 161–174. doi: 10.1016/j.neubiorev.2014.02.015

Stella, N. (2009). Endocannabinoid signaling in microglial cells. *Neuropharmacology* 56(Suppl. 1), 244–253. doi: 10.1016/j.neuropharm.2008.07.037

Stevens, B., Allen, N. J., Vazquez, L. E., Howell, G. R., Christopherson, K. S., Nouri, N., et al. (2007). The classical complement cascade mediates CNS synapse elimination. *Cell* 131, 1164–1178. doi: 10.1016/j.cell.2007.10.036

Suzuki, K., Sugihara, G., Ouchi, Y., Nakamura, K., Futatsubashi, M., Takebayashi, K., et al. (2013). Microglial activation in young adults with autism spectrum disorder. *JAMA Psychiatry* 70, 49–58.

Tang, G., Gudsnuk, K., Kuo, S. H., Cotrina, M. L., Rosoklija, G., Sosunov, A., et al. (2014). Loss of mTOR-dependent macroautophagy causes autistic-like synaptic pruning deficits. *Neuron* 83, 1131–1143. doi: 10.1016/j.neuron.2014.07.040

Vargas, D. L., Nascimbene, C., Krishnan, C., Zimmerman, A. W., and Pardo, C. A. (2005). Neuroglial activation and neuroinflammation in the brain of patients with autism. *Ann. Neurol.* 57, 67–81. doi: 10.1002/ana.20315

Voineagu, I., Wang, X., Johnston, P., Lowe, J. K., Tian, Y., Horvath, S., et al. (2011). Transcriptomic analysis of autistic brain reveals convergent molecular pathology. *Nature* 474, 380–384. doi: 10.1038/nature10110

Wang, M., Li, H., Takumi, T., Qiu, Z., Xu, X., Yu, X., et al. (2017). Distinct defects in spine formation or pruning in two gene duplication mouse models of autism. *Neurosci. Bull.* 33, 143–152. doi: 10.1007/s12264-017-0111-8

Wolf, Y., Boura-Halfon, S., Cortese, N., Haimon, Z., Sar Shalom, H., Kuperman, Y., et al. (2017). Brown-adipose-tissue macrophages control tissue innervation and homeostatic energy expenditure. *Nat. Immunol.* 18, 665–674. doi: 10.1038/ni.3746

Wu, C. S., Jew, C. P., and Lu, H. C. (2011). Lasting impacts of prenatal cannabis exposure and the role of endogenous cannabinoids in the developing brain. *Future Neurol.* 6, 459–480. doi: 10.2217/fnl.11.27

Yang, I., Han, S. J., Kaur, G., Crane, C., and Parsa, A. T. (2010). The role of microglia in central nervous system immunity and glioma immunology. *J. Clin. Neurosci.* 17, 6–10. doi: 10.1016/j.jocn.2009.05.006

Zhan, Y., Paolicelli, R. C., Sforazzini, F., Weinhard, L., Bolasco, G., Pagani, F., et al. (2014). Deficient neuron-microglia signaling results in impaired functional brain connectivity and social behavior. *Nat. Neurosci.* 17, 400–406. doi: 10.1038/nn.3641

Zhao, H., Zhu, C., and Huang, D. (2018). Microglial activation: an important process in the onset of epilepsy. *Am. J. Transl. Res.* 10, 2877–2889.

Zuardi, A. W., Crippa, J. A., Hallak, J. E., Bhattacharyya, S., Atakan, Z., Martin-Santos, R., et al. (2012). A critical review of the antipsychotic effects of cannabidiol: 30 years of a translational investigation. *Curr. Pharm. Des.* 18, 5131–5140. doi: 10.2174/138161212802884681

Zuckerman, B., Frank, D. A., Hingson, R., Amaro, H., Levenson, S. M., Kayne, H., et al. (1989). Effects of maternal marijuana and cocaine use on fetal growth. *N. Engl. J. Med.* 320, 762–768. doi: 10.1056/nejm198903233201203

Conflict of Interest Statement: The authors declare that the research was conducted in the absence of any commercial or financial relationships that could be construed as a potential conflict of interest.

frontiers in Cellular Neuroscience

ORIGINAL RESEARCH
published: 11 October 2019
doi: 10.3389/fncel.2019.00460

The Opening of Connexin 43 Hemichannels Alters Hippocampal Astrocyte Function and Neuronal Survival in Prenatally LPS-Exposed Adult Offspring

*Carolina E. Chávez, Juan E. Oyarzún, Beatriz C. Avendaño, Luis A. Mellado, Carla A. Inostroza, Tanhia F. Alvear and Juan A. Orellana**

Departamento de Neurología, Facultad de Medicina, Escuela de Medicina and Centro Interdisciplinario de Neurociencias, Pontificia Universidad Católica de Chile, Santiago, Chile

OPEN ACCESS

Edited by:
Yu Tang, National Clinical Research Center for Geriatric Disorders, Xiangya Hospital, Central South University, China

Reviewed by:
Daniele Nosi, University of Florence, Italy
Marijke De Bock, Ghent University, Belgium
Gertrudis Perea, Cajal Institute (CSIC), Spain

***Correspondence:**
Juan A. Orellana
jaorella@uc.cl

Specialty section:
This article was submitted to Non-Neuronal Cells, a section of the journal Frontiers in Cellular Neuroscience

Received: *07 May 2019*
Accepted: *27 September 2019*
Published: *11 October 2019*

Citation:
Chávez CE, Oyarzún JE, Avendaño BC, Mellado LA, Inostroza CA, Alvear TF and Orellana JA (2019) The Opening of Connexin 43 Hemichannels Alters Hippocampal Astrocyte Function and Neuronal Survival in Prenatally LPS-Exposed Adult Offspring. Front. Cell. Neurosci. 13:460. doi: 10.3389/fncel.2019.00460

Clinical evidence has revealed that children born from mothers exposed to viral and bacterial pathogens during pregnancy are more likely to suffer various neurological disorders including schizophrenia, autism bipolar disorder, major depression, epilepsy, and cerebral palsy. Despite that most research has centered on the impact of prenatal inflammation in neurons and microglia, the potential modifications of astrocytes and neuron-astrocyte communication have received less scrutiny. Here, we evaluated whether prenatally LPS-exposed offspring display alterations in the opening of astrocyte hemichannels and pannexons in the hippocampus, together with changes in neuroinflammation, intracellular Ca^{2+} and nitric oxide (NO) signaling, gliotransmitter release, cell arborization, and neuronal survival. Ethidium uptake recordings revealed that prenatal LPS exposure enhances the opening of astrocyte Cx43 hemichannels and Panx1 channels in the hippocampus of adult offspring mice. This enhanced channel activity occurred by a mechanism involving a microglia-dependent production of IL-1β/TNF-α and the stimulation of p38 MAP kinase/iNOS/$[Ca^{2+}]_i$-mediated signaling and purinergic/glutamatergic pathways. Noteworthy, the activity of Cx43 hemichannels affected the release of glutamate, $[Ca^{2+}]_i$ handling, and morphology of astrocytes, whereas also disturbed neuronal function, including the dendritic arbor and spine density, as well as survival. We speculate that excitotoxic levels of glutamate triggered by the activation of Cx43 hemichannels may contribute to hippocampal neurotoxicity and damage in prenatally LPS-exposed offspring. Therefore, the understanding of how astrocyte-neuron crosstalk is an auspicious avenue toward the development of broad treatments for several neurological disorders observed in children born to women who had a severe infection during gestation.

Keywords: neuroinflammation, hemichannel, connexin, glia, pannexin

INTRODUCTION

Environmental factors during early development have a crucial impact on brain function, causing individual differences that could lead to behavioral alteration and increased risk for neurological diseases over the lifetime (Faa et al., 2016). One of the early experiences that affect the brain outcome is the maternal infection, which impairs the complex immune harmony between the maternal and fetal environments, leading to a disrupted immune profile in the developing brain (Gumusoglu and Stevens, 2019). Indeed, clinical evidence has revealed that children born from mothers exposed to viral and bacterial pathogens during pregnancy are more likely to suffer various neurological disorders such as schizophrenia, autism bipolar disorder, major depression, epilepsy, and cerebral palsy (Bergdolt and Dunaevsky, 2018). Most of these epidemiological data have been reproduced in rodent models linked to the administration of lipopolysaccharide (LPS) during gestation (Boksa, 2010).

Although the offspring from LPS-exposed pregnant rodents displays a wide spectrum of brain abnormalities, including behavioral and cognitive changes, anatomical abnormalities, altered synaptic transmission, and immune disturbances (Golan et al., 2005; Rousset et al., 2006; Escobar et al., 2011), the involved mechanisms remain unknown. Moreover, most research has centered on the impact of prenatal inflammation in neurons and microglia, however, the potential modifications of astrocytes and neuron-astrocyte communication have received less scrutiny. Astrocytes encompass the most ubiquitous glial cell type and are endowed with the ability to sense neuronal function and react to it by releasing biomolecules termed "gliotransmitters" (e.g., glutamate, ATP, and D-serine) (Perea et al., 2009). Brain function is highly dependent on astrocytes, as they govern the energy supply to neurons (lactate) along with controlling the homeostatic balance of extracellular pH, neurotransmitters and ions, as well as modulating the redox response and intracellular Ca^{2+} concentration ($[Ca^{2+}]_i$) signaling (Santello et al., 2019). During brain disease, astrocytes undergo a protective cell reaction called "reactive astrogliosis," however, when damage turns persistent, this response could disturb astrocyte-to-neuron communication and facilitate the recruitment of the innate immune response (Pekny and Pekna, 2014).

Despite that is known that prenatal LPS exposure triggers reactive astrogliosis (Hao et al., 2010; Zager et al., 2015), the signaling that shed light on this phenomenon and whether other astrocytic properties (e.g., gliotransmitter release, $[Ca^{2+}]_i$ dynamics, NO production) are disturbed remain poorly understood. Current studies suggest that cellular cascades associated to hemichannels and pannexons are pivotal for astroglial function and dysfunction (Abudara et al., 2018). Hemichannels are plasma membrane channels composed by the oligomerization of six connexin monomers around a central pore that permit the diffusion of ions and small molecules, acting as a signaling route for communication between the cytoplasmic and extracellular compartments (Abudara et al., 2018). On the other hand, pannexins channels or pannexons are made of the oligomerization of pannexins, a three-member protein family with similar secondary and tertiary structures than connexins and with the capacity to form plasma membrane channels (Dahl, 2018).

In astrocytes, hemichannels and pannexons permit the release of gliotransmitters that have been found crucial for synaptic transmission and plasticity, as well as behavior and memory (Stehberg et al., 2012; Ardiles et al., 2014; Chever et al., 2014; Walrave et al., 2016; Meunier et al., 2017). However, during pathological conditions, the permanent activity of these channels has been linked to the homeostatic disturbances occurring in the pathogenesis and progression of multiple diseases (Salameh et al., 2013; Orellana et al., 2016; Leybaert et al., 2017). In a previous study, using neonatal primary cell cultures, we demonstrated that astrocytes obtained from the offspring of LPS-exposed dams show an elevated opening of hemichannels and pannexons (Avendano et al., 2015). Nevertheless, whether prenatal LPS exposure affects the opening of these channels in the adult offspring and the possible impact of this on astrocyte function and neuronal survival is still ignored. Here, by performing studies in the stratum radiatum of the hippocampus, we found that prenatal LPS exposure increases the activity of astrocyte connexin 43 (Cx43) hemichannels and pannexin-1 (Panx1) channels *ex vivo* in acute brain slices from adult offspring mice. Relevantly, the opening of Cx43 hemichannels affected the release of glutamate, $[Ca^{2+}]_i$ handling, and morphology of astrocytes, whereas also impaired the dendritic arbor and spine density, as well as neuronal survival.

MATERIALS AND METHODS

Reagents and Antibodies

The mimetic peptides gap19 (KQIEIKKFK, intracellular loop domain of Cx43), gap19^{I130A} (KQAEIKKFK, negative control), Tat-gap19 (YGRKKRRQRRR-KQIEIKKFK, intracellular loop domain of Cx43), Tat-gap19^{I130A} (YGRKKRRQRRR-KQAEIKKFK, negative control), Tat-L2 (YGRKKRRQRRR-DGANVDMHLKQIEIKKFKYGIEEHGK, second intracellular loop domain of Cx43), Tat-L2$^{H126K/I130N}$ (YGRKKRRQRRR-DGANVDMKLKQNEIKKFKYGIEEHGK, negative control), ^{10}panx1 (WRQAAFVDSY, first extracellular loop domain of Panx1) and ^{10}panx1^{src} (FSVYWAQADR, scrambled peptide) were obtained from Genscript (New Jersey, United States). HEPES, water (W3500), minocycline, SB203580, polyclonal anti-Cx43 antibody, anti-glial fibrillary acidic protein (GFAP) monoclonal antibody, minocycline, oATP, ethidium (Etd) bromide (Ex-Max 493 nm/Em-Max 620 nm), sulforhodamine 101 (SR101) (Ex-Max 586 nm/Em-Max 605 nm) and probenecid (Prob) were purchased from Sigma-Aldrich (St. Louis, MO, United States). A740003, U-73122, 2-APB, MTEP, SIB-1757, LN-6, and A740003 were obtained from Tocris (Bristol, United Kingdom). Fluo-4-AM (Ex-Max 494 nm/Em-Max 506 nm), DAF-FM diacetate (Ex-Max 495 nm/Em-Max 515 nm), monoclonal anti-Iba-1 antibody, BAPTA-AM, diamidino-2-phenylindole (DAPI) (Ex-Max 359 nm/Em-Max 461 nm), goat anti-mouse Alexa Fluor 488 (Ex-Max 495 nm/Em-Max 519 nm) were obtained from Thermofisher (Waltham, MA, United States). Fluoro-Jade C (F-Jade) (Ex-Max 485 nm/Em-Max 525 nm) were obtained

from Chemicon (Martinsried/Munich, Germany). A soluble form of the TNF-α receptor (sTNF-αR1) and a recombinant receptor antagonist for IL-1β (IL-1ra) were from R&D Systems (Minneapolis, MN, United States).

Animals

The animals were treated and handled according to the National Institutes of Health guidelines (NIH, Baltimore, MD, United States). The experimental procedures were approved by the Bioethical and Biosafety Committee of the Faculty of Biological Sciences at the Pontificia Universidad Católica de Chile. Mice of 8–9 weeks of age were housed in cages in a temperature-controlled (24°C) and humidity-controlled vivarium under a 12 h light/dark cycle (lights on 8:00 a.m.), with *ad libitum* access to food and water. The experiments performed in this study involved the following number of offspring animals per group of treatment: control (54), prenatal LPS (78), prenatal LPS + Tat-gap19 (6) and prenatal LPS + Tat-gap19^{I130A} (6) (see below for details).

Prenatal LPS Exposure Protocol and Mimetic Peptide *in vivo* Administration

The protocol of inflammatory stimulation was applied on gestation day 17. Pregnant mice were randomly assigned to one of two groups: (1) control (0.9% NaCl, i.p. injection) and (2) prenatal LPS (0.01 μg/g *E. Coli* LPS, i.p. injection). Given that prenatal LPS inflammation may induce sex-specific brain effects in the offspring (Makinson et al., 2017), we used only male offspring in our studies. Following full term delivery male offspring were used to prepare acute brain slices. In some *in vivo* experiments, we used the gap19 mimetic peptide coupled to the TAT membrane translocation motif (Tat-gap19), which is known to cross the blood-brain barrier (Abudara et al., 2014). Although gap19 contains the KKFK sequence that is a known cell-membrane translocation motif that facilitates plasma membrane permeability (Carrigan and Imperiali, 2005), we used the TAT version of this peptide in order to increase its cell membrane permeability and chances to interact with its union site: the intracellular C-terminal tail of Cx43 (Abudara et al., 2014). An I130A-modified gap19 analog (Tat-gap19^{I130A}) was employed as a negative control peptide because amino acid I130 is implicated in the formation of hydrogen bonds and thereby crucial for gap19 activity (Wang et al., 2013). Accordingly, Tat-Gap19^{I130A} exerts no inhibitory effects on Cx43 hemichannels (Wang et al., 2013). Tat-gap19 (23 mg/kg), Tat-gap19^{I130A} (23 mg/kg) or saline solution were administrated via intraperitoneal (i.p.) injections beginning on PND 30, as has been previously described to be useful in acute and long-lasting administration in rodents (Crespo Yanguas et al., 2018; Chen et al., 2019; Maatouk et al., 2019). A second dose was given on PND45 followed by injections in PND 60, 75, 90, and 105.

Acute Brain Slices

Mice were anesthetized under isoflurane, decapitated and brains were extracted and cut into coronal slices (300 μm) using a vibratome (Leica, VT1000GS; Leica, Wetzlar, Germany) filled with ice-cold slicing solution containing (in mM): sucrose (222); KCl (2.6); $NaHCO_3$ (27); $NaHPO_4$ (1.5); glucose (10); $MgSO_4$ (7); $CaCl_2$ (0.5) and ascorbate (0.1), bubbled with 95% O_2/5% CO_2, pH 7.4. Then, the slices were transferred at room temperature (20–22°C) to a holding chamber in ice-cold artificial cerebral spinal fluid (ACSF) containing (in mM): NaCl (125), KCl (2.5), glucose (25), $NaHCO_3$ (25), NaH_2PO_4 (1.25), $CaCl_2$ (2), and $MgCl_2$ (1), bubbled with 95% O_2/5% CO_2, pH 7.4, for a stabilization period of 60 min before dye uptake experiments (see below).

Treatments

Some acute brain slices were pre-incubated for 15 min before and during experiments with the following agents: mimetic peptides against Cx43 hemichannels (Tat-L2 and gap19, 100 μM) and pannexin1 (Panx1) channels (^{10}panx1, 100 μM), Prob (pannexin channel blocker, 500 μM), minocycline (inhibitor of microglial activation, 50 nM), sTNF-αR1 (soluble form of the receptor that binds TNF-α, 300 ng/ml), IL-1ra (IL-1β receptor endogenous blocker, 300 ng/ml), SB203580 (p38 MAP kinase inhibitor, 1 μM), L-N6 (iNOS inhibitor, 1 μM), A740003 ($P2X_7$ receptor blocker, 200 nM), oATP (general P2X receptor blocker, 200 μM), BAPTA-AM (intracellular Ca^{2+} chelator, 10 μM), MTEP (selective $mGluR_5$ antagonist, 50 nM), SIB-1757 (selective $mGluR_5$ antagonist, 5 μM), U-73122 (selective phospholipase C (PLC) inhibitor, 5 μM), 2-APB (inhibitor of IP_3 receptor antagonist, 50 μM), tetrodotoxin (TTX, 0. 5 μM).

Dye Uptake in Acute Brain Slices and Confocal Microscopy

For dye uptake and *ex vivo* "snapshot" experiments, acute brain slices were incubated with 5 μM ethidium (Etd) for 10 min in a chamber filled with ACSF and bubbled with 95% O_2/5% CO_2, pH 7.4. Afterward, the slices were washed three times (5 min each) with ACSF, and fixed at room temperature with 4% paraformaldehyde for 60 min, rinsed once with 0.1 mM glycine in phosphate buffered saline (PBS) for 5 min and then twice with PBS for 10 min with gentle agitation. Then, the slices were incubated two times for 30 min each with a blocking solution (PBS, gelatin 0.2%, Triton-X 100 1%) at room temperature. Afterward, the slices were incubated overnight at 4°C with anti-GFAP monoclonal antibody (1:500, Sigma) to detect astrocytes. Additionally, some slices not previously subjected to Etd uptake were incubated overnight at 4°C with anti-Iba-1 monoclonal antibody (1:500, Thermofisher) to detect microglia or anti-polyclonal Cx43 antibody (1:400, SIGMA) to detect Cx43. Later, the slices were washed three times (10 min each) with blocking solution and then incubated for 2 h at room temperature with goat anti-mouse Alexa Fluor 488 (1:1000) antibody and Hoechst 33342. Further, the slices were washed three times (10 min each) in PBS and then mounted in Fluoromount, cover-slipped and examined in a confocal laser-scanning microscope (Eclipse Ti-E C2, Nikon, Japan). Stacks of consecutive confocal images were taken with 40X objective at 100 nm intervals were acquired sequentially with three lasers (in nm: 408, 488, and 543), and Z projections were reconstructed using Nikon confocal

software (NIS-elements) and ImageJ software. At least six cells per field were selected from at least three fields in each brain slice. To assess the fluorescent intensity and distribution of Cx43 in astrocytes, stacks of consecutive confocal images were taken with the same confocal microscope, but with a 60X oil immersion objective (1.4 NA) at 200 nm intervals. Images were acquired sequentially with three lasers (in nm: 488 and 543), and Z projections were reconstructed using Nikon confocal software (NIS-elements). Image analysis of Z projections was then performed with ImageJ software. Cx43 intensity in areas close to the plasma membrane and cytoplasm was modeled by using the Otsu plugin for automatic image thresholding and the "enlarge" function of ImageJ. With the latter, we created a 10-pixel extension from the contour of the intracellular GFAP signal of each selected astrocyte to obtain an approximation of the plasma membrane area. Dye uptake or Cx43 fluorescence was calculated with the following formula: Corrected fluorescence = Integrated Density – ([Area of selected cell] x [Mean fluorescence of background readings]).

Enzyme-Linked Immunosorbent Assay (ELISA)

ELISA assays were performed to determine the amount of TNF-α and IL-1β in the hippocampus. Mice were anesthetized with ketamine/xylazine (10:1 mg/kg of body weight, i.p.) and then perfused and decapitated. Afterward the hippocampus was removed and homogenized with an Ultra-Turrax homogenizer in buffer containing Tris-HCl 100 mM pH 7.4, EDTA 5 mM, SDS 1%, PMSF 1 μM and the protease inhibitor cocktail (ratio: 0.1 g hippocampus tissue: 1 ml lysis buffer) (Pierce, Rockford, IL, United States). Protein concentrations were determined by using a detergent-compatible Bio-Rad protein assay kit (Bio-Rad, Richmond, CA, United States). Then, the samples were centrifuged at 14,000 g for 10 min. Supernatants were collected and protein content assayed by BCA method. Cytokine levels were determined by sandwich ELISA, according to the manufacturer's protocol (IL-1β and TNF-α EIA kit, Enzo Life Science, United States). For the assay, 100 μl of samples were added per ELISA plate well and incubated 4°C overnight. A calibration curve with recombinant cytokine was included. Detection antibody was incubated at room temperature for 2 h and the reaction developed with avidin–HRP and substrate solution. Absorbance was measured at 450 nm with reference to 570 nm with the microplate reader Synergy HT (Biotek Instruments). The results were normalized by protein amount.

$[Ca^{2+}]_i$ and NO Imaging

Acute brain slices were incubated for 20 min at 34°C in ACSF solution containing 1 μM SR101, washed and processed for Fluo-4 AM (Ca^{2+} indicator) or DAF-FM (NO indicator) loading. For that, acute slices were incubated for 60 min at 37°C in ACSF containing 0.02% Pluronic F-127 and 5 μM Fluo-4 AM or 5 μM DAF-FM. Then, slices were transferred on the stage of a confocal laser scanning microscope and Ca^{2+} or NO measurements were carried out for 20 min. Fluo-4 or DAF-FM were excited with an argon laser (488 nm) and emission was filtered with a 515 ± 15 nm filter, whereas SR101 was excited with a HeNe green laser (543 nm) and emission was filtered with a 605 ± 75 nm filter. Acquisitions were carried out in the frame-scanning mode at 1 frame every 2 s with a 60x objective (NA 0.95; Nikon, Tokyo, Japan) on an Eclipse microscope (Nikon Instruments, Tokyo, Japan) equipped with and confocal head (confocal C2 head, Nikon) and controlled by the NIS-element software. The NO/Ca^{2+} imaging data was analyzed using FIJI-IMAGE-J programs. Images with obvious motion were excluded for analysis. ROIs in astrocytes, including somata and processes, were manually identified on the basis of morphology. Fluorescence intensity was calculated with the following formula: Corrected total cell fluorescence = Integrated Density – ([Area of selected cell] × [Mean fluorescence of background readings]). At least four cells per field were selected from at least three fields in each brain slice. For spontaneous $[Ca^{2+}]_i$ oscillations, the peaks were detected using the algorithm developed by Igor Pro from WaveMetrics. The frequency and amplitude were calculated and measured.

Measurement of Extracellular ATP and Glutamate Concentration

Acute hippocampal slices were immersed in oxygenated ACSF (as above), pH 7.4, at room temperature (20–22°C) for 30 min either under control conditions or exposed to different agents. Then, extracellular ATP was measured using a luciferin/luciferase bioluminescence assay kit (Sigma-Aldrich, St. Louis, MO, United States), while extracellular levels of glutamate were determined using an enzyme-linked fluorimetric assay (Sigma-Aldrich, St. Louis, MO, United States). The amount of glutamate and ATP in each sample was inferred from standard curves. Briefly, after the experiments, the slices were washed twice with ACSF solution and sonicated in ice-cold PBS containing 5 μM EDTA, Halt (78440) and T-PER protein extraction cocktail (78510) according to manufacturer instructions (Pierce, Rockford, IL, United States). Total proteins from tissue homogenates were measured using the Bio-Rad protein assay.

Golgi Staining

Mice were deeply anesthetized with isoflurane (4%) before euthanizing by decapitation. Brains were removed quickly from the skull to avoid any damage to the tissue. After rinsing, the tissue was sliced in approximately 10 mm thick blocks. The blocks were stained with the FD Rapid GolgiStain™ kit (FD NeuroTechnologies, Ellicott City, MD, United States). They were first immersed in the impregnation solution (A and B) which was replaced after 6–12 h and then kept in dark for 15–16 days. Afterward, the blocks were put in Solution C which was replaced after 24 h and kept in dark for the next 48–60 h. Cryomicrotome (Microm Thermo Scientific, Walldorf, Germany) was used to cut 200 μm thick slices. Slices were mounted on a gelatin-coated microscope slides, stained, and dehydrated and coverslipped with Permount. Tissue preparation and staining were all done by the same person following the FD Rapid GolgiStain™ kit manufacturer's protocol. Neuronal dendritic arbors and

spines were imaged using motorized microscope-computer based system and the MFB Stereo Investigator software version 11 (MBF–Bioscience, Williston, ND, United States). System was composed of z-axis motorized Olympus BX51 microscope equipped with x-y motorized stage guided by MAC5000 stage controller (Ludl Electronic Products Ltd., Hawthorne, NY, United States).

Morphometry and Sholl Analysis

Image processing of slices labeled for microglia (Iba-1 immunostaining), astrocytes (GFAP immunostaining) or neurons (golgi staining) was performed using the Fiji-ImageJ software (Schindelin et al., 2012). All samples were coded and analyzed randomly by a researcher blinded to animal number and condition. A minimum of 10 cells from each animal where chosen for analysis and their image data were imported using the BioFormats plugin and then channels separated with the Split channels tool. Later, the Iba-1, GFAP or golgi channel were selected and Z-axis projection of the sum of planes was performed using the Z projection tool. Afterward, microglia, astrocytes or neurons were selected and cut with the crop tool to facilitate their analysis when they fulfilled the following criteria: (i) presence of untruncated processes, (ii) consistent and strong staining along the entire arborization field, and (iii) relative isolation from neighboring cells to avoid overlap. Afterward, signal was segmented with the threshold tool and converted to binary mask before its skeletonization with the skeletonize tool. The latter tool allowed to obtain segment length and any possible bifurcation of the skeletonized image analyzed with the Fiji-ImageJ software. Due their complexity, drawings of neurons were done before skeletonization by using the Neuromantic software (Myatt et al., 2012), which allow the semi-manual or semi-automatic reconstruction of neurons from single images or image stacks. Then various features were measured including maximum and total branch length of cell processes, number of terminals, maximum path distance (maximum length of a path between the soma and terminal dendrites), as well as the number of branches were measured with the AnalizeSkeleton plugin of Fiji-ImageJ and/or the Neuromantic software. Further, the plugin Sholl analysis of Fiji-ImageJ was used to place concentric circles around the cell starting from the soma and radiating outward at increasing radial increments of 5 μm (Sholl, 1953). Different parameters were measured including the numbers of intersections (points where the cellular processes cross concentric rings), area under the Sholl curve, the maximum number of intersections, the radius of highest count of intersections (maximum intersect. radius) and the sum of intersections divided by intersecting radii (mean of intersections).

Spine Density Estimation

Dendrite spine counting was conducted blind to the experimental condition. Measurements were obtained from the CA1 area of the dorsal hippocampus, whereas secondary or tertiary dendrite branches from the apical part (stratum radiatum) and from the basal part (stratum oriens) of the pyramidal cells were analyzed. Dendrite fragments chosen for analysis had to meet the following criteria: (i) good staining and impregnation without breaks, (ii) location about 150 μm (apical part) or about 40 μm (basal part) from the soma, (ii) branch fragments must be in the same focus plane and have a length about 30 μm (20–50 μm), and (iv) the branch fragment must be relatively straight to minimize errors connected with length measuring. About 8 fragments per brain were analyzed and spines were counted in the Fiji-ImageJ software. Afterward, signal was segmented with the threshold tool and converted to binary mask before its skeletonization with the skeletonize tool. The latter tool allowed to obtain segment length and the number of spines using the semiautomatic counting plugin of the Fiji-ImageJ software.

Neuronal Death Quantification

Acute brain slices were fixed in 40% ethanol at 4°C for 5 min, treated with 0.1% Triton X-100 in PBS for 10 min and rinsed twice with distilled water. Preparations were incubated with 0.001% F-Jade in distilled water and gently shaken for 30 min in the dark. Later, F-Jade was removed and slices were incubated with anti-GFAP monoclonal antibody (Sigma, 1:400) diluted in 0.1% PBS-Triton X-100 with 2% NGS at 4°C overnight. After five rinses in 0.1% PBS-Triton X-100, slices were incubated with goat anti-mouse IgG Alexa Fluor 488 (1:1000) at room temperature for 50 min. After several washes, coverslips were mounted in DAKO fluorescent mounting medium and examined with a confocal laser-scanning microscope (Olympus, Fluoview FV1000, Tokyo, Japan).

Statistical Analysis

For each data group, results were expressed as mean ± standard error (SEM); n refers to the number of independent experiments. Detailed statistical results were included in the figure legends. Statistical analyses were performed using GraphPad Prism (version 7, GraphPad Software, La Jolla, CA, United States). Normality and equal variances were assessed by the Shapiro–Wilk normality test and Brown–Forsythe test, respectively. Unless otherwise stated, data that passed these tests were analyzed by unpaired *t*-test in case of comparing two groups, whereas in case of multiple comparisons, data were analyzed by one or two-way analysis of variance (ANOVA) followed, in case of significance, by a Tukey's *post hoc* test. When data were heteroscedastic as well as not normal and with unequal variances, we used Mann–Whitney test in case of comparing two groups, whereas in case of multiple comparisons data are analyzed by Kruskal–Wallis test followed, in case of significance, by Dunn's *post hoc* test. A probability of $P < 0.05$ was considered statistically significant.

RESULTS

Prenatal LPS Exposure Enhances the Opening of Cx43 Hemichannels and Panx1 Channels in the Hippocampus of Adult Offspring Mice

The offspring of LPS-exposed dams exhibit alterations in hippocampal-dependent synaptic plasticity and memory

(Hao et al., 2010; Kelley et al., 2017), as well as increased neuronal death and astrogliosis (Ling et al., 2002; Zager et al., 2015). Because the exacerbated activity of astrocyte hemichannels and pannexons impact synaptic impairment, neuronal loss and astrogliosis in the hippocampus (Abudara et al., 2015; Yi et al., 2016; Gomez et al., 2018), we examined whether prenatal LPS exposure modulates the functional activity of these channels in the hippocampal CA1 region of the offspring. For that reason, we investigated hemichannel and pannexon activity by measuring ethidium (Etd) uptake in acute brain slices from the offspring mice following different months after birth. Etd enters to the cytosol of activated cells through selective large-pore channels, including hemichannels and pannexons. After its intercalation with base pairs of DNA and RNA, Etd becomes fluorescent, denoting channel activity (Johnson et al., 2016). Etd uptake by GFAP-positive astrocytes on acute brain slices was studied taking "snapshot" images in the stratum radiatum of the hippocampal CA1 region.

Astrocytes analyzed in acute brain slices from control offspring displayed a weak Etd uptake in the stratum radiatum (**Figure 1A**). Nonetheless, 4 months old offspring mice from LPS-exposed dams exhibited hippocampal astrocytes with increased Etd uptake compared to control conditions (∼900%, **Figures 1A–C**). Temporal analysis of these responses showed that astroglial Etd uptake rapidly increased 1 month after birth in prenatally LPS-exposed offspring and reached a maximum in 4 months old offspring (**Figure 1C**). Thus, hereinafter and unless otherwise stated, this postnatal period was used in all further experiments throughout this study. Because Cx43 hemichannels and Panx1 channels are pivotal pathways for dye passage in astrocytes (Contreras et al., 2002; Iglesias et al., 2009), the potential involvement of these channels in the prenatal LPS-induced astroglial Etd uptake was investigated. Accordingly, acute brain slices were pre-incubated for 15 min before and during Etd uptake recordings with a battery of diverse pharmacological molecules. Tat-L2 (100 μM) and gap19 (100 μM); two mimetic peptides that inhibit Cx43 hemichannels by biding the intracellular L2 loop of Cx43 (Iyyathurai et al., 2013); strongly blunted the prenatal LPS-evoked Etd uptake in hippocampal astrocytes to ∼30 and 26% compared to 100% of the maximum response, respectively (**Figure 1D**). Moreover, an adapted Tat-L2 ($Tat\text{-}L2^{H126K/I130N}$), in which 2 aa essential for binding of L2 to the CT tail of Cx43 are mutated, did not cause an equivalent inhibitory response (**Figure 1D**). Equivalently, we noted that an inactive structure of gap19 containing the I130A modification ($gap19^{I130A}$), failed to reduce the prenatal LPS-dependent Etd uptake in astrocytes (**Figure 1D**). To elucidate the participation of Panx1 channels to the prenatal LPS-induced Etd uptake in hippocampal astrocytes, we employed the mimetic peptide ^{10}panx1 with an amino acid sequence homologous to the first extracellular loop domain of Panx1 (Pelegrin and Surprenant, 2006), as well as probenecid. ^{10}panx1 (100 μM) and probenecid (500 μM) but not a scrambled peptide for ^{10}panx1 partially counteracted the prenatal LPS-mediated astrocyte Etd uptake (**Figure 1D**). Collectively, this evidence suggests that prenatal LPS exposure augments the opening of astrocyte

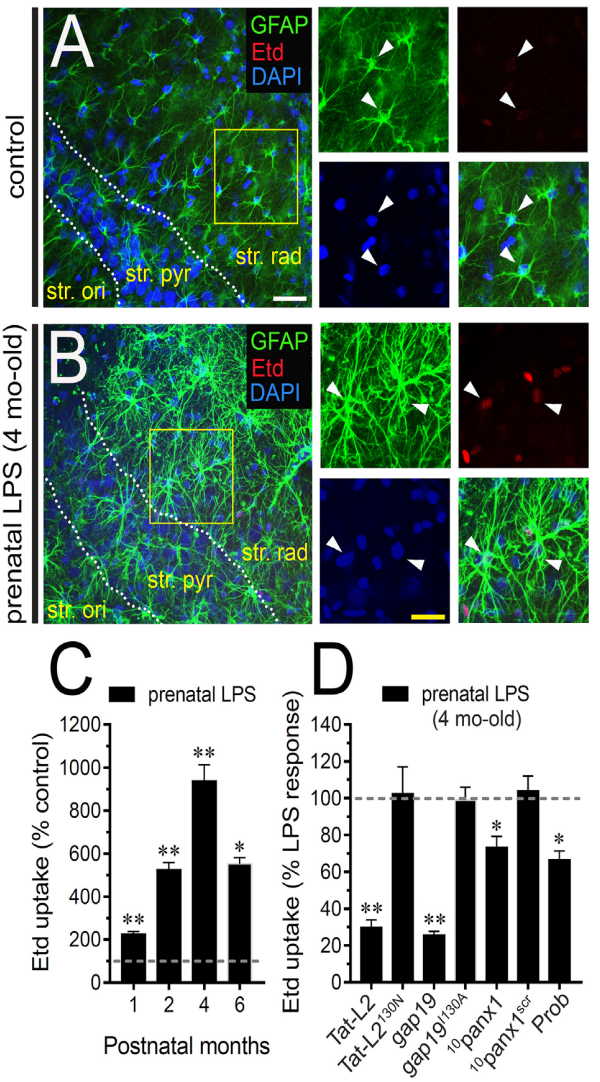

FIGURE 1 | Prenatal LPS exposure augments the activity of Cx43 hemichannels and Panx1 channels by astrocytes on offspring hippocampus. Representative images showing GFAP (green), Etd (red) and DAPI (blue) staining in the hippocampus of control offspring **(A)** or prenatally LPS-exposed offspring **(B)** of 4 months old. Insets of astrocytes were taken from the area depicted within the yellow squares in **(A,B)**. **(C)** Averaged data of Etd uptake normalized to control conditions (dashed line) by hippocampal astrocytes in acute slices from prenatally LPS-exposed offspring after following different postnatal periods. $^{**}p < 0.0001$, $^{*}p < 0.001$ versus control, one-way ANOVA Tukey's *post hoc* test, mean ± S.E.M., $n = 3$. **(D)** Averaged data normalized to the maximal effect (dashed line) induced by prenatal LPS exposure on Etd uptake by hippocampal astrocytes in acute slices from 4 months old offspring exposed to the following pharmacological agents: 100 μM Tat-L2, 100 μM $Tat\text{-}L2^{H126K/I130N}$, 100 μM gap19, 100 μM $gap19^{I130A}$, 100 μM ^{10}panx1, 100 μM $^{10}panx1^{scrb}$ and 500 μM Probenecid (Prob). $^{**}p < 0.0001$, $^{*}p < 0.05$ versus LPS, one-way ANOVA Tukey's *post hoc* test, mean ± S.E.M., $n = 3$. Calibration bars: white bar = 180 μm; yellow bar: 100 μm.

Cx43 hemichannels and Panx1 channels in the hippocampus from the adult offspring.

Activation of Microglia and IL-1β/TNF-α/p38 MAP Kinase/iNOS Signaling Contribute to the Opening of Astrocyte Cx43 Hemichannels in Prenatally LPS-Exposed Adult Offspring

Given that release of inflammatory cytokines is critical for modulating molecular, morphological and functional properties of astrocytes during pathological conditions (Agulhon et al., 2012), we evaluated whether prenatal LPS exposure could modulate the hippocampal levels of these cytokines in the offspring. During the 1 month period after birth, the hippocampus of prenatally LPS-exposed offspring showed a strong ∼5.5-fold increase in IL-1β levels compared to control that then dropped progressively in the following months (**Figure 2A**). Likewise, prenatal LPS exposure triggered a prominent 2.5-fold increase in hippocampal TNF-α levels of 1 month old offspring, which was slightly decreasing over time (**Figure 2B**). One of the major sources of cytokine production in the brain is the microglia and its activation has been observed along with neuroinflammation in prenatally LPS-exposed offspring (Schaafsma et al., 2017). Given that activation of microglia occurs along with changes in their morphology (Kettenmann et al., 2011), we measured the total branch length and branch points of microglial processes at the stratum radiatum. Analysis starting at the cell body throughout the end of each process, permit us to calculate the sum of all branch lengths and number of branch points of each microglia arbor. We found that prenatal LPS exposure reduced the branch points and the total length of microglial processes in the 4 months old offspring hippocampus (**Figures 2C,D**). Relevantly, microglia processes from prenatally LPS-exposed offspring showed similar branch points and length than their control counterparts when brain slices were treated with 50 nM minocycline (**Figures 2C,D**), a molecule that attenuates microglial activation (Kim and Suh, 2009).

To explore deeper the arbor complexity of microglia in the prenatally LPS-exposed offspring, we employed a Sholl analysis, which consists in place concentric rings at established intervals from the soma to then count branch intersections at each ring. We observed that hippocampal microglia of the offspring of LPS-exposed dams are significantly different from those of control offspring (**Figures 2E–K**). Particularly, during 4 months after birth, a dramatical reduction in the number of intersections between branches and Sholl rings was detected in hippocampal microglia of prenatally LPS-exposed offspring (**Figure 2E**). Prenatal LPS exposure also reduced microglial branch complexity as measured by the area under the Sholl curve for the total number of branch intersections at 5–60 μm from the soma (**Figure 2L**). Furthermore, hippocampal microglia of the offspring of LPS-exposed dams also exhibited decreased values in the maximum number of intersections, the radius of highest count of intersections (maximum intersect. radius) and the sum of intersections divided by intersecting radii (mean of intersections) (**Figures 2M–O**). Relevantly, minocycline treatment greatly prevented not only the arbor reduction and altered morphology observed in hippocampal microglia from prenatally LPS-exposed offspring (**Figures 2E–O**), but also the increased production of IL-1β and TNF-α occurring in these conditions (**Figure 2P**).

On the other hand, we found that minocycline prominently blunted the prenatal LPS-induced Etd uptake in hippocampal astrocytes, whereas pretreatment with a soluble form of TNF-α receptor that binds TNF-α (sTNF-aR1) and a recombinant antagonist for IL-1β receptor (IL-1ra) caused equivalent responses (**Figure 2Q**). It is known that IL-1β and TNF-α along with p38 MAP kinase activation, lead to NO-dependent S-nitrosylation of astrocytic Cx43 hemichannels, increasing their activity (Retamal et al., 2007). In this line, we found that the prenatal LPS-induced Etd uptake in hippocampal astrocytes was prominently tackled by blocking p38 MAP kinase with 10 μM SB202190 or of iNOS by 5 μM L-N6 (**Figure 2Q**). Altogether, these observations reveal that TNF-α/IL-1β and activation of iNOS/p38 MAP kinase pathways appear to be pivotal for the prenatal LPS-evoked opening of astrocyte Cx43 hemichannels but not Panx1 channels in the hippocampus. Accordingly, the Cx43 hemichannel blocker gap19 failed to trigger any additive inhibition in the prenatal LPS-induced Etd uptake when slices were treated with minocycline (**Figure 2Q**). By contrast, the Panx1 channel blocker ^{10}panx1 caused an additive inhibition when slices were stimulated with minocycline (**Figure 2Q**), suggesting that pannexon activity is not linked to the release of cytokines from activated microglia.

Prior studies have described that opening of Panx1 channels relies on direct protein-protein interactions with $P2X_7$ receptors ($P2X_7Rs$) (Iglesias et al., 2008). According with this evidence, we found that 200 nM A740003, a selective $P2X_7R$ antagonist, caused a partial reduction in the prenatal LPS-induced Etd uptake in hippocampal astrocytes (**Figure 2Q**), which was close to the inhibitory effect induced by Panx1 channel blockers (**Figure 1D**). Relevantly, ^{10}panx1 did not evoke any additive inhibition on Etd uptake of that caused by A740003 (**Figure 2Q**), underscoring the possibility that prenatal LPS-induced opening of Panx1 channels could take place via the activation of $P2X_7Rs$.

Prenatal LPS Exposure Increases the Astrocyte Production of NO and the Release of ATP via Panx1 Channels in the Offspring Hippocampus

Given that NO opens Cx43 hemichannels (Retamal et al., 2006) and because inhibition of iNOS with LN-6 greatly reduced the Etd uptake caused by prenatal LPS exposure in hippocampal astrocytes (**Figure 2Q**), we tested if this condition could affect NO production in the offspring hippocampus. DAF-FM (NO indicator) and SR101 (astrocyte marker) fluorescence imaging revealed that hippocampal astrocytes from prenatally LPS-exposed offspring showed a ∼2.5-fold augment in basal NO production compared to control conditions (**Figures 3A–C**). The fact that LN-6 totally suppressed the prenatal-LPS-induced

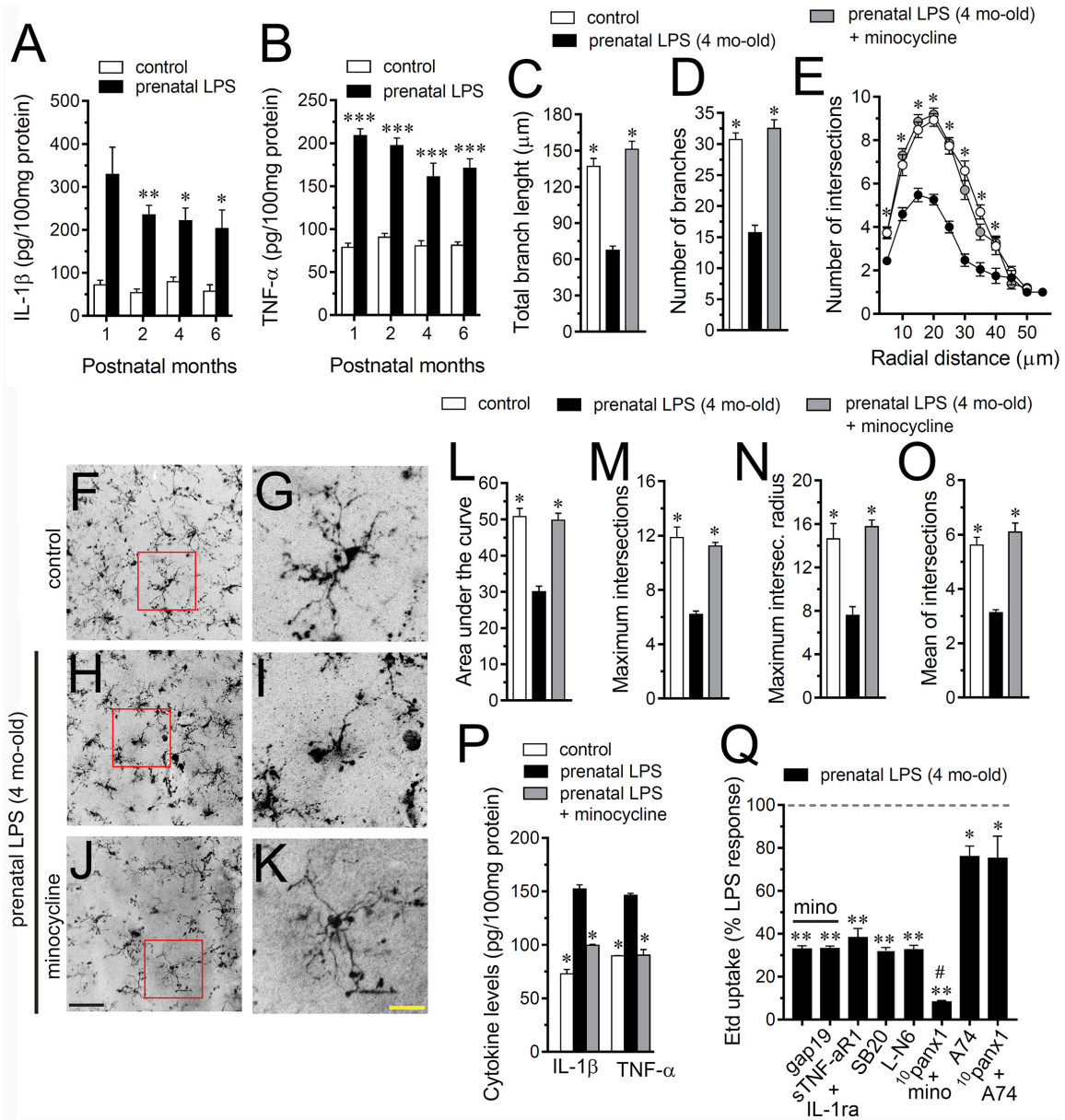

FIGURE 2 | Microglia and IL-1β/TNF-α/p38 MAP kinase/iNOS signaling participate in the prenatal LPS-induced opening of astrocyte Cx43 hemichannels on offspring hippocampus. Averaged data of hippocampal levels of IL-1β **(A)** and TNF-α **(B)** from control offspring (white bars) or prenatally LPS-exposed offspring (black bars) following different postnatal periods. ***$p < 0.0001$, **$p < 0.005$, *$p < 0.05$ versus control, two-way ANOVA Bonferroni's *post hoc* test, mean ± S.E.M., $n = 3$. **(C,D)** Averaged data of total branch length **(C)** and number of branches **(D)** by hippocampal microglia in acute slices from control offspring (white bars) or prenatally LPS-exposed offspring (black bars) of 4 months old. Also shown are the effects of treatment with 50 nM minocycline for 2 h in acute slices prenatally LPS-exposed offspring of 4 months old (gray bars). *$p < 0.0001$ versus LPS, one-way ANOVA Dunnett's *post hoc* test, mean ± S.E.M., $n = 3$. **(E)** Averaged data of Sholl analysis by hippocampal microglia from control offspring (white circles) or prenatally LPS-exposed offspring of 4 months old alone (black circles) or plus treatment with 50 nM minocycline (gray circles). *$p < 0.001$ versus LPS, two-way ANOVA Tukey's *post hoc* test, mean ± S.E.M., $n = 3$. **(F–K)** Representative Iba-1 (black) positive hippocampal microglia in acute slices from control offspring **(F,G)** or prenatally LPS-exposed offspring of 4 months old alone **(H,I)** or plus treatment with 50 nM minocycline **(J,K)**. Insets of microglia **(G,I,K)** were taken from the area depicted within the red squares in **(F,H,J)**. **(L–O)** Averaged data of area under the curve of Sholl analysis **(L)**, maximum intersection **(M)**, maximum intersection radius **(N)**, and mean of intersections **(O)** by hippocampal microglia from control offspring (white bars) or prenatally LPS-exposed offspring of 4 months old alone (black bars) or plus treatment with 50 nM minocycline (gray bars). *$p < 0.0001$ versus LPS, one-way ANOVA Dunnett's *post hoc* test, mean ± S.E.M., $n = 3$. **(P)** Averaged data of hippocampal levels of IL-1β and TNF-α from control offspring (white bars) or prenatally LPS-exposed offspring of 4 months old alone (black bars) or plus treatment with 50 nM minocycline (gray bars). ***$p < 0.0001$, versus control, two-way ANOVA Bonferroni's *post hoc* test, mean ± S.E.M., $n = 3$. **(Q)** Averaged data normalized to the maximal effect (dashed line) induced by prenatal LPS exposure on Etd uptake by hippocampal astrocytes in acute slices from 4 months old offspring exposed to the following pharmacological agents: 50 nM minocycline, 50 nM minocycline + 100 μM gap19, sTNF-αR1 + IL-1ra (300 ng/ml each), 1 μM SB203580, 1 μM L-N6, 50 nM minocycline + 100 μM ^{10}panx1, 200 nM A740003 or 100 μM ^{10}panx1 + 200 nM A740003. **$p < 0.0001$, *$p < 0.005$ versus LPS, $^{\#}p < 0.0001$ versus minocycline, one-way ANOVA Dunnett's *post hoc* test, mean ± S.E.M., $n = 3$. Calibration bars: black bar = 180 μm; yellow bar: 80 μm.

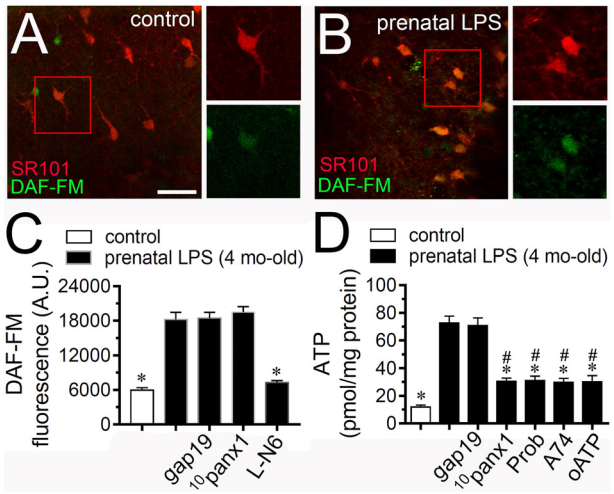

FIGURE 3 | Prenatal LPS exposure increases the production of NO by astrocytes and the Panx1 channel-dependent release of ATP on offspring hippocampus. Representative images showing SR101 (red) and DAF-FM (green) staining by hippocampal astrocytes in acute slices from control offspring **(A)** or prenatally LPS-exposed offspring **(B)** of 4 months old. Insets of astrocytes were taken from the area depicted within the red squares in **(A,B)**. **(C)** Averaged of DAF-FM signal fluorescence by astrocytes in acute slices from control offspring (white bar) or prenatally LPS-exposed offspring of 4 months old alone (black bars) or in combination with the following pharmacological agents: 100 μM gap19, 100 μM ^{10}panx1 and 1 μM L-N6. $^{*}p < 0.0001$ versus LPS, one-way ANOVA Tukey's *post hoc* test, mean ± S.E.M., $n = 3$. **(D)** Averaged data of ATP release by acute hippocampal slices from control offspring (white bar) or prenatally LPS-exposed offspring of 4 months old alone (black bars) or in combination with the following blockers: 100 μM gap19, 100 μM ^{10}panx1 and 1 μM L-N6. $^{*}p < 0.0001$ versus LPS, $^{\#}p < 0.0001$ versus control, one-way ANOVA Tukey's *post hoc* test, mean ± S.E.M., $n = 3$. Calibration bar = 85 μm.

production of NO indicates that iNOS is the major contributor to this response (**Figure 3C**). A previous study has related the opening of Panx1 channels with the production of NO (Orellana et al., 2013). In opposition to this finding, we observed that neither ^{10}panx1 nor gap19 were effective in to prevent the prenatal-LPS-induced production of NO (**Figure 3C**), suggesting that Panx1 channels and Cx43 hemichannels and are not involved in this response.

iNOS stimulation is crucial for the hemichannel/pannexon-dependent release of ATP from astrocytes occurring after LPS treatment (Avendano et al., 2015). With this in mind and given that A740003, a selective antagonist of $P2X_7$Rs, counteracted the astrocyte Etd uptake triggered by prenatal LPS exposure (**Figure 2Q**), we investigated if this condition could impact the release of ATP in the offspring hippocampus. Measurements of extracellular ATP levels with the luciferin/luciferase bioluminescence assay showed that prenatal LPS exposure dramatically augmented the release of ATP in ∼7-fold in the offspring hippocampus compared to control conditions (**Figure 3D**). Importantly, probenecid or ^{10}panx1 but not gap19 markedly reduced the release of ATP caused by prenatal LPS exposure (from ∼73 pmol/mg to ∼30 pmol/mg and ∼31 pmol/mg, respectively) (**Figure 3D**). Similarly, 200 μM oATP or 200 nM A740003 prominently reduced the prenatal LPS-evoked release of ATP (**Figure 3B**).

Cx43 Hemichannel Opening Evoked by Prenatal LPS Exposure Contributes to $[Ca^{2+}]_i$ and Glutamatergic Signaling on Offspring Hippocampus

At the next step, we decided to analyze the effect of hemichannel/pannexon blockers on astroglial $[Ca^{2+}]_i$ in prenatally LPS-exposed offspring. As indicated by the assessment of Fluo-4 (Ca^{2+} indicator) and SR101, hippocampal astrocytes from offspring of LPS-exposed dams showed a 3-fold augment in basal levels of Ca^{2+} signal compared to control astrocytes (**Figures 4A–C**). Importantly, blockade of Cx43 hemichannels with Tat-L2 or gap19 dramatically suppressed the prenatal LPS-mediated increase in astroglial $[Ca^{2+}]_i$ in the hippocampus (**Figure 4C**). Similar observations were obtained upon treatment with minocycline but not with probenecid or ^{10}panx1 (**Figure 4C**). Altogether these findings indicate that microglial-dependent opening of Cx43 hemichannels but not Panx1 channels participate in the prenatal LPS-induced increase in astroglial $[Ca^{2+}]_i$ in the hippocampus.

Glutamate modulates $[Ca^{2+}]_i$ dynamics in astrocytes, particularly through the stimulation of metabotropic glutamate receptors (mGluRs) and subsequent release of Ca^{2+} from intracellular stores (Bradley and Challiss, 2012). Here, we found that prenatal LPS-evoked $[Ca^{2+}]_i$ response was prominently blunted by 50 nM MTEP or 5 μM SIB-1757, being the latter two selective antagonists of $mGluR_5$ (**Figure 4C**). Noteworthy, selective blockade of phospholipase C (PLC) or IP_3 receptors with 5 μM U73122 or 50 μM APB, respectively, as well as chelation of $[Ca^{2+}]_i$ with 10 μM BAPTA-AM, strikingly counteracted the increase in astroglial $[Ca^{2+}]_i$ triggered by prenatal LPS exposure (**Figure 4C**). On the other hand, inhibition of $P2X_7$Rs with oATP or A740003 caused a slight reduction in the prenatal LPS-induced astroglial $[Ca^{2+}]_i$ signal (**Figure 4C**). This could imply that astroglial $[Ca^{2+}]_i$ response resulting from prenatal LPS exposure is a consequence of the Cx43 hemichannel-dependent release of glutamate and further stimulation of $mGluR_5$ rather than signaling via Panx1 channels. Consistent with this notion, we saw that prenatal LPS exposure induced a 7-fold increase in the release of glutamate in the offspring hippocampus, a response that was totally blunted by Tat-L2 or gap19 but not with probenecid or ^{10}panx1 (**Figure 4D**). Further, we tested whether $[Ca^{2+}]_i$ and $mGluR_5$ signaling were implicated in the Etd uptake observed in hippocampal astrocytes from prenatally LPS-exposed offspring. BAPTA-AM, but not inhibition of PLC, IP_3 receptors or $mGluR_5$, significantly reduced the prenatal LPS-induced Etd uptake in hippocampal astrocytes (**Figure 4E**). In this scenario, we further performed the analysis of spontaneous $[Ca^{2+}]_i$ oscillations in astrocytes. We found that prenatal LPS exposure increase the number of spontaneous astroglial $[Ca^{2+}]_i$ oscillations and their amplitude in the offspring hippocampus, a response that was totally blunted by BAPTA-AM but not by gap19,

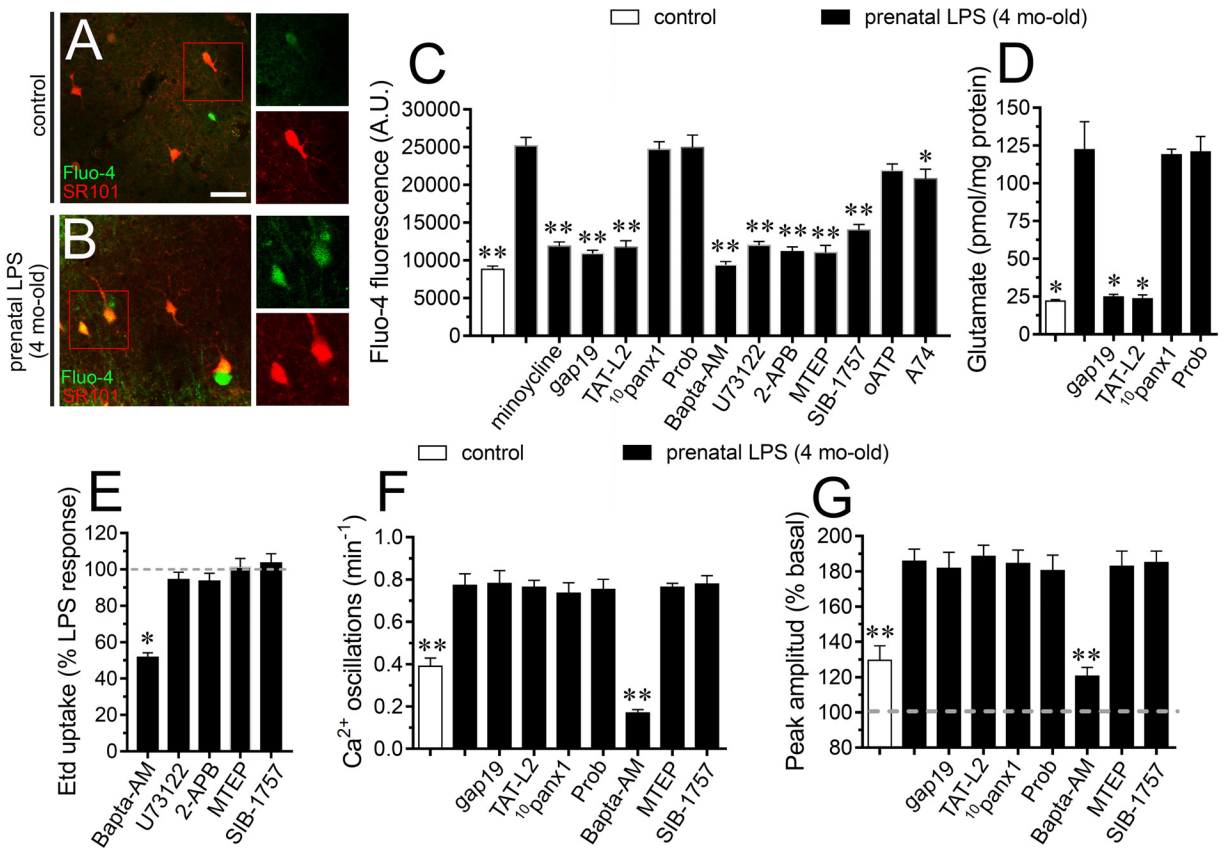

FIGURE 4 | Prenatal LPS-induced opening of Cx43 hemichannels increases $[Ca^{2+}]_i$ and glutamatergic signaling on offspring hippocampus. Representative images showing SR101 (red) and Fluo-3 (green) staining by hippocampal astrocytes in acute slices from control offspring **(A)** or prenatally LPS-exposed offspring **(B)** of 4 months old. Insets of astrocytes were taken from the area depicted within the red squares in (A,B). **(C)** Averaged of basal Fluo-4 signal fluorescence by hippocampal astrocytes in acute slices from control offspring (white bar) or prenatally LPS-exposed offspring of 4 months old alone (black bars) or in combination with the following pharmacological agents: 50 nM minocycline, 100 μM gap19, 100 μM Tat-L2, 100 μM ^{10}panx1, 500 μM Probenecid (Prob), 10 μM Bapta-AM, 5 μM U-73122, 50 μM 2-APB, 50 nM MTEP, 5 μM SIB-1757, 200 μM oATP and 200 nM A740003. $^{**}p < 0.0001$, $^{*}p < 0.005$ versus LPS, one-way ANOVA Tukey's *post hoc* test, mean ± S.E.M., $n = 3$. **(D)** Averaged data of glutamate release by acute hippocampal slices from control offspring (white bar) or prenatally LPS-exposed offspring of 4 months old alone (black bars) or in combination with the following blockers: 100 μM gap19, 100 μM Tat-L2, 100 μM ^{10}panx1, 500 μM Probenecid (Prob). $^{*}p < 0.0001$ versus LPS, one-way ANOVA Tukey's *post hoc* test, mean ± S.E.M., $n = 3$. **(E)** Averaged data normalized to the maximal effect (dashed line) induced by prenatal LPS exposure on Etd uptake by hippocampal astrocytes in acute slices from 4 months old offspring exposed to the following pharmacological agents: 10 μM Bapta-AM, 5 μM U-73122, 50 μM 2-APB, 50 nM MTEP, and 5 μM SIB-1757. $^{*}p < 0.0001$ versus LPS, one-way ANOVA Tukey's *post hoc* test, mean ± S.E.M., $n = 3$. **(F)** Averaged of spontaneous $[Ca^{2+}]_i$ oscillations by hippocampal astrocytes in acute slices from control offspring (white bar) or prenatally LPS-exposed offspring of 4 months old alone (black bars) or in combination with the following pharmacological agents: 100 μM gap19, 100 μM Tat-L2, 100 μM ^{10}panx1, 500 μM Probenecid (Prob), 10 μM Bapta-AM, 50 nM MTEP or 5 μM SIB-1757. $^{**}p < 0.005$ versus LPS, one-way ANOVA Tukey's *post hoc* test, mean ± S.E.M., $n = 3$. **(G)** Averaged of peak amplitude of spontaneous $[Ca^{2+}]_i$ oscillations by hippocampal astrocytes in acute slices from control offspring (white bar) or prenatally LPS-exposed offspring of 4 months old alone (black bars) or in combination with the following pharmacological agents: 100 μM gap19, 100 μM Tat-L2, 100 μM ^{10}panx1, 500 μM Probenecid (Prob), 10 μM Bapta-AM, 50 nM MTEP or 5 μM SIB-1757. $^{**}p < 0.005$ versus LPS, one-way ANOVA Tukey's *post hoc* test, mean ± S.E.M., $n = 3$. Calibration bar = 85 μm.

Tat-L2, ^{10}panx1, probenecid, MTEP or SIB-1757 (**Figure 4F**). Similar responses were observed when the peak amplitude of spontaneous astroglial $[Ca^{2+}]_i$ oscillations was analyzed (**Figure 4G**). To figure out the possible contribution of neurons to these responses, we performed the above experiments in presence of 0.5 μM TTX. We found that TTX did not affect the prenatal LPS-induced changes in NO and $[Ca^{2+}]_i$ levels, as well as the release of glutamate, suggesting that neurons do not participate in these processes under these conditions (**Supplementary Figures S1A–E**). Collectively, these data suggest that spontaneous $[Ca^{2+}]_i$ oscillations evoked by prenatal LPS exposure are likely necessary for the opening of astroglialCx43 hemichannels, whereas the subsequent release of glutamate through them is needed for the increase in basal $[Ca^{2+}]_i$ via the activation of $mGluR_5$ receptors. Although previous studies have associated the channel-dependent Etd uptake with changes in the distribution of Cx43 in astrocytes (Avendano et al., 2015), we found that prenatal LPS exposure did not alter the total amount or distribution of Cx43 in hippocampal astrocytes (**Supplementary Figures S2A–G**).

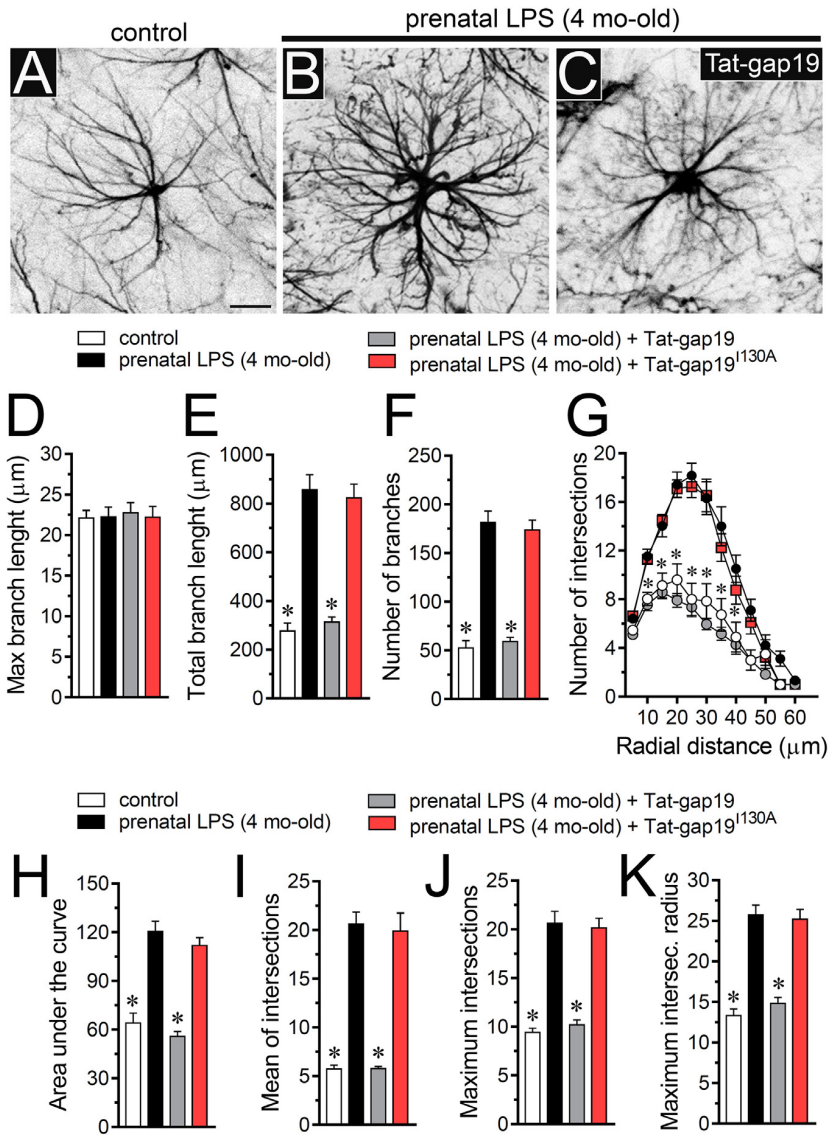

FIGURE 5 | Prenatal LPS exposure increases the arborization of hippocampal astrocytes in the offspring by a mechanism involving the activation of Cx43 hemichannels. **(A–C)** Representative GFAP (black) positive hippocampal astrocytes from control offspring **(A)** or prenatally LPS-exposed offspring of 4 months old alone **(B)** or plus the *in vivo* administration of 23 mg/kg Tat-gap19 **(C)**. **(D–F)** Averaged data of maximum branch length **(D)**, total branch length **(E)** and number of branches **(F)** by hippocampal astrocytes in acute slices from control offspring (white bars) or prenatally LPS-exposed offspring (black bars) of 4 months old. Also shown are the effects of *in vivo* administration of 23 mg/kg Tat-gap19 (gray bars) or its inactive form: 23 mg/kg Tat-gap19^{I130A} (red bars). *$p < 0.0001$ versus LPS, one-way ANOVA Dunnett's *post hoc* test, mean ± S.E.M., $n = 3$. **(G)** Averaged data of Sholl analysis by hippocampal astrocytes from control offspring (white circles) or prenatally LPS-exposed offspring of 4 months old alone (black circles) or plus the *in vivo* administration of 23 mg/kg Tat-gap19 (gray circles) or 23 mg/kg Tat-gap19^{I130A} (red circles). *$p < 0.001$ versus LPS, two-way ANOVA Tukey's *post hoc* test, mean ± S.E.M., $n = 3$. **(H–K)** Averaged data of area under the curve of Sholl analysis **(H)**, maximum intersection **(I)**, maximum intersection radius **(J)**, and mean of intersections **(K)** by hippocampal astrocytes from control offspring (white bars) or prenatally LPS-exposed offspring of 4 months old alone (black bars) or plus the *in vivo* administration of 23 mg/kg Tat-gap19 (gray bars) or 23 mg/kg Tat-gap19^{I130A} (red bars). *$p < 0.0001$ versus LPS, one-way ANOVA Dunnett's *post hoc* test, mean ± S.E.M., $n = 3$. Calibration bar = 40 μm.

Activation of Cx43 Hemichannels Contributes to Increased Arborization of Hippocampal Astrocytes in Prenatally LPS-Exposed Offspring

One of the crucial aspects of reactive astrogliosis is the hypertrophy of cellular processes accompanied by crucial changes in the arborization and morphology of astrocytes (Pekny and Pekna, 2014). To understand whether the above described prenatal LPS-induced changes in astrocytes are accompanied by alterations in their arborization, we analyzed the maximum and total branch length of astroglial processes at the stratum radiatum (**Figures 5A–E**). Similar to the previous measurements made in microglia, we calculated the longest branch and the sum of all

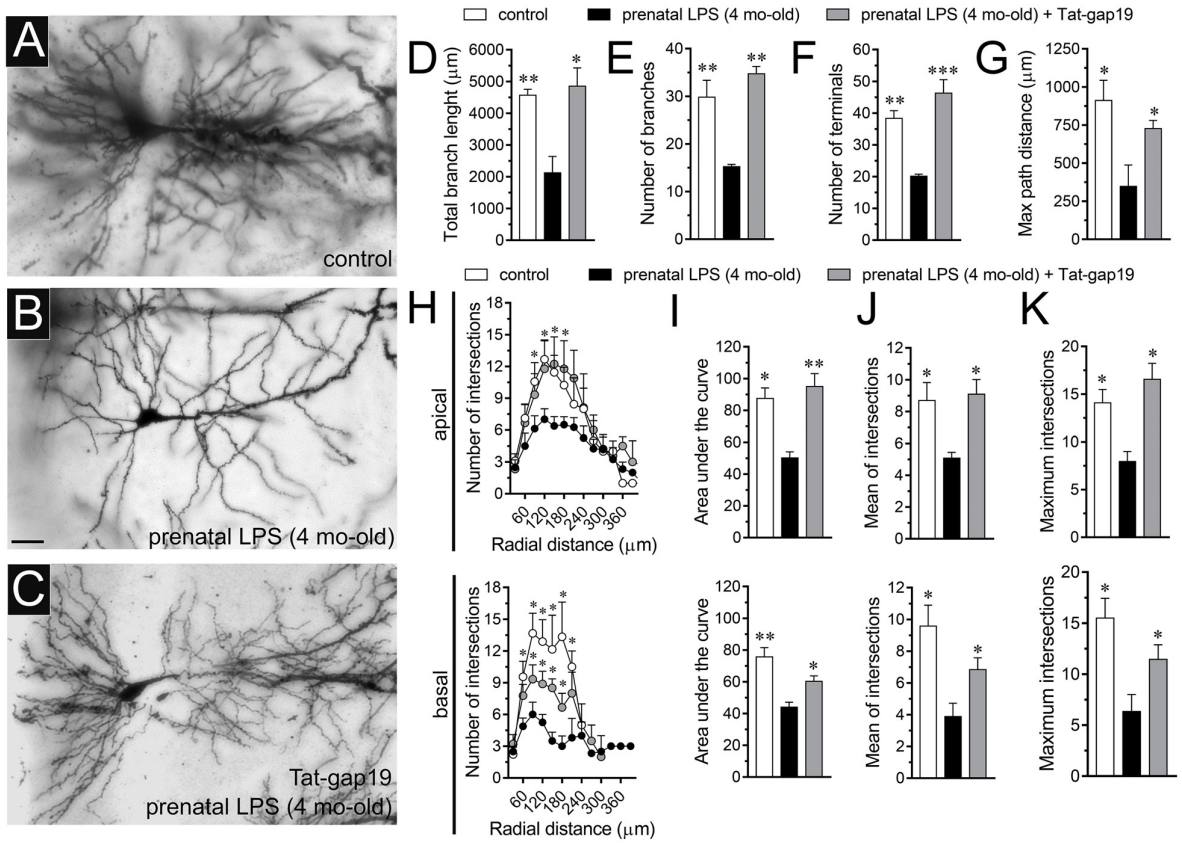

FIGURE 6 | Prenatal LPS exposure increases the arborization of CA1 pyramidal neurons in the offspring by a mechanism involving the activation of Cx43 hemichannels. **(A–C)** Representative golgi (black) staining by CA1 pyramidal neurons from control offspring **(A)**, prenatally LPS-exposed offspring of 4 month old alone **(B)** or in combination with the *in vivo* administration of 23 mg/kg Tat-gap19 **(C)**. **(D–G)** Averaged data of total branch length **(D)**, number of branches **(E)**, number of terminals **(F),** and maximum path distance **(G)** by CA1 pyramidal neurons from control offspring (white bars) or prenatally LPS-exposed offspring of 4 months old alone (black bars) or in combination with the *in vivo* administration of 23 mg/kg Tat-gap19 (gray bars). $*p < 0.05$, $**p < 0.01$, $***p < 0.005$ versus LPS, one-way ANOVA Dunnett's *post hoc* test, mean ± S.E.M., $n = 3$. **(H)** Averaged data of Sholl analysis by apical (upper panel) and basal (bottom panel) dendritic arbor of CA1 pyramidal neurons from control offspring (white circles) or prenatally LPS-exposed offspring of 4 months old alone (black circles) or plus the *in vivo* administration of 23 mg/kg Tat-gap19 (gray circles). $*p < 0.05$ versus LPS, two-way ANOVA Tukey's *post hoc* test, mean ± S.E.M., $n = 3$. **(I–K)** Averaged data of area under the curve of Sholl analysis **(I)**, mean of intersections **(J)** and maximum intersection **(K)** by apical (upper panel) and basal (bottom panel) dendritic arbor of CA1 pyramidal neurons from control offspring (white bars) or prenatally LPS-exposed offspring of 4 months old alone (black bars) or plus the *in vivo* administration of 23 mg/kg Tat-gap19 (gray bars). $*p < 0.05$, $**p < 0.01$ versus LPS, one-way ANOVA Tukey's *post hoc* test, mean ± S.E.M., $n = 3$. Calibration bar = 45 μm.

branch lengths of each astrocyte arbor, which were depicted as maximum and total branch length, respectively. Measurements of cell arbor disclosed that maximum branch length remained without alterations between hippocampal astrocytes from control and prenatally LPS-exposed offspring (**Figure 5D**). Nonetheless, astrocytes from prenatally LPS-exposed offspring exhibited a ∼2-fold increase in both total branch length (**Figure 5E**) and the number of branches (**Figure 5F**). Sholl analysis demonstrated that hippocampal astrocytes from the offspring of LPS-exposed dams showed more complex arbors than in control animals (**Figures 5A–C,G**). Specifically, in these astrocytes, both the number of intersections between branches and Sholl rings, as well as the area under the Sholl curve were increased (**Figures 5G,H**). Prenatal LPS exposure triggered equivalent augmented values in the maximum number of intersections, the radius of the highest count of intersections and mean of intersections (**Figures 5I–K**). These findings suggest that prenatal LPS enhance the complexity of astrocyte branch arbors in the hippocampus of prenatally LPS-exposed offspring.

To unveil the contribution of Cx43 hemichannel activity in prenatal LPS-induced increase in branch arbor complexity, we injected prenatally LPS-exposed offspring mice during postnatal months with the gap19 mimetic peptide containing the cell-penetrating TAT linker (Tat-gap19; 23 mg/kg, see section Materials and methods), which crosses the blood-brain barrier (BBB) (Abudara et al., 2014). Notably, Tat-gap19 completely prevented the prenatal LPS-induced increase in diverse arbor parameters, including total branch length (**Figure 5E**), number of branches (**Figure 5F**), arbor complexity (**Figure 5G**), the area under the Sholl curve (**Figure 5H**), mean of intersections (**Figure 5I**), maximum number of intersections (**Figure 5J**), and the radius of highest count of intersections (**Figure 5K**). Relevantly, the inactive form of Tat-gap19 containing the I130A modification (TAT-gap19^{I130A}) induced no effect on the prenatal

LPS-mediated increase on astrocyte arborization (**Figures 5D–K**). These findings suggest that opening of Cx43 hemichannels is crucial for the prenatal LPS-mediated increment in astrocyte arbor branch complexity in the offspring hippocampus.

The Opening of Cx43 Hemichannels Is Required for the Prenatal LPS-Mediated Reduction in Arbor Branch Complexity and Dendritic Spine Density of Hippocampal Pyramidal Neurons in the Offspring

Hippocampal synaptic dysfunction has been linked with retraction of dendrites pyramidal neurons, as well as loss of synapses in diverse neurological disorders (Luo and O'Leary, 2005; Riccomagno and Kolodkin, 2015). Nonetheless, whether prenatal LPS exposure causes dendritic retraction and spine density reduction in the hippocampus have not been studied in detail (Fernandez de Cossio et al., 2017). Here, analysis of dendritic arbor (**Figures 6A–C**) showed that prenatal LPS exposure caused a ∼2-fold decrease in total branch length (**Figure 6D**), number of branches (**Figure 6E**) and the number of terminals (**Figure 6F**) in CA1 pyramidal neurons. These neurons also exhibited a decrease in the maximum path distance between the soma and terminal dendrites when compared with their control counterparts (**Figure 6G**). A precise Sholl analysis underscored that CA1 pyramidal neurons from the offspring of LPS-exposed dams displayed a ∼2-fold decline in arbor complexity in both basal and apical dendrites (**Figure 6H**). Indeed, prenatal LPS exposure diminished the area under the Sholl curve (**Figure 6I**), the mean of intersections between branches and Sholl rings (**Figure 6J**), as well as the maximum number of intersections (**Figure 6K**). Of note, dendritic retraction evoked by prenatal LPS exposure was accompanied by decreased spine density in apical but not basal dendrites of CA1 pyramidal neurons (**Figures 7A–D**).

Consistent with what occurred in hippocampal astrocytes, *in vivo* treatment with Tat-gap19 strongly counteracted the prenatal LPS-induced decrease in arborization, although this inhibitory response was more effective in apical rather than basal dendritic arbor (**Figures 6H–K**). In addition, Tat-gap19 also totally blunted the prenatal LPS-induced decrease in spine density in apical dendrites of CA1 pyramidal neurons (**Figure 7D**). TAT-gap19^{I130A}, the inactive form of Tat-gap19, did not change the prenatal LPS-mediated reduction in the neuronal pyramidal arbor or spine density (not shown). Altogether these findings argue for a crucial role of Cx43 hemichannels in the prenatal LPS-mediated reduction of dendritic arbor and spine density of CA1 pyramidal neurons.

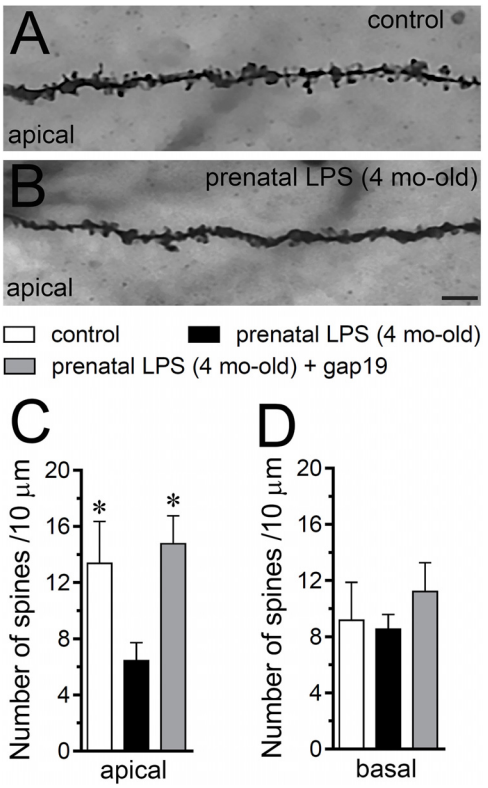

FIGURE 7 | Prenatal LPS exposure increases spine density in apical but not basal dendrites of CA1 pyramidal neurons, a response based on the activation of Cx43 hemichannels. **(A,B)** Representative golgi (black) staining by apical dendrites of CA1 pyramidal neurons from control offspring **(A)** or prenatally LPS-exposed offspring of 4 months old **(B)**. **(C,D)** Averaged data of the number of apical **(A)** or basal **(B)** dendritic spines by CA1 pyramidal neurons from control offspring (white bars) or prenatally LPS-exposed offspring of 4 months old alone (black bars) or in combination with the *in vivo* administration of 23 mg/kg Tat-gap19 (gray bars). *$p < 0.05$ versus LPS, one-way ANOVA Tukey's *post hoc* test, mean ± S.E.M., $n = 3$. Calibration bar = 3 µm.

Cx43 Hemichannels Participate in the Prenatal LPS-Induced Neuronal Death in Hippocampal Slices

It is well established that prenatal-LPS exposure triggers neuronal death in the offspring (Ling et al., 2002; Hao et al., 2010) and diverse studies have proposed that uncontrolled release of substances via opening of astrocyte Cx43 hemichannels could be toxic for neighboring neurons (Orellana et al., 2011; Yi et al., 2016). With this in mind, we evaluated if prenatal LPS exposure could induce cell death in CA1 pyramidal neurons and whether Cx43 hemichannels are involved in this process. In control offspring, most pyramidal neurons were negative for F-Jade staining (∼3 neurons/field) and most astrocytes displayed a normal grade of GFAP expression (**Figures 8A–C,J,K**). However, prenatally LPS-exposed offspring exhibited a ∼10-fold augment in CA1 pyramidal neurons displaying F-Jade staining, which was accompanied by a qualitative augment in GFAP reactivity (**Figures 8D–F,J,K**). Relevantly, *in vivo* treatment with Tat-gap19 greatly tackled both the prenatal LPS-induced F-Jade staining of CA1 pyramidal neurons (to ∼8 neurons/field) and the enchanced reactivity of GFAP (in ∼40%) in hippocampal slices (**Figures 8G–K**). In the presence of TAT-gap19^{I130A}, the F-Jade staining by CA1 pyramidal neurons remained unaltered in prenatally LPS-exposed offspring (**Figures 8J,K**). The above data suggest that

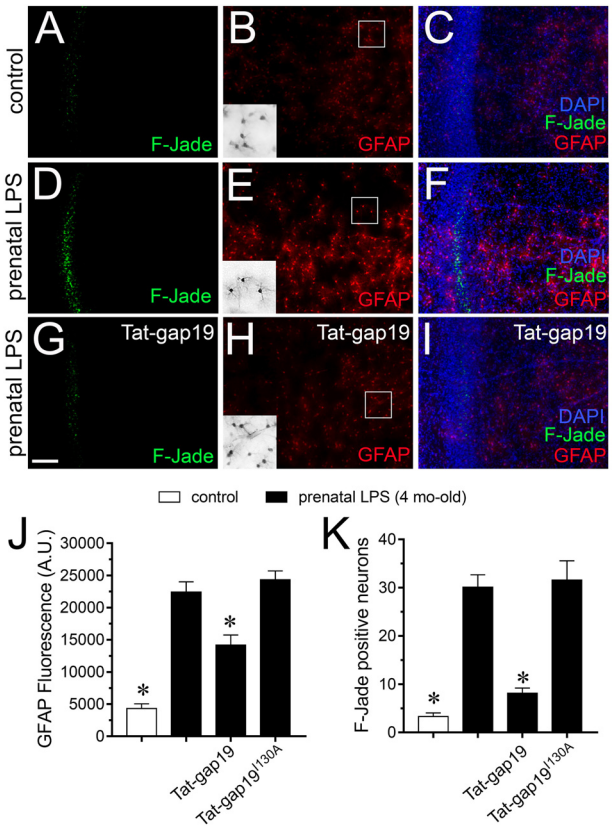

FIGURE 8 | Cx43 hemichannel contributes to neuronal death evoked by prenatal LPS exposure on offspring hippocampus. **(A–I)** Representative images depicting Fluoro-Jade (F-Jade, green), GFAP (red) and DAPI (blue) staining in acute slices from control offspring **(A–C)** or prenatally LPS-exposed offspring of 4 months old alone **(D–F)** or in combination with the *in vivo* administration of 23 mg/kg Tat-gap19 **(G–I)**. Insets of gray scale GFAP staining for astrocytes are shown from the area depicted within the white squares in **(B,E,H)**. **(J)** Averaged data of GFAP fluorescence per field in acute slices from control offspring (white bars) or prenatally LPS-exposed offspring of 4 months old alone (black bars) or in combination with the *in vivo* administration of 23 mg/kg Tat-gap19 (gray bars). *$p < 0.01$ versus LPS, one-way ANOVA Tukey's *post hoc* test, mean ± S.E.M., $n = 3$. **(K)** Averaged number of F-Jade-positive CA1 pyramidal neurons per field in acute slices from control offspring (white bars) or prenatally LPS-exposed offspring of 4 months old alone (black bars) or in combination with the *in vivo* administration of 23 mg/kg Tat-gap19 (gray bars). *$p < 0.001$ versus LPS, one-way ANOVA Tukey's *post hoc* test, mean ± S.E.M., $n = 3$. Calibration bar = 100 μm.

Cx43 hemichannels are main contributors to the hippocampal neuronal death caused by prenatal LPS exposure in the offspring.

DISCUSSION

In this work, we reported that prenatal LPS exposure augments the activity of astrocyte Cx43 hemichannels and Panx1 channels in the hippocampus of adult offspring mice. This enhanced channel activity occurred by a mechanism involving a microglia-dependent production of IL-1β/TNF-α and the stimulation of p38 MAPK/iNOS/$[Ca^{2+}]_i$-mediated pathways and purinergic/glutamatergic signaling. Noteworthy, the opening of Cx43 hemichannels affected the release of glutamate, $[Ca^{2+}]_i$ handling, and morphology of astrocytes, whereas also disturbed neuronal function, including the dendritic arbor and spine density, as well as survival.

Previous evidence indicates that prenatal LPS exposure triggers diverse disturbances in the offspring brain, including alterations in hippocampal-dependent synaptic plasticity and memory (Golan et al., 2005; Escobar et al., 2011; Kelley et al., 2017), as well as increased neuronal death and astrogliosis (Ling et al., 2002; Hao et al., 2010; Zager et al., 2015; Cho et al., 2018). This study suggests that part of the above-mentioned abnormalities induced by prenatal LPS exposure could take place by the persistent opening of astrocyte Cx43 hemichannels and/or Panx1 channels within the hippocampus. As assayed by Etd uptake in acute brain slices, we found that a single LPS injection during pregnancy increases the opening of Cx43 hemichannels and Panx1 channels in hippocampal astrocytes from the stratum radiatum in the offspring. These responses were prominently inhibited by Tat-L2 or gap19, whereas probenecid or ^{10}panx1 showed a partial inhibitory effect. Thus, Cx43 hemichannels rather than Panx1 channels were the major responsible for the prenatal LPS-induced Etd uptake in astrocytes. The latter is consistent with the enhanced activity reported for both channels in astrocyte cultures obtained from prenatally LPS-exposed neonates (Avendano et al., 2015), as well as astrocytes from different animal pathological models such as neuropathic pain (Tonkin et al., 2018), Alzheimer's disease (Yi et al., 2016), epileptic seizures (Santiago et al., 2011), spinal cord injury (Garre et al., 2016), and acute brain infection (Karpuk et al., 2011).

How does prenatal LPS exposure trigger the opening of Cx43 hemichannels and Panx1 channels in hippocampal astrocytes *ex vivo*? Multiple lines of evidence indicate that environmental factors during early development impact the future inflammatory balance and immunity response of the offspring (Boksa, 2010). Here, we observed that prenatal LPS exposure induced a microglia-dependent long-lasting production of both IL-1β and TNF-α on offspring hippocampus. The latter response was accompanied by a profound retraction of microglia cellular processes compatible with amoeboid features typical of activated microglia. This is in agreement with the presence of activated microglia as well as with upregulated levels of IL-1β and TNF-α in the offspring's brain of LPS-exposed dams (Boksa, 2010). In addition, our experiments showed that minocycline, a molecule that attenuates microglial activation, or inhibition of IL-1β/TNF-α signaling, dramatically suppressed the prenatal LPS-induced opening of astrocytic Cx43 hemichannels but not Panx1 channels on offspring hippocampus. These findings harmonize with prior studies showing that release of IL-1β and TNF-α from activated microglia causes the activation of astroglial Cx43 hemichannels (Retamal et al., 2007). Thereby, in our system, the opening of astroglial Cx43 hemichannels likely resulted from the IL-1β/TNF-α-mediated activation of p38 MAP kinase and further iNOS-dependent S-nitrosylation of Cx43, as has been previously described (Retamal et al., 2006; Retamal et al., 2007) (**Figure 9**). In accord with this hypothesis, we detected that prenatal LPS-induced astroglial Etd uptake was strongly

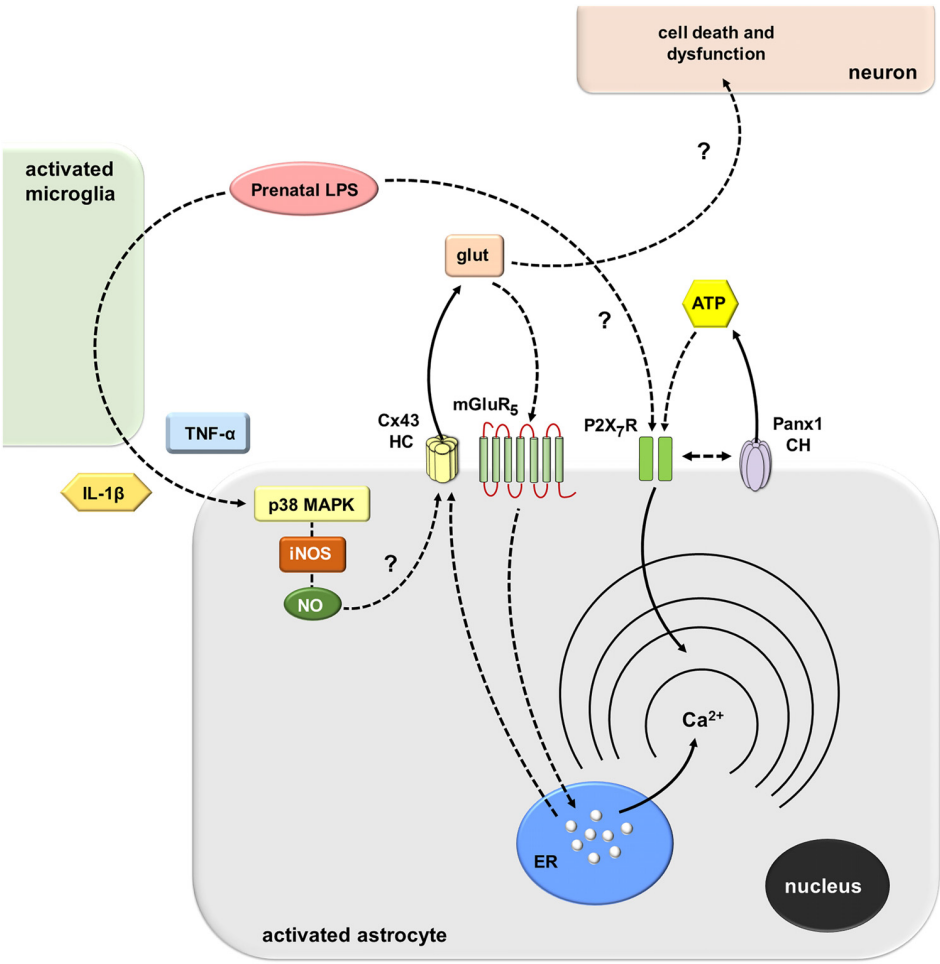

FIGURE 9 | Schematic diagram showing the possible pathways involved in the prenatal LPS-induced activation of Cx43 hemichannels/Panx1 channels and its consequences for astroglial function and neuronal survival. Prenatal LPS exposure activates microglia, resulting in the release of IL-1β and TNF-α. Both cytokines stimulate astrocytes, leading to the activation of a p38MAPK/iNOS-dependent pathway and further production of NO. The latter likely induces unknown mechanisms that cause opening of Cx43 hemichannels enabling the release of glutamate. Glutamate released via Cx43 hemichannels activates $mGluR_5$ receptors resulting in the stimulation of IP_3 receptors and further release of Ca^{2+} stored in the endoplasmic reticulum. In parallel, the activation of astroglial $P2X_7$ receptors lead to the opening of Panx1 channels and further release of ATP, possibly through direct protein-to-protein interactions. Relevantly, the modulation of $[Ca^{2+}]_i$ dynamics evoked by Cx43 hemichannels may alter astroglial morphology (not depicted), whereas the excitotoxic release of glutamate through Cx43 hemichannels may affect neuronal arborization and survival by unknown mechanisms.

blunted by blocking p38 MAP kinase or iNOS. In the same line, hippocampal astrocytes from prenatally LPS-exposed offspring showed increased levels of NO production, as measured by DAF-FM signal. Of note, this response was totally blunted by the inhibition of iNOS but not by blockers of Cx43 hemichannels or Panx1 channels, suggesting that these channels do not participate in astrocyte NO production caused by prenatal LPS exposure.

A cornerstone underlying the opening of Panx1 channels came from their close association with $P2X_7$Rs (Dahl, 2018). Indeed, Panx1 co-immunoprecipitates with $P2X_7$Rs (Pelegrin and Surprenant, 2006; Poornima et al., 2012), and proline 451 in the C-terminal tails of these receptors has been found crucial in this interaction (Iglesias et al., 2008; Sorge et al., 2012). In this context, our experiments showed that activation of $P2X_7$Rs and opening of astrocytic Panx1 channels are part of the mechanism involved in the prenatal LPS-induced release of ATP on offspring hippocampus. In concordance with these findings, previous studies have described that ATP triggers its own release via $P2X_7$Rs and further activation of Panx1 channels (Iglesias et al., 2009; Garre et al., 2016). The fact that Panx1 channels contribute to the prenatal LPS-induced Etd uptake and release of ATP but not glutamate is puzzling. One possibility is that despite that both channels may be permeable to Etd, they differ in their contribution to the release of ATP and glutamate in our system. Although this seems paradoxical, recent studies have demonstrated that hemichannels and pannexons do not act as freely permeable non-selective pores, but they select permeants in an isoform-specific form (Hansen et al., 2014a,b; Nielsen et al., 2017). Thus, fluorescent dye uptake cannot be employed as an indicator of

permeability to ions or small biologically relevant molecules. Alternatively, other explanation to these findings may imply that another cell type, expressing functional Panx1 channels may be responsible for the Panx1-dependent release of ATP and Etd uptake found in astrocytes in the hippocampus. Regardless of its source, we can speculate that ATP may activate distant astrocytes and/or neurons in a paracrine manner, triggering Ca^{2+} responses that could rely on the reactive profile of astrocytes (Butt, 2011). If so, the stimulation of purinergic receptors could be shut down by diffusion of ATP to distant areas as well as by desensitization of P2Y receptors and degradation of extracellular ATP by exonucleases. Simultaneously, a negative feedback loop is the counteracting effect that could be evoked by ATP on Panx1 channels (Qiu and Dahl, 2009).

How does Cx43 hemichannel opening affect Ca^{2+} signaling? Hemichannels are permeable to Ca^{2+} (De Bock et al., 2012; Fiori et al., 2012). In this scenario, alterations on $[Ca^{2+}]_i$ handling linked to astrocyte hemichannel opening could be pivotal in the potential vicious cycle underpinning astrocyte dysfunction in the prenatally LPS-exposed offspring. Supporting this idea, we found that prenatal LPS exposure increased the basal $[Ca^{2+}]_i$ and the number and amplitude of spontaneous oscillations by astrocytes on offspring hippocampus. Notably, the increase of spontaneous astroglial $[Ca^{2+}]_i$ oscillations and their amplitude was totally blunted by BAPTA-AM but not by gap19, Tat-L2, ^{10}panx1, probenecid, MTEP or SIB-1757. Moreover, the increase in basal $[Ca^{2+}]_i$ evoked by prenatal LPS exposure was dependent on the microglia-mediated opening of Cx43 hemichannels and subsequent stimulation of $mGluR_5$, but not activation of Panx1 channels. Collectively, these data suggest that spontaneous $[Ca^{2+}]_i$ oscillations evoked by prenatal LPS exposure are necessary for the opening of astroglialCx43 hemichannels, which result in the release of glutamate and the subsequent downstream increase of basal $[Ca^{2+}]_i$ via intracellular stores (**Figure 9**). Consistent with this, selective blockade of PLC or IP_3 receptors, as well as chelation of $[Ca^{2+}]_i$, strongly blunted the increase in basal astroglial $[Ca^{2+}]_i$ triggered by prenatal LPS exposure. Furthermore, prenatal LPS exposure enhanced the release of glutamate on offspring hippocampus, a response completely dependent on the opening of Cx43 hemichannels but not Panx1 channels. These data concord with previous studies showing the release of glutamate via activation of Cx43 hemichannels (Ye et al., 2003) and with the fact that $mGluR_5$ controls $[Ca^{2+}]_i$ responses in astrocytes (Panatier and Robitaille, 2016). Previous studies have described that opening of Cx43 hemichannels is regulated by $[Ca^{2+}]_i$ (De Bock et al., 2012; Meunier et al., 2017). In this line, we noted that chelation of $[Ca^{2+}]_i$ reduced the prenatal LPS-induced Etd uptake by astrocytes on offspring hippocampus, whereas inhibition of $mGluR_5$, PLC or IP_3 receptor did not affect this response.

In the inflamed brain, among other disturbances, astrocytes and neurons undergo the remodeling of their dendritic arbor as well as several morphological changes (Luo and O'Leary, 2005; Pekny and Pekna, 2014; Riccomagno and Kolodkin, 2015). In this work, we detected for the first time that prenatal LPS exposure augments the complexity of astrocyte branch arbors on offspring hippocampus, whereas in neurons occurred the opposite. This evidence harmonizes with studies reporting that neuropathological conditions augment the arborization of hippocampal astrocytes (Beauquis et al., 2013; Chun et al., 2018) and induce dendritic retraction of CA1 pyramidal neurons (Christian et al., 2011; Burak et al., 2018). Usually, the reduction in neurite arborization lined to the loss of branching and a decline in total neurite lengths is accompanied by a decrease in synaptic number and retraction of dendritic spines (Luo and O'Leary, 2005; Rossi and Volterra, 2009). In this context, our experiments revealed that dendritic retraction of CA1 pyramidal neurons triggered by prenatal LPS occurred in parallel with a reduction in the number of apical but not basal dendritic spines in these neurons. It is not clear why the dendritic spine density of basal dendrites is not altered by prenatal LPS exposure. However, this evidence are supported by prior studies describing the layer-specific spine density of CA1 pyramidal neurons (Spruston, 2008) and the opposite regulation of this feature between apical and basal dendrites during different pathological conditions (Hyer and Glasper, 2017; Maynard et al., 2017).

Remarkably, the prenatal LPS-induced alterations on arborization and morphology of astrocytes and neurons were dramatically counteracted with the administration of a specific blocker of Cx43 hemichannels that crosses the BBB. Thus, prenatal LPS exposure elicits divergent morphological effects on offspring astrocytes and neurons that likely reflect their inflammatory status, a phenomenon in which the opening of Cx43 hemichannels seems to be crucial. Substantial levels of glutamate at the synaptic cleft could be neurotoxic under pathological conditions (Lau and Tymianski, 2010). In this context, recent evidence indicates that glutamate released by a mechanism implicating the opening of astroglial Cx43 hemichannels could reduce neuronal survival (Orellana et al., 2011; Yi et al., 2016). Here, we observed that selective inhibition of Cx43 hemichannels greatly prevents the prenatal LPS-induced death of CA1 pyramidal neurons on offspring hippocampus. The latter suggests that Cx43 hemichannels likely contribute to neuronal damage either by altering astrocyte functions (e.g., $[Ca^{2+}]_i$ handling) and/or through the release of excitotoxic amounts of glutamate. Supporting this idea, the prenatal LPS-induced overexpression of GFAP, $[Ca^{2+}]_i$ increase and release of glutamate was strongly blunted by blocking Cx43 hemichannels. Excitotoxic levels of glutamate along with a dysfunctional astroglial partnership plausibly could cause neuronal damage via osmotic and $[Ca^{2+}]_i$ imbalance, as well as caspase activation (Orellana et al., 2011; Moidunny et al., 2016) (**Figure 9**).

Our findings suggest that opening of astrocyte Cx43 hemichannels occurs at early phases of postnatal life in prenatally LPS-exposed offspring and is accompanied by hippocampal neuroinflammation, as well as diverse astrocyte and neuronal alterations in function and morphology. Future studies are needed in order to elucidate whether astroglial hemichannel/pannexon opening evoked by prenatal LPS exposure may also take place at fetal stages. We speculate that excitotoxic levels of glutamate triggered by the activation of Cx43 hemichannels may contribute to the hippocampal neurotoxicity and damage in prenatally LPS-exposed offspring. Therefore, the

understanding of how astrocyte-neuron crosstalk is affected in prenatally LPS-exposed offspring is a promising avenue toward the development of common therapies for several neurological disorders observed in children born to women who had a severe infection during pregnancy.

DATA AVAILABILITY STATEMENT

The datasets generated for this study are available on request to the corresponding author.

ETHICS STATEMENT

This study was carried out in accordance with the recommendations of "Protocolo de Cuidado y Uso Animal del Comité Ético Cienífico para el Cuidado de Animales y Ambiente." The protocol was approved by the "Comité Ético Científico para el Cuidado de Animales y Ambiente" of the Ponificia Universidad Católica de Chile.

AUTHOR CONTRIBUTIONS

CC, JEO, BA, LM, CI, TA, and JAO conceived, performed, and analyzed the experiments. JAO wrote and edited the manuscript. All authors read and approved the final manuscript.

FUNDING

This work was supported by (i) the Comisión Nacional de Investigación Científica y Tecnológica (CONICYT) and Fondo Nacional de Desarrollo Científico y Tecnológico (FONDECYT) Grant 1160710 (to JAO) and (ii) the CONICYT and Programa de Investigación Asociativa (PIA) Grant Anillo de Ciencia y Tecnología ACT1411 (to JAO).

ACKNOWLEDGMENTS

CONICYT, PIA, FONDECYT, and Pontificia Universidad Católica de Chile.

SUPPLEMENTARY MATERIAL

The Supplementary Material for this article can be found online at: https://www.frontiersin.org/articles/10.3389/fncel.2019.00460/full#supplementary-material

FIGURE S1 | Neurons do not contribute to the prenatal LPS-induced changes in astroglial function observed in the offspring hippocampus. **(A)** Averaged of DAF-FM signal fluorescence by astrocytes in acute slices from control offspring (white bar) or prenatally LPS-exposed offspring of 4 months old alone (black bars) or in combination with 0.5 μM TTX and the following pharmacological agents: 100 μM gap19, 100 μM ^{10}panx1 and 1 μM L-N6. *$p < 0.0001$ versus LPS, one-way ANOVA Tukey's *post hoc* test, mean ± S.E.M., $n = 3$. **(B)** Averaged of basal Fluo-4 signal fluorescence by hippocampal astrocytes in acute slices from control offspring (white bar) or prenatally LPS-exposed offspring of 4 months old alone (black bars) or in combination with 0.5 μM TTX and the following pharmacological agents: 50 nM minocycline, 100 μM gap19, 100 μM Tat-L2, 100 μM ^{10}panx1, 500 μM Probenecid (Prob), 10 μM Bapta-AM, 5 μM U-73122, 50 μM 2-APB, 50 nM MTEP, 5 μM SIB-1757, 200 μM oATP, and 200 nM A740003. **$p < 0.0001$, *$p < 0.005$ versus LPS, one-way ANOVA Tukey's *post hoc* test, mean ± S.E.M., $n = 3$. **(C)** Averaged data of glutamate release by acute hippocampal slices from control offspring (white bar) or prenatally LPS-exposed offspring of 4 months old alone (black bars) or in combination with 0.5 μM TTX and the following blockers: 100 μM gap19, 100 μM Tat-L2, 100 μM ^{10}panx1, 500 μM Probenecid (Prob). *$p < 0.0001$ versus LPS, one-way ANOVA Tukey's *post hoc* test, mean ± S.E.M., $n = 3$. **(D)** Averaged of spontaneous $[Ca^{2+}]_i$ oscillations by hippocampal astrocytes in acute slices from control offspring (white bar) or prenatally LPS-exposed offspring of 4 months old alone (black bars) or in combination with 0.5 μM TTX and the following pharmacological agents: 100 μM gap19, 100 μM Tat-L2, 100 μM ^{10}panx1, 500 μM Probenecid (Prob), 10 μM Bapta-AM, 50 nM MTEP or 5 μM SIB-1757. **$p < 0.005$ versus LPS, one-way ANOVA Tukey's *post hoc* test, mean ± S.E.M., $n = 3$. **(E)** Averaged of peak amplitude of spontaneous $[Ca^{2+}]_i$ oscillations by hippocampal astrocytes in acute slices from control offspring (white bar) or prenatally LPS-exposed offspring of 4 months old alone (black bars) or in combination with 0.5 μM TTX and the following pharmacological agents: 100 μM gap19, 100 μM Tat-L2, 100 μM ^{10}panx1, 500 μM Probenecid (Prob), 10 μM Bapta-AM, 50 nM MTEP or 5 μM SIB-1757. **$p < 0.005$ versus LPS, one-way ANOVA Tukey's *post hoc* test, mean ± S.E.M., $n = 3$.

FIGURE S2 | Prenatal LPS exposure does not affect total level and distribution of Cx43 in astrocytes. **(A,B)** Representative confocal images depicting GFAP (green) and Cx43 (red) staining by astrocytes in acute slices from control offspring **(A)** or prenatally LPS-exposed offspring of 4-month old **(B)**. **(C–F)** Insets of astrocytes and examples of draws for staining analysis were taken from the area depicted within the white squares in **(A,B)**. Calibration bars: white = 120 μm; yellow = 20 μm. **(G)** Quantification of membrane, intracellular and total staining of Cx43 by astrocytes in acute slices from control offspring (white bars) or prenatally LPS-exposed offspring of 4 months old (black bars). Data were obtained from at least three independent experiments with three or more repeats each one (≥20 cells analyzed for each repeat).

REFERENCES

Abudara, V., Bechberger, J., Freitas-Andrade, M., De Bock, M., Wang, N., Bultynck, G., et al. (2014). The connexin43 mimetic peptide Gap19 inhibits hemichannels without altering gap junctional communication in astrocytes. *Front. Cell. Neurosci.* 8:306. doi: 10.3389/fncel.2014.00306

Abudara, V., Retamal, M. A., Del Rio, R., and Orellana, J. A. (2018). Synaptic functions of hemichannels and pannexons: a double-edged sword. *Front. Mol. Neurosci.* 11:435. doi: 10.3389/fnmol.2018.00435

Abudara, V., Roux, L., Dallerac, G., Matias, I., Dulong, J., Mothet, J. P., et al. (2015). Activated microglia impairs neuroglial interaction by opening Cx43 hemichannels in hippocampal astrocytes. *Glia* 63, 795–811. doi: 10.1002/glia.22785

Agulhon, C., Sun, M. Y., Murphy, T., Myers, T., Lauderdale, K., and Fiacco, T. A. (2012). Calcium signaling and gliotransmission in normal vs. reactive astrocytes. *Front. Pharmacol.* 3:139. doi: 10.3389/fphar.2012.00139

Ardiles, A. O., Flores-Munoz, C., Toro-Ayala, G., Cardenas, A. M., Palacios, A. G., Munoz, P., et al. (2014). Pannexin 1 regulates bidirectional hippocampal synaptic plasticity in adult mice. *Front. Cell. Neurosci.* 8:326. doi: 10.3389/fncel.2014.00326

Avendano, B. C., Montero, T. D., Chavez, C. E., Von Bernhardi, R., and Orellana, J. A. (2015). Prenatal exposure to inflammatory conditions increases Cx43 and Panx1 unopposed channel opening and activation of astrocytes in the offspring effect on neuronal survival. *Glia* 63, 2058–2072. doi: 10.1002/glia.22877

Beauquis, J., Pavia, P., Pomilio, C., Vinuesa, A., Podlutskaya, N., Galvan, V., et al. (2013). Environmental enrichment prevents astroglial pathological changes in

the hippocampus of APP transgenic mice, model of Alzheimer's disease. *Exp. Neurol.* 239, 28–37. doi: 10.1016/j.expneurol.2012.09.009

Bergdolt, L., and Dunaevsky, A. (2018). Brain changes in a maternal immune activation model of neurodevelopmental brain disorders. *Prog. Neurobiol.* 175, 1–19. doi: 10.1016/j.pneurobio.2018.12.002

Boksa, P. (2010). Effects of prenatal infection on brain development and behavior: a review of findings from animal models. *Brain Behav. Immun.* 24, 881–897. doi: 10.1016/j.bbi.2010.03.005

Bradley, S. J., and Challiss, R. A. (2012). G protein-coupled receptor signalling in astrocytes in health and disease: a focus on metabotropic glutamate receptors. *Biochem. Pharmacol.* 84, 249–259. doi: 10.1016/j.bcp.2012.04.009

Burak, K., Lamoureux, L., Boese, A., Majer, A., Saba, R., Niu, Y., et al. (2018). MicroRNA-16 targets mRNA involved in neurite extension and branching in hippocampal neurons during presymptomatic prion disease. *Neurobiol. Dis.* 112, 1–13. doi: 10.1016/j.nbd.2017.12.011

Butt, A. M. (2011). ATP: a ubiquitous gliotransmitter integrating neuron-glial networks. *Semin. Cell Dev. Biol.* 22, 205–213. doi: 10.1016/j.semcdb.2011.02.023

Carrigan, C. N., and Imperiali, B. (2005). The engineering of membrane-permeable peptides. *Anal. Biochem.* 341, 290–298. doi: 10.1016/j.ab.2005.03.026

Chen, B., Yang, L., Chen, J., Chen, Y., Zhang, L., Wang, L., et al. (2019). Inhibition of Connexin43 hemichannels with Gap19 protects cerebral ischemia/reperfusion injury via the JAK2/STAT3 pathway in mice. *Brain Res. Bull.* 146, 124–135. doi: 10.1016/j.brainresbull.2018.12.009

Chever, O., Lee, C. Y., and Rouach, N. (2014). Astroglial connexin43 hemichannels tune basal excitatory synaptic transmission. *J. Neurosci.* 34, 11228–11232. doi: 10.1523/JNEUROSCI.0015-14.2014

Cho, J. W., Jung, S. Y., Kim, D. Y., Chung, Y. R., Choi, H. H., Jeon, J. W., et al. (2018). PI3K-Akt-Wnt pathway is implicated in exercise-induced improvement of short-term memory in cerebral palsy rats. *Int. Neurourol. J.* 22, S156–S164. doi: 10.5213/inj.1836224.112

Christian, K. M., Miracle, A. D., Wellman, C. L., and Nakazawa, K. (2011). Chronic stress-induced hippocampal dendritic retraction requires CA3 NMDA receptors. *Neuroscience* 174, 26–36. doi: 10.1016/j.neuroscience.2010.11.033

Chun, H., An, H., Lim, J., Woo, J., Lee, J., Ryu, H., et al. (2018). Astrocytic proBDNF and tonic GABA distinguish active versus reactive astrocytes in hippocampus. *Exp. Neurobiol.* 27, 155–170. doi: 10.5607/en.2018.27.3.155

Contreras, J. E., Sánchez, H. A., Eugenin, E. A., Speidel, D., Theis, M., Willecke, K., et al. (2002). Metabolic inhibition induces opening of unapposed connexin 43 gap junction hemichannels and reduces gap junctional communication in cortical astrocytes in culture. *Proc. Natl. Acad. Sci. U.S.A.* 99, 495–500. doi: 10.1073/pnas.012589799

Crespo Yanguas, S., Da Silva, T. C., Pereira, I. V. A., Willebrords, J., Maes, M., Sayuri Nogueira, M., et al. (2018). TAT-Gap19 and carbenoxolone alleviate liver fibrosis in mice. *Int. J. Mol. Sci.* 19:E817. doi: 10.3390/ijms19030817

Dahl, G. (2018). The Pannexin1 membrane channel: distinct conformations and functions. *FEBS Lett.* 592, 3201–3209. doi: 10.1002/1873-3468.13115

De Bock, M., Wang, N., Bol, M., Decrock, E., Ponsaerts, R., Bultynck, G., et al. (2012). Connexin 43 hemichannels contribute to cytoplasmic Ca2+ oscillations by providing a bimodal Ca2+-dependent Ca2+ entry pathway. *J. Biol. Chem.* 287, 12250–12266. doi: 10.1074/jbc.M111.299610

Escobar, M., Crouzin, N., Cavalier, M., Quentin, J., Roussel, J., Lante, F., et al. (2011). Early, time-dependent disturbances of hippocampal synaptic transmission and plasticity after in utero immune challenge. *Biol. Psychiatry* 70, 992–999. doi: 10.1016/j.biopsych.2011.01.009

Faa, G., Manchia, M., Pintus, R., Gerosa, C., Marcialis, M. A., and Fanos, V. (2016). Fetal programming of neuropsychiatric disorders. *Birth Defects Res. C Embryo Today* 108, 207–223. doi: 10.1002/bdrc.21139

Fernandez de Cossio, L., Guzman, A., Van Der Veldt, S., and Luheshi, G. N. (2017). Prenatal infection leads to ASD-like behavior and altered synaptic pruning in the mouse offspring. *Brain Behav. Immun.* 63, 88–98. doi: 10.1016/j.bbi.2016.09.028

Fiori, M. C., Figueroa, V., Zoghbi, M. E., Saez, J. C., Reuss, L., and Altenberg, G. A. (2012). Permeation of calcium through purified connexin 26 hemichannels. *J. Biol. Chem.* 287, 40826–40834. doi: 10.1074/jbc.M112.383281

Garre, J. M., Yang, G., Bukauskas, F. F., and Bennett, M. V. (2016). FGF-1 triggers pannexin-1 hemichannel opening in spinal astrocytes of rodents and promotes inflammatory responses in acute spinal cord slices. *J. Neurosci.* 36, 4785–4801. doi: 10.1523/JNEUROSCI.4195-15.2016

Golan, H. M., Lev, V., Hallak, M., Sorokin, Y., and Huleihel, M. (2005). Specific neurodevelopmental damage in mice offspring following maternal inflammation during pregnancy. *Neuropharmacology* 48, 903–917. doi: 10.1016/j.neuropharm.2004.12.023

Gomez, G. I., Falcon, R. V., Maturana, C. J., Labra, V. C., Salgado, N., Rojas, C. A., et al. (2018). Heavy alcohol exposure activates astroglial hemichannels and pannexons in the hippocampus of adolescent rats: effects on neuroinflammation and astrocyte arborization. *Front. Cell. Neurosci.* 12:472. doi: 10.3389/fncel.2018.00472

Gumusoglu, S. B., and Stevens, H. E. (2019). Maternal inflammation and neurodevelopmental programming: a review of preclinical outcomes and implications for translational psychiatry. *Biol. Psychiatry* 85, 107–121. doi: 10.1016/j.biopsych.2018.08.008

Hansen, D. B., Braunstein, T. H., Nielsen, M. S., and Macaulay, N. (2014a). Distinct permeation profiles of the connexin 30 and 43 hemichannels. *FEBS Lett.* 588, 1446–1457. doi: 10.1016/j.febslet.2014.01.036

Hansen, D. B., Ye, Z. C., Calloe, K., Braunstein, T. H., Hofgaard, J. P., Ransom, B. R., et al. (2014b). Activation, permeability, and inhibition of astrocytic and neuronal large pore (hemi)channels. *J. Biol. Chem.* 289, 26058–26073. doi: 10.1074/jbc.M114.582155

Hao, L. Y., Hao, X. Q., Li, S. H., and Li, X. H. (2010). Prenatal exposure to lipopolysaccharide results in cognitive deficits in age-increasing offspring rats. *Neuroscience* 166, 763–770. doi: 10.1016/j.neuroscience.2010.01.006

Hyer, M. M., and Glasper, E. R. (2017). Separation increases passive stress-coping behaviors during forced swim and alters hippocampal dendritic morphology in California mice. *PLoS One* 12:e0175713. doi: 10.1371/journal.pone.0175713

Iglesias, R., Dahl, G., Qiu, F., Spray, D. C., and Scemes, E. (2009). Pannexin 1: the molecular substrate of astrocyte "hemichannels". *J. Neurosci.* 29, 7092–7097. doi: 10.1523/JNEUROSCI.6062-08.2009

Iglesias, R., Locovei, S., Roque, A., Alberto, A. P., Dahl, G., Spray, D. C., et al. (2008). P2X7 receptor-Pannexin1 complex: pharmacology and signaling. *Am. J. Physiol. Cell Physiol.* 295, C752–C760. doi: 10.1152/ajpcell.00228.2008

Iyyathurai, J., D'hondt, C., Wang, N., De Bock, M., Himpens, B., Retamal, M. A., et al. (2013). Peptides and peptide-derived molecules targeting the intracellular domains of Cx43: gap junctions versus hemichannels. *Neuropharmacology* 75, 491–505. doi: 10.1016/j.neuropharm.2013.04.050

Johnson, R. G., Le, H. C., Evenson, K., Loberg, S. W., Myslajek, T. M., Prabhu, A., et al. (2016). Connexin hemichannels: methods for dye uptake and leakage. *J. Membr. Biol.* 249, 713–741. doi: 10.1007/s00232-016-9925-y

Karpuk, N., Burkovetskaya, M., Fritz, T., Angle, A., and Kielian, T. (2011). Neuroinflammation leads to region-dependent alterations in astrocyte gap junction communication and hemichannel activity. *J. Neurosci.* 31, 414–425. doi: 10.1523/JNEUROSCI.5247-10.2011

Kelley, M. H., Wu, W. W., Lei, J., Mclane, M., Xie, H., Hart, K. D., et al. (2017). Functional changes in hippocampal synaptic signaling in offspring survivors of a mouse model of intrauterine inflammation. *J. Neuroinflammation* 14:180. doi: 10.1186/s12974-017-0951-1

Kettenmann, H., Hanisch, U. K., Noda, M., and Verkhratsky, A. (2011). Physiology of microglia. *Physiol. Rev.* 91, 461–553. doi: 10.1152/physrev.00011.2010

Kim, H. S., and Suh, Y. H. (2009). Minocycline and neurodegenerative diseases. *Behav. Brain Res.* 196, 168–179. doi: 10.1016/j.bbr.2008.09.040

Lau, A., and Tymianski, M. (2010). Glutamate receptors, neurotoxicity and neurodegeneration. *Pflugers Arch.* 460, 525–542. doi: 10.1007/s00424-010-0809-1

Leybaert, L., Lampe, P. D., Dhein, S., Kwak, B. R., Ferdinandy, P., Beyer, E. C., et al. (2017). Connexins in cardiovascular and neurovascular health and disease: pharmacological implications. *Pharmacol. Rev.* 69, 396–478. doi: 10.1124/pr.115.012062

Ling, Z., Gayle, D. A., Ma, S. Y., Lipton, J. W., Tong, C. W., Hong, J. S., et al. (2002). In utero bacterial endotoxin exposure causes loss of tyrosine hydroxylase neurons in the postnatal rat midbrain. *Mov. Disord.* 17, 116–124. doi: 10.1002/mds.10078

Luo, L., and O'Leary, D. D. (2005). Axon retraction and degeneration in development and disease. *Annu. Rev. Neurosci.* 28, 127–156. doi: 10.1146/annurev.neuro.28.061604.135632

Maatouk, L., Yi, C., Carrillo-De Sauvage, M. A., Compagnion, A. C., Hunot, S., Ezan, P., et al. (2019). Glucocorticoid receptor in astrocytes regulates midbrain dopamine neurodegeneration through connexin hemichannel activity. *Cell Death Differ* 26, 580–596. doi: 10.1038/s41418-018-0150-3

Makinson, R., Lloyd, K., Rayasam, A., Mckee, S., Brown, A., Barila, G., et al. (2017). Intrauterine inflammation induces sex-specific effects on neuroinflammation, white matter, and behavior. *Brain Behav. Immun.* 66, 277–288. doi: 10.1016/j.bbi.2017.07.016

Maynard, K. R., Hobbs, J. W., Sukumar, M., Kardian, A. S., Jimenez, D. V., Schloesser, R. J., et al. (2017). Bdnf mRNA splice variants differentially impact CA1 and CA3 dendrite complexity and spine morphology in the hippocampus. *Brain Struct. Funct.* 222, 3295–3307. doi: 10.1007/s00429-017-1405-3

Meunier, C., Wang, N., Yi, C., Dallerac, G., Ezan, P., Koulakoff, A., et al. (2017). Contribution of astroglial Cx43 hemichannels to the modulation of glutamatergic currents by D-serine in the mouse prefrontal cortex. *J. Neurosci.* 37, 9064–9075. doi: 10.1523/JNEUROSCI.2204-16.2017

Moidunny, S., Matos, M., Wesseling, E., Banerjee, S., Volsky, D. J., Cunha, R. A., et al. (2016). Oncostatin M promotes excitotoxicity by inhibiting glutamate uptake in astrocytes: implications in HIV-associated neurotoxicity. *J. Neuroinflammation* 13:144. doi: 10.1186/s12974-016-0613-8

Myatt, D. R., Hadlington, T., Ascoli, G. A., and Nasuto, S. J. (2012). Neuromantic - from semi-manual to semi-automatic reconstruction of neuron morphology. *Front. Neuroinform.* 6:4. doi: 10.3389/fninf.2012.00004

Nielsen, B. S., Alstrom, J. S., Nicholson, B. J., Nielsen, M. S., and Macaulay, N. (2017). Permeant-specific gating of connexin 30 hemichannels. *J. Biol. Chem.* 292, 19999–20009. doi: 10.1074/jbc.M117.805986

Orellana, J. A., Froger, N., Ezan, P., Jiang, J. X., Bennett, M. V., Naus, C. C., et al. (2011). ATP and glutamate released via astroglial connexin 43 hemichannels mediate neuronal death through activation of pannexin 1 hemichannels. *J. Neurochem.* 118, 826–840. doi: 10.1111/j.1471-4159.2011.07210.x

Orellana, J. A., Montero, T. D., and Von Bernhardi, R. (2013). Astrocytes inhibit nitric oxide-dependent Ca(2+) dynamics in activated microglia: involvement of ATP released via pannexin 1 channels. *Glia* 61, 2023–2037. doi: 10.1002/glia.22573

Orellana, J. A., Retamal, M. A., Moraga-Amaro, R., and Stehberg, J. (2016). Role of astroglial hemichannels and pannexons in memory and neurodegenerative diseases. *Front. Integr. Neurosci.* 10:26. doi: 10.3389/fnint.2016.00026

Panatier, A., and Robitaille, R. (2016). Astrocytic mGluR5 and the tripartite synapse. *Neuroscience* 323, 29–34. doi: 10.1016/j.neuroscience.2015.03.063

Pekny, M., and Pekna, M. (2014). Astrocyte reactivity and reactive astrogliosis: costs and benefits. *Physiol. Rev.* 94, 1077–1098. doi: 10.1152/physrev.00041.2013

Pelegrin, P., and Surprenant, A. (2006). Pannexin-1 mediates large pore formation and interleukin-1beta release by the ATP-gated P2X7 receptor. *EMBO J.* 25, 5071–5082. doi: 10.1038/sj.emboj.7601378

Perea, G., Navarrete, M., and Araque, A. (2009). Tripartite synapses: astrocytes process and control synaptic information. *Trends Neurosci.* 32, 421–431. doi: 10.1016/j.tins.2009.05.001

Poornima, V., Madhupriya, M., Kootar, S., Sujatha, G., Kumar, A., and Bera, A. K. (2012). P2X7 receptor-pannexin 1 hemichannel association: effect of extracellular calcium on membrane permeabilization. *J. Mol. Neurosci.* 46, 585–594. doi: 10.1007/s12031-011-9646-8

Qiu, F., and Dahl, G. (2009). A permeant regulating its permeation pore: inhibition of pannexin 1 channels by ATP. *Am. J. Physiol. Cell Physiol.* 296, C250–C255. doi: 10.1152/ajpcell.00433.2008

Retamal, M. A., Cortes, C. J., Reuss, L., Bennett, M. V., and Saez, J. C. (2006). S-nitrosylation and permeation through connexin 43 hemichannels in astrocytes: induction by oxidant stress and reversal by reducing agents. *Proc. Natl. Acad. Sci. U.S.A.* 103, 4475–4480. doi: 10.1073/pnas.0511118103

Retamal, M. A., Froger, N., Palacios-Prado, N., Ezan, P., Saez, P. J., Saez, J. C., et al. (2007). Cx43 hemichannels and gap junction channels in astrocytes are regulated oppositely by proinflammatory cytokines released from activated microglia. *J. Neurosci.* 27, 13781–13792. doi: 10.1523/jneurosci.2042-07.2007

Riccomagno, M. M., and Kolodkin, A. L. (2015). Sculpting neural circuits by axon and dendrite pruning. *Annu. Rev. Cell Dev. Biol.* 31, 779–805. doi: 10.1146/annurev-cellbio-100913-013038

Rossi, D., and Volterra, A. (2009). Astrocytic dysfunction: insights on the role in neurodegeneration. *Brain Res. Bull.* 80, 224–232. doi: 10.1016/j.brainresbull.2009.07.012

Rousset, C. I., Chalon, S., Cantagrel, S., Bodard, S., Andres, C., Gressens, P., et al. (2006). Maternal exposure to LPS induces hypomyelination in the internal capsule and programmed cell death in the deep gray matter in newborn rats. *Pediatr. Res.* 59, 428–433. doi: 10.1203/01.pdr.0000199905.08848.55

Salameh, A., Blanke, K., and Dhein, S. (2013). Mind the gap! Connexins and pannexins in physiology, pharmacology and disease. *Front. Pharmacol.* 4:144. doi: 10.3389/fphar.2013.00144

Santello, M., Toni, N., and Volterra, A. (2019). Astrocyte function from information processing to cognition and cognitive impairment. *Nat. Neurosci.* 22, 154–166. doi: 10.1038/s41593-018-0325-8

Santiago, M. F., Veliskova, J., Patel, N. K., Lutz, S. E., Caille, D., Charollais, A., et al. (2011). Targeting pannexin1 improves seizure outcome. *PLoS One* 6:e25178. doi: 10.1371/journal.pone.0025178

Schaafsma, W., Basterra, L. B., Jacobs, S., Brouwer, N., Meerlo, P., Schaafsma, A., et al. (2017). Maternal inflammation induces immune activation of fetal microglia and leads to disrupted microglia immune responses, behavior, and learning performance in adulthood. *Neurobiol. Dis.* 106, 291–300. doi: 10.1016/j.nbd.2017.07.017

Schindelin, J., Arganda-Carreras, I., Frise, E., Kaynig, V., Longair, M., Pietzsch, T., et al. (2012). Fiji: an open-source platform for biological-image analysis. *Nat. Methods* 9, 676–682. doi: 10.1038/nmeth.2019

Sholl, D. A. (1953). Dendritic organization in the neurons of the visual and motor cortices of the cat. *J. Anat.* 87, 387–406.

Sorge, R. E., Trang, T., Dorfman, R., Smith, S. B., Beggs, S., Ritchie, J., et al. (2012). Genetically determined P2X7 receptor pore formation regulates variability in chronic pain sensitivity. *Nat. Med.* 18, 595–599. doi: 10.1038/nm.2710

Spruston, N. (2008). Pyramidal neurons: dendritic structure and synaptic integration. *Nat. Rev. Neurosci.* 9, 206–221. doi: 10.1038/nrn2286

Stehberg, J., Moraga-Amaro, R., Salazar, C., Becerra, A., Echeverria, C., Orellana, J. A., et al. (2012). Release of gliotransmitters through astroglial connexin 43 hemichannels is necessary for fear memory consolidation in the basolateral amygdala. *FASEB J.* 26, 3649–3657. doi: 10.1096/fj.11-198416

Tonkin, R. S., Bowles, C., Perera, C. J., Keating, B. A., Makker, P. G. S., Duffy, S. S., et al. (2018). Attenuation of mechanical pain hypersensitivity by treatment with Peptide5, a connexin-43 mimetic peptide, involves inhibition of NLRP3 inflammasome in nerve-injured mice. *Exp. Neurol.* 300, 1–12. doi: 10.1016/j.expneurol.2017.10.016

Walrave, L., Vinken, M., Albertini, G., De Bundel, D., Leybaert, L., and Smolders, I. J. (2016). Inhibition of Connexin43 hemichannels impairs spatial short-term memory without affecting spatial working memory. *Front. Cell. Neurosci.* 10:288. doi: 10.3389/fncel.2016.00288

Wang, N., De Vuyst, E., Ponsaerts, R., Boengler, K., Palacios-Prado, N., Wauman, J., et al. (2013). Selective inhibition of Cx43 hemichannels by Gap19 and its impact on myocardial ischemia/reperfusion injury. *Basic Res. Cardiol.* 108:309. doi: 10.1007/s00395-012-0309-x

Ye, Z. C., Wyeth, M. S., Baltan-Tekkok, S., and Ransom, B. R. (2003). Functional hemichannels in astrocytes: a novel mechanism of glutamate release. *J. Neurosci.* 23, 3588–3596. doi: 10.1523/jneurosci.23-09-03588.2003

Yi, C., Mei, X., Ezan, P., Mato, S., Matias, I., Giaume, C., et al. (2016). Astroglial connexin43 contributes to neuronal suffering in a mouse model of Alzheimer's disease. *Cell Death Differ.* 23, 1691–1701. doi: 10.1038/cdd.2016.63

Zager, A., Peron, J. P., Mennecier, G., Rodrigues, S. C., Aloia, T. P., and Palermo-Neto, J. (2015). Maternal immune activation in late gestation increases neuroinflammation and aggravates experimental autoimmune encephalomyelitis in the offspring. *Brain Behav. Immun.* 43, 159–171. doi: 10.1016/j.bbi.2014.07.021

Conflict of Interest: The authors declare that the research was conducted in the absence of any commercial or financial relationships that could be construed as a potential conflict of interest.

frontiers in Cellular Neuroscience

MINI REVIEW
published: 11 October 2019
doi: 10.3389/fncel.2019.00453

The Role of Neuronal Factors in the Epigenetic Reprogramming of Microglia in the Normal and Diseased Central Nervous System

*Tatyana Veremeyko[1], Amanda W. Y. Yung[1], Marina Dukhinova[1,2], Tatyana Strekalova[3,4,5] and Eugene D. Ponomarev[1,6]**

[1] School of Biomedical Sciences, Faculty of Medicine, The Chinese University of Hong Kong, Shatin, Hong Kong, [2] Synthetic and Systems Biology for Biomedicine, Italian Institute of Technology (IIT), Genoa, Italy, [3] Department of Psychiatry and Neuropsychology, Maastricht University, Maastricht, Netherlands, [4] Institute of General Pathology and Pathophysiology, Moscow, Russia, [5] Laboratory of Psychiatric Neurobiology and Department of Normal Physiology, Institute of Molecular Medicine, Sechenov First Moscow State Medical University, Moscow, Russia, [6] Kunming Institute of Zoology, Chinese University of Hong Kong Joint Laboratory of Bioresources and Molecular Research in Common Diseases, Chinese Academy of Sciences, Kunming, China

OPEN ACCESS

Edited by:
Xuping Li,
Houston Methodist Research Institute, United States

Reviewed by:
Maria Angeles Arevalo,
Spanish National Research Council (CSIC), Spain
Gyun Jee Song,
Catholic Kwandong University, South Korea

***Correspondence:**
Eugene D. Ponomarev
eponomarev@cuhk.edu.hk;
eugpon@gmail.com

Specialty section:
This article was submitted to Non-neuronal Cells, a section of the journal Frontiers in Cellular Neuroscience

Received: *14 June 2019*
Accepted: *23 September 2019*
Published: *11 October 2019*

Citation:
Veremeyko T, Yung AWY, Dukhinova M, Strekalova T and Ponomarev ED (2019) The Role of Neuronal Factors in the Epigenetic Reprogramming of Microglia in the Normal and Diseased Central Nervous System. Front. Cell. Neurosci. 13:453. doi: 10.3389/fncel.2019.00453

Twenty years ago, the scientific community exhibited relatively little interest in the study of microglial cells. However, recent technical and conceptual advances in this field have greatly increased interest in the basic biology of these cells within various neurodegenerative diseases, including multiple sclerosis, Alzheimer's disease, and traumatic brain/spinal cord injuries. The main functions of these cells in the normal central nervous system (CNS) remain poorly understood, despite considerable elucidation of their roles in pathological conditions. Microglia populate the brain before birth and remain in close lifelong contact with CNS-resident cells under the influence of the local microenvironment. Within the CNS parenchyma, microglia actively interact with two main cell types, astrocytes and neurons, which produce many factors that affect microglia phenotypes in the normal CNS and during neuroinflammation. These factors include interleukin (IL)-34, macrophage colony-stimulating factor, transforming growth factor-β, and IL-4, which promote microglial expansion, survival, and differentiation to an anti-inflammatory phenotype in the normal CNS. Under inflammatory conditions, however, astrocytes produce several pro-inflammatory factors that contribute to microglial activation. The interactions of microglia with neurons in the normal and diseased CNS are especially intriguing. Microglia are known to interact actively with neurons by facilitating axonal pruning during development, while neurons provide specific factors that alter microglial phenotypes and functions. This review focuses mainly on the roles of soluble neuronal factors that affect microglial phenotypes and functions and the possible involvement of these factors in the pathology of neurodegenerative diseases.

Keywords: microglia, neurons, neuroinflammation, transcriptional regulation, microRNA

INTRODUCTION

Microglia are central nervous system (CNS)-resident myeloid cells that originate from common erythro-myeloid progenitors (EMPs), which themselves originate from embryonic stem cells (ESCs) in the yolk. Microglia populate the brain during early fetal development (Kierdorf et al., 2013; Ponomarev et al., 2013). Later, microglia harbor the ability to self-renew locally and remain in the CNS microenvironment throughout life, where they comprise 10–15% of all cells in the brain and spinal cord. In this respect, microglia differ from resident macrophages in other tissues, which originate from hematopoietic stem cells (HSCs) (Li and Barres, 2018), although resident myeloid Langerhans cells in several tissues, such as the skin, represent a mixture of cells derived from ESCs and HSCs (Collin and Milne, 2016). Under pathological conditions such as irradiation or inflammation, HSC-derived myeloid cells may also enter the CNS and acquire the characteristics of ESC-derived microglia, thus leading to a mixed population of HSC- and ESC-derived CNS-resident macrophages similar to that of dermal Langerhans cells (Ponomarev et al., 2013).

Currently, we understand that the phenotypes and functions of microglia are influenced strongly by the local CNS microenvironment. Even in a diseased CNS, microglia in unaffected areas exhibit a normal phenotype and are referred to as homeostatic microglia, whereas microglia proximal to the damaged area exhibit a distinct disease-associated phenotype (Dubbelaar et al., 2018). Under normal conditions, homeostatic microglia are maintained at appropriate densities in various regions of the brain, mostly via local self-renewal (Li and Barres, 2018; Hammond et al., 2019). During disease, microglia in damaged areas often exhibit heterogeneous and mixed-activation phenotypes and may play a beneficial or detrimental role, depending on the area, extent, and nature of neuronal damage and the stage of the disease (Li and Barres, 2018; Szepesi et al., 2018; Hammond et al., 2019). Therefore, it is important to understand how the phenotypes and functions of microglia are determined by specific signals from other CNS-resident cells, such as astrocytes and neurons. This review discusses the nature of such signals and mechanisms of adaptation to the local microenvironment.

EPIGENETIC CHANGES MEDIATE ADAPTATION OF THE MICROGLIA TO TISSUE-SPECIFIC MICROENVIRONMENTS

Modern studies have demonstrated that the adaptation of macrophages to local tissue microenvironments is mediated by epigenetic changes in chromatin (i.e., chromatin remodeling). This process enables the binding of several key transcription factors (TFs) that mediate microglial differentiation (Gosselin et al., 2017; Holtman et al., 2017). Like other tissue-resident macrophages, microglia reside in the CNS under the influence of tissue-derived factors that drive the expression of lineage-specific TFs such as PU.1 and CEBPα (Gosselin et al., 2014). Both CEBPα and PU.1 are induced by macrophage colony-stimulating factor-1 (CSF-1) or its analog, interleukin (IL)-34 (Ponomarev et al., 2013), which are produced by astrocytes and neurons (Frei et al., 1992; Mizuno et al., 2011). These factors drive the survival, renewal, and lineage-specific differentiation of microglia (Li and Barres, 2017). In addition to lineage-specific TFs, tissue-specific TFs complement and modulate the functions of core lineage-specific factors (Gosselin et al., 2014; Holtman et al., 2017), including SMAD family TFs driven by transforming growth factor (TGF) β, which is produced by astrocytes and neurons (Dobolyi et al., 2012). We found that mature microglia very strongly express TGFβ1 mRNA (unpublished observation), indicating that self-TGFβ1 could maintain SMAD2/3 expression in an autocrine manner. Several other factors, including but not limited to V-Maf musculoaponeurotic fibrosarcoma oncogene homolog B (MAFB), interferon response factor (IRF)8, Sal-like (SALL)1, and peroxisome proliferator-activated receptor (PPAR)γ, contribute to the transcriptional control of microglia identity in the normal CNS (Gosselin et al., 2014, 2017; Holtman et al., 2017). Under inflammatory conditions, other inducible TFs, such as nuclear factor (NF)κB, NF-of activated T cells (AT), and signal transducer and activator of transcription (STAT)1/3, contribute further to the phenotypes of activated microglia (Holtman et al., 2017). The cooperative binding of various lineage- and tissue-specific TFs, such as PU.1, CEBPα, IRF8, SMAD2/3, and SALL1, induce the modification of chromatin and generation of primed enhancers for gene expression, which is characterized by monomethylated H3K4 (H3K4me1). In the diseased CNS, inflammatory stimuli [e.g., IL-6, tumor necrosis factor (TNF)] induces the binding of additional factors, such as NFκB, NF-AT, and STAT1/3, and the acetylation of H3K27 (H3K27Ac) (Holtman et al., 2017). Thus, the actions of multiple TFs induce epigenetic changes that lead to the remodeling of chromatin and the formation of a specific mature microglial phenotype. The exact mechanism underlying this highly complex process remains elusive.

EPIGENETIC CHANGES IN THE ACTIVATION AND POLARIZATION OF MACROPHAGES AND MICROGLIA

The phenotypes and functions of immune cells such as microglia and macrophages depend on the type of activation. One example is the existence of pro-inflammatory M1-like macrophages, which are activated by interferon (IFN)γ and/or lipopolysaccharide (LPS), and M2-like macrophages, which are activated by IL-4 and/or IL-13 and associated with the resolution of inflammation and repair of damaged tissues (Sica and Mantovani, 2012; Ley, 2017). The phenotypes of M1 and M2 macrophages are plastic, and the existing model of the activation and polarization spectrum oversimplifies the M1–M2 phenotypic dichotomy, especially *in vivo* (Martinez and Gordon, 2014; Ransohoff, 2016). Nevertheless, *in vitro* studies have clearly delineated a distinct pattern of specific TF expression in M1 macrophages, which is characterized by STAT1, STAT2,

IRF4, and NFκB. In contrast, the M2 macrophage phenotype is mediated by STAT6, GATA3, and PPARγ (Lawrence and Natoli, 2011; Cherry et al., 2014; Li et al., 2018). Regarding specific markers, M1 macrophages express nitric oxide (NO) produced by the enzyme NOS2, high levels of major histocompatibility (MHC) class II and CD86 receptors, and the cytokines TNF and IL-6. In contrast, M2 macrophages express arginase (Arg1), extracellular matrix-binding lectin (Ym1/Chi3l3), and the chemokine CCL22, a heparin-binding protein (Lawrence and Natoli, 2011; Krzyszczyk et al., 2018).

Histone methylation and acetylation are associated with both the M1 and M2 states of activated macrophages and microglia (Cheray and Joseph, 2018; Groot and de Pienta, 2018). The methylation of H4R3 has been shown to positively regulate M2 by inducing the expression of the M2-associated TF PPARγ in mouse peritoneal macrophages (PMs) activated with IL-4 (Tikhanovich et al., 2017). H3K4 methylation also positively regulates M2 polarization in human macrophages activated with M-CSF and IL-4 (Kittan et al., 2013). The enzyme JMJD3, known also as H3K27 demethylase, has been shown to be critical to the upregulation of IRF4 and Arg1 in mouse bone marrow-derived macrophages (BMDMs) stimulated with IL-4 (Satoh et al., 2010). The expression of JMJD3 is also upregulated in IL-4-treated mouse microglia, leading to H3K27 demethylation (Tang et al., 2014). Moreover, the acetylation of H3K9 and H3K14 in the *Tnf, Il6*, *Nos2*, and *H2Ab* (MHC class II) promoter regions is a critical inducer of the expression of these M1-associated molecules in LPS-stimulated mouse microglia (Chauhan et al., 2015).

Similar to other tissues, the CNS produces IL-4 via neurons and possibly astrocytes. This cytokine contributes to the expression of M2-like markers and may also induce the expression of the M2-associated TF PPARγ in mature microglia (Veremeyko et al., 2015, 2018b; Zhao et al., 2015). We found that normal microglia express Ym1 in a CNS-derived IL-4-dependent manner (Ponomarev et al., 2007). More recent studies based on single-cell RNA sequencing demonstrated that mouse microglia express *Arg1*, especially during the embryonic and early postnatal stages (Hammond et al., 2019). However, the initial concept of microglial polarization was criticized recently, as microglia were shown to express M1 and M2 markers simultaneously at the single-cell level (Ransohoff, 2016). We found this unsurprising, as we discovered long ago that microglia exhibited dual activation and an M1/M2 mixed phenotype in the context of experimental autoimmune encephalitis (Ponomarev et al., 2007). We believe that criticism of the concept of microglial polarization was mainly due to the misconception that microglia must exist in one of two mutually exclusive states (M1 or M2). More recent studies of macrophages and microglia demonstrated that these activation states are impermanent and somewhat dynamic. We also demonstrated that IL-4-activated macrophages exhibit a high level of plasticity, and that this is due to a high level of Egr2, which enables the cells to react to other activation stimuli (Veremeyko et al., 2015). Interestingly, mouse and human microglia express multiple early response genes, including Egr2, even at a single-cell level, which suggests a high level of cellular plasticity (Masuda et al., 2019). Importantly, therefore, microglia are exposed to a milieu of different cytokines (e.g., IL-4, TNF) during inflammation, and the state of activation represents a dynamic superposition of different activation pathways, rather than the mutual exclusion of the M1 and M2 states.

ROLE OF MICRORNA IN MICROGLIAL PHENOTYPES AND FUNCTIONS

In addition to histone methylation and acetylation, other epigenetic mechanisms regulate gene expression in microglia. One well-known mechanism involves the suppressive actions of regulatory microRNAs (miRNAs) against gene expression. MiRNAs are short (22–23 nucleotides) non-coding RNAs that bind complementarily to the mRNAs of target genes and either repress the translation or induce the degradation of these mRNAs (Ponomarev et al., 2013). In both cases, translation of the target gene and protein expression are decreased. The roles of miRNAs in microglial functions were reviewed recently (Guo et al., 2019). Moreover, a recent study demonstrated the microglial–neuronal transfer of exosome-associated miRNAs. M1-activated microglia were shown to produce extracellular vesicles containing the microglia-specific miRNA miR-146a-5p, which is not detected in neurons. Upon transfer, this miRNA downregulated the expression of the genes encoding presynaptic synaptotagmin-1 and postsynaptic neuroligin-1 (Prada et al., 2018). In this review, we focus on the roles of two neuronal miRNAs, miR-124 and miR-9, which are transferred from neurons to microglia and/or macrophages. Our screening of microRNAs that are expressed in microglia but not in resident PMs or BMDMs revealed the strong expression of miR-124 in the microglia (Ponomarev et al., 2011). Interestingly, miR-124 is expressed strongly in neurons and is responsible for the differentiation of neuronal progenitor cells (NPCs) into mature neurons (Ponomarev et al., 2013). We determined that miR-124 targeted CEBPα, a critical TF for macrophage and microglial differentiation. CEBPα was expressed in mouse embryonic (until E14) and early postnatal microglia (E15–P14) but not in mature microglia (P60), whereas miR-124 was expressed strongly in mature microglia, but not in embryonic and early postnatal microglia. The transfection of BMDMs with miR-124 decreased the expression of CEBPα and PU.1 and the pro-inflammatory cytokines TNF and IL-6, and increased the expression of the anti-inflammatory factors Arg1, Fizz1, and TGFβ1 (Ponomarev et al., 2011). Indeed, exposure to the pro-inflammatory stimuli TNF and IL-6 increased the expression and DNA binding of CEBPα and PU.1, which in turn increased the induction of downstream gene expression (Crotti et al., 2014). The upregulation of Arg1, Fizz1, and TGFβ1 in macrophages transfected with miR-124 was consistent with the phenotypes of M2-like macrophages activated with IL-4 or IL-13 (Ponomarev et al., 2011). Indeed, we found that IL-4 or IL-13 induced the expression of longer pre-miR-124 transcripts in BMDMs and lung resident macrophages in a STAT6-dependent manner, whereas this process was not observed in mature microglia from a normal CNS (Veremeyko et al., 2013). Therefore, the microglial expression of neuronal miR-124 was upregulated via mechanisms other than the intrinsic transcription of longer miR-124 precursors and subsequent

processing and maturation into functional miR-124. Further experiments indicated the horizontal transfer of miR-124 and miR-9 from neurons to microglia (Veremeyko et al., 2018a). Similar to miR-124, miR-9 is expressed strongly in neurons. This miRNA deactivates macrophages and microglia by targeting NFκB, the expression of which is induced in microglia by inflammatory stimuli (Veremeyko et al., 2018a). Therefore, both miR-124 and miR-9 promote an anti-inflammatory phenotype in the normal CNS. These findings also indicate that normal neurons send continuous signals to microglia to maintain the latter cells in a quiescent state.

HORIZONTAL TRANSFER OF MIRNA FROM NEURONS TO MICROGLIA

Our understanding of the induction of miR-124 expression in mature microglia led us to hypothesize that this miRNA is transferred from mature neurons to microglia. Although previous reports described the transfer of miRNA between cell types (Barteneva et al., 2013, 2017), most demonstrated the transfer of miRNAs via exosomes or microparticles (Zhang et al., 2015). We investigated in detail the presence of the neuronally abundant microRNAs, miR-124 and miR-9, in the extracellular space. Notably, both miR-124 and miR-9 were secreted actively by electrically active neurons, which was confirmed by using tetrodotoxin (TTX) to block secretion (Veremeyko et al., 2018a). However, both miRNAs were secreted in various forms, including naked single-strand RNA (ssRNA), naked double-strand RNA (dsRNA), and ssRNA or dsRNA complexed with proteins, and within exosomes. Importantly, some proportion of miR-9 was co-localized with exosomes, whereas miR-124 was not associated with exosomes. Rather, miR-124 formed complexes with high-density lipoproteins (HDLs), which are produced in the CNS by astrocytes. These HDL–miR-124 complexes translocated efficiently into the cytoplasm of microglia and macrophages via scavenger receptors. This finding highlights an important mechanism by which functional neurons send continuous signals to the microglia to provide instruction and maintain a resting (non-activated) phenotype in the normal CNS (Veremeyko et al., 2018a). We propose that neuronal electric and synaptic activity decreases, miR-124 and miR-9 secretions are blocked, and the microglial phenotype shifts from resting to activated during neurodegeneration.

ANALOGOUS REGULATION OF GENE EXPRESSION IN MICROGLIA AND NEURONS

We hypothesized that gene expression is regulated similarly, in neurons and microglia, as both cell types are closely associated with each other and exposed to the same microenvironment. Several findings support our hypothesis. First, we observed that microglia express neuronal miRNAs such as miR-124 and miR-9 (Veremeyko et al., 2018a). Second, microglia produce neuronal trophic factors such as brain-derived neurotrophic factor (BDNF) (Parkhurst et al., 2013). Third, microglia express Egr1, c-Jun, and c-Fos, which are products of neuronal early response genes (Holtman et al., 2017). Fourth, microglia express Sall1, which, together with Egr1, is associated with neuronal maturation and synaptic pruning (Buttgereit et al., 2016). Egr1, c-Jun, and c-Fos are hallmarks of neuronal synaptic activity (Dukhinova et al., 2018), while Egr2 is involved in macrophage activation, polarization, and plasticity (Veremeyko et al., 2015). However, c-Fos forms complexes with c-Jun to form activator protein-1 (AP-1), a very potent TF associated with macrophage activation (Hop et al., 2018). AP-1 induces the expression of pro-inflammatory genes in macrophages and microglia (Matcovitch-Natan et al., 2016; Holtman et al., 2017). Alone, c-Fos suppresses the expression of M1-associated genes such as *Nos2*, *Tnf*, and *Il6* (Okada, 2003; Ray et al., 2006). CEBPβ is another interesting TF that is regulated in macrophages by Egr1–3 and the cAMP pathway (Veremeyko et al., 2015, 2018b). CEBPβ is important for cortical neurogenesis and may thus induce the expression of both myeloid and neuronal genes (Ménard et al., 2002). Sall1 also regulates cortical neurogenesis (Harrison et al., 2012) and serves as a unique marker of microglia. The miRNA miR-124 inactivates the transcriptional repressor REST, which in turn inhibits the expression of neuronal genes in non-neuronal cell types (Visvanathan et al., 2007). Mir-124 is expressed in microglia and M2 macrophages. Sall1-deficient or miR-124 inhibitor-treated microglia lose their processes that are typical for adult microglia in normal CNS (ramified form) and take a more activated amoeboid form, indicating that the resting microglial phenotype might be maintained by neuronal genes (Ponomarev et al., 2011; Koso et al., 2016, 2018). In other words, neurons and mature microglia share similar expression patterns for several genes. We believe that these neuronal genes may contribute to the unique phenotypes of microglia in the CNS. However, the induction of neuronal gene expression in microglia remains unclear and must be addressed. We propose that neuronal gene expression in microglia is associated with similar epigenetic changes that occur in both cell types during development. During neural lineage commitment, H3K27 in the promoter regions of many neural lineage genes is demethylated by the enzyme JMJD3 (Choi et al., 2015), similar to the effects of IL-4 on mouse BMDMs. Simultaneously, H3K27 is methylated in non-neuronal cells (including non-activated peripheral macrophages) (Satoh et al., 2010). These findings indicate similar epigenetic changes in microglia, M2 macrophages, and neuronal cells.

Besides the demethylation of H3K27 in M2 macrophages, miR-124 is upregulated by the IL-4 and cAMP pathways in mouse BMDM (Veremeyko et al., 2018b), while microglia receive horizontal transfers of miR-124 and miR-9 from neurons (Veremeyko et al., 2018a). Therefore, we propose that neuronal miR-124 and miR-9 inhibit REST in microglia, leading to the expression of several neuronal genes, similar to the consequences of miR-124 and miR-9 overexpression in fibroblasts (Lee et al., 2018). As the deactivation of REST and upregulation of miR-124 were shown to be associated with the modification of the neuronal BAF chromatin remodeling complex during neuronal

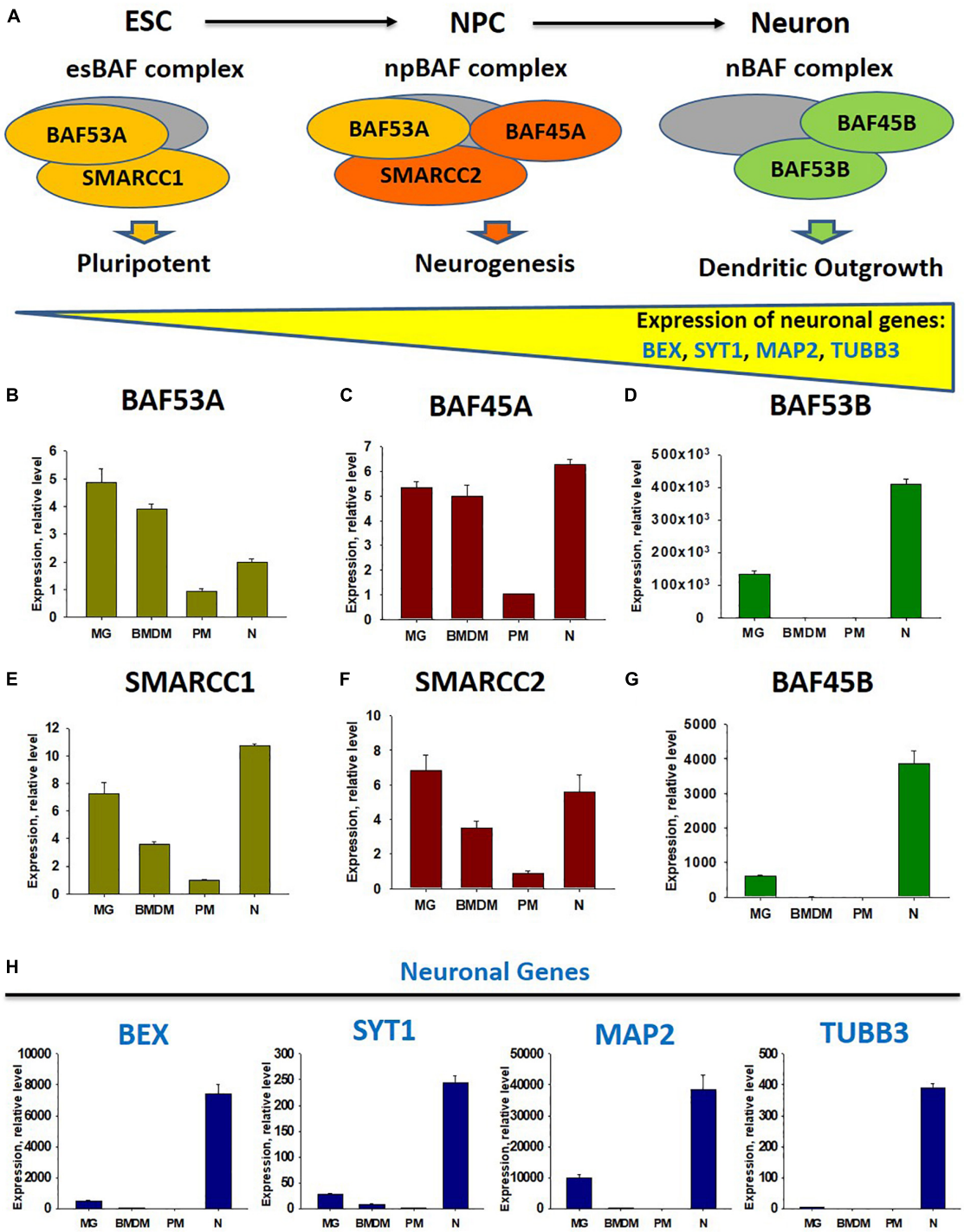

FIGURE 1 | Comparison of expression of factors of chromatin remodeling BAF complexes at the stage of embryonic stems cells (esBAF), neuronal progenitor cells (npBAF), and neurons (nBAF) as well as analysis of expression neuronal genes in microglia, bone marrow-derived macrophages, peritoneal macrophages, and cultured cortical neurons. **(A)** Schematic diagram of Brm/Brg-associated factor (BAF) chromatin remodeling complex for three stages of neuronal differentiation from embryonic stem cells (ESC) to neuronal progenitor cells (NPC) and to mature neurons (Neuron) (Adapted from "Epigenetic regulation of neural differentiation from embryonic stem cells" by Atsushi Shimomura and Eri Hashino with permission. 2013 Shimomura A., Hashino E. Published in *Trends in Cell Signaling Pathways in Neuronal Fate Decision* under CC BY 3.0 license. Available from: htpp://dx.doi.org/10.5772/53650). **(B–G)** Expression of factors of BAF complex *BAF53A* **(B)**, *BAF45A* **(C)**, *BAF53B* **(D)**, *SMARCC1* **(E)**, *SMARCC2* **(F)**, and *BAF45B* **(G)** in microglia (MG), bone marrow-derived macrophages (BMDM), peritoneal macrophages (PM), and cultured cortical neurons (N). **(H)** Expression of neuronal genes *BEX*, *SYT1*, *MAP2*, and *TUBB3 in* microglia (MG), bone marrow-derived macrophages (BMDF), peritoneal macrophages (PM), and cultured cortical neurons (N).

TABLE 1 | Neuron-derived soluble factors that affect the activation state of microglia in normal CNS and during neuroinflammation and neurodegeneration.

Class of mediators	Neuron-derived mediators	Changes during neuroinflammation/ neurodegeneration	Effect on microglia
Cytokines	IL-4	Decreased	Promote anti-inflammatory phenotype and expression of: Ym1, Fizz1, TGFβ1 (Veremeyko et al., 2015, 2018b; Zhao et al., 2015; Cheray and Joseph, 2018)
	TGFβ1	Decreased	Promote homeostatic phenotype of microglia in normal adult CNS (Dobolyi et al., 2012)
	IL-34	Increased	Homeostatic maintenance, proliferation, and survival of microglia (Frei et al., 1992; Mizuno et al., 2011; Ponomarev et al., 2013)
Chemokines	CCL2	Increased	Microglia migration, activation, and proliferation (Haas et al., 2019)
	CXCL12	Increased	Microglia migration and activation (Haas et al., 2019)
	CX3CL1 (soluble form)	Decreased	Deactivate microglia (Haas et al., 2019)
Growth Factors	NGF	Increased	Promote anti-inflammatory phenotype of microglia (Fodelianaki et al., 2019)
	BDNF	Increased	Suppress release of NO in microglia. Promote anti-inflammatory phenotype (Lai et al., 2018)
Neurotransmitters	Serotonin (5HT)	Decreased during TBI-induced neuroinflammation	Decreased IFNγ-induced activation of macrophages and possibly microglia (Liu et al., 2016)
	Dopamine	Decreased	Possibly suppress microglia activation via DR2 (Liu et al., 2016)
	Glutamate	Decreased	Promote microglia activation and expression of TNF and NO (Liu et al., 2016)
	GABA	Decreased	Inhibit microglia activation and release LPS-induced TNF and IL-6 (Liu et al., 2016)
Low-molecular-weight mediators	ATP	Increased	Activate microglia (Davalos et al., 2005)
microRNAs	miR-124 miR-9	Decreased Decreased	Deactivate microglia (Veremeyko et al., 2018a)
Complement	C3	Increased	Mediate synaptic pruning by microglia (Luchena et al., 2018)
	C1q	Increased	

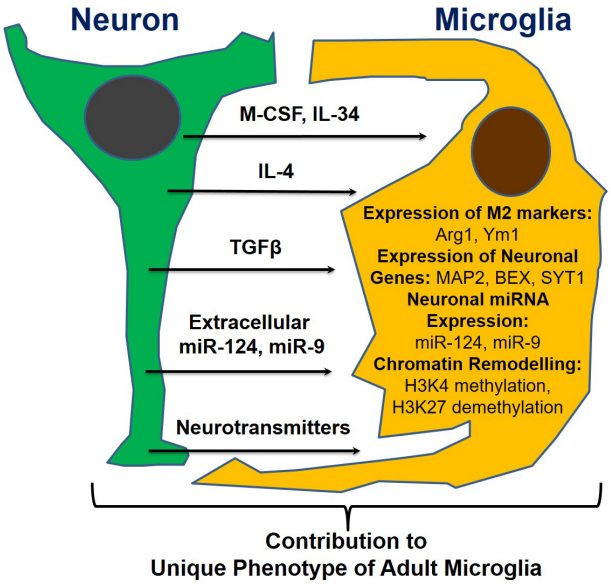

FIGURE 2 | Neuronal soluble factors that determine the ultimate phenotype of microglia in the normal or diseased CNS.

lineage commitment (Choi et al., 2015), we hypothesized that BAF would also be modified in the microglia, compared with non-activated BMDM. To test this hypothesis, we investigated the neuronal BAF chromatin remodeling complex (Choi et al., 2015), which regulates the expression of neuronal genes during differentiation from embryonic stem cells (ESCs) to neuronal progenitor cells (NPCs) from NPCs to mature neurons (Shimomura and Hashino, 2013), in neurons, peritoneal macrophages (PMs), BMDMs, and microglia (**Figure 1A**). In the ESC stage, the esBAF complex exists, and the co-factors *BAF53A* and *SMARCC1* are expressed predominantly. In the NPC stage, the npBAF complex retains *BAF53A* but includes two new factors, *BAF45A* and *SMARCC2*. Finally, in mature neurons, the nBAF complex comprises *BAF45B* and *BAF53B*. The expression of the neuronal genes *BEX*, *SYT1*, *MAP2*, and *TUBB3* increased gradually during the ESC→NPC→neuron transition path (**Figure 1A**). We similarly compared the expression levels of transcripts encoding factors in the esBAF, npBAF, and nBAF complexes in mature microglia, BMDMs, PMs, and cultured mature cortical neurons, as described in our earlier studies (Veremeyko et al., 2015, 2018a; Dukhinova et al., 2018, 2019). We observed a similar expression of *BAF53A* and *SMARCC1*, which encode esBAF components, between microglia and neurons and

between microglia and BMDMs. However, these genes were expressed at significantly higher levels in microglia than in PMs (**Figures 1B,E**). We observed a similar pattern in the expression of *BAF45A* and *SMARCC2*, which encode npBAF components. These genes were expressed similarly in microglia and neurons, at similar or slightly higher levels in microglia relative to BMDMs, and at significantly higher levels in microglia than in PMs (**Figures 1C,F**). However, *BAF53B* and *BAF45B*, which encode nBAF components, were only expressed at detectable levels in neurons and microglia, but not BMDMs and PMs (**Figures 1D,G**). The neuronal genes *BEX*, *SYT1*, and *MAP2* were expressed in neurons and microglia, but not in BMDMs and PMs (**Figure 1H**). *TUBB3*, the most abundant neuronal gene, was not expressed in microglia, indicating that the previous results could not be attributed to the contamination of microglia preparations with neuronal cells (**Figure 1H**, *TUBB3*). Therefore, in contrast with other macrophages, microglia express factors associated with the nBAF complex, as well as several neuronal genes. Although the roles of neuronal gene products such as MAP2 in the microglial phenotype remain unclear, we propose that these factors contribute to the unique phenotype of mature microglia in the normal CNS.

ROLES OF NEURONAL SOLUBLE FACTORS IN THE MAINTENANCE OF THE MICROGLIAL PHENOTYPE

Following our discovery of the horizontal transfer of neuronal miR-9 and miR-124 from electrically active neurons to microglia, we hypothesized that the microglial phenotype is influenced strongly by soluble neuronal factors (**Table 1** and **Figure 2**). Accordingly, these soluble neuronal factors exhibit great potential for future therapeutic interventions targeting neurodegenerative diseases. Both astrocytes and neurons can produce IL-4, TGFβ1, and IL-34, which greatly affect the microglial phenotype, as discussed previously (**Table 1**). Neuronal IL-4 might further contribute to H3K27 demethylation in microglia (Cheray and Joseph, 2018). Neurons also produce the chemokines CCL2, CCL12, and CX3CL1 (both membrane-bound and soluble forms), which can induce microglial migration toward neurons (CCL2 and CCL12) and microglial deactivation (CX3CL1) (Haas et al., 2019). Neuronal growth factor (NGF) and BDNF also contribute to the anti-inflammatory microglial phenotype (**Table 1**; Lai et al., 2018; Fodelianaki et al., 2019). Neurotransmitters are other important molecules released by electrically active neurons that can directly affect microglia. Common neurotransmitters, such as serotonin, dopamine, and GABA, deactivate microglia, while glutamate activates these cells (**Table 1**; Liu et al., 2016). ATP is released by activated and damaged neurons and contributes to microglial activation and inflammation (Davalos et al., 2005). The neuronal microRNAs miR-124 and miR-9 are transferred to the microglial cytoplasm, where they downregulate the expression of CEBPα and NFκB and deactivate the cells (**Table 1**; Veremeyko et al., 2018a). Finally, the complement components C1q and C3 mediate neuronal axonal pruning by microglia via complement receptors (**Table 1**). Interestingly, C1q expression is induced in neurons via a TGFβ1-mediated mechanism, while C3 is present in neuronal synapses (Luchena et al., 2018). In summary, many factors, including pro- and anti-inflammatory stimuli, affect communication between neurons and microglia. The balance of these stimuli determines the ultimate phenotype of microglia in the normal or diseased CNS (**Figure 2**).

CONCLUDING REMARKS

Microglia represent a unique population of resident myeloid cells in the CNS. The phenotypes of these cells are influenced strongly by the local microenvironment and determined by the specific regulation of gene expression at the epigenetic level. Currently, neuronal cells are thought to actively influence the phenotypes of microglia. In the normal CNS, electrically and synaptically active neurons maintain microglia in a deactivated state, whereas changes in the balance of inhibitory vs. activating stimuli in the contexts of neuroinflammatory and neurodegenerative diseases cause immediate changes in the microglial phenotype and induce activation. A further understanding of the interactions of neurons and microglia in the normal CNS would ultimately lead to the discovery of new pathways. This information would suggest potential mechanisms by which homeostasis could be restored in pathological settings, as well as potential treatment options for neurodegenerative diseases such as multiple sclerosis, Alzheimer's disease, and Parkinson's disease.

AUTHOR CONTRIBUTIONS

TV and EP conceived the review and study. TV, AY, and MD performed the experiments. TV, TS, and EP analyzed the data. TS and EP prepared the manuscript.

FUNDING

This work was supported by Research Grant Council–General Research Fund, reference no. 14113316 (Hong Kong Government, Hong Kong), and by Research Grant Council–Areas of Excellence Fund grant (Hong Kong Government, Hong Kong), reference no. AoE/M-604/16.

REFERENCES

Barteneva, N. S., Baiken, Y., Fasler-Kan, E., Alibek, K., Wang, S., Maltsev, N., et al. (2017). Extracellular vesicles in gastrointestinal cancer in conjunction with microbiota: on the border of kingdoms. *Biochim. Biophys. Acta Rev. Cancer* 1868, 372–393. doi: 10.1016/j.bbcan.2017.06.005

Barteneva, N. S., Fasler-Kan, E., Bernimoulin, M., Stern, J. N. H., Ponomarev, E. D., Duckett, L., et al. (2013). Circulating microparticles: square the circle. *BMC Cell Biol.* 14:23. doi: 10.1186/1471-2121-14-23

Buttgereit, A., Lelios, I., Yu, X., Vrohlings, M., Krakoski, N. R., Gautier, E. L., et al. (2016). Sall1 is a transcriptional regulator defining microglia identity and function. *Nat. Immunol.* 17, 1397–1406. doi: 10.1038/ni.3585

Chauhan, A., Quenum, F. Z., Abbas, A., Bradley, D. S., Nechaev, S., Singh, B. B., et al. (2015). Epigenetic modulation of microglial inflammatory gene loci in helminth-induced immune suppression: implications for immune regulation in neurocysticercosis. *ASN Neuro* 7:1759091415592126. doi: 10.1177/1759091415592126

Cheray, M., and Joseph, B. (2018). Epigenetics control microglia plasticity. *Front. Cell Neurosci.* 12:243. doi: 10.3389/FNCEL.2018.00243

Cherry, J. D., Olschowka, J. A., and O'Banion, M. K. (2014). Neuroinflammation and M2 microglia: the good, the bad, and the inflamed. *J. Neuroinflammation* 11:98. doi: 10.1186/1742-2094-11-98

Choi, K.-Y., Yoo, M., and Han, J.-H. (2015). Toward understanding the role of the neuron-specific BAF chromatin remodeling complex in memory formation. *Exp. Mol. Med.* 47, e155–e155. doi: 10.1038/emm.2014.129

Collin, M., and Milne, P. (2016). Langerhans cell origin and regulation. *Curr. Opin. Hematol.* 23, 28–35. doi: 10.1097/MOH.0000000000000202

Crotti, A., Benner, C., Kerman, B. E., Gosselin, D., Lagier-Tourenne, C., Zuccato, C., et al. (2014). Mutant huntingtin promotes autonomous microglia activation via myeloid lineage-determining factors. *Nat. Neurosci.* 17, 513–521. doi: 10.1038/nn.3668

Davalos, D., Grutzendler, J., Yang, G., Kim, J. V., Zuo, Y., Jung, S., et al. (2005). ATP mediates rapid microglial response to local brain injury in vivo. *Nat. Neurosci.* 8, 752–758. doi: 10.1038/nn1472

Dobolyi, A., Vincze, C., Pál, G., and Lovas, G. (2012). The neuroprotective functions of transforming growth factor beta proteins. *Int. J. Mol. Sci.* 13, 8219–8258. doi: 10.3390/IJMS13078219

Dubbelaar, M. L., Kracht, L., and Eggen, B. J. L. (2018). Boddeke EWGM. The kaleidoscope of microglial phenotypes. *Front. Immunol.* 9:1753. doi: 10.3389/fimmu.2018.01753

Dukhinova, M., Kuznetsova, I., Kopeikina, E., Veniaminova, E., Yung, A. W. Y. Y., Veremeyko, T., et al. (2018). Platelets mediate protective neuroinflammation and promote neuronal plasticity at the site of neuronal injury. *Brain Behav. Immun.* 74, 7–27. doi: 10.1016/j.bbi.2018.09.009

Dukhinova, M., Veremeyko, T., Yung, A. W. Y., Kuznetsova, I. S., Lau, T. Y. B., Kopeikina, E., et al. (2019). Fresh evidence for major brain gangliosides as a target for the treatment of Alzheimer's disease. *Neurobiol. Aging* 77, 128–143. doi: 10.1016/j.neurobiolaging.2019.01.020

Fodelianaki, G., Lansing, F., Bhattarai, P., Troullinaki, M., Zeballos, M. A., Charalampopoulos, I., et al. (2019). Nerve growth factor modulates LPS-induced microglial glycolysis and inflammatory responses. *Exp. Cell Res.* 377, 10–16. doi: 10.1016/J.YEXCR.2019.02.023

Frei, K., Nohava, K., Malipiero, U. V., Schwerdel, C., and Fontana, A. (1992). Production of macrophage colony-stimulating factor by astrocytes and brain macrophages. *J. Neuroimmunol.* 40, 189–195. doi: 10.1016/0165-5728(92)90133-6

Gosselin, D., Link, V. M., Romanoski, C. E., Fonseca, G. J., Eichenfield, D. Z., Spann, N. J., et al. (2014). Environment drives selection and function of enhancers controlling tissue-specific macrophage identities. *Cell* 159, 1327–1340. doi: 10.1016/j.cell.2014.11.023

Gosselin, D., Skola, D., Coufal, N. G., Holtman, I. R., Schlachetzki, J. C. M., Sajti, E., et al. (2017). An environment-dependent transcriptional network specifies human microglia identity. *Science* 356:eaal3222. doi: 10.1126/science.aal3222

Groot, A. E., and de Pienta, K. J. (2018). Epigenetic control of macrophage polarization: implications for targeting tumor-associated macrophages. *Oncotarget* 9, 20908–20927. doi: 10.18632/ONCOTARGET.24556

Guo, Y., Hong, W., Wang, X., Zhang, P., Körner, H., Tu, J., et al. (2019). MicroRNAs in microglia: how do microRNAs affect activation, inflammation, polarization of microglia and mediate the interaction between microglia and glioma? *Front. Mol. Neurosci.* 12:125. doi: 10.3389/fnmol.2019.00125

Haas, A. H., de, Weering, H. R. J., van, Jong, E. K., de Boddeke, H. W. G. M., et al. (2019). Neuronal chemokines: versatile messengers in central nervous system cell interaction. *Mol. Neurobiol.* 36, 137–151. doi: 10.1007/S12035-007-0036-8

Hammond, T. R., Dufort, C., Dissing-Olesen, L., Giera, S., Young, A., Wysoker, A., et al. (2019). Single-cell RNA sequencing of microglia throughout the mouse lifespan and in the injured brain reveals complex cell-state changes. *Immunity* 50, 253.e6–271.e6. doi: 10.1016/j.immuni.2018.11.004

Harrison, S. J., Nishinakamura, R., Jones, K. R., and Monaghan, A. P. (2012). Sall1 regulates cortical neurogenesis and laminar fate specification in mice: implications for neural abnormalities in Townes–Brocks syndrome. *Dis. Model Mech.* 5, 351–365. doi: 10.1242/dmm.002873

Holtman, I. R., Skola, D., and Glass, C. K. (2017). Transcriptional control of microglia phenotypes in health and disease. *J. Clin. Invest.* 127, 3220–3229. doi: 10.1172/JCI90604

Hop, H. T., Arayan, L. T., Huy, T. X. N., Reyes, A. W. B., Vu, S. H., Min, W., et al. (2018). The key role of c-Fos for immune regulation and bacterial dissemination in brucella infected macrophage. *Front. Cell Infect Microbiol.* 8:287. doi: 10.3389/fcimb.2018.00287

Kierdorf, K., Erny, D., Goldmann, T., Sander, V., Schulz, C., Perdiguero, E. G., et al. (2013). Microglia emerge from erythromyeloid precursors via Pu.1- and *Irf*8-dependent pathways. *Nat. Neurosci.* 16, 273–280. doi: 10.1038/nn.3318

Kittan, N. A., Allen, R. M., Dhaliwal, A., Cavassani, K. A., Schaller, M., Gallagher, K. A., et al. (2013). Cytokine induced phenotypic and epigenetic signatures are key to establishing specific macrophage phenotypes. *PLoS One* 8:e78045. doi: 10.1371/journal.pone.0078045

Koso, H., Nishinakamura, R., and Watanabe, S. (2018). Sall1 regulates microglial morphology cell autonomously in the developing retina. *Adv. Exp. Med. Biol.* 1074, 209–215. doi: 10.1007/978-3-319-75402-4_26

Koso, H., Tsuhako, A., Lai, C.-Y., Baba, Y., Otsu, M., Ueno, K., et al. (2016). Conditional rod photoreceptor ablation reveals Sall1 as a microglial marker and regulator of microglial morphology in the retina. *Glia* 64, 2005–2024. doi: 10.1002/glia.23038

Krzyszczyk, P., Schloss, R., Palmer, A., and Berthiaume, F. (2018). The role of macrophages in acute and chronic wound healing and interventions to promote pro-wound healing phenotypes. *Front. Physiol.* 9:419. doi: 10.3389/fphys.2018.00419

Lai, S.-W., Chen, J.-H., Lin, H.-Y., Liu, Y.-S., Tsai, C.-F., Chang, P.-C., et al. (2018). Regulatory effects of neuroinflammatory responses through brain-derived neurotrophic factor signaling in microglial cells. *Mol. Neurobiol.* 55, 7487–7499. doi: 10.1007/s12035-018-0933-z

Lawrence, T., and Natoli, G. (2011). Transcriptional regulation of macrophage polarization: enabling diversity with identity. *Nat. Rev. Immunol.* 11, 750–761. doi: 10.1038/nri3088

Lee, S. W., Oh, Y. M., Lu, Y.-L., Kim, W. K., and Yoo, A. S. (2018). MicroRNAs overcome cell fate barrier by reducing EZH2-controlled REST stability during neuronal conversion of human adult fibroblasts. *Dev. Cell* 46, 73.e7–84.e7. doi: 10.1016/j.devcel.2018.06.007

Ley, K. (2017). M1 means kill. M2 means heal. *J. Immunol.* 199, 2191–2193. doi: 10.4049/JIMMUNOL.1701135

Li, H., Jiang, T., Li, M.-Q., Zheng, X.-L., and Zhao, G.-J. (2018). Transcriptional regulation of macrophages polarization by microRNAs. *Front. Immunol.* 9:1175. doi: 10.3389/fimmu.2018.01175

Li, Q., and Barres, B. A. (2017). Microglia and macrophages in brain homeostasis and disease. *Nat. Rev. Immunol.* 18, 225–242. doi: 10.1038/nri.2017.125

Li, Q., and Barres, B. A. (2018). Microglia and macrophages in brain homeostasis and disease. *Nat. Rev. Immunol.* 18, 225–242. doi: 10.1038/nri.2017.125

Liu, H., Leak, R. K., and Hu, X. (2016). Neurotransmitter receptors on microglia. *Stroke Vasc Neurol.* 1, 52–58. doi: 10.1136/svn-2016-000012

Luchena, C., Zuazo-Ibarra, J., Alberdi, E., Matute, C., and Capetillo-Zarate, E. (2018). Contribution of neurons and glial cells to complement-mediated synapse removal during development, aging and in Alzheimer's disease. *Mediators Inflamm.* 2018, 1–12. doi: 10.1155/2018/2530414

Martinez, F. O., and Gordon, S. (2014). The M1 and M2 paradigm of macrophage activation: time for reassessment. *F1000Prime Rep.* 6:13. doi: 10.12703/P6-13

Masuda, T., Sankowski, R., Staszewski, O., Böttcher, C., Amann, L., Sagar, et al. (2019). Spatial and temporal heterogeneity of mouse and human microglia at single-cell resolution. *Nature* 566, 388–392. doi: 10.1038/s41586-019-0924-x

Matcovitch-Natan, O., Winter, D. R., Giladi, A., Vargas Aguilar, S., Spinrad, A., Sarrazin, S., et al. (2016). Microglia development follows a stepwise program to regulate brain homeostasis. *Science* 353, aad8670. doi: 10.1126/science.aad8670

Ménard, C., Hein, P., Paquin, A., Savelson, A., Yang, X. M., Lederfein, D., et al. (2002). An essential role for a MEK-C/EBP pathway during growth factor-regulated cortical neurogenesis. *Neuron* 36, 597–610. doi: 10.1016/S0896-6273(02)01026-7

Mizuno, T., Doi, Y., Mizoguchi, H., Jin, S., Noda, M., Sonobe, Y., et al. (2011). Interleukin-34 selectively enhances the neuroprotective effects of microglia to attenuate oligomeric amyloid-β neurotoxicity. *Am. J. Pathol.* 179, 2016–2027. doi: 10.1016/j.ajpath.2011.06.011

Okada, S. (2003). Dominant-negative effect of the c-fos family gene products on inducible NO synthase expression in macrophages. *Int. Immunol.* 15, 1275–1282. doi: 10.1093/intimm/dxg126

Parkhurst, C. N., Yang, G., Ninan, I., Savas, J. N., Yates, J. R., Lafaille, J. J., et al. (2013). Microglia promote learning-dependent synapse formation through brain-derived neurotrophic factor. *Cell* 155, 1596–1609. doi: 10.1016/j.cell.2013.11.030

Ponomarev, E. D., Maresz, K., Tan, Y., and Dittel, B. N. (2007). CNS-derived interleukin-4 is essential for the regulation of autoimmune inflammation and induces a state of alternative activation in microglial cells. *J. Neurosci.* 27, 10714–10721. doi: 10.1523/JNEUROSCI.1922-07.2007

Ponomarev, E. D., Veremeyko, T., Barteneva, N., Krichevsky, A. M., and Weiner, H. L. (2011). MicroRNA-124 promotes microglia quiescence and suppresses EAE by deactivating macrophages via the C/EBP-α-PU.1 pathway. *Nat. Med.* 17, 64–70. doi: 10.1038/nm.2266

Ponomarev, E. D., Veremeyko, T., and Weiner, H. L. (2013). MicroRNAs are universal regulators of differentiation, activation, and polarization of microglia and macrophages in normal and diseased CNS. *Glia* 61, 91–103. doi: 10.1002/glia.22363

Prada, I., Gabrielli, M., Turola, E., Iorio, A., D'Arrigo, G., Parolisi, R., et al. (2018). Glia-to-neuron transfer of miRNAs via extracellular vesicles: a new mechanism underlying inflammation-induced synaptic alterations. *Acta Neuropathol.* 135, 529–550. doi: 10.1007/s00401-017-1803-x

Ransohoff, R. M. (2016). A polarizing question: do M1 and M2 microglia exist. *Nat. Neurosci.* 19, 987–991. doi: 10.1038/nn.4338

Ray, N., Kuwahara, M., Takada, Y., Maruyama, K., Kawaguchi, T., Tsubone, H., et al. (2006). c-Fos suppresses systemic inflammatory response to endotoxin. *Int. Immunol.* 18, 671–677. doi: 10.1093/intimm/dxl004

Satoh, T., Takeuchi, O., Vandenbon, A., Yasuda, K., Tanaka, Y., Kumagai, Y., et al. (2010). The Jmjd3-Irf4 axis regulates M2 macrophage polarization and host responses against helminth infection. *Nat. Immunol.* 11, 936–944. doi: 10.1038/ni.1920

Shimomura, A., and Hashino, E. (2013). "Epigenetic regulation of neural differentiation from embryonic stem cells," in *Trends in Cell Signaling Pathways in Neuronal Fate Decision*, ed. S. Wislet (London: IntechOpen Limited), 305–325.

Sica, A., and Mantovani, A. (2012). Macrophage plasticity and polarization: in vivo veritas. *J. Clin. Invest* 122, 787–795. doi: 10.1172/JCI59643

Szepesi, Z., Manouchehrian, O., Bachiller, S., and Deierborg, T. (2018). Bidirectional microglia–neuron communication in health and disease. *Front. Cell Neurosci.* 12:323. doi: 10.3389/fncel.2018.00323

Tang, Y., Li, T., Li, J., Yang, J., Liu, H., Zhang, X. J., et al. (2014). Jmjd3 is essential for the epigenetic modulation of microglia phenotypes in the immune pathogenesis of Parkinson's disease. *Cell Death. Differ.* 21, 369–380. doi: 10.1038/cdd.2013.159

Tikhanovich, I., Zhao, J., Olson, J., Adams, A., Taylor, R., Bridges, B., et al. (2017). Protein arginine methyltransferase 1 modulates innate immune responses through regulation of peroxisome proliferator-activated receptor γ-dependent macrophage differentiation. *J. Biol. Chem.* 292, 6882–6894. doi: 10.1074/JBC.M117.778761

Veremeyko, T., Kuznetsova, I. S., Dukhinova, M., Yung, A. W. Y., Kopeikina, E., Barteneva, N. S. P. E., et al. (2018a). Neuronal extracellular microRNAs miR-124 and miR-9 mediate cell–cell communication between neurons and microglia. *J. Neurosci. Res.* 97, 162–184. doi: 10.1002/jnr.24344

Veremeyko, T., Yung, A. W. Y., Dukhinova, M., Kuznetsova, I. S., Pomytkin, I., Lyundup, A., et al. (2018b). Cyclic AMP pathway suppress autoimmune neuroinflammation by inhibiting functions of encephalitogenic CD4 T cells and enhancing M2 macrophage polarization at the site of inflammation. *Front. Immunol.* 9:50. doi: 10.3389/fimmu.2018.00050

Veremeyko, T., Siddiqui, S., Sotnikov, I., Yung, A., and Ponomarev, E. D. (2013). IL-4/IL-13-dependent and independent expression of miR-124 and its contribution to M2 phenotype of monocytic cells in normal conditions and during allergic inflammation. *PLoS One* 8:e81774. doi: 10.1371/journal.pone.0081774

Veremeyko, T., Yung, A. W. Y., Anthony, D. C., Strekalova, T., and Ponomarev, E. D. (2015). Early growth response gene-2 is essential for M1 and M2 macrophage activation and plasticity by modulation of the transcription factor CEBPβ. *Front. Immunol.* 9:2515. doi: 10.3389/fimmu.2018.02515

Visvanathan, J., Lee, S., Lee, B., Lee, J. W., and Lee, S.-K. (2007). The microRNA miR-124 antagonizes the anti-neural REST/SCP1 pathway during embryonic CNS development. *Genes Dev.* 21, 744–749. doi: 10.1101/gad.1519107

Zhang, J., Li, S., Li, L., Li, M., Guo, C., Yao, J., et al. (2015). Exosome and exosomal microRNA: trafficking, sorting, and function. *Genom. Proteom. Bioinforma* 13, 17–24. doi: 10.1016/j.gpb.2015.02.001

Zhao, X., Wang, H., Sun, G., Zhang, J., Edwards, N. J., and Aronowski, J. (2015). Neuronal interleukin-4 as a modulator of microglial pathways and ischemic brain damage. *J. Neurosci.* 35, 11281–11291. doi: 10.1523/JNEUROSCI.1685-15.2015

Conflict of Interest: The authors declare that the research was conducted in the absence of any commercial or financial relationships that could be construed as constituting a potential conflict of interest.

frontiers in Cellular Neuroscience

PERSPECTIVE
published: 14 November 2019
doi: 10.3389/fncel.2019.00504

Differences of Microglia in the Brain and the Spinal Cord

*Fang-Ling Xuan[1], Keerthana Chithanathan[1], Kersti Lilleväli[1], Xiaodong Yuan[2] and Li Tian[1,3]**

[1] *Department of Physiology, Faculty of Medicine, Institute of Biomedicine and Translational Medicine, University of Tartu, Tartu, Estonia,* [2] *Department of Neurology, Kailuan General Hospital, North China University of Science and Technology, Tangshan, China,* [3] *Psychiatry Research Centre, Beijing HuiLongGuan Hospital, Peking University, Beijing, China*

Microglia were previously regarded as a homogenous myeloid cell lineage in the mammalian central nervous system (CNS). However, accumulating evidences show that microglia in the brain and SC are quite different in development, cellular phenotypes and biological functions. Although this is a very interesting phenomenon, the underlying mechanisms and its significance for neurological diseases in association with behavioral and cognitive changes are still unclear. How microglia differ between these two regions and whether such diversity may contribute to CNS development and functions as well as neurological diseases will be discussed in this Perspective.

Keywords: microglia, spinal cord, brain, neuroinflammation, neurological diseases

OPEN ACCESS

Edited by:
Yu Tang,
Central South University, China

Reviewed by:
Hidetoshi Saitoh,
Kyushu University, Japan
Melanie Greter,
University of Zurich, Switzerland

****Correspondence:***
Li Tian
li.tian@ut.ee

Specialty section:
This article was submitted to Non-Neuronal Cells, a section of the journal Frontiers in Cellular Neuroscience

Received: *15 June 2019*
Accepted: *25 October 2019*
Published: *14 November 2019*

Citation:
Xuan F-L, Chithanathan K, Lilleväli K, Yuan X and Tian L (2019) Differences of Microglia in the Brain and the Spinal Cord. Front. Cell. Neurosci. 13:504. doi: 10.3389/fncel.2019.00504

INTRODUCTION

Microglia are important for building and defending the central nervous system (CNS) (Tay et al., 2017) are considered the most dynamic glial cell type in the CNS to sense and adapt to their surroundings, thereby giving them a complex feature of heterogeneity (Nayak et al., 2014). However, the implication of spatial heterogeneity of microglia in normal CNS functions and diseases is still evasive. Although the past years have witnessed a dramatic growth of attention on microglial functions in the CNS, evidence available for this Perspective is rather limited, because most microglial studies have investigated only the brain and have used disease models concerning the brain or the spinal microglial functions separately, and a direct comparison between the brain and the spinal cord (SC) under basal or diseased condition is rare. The aim of this paper is hence to provide an updated available knowledge on microglial differences between the brain and the SC and to discuss its potential application for treating neurological diseases. Besides region-specific features, microglia are also increasingly known to differ temporally and between genders, but these other heterogenous aspects will not be focused here and readers are referred to other recent reviews (Mapplebeck et al., 2016; Silvin and Ginhoux, 2018; Rahimian et al., 2019).

DIFFERENCES IN DEVELOPMENT AND PHENOTYPES OF MICROGLIA IN THE BRAIN VERSUS IN THE SC

Using various immunohistochemical markers for microglia, including tomato lectin, CD45, CD68, major histocompatibility complex (MHC)-II, CD11b/c (OX-42), and ionized calcium-binding

adaptor molecule-1 (Iba1), researchers have observed generally similar developmental aspects of microglia in their entrance and colonization in the brain and the SC, but minor differences exist (Rezaie and Male, 1999). In a study comparing cell populations in the lumbar locomotor region of the spinal cord and in the brainstem motor nucleus of new-born rats, Cifra et al. (2012) observed less than 10% of microglia in the neonate brainstem but very few microglia in the spinal gray matter (**Table 1**). Moreover, an earlier study discovered that microglial density in the adult colony-stimulating factor (CSF)1-deficient mice was specifically decreased by 86.4% in the white matter tract of the spinal dorsal column compared with that in age-matched wild-type controls, whereas the decrease was much less (24.0%) in the gray matter of cerebral cortex (Kondo and Duncan, 2009). This suggests that spinal microglia respond to CSF1-dependent cell proliferation more sensitively than cortical microglia, but whether this is due to the differential expression of CSF1 and/or its receptor in different CNS regions is unclear. A very recent study comparing cerebellar and cerebral microglia in CSF1-deficient mice also confirmed that CSF1 depletion did not affect microglia in the forebrain (Kana et al., 2019). Nevertheless, CSF1 is more enriched in the brain than the spinal cord. IL-34, an alternative ligand for CSF1R, is also highly expressed in the brain compared to the spinal cord and is critical for developing cerebral microglia, in contrast to CSF1 (Greter et al., 2012; Wang et al., 2012). However, whether it is dispensable for spinal microglia development or not is unclear. In another recent study using a diphtheria toxin receptor (DTR)-based genetic depletion approach for adult mice, Bruttger et al., 2015) further revealed that while microglia were rapidly ablated in all studied areas, e.g., the cortex, cerebellum and SC, within 3 days, residual microglia recovered more rapidly in the SC than in the cortex within 7 days, providing another evidence on the sensitivity of spinal microglia to changes in environmental cues.

TABLE 1 | Differences in regional features of brain versus spinal microglia.

Features	Brain versus SC	References
Entrance	• <10% of total brainstem cells but few microglia in the SC in rats at P4; • Entrance in the cerebrum at GW4-8 but in the SC at GW9-16 in humans;	Monier et al., 2007; Cifra et al., 2012
Proliferation	• Spinal microglia more sensitive to CSF1 and genetic ablation; • Cerebral microglia less responsive to CSF1;	Kondo and Duncan, 2009; Bruttger et al., 2015; Kana et al., 2019
Receptors and genes	• Lower expression of CSF1 and IL34 in the SC; • Higher levels of CD11b, CD45, CD86, CCR9 and MHCII but lower level of CD172a in the SC; • *Fos* and *Kif* genes more enriched in the SC; • $CST3^{-}SPARC^{-}IBA1^{+}$ microglia more enriched in the juvenile SC;	de Haas et al., 2008; Olson, 2010; Wang et al., 2012; Li et al., 2016; Gosselin et al., 2017; Masuda et al., 2019
Response to injury	• *CD68*, *C1qb*, *C3*, *C4a* and *Tgfb1* upregulated in the SC but downregulated in the cortex after SNI; • BDNF upregulated in the SC but downregulated in the hippocampus and no difference in change of TNF after SNI; • Inflammatory response greater in the SC after trauma.	Schnell et al., 1999; Batchelor et al., 2008; Li et al., 2016; Liu et al., 2017

Importantly, much of the knowledge on developmental features of microglia in the SC comes from previous studies on human post-mortem samples (**Table 1**). In the developing human CNS, both brain and SC microglial progenitors are suggested to enter their respective eminence from the meninges (Rezaie and Male, 1999; Monier et al., 2007). However, Rezaie and Male (1999) found that human amoeboid-like microglia-macrophages appeared in the SC at gestational weeks (GW)9 and peaked at GW16, which is later than entrance in the cerebrum at GW4-8 as described by Monier et al. (2007). Morphologically, Hutchins et al. found that during GW18-24, gray matter microglia were ramified while white matter microglia were amoeboid in the SC (Hutchins et al., 1992). Since morphological maturation of microglia- macrophage precursors stages a step-wise amoeboid, intermediate, and ramified transition (Verney et al., 2010), this indicates an inside-out migratory route of microglia-macrophage progenitors in the SC, which also resembles the early developmental cerebrum (Monier et al., 2007; Verney et al., 2010). McKay et al. found that morphologies of microglia even differed between the dorsal and ventral horns within the spinal gray matter in adult rats (McKay et al., 2007), with both microglial size (length between the tips of the two longest processes through the soma) and soma area smaller in the dorsal horn (DH) than in the ventral horn.

Other microglial phenotypes may also differ from those in the brain at adulthood (**Table 1**). Fundamental gene expression differences in microglia between the brain and SC have been particularly noticed. For instance, de Haas et al. made a pilot comparison of the protein expression of several microglial molecules among the mouse hippocampus, cerebral cortex, cerebellum and SC, and observed that levels of CD11b, CD45, CD86, and CCR9 were higher in the SC as compared to other regions (de Haas et al., 2008). A later study similarly found higher levels of several immune molecules on spinal microglia than their counterparts in the brain both at steady state and upon viral infection (Olson, 2010). We previously also confirmed that microglial expression of CD11b/c and MHCII were constitutively higher in the SC than in the cerebral cortex and thalamus, which conversely expressed more abundantly CD172a (SIRPα), an inhibitory immune receptor (Li et al., 2016).

Using genome-wide chromatin gene expression profiling and/or single-cell RNA sequencing (scRNAseq) analysis, three recent pivotal studies included microglia in the SC (Matcovitch-Natan et al., 2016; Gosselin et al., 2017). Matcovitch-Natan et al. (2016) provided seminal evidence that microglia underwent a three-step developmental program - early, pre-, and adult microglia across the mouse brain. Gosselin et al. (2017) examined the transcriptomes and epigenetic landscapes of human microglia isolated from surgically resected brain tissue *ex vivo* and after transition to an *in vitro* environment, and studied transcriptomes of various mouse CNS regions. However, neither study specifically addressed regional aspects

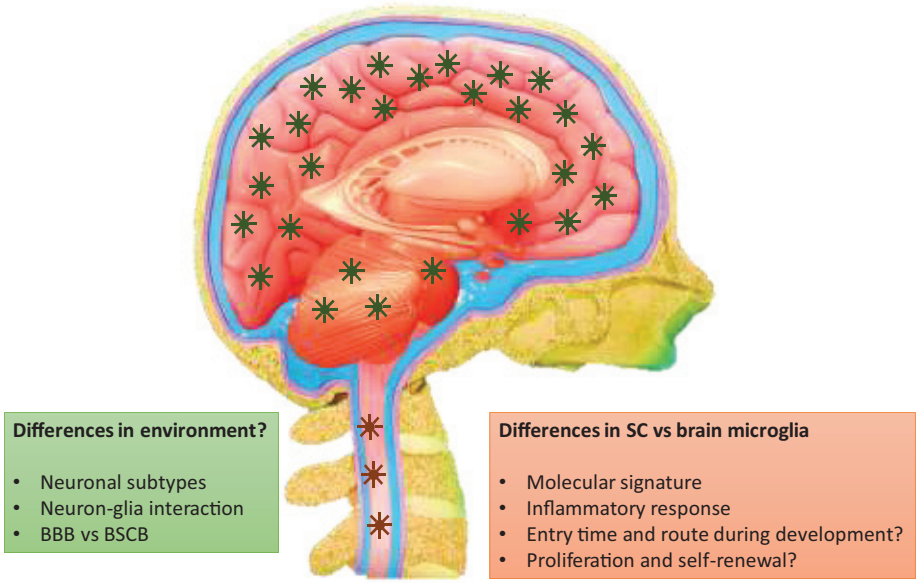

FIGURE 1 | Differences between brain and spinal microglia and the potential contributing factors.

of spinal microglial transcriptomic features in development and adulthood. In the study of Gosselin et al., gene family members of *Fos* and *Kif* seemed to be more enriched in the SC than the brain as a function of development in mice (Gosselin et al., 2017). Very recently, Masuda et al. (2019) made a thorough scRNAseq analysis of mouse microglia across different CNS regions, including the SC, in embryonic, juvenile and adult stages and found that compared to juvenile microglia, adult microglial clusters showed a more homogenous distribution across regions. Although the authors did not focus on the SC in particular either, their results demonstrated that a minor cluster (C7, representing $CST3^{-}SPARC^{-}IBA1^{+}$ microglia) was more prevalent in the juvenile SC and cerebellum as well as in the adult cerebellum and corpus callosum compared to the cortex and hippocampus (Masuda et al., 2019). These studies nevertheless provide some first clues on whether differentiation of microglia is orchestrated synchronically in different CNS regions across different developmental stages.

It is still unclear what underlies the fundamental difference between spinal and brain microglia and whether this is mainly caused by intrinsic or extrinsic factors (**Figure 1**). Guiding cues that drive the differences of microglia between the brain and the SC may come from the peripheral circulation, as blood-derived molecules penetrate the blood-brain barrier (BBB) and the blood-SC barrier (BSCB) in different manners (Abbott et al., 2010; Bartanusz et al., 2011). The BSCB is generally considered as the morphological extension of the BBB into the SC. Nevertheless, evidences suggest that structural and functional differences exist between them, so that the BSCB has higher permeability and lower expressions of tight junction proteins, such as ZO-1 and Occludin, and adherence junction proteins, such as VE-cadherin and β-catenin (reviewed in Bartanusz et al., 2011). It is noteworthy that glial cell types themselves may contribute to the morphological and functional differences between the BBB and BSCB.

MICROGLIAL REGIONAL HETEROGENEITY IN NEUROINFLAMMATORY CNS DISEASES

Although unconfirmed yet, it is highly expected that basal differences of microglia between the SC and the brain may contribute to the onset, development and treatment response of respective CNS diseases. Such differences are parallel to the facts that the brain and the SC play non-redundant roles in high-order functions of vertebrates and hence require different neurotransmission signals and regional connections. Knowledge on spinal microglia-mediated neuroinflammation and in comparison to brain microglia, however, has been mostly derived from studies on neurological conditions so far, namely traumatic brain injury (TBI), spinal cord injury (SCI), as well as spinal nerve injury models (Details on the respective models are provided in these recent reviews (Zhang and Gensel, 2014; Gensel and Zhang, 2015; Hu et al., 2015; Martini and Willison, 2016; Jassam et al., 2017; Cox, 2018; **Table 1**). Subtle to dramatic pathological and neuroinflammatory differences exist among different models. For instance, TBI is regarded as a diffuse injury, whereas spinal cord injury and stroke are anatomically discrete (Cox, 2018). Whether microglia contribute to such differences is currently unknown. In a recent study using spared nerve injury (SNI) model in mice, Liu et al. showed opposite changes in dendritic lengths and spine densities between hippocampal CA1 pyramidal neurons and spinal neurons along with differential expression of hippocampal and spinal brain-derived neurotrophic factor (BDNF) after SNI,

which was prevented by genetic deletion of tumor necrosis factor (TNF) receptor 1, a microglia-enriched cytokine receptor, and by inhibition or ablation of microglia (Liu et al., 2017). It is intriguing how the same TNF receptor can play opposite roles in regulation of neurons at different sites but differential microglial reaction after SNI would be expected. In line with this notion, using a similar SNI rat model, we earlier had observed that baseline differences of spinal and cortical microglia in $CD172a^+$ and $MHCII^+$ subpopulations as well as in expression of microglial activation genes underlined their differential responses to SNI as well as to the analgesic effect of minocycline, so that genes involved in M2 polarization and phagocytosis were upregulated in the spinal dorsal horn after SNI compared to Sham, but were downregulated in the cortex (Li et al., 2016). However, Liu et al. found that SNI increased TNF-α levels in both the hippocampus and the ipsilateral spinal dorsal horn compared with shams, which was also similarly dampened by minocycline treatment and by DTR-mediated genetic depletion of microglia (Liu et al., 2017), implying similar activation responses of spinal and hippocampal microglia to SNI. Causes for discrepancies in these studies need to be further examined.

Studies on TBI and SCI have reported that acute inflammatory response to traumatic injury is significantly greater in the SC than in the cerebral cortex. A more careful dissection on these differences was thoroughly provided in an earlier review (Zhang and Gensel, 2014) and therefore we will not reiterate here but only give a couple of exemplar evidences briefly. For instance, Schnell et al. originally found that myeloid recruitment to the lesion site and the surrounding parenchyma was significantly higher in the SC than in the brain. The area of BBB breakdown was substantially larger and vascular damage persisted longer in the SC (Schnell et al., 1999). A later study consistently found that, one week after mechanical injuries to both the gray and white matters, microglial response was significantly greater in the SC compared to the brain (Batchelor et al., 2008). In addition, a greater inflammatory response in the white matter compared to the gray matter within both the brain and SC was observed (McKay et al., 2007; Batchelor et al., 2008). In an *in vitro* cell culture study on morphological properties and secretion of inflammatory and trophic effectors by microglia derived from the brain or spinal cord of neonatal rats, Baskar Jesudasan et al. (2014) demonstrated that spinal microglia assumed a less inflammatory phenotype after lipopolysaccharide-induced activation, with reduced release of proinflammatory cytokines and nitric oxide, a less amoeboid morphology, and reduced phagocytosis relative to brain-derived microglia. These results suggest that local instead of global microglia-modulatory and/or anti-inflammatory strategies targeting microglia more specifically may be more valuable to reduce damages caused by local microglial activation in treating SC-related neurological diseases.

DISCUSSION

Brain microglia may be more important for regulating neuron-mediated cognition and emotion, whereas spinal microglia more relevant for controlling neuron-mediated sensory-motor functions. This may commit brain and spinal microglia to different CNS conditions, e.g., psychiatric and mental disorders versus sensory-motor neurological diseases. It is doubtless that more and more researchers are recognizing the existence of microglial regional specificity, but more vigorous investigations are still required for us to more deeply understand this interesting phenomenon.

AUTHOR CONTRIBUTIONS

All authors listed have made a substantial, direct and intellectual contribution to the work, and approved it for publication.

FUNDING

LT acknowledges the Beijing Municipal Science and Technology Commission No. Z171100001017021, and the Estonian Research Council-European Union Regional Developmental Fund Mobilitas Pluss Program No. MOBTT77.

REFERENCES

Abbott, N. J., Patabendige, A. A., Dolman, D. E., Yusof, S. R., and Begley, D. J. (2010). Structure and function of the blood-brain barrier. *Neurobiol. Dis.* 37, 13–25.

Bartanusz, V., Jezova, D., Alajajian, B., and Digicaylioglu, M. (2011). The blood-spinal cord barrier: morphology and clinical implications. *Ann. Neurol.* 70, 194–206. doi: 10.1002/ana.22421

Baskar Jesudasan, S. J., Todd, K. G., and Winship, I. R. (2014). Reduced inflammatory phenotype in microglia derived from neonatal rat spinal cord versus brain. *PLoS One* 9:e99443. doi: 10.1371/journal.pone.0099443

Batchelor, P. E., Tan, S., Wills, T. E., Porritt, M. J., and Howells, D. W. (2008). Comparison of inflammation in the brain and spinal cord following mechanical injury. *J. Neurotrauma* 25, 1217–1225. doi: 10.1089/neu.2007.0308

Bruttger, J., Karram, K., Wortge, S., Regen, T., Marini, F., Hoppmann, N., et al. (2015). Genetic cell ablation reveals clusters of local self-renewing microglia in the mammalian central nervous system. *Immunity* 43, 92–106. doi: 10.1016/j.immuni.2015.06.012

Cifra, A., Mazzone, G. L., Nani, F., Nistri, A., and Mladinic, M. (2012). Postnatal developmental profile of neurons and glia in motor nuclei of the brainstem and spinal cord, and its comparison with organotypic slice cultures. *Dev. Neurobiol.* 72, 1140–1160. doi: 10.1002/dneu.20991

Cox, C. S. Jr. (2018). Cellular therapy for traumatic neurological injury. *Pediatr. Res.* 83, 325–332. doi: 10.1038/pr.2017.253

de Haas, A. H., Boddeke, H. W., and Biber, K. (2008). Region-specific expression of immunoregulatory proteins on microglia in the healthy CNS. *Glia* 56, 888–894. doi: 10.1002/glia.20663

Gensel, J. C., and Zhang, B. (2015). Macrophage activation and its role in repair and pathology after spinal cord injury. *Brain Res.* 1619, 1–11. doi: 10.1016/j.brainres.2014.12.045

Gosselin, D., Skola, D., Coufal, N. G., Holtman, I. R., Schlachetzki, J. C. M., Sajti, E., et al. (2017). An environment-dependent transcriptional network specifies human microglia identity. *Science* 356:eaal3222. doi: 10.1126/science.aal3222

Greter, M., Lelios, I., Pelczar, P., Hoeffel, G., Price, J., Leboeuf, M., et al. (2012). Stroma-derived interleukin-34 controls the development and maintenance of

langerhans cells and the maintenance of microglia. *Immunity* 37, 1050–1060. doi: 10.1016/j.immuni.2012.11.001

Hu, X., Leak, R. K., Shi, Y., Suenaga, J., Gao, Y., Zheng, P., et al. (2015). Microglial and macrophage polarization-new prospects for brain repair. *Nat. Rev. Neurol.* 11, 56–64. doi: 10.1038/nrneurol.2014.207

Hutchins, K. D., Dickson, D. W., Rashbaum, W. K., and Lyman, W. D. (1992). Localization of microglia in the human fetal cervical spinal cord. *Brain Res. Dev. Brain Res.* 66, 270–273. doi: 10.1016/0165-3806(92)90091-a

Jassam, Y. N., Izzy, S., Whalen, M., McGavern, D. B., and El Khoury, J. (2017). Neuroimmunology of traumatic brain injury: time for a paradigm shift. *Neuron* 95, 1246–1265. doi: 10.1016/j.neuron.2017.07.010

Kana, V., Desland, F. A., Casanova-Acebes, M., Ayata, P., Badimon, A., Nabel, E., et al. (2019). CSF-1 controls cerebellar microglia and is required for motor function and social interaction. *J. Exp. Med.* 216, 2265–2281. doi: 10.1084/jem.20182037

Kondo, Y., and Duncan, I. D. (2009). Selective reduction in microglia density and function in the white matter of colony-stimulating factor-1-deficient mice. *J. Neurosci. Res.* 87, 2686–2695. doi: 10.1002/jnr.22096

Li, Z., Wei, H., Piirainen, S., Chen, Z., Kalso, E., Pertovaara, A., et al. (2016). Spinal versus brain microglial and macrophage activation traits determine the differential neuroinflammatory responses and analgesic effect of minocycline in chronic neuropathic pain. *Brain Behav. Immun.* 58, 107–117. doi: 10.1016/j.bbi.2016.05.021

Liu, Y., Zhou, L. J., Wang, J., Li, D., Ren, W. J., Peng, J., et al. (2017). TNF-alpha differentially regulates synaptic plasticity in the hippocampus and spinal cord by microglia-dependent mechanisms after peripheral nerve injury. *J. Neurosci.* 37, 871–881. doi: 10.1523/JNEUROSCI.2235-16.2016

Mapplebeck, J. C., Beggs, S., and Salter, M. W. (2016). Sex differences in pain: a tale of two immune cells. *Pain* 157(Suppl. 1), S2–S6. doi: 10.1097/j.pain.0000000000000389

Martini, R., and Willison, H. (2016). Neuroinflammation in the peripheral nerve: cause, modulator, or bystander in peripheral neuropathies? *Glia* 64, 475–486. doi: 10.1002/glia.22899

Masuda, T., Sankowski, R., Staszewski, O., Bottcher, C., Amann, L., Sagar, C., et al. (2019). Spatial and temporal heterogeneity of mouse and human microglia at single-cell resolution. *Nature* 566, 388–392. doi: 10.1038/s41586-019-0924-x

Matcovitch-Natan, O., Winter, D. R., Giladi, A., Vargas Aguilar, S., Spinrad, A., Sarrazin, S., et al. (2016). Microglia development follows a stepwise program to regulate brain homeostasis. *Science* 353:aad8670. doi: 10.1126/science.aad8670

McKay, S. M., Brooks, D. J., Hu, P., and McLachlan, E. M. (2007). Distinct types of microglial activation in white and grey matter of rat lumbosacral cord after mid-thoracic spinal transection. *J. Neuropathol. Exp. Neurol.* 66, 698–710. doi: 10.1097/nen.0b013e3181256b32

Monier, A., Adle-Biassette, H., Delezoide, A. L., Evrard, P., Gressens, P., and Verney, C. (2007). Entry and distribution of microglial cells in human embryonic and fetal cerebral cortex. *J. Neuropathol. Exp. Neurol.* 66, 372–382. doi: 10.1097/nen.0b013e3180517b46

Nayak, D., Roth, T. L., and McGavern, D. B. (2014). Microglia development and function. *Annu. Rev. Immunol.* 32, 367–402. doi: 10.1146/annurev-immunol-032713-120240

Olson, J. K. (2010). Immune response by microglia in the spinal cord. *Ann. N. Y. Acad. Sci.* 1198, 271–278. doi: 10.1111/j.1749-6632.2010.05536.x

Rahimian, R., Cordeau, P. Jr., and Kriz, J. (2019). Brain response to injuries: when microglia go sexist. *Neuroscience* 405, 14–23. doi: 10.1016/j.neuroscience.2018.02.048

Rezaie, P., and Male, D. (1999). Colonisation of the developing human brain and spinal cord by microglia: a review. *Microsc. Res. Tech.* 45, 359–382. doi: 10.1002/(sici)1097-0029(19990615)45:6<359::aid-jemt4>3.3.co;2-4

Schnell, L., Fearn, S., Klassen, H., Schwab, M. E., and Perry, V. H. (1999). Acute inflammatory responses to mechanical lesions in the CNS: differences between brain and spinal cord. *Eur. J. Neurosci.* 11, 3648–3658. doi: 10.1046/j.1460-9568.1999.00792.x

Silvin, A., and Ginhoux, F. (2018). Microglia heterogeneity along a spatio-temporal axis: more questions than answers. *Glia* 66, 2045–2057. doi: 10.1002/glia.23458

Tay, T. L., Savage, J. C., Hui, C. W., Bisht, K., and Tremblay, M. E. (2017). Microglia across the lifespan: from origin to function in brain development, plasticity and cognition. *J. Physiol.* 595, 1929–1945. doi: 10.1113/JP272134

Verney, C., Monier, A., Fallet-Bianco, C., and Gressens, P. (2010). Early microglial colonization of the human forebrain and possible involvement in periventricular white-matter injury of preterm infants. *J. Anat.* 217, 436–448. doi: 10.1111/j.1469-7580.2010.01245.x

Wang, Y., Szretter, K. J., Vermi, W., Gilfillan, S., Rossini, C., Cella, M., et al. (2012). IL-34 is a tissue-restricted ligand of CSF1R required for the development of Langerhans cells and microglia. *Nat. Immunol.* 13, 753–760. doi: 10.1038/ni.2360

Zhang, B., and Gensel, J. C. (2014). Is neuroinflammation in the injured spinal cord different than in the brain? Examining intrinsic differences between the brain and spinal cord. *Exp. Neurol.* 258, 112–120. doi: 10.1016/j.expneurol.2014.04.007

Conflict of Interest: The authors declare that the research was conducted in the absence of any commercial or financial relationships that could be construed as a potential conflict of interest.

Advantages of publishing in Frontiers

OPEN ACCESS
Articles are free to read for greatest visibility and readership

FAST PUBLICATION
Around 90 days from submission to decision

HIGH QUALITY PEER-REVIEW
Rigorous, collaborative, and constructive peer-review

TRANSPARENT PEER-REVIEW
Editors and reviewers acknowledged by name on published articles

Frontiers
Avenue du Tribunal-Fédéral 34
1005 Lausanne | Switzerland

Visit us: www.frontiersin.org
Contact us: info@frontiersin.org | +41 21 510 17 00

REPRODUCIBILITY OF RESEARCH
Support open data and methods to enhance research reproducibility

DIGITAL PUBLISHING
Articles designed for optimal readership across devices

FOLLOW US
@frontiersin

IMPACT METRICS
Advanced article metrics track visibility across digital media

EXTENSIVE PROMOTION
Marketing and promotion of impactful research

LOOP RESEARCH NETWORK
Our network increases your article's readership